



## The electrospinning of xanthan gum: from solution to nanofiber formation

**Shekarforoush, Elhamalsadat; Mendes, Ana Carina Loureiro; Chronakis, Ioannis S.**

*Published in:*  
ANNIC 2017 - Book of abstracts

*Publication date:*  
2017

*Document Version*  
Publisher's PDF, also known as Version of record

[Link back to DTU Orbit](#)

*Citation (APA):*  
Shekarforoush, E., Mendes, A. C. L., & Chronakis, I. S. (2017). The electrospinning of xanthan gum: from solution to nanofiber formation. In *ANNIC 2017 - Book of abstracts* (pp. 235-235). [632].

---

### General rights

Copyright and moral rights for the publications made accessible in the public portal are retained by the authors and/or other copyright owners and it is a condition of accessing publications that users recognise and abide by the legal requirements associated with these rights.

- Users may download and print one copy of any publication from the public portal for the purpose of private study or research.
- You may not further distribute the material or use it for any profit-making activity or commercial gain
- You may freely distribute the URL identifying the publication in the public portal

If you believe that this document breaches copyright please contact us providing details, and we will remove access to the work immediately and investigate your claim.



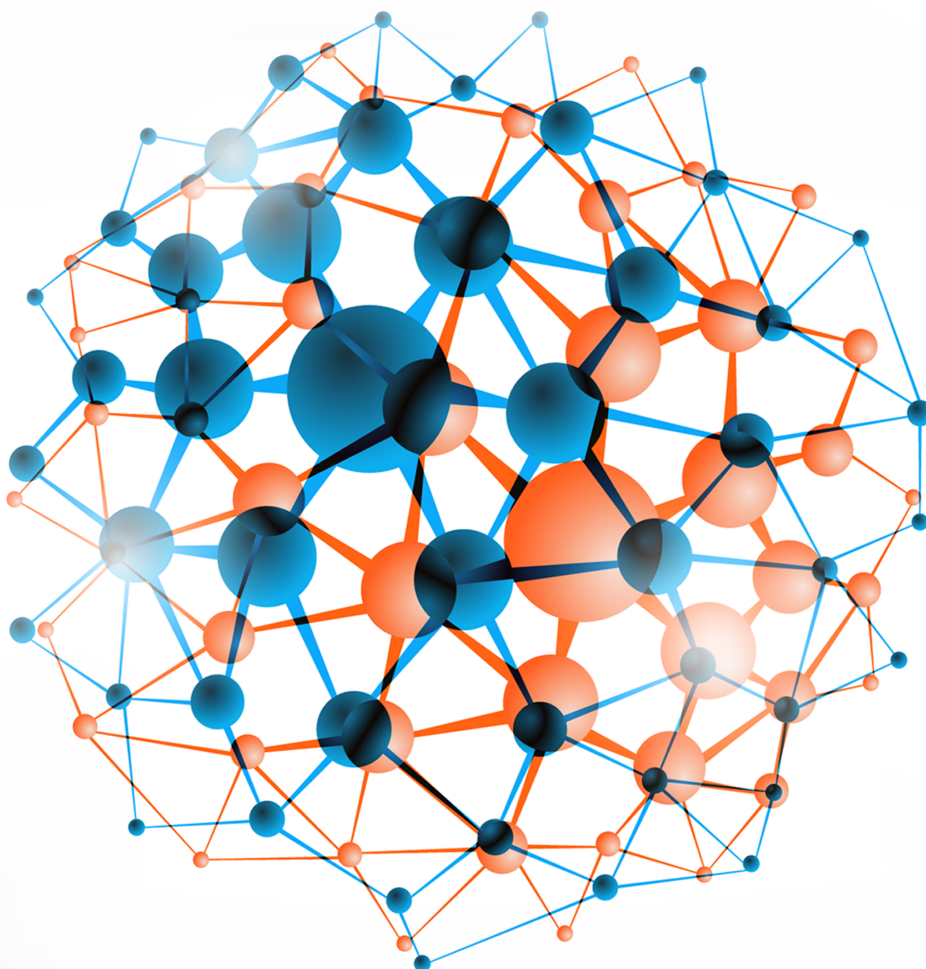
# ANNIC 2017

APPLIED NANOTECHNOLOGY AND NANOSCIENCE  
INTERNATIONAL CONFERENCE

## BOOK OF ABSTRACTS

ROME

Oct 18-20, 2017



Prem 

[premc.org](http://premc.org)

# Table of Contents

<b>Triboelectric Nanogenerators and Tribotronics</b>	<b>1</b>
<u>Prof. Sang-Woo Kim</u>	
<b>2-Dimensional Composites Based On Graphene For Applications In Electronics, Mechanics Or Energy Storage</b>	<b>2</b>
<u>Prof. Vincenzo Palermo</u>	
<b>New approaches for exploiting electron and photon beams inside a TEM for nanoscale characterization</b>	<b>3</b>
<u>Prof. Odile Stéphan</u>	
<b>Fano resonances tuned at Lifshitz transitions in superconducting nanofilaments, a new physics at the crossover between quantum nanomaterials and quantum biology</b>	<b>4</b>
<u>Prof. Antonio Bianconi</u>	
<b>Pd-Cu Core/shell Nanoparticles as an Efficient Catalyst for Fuel Cell applications</b>	<b>5</b>
<u>Mr. Ji Liu, Dr. Xiaofeng Fan, Prof. Changqing Sun, Prof. Weiguang Zhu</u>	
<b>Combination of far-field and near-field electrospinning for “ribs like structures”</b>	<b>6</b>
<u>Mr. Jan Klemes, Dr. Adela Kotzianova, Ms. Julie Bystronova, Dr. Marek Pokorny, Mr. Ondrej Zidek, Dr. Vladimír Velebný</u>	
<b>Surface Enhanced Raman Spectroscopy: silver/gold nanoparticles deposited on graphene monolayers</b>	<b>8</b>
<u>Dr. Věra Jandová, Dr. Martin Koštejn, Dr. Oleksiy Lyutakov, Dr. Radmila Tomovska, Dr. Radek Fajgar</u>	
<b>Development of thermo-responsive magnetic nanoparticles for Cryptosporidium oocyst recovery</b>	<b>9</b>
<u>Dr. Takahiro SEKIKAWA, Dr. Noriyuki OHNISHI, Dr. Xiaomao XIE</u>	
<b>A facile green synthesis of graphene/AuNP/PEDOT:PSS nanocomposite and its application in electrochemical sensor</b>	<b>10</b>
<u>Ms. Paweena Pananon, Mr. Chakrit Sriprachuabwong, Dr. Anurat Wisitsorrat, Dr. Piyachat Chuysinuan, Dr. Adisorn Tuantranont, Prof. Patchareenart Saparpakorn, Dr. Decha Dechtrirat</u>	
<b>Facile synthesis of hybrid nano-alloy catalysts for fuel cell electrodes</b>	<b>11</b>
<u>Dr. Heeyeon Kim, Mr. Guk-hyeon Kwon, Dr. Ji-haeng Yu</u>	
<b>Effect of gas species on the flow rate through porous materials consisting of micro-/nanoscale structures</b>	<b>12</b>
<u>Dr. Guang Yang, Mr. Yiye Huang, Ms. Rongrong Lv, Prof. Bernhard Weigand, Mr. Kilian Weishaupt, Prof. Rainer Helmig, Dr. Alexandros Terzis, Prof. Jingyi Wu</u>	
<b>Remote control of light-triggered virotherapy</b>	<b>13</b>
<u>Prof. S.-Ja Tseng</u>	
<b>Development of Core-shell SiC nanoparticles for Ti-based nanocomposite alloys for additive manufacturing techniques</b>	<b>14</b>
<u>Dr. Maria Dolores Marcos-Martinez, Dr. Mariajose Lopez-Tendero, Dr. Luis Angel Villaescusa-Alonso, Dr. Elena Aznar-Gimeno, Mrs. Angela Rives-Monparler, Mr. Santiago Sanchez-Cabezas, Mr. Andy Sanchez-Montoto, Mrs. Sarai Pradas, Mr. Alejandro Cuenca-Bustos</u>	

<b>Singlet oxygen sensitized delayed fluorescence as tool for estimation of photooxidation properties and oxygen sensing.</b>	<b>15</b>
<u>Dr. Petr Henke, Prof. Jiří Mosinger, Dr. Pavel Kubát</u>	
<b>Silver nanocubes-based sensor for mercury detection in water samples.</b>	<b>16</b>
<u>Ms. Justyna Matyjewicz, Dr. Adam Lesniewski, Dr. Joanna Niedziolka-Jonsson</u>	
<b>The Structure and Properties of Ink-jet Printed Photo-curable in-situ polymerization Cationic Aqueous Dispersion Polyurethane Acrylate/Silica</b>	<b>18</b>
<u>Mr. Yiding Meng, Prof. Jianzhong Shao, Mr. Chenglong Wang, Dr. Yi Huang</u>	
<b>Evaluation of the subcutaneous administration route for human serum albumin nanoparticles in mice</b>	<b>20</b>
<u>Mr. Alejandro Manzanares, Dr. Lino Sánchez-Segura, Dr. Ramón Carriles, Dr. Yolanda Alvarado-Caudillo, Dr. Agustino Martínez-Antonio, Mrs. Dalia Rodríguez-Ríos, Dr. Gloria Barbosa-Sabanero, Dr. Gertrud Lund, Prof. Silvio Zaina</u>	
<b>Fine tuning of the electro-spinning process for novel nano-fibrous elastomerscaffolds</b>	<b>21</b>
<u>Dr. Vera Graup, Mr. Wenhui Song, Mr. Arnold Darbyshire</u>	
<b>Hydrogenization of fullerenes as a method of storage of hydrogen</b>	<b>23</b>
<u>Ms. Zhuldyz Otarbay, Dr. Maratbek Gabdullin, Mr. Yerassyl Yerlanuly, Mr. Daniyar Ismailov, Prof. Khabybulla Abdullyn</u>	
<b>Fiber optic sensor reduced by chemical etching for measuring refractive index of sucrose solutions</b>	<b>24</b>
<u>Dr. P. Zaca-Morán, Dr. J. P. Padilla-martínez, Mr. J. M. Pérez-Corte, Dr. J. G. Ortega-mendoza, Dr. F. Chávez, Dr. G. F. Pérez-sánchez, Mr. N. Morales</u>	
<b>Unoccupied electronic states of few-layer graphene</b>	<b>25</b>
<u>Dr. pierfrancesco riccardi, Dr. Antonio Sindona</u>	
<b>Magnetron sputter deposition of thin VO<sub>2</sub> films onto polycrystalline substrate</b>	<b>26</b>
<u>Dr. Sergey Maklakov, Prof. Sergey A. Maklakov, Mr. Victor Polozov, Mr. Alexey Mishin, Prof. Ilya Ryzhikov, Prof. Vladimir Kisel</u>	
<b>Rapid thermal process by RF heating of nano-graphene layer/silicon substrate structure: Heat explosion theory approach</b>	<b>27</b>
<u>Dr. Misha Sinder, Prof. Joshua Pelleg, Prof. Victor Meerovich, Prof. Vladimir Sokolovsky</u>	
<b>Characterization and Comparison of Photocatalytic Activity Silver Ion doped on TiO<sub>2</sub>(TiO<sub>2</sub>/Ag<sup>+</sup>) and Silver Ion doped on Black TiO<sub>2</sub>(Black TiO<sub>2</sub>/Ag<sup>+</sup>)</b>	<b>28</b>
<u>Ms. Jin Yi Kim, Mr. Ho Hyung Sim, Mrs. SINAEE SONG, Ms. Yeoung Ah Noh, Mr. Hong Woon Lee, Prof. Hee Taik Kim</u>	
<b>Structural, morphological and optical investigation of sol-gel Au-doped ZnO nanostructured thin films.</b>	<b>30</b>
<u>Ms. Lydia OUAREZ, Prof. Azeddine CHELOUCHE, Dr. Tahar TOUAM, Dr. David BARBA, Prof. Rachid MAHIOU, Prof. Djamel DJOUADI, Prof. Federico ROSEI</u>	
<b>Feasibility of low-loss and high-speed plasmonic components and circuits</b>	<b>32</b>
<u>Prof. Mitsuo Fukuda, Mr. Yuuta Tonooka, Mr. Tomoaki Inoue, Mr. Shinya Okahisa, Dr. Yuya Ishii</u>	
<b>Influence of zinc oxide nanofillers on the mechanical properties of PDMS</b>	<b>33</b>
<u>Ms. Karina Jeronimo, Prof. Vasileios Koutsos, Dr. Enrico Mastropaolo</u>	

<b>Pd surface functionalization of 3D electroformed Ni and Ni-Mo alloy metallic nanofoams for hydrogen production</b>	<b>35</b>
<u>Dr. Aurora PETICA, Mr. Danut Balan, Dr. Florentina Golgovici, Prof. Marius Enachescu, Dr. Liana Anicai</u>	
<b>Nanofiber biomass carriers as effective tool for environmental monitoring and technical applications</b>	<b>36</b>
<u>Dr. Lukáš Dvořák, Ms. Magda Nechanická, Ms. Denisa Vlková, Dr. Jan Dolina, Mrs. Iva Dolinová</u>	
<b>Suppressing spontaneous polarization of p-GaN by graphene oxide passivation: enhanced light output of flexible UV-LED</b>	<b>37</b>
<u>Ms. Sooyeon JEONG, Dr. Seung Yol Jeong</u>	
<b>Facile fabrication of non-iridescence structural colored films with high stability and superhydrophobic/oleophobic properties</b>	<b>38</b>
<u>Dr. Yichen Li, Prof. Lan Zhou, Dr. Guojin Liu, Prof. Jianzhong Shao</u>	
<b>Effects on the nanostructure of additive materials in complex solutions</b>	<b>39</b>
<u>Dr. Scott Jamieson</u>	
<b>Design and Analysis of non-linear properties of photonic crystal fiber with Various Doping Concentration</b>	<b>40</b>
<u>Dr. Mohamed Benhaddad, Dr. Fouad Kerrou, Prof. Ouanassa Benabbes</u>	
<b>Fluorescence Active Carbon Nano Spindles Used as a Probe for the Selective Detection of Escherichia coli DNA</b>	<b>41</b>
<u>Mr. sabyasachi Chatterjee, Mr. Anurag Roy, Mr. Srikrishna Pramanik, Dr. Parukuttyamma Sujatha Devi, Dr. Gopinatha Suresh Kumar</u>	
<b>Bi11VO19-VO2 microstructure and its visible light driven photocatalytic performance in organic dye degradation</b>	<b>42</b>
<u>Mrs. Arini Nuran Zulkifili, Prof. Shinji Kimijima, Prof. Jinhua Ye</u>	
<b>Development of NO2 sensor by fungal-ZnFe2O4 at room temperature</b>	<b>43</b>
<u>Mr. Goutham Solleti, Ms. Kruthi Doriya, Dr. Devarai Santhosh Kumar, Prof. Kalagadda Venkateswara Rao</u>	
<b>Photoelectrochemical hydrogen production by decorated metal oxides</b>	<b>44</b>
<u>Mr. Nurlan Bakranov, Dr. Sarkyt Kudaibergenov, Prof. Niazbek Ibraev</u>	
<b>Phase-Controlled Synthesis of Bismuth oxide Polymorphs towards Removal of Environmental Pollutants</b>	<b>45</b>
<u>Dr. Anandan Sambandam</u>	
<b>Effect of doping concentration of lanthanide nanoparticle on homeotropic liquid crystal alignment</b>	<b>46</b>
<u>Mr. Seok Gon Hwang, Mr. Chan-woo Oh, Mr. Eungon Park, Prof. Hong-Gyu Park</u>	
<b>Relaxation dynamics of a multihierarchical polymer network based on Vicsek fractal and dendrimer</b>	<b>47</b>
<u>Dr. Aurel Jurjiu</u>	
<b>Formation of various types of nanostructures on germanium surface by nanosecond laser pulses</b>	<b>48</b>
<u>Mr. Sergei Mikolutskiy, Mr. Radmir Khasaya, Mr. Yury Khomich, Dr. Vladimir Yamshchikov</u>	
<b>Highly efficient electrocatalysts by N-, S-doping of mesoporous carbons for enhanced oxygen reduction reaction</b>	<b>50</b>
<u>Mr. Riccardo Argurio, Prof. Zheng Xiao Guo, Dr. Yun Zong</u>	
<b>On low-dimensional models at NMR line shape analysis in nanomaterial systems</b>	<b>51</b>
<u>Prof. Mikhail Kucherov, Dr. Oleg V. Falaleev</u>	

<b>Hybrid epoxy nanocomposites reinforced with 1D &amp; 2D carbon nanomaterials: Thermomechanical and electrical properties.</b>	<b>52</b>
<u>Mr. Juventino López Barroso, Dr. José Luis Rivera Armenta, Dr. Ana Laura Martínez Hernández, Dr. Armando Almendarez Camarillo, Dr. Perla Elvia García Casillas, Dr. Carlos Velasco Santos</u>	
<b>Indium-saving effect and physical properties of transparent conductive multilayers</b>	<b>53</b>
<u>Prof. Midori Kawamura, Dr. Takayuki Kiba, Prof. Yoshio Abe, Dr. Kyung Ho Kim</u>	
<b>Kinetics of the melting front movement in process of centrifugal induction surfacing of powder material with nanoscale modifiers</b>	<b>54</b>
<u>Mr. Ihar Sasnouski, Mr. Artsiom Kurylionak</u>	
<b>Stretchable and flexible thermoelectric polymer composites</b>	<b>56</b>
<u>Dr. Petr Slobodian, Dr. Jiri Matyas, Dr. Robert Olejnik, Dr. Pavel Riha</u>	
<b>Synthesis and application of magnetic catalyst for hydrogenation reaction</b>	<b>57</b>
<u>Mr. Po-Wei Lan, Prof. Chuh-yung Chen, Prof. Cheng-Chien Wang</u>	
<b>The effect of surface modification with silane coupling agent on blue-light curable inkjet printing of TiO<sub>2</sub> particles as white inks</b>	<b>58</b>
<u>Mr. Chenglong Wang, Prof. Jianzhong Shao, Mr. Yiding Meng</u>	
<b>Influence of gas flow ratio on formation of silicon nanocrystals in SiN<sub>x</sub>:H</b>	<b>59</b>
<u>Mrs. Faiza Tiour, Dr. bedra Benyahia, Dr. Nouredine Brihi, Dr. Ali Sari, Dr. Brahim Mahmoudi, Mrs. Isa Menous</u>	
<b>Cytotoxicity of graphene oxide in human endothelial cells</b>	<b>60</b>
<u>Ms. Na Geum Lee, Dr. Young-Lai Cho, Dr. Jeong-ki Min</u>	
<b>Anti-bacterial and anti-cancerous potential of medicinal plant mediated biofabricated nanoparticles: A question to its selective cytotoxicity?</b>	<b>63</b>
<u>Mr. Parth Sarthi Nayak, Mr. Manish Sharma, Dr. Suman Jha</u>	
<b>Theoretical study on the origins of the gap bowing in CaxMg<sub>1-x</sub>S alloys</b>	<b>65</b>
<u>Dr. Boutarfa Bariza</u>	
<b>Large scale roll-to-roll coating process to enhance the optical and electrical properties for transparent conductive single-walled carbon nanotube /silver nanowire hybrid film</b>	<b>66</b>
<u>Prof. Kwan Han Yoon, Prof. Young Sil Lee</u>	
<b>Fast and large-scale synthesis of 2D molybdenum trioxide (MoO<sub>3</sub>) nanosheets for ion-exchange battery applications</b>	<b>67</b>
<u>Mrs. Anousha Khamsavi, Mr. Mahdi Sasar, Dr. Yaser Abdi</u>	
<b>Epoxide-based organic inorganic nano-hybrid materials using surface modifier-free hybridization method toward highly effective filling of ZrO<sub>2</sub> nano-particles</b>	<b>68</b>
<u>Mr. Kazushi Enomoto, Dr. Moriya Kikuchi, Prof. Atsushi Narumi, Prof. Seigou Kawaguchi</u>	
<b>Comparison between layering NbSe<sub>2</sub> and rod characteristic of MgB<sub>2</sub> by investigation of elastic constants</b>	<b>70</b>
<u>Ms. Asiye Shokri, Dr. Ahmad Yazdani, Mr. behrad barakati</u>	

<b>Multifunctional graphene (RGO) wrapped Au plasmonic nanostructure: Giant enhanced photoluminescence, excellent visible-light assisted photodetection along with its application towards electrochemical non-enzymatic H<sub>2</sub>O<sub>2</sub> and AA biosensor</b>	<b>71</b>
<u>Mr. Sumit Majumder, Dr. Sanjay Kumar, Prof. Sangam Banerjee</u>	
<b>Metamaterials based on mixture of Au and CdZnSe/ZnS nanoparticles for future sensorics</b>	<b>73</b>
<u>Dr. Elena Ushakova, Dr. Sergei Cherevkov, Ms. Tatiana Kormilina, Dr. Aliaksei Dubavik, Mr. Mikhail Baranov, Dr. Aleksandr Litvin, Prof. Anatoly Fedorov, Prof. Alexander Baranov</u>	
<b>Stabilization of silver nanoparticles with dyes for optical limiting</b>	<b>74</b>
<u>Dr. Cordula Hege, Dr. Olivier Muller, Ms. Stefanie Dengler, Dr. Bernd Eberle, Mr. Lionel Merlat</u>	
<b>Tubular gold nanoparticle assemblies</b>	<b>75</b>
<u>Mr. Priyadarshi Ranjan, Dr. Ronit Popovitz-biro, Dr. Iddo Pinkas, Dr. Sidney Cohen, Dr. Michal Lahav, Prof. Reshef Tenne, Prof. Milko van der Boom</u>	
<b>In situ synthesis of plasmonic and magnetic nanoparticles in polymer thin films under laser and solar irradiation</b>	<b>76</b>
<u>Mr. Elie Nadal, Mr. Laurent Peres, Dr. Noémi Barros, Prof. Marc Respaud, Dr. Katerina Soulantica, Prof. Hamid Kachkachi</u>	
<b>The dynamical and thermodynamic properties of the Pöschl-Teller oscillator in Quantum Engines.</b>	<b>77</b>
<u>Dr. Enock Oluwole OLADIMEJI, Prof. Rudoy Yuri G</u>	
<b>Electroactive Self-Assembled-Monolayer for Smart Functional Surfaces</b>	<b>78</b>
<u>Ms. Maria Serena Maglione, Dr. Stefano Casalini, Dr. Stamatis Georgakopoulos, Dr. Nuria Crivillers, Dr. Concepción Rovira, Dr. Marianna Barbalinardo, Mr. Vitaliy Parkula, Dr. Pierpaolo Greco, Dr. Marta Mas-Torrent</u>	
<b>Magnetic, thermal and luminescence properties in room-temperature nanosecond electron-irradiated various metal oxide nanopowders</b>	<b>79</b>
<u>Prof. Sergey Sokovnin, Dr. Vladislav Il'ves, Mr. Michail Balezin</u>	
<b>High performance nanowire based field effect transistors for sensing applications</b>	<b>81</b>
<u>Dr. Camelia Florica, Dr. Andreea Costas, Dr. Nicoleta Preda, Dr. Elena Matei, Dr. Ionut Enculescu</u>	
<b>Assessment on Lattice Thermal Transport Properties of Functionalized MXene Structures</b>	<b>82</b>
<u>Dr. Sevil Sarikurt, Dr. Deniz Cakir, Dr. Murat Keceli, Dr. Cem Sevik</u>	
<b>Continuous production of monodisperse nanoparticles assemblies by an in-flow ligand desorption method.</b>	<b>83</b>
<u>Dr. Jenny Merlin, Dr. Steven Ferguson, Dr. Dermot F. Brougham</u>	
<b>Highly reliable controllability of quadruple-level-cell operation in HfO<sub>2</sub> based resistive switching device</b>	<b>84</b>
<u>Dr. Gun Hwan Kim, Dr. Bo Keun Park, Dr. Taek-mo Chung, Dr. Young Kuk Lee</u>	
<b>Light-funnel arrays for photovoltaic applications: a novel approach toward absorption enhancement of the solar radiation</b>	<b>86</b>
<u>Dr. Gil Shalev, Mr. Gilad Marko, Mr. Tamir Gabay, Mr. Yuval Nissan</u>	
<b>Point Defect-Passivated MoS<sub>2</sub> Nanosheet-Based High Performance Piezoelectric Nanogenerator</b>	<b>88</b>
<u>Dr. Sang A Han, Prof. Sang-Woo Kim</u>	

<b>Electron Beam-Induced Transformation of Cesium Lead Halide Perovskite Nanocrystals</b>	<b>89</b>
<u>Dr. Zhiya Dang, Mr. Javad Shamsi, Mr. Muhammad Imran, Mr. Quinten Akkerman, Dr. Giovanni Bertoni, Dr. Rosaria Brescia, Prof. Liberato Manna</u>	
<b>Synthesis and characterization of Pd nanocatalyst at W based support for low temperature fuel cells application</b>	<b>91</b>
<u>Dr. Nevenka Elezovic, Mrs. Mila Krstajic Pajic, Dr. Piotr Zabinski, Dr. Peter Ercius, Prof. Velimir Radmilovic, Prof. Nedeljko Krstajic</u>	
<b>Effect of Mechanically-Induced Doping With 10 wt.% TiO<sub>2</sub> on the Hydrogen Uptake/Release Kinetics of Commercial MgH<sub>2</sub> Powders</b>	<b>93</b>
<u>Ms. shorouq ahmed</u>	
<b>Carbon nanofibers: A new adsorbent for Au (III)</b>	<b>95</b>
<u>Dr. Irene Garcia Diaz, Dr. Felix Antonio Lopez, Dr. Francisco José Alguacil</u>	
<b>On the interaction of TEMPO radicals with gold clusters</b>	<b>97</b>
<u>Dr. Carolina Aliaga, Dr. Marcos Rezende, Ms. Camila Pastene</u>	
<b>Fluorescence enhancement via excitation of bright and dark modes in 2D plasmonic nanostructures</b>	<b>98</b>
<u>Mr. Alexey Shaymanov, Mr. Igor Nechepurenko, Mr. Alexander Baburin, Mr. Kirill Khabarov, Mr. Elena Ryzhova, Mr. Alexander Dorofeenko, Dr. Peter Tananaev, Dr. George Yankovskij, Dr. Ilya Rodionov, Dr. Alexander Baryshev</u>	
<b>Plasmonic Enhanced Upconversion Nanostructure for Anti-counterfeit Devices</b>	<b>99</b>
<u>Mrs. KISUN PARK, Dr. Ho Seong Jang, Dr. Il Ki Han, Prof. Dongjin Byun, Dr. Hyungduk Ko</u>	
<b>Suppression and Enhancement of Deep Level Emission of ZnO on Si<sup>4+</sup> &amp; V<sup>5+</sup> substitution</b>	<b>100</b>
<u>Ms. Tulika Srivastava, Mr. Gaurav Bajpai, Dr. Somaditya Sen</u>	
<b>On-chip Synthesis of Nanoporous Silver Microstructures (np-AgMSs) as Mesoporous Materials for SERS Substrate Application.</b>	<b>101</b>
<u>Ms. Duangtip Lawanstien, Dr. Kanet Wongravee, Dr. Mopichar Srisa-art</u>	
<b>Conducting Polymer Nanospheres of High Electrochemical Activity – Synthesis and Sensor Applications</b>	<b>103</b>
<u>Prof. Agata Michalska, Prof. Krzysztof Maksymiuk</u>	
<b>Band edge corrections of semiconductor alloys for buffers nano-materials based solar cells</b>	<b>104</b>
<u>Dr. OUARAB Nouredine</u>	
<b>Carbon nanomaterials: Adsorbents for organic contaminants in wastewater</b>	<b>105</b>
<u>Mrs. Ana Lopez Fernandez, Dr. Irene Garcia Diaz, Dr. Lorena Alcaraz, Prof. Miguel Angel Casermeiro, Dr. Félix López</u>	
<b>Determination of permeability of ultra-fine cupric oxide aerosol through military filters and protective filters</b>	<b>107</b>
<u>Ms. Eva Kellnerová, Dr. Zbyněk Večeřa, Prof. Josef Kellner, Dr. Tomáš Zeman, Dr. Josef Navratil</u>	
<b>Enhancing the performance of water treatment polyethersulfone membranes using graphene materials</b>	<b>109</b>
<u>Prof. Ahmed Abdala</u>	
<b>Controlling Hydrophilicity of Titanium Dioxide for Self-cleaning Surfaces</b>	<b>111</b>
<u>Mr. Abdullah Alkandary, Dr. feras alzubi</u>	



<b>Synthesis, mechanistic studies and technological innovation of applying oxide nanomaterials in wastewater treatment by flotation</b>	<b>113</b>
<u>Prof. Cristina Covaliu, Prof. Gigel Paraschiv, Prof. Laura Toma, Prof. Eugeniu Vasile</u>	
<b>Structural and optical properties of SiC-SiO<sub>2</sub> nanocomposite thin films</b>	<b>114</b>
<u>Dr. isma bozetine, Dr. Aissa Keffous, Dr. Samira Kaci, Mr. Menari Hamid, Mr. Amar Manseri</u>	
<b>N-DOPED TiO<sub>2</sub>/CdS NANOCOMPOSITE FILMS: SILAR SYNTHESIS, CHARACTERIZATION AND APPLICATION IN QUANTUM DOTS SOLAR CELL</b>	<b>115</b>
<u>Prof. Kristian Handoyo Sugiyarto, Dr. Cahyorini Kusumawardani, Prof. Anti Kolonial Prodjosantoso</u>	
<b>Liposome-based Multifunctional glioblastoma-Targeted drug delivery</b>	<b>116</b>
<u>Dr. Beatrice Formicola, Dr. Lorena Passoni, Prof. Michela Matteoli, Dr. Maria Gregori, Dr. Francesca Re, Prof. Massimo Masserini</u>	
<b>Alteration of temoporfin pharmacokinetics by <math>\beta</math>-cyclodextrin derivatives</b>	<b>118</b>
<u>Dr. Igor Yankovsky, Mr. Ilya Yakavets, Dr. Henri-Pierre Lassalle, Dr. Lina Bezdetnaya, Dr. Vladimir Zorin</u>	
<b>A Highly Promising Treatment Option for Glioblastoma Using Dual-Epitope Decorated Therapeutic Nanoparticles</b>	<b>120</b>
<u>Dr. Sheikh Mohamed Mohamed, Dr. Srivani Veerananarayanan, Prof. Yasushi Sakamoto, Prof. Toru Maekawa, Prof. Sakthi Kumar D</u>	
<b>Biodegradable multiliposomal carriers with controllable stability in water-salt media</b>	<b>121</b>
<u>Dr. Olga Zaborova, Dr. Andrey Sybachin, Prof. Timothy Deming, Prof. Alexander Yaroslavov</u>	
<b>Mechanical properties of nanoparticles affecting interactions with tumor cells</b>	<b>122</b>
<u>Dr. Ofra Benny</u>	
<b>Nanoclusters of self-assembled quantum dots driven by fluorine-fluorine interactions as delivery platform for enzymes</b>	<b>124</b>
<u>Dr. Carolina Carrillo Carrion, Dr. Mónica Carril, Prof. Wolfgang Parak</u>	
<b>Magnetically Targeted Delivery of Sorafenib to Liver Using Solid Lipid Nanoparticles for Treatment of Hepatocellular Carcinoma</b>	<b>126</b>
<u>Dr. Nicoletta Depalo, Mr. Fabio Vischio, Ms. Ilaria Arduino, Ms. Silvia Villa, Prof. Fabio Canepa, Dr. Elisabetta Fanizza, Prof. Byung Chul Lee, Dr. Valentino Laquintana, Prof. Angela Lopodota, Dr. Annalisa Cutrignelli, Dr. Maria Principia Scavo, Dr. Marinella Striccoli, Prof. Angela Agostiano, Dr. M. Lucia Curri, Dr. Nunzio Denora</u>	
<b>Hybrid organic-inorganic materials as precursors for water splitting electrocatalysts</b>	<b>127</b>
<u>Mr. Rui Zhang, Dr. Patricia Russo, Prof. Nicola PINNA</u>	
<b>Charge dynamics in composite systems for advanced applications</b>	<b>128</b>
<u>Prof. Alberto Vomiero</u>	
<b>Radical Properties in Functional Oxide Thin Films from Insulators to Superconductors</b>	<b>129</b>
<u>Prof. Judith Driscoll</u>	
<b>2D Semiconductor nanostructures at atomic scale</b>	<b>130</b>
<u>Prof. Jordi Arbiol</u>	



<b>Design of screen-printed carbon electrodes on nanocellulose membranes</b>	<b>131</b>
<u>Dr. Robson Silva</u> , Dr. Deivy Wilson, Dr. Rafael R. Domenegueti, Dr. Sidney J. L. Ribeiro, Dr. Osvaldo N. Oliveira Jr.	
<b>Achieving higher sensitivity of CdS-based SAW sensor detecting visual light</b>	<b>132</b>
<u>Mr. Byungmoon Lee</u> , Mr. Jin Woo Lee, Mr. Jong Woo Kim, Mr. Jinkee Hong, Prof. Byeong-kwon Ju	
<b>Investigation of etchant composition on the contact angle and morphology of the black silicon, formed by MACE with Ni</b>	<b>134</b>
<u>Ms. Olga Volovlikova</u> , Mr. Sergey Gavrilov, Mr. Gennady Silakov, Mr. Artem Sysa, Ms. Yana Grishina, Ms. Yulia Shilyaeva	
<b>Lateral epitaxial heterojunctions in single nanowires fabricated by masked cation exchange</b>	<b>136</b>
<u>Dr. Sedat Dogan</u> , Dr. Stefan Kudera, Dr. Zhiya Dang, Dr. Francisco Palazon, Dr. Urko Petralanda, Dr. Sergey Artyukhin, Dr. Luca De Trizio, Prof. Liberato Manna, Prof. Roman Krahne	
<b>One-step synthesis of porous carbon nanosheets with controllable pore size and their dye adsorption performances</b>	<b>137</b>
<u>Mrs. Jiyoung Lee</u> , Ms. Yeong A. Lee, Dr. Chung-Yul Yoo, Dr. Jung Joon Yoo, Dr. Hana Yoon, Prof. Bongsoo Kim	
<b>Liposomes decorated with G-Quadruplex Decoy Oligonucleotides: Their Nanoparticle Delivery and efficient Bioactivity in Pancreatic Cancer Cells</b>	<b>138</b>
Dr. Susanna Cogoi, Dr. Ulla Jakobsen, <u>Dr. Erik Pedersen</u> , Prof. Luigi Xodo, Dr. Stefan Vogel	
<b>Silicon Nanowires for Water Splitting</b>	<b>139</b>
<u>Dr. Vladislav Dřínek</u> , Dr. Pavel Dytrych, Dr. Radek Fajgar, Dr. Mariana Klementová	
<b>Magnetic thermometer: thermal effect on the dynamics of agglomeration of magnetite nanoparticles by magnetic field</b>	<b>141</b>
<u>Prof. Hackjin Kim</u>	
<b>Hydrogenation/ Dehydrogenation Kinetics Behaviors of MgH<sub>2</sub> Powders Doped With 10wt % ZnO Nanoparticles</b>	<b>143</b>
<u>Ms. shorouq ahmed</u>	
<b>An investigation into the effect of thickness and annealing temperature on RF sputtered ZnO thin film properties for photonic applications</b>	<b>145</b>
Mr. Abderaouf NAMOUNE, Dr. Tahar TOUAM, <u>Dr. Laid HAMMICHE</u> , Prof. Azeddine CHELOUCHE, Prof. Djamal DJOUADI	
<b>Effects of (Ce, Cu) co-doping on the structural and optical properties of ZnO aerogels synthesized in supercritical ethanol</b>	<b>146</b>
<u>Prof. Djamal DJOUADI</u> , Mrs. Ouidette SLIMI, Dr. Laid HAMMICHE, Prof. Azeddine CHELOUCHE, Dr. Tahar TOUAM	
<b>Simple morphological control over functional diversity of SERS materials</b>	<b>147</b>
<u>Dr. Anna Semenova</u> , Dr. Alexander Barantchikov, Prof. Vladimir Ivanov, Prof. Eugene Goodilin	
<b>NFFA-Europe: enhancing European competitiveness in nanoscience research and innovation</b>	<b>149</b>
<u>Dr. Flavio Carsughi</u>	

<b>The effect of Silicon Quantum Dots on Different Cell Types</b>	<b>150</b>
Ms. Tereza Belinova, <u>Dr. Iva Machová</u> , Ms. Lucie Vrabcová, Dr. Anna Fuciková, Prof. Jan Valenta, Dr. Hiroshi Sugimoto, Dr. Minoru Fujii, Dr. Marie Hubalek Kalbacova	
<b>Nanostructured zeolites for heavy metals removal from wastewater</b>	<b>151</b>
<u>Prof. Cristina Covaliu</u> , Prof. Gigel Paraschiv, Prof. Eugeniu Vasile, Prof. Ecaterina Matei	
<b>High-contrast-resolution single nanoparticle spectroscopy with MEMS-scanning mirrors based polarization-interferometric laser microscope</b>	<b>153</b>
<u>Prof. Chikara Egami</u> , Mr. Yuki Hata	
<b>Effect of thickness on physical and waveguiding properties of nanostructured AZO thin films by a sol-gel dip-coating method</b>	<b>154</b>
Mrs. Khamsa NECIB, Dr. Tahar TOUAM, <u>Prof. Azeddine CHELOUCHE</u> , Ms. Lydia OUAREZ, Prof. Djamal DJOUADI, Dr. Laid HAMMICHE	
<b>Rapid Isolation and Diagnosis of Brain Injury Marker in Plasma by SERS Nanosensor</b>	<b>156</b>
<u>Mr. Waleed Hassanain</u> , Dr. Sivanesan Arumugam, Dr. Emad Kiriakous, Prof. Godwin Ayoko, Prof. Martin Sillence	
<b>Glucose oxidase immobilization studies on boron doped CVD diamond coatings</b>	<b>158</b>
<u>Prof. Rui Silva</u> , Dr. Miguel Neto, Dr. Ana Piedade, Dr. Filipe Oliveira	
<b>Surface Modification of Porous Silicon Carbide by formation of a Functionalized Polymer</b>	<b>160</b>
<u>Mrs. Lamia TALBI</u>	
<b>Characterization of local atomic structure in Co/Zn based ZIFs by XAFS</b>	<b>161</b>
<u>Ms. Yulia Podkovyrina</u> , Ms. Vera Butova, Ms. Elena Bulanova, Dr. Andriy Budnik, Prof. Alexander Soldatov, Prof. Carlo Lamberti	
<b>Highly controlled nanoporous Ag electrode by vaporization control of 2-Ethoxyethanol for a flexible supercapacitor application</b>	<b>163</b>
<u>Mr. Jinwoo Lee</u> , Mr. Jinhyeong Kwon, Mr. Habeom Lee, Prof. Seung Hwan Ko	
<b>Adherence of amino acids functionalized iron oxide nanoparticles on bacterial models E. coli and B. subtilis</b>	<b>165</b>
Dr. Wiliam Trujillo, Ms. jacquelyne zarria romero, Dr. J. Pino Gaviño, <u>Ms. Lucila Menacho</u> , Dr. M. Coca Calderón, <u>Dr. Angel Bustamante</u>	
<b>Dynamic Consolidation and Investigation of Nanostructural W-Cu / W-Y Cylindrical Billets</b>	<b>166</b>
<u>Dr. Bagrat Godibadze</u> , Dr. Akaki Peikrishvili, Dr. Elguja Chagelishvili, Mr. Avtandil Dgebuadze, Dr. Grigor Mamniashvili	
<b>Unraveling the ultrafast fluorescence properties of copper nanoclusters synthesized within the nanopool of reverse micelles</b>	<b>167</b>
<u>Mr. Raj Kumar Koninti</u> , Mr. Partha Hazra	
<b>Graphene/styrene-isoprene-styrene copolymer composite thin film as a flexible microstrip antenna for heptane vapors detection</b>	<b>169</b>
Dr. Robert Olejnik, Dr. Jiri Matyas, <u>Dr. Petr Slobodian</u> , Dr. Pavel Riha	

<b>Understanding of two distinct and independent mechanisms of apoptosis and autophagy-mediated necrosis in human endothelial cells to determine size allowance of silica nanoparticles for biomedical application</b>	<b>170</b>
Dr. Young-Lai Cho, <u>Ms. Na Geum Lee</u> , Dr. Kwang-hee Bae	
<b>Wireless electronic manometer based on nanomaterials</b>	<b>172</b>
<u>Ms. Zhuldyz Otarbay</u> , Ms. Dilyara Abay, Ms. Madengul Token, Dr. Mukhit Muratov, Mr. Daniyar Ismailov, Mr. Nazim Guseinov, Dr. Maratbek Gabdullin	
<b>Antibiotic-Encapsulated Poly(lactic acid) Particles integrated in Porous Gelatin Scaffolds for Tissue Engineering Applications</b>	<b>173</b>
<u>Dr. Patcharakamon Nooeaid</u> , Dr. Piyachat Chuysinuan, Dr. Chalanan Pengsuk, Dr. Decha Dechtrirat, Prof. Supanna Techasakul	
<b>Microstructure Characterization of Mechanically-Induced Synthesizing of Zinc Metatitanate</b>	<b>174</b>
<u>Dr. Latifah Alhajji</u>	
<b>Cytochrome P450 genes expression in HepG2 cells after treatment with nanostructures of different allotropic forms of carbon</b>	<b>175</b>
<u>Ms. Barbara Strojny</u> , Dr. Marta Grodzik, Ms. Malwina Sosnowska, Mr. Jarosław Szczepaniak, Dr. Marta Kutwin, Dr. Sławomir Jaworski, Ms. Natalia Kurantowicz, Dr. Mateusz Wierzbicki, Dr. Anna Hotowy, Prof. Ewa Sawosz	
<b>Anti-inflammatory properties of new hybrid biomaterials based on silver nanoparticles and polyphenols from European elderberry fruits</b>	<b>176</b>
<u>Prof. Luminita David</u> , Dr. Bianca Moldovan, Mrs. Nicoleta Decea, Prof. Gabriela Adriana Filip	
<b>Microstructure analysis of differently shaped nanocrystalline (Fe,Y)3O4</b>	<b>177</b>
<u>Dr. Bratislav Antic</u>	
<b>Material Science and Nanotechnology Application in Biomedical Practice.</b>	<b>178</b>
Dr. Sidorenko Evgeny, <u>Dr. Musina Alvina</u>	
<b>Luminescent Dye-Doped Polymer Nanofibers Produced by Electrospinning Technique</b>	<b>179</b>
Dr. Monica Enculescu, Mr. Alex Evangelidis, <u>Dr. Ionut Enculescu</u>	
<b>Poly (lactic acid) (PLA) electrospun nanofibers containing rice extracts for biomedical applications</b>	<b>180</b>
<u>Dr. Piyachat Chuysinuan</u> , Mr. Nitirat Chimnoi, Mrs. Lalita Pattani, Mrs. Panita Khlaychan, Dr. Patcharakamon Nooeaid, Prof. Supanna Techasakul	
<b>Observation of partial relaxation mechanisms via anisotropic strain relief on epitaxial islands using semiconductor nanomembranes</b>	<b>181</b>
<u>Ms. Bárbara Rosa</u> , Ms. Lucas Marçal, Dr. Rodrigo Andrade, Dr. Luciana Dornelas, Prof. Wagner N Rodrigues, Prof. Patricia Lustoza, Prof. Maurício Pires, Prof. Ricardo W Nunes, Prof. Ângelo Malachias	
<b>The effects of biofunctionalized silver nanoparticles with polyphenols from Cornus Mas in experimental inflammation</b>	<b>183</b>
<u>Prof. Gabriela Adriana Filip</u> , Prof. Simona Clichici, Mrs. Nicoleta Decea, Dr. Ioana Baldea, Dr. Diana Olteanu, Dr. Ramona Suharoschi, Dr. Ioana Scrobota, Dr. Mihai Cenariu, Dr. Bianca Moldovan, Prof. Luminita David	
<b>Magnetic and Structural Properties of the Maghemite Core-Shell Nanoparticles at Elevated Temperatures</b>	<b>184</b>
Mr. Ihor Syvorotka, Mr. Stepan Hurskyy, <u>Prof. Sergii Ubizskii</u> , Prof. Leonid Vasylechko	

<b>Development of a thermo-reversible in situ forming implant associated with Nanostructured Lipid Carriers (NLC) as sustained delivery system for estradiol valerate.</b>	<b>185</b>
<u>Mrs. María Teresa Pineda Hernández, Dr. Flora Adriana Ganem Rondero</u>	
<b>Shock Assisted Liquid Phase Consolidation of Nanostructured W-Ag Composites</b>	<b>186</b>
<u>Dr. Akaki Peikrishvili, Dr. George Tavadze, Dr. Bagrat Godibadze, Dr. Elguja Chagelishvili, Mr. Avtandil Dgebuadze</u>	
<b>Graphene-based nanocomposites decorated with silver nanoparticles as antibacterial agent</b>	<b>187</b>
<u>Dr. Sławomir Jaworski, Dr. Mateusz Wierzbicki, Prof. Ewa Sawosz, Dr. Marta Kutwin, Ms. Barbara Strojny, Ms. Natalia Kurantowicz, Dr. Marta Grodzik</u>	
<b>Thermophysical properties of nanofluids containing nanodiamonds/graphite mixture with various ash fractions</b>	<b>188</b>
<u>Dr. Gawęł Żyła, Mr. Jacek Fal, Dr. Patrice Estellé</u>	
<b>Water purification via traditional pottery impregnated with silver nanoparticles</b>	<b>189</b>
<u>Dr. Heli Piedra-gil, Dr. Juan Antonio Hoyoz-guzman, Dr. Lesli Ortega-arroyo, Dr. Jorge Humberto Vargas-aparicio, Dr. Maria Sanchez-góngora, Dr. Teresita Cardona-juárez, Dr. Eduardo San Martín, Dr. Luz Perez-rea, Dr. Fabio Vengoechea, Dr. Victor M Castaño</u>	
<b>Electrodeposition of Sn-rGO composites involving choline chloride – ethylene glycol ionic liquids with applications in electronics</b>	<b>190</b>
<u>Mrs. Stefania Costovici, Mr. Dan Balan, Ms. Oana Brincoveanu, Prof. Teodor Visan, Dr. Liana Anicai, Prof. Marius Enachescu</u>	
<b>Niobium oxide nanocolumns formed via anodic alumina with modulated pore diameters</b>	<b>192</b>
<u>Dr. Andrei Pligovka, Ms. Anna Zakhlebayeva, Mr. Andrei Lazavenka</u>	
<b>Light-induced oxygen sensing using a ZnO/GO based oxygen sensor</b>	<b>193</b>
<u>Mr. Mahdi Sasar, Mrs. Anousha Khamsavi, Mr. Yusef Khosravi, Dr. Yaser Abdi</u>	
<b>Growth of a highly c-axis oriented AlN thin films</b>	<b>195</b>
<u>Dr. Nabila Redjda, Prof. Mouhamed Azzaz, Dr. Nouredine Gabouze, Dr. Olivier Tottereau, Mr. Hamid Menari, Dr. Bendiba Guedouar</u>	
<b>Synthesis of nanocrystalline <math>\alpha</math>-Fe<sub>2</sub>O<sub>3</sub> by using thermal Oxidation of Fe Films</b>	<b>196</b>
<u>Ms. Ghania Fortas, Dr. Nouredine Gabouze, Prof. Nacereddine Haine, Mr. Amar Manseri, Prof. Mourad Zergoug, Mr. Menari Hamid, Dr. Sam Sabrina, Mr. Hocine Cheraga, Dr. isma bozetine</u>	
<b>Polyamide/Polyethylene/ Oxidized Graphite Nanocomposites With Functional Compatibilizers: Characterization By Physico-Mechanical Tests And Atr-Ftir Spectrometry</b>	<b>197</b>
<u>Dr. Alexandrescu Laurentia, Mr. Mihai Georgescu, Dr. Maria Sonmez, Dr. Anton Ficai, Dr. Denisa Ficai, Mr. Ligian Tudoroiu, Dr. Roxana Trusca</u>	
<b>Composite Material Polystyrene activated carbon for Water Purification</b>	<b>198</b>
<u>Dr. Abdelhak Maghchiche</u>	
<b>Electrical properties of thin films deposited from TMS/O<sub>2</sub> in Microwave Multipolar Plasma reactor</b>	<b>199</b>
<u>Mr. Kihel Mouloud, Prof. Salah Sahli, Prof. Patrice Raynaud, Dr. Mohamed Benhaddad, Dr. Fermi Youcef</u>	
<b>Magneto-thermal competition on interface effect of urea-nano size magnetite formation</b>	<b>200</b>
<u>Dr. Ahmad Yazdani, Ms. samira sharifi</u>	

<b>Poly(3,4-ethylenedioxythiophene)-Single Walled Carbon Nanohorns Composite Coatings for Neural Sensing and Stimulation</b>	<b>201</b>
<u>Dr. stefano carli</u> , Mrs. Linda Lambertini, Dr. Elena Zucchini, Dr. Francesca Ciarpella, Dr. Alice Scarpellini, Dr. Mirko Prato, Dr. Elisa Castagnola, Dr. Davide Ricci, Prof. Luciano Fadiga	
<b>Synthesis ABA Triblock Copolymers by Complex Living Free Radical Polymerization</b>	<b>203</b>
<u>Mrs. PIN-CHEN LEE</u> , Prof. Chuh-yung Chen, <u>Prof. Cheng-Chien Wang</u>	
<b>Nanofibrous Waterproof Breathable Protective Clothing</b>	<b>205</b>
Mr. Fouad J. Maksoud, Mr. Mohammad Lameh, Mr. Sary Fayyad, Dr. Nagham Ismail, <u>Dr. Ali Tehrani</u> , Prof. Nesreen Ghaddar, Prof. Kamel Ghali	
<b>Concepts of Novel Infrared Photodetectors Based on van der Waals/Graphene Heterostructures</b>	<b>207</b>
<u>Dr. Maxim Ryzhii</u> , Prof. Victor Ryzhii, Prof. Taiichi Otsuji, Prof. Michael Shur	
<b>Nonlinear behavior of fluid conveying single-walled carbon nanotubes with a geometrical imperfection</b>	<b>209</b>
<u>Ms. Liu Chenxin</u> , Prof. Ni Qiao	
<b>A new biochemical approach for controlled release of dexamethasone from functionalized PEDOT coatings for neural applications.</b>	<b>210</b>
<u>Dr. stefano carli</u> , Prof. Claudio Trapella, Mrs. Linda Lambertini, Dr. Anna Fantinati, Dr. Elisa Castagnola, Ms. Claudia Cea, Ms. Surabhi Nimbalkar, Dr. Alice Scarpellini, Dr. Mirko Prato, Prof. Sam Kassegne, Dr. Davide Ricci, Prof. Luciano Fadiga	
<b>Microfluidic synthesis of multifunctional liposomes for targeted drug delivery</b>	<b>212</b>
<u>Mr. Rui Ran</u>	
<b>Potential environmental risk of <sup>223</sup>Ra-labelled hydroxyapatite nanoparticles.</b>	<b>214</b>
<u>Prof. Stanislav Smrcek</u> , Mr. Pavel Nykl, Ms. Tereza Krmelová, Dr. Martin Vlk, Prof. Ján Kozempel	
<b>Antibacterial nanosilver: defeating resistance, prolonged effects, mechanisms, and potential applications</b>	<b>215</b>
<u>Ms. Dina Mosselhy</u> , Ms. Henrika Granbhom, Dr. Ulla Hynönen, Dr. Yanling Ge, Prof. Airi Palva, Prof. Katrina Nordström, Prof. Simo-Pekka Hannula	
<b>Proteins immobilized on nanoparticles – determination of the surface coverage</b>	<b>216</b>
<u>Dr. Jaroslaw Grobelny</u> , Dr. Katarzyna Ranoszek-Soliwoda, Ms. Ewa Czechowska, Dr. Emilia Tomaszewska, Dr. Grzegorz Celichowski, Prof. Janusz Szemraj	
<b>Nanomedicines as photodynamic therapy for cancer</b>	<b>217</b>
<u>Dr. Swati Biswas</u> , Ms. Preeti Jha, Dr. Balaram Ghosh, Dr. Vladimir Zorin	
<b>Stability enhancement in organic photovoltaics: in-situ structural/morphological monitoring approach applied to plasmonic devices</b>	<b>218</b>
<u>Dr. Barbara Paci</u> , Dr. Amanda Generosi, Dr. George Kakavelakis, Mr. Marco Guaragno, Dr. Valerio Rossi Albertini, Dr. Emmanuel Stratakis, Prof. Emmanuel Kymakis	
<b>Ligand Induced Shape Control of Cesium Lead Bromide Nanocrystals by Post Synthetic Treatments</b>	<b>220</b>
<u>Dr. Elisabetta Fanizza</u> , Ms. Francesca Cascella, Dr. Annamaria Panniello, Dr. Leonardo Triggiani, Dr. Nicoletta Depalo, Dr. Cinzia Giannini, Dr. Davide Altamura, Prof. Angela Agostiano, Dr. M. Lucia Curri, Dr. Marinella Striccoli	

<b>Size and temperature effect on the photoluminescent properties of Europium-doped silica nanoparticles</b>	<b>221</b>
<u>Dr. Hussein Fneich</u> , Dr. Nathalie Gaumer, Prof. Stephane Chaussedent, Mr. Manuel Vermillac, Dr. Wilfried Blanc, Prof. Ahmad Mehdi	
<b>Broadband Nonlinear Optical Response of Colloidal Carbon Nanohorns</b>	<b>223</b>
<u>Ms. Stefanie Dengler</u> , Dr. Olivier Muller, Dr. Cordula Hege, Dr. Bernd Eberle	
<b>Influence of aggregation on magnetic and optical properties of CoFe<sub>2</sub>O<sub>4</sub> superparamagnetic nanoparticles</b>	<b>225</b>
<u>Dr. Yulia Gromova</u> , Prof. Vladimir Maslov, Mr. Mikhail Baranov, Dr. Raquel Serano, Mrs. Vera Kuznetsova, Dr. Finn Purcell-milton, Prof. Yurii Gun'ko, Prof. Alexander Baranov, Prof. Anatoly Fedorov	
<b>Nanocrystals of GeSn alloys in oxide matrix for optoelectronic applications</b>	<b>226</b>
<u>Dr. Ionel STAVARACHE</u> , Dr. Adrian SLAV, Dr. Mariana BRAIC, Dr. Valentin Serban TEODORESCU, Dr. Petronela PREPELITA, Dr. Catalin PALADE, Dr. Ana-Maria LEPADATU, Dr. Sorina LAZANU, Dr. Magdalena Lidia CIUREA, Ms. Daniela STANGE, Dr. Dan Mihai BUCA, Dr. Toma STOICA	
<b>Water stable nanofibrous tubes from hyaluronan derivative and nanocrystalline cellulose</b>	<b>227</b>
<u>Dr. Adela Kotzianova</u> , Mr. Jan Klemes, Mr. Ondrej Zidek, Dr. Marek Pokorny, Dr. Gloria Huerta-Angeles, Dr. Vladimir Velebny	
<b>Preparation of Hollow Cationic-Poly(cyclodextrin) Nanoparticles through Colloidal Templating</b>	<b>229</b>
<u>Dr. Sabrina Belbekhouche</u> , Ms. Imane El Joukhar, Prof. Benjamin Carbonnier	
<b>Biodistribution and quantitation of metal oxide nanoparticle at the subcellular level using confocal Raman microscopy</b>	<b>230</b>
<u>Dr. Vincenzo Calcagno</u> , Mrs. Carolin Merker, Dr. Jana Fleddermann, Dr. José Barzola Quiquia, Mr. Thomas Meyer, Prof. Jan Meijer, Dr. Irina Estrela-lopis	
<b>Rediscovering mechanochemistry: new opportunities in the synthesis of nanocomposites by High Energy Ball Milling</b>	<b>232</b>
<u>Dr. Alessandra Scano</u> , Dr. Martina Pilloni, Dr. Valentina Cabras, Mr. Federico Ebau, Dr. Maria Letizia Manca, Prof. Anna Maria Fadda, Prof. Guido Ennas	
<b>Nanoparticles of copper salts by in-situ surface modification and their effectiveness in antibacterial activity</b>	<b>233</b>
<u>Dr. Esin Akarsu</u> , Dr. Ömer Kesmez	
<b>Highly versatile metal-organic frameworks</b>	<b>234</b>
<u>Dr. Maria Chiara di Gregorio</u> , Dr. Linda J. W. Shimon, Dr. Lothar Houben, Dr. Vlad Brumfeld, Dr. Michal Lahav, Prof. Milko van der Boom	
<b>The electrospinning of xanthan gum: from solution to nanofiber formation</b>	<b>235</b>
<u>Ms. Elhamalsadat Shekarforoush</u> , Dr. Ana Carina Loureiro Mendes, Prof. Ioannis S. Chronakis	
<b>Engineering of the highly active low-temperature oxidation ceria based catalyst – surface structures and bulk doping.</b>	<b>236</b>
<u>Dr. Roman Gulyaev</u> , Dr. Sergey Malykhin, Dr. Arcady Ishchenko, Dr. Tatyana Kardash, Dr. Alexandra Ivanova	
<b>Direct access to primary amines and particle morphology control in nanoporous CO<sub>2</sub> sorbents</b>	<b>237</b>
<u>Ms. Nesibe A Dogan</u> , Dr. Ercan Ozdemir, Dr. Cafer T Yavuz	

<b>Preparation of Ceria Nanoparticles by Precipitation Method and Investigation of their Defect Characteristics</b>	239
<u>Mr. Zhao Liu</u>	
<b>Nanocrystalline TiC Powers For Improving The Hydrogenation/Dehydrogenation Behaviors of MgH<sub>2</sub></b>	240
<u>Ms. shorouq ahmed</u>	
<b>Tailoring Cu nanoparticles using the spinning disc reactor for methanol synthesis</b>	242
<u>Mr. Christian Ahoba-Sam</u> , Dr. Kamelia V.K. Boodhoo, Prof. Unni Olsbye, Prof. Klaus-joachim Jens	
<b>Self-assembled transient networks of surfactant based nano-worms</b>	243
<u>Dr. Vyacheslav Molchanov</u> , Mr. Alexander Kwiatkowski, Prof. Olga Philippova	
<b>PDMS membranes loaded with TiO<sub>2</sub>NPs for antibacterial activity</b>	244
Dr. Valentina Caratto, <u>Dr. Stefano Alberti</u> , Prof. Silvia Vicini, Prof. Maila Castellano, Dr. Marco Mauri, Prof. Maurizio Ferretti	
<b>Flexible, stretchable and healable electronics</b>	246
<u>Prof. Fabio Ciccoira</u>	
<b>Novel BROADSPECTRUM Antivirals</b>	248
<u>Prof. Francesco Stellacci</u>	
<b>Engineered nanomaterial interactions with biological exudates – do we need to redesign standard testing approaches for nanomaterials?</b>	249
<u>Prof. Iseult Lynch</u>	
<b>Labs, Cells and Organs on Chip.</b>	250
<u>Prof. albert van den berg</u>	
<b>SAW sensor based on ZnO thin film for ultraviolet light measurement</b>	251
<u>Mr. seawhan choi</u> , Mr. Kunnyun Kim, Ms. Yeon Hwa Kwak, Prof. Byeong-kwon Ju	
<b>Optical Absorption Caused by Periodic Antenna Array-induced Surface Plasmons in the Mid-infrared Range</b>	252
<u>Dr. Kenichi Kasahara</u>	
<b>Investigation of the phase formation from nickel-modified nanostructured silicon</b>	254
<u>Ms. Olga Volovlikova</u> , Ms. Yulia Shilyaeva, Ms. Alexandra Berezkina, Mr. Sergey Gavrilov	
<b>Development of long-circulating nanoparticles for ATP delivery</b>	255
<u>Dr. Patricia Diaz</u> , Dr. Juan Huidobro-Toro	
<b>Colloidal synthesis of metastable AuCuS phase nanocrystals and in-situ TEM heating study of their transformation</b>	256
<u>Mr. Muhammad Imran</u> , Prof. Liberato Manna, Dr. Rosaria Brescia	
<b>Collagen/hydroxyapatite nanostructured layers with controlled release of different antimicrobial agents: the release kinetics, antimicrobial activity and cytocompatibility</b>	257
<u>Dr. Tomas Suchy</u> , Dr. Monika Supova, Dr. Eva Klapkova, Dr. Vaclava Adamkova, Dr. Rastislav Ballay, Dr. Frantisek Denk, Dr. Marek Pokorny, Dr. Pavla Sauerova, Dr. Marie Hubalek Kalbacova	



<b>Thermoluminescent and dosimetric properties of Mn-doped YAP nanoceramics</b>	259
Dr. Nataliya Martynyuk, Dr. Yaroslav Zhydachevskyy, Dr. Anatolii Popov, Dr. Dmytro Sugak, Dr. Pawel Bilski, Prof. Sergii Ubizskii, Prof. Marek Berkowski, Prof. Andrzej Suchocki	
<b>Spin injection from a semiconductor to a 3D topological insulator: a pathway for hybrid opto-spintronics</b>	260
Mr. Y.Q. Huang, Dr. Y.X. Song, Prof. S.M. Wang, Prof. I.A. Buyanova, <u>Prof. Weimin M. Chen</u>	
<b>Magnetically guided viral transduction of gene-based sensitization for localized photodynamic therapy to overcome multi drug resistance in breast cancer cells</b>	261
<u>Prof. Zi-Xian Liao</u>	
<b>Plasmonic Nanostructures for IR Photodetectors</b>	262
<u>Dr. Dana Cristea</u> , Dr. Paula Obreja, Dr. Adrian Dinescu, Dr. Roxana Tomescu	
<b>Fabrication of composite cathodes by electrodeposition for solid oxide fuel cells</b>	264
<u>Mr. Saeed ur Rehman</u> , Dr. Rak-hyun Song, Dr. Seok-joo Park, Dr. Tak-hyung Lim, Dr. Jong-eun Hong, Dr. Jon-won Lee, Dr. Seung-bok Lee	
<b>Formation of crystal nuclei in small volumes near critical supercooling</b>	265
<u>Dr. Zdeněk Kožíšek</u> , Prof. Pavel Demo	
<b>Zein-phosphatidylcholine mixed nanoparticles as a hydrophobic drug carrier</b>	266
<u>Dr. Soon-seok Hong</u> , Prof. Soo-jeong Lim	
<b>Dynamics of a Sierpinski-dendrimer type polymer network</b>	267
<u>Dr. Flaviu Turcu</u> , Dr. Aurel Jurjiu, Mr. Teodor Biter	
<b>Magnetic and magneto-optical properties of Co<sub>1</sub>xDy<sub>x</sub>Fe<sub>20</sub> nanoparticles and thin films synthesized by co- precipitation</b>	268
<u>Ms. maryam karimi</u>	
<b>Design and Simulation of SAW sensor for Photo Sensing</b>	269
<u>Mr. Jong Woo Kim</u> , Mr. Jin Woo Lee, Mr. Byungmoon Lee, Mr. Jinkee Hong, Prof. Byeong-kwon Ju	
<b>Graphene like ZnO 2D structure from semiconductor to conductor behavior by doping F</b>	270
Dr. Ahmad Yazdani, <u>Mr. behrad barakati</u> , Mrs. Asiye Shokri	
<b>SYNTHESIS AND CHARACTERIZATION OF PEPTIDE LOADED NANOPARTICLES FOR USE IN NEW GENERATION VACCINE SYSTEMS</b>	271
Ms. Elif F. Yilmaz, Ms. Pelin Pelit Arayıcı, <u>Dr. Mesut Karahan</u> , Dr. Zeynep Mustafaeva	
<b>Study of Spectroscopic Properties of Nanosized Particles of Core-shell Morphology</b>	272
<u>Dr. Tamar Bzhalava</u> , Prof. Paata Kervalishvili	
<b>A new peptide-based fluorescent probe selective for mercury(II)</b>	274
<u>Dr. Giuliana Donadio</u> , Dr. Rosario Oliva, Dr. Marialuisa Siepi, Prof. Pompea Del Vecchio, Prof. Luigi Petraccone, Prof. Ezio Ricca, Prof. Rachele Istatico, Ms. Mariamichela Lanzilli, Prof. Eugenio Notomista	
<b>Biodegradable Ultrafine Nanoparticles of Poly(Methyl Methacrylate-co- Methacrylic Acid) Prepared via Semicontinuous Heterophase Polymerization</b>	275
<u>Mrs. Hened Saade</u> , Dr. R. Guillermo López	
<b>Computational study on the structure, stability, and growth of supported gold nanoparticles</b>	276
<u>Dr. Julien Engel</u> , Ms. Samantha Francis, Dr. Alberto Roldan	



<b>Temperature-dependent Emission Properties of CdSe/CdS/CdTe Core/Crown Nanoplatelets</b>	277
<u>Mrs. palvasha ijaz, Dr. Ilaria Angeloni, Dr. Guillaume Bertrand, Dr. Iwan Moreels</u>	
<b>Influence of Au nanoparticles for enhanced performance of quantum dot light-emitting diodes</b>	278
<u>Prof. Jiwan Kim</u>	
<b>Fluorescent triazolyl-coumarin carbon spheres synthesized from waste tyres for Fe<sup>3+</sup> detection</b>	279
<u>Ms. Jacolien Du Plessis, Dr. Neliswa Mama, Prof. Vincent Nyamori</u>	
<b>Advanced nanocomposite materials for Oil &amp; Gas production</b>	281
<u>Ms. Chinyere Okolo, Dr. Fawad Inam</u>	
<b>Biocompatible and functionalized electrospun fibers</b>	282
<u>Dr. Elena Matei, Mrs. Mihaela Oancea, Mr. Alexandru Evanghelidis, Dr. Ionut Enculescu</u>	
<b>Catalytic activity of bimetallic AuPd alloys supported MgO and MnO<sub>2</sub> nanostructures and their role in selective aerobic oxidation of alcohols</b>	283
<u>Dr. Hamed Alshammari</u>	
<b>Colloidal Synthesis of Bipolar Off-Stoichiometric Gallium Iron Oxide Spinel-Type Nanocrystals with Near-IR Plasmon Resonance</b>	284
<u>Dr. Carmine Urso, Dr. Mariam Barawi, Dr. Roberto Gaspari, Dr. Gianluca Sirigu, Dr. Ilka Kriegel, Dr. Margherita Zavelani-rossi, Dr. Francesco Scotognella, Dr. Michele Manca, Dr. Mirko Prato, Dr. Luca De Trizio, Prof. Liberato Manna</u>	
<b>Local atomic and electronic structure of Cu (I,II) binding site in amyloid beta peptide: theoretical HERFD XANES study</b>	285
<u>Mrs. Maria Kremennaya, Dr. Mikhail Soldatov, Ms. Yulia Podkovyrina, Mrs. Irina Dadasheva</u>	
<b>Effects of the compliance current on the resistive switching behavior of arsenic telluride thin films</b>	286
<u>Prof. Taeho Kim, Prof. hyunchul Sohn, Mr. Jinyeol Lee, Ms. Dayoon Lee, Mr. Jaeyeon Kim</u>	
<b>Characterization of Polycaprolactone and Rice Husk Silica Composite (PCL-SiO<sub>2</sub>) by E-Spinning to Apply Supporter for Drug Release</b>	288
<u>Mrs. SINA E SONG, Ms. Yeoung Ah Noh, Ms. Jin Yi Kim, Prof. Hee Taik Kim</u>	
<b>Analysis of Ge/GaAs heterojunction-based PN junction tunneling field-effect transistor with dual-metal-gate structure for high-performance and low-power applications</b>	290
<u>Mr. Jae Hwa Seo, Mr. Young Jun Yoon, Mr. Min Su Cho, Prof. In Man Kang</u>	
<b>All Optical Programmable Logic Array (PLA)</b>	291
<u>Dr. Dawit Hailu</u>	
<b>Detection of organic vapors on sputtered and annealed thin Au films</b>	292
<u>Dr. Ondrej Kvitek, Mr. Vojtech Kopacek, Dr. Alena Reznickova, Prof. Vaclav Svorcik</u>	
<b>Investigation on Nonlinear Optical Properties of MoS<sub>2</sub> Nanoflake, Grown on Silicon and Quartz Substrates</b>	294
<u>Mrs. samaneh bayesteh, Dr. Seyedeh Zahra Mortazavi, Dr. Ali Reyhani</u>	
<b>Pegylated and amphiphilic Chitosan coated manganese ferrite nanoparticles for pH-sensitive delivery of methotrexate: synthesis and characterization</b>	296
<u>Mrs. leila karimi</u>	

<b>UV-spectroscopy Method for Detecting the Chitosan Nanoparticles Formation</b>	<b>298</b>
Dr. Palanirajan Vijayaraj Kumar, Mr. Marwan Abdelmahmoud Abdelkarim Maki, Dr. Lee Ming Tatt, Dr. Yeong Siew Wei, Prof. Abu Bakar Bin Abdul Majeed	
<b>SYNTHESIS OF A NEW SPIRONUCLEOSIDE: SULFAHYDANTOCIDINE</b>	<b>299</b>
Dr. Fatma-Zohra SMAINE, Dr. Jean-yves Winum	
<b>Fabrication and characterization of Rice Husk Aerogel-Polydimethylsiloxane (PDMS) Insulation Film</b>	<b>300</b>
Ms. Yeoung Ah Noh, Mrs. SINA SONG, Ms. Jin Yi Kim, Prof. Hee Taik Kim	
<b>A built-in sensor with carbon nanotubes coated by Ag clusters for deformation monitoring of glass fiber/epoxy composites</b>	<b>301</b>
Dr. Petr Slobodian, Dr. Pavel Riha, Dr. Robert Olejnik, Dr. Jiri Matyas, Ms. Silvia Pertegas, Prof. Ralf Schledjewski	
<b>The effect of processing variables on the morphology of electrospun nanofibers</b>	<b>302</b>
Dr. Muhammad Ali Zulfikar, Mrs. Irlin Afrianingsih, Dr. Muhamad Nasir, Dr. Anita Alni	
<b>In a SiNx-based membrane for EUV pellicle, Evaluation of Stress Variation and Mechanical Strength According to Film Deposition Process Conditions</b>	<b>303</b>
Mr. Gi-sung Lee, Mr. Kwang-hee Kim, Mr. Dong-wook Lee, Mr. Hae-chul Hwang, Mr. Nam-soo Park, Mr. Hee-oh Kang, Mrs. Kyung-jin Park, Mr. Changho Seo	
<b>Angle aligned electrospun metal fibers and its potential for stretchable electrodes for wearable electronics.</b>	<b>304</b>
Dr. doo-hyeb youn, Dr. Changbong Yeon, Dr. Sun Jin Yun	
<b>Investigation on the Effect of Preparation Techniques of Anatase on its Structural and Optical Properties</b>	<b>305</b>
Mrs. Zakiya Rashid, Ms. Faten Almutawa, Dr. Latifah Alhajji	
<b>Facile photocatalyst sedimentation: Utilizing isoelectric point for immediate TiO<sub>2</sub> nanoparticles separation.</b>	<b>306</b>
Dr. Entesar Al-Hetlani, Mr. Mohamed O. Amin, Dr. Metwally Madkour	
<b>Thermal and non-thermal explosion in metals ablation by femtosecond laser pulse: classical approach of the Two Temperature Model</b>	<b>307</b>
Mr. Ahmed Abdelmalek, Dr. Zeyneb Bedrane	
<b>Local electronic interaction effects on Dynamical and static spin susceptibilities of doped gapped graphene nanoribbon</b>	<b>308</b>
Dr. Hamed Rezania	
<b>The method of synthesizing of superhydrophobic surfaces by PECVD</b>	<b>310</b>
Ms. Zhuldyz Otarbay, Dr. Sagi Orazbayev, Dr. Maratbek Gabdullin, Dr. Merlan Dosbolayev, Prof. Tlekkabul Ramazanov, Mr. Askar Zhunisbekov, Mr. Dulat Omirbekov	
<b>Shift of semimetal-semiconductor band direction on “0 1 1” to “1 1 1” Bismuth quazi-two- dimension system</b>	<b>311</b>
Dr. Ahmad Yazdani, Mr. Sajad Hamreh	
<b>Metal nanolayer deposited highly stable Ag thin films and their optical properties</b>	<b>312</b>
Prof. Midori Kawamura, Dr. Takayuki Kiba, Prof. Yoshio Abe, Dr. Kyung Ho Kim, Prof. Hiroshi Murotani	

<b>Phisico-chemical properties of zinc coating with modified detonation nano diamonds additives</b>	<b>313</b>
<u>Ms. Elvina Osmanova, Ms. Ksenia Svir</u>	
<b>Fabrication Techniques for Platelet-Functionalized Nanofibers</b>	<b>314</b>
<u>Ms. Karolina Vocetkova, Mr. Matej Buzgo, Ms. Vera Sovkova, Prof. Evzen Amler</u>	
<b>Testing the Biocompatibility of Fully Porous Ceramics for Bone Tissue Engineering</b>	<b>315</b>
<u>Ms. Vera Lukasova, Mr. Premysl Stastny, Mr. Martin Trunec</u>	
<b>Collagen type I based foamed scaffold for bone defects therapy</b>	<b>316</b>
<u>Ms. Veronika Blahnova, Dr. Eva Filova, Ms. Veronika Svachova, Mr. Martin Trunec, Dr. Lucy Vojtova, Prof. Evzen Amler</u>	
<b>Investigation on the piezoelectrical properties of single layered MoS<sub>2</sub> at various conditions</b>	<b>317</b>
<u>Dr. Ahrum Sohn, Mr. Seung Choi, Mr. Tae-Ho Kim, Dr. Sang A Han, Prof. Sang-Woo Kim</u>	
<b>Novel magnetic nanoadsorbents for wastewater remediation</b>	<b>318</b>
<u>Dr. Alex Fabiano Campos, Ms. Helena Augusta Lisboa de Oliveira, Mr. Paulo H. M. Brito, Dr. Renata Aquino, Dr. Franciscarlos G. da Silva, Dr. Jerome Depeyrot</u>	
<b>Enhancing the Pozzolanicity of Jordanian Volcanic Tuffs using Calcium Carbonate Nanoparticles</b>	<b>319</b>
<u>Dr. Ayman Ababneh, Prof. Borhan Aldeen Albiss, Ms. Tasneem Lafi</u>	
<b>Effect of Metallic Thin-films' Type on Sessile Droplet Contact Angle</b>	<b>320</b>
<u>Dr. feraz alzub, Mr. Abdullah Alkandary</u>	
<b>A Sustainable Green Biosynthesis of Silver Nanoparticles Using Plant Leaves Extracts</b>	<b>322</b>
<u>Prof. Muna AbuDalo, Mr. Ismaeel Al-mheidat, Mrs. Alham Al-shurafat, Mrs. Colleen Grinham, Mrs. Vinka Oyanedel-Craver</u>	
<b>Relevance of LiPF<sub>6</sub> as Etching Agent of LiMnPO<sub>4</sub> Colloidal Nanocrystals for High Rate Performing Li-ion Battery Cathodes</b>	<b>323</b>
<u>Ms. Lin Chen, Dr. Enrico Dilella, Dr. Andrea Paoletta, Dr. Giovanni Bertoni, Dr. Alberto Ansaldo, Dr. Massimo Colombo, Mr. Sergio Marras, Prof. Bruno Scrosati, Prof. Liberato Manna, Dr. Simone Monaco</u>	
<b>The new investigation on CTAB synthesis of vanadium oxide nanorods</b>	<b>324</b>
<u>Mr. Alireza Behfar, Prof. Theodore Betley, Prof. Cynthia Friend</u>	
<b>Magnetic and electrical performance of atomic layer deposited nanolaminates</b>	<b>325</b>
<u>Dr. Aile Tamm, Mr. Kristjan Kalam, Mr. Mats Mikkor, Ms. Helina Seemen, Dr. Mihkel Rähn, Prof. Kaupo Kukli, Mr. Joosep Link, Dr. Raivo Stern, Dr. Helena Castán, Prof. Salvador Dueñas</u>	
<b>Interfacial self-reaction during atomic layer deposition of Al<sub>2</sub>O<sub>3</sub> on oxidized black phosphorus and improved electrical properties by stable surface chemical structure</b>	<b>327</b>
<u>Mr. Dae-Kyoung KIM, Mr. Jimin CHAE, Mr. Hanbum PARK, Prof. Mann-Ho CHO</u>	
<b>Fabrication of Self-Organized Precisely Tunable Plasmonic SERS Substrates via Glancing Angle Deposition</b>	<b>328</b>
<u>Dr. Oral Ualibek, Dr. Ehsan Rezvani, Dr. Brendan Bulfin, Prof. Igor Shvets, Dr. Gulnar Sugurbekova</u>	
<b>Preparation of Novel Nanocomposites Modified with Hybrid Nano-Reinforcements</b>	<b>330</b>
<u>Mr. Ayad Mahuof, Dr. George Kotsikos, Prof. Geoff Gibson</u>	

<b>Development of super repellent nano-composite coatings based on functionalised nano-silica.</b>	<b>332</b>
<u>Prof. Geraldine Durand</u> , Prof. Alan Taylor, Ms. Marta Alvarez, Ms. Nadia Sid, Ms. Maria Linzoain, Dr. Anna Wojdyla-cieslak, Mr. Angelo La Rosa	
<b>Far-Red Fluorescent carbon nano-onions for high-resolution cellular imaging</b>	<b>333</b>
<u>Mr. Adalberto Camisasca</u> , Dr. Stefania Lettieri, Dr. Marta D amora, Prof. Silvia Giordani	
<b>Biomimetic design, fabrication and development of nano-microstructured layered urine bladder scaffolds for bladder tissue engineering</b>	<b>335</b>
<u>Dr. Fatemeh Ajallouei</u>	
<b>Scanning tunneling spectroscopy investigation of van der Waals based metal/semiconductor interfaces</b>	<b>336</b>
Dr. toai le quang, Dr. Vladimir Cerchez, Dr. Karol Nogajewski, Prof. Marek Potemski, Dr. Minh Tuan Dau, Prof. Matthieu Jamet, Prof. Pierre Mallet, Prof. Jean-yves Veuillen	
<b>Nonlinear behavior and buckling of double-carbon nanotubes systems conveying fluid</b>	<b>338</b>
<u>Dr. Kun Zhou</u> , Prof. Ni Qiao	
<b>Facile synthesis of MoS<sub>2</sub>-flakes/amorphous-carbon composite as anode for lithium-ion batteries</b>	<b>339</b>
<u>Mr. Duc Anh Dinh</u>	
<b>Printing Three-dimensional Conducting Polymer Structures Using Scanned Nanopipettes with Submicron Resolution</b>	<b>341</b>
<u>Mr. Alex Wibawa</u> , Dr. Pavel Novak	
<b>Controlling Charge Transport in Molecular Electronics by Tuning the Molecular Conformation of Floppy Molecules Self-Assembled in Monolayers Adsorbed on Electrodes</b>	<b>343</b>
<u>Dr. Ioan Baldea</u>	
<b>Optical fiber meta-tips</b>	<b>345</b>
<u>Dr. Maria Principe</u> , Prof. Marco Consales, Dr. Alberto Micco, Dr. Alessio Crescitelli, Dr. Giuseppe Castaldi, Dr. Emanuela Esposito, Dr. Vera La Ferrara, Prof. Antonello Cutolo, Prof. Vincenzo Galdi, Prof. Andrea Cusano	
<b>Staphylococcus aureus Exotoxin Detection Using Potentiometric Nanobiosensor(MIP) based on Microbial Electrode Approach with Effects of pH and Temperature</b>	<b>347</b>
<u>Dr. HAMED AHARI</u> , Dr. Mehdi Hedayati, Dr. Amirali Anvar, Dr. Behrouz Akbari-adergani, Prof. Hedayat Hosseini, Dr. Shapour Kakoolaki	

# Triboelectric Nanogenerators and Tribotronics

Wednesday, 18th October - 09:05 - Plenary Speeches - Auditorium - Oral - Abstract ID: 844

***Prof. Sang-Woo Kim***<sup>1</sup>

*1. Sungkyunkwan University*

Energy harvesting systems based on piezoelectric and triboelectric nanomaterials are in great demand, as they can provide routes for the development of self-powered devices which are highly flexible, stretchable, mechanically durable, and can be used in a wide range of applications. Our recent research interest mainly focuses on the fabrication of piezoelectric and triboelectric power generators based on various kinds of nanomaterials. Flexible generators exhibit good performances and are easy to integrate which make it the perfect candidate for many applications, and therefore crucial to develop. In this presentation, I firstly introduce the fundamentals and possible device applications of triboelectric power generators, including their basic operation modes. Then the different improvement parameters will be discussed. As main topics, I will present a couple of recent achievements regarding highly stretchable piezoelectric-pyroelectric hybrid nanogenerators (NGs), transparent flexible graphene triboelectric NGs (TENGs), textile-based wearable TENGs, etc.

References:

- "Fully Stretchable Textile Triboelectric Nanogenerator with Knitted Fabric Structures", ACS Nano (online, 2017)
- "Rewritable ghost floating gates by tunnelling triboelectrification for two-dimensional electronics", Nature Commun. 8, 15891 (2017)
- "High-Performance Triboelectric Nanogenerators Based on Solid Polymer Electrolytes with Asymmetric Pairing of Ions", Adv. Energy Mater. 7, 1700289 (2017)
- "High-Performance Piezoelectric, Pyroelectric, and Triboelectric Nanogenerators Based on P(VDF-TrFE) with Controlled Crystallinity and Dipole Alignment", Adv. Funct. Mater. 27, 1700702 (2017)
- "Boosting Power-Generating Performance of Triboelectric Nanogenerators via Artificial Control of Ferroelectric Polarization and Dielectric Properties", Adv. Energy Mater. 7, 1600988 (2017)
- "Graphene Tribotronics for Electronic Skin and Touch Screen Applications", Adv. Mater. 29, 1603544 (2017)
- "Triboelectrification-Induced Large Electric Power Generation from a Single Moving Droplet on Graphene/Polytetrafluoroethylene", ACS Nano 10, 7297 (2016)
- "Controllable Charge Transfer by Ferroelectric Polarization Mediated Triboelectricity", Adv. Funct. Mater. 26, 3067 (2016)
- "Shape memory polymer-based self-healing triboelectric nanogenerator", Energy Environ. Sci. 8, 3605 (2015)
- "Control of Skin Potential by Triboelectrification with Ferroelectric Polymers", Adv. Mater. 27, 5553 (2015)
- "Nanopatterned Textile-Based Wearable Triboelectric Nanogenerator", ACS Nano 9, 3501 (2015)
- "Transparent Flexible Graphene Triboelectric Nanogenerators", Adv. Mater. 26, 3918 (2014)
- "Hydrophobic Sponge Structure-Based Triboelectric Nanogenerator", Adv. Mater. 29, 5037 (2014)

## 2-Dimensional Composites Based On Graphene For Applications In Electronics, Mechanics Or Energy Storage

Wednesday, 18th October - 09:40 - Plenary Speeches - Auditorium - Oral - Abstract ID: 38

***Prof. Vincenzo Palermo***<sup>1</sup>

*1. National Research Council of Italy, CNR-ISOF, Bologna*

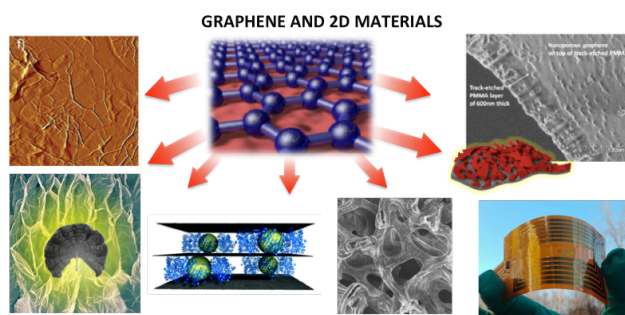
At the beginning of its exciting life, graphene was mostly a game for physicists. Due to the difficulty of producing sufficient amounts of high-quality graphene, researchers used single sheets of graphene exfoliated with adhesive tape, in very simple geometries, to study the properties of this new material. Later on, new methods to produce graphene on large scale were developed, based on the chemical processing of graphite in solution or on the chemical growth of graphene on metals.

Using chemistry it is possible to effectively tailor this poorly soluble and almost chemically inert material into a wide variety of forms. During the last years, the chemistry of graphene has played an ever increasing role in the controlled functionalization, large-scale production, processing and in numerous applications of such material, being also used to produce new 2D materials beyond graphene.

In this talk, I will describe how we use covalent, supramolecular and electrochemical techniques to obtain graphene-based solutions and process them in novel composite materials. We exploit in this way the 2-dimensional nature of these materials to produce porous membranes, thin coatings, foams or polymer composites for applications in electronics, mechanics or energy storage.

### BIBLIOGRAPHY

1. *Electrochemical Functionalization of Graphene at the Nanoscale with Self-Assembling Diazonium Salts.* **ACS Nano**, (2016) **10**, 7125.
2. *Graphene-based coatings on polymer films for gas barrier applications.* **Carbon**, (2016) **96**, 503.
3. *Large area fabrication of self-standing nanoporous graphene-on-PMMA substrate.* **Materials Letters**, (2016) **184**, 47.
4. *Supramolecular self-assembly of graphene oxide and metal nanoparticles into stacked multilayers by means of a multitasking protein ring.* **Nanoscale**, (2016) **8**, 6739.
5. *Electrochemically exfoliated graphene oxide/iron oxide composite foams for lithium storage, produced by simultaneous graphene reduction and Fe(OH)(3) condensation.* **Carbon**, (2015) **84**, 254.
6. *REVIEW: Nanoscale Mechanics of Graphene and Graphene Oxide in Composites: A Scientific and Technological Perspective.* **Advanced Materials**, (2016) **28**, 6232.



Graphene and 2d materials.png

# **New approaches for exploiting electron and photon beams inside a TEM for nanoscale characterization**

---

Wednesday, 18th October - 10:45 - Plenary Speeches - Auditorium - Oral - Abstract ID: 843

---

***Prof. Odile Stéphan*** <sup>1</sup>

*1. University of Paris-Sud*

Coming soon

# **Fano resonances tuned at Lifshitz transitions in superconducting nanofilaments, a new physics at the crossover between quantum nanomaterials and quantum biology**

---

Wednesday, 18th October - 11:25 - Plenary Speeches - Auditorium - Oral - Abstract ID: 845

---

**Prof. Antonio Bianconi**<sup>1</sup>

*1. RICMASS*

Coming soon



---

## Pd-Cu Core/shell Nanoparticles as an Efficient Catalyst for Fuel Cell applications

---

Wednesday, 18th October - 13:30 - Poster Session - Hall & Room 3 - Poster - Abstract ID: 441

---

***Mr. Ji Liu<sup>1</sup>, Dr. Xiaofeng Fan<sup>2</sup>, Prof. Changqing Sun<sup>1</sup>, Prof. Weiguang Zhu<sup>1</sup>***

*1. Nanyang Technological University, 2. Jilin University*

Designing new materials for heterogeneous catalysis is interesting and challenging in surface science. For years, scientists have found out that bimetallic system can achieve better catalytic performance due to effects such as ligand effect and ensemble effect. Since the reactivity of bimetallic overlayer can be tailored by substrate, the bimetallic nanoparticle with core/shell structure is promising due to its easy way of the formation with the effect of phase separation. Recent studies have proved that Pd-based intermetallic nanoparticle has the potential to serve as a non-Pt catalyst for fuel oxidation and oxygen reduction reaction.<sup>1</sup>

In this paper, we have studied the catalytic activity of PdCu nanoparticle for CO oxidation and oxygen reduction reaction by density functional theory calculations. Two structures have been proposed, including face-centered tetragonal (fct) PdCu/Pd nanoparticle and face-centered cubic (fcc) PdCu bimetallic surface alloy. Fct-Pd/Cu/Pd structure consists of ordered alloy distribution PdCu as core and thin overlayer Pd as shell; fcc-PdCu bimetallic surface alloy structure includes three-layer Cu(111) substrate as core and thin overlayer Pd as shell.

We have found out that the adsorption energies and catalytic activities depend largely on the electronic structure of surface Pd atoms near the Fermi level which is affected and modified by core. A linear relationship is found between the adsorption energy ( $E_{ad}$ ) and the d-band center ( $\epsilon_d$ ) for fcc-PdCu bimetallic alloy with increasing Pd overlayer up to three layers at most. With nudged elastic band method, we have calculated the energy barriers for O<sub>2</sub> dissociation on fct-PdCu/Pd nanoparticle and CO oxidation with atomic O on fcc-PdCu bimetallic alloy. With Sabatier principle and volcano curve, we have predicted the activity of ORR and CO oxidation for both structures by adopting the model proposed by Nørskov.<sup>2</sup> We hope our work can shed some lights on the design of bimetallic nanoparticles towards superior catalytic catalysis.

### References

1. Wang, Chenyu, et al. "Size-dependent disorder–order transformation in the synthesis of monodisperse inter-metallic PdCu nanocatalysts." *ACS nano* 10.6 (2016): 6345-6353.
2. Stamenkovic, Vojislav, et al. "Changing the activity of electrocatalysts for oxygen reduction by tuning the surface electronic structure." *Angewandte Chemie* 118.18 (2006): 2963-2967.

# Combination of far-field and near-field electrospinning for “ribs like structures”

Wednesday, 18th October - 13:30 - Poster Session - Hall & Room 3 - Poster - Abstract ID: 209

**Mr. Jan Klemes<sup>1</sup>, Dr. Adela Kotzianova<sup>1</sup>, Ms. Julie Bystronova<sup>1</sup>, Dr. Marek Pokorný<sup>1</sup>, Mr. Ondrej Zidek<sup>1</sup>, Dr. Vladimír Velebný<sup>1</sup>**

*1. Contipro a.s.*

In terms of biomaterials, there are many factors that play a key role in the interaction of the material with its surrounding. Besides the composition itself, the structure of the biomaterial surface is crucial. It mediates contact with the environment and determines how the material will interact with its surroundings (e.g. tissue, cells). One way how to influence the properties of a biomaterial is to make a pattern on its surface. The presented work describes a developed device and a method for preparation new regular polymer structures containing nano/micro fibers and parallel micropatterning.

Electrospinning (ES) is a method for preparation of nano- and micro- fiber substrates. Fibers within this substrate could be highly oriented or arranged in no order. The materials prepared in this way are used, mainly in the form of planar scaffolds, for the determination of the basic principles of interaction between fibrous biomaterials surfaces and adherent cells. A modification of the classical electrospinning is a method called near-field electrospinning (NFES). Unlike ES, this method uses a deposition zone of only few millimeters and thus allows precise surface modification by depositing of parallel micro-sized polymer structures with a high degree of repeatability. Moreover, this method allows controlling more specific parameters such as the width of patterns or their spacing. These parameters could play a significant role in terms of cell behavior.

This work describes a developed device combining both mentioned methods - ES and NFES. The device, respectively a combination of both methods, allowed us preparation of the new regular structures containing nano/micro fibers as a substrate and parallel micropatterning. These “ribs like structures” represent a unique form of surface modification which may significantly influence behavior of a biomaterial and its interaction with its surrounding e.g. cells. Structures could be prepared from a wide range of polymeric materials, that can chemically interact or be inert to each other and thus further influence interaction. Prepared biomaterials can be used in the fields of cell culture, drug release, tissue engineering, and surface modification for biosensors and bioelectronics.

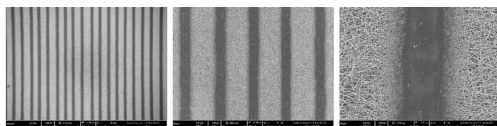


Fig. 1 Patterned nanofibrous substrate in SEM images with different magnification.

Fig 1.png

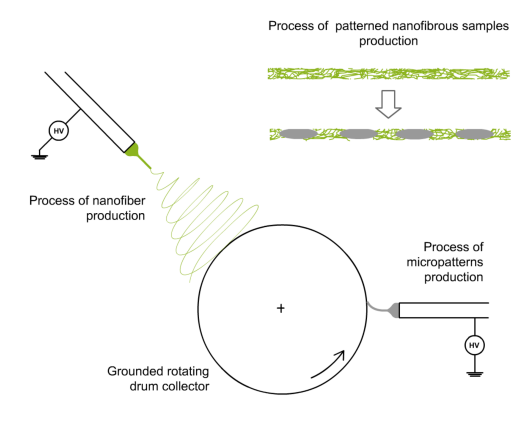


Fig. 2 Scheme of the developed technique and its processing.

Fig 2.png

"This project has received funding from the European Union's Seventh Framework Programme for research, technological development and demonstration under grant agreement no. 602694 (IMMODGEL)."

Funding information.png

---

## Surface Enhanced Raman Spectroscopy: silver/gold nanoparticles deposited on graphene monolayers

---

Wednesday, 18th October - 13:30 - Poster Session - Hall & Room 3 - Poster - Abstract ID: 285

---

***Dr. Věra Jandová<sup>1</sup>, Dr. Martin Koštejn<sup>1</sup>, Dr. Oleksiy Lyutakov<sup>2</sup>, Dr. Radmila Tomovska<sup>3</sup>, Dr. Radek Fajgar<sup>1</sup>***

*1. Institute of Chemical Process Fundamentals of CAS, v.v.i., Czech Republic, 2. Department of Solid State Engineering, University of Chemistry and Technology, Prague, 3. Institute for Polymer Materials, POLYMAT, The University of the Basque Country Donostia-San Sebastián*

Surface Enhanced Raman Spectroscopy (SERS) seems to be one of the most powerful analytical tools for monitoring of environmental contaminants at low concentrations. Increasing the intensity of Raman signal has been regularly observed to be as high as  $10^{14}$  for optimized systems, reaching up to single molecule detection level.

We present results of SERS study using two excitation wavelengths observed primarily for analytes adsorbed onto silver and gold nanoparticles deposited on monolayered graphene.

The metals provide localized surface plasmon resonance, considerably increasing local electromagnetic field and combination with graphene based materials are expected better SERS performances due to concentration effect through a  $\pi$ - $\pi$  stacking.

Graphene monolayer was prepared by the conventional CVD technique on a Cu substrate ( $\text{CH}_4/\text{H}_2$ , 800 °C). The Cu/graphene sheet was then accommodated in a glass reactor and the surface was covered by Ag or Au nanoparticles. The laser ablation (ArF excimer laser, 193 nm, 100 mJ/pulse) of elemental metal targets was used to cover graphene surface by nanoparticles with diameters up to 25 nm. The deposition process was optimized (deposition time, pressure of a background gas) to obtain the best SERS performance. Deposition in vacuum was found to afford completely graphitized samples due to excess energy of the metal atoms/clusters, reaching the graphene surface. The deposition of metal nanoparticles was therefore conducted at pressures 2 - 15 Pa of helium. At 10 Pa the metal nanoparticles were deposited onto the graphene surface without its graphitization. The prepared SERS substrates were characterized by scanning and transmission electron microscopies, electron and x-ray diffractions and by spectroscopy techniques (UV-Vis, FTIR, Raman and XPS). SERS studies were performed using excitation wavelengths 473 nm (Ag based substrates) and 532 nm (Au based substrates). Raman spectra of the model compounds (Rhodamine 6G, Fluoresceine, methylene blue, aminothiophenole) will be presented.

# Development of thermo-responsive magnetic nanoparticles for *Cryptosporidium* oocyst recovery

Wednesday, 18th October - 13:30 - Poster Session - Hall & Room 3 - Poster - Abstract ID: 525

**Dr. Takahiro SEKIKAWA<sup>1</sup>, Dr. Noriyuki OHNISHI<sup>2</sup>, Dr. Xiaomao XIE<sup>3</sup>**

**1. University of Shizuoka, 2. JNC Petrochemical Corporation, 3. Yokohama Research Center, JNC Corporation**

A protozoan parasite *Cryptosporidium* is shed in the feces of humans and other animals. *Cryptosporidium* oocysts have a robust wall, which is resistant to many environmental factors as well as to normal disinfection processes for tap water. We have developed a process called surfactant extraction treatment (SET) that can extract nucleic acids from the oocyst using only surfactants in order to simplify the method for oocysts detection (Sekikawa, *Wat Sci Tech:Water Suppl*, 17(1), 161-168, 2017).

Thermo-responsive magnetic nanoparticles (MNPs) show a property of reversible phase transition between dispersion and aggregation depending on temperature. In this study, we tried to develop thermo-responsive MNPs for recovering oocysts from water samples in order to apply the MNPs to the SET method. Thermo-responsive MNPs for recovering the oocysts were made from a combination of thermo-responsive MNPs (JNC Corporation) and *Cryptosporidium parvum* monoclonal antibody (Cryp-a-Glo biotin, Waterborne) (Fig. 1). Oocysts recovered by the MNPs were supplied to a SET tube directly. Subsequently, 18S rDNA extracted by SET was amplified using a quantitative PCR assay. As a result, we were able to recover oocysts using the MNPs and detected DNA in the oocysts.

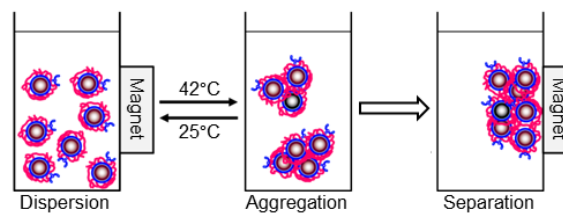


**Figure 1** The *Cryptosporidium parvum* oocyst recovery method using thermo-responsive magnetic nanoparticles

Fig. 1.png

---

## A facile green synthesis of graphene/AuNP/PEDOT:PSS nanocomposite and its application in electrochemical sensor

---

Wednesday, 18th October - 13:30 - Poster Session - Hall & Room 3 - Poster - Abstract ID: 535

---

**Ms. Paweena Pananon<sup>1</sup>, Mr. Chakrit Sriprachuabwong<sup>2</sup>, Dr. Anurat Wisitsorrat<sup>2</sup>, Dr. Piyachat Chuysinuan<sup>3</sup>, Dr. Adisorn Tuantranont<sup>2</sup>, Prof. Patchareenart Saparpakorn<sup>1</sup>, Dr. Decha Dechtrirat<sup>1</sup>**

*1. kasetsart University, 2. National Sciences and Technology Development Agency (NSTDA), 3. Chulabhorn Research Institute*

A facile and green chemical method was developed to prepare a graphene/gold nanoparticle/PEDOT:PSS nanocomposite. Firstly, graphene (GP) was prepared by electrolytic exfoliation of graphite in an aqueous polystyrene sulfonate (PSS) solution. After adding HAuCl<sub>4</sub> and EDOT monomer to the GP/PSS dispersion, gold nanoparticles and PEDOT were formed simultaneously via in-situ reduction of HAuCl<sub>4</sub> and oxidative polymerization of EDOT. The resulting as-prepared GP/AuNP/PEDOT:PSS dispersion was drop-casted on a glassy carbon electrode (GCE) and the resulting electrode was then used to detect dopamine (DA) and uric acid (UA). The morphology and structure of the nanocomposite were characterized by a transmission electron microscope (TEM), a scanning electron microscope (SEM), Raman spectroscopy, FTIR spectroscopy and X-ray diffraction (XRD). In comparison to a bare GCE, the graphene/AuNP/PEDOT:PSS modified electrode showed considerably higher electrocatalytic activities toward the oxidation of dopamine (DA) and uric acid (UA) with an increase in peak currents and a decrease in electrode overpotentials. Moreover, the oxidation of a common interfering agent such as ascorbic acid (AA) could be greatly suppressed by the resulting modified electrode. Using differential pulse voltammetry (DPV), selective determination of dopamine and uric acid in the presence of ascorbic acid could be achieved with a peak potential separation of 110 mV between DA and UA. The sensor exhibited wide linear responses for DA and UA in the ranges of 1 nM to 300  $\mu$ M and 10  $\mu$ M to 1 mM with detection limits (S/N = 3) of 100 pM and 10  $\mu$ M, respectively. The established sensor showed excellent reproducibility and high stability over at least 2 months without any significant change in its electrochemical response. There was also no electrode fouling observed, even after 25 successive scans. Furthermore, the proposed sensor was successfully used to determine DA and UA in real samples with satisfactory recovery results.

---

## Facile synthesis of hybrid nano-alloy catalysts for fuel cell electrodes

---

Wednesday, 18th October - 13:30 - Poster Session - Hall & Room 3 - Poster - Abstract ID: 548

---

***Dr. Heeyeon Kim<sup>1</sup>, Mr. Guk-hyeon Kwon<sup>1</sup>, Dr. Ji-haeng Yu<sup>2</sup>***

*1. Korea Institute of Energy Research (KIER), 2. Korea Institute of Energy Research (KIER)*

In order to solve the environmental problem, there are growing interests in the use of clean energy. Hydrogen fuel cells have been widely touted as an environmentally-friendly alternative to conventional fossil fuels and they are expected to become one of the major power resources using hydrogen energy. Hydrogen fuel cells are a clean, reliable, quiet, and efficient source of high-quality electric power. They use hydrogen as a fuel to drive an electrochemical process that produces electricity, with water and heat as the only by-products. However, high cost of electrode materials is a bottle neck to commercialization of the system. In the case of polymer electrolyte membrane fuel cells (PEMFC), Pt catalyst with high performance and long-term stability is essentially needed. We have developed new synthesis techniques of hybrid nano-alloy catalysts using chemical vapor deposition (CVD) technique. The alloy catalysts synthesized by single-step CVD or sequential CVD processes showed higher performance with long-term stability compared to commercial Pt/C catalysts. These techniques for the synthesis of bimetallic nano-alloys are efficient for the quick, simple and easy synthesis of optimal catalytic structure. Acknowledgment. This work was supported by the Research and Development Program of Korea Institute of Energy Research (KIER/B6-2452, B7-2417-01).

# Effect of gas species on the flow rate through porous materials consisting of micro-/nanoscale structures

Wednesday, 18th October - 13:30 - Poster Session - Hall & Room 3 - Poster - Abstract ID: 569

**Dr. Guang Yang<sup>1</sup>, Mr. Yiye Huang<sup>2</sup>, Ms. Rongrong Lv<sup>2</sup>, Prof. Bernhard Weigand<sup>1</sup>, Mr. Kilian Weishaupt<sup>1</sup>, Prof. Rainer Helmig<sup>1</sup>, Dr. Alexandros Terzis<sup>1</sup>, Prof. Jingyi Wu<sup>2</sup>**

1. University of Stuttgart, 2. Shanghai Jiao Tong University

Gas transport in porous materials is of scientific and technological interest due to its direct applicability in many industrial processes, environmental flows as well as biological applications. However, if the length scales of the pores are small enough, the gas permeability differs from the intrinsic permeability of the porous material, which is caused by the Klinkenberg effect. In this study, pressure driven gas transport characteristics in porous materials with micro-/nanoscale pores are investigated by the direct simulation Monte Carlo method. Different gas species, nitrogen, helium, argon and methane, are considered as the working fluid, and the pore-length of the material varies from 5nm to 400nm. Pore scale flow patterns are obtained for various Knudsen numbers, and the mass flow rates are integrated, where the 'Knudsen Paradox' has been observed. The apparent permeability, as calculated based on the Darcy's law, are correlated. The accuracy of widely used Klinkenberg correlations are also evaluated by the present data.

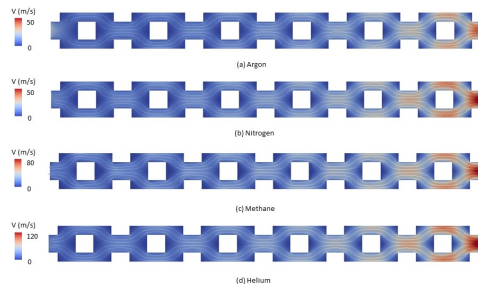


Figure1 Flow patterns for different gases

Figure1 flow patterns for different gases.jpg

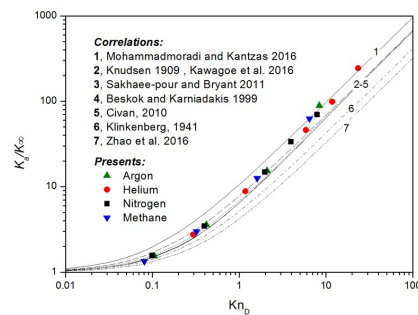


Figure 2 Permeability ratio for various Knudsen numbers

Figure 2 permeability ratio for various knudsen numbers.jpg



# Remote control of light-triggered virotherapy

Wednesday, 18th October - 13:30 - Poster Session - Hall & Room 3 - Poster - Abstract ID: 586

**Prof. S.-Ja Tseng<sup>1</sup>**

*1. Graduate Institute of Oncology, National Taiwan University College of Medicine*

Clinical virotherapy has been successfully approved for use in cancer treatment by the US Food and Drug Administration (FDA), however a number of improvements are still sought to more broadly develop virotherapy. A particular challenge is to administer viral therapy systemically and overcome limitations in intra-tumoral injection, especially for complex tumor within sensitive organs. To achieve this however, a technique is required that delivers the virus to tumor before the body's natural self defense eradicates the virus prematurely. Here we show that recombinant adeno-associated virus serotype 2 (AAV2) chemically conjugated with iron oxide nanoparticles (~5 nm) have remarkable ability to be remotely guided under magnetic field (Figure 1). Transduction is achieved with micro-scale precision. Furthermore, a gene for production of the photosensitive protein KillerRed was introduced into the AAV2 genome to enable photo-dynamic therapy (PDT); or light-triggered virotherapy. In vivo experiments revealed that magnetic guidance of "ironized" AAV2-KillerRed injected by tail vein in conjunction with PDT significantly decreases the tumor growth via apoptosis (Figure 2). We have demonstrated specificity in anti-tumor effects with light-triggered virotherapy achieved with remotely guided "Ironized" virus delivery. Such a technological concept could be harnessed to improve therapeutic efficacy and accuracy with systemic delivery via the bloodstream. There are several distinguishing features of our Ironized AAV2, such as targeted delivery, light-triggered activation of virotherapy, lack of recombination and genomic integration, and strong pre-clinical safety record, that define potential advantages of this concept. Furthermore, magnetic resonance imaging (MRI) instruments can be applied to create pulsed magnetic field gradients in desired direction, and it may provide the prospect of shaping the accumulation within an internal 3D volume. This proof-of-principle demonstrates guided and highly localized micro-scale, light-triggered virotherapy.

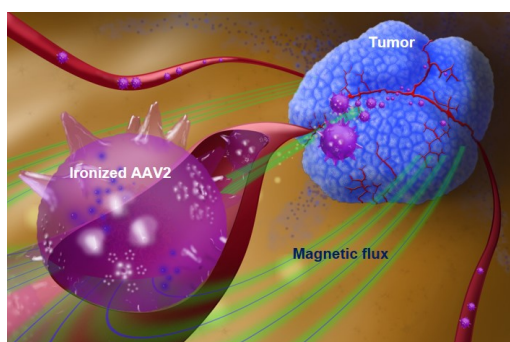


Figure 1.jpg

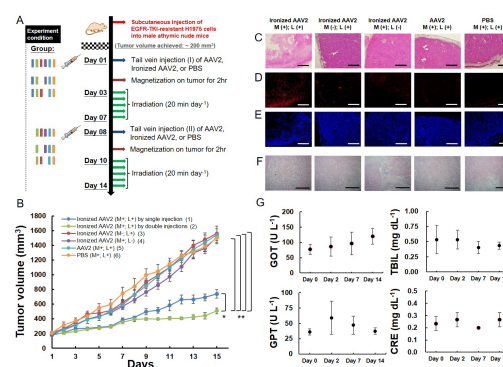


Figure 2.jpg

# Development of Core-shell SiC nanoparticles for Ti-based nanocomposite alloys for additive manufacturing techniques

Wednesday, 18th October - 13:30 - Poster Session - Hall & Room 3 - Poster - Abstract ID: 603

**Dr. Maria Dolores Marcos-Martinez<sup>1</sup>, Dr. Mariajose Lopez-Tendero<sup>2</sup>, Dr. Luis Angel Villaescusa-Alonso<sup>1</sup>, Dr. Elena Aznar-Gimeno<sup>1</sup>, Mrs. Angela Rives-Monparler<sup>1</sup>, Mr. Santiago Sanchez-Cabezas<sup>1</sup>, Mr. Andy Sanchez-Montoto<sup>1</sup>, Mrs. Sarai Pradas<sup>2</sup>, Mr. Alejandro Cuenca-Bustos<sup>2</sup>**  
 1. Centro de Reconocimiento Molecular y Desarrollo Tecnológico (IDM), Unidad Mixta Universitat Politècnica de València, Universitat de València, Spain. Departamento de Química, Universitat Politècnica de Valencia, Valencia, Spain, 2. Laurentia Technologies, Paterna-Valencia, Spain

**Introduction.** The use of nanoparticles in 3D printing is progressing rapidly, and polymeric materials have benefited from the addition of carbon nanotubes, graphene, etc. to improve mechanical properties and contribute to lightweight. Unfortunately, to get an effective dispersion of nanoparticles in order to take maximum advantage, high energy processes are required and even these do not provide the expected mechanical performance. NANOTUN3D EU project [1] aims to improve the mechanical performance of Ti64 alloys by effective dispersion of SiC NPs. NANOTUN3D will provide an innovative concept to solve that limitation and improve the dispersion of SiC nanoparticles based on core-shell structures.

**Results and discussion.** The synthesis of core-shell nanoparticles was based on the direct formation of metal oxides on top of SiC nanoparticles by acidic hydrolysis of precursors. Nanoparticulated SiC material as core was characterized by X-ray diffraction, and transmission electron microscopy. The homogeneity of the metal oxide shell has been analysed by means of the Scanning Transmission Electron Microscopy (STEM) coupled with energy-dispersive X-ray spectroscopy (EDS) techniques. Characterization revealed that SiC nanoparticles corresponds with desired b-SiC phase with an average size around 42nm. STEM image 1 correspond to a preparation of MO<sub>2</sub>@SiC core-shell nanoparticles with a Si:M molar ratio of 9.4 and shows a total overlapping of the two X-ray signals coming from metal and silicon atoms. This study confirmed that shell with 10 nm thickness was homogeneously distributed on SiC nanoparticles.

**Conclusions.** Homogeneous precipitation of metal oxides in the presence of the SiC nanoparticles produces a homogeneous thin shell which can contribute to improve their dispersion into Ti6Al4V metal powder for additive manufacturing techniques. Obtained core-shell nanoparticles have been scale-up at a pilot level and next stage is the application of those nanoparticles to the production of a Ti6Al4V metal powder to be processed by additive manufacturing techniques with powder bed fusion –selective laser melting (SLM) and electron beam melting (EBM)- with enhanced structural performance versus standard alloy

[1] NANOTUN3D project funded by EU H2020 Programme under grant agreement n° 685952. <http://www.nanotun3d.eu>



Image 1. Representative image of MO<sub>2</sub>@SiC core-shell nanoparticle obtained in the electron transmission microscope working in STEM-EDX mode using the mapping tool.

Image-laurentia.jpg

# Singlet oxygen sensitized delayed fluorescence as tool for estimation of photooxidation properties and oxygen sensing.

Wednesday, 18th October - 13:30 - Poster Session - Hall & Room 3 - Poster - Abstract ID: 205

**Dr. Petr Henke<sup>1</sup>, Prof. Jiří Mosinger<sup>1</sup>, Dr. Pavel Kubát<sup>2</sup>**

1. Faculty of Science, Charles University, 2. J. Heyrovsky Institute of Physical Chemistry, Academy of Sciences of the Czech Republic

The singlet oxygen sensitized delayed fluorescence (SODF) is relatively rare phenomenon observed for some fluorescent photosensitizers. SODF is generated from repopulated  $S_1$  excited states of the photosensitizer from its long-lived triplet states by singlet oxygen ( $O_2(^1\Delta_g)$ ) nearby formed *via* photosensitized reaction. The prerequisites of SODF include high concentration of fluorescent photosensitizer with longer lived triplet states, proper energy of the triplet states and high concentration of  $O_2(^1\Delta_g)$  generated in close proximity of the triplets. SODF can be finding on polymer nanomaterials enriched with porphyrin photosensitizers. These materials have potential broad applications in medicine due antibacterial and antiviral properties of photogenerated  $O_2(^1\Delta_g)$ .<sup>1,2</sup> Herein we report the study of sulfonated polystyrene nanoparticles (NPs) with encapsulated hydrophobic 5,10,15,20-tetraphenylporphyrin or ionically entangled tetracationic 5,10,15,20-tetrakis(N-methylpyridinium-4-yl)porphyrin. A simple nanoprecipitation method was used for preparation of stable NPs from sulfonated electrospun nanofiber membranes. The materials were studied by microscopic methods, dynamic light scattering, steady state and time-resolved absorption and fluorescence spectroscopy. Photooxidation ability was measured as kinetic of photodegradation of uric acid or formation of  $I_3^-$  in iodide test.

These photoactive nanoparticles exhibit an effective photogeneration of  $O_2(^1\Delta_g)$  under irradiation by visible light leading to strong signal of SODF. Photophysical evaluation reveal that SODF of nanoparticles depends on the mode of photosensitizer bounding, concentration of photosensitizer and dissolved oxygen  $O_2(^3\Sigma_g^-)$  and the temperature in aqueous solutions. Applications of SODF toward dissolved oxygen sensing and monitoring of photooxidation ability in aqueous media are demonstrated and discussed.

Acknowledgment:

This work was supported by the Czech Science Foundation (16-15020S) and by Operational programme Research, Development and Education, Charles University Centre of Advanced Materials, CZ.02.1.01/0.0/0.0/15\_003/0000417.

References:

- [1] Henke P., Kozak H., Artemenko A., Kubát P., Forstová J., Mosinger J., ACS Appl. Mater. Interfaces, 6, 15 (2014).
- [2] Henke P., Kirakci K., Kubát P., Fraiberk M., Forstová J., Mosinger J., ACS Appl. Mater. Interfaces, 8, 38 (2016).

---

## Silver nanocubes-based sensor for mercury detection in water samples.

---

Wednesday, 18th October - 13:30 - Poster Session - Hall & Room 3 - Poster - Abstract ID: 242

---

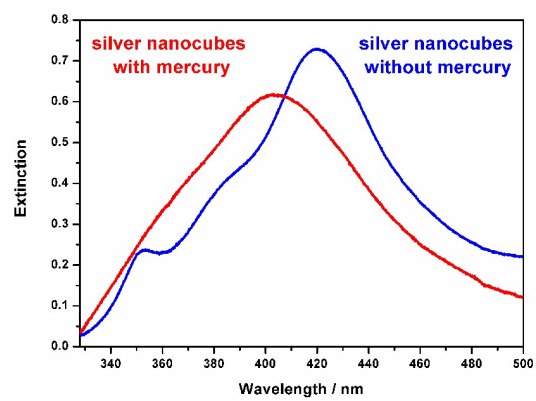
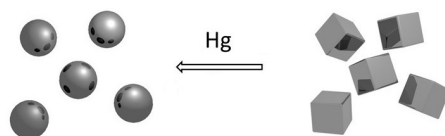
***Ms. Justyna Matyjewicz<sup>1</sup>, Dr. Adam Lesniewski<sup>1</sup>, Dr. Joanna Niedziolka-Jonsson<sup>1</sup>***

*1. Institute of Physical Chemistry, Polish Academy of Science*

Mercury is a commonly known environmental pollutant that can cause severe harm to humans and animals. One of the main sources of chronic low-level mercury exposure is fish and shellfish consumption. Mercury is metabolized by the bacteria or algae and enters the food chain, to be consumed by water organisms and finally by humans. Due to potential danger of mercury poisoning, it is very important to monitor this element concentration in water samples.

Various classical analytical methods have been proposed for mercury detection. However, most of them are usually complex and need time consuming pre-treatment, pre-concentration and separation steps. Many systems utilize mercury's unique capability to form amalgams with gold and silver. The amalgamation process significantly influences localized surface plasmon resonance (LSPR) spectrum of the nanostructures. Since the measurements require only a spectrophotometer as an instrument, LSPR-based methods have been developed as fast, simple, and low cost technology.

In our work a new, selective AgNCs-based mercury sensor have been developed. The silver nanocubes were synthesized by polyol reduction. Addition of aqueous NaBH<sub>4</sub> is necessary to reduce Hg<sup>2+</sup> to Hg(0). Aqueous solutions of HgCl<sub>2</sub> were added to AgNCs in the presence of NaBH<sub>4</sub> and the UV-vis spectra have been measured. The HgCl<sub>2</sub> concentration range was  $1 \times 10^{-17}$  –  $1 \times 10^{-5}$  M. The detection limit of AgNCs-sensor was  $1 \times 10^{-16}$  M, which is significantly lower comparing to the others already published silver nanoparticles-based mercury sensors. The new sensor has been demonstrated to be selective against Fe<sup>2+</sup>, Cu<sup>2+</sup>, Co<sup>2+</sup>, Zn<sup>2+</sup>, Ni<sup>2+</sup> and Mg<sup>2+</sup>. The potential application of AgNCs-sensor may be investigation of Hg<sup>2+</sup> in natural waters e.g. Baltic Sea. We have also investigated mercury detection by silver nanocubes suspended in NaCl water solutions. The silver nanocubes did not precipitate at the high concentration of NaCl and the shape of peaks remained the same as in water. After addition of HgCl<sub>2</sub> to AgNCs/NaBH<sub>4</sub> the sensor was still sensitive to the mercury also in the low concentration of HgCl<sub>2</sub>.



Abstrakt jmatyjewicz.jpg

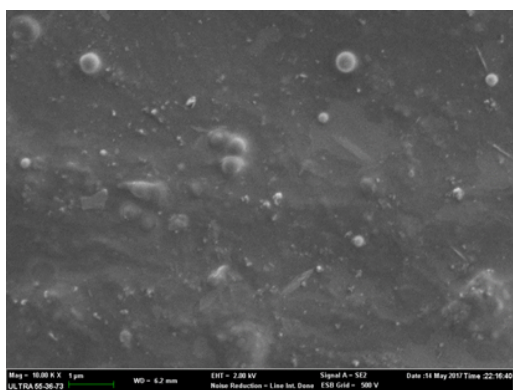
# The Structure and Properties of Ink-jet Printed Photo-curable in-situ polymerization Cationic Aqueous Dispersion Polyurethane Acrylate/Silica

Wednesday, 18th October - 13:30 - Poster Session - Hall & Room 3 - Poster - Abstract ID: 396

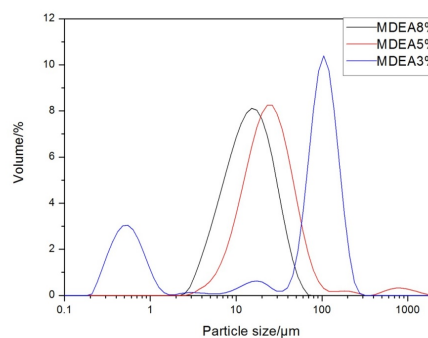
**Mr. Yiding Meng<sup>1</sup>, Prof. Jianzhong Shao<sup>1</sup>, Mr. Chenglong Wang<sup>1</sup>, Dr. Yi Huang<sup>1</sup>**

**1. Zhejiang Sci-Tech University**

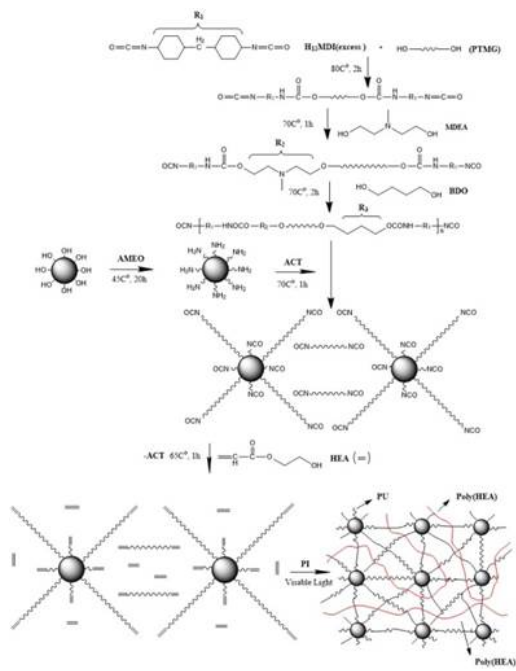
A series of photo-curable in-situ polymerization cationic aqueous dispersion polyurethane acrylate/Silica for digital ink-jet printing was designed and synthesized by incorporating N-Methyldiethanolamine (MDEA) as the hydrophilic chain extender, 2-hydroxyethyl acrylate (HEA) as Photosensitive reactive capping agent and in-situ grafted by 3-Aminopropyltriethoxysilane (AMEO) modified Silica at the end of macromolecular chain. The structure of synthesized PUAs oligomer were confirmed by infrared spectroscopic analysis, <sup>1</sup>H-NMR, and free NCO root titration. The characterization of rheology and laser particle size analysis indicated the oligomer is a typical shear thinning polymer fluid while the WPU/Silica can emulsify stably in the system of water and salted by acetic acid (Ac) which having a solid content of 33%. Silica was well dispersed in organic particles. The system had excellent compatibility and storage stability. The dispersions were effectively cured under Blue light/UV LED lamp, initiated by 3% of Diphenyl(2,4,6-trimethylbenzoyl)phosphine oxide (TPO) and copolymerized with acrylate. The investigation illustrated the Photo-curable in-situ polymerization Cationic waterborne Polyurethane Acrylate/Silica film effectively forming a semi-interpenetrating network system to achieve rapid curing coating. The results showed the product cured by WPU/Silica dispersion of R=1.5 mixed with equimolar HEA obtained low yellowing, the maximum breaking strength, high elongation at break, Low modulus, high thermal decomposition temperature, high crystallization temperature of hard segment, low glass transition temperature of soft segment, high degree of phase separation, better optically transparent performance, which can widely be applied for 3D digital ink-jet printing.



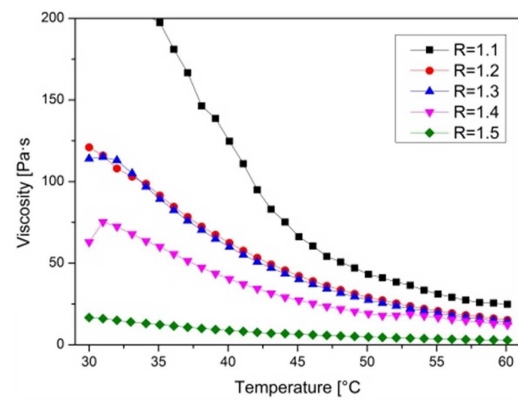
S.png



2.jpg



4.jpg



V.jpg



---

## Evaluation of the subcutaneous administration route for human serum albumin nanoparticles in mice

---

Wednesday, 18th October - 13:30 - Poster Session - Hall & Room 3 - Poster - Abstract ID: 789

---

**Mr. Alejandro Manzanares<sup>1</sup>, Dr. Lino Sánchez-Segura<sup>1</sup>, Dr. Ramón Carriles<sup>2</sup>, Dr. Yolanda Alvarado-Caudillo<sup>3</sup>, Dr. Agustino Martínez-Antonio<sup>1</sup>, Mrs. Dalia Rodríguez-Ríos<sup>1</sup>, Dr. Gloria Barbosa-Sabanero<sup>3</sup>, Dr. Gertrud Lund<sup>1</sup>, Prof. Silvio Zaina<sup>3</sup>**

*1. CINVESTAV Irapuato Unit, 2. CIO, 3. University of Guanajuato*

**Introduction.** One of our group's current efforts is to effectively target the DNA methylome of the atherosclerotic lesion. Part of our strategy is to employ macrophage-targeted human serum albumin (HSA) nanoparticles (HSA-NPs) as carriers for epigenetic modifiers. Lateral tail vein injection is traditionally used to deliver drugs to the vascular system, yet it poses practical and ethical challenges when repeated administrations are performed in dark-skinned C57BL/6 mice. Here, we evaluate the subcutaneous (s.c.) route as an alternative. To our knowledge, similar studies have been conducted for HSA-conjugated drugs and oxidation-stressed (aggregated) HSA, but not HSA-NPs *per se*.

**Methods.** HSA-NP physico-chemical properties (size, Z-potential) were determined by standard methods. ApoE-null mice (n=3) received one s.c. injection of 150 µg HSA-NP in 150 µl PBS. Peripheral blood was obtained by tail tip bleeding immediately before injection (time 0) and at 4, 8, 24 and 48 h post-injection (h.p.i.). The presence of HSA-NPs in peripheral blood was assessed by dot-blot or Western blotting with a specific anti-HSA monoclonal antibody.

**Results and Discussion.** HSA-NP size ranged 162-724 nm. Their Z-potential was -35.9 mV at pH 9, and remained negative in the 5-9 pH range. Following s.c. administration, HSA was present in peripheral blood and showed a significant h.p.i.-dependent increase ( $p=4 \times 10^{-5}$ ). We speculated that the latter effect might have been due to time-dependent increase of endogenous serum albumin expression, particularly since the extent of antibody cross reactivity was unknown. Yet, no concomitant change in peripheral blood 60-80 kDa protein expression was observed using the same antibody, thus ruling out the occurrence of such an artifact. By comparison with a HSA standard reference, we estimate that ~20% of the injected HSA-NPs is recovered in the bloodstream at 48 h.p.i. The s.c. route is therefore practical and effective to deliver HSA-NPs to the vascular tissue.



---

## Fine tuning of the electro-spinning process for novel nano-fibrous elastomerscaffolds

---

Wednesday, 18th October - 13:30 - Poster Session - Hall & Room 3 - Poster - Abstract ID: 794

---

*Dr. Vera Graup<sup>1</sup>, Mr. Wenhui Song<sup>1</sup>, Mr. Arnold Darbyshire<sup>1</sup>*

*1. University College London*

### Introduction

Electrospinning is a widely-known fabrication technique for nanofibers. With the emerging of novel, nano-structured polymers, this process needs to be re-evaluated and modified to produce replicable, consistent results for each type of materials.

This project focuses on the production and characterisation of nano-fibrous scaffold from a novel, biodegradable polyurethane-based nanocomposite using electrospinning. To create a stable jet stream and generate reproducible fibers, the solution formulation, environmental factors such as temperature and humidity and solution factors such as solvent and polymer-composition were investigated.

### Methods

POSS-terminated aliphatic polyester-urethane-urea (PEUU-POSS) solution was produced in-house at a concentration of 18%(DMAc). A custom made electrospinning set up, allowing us to monitor and control humidity and temperature, was used.

Random fibers were generated at a distance of 35cm, a voltage of 13kV and a flow rate of 1ml/h. To characterise the produced scaffolds a degradation profile was determined by immersing the scaffolds in PBS. Mechanical properties, changes in surface wettability(contact angle) after electrospinning were also evaluated.

### Results

The recorded humidity ranged from 35% to 51%, Temperatures ranged from 20C to 30C. Fibres were obtained at a distance of 35cm, a voltage of 13kV and a flow rate of 1ml/h if humidity was under 39%, between 39% and 49% individual particles were created, above 50% wet patches with no morphology appeared. Temperatures above 25C at all humidities created stable fibres, while at lower temperatures fibre formation was dependent on the surrounding temperature.

The stable, native scaffolds(Figure 1) showed a fibre-diameter in a range of 500 nm to  $1.1 \pm 0.36$   $\mu$ m, a Young's Modulus of  $6 \pm 1.6$  kPa and super high ultimate strain 575%. Contact angle measurement for random scaffolds returned hydrophobic readings of  $119.4 \pm 8.28^\circ$ , which decreased over the course of a 5-week degradation study. Weight decreased by nearly 50% during the first two weeks and then plateaued. UV spectrum analysis showed an increase of break down products of polymer.

### Discussion

PEUU-POSS is a promising novel biodegradable polymer with remarkable hyperplastic-mechanical properties. Further work is required into its processing, which is currently limited by the selection of solvents.

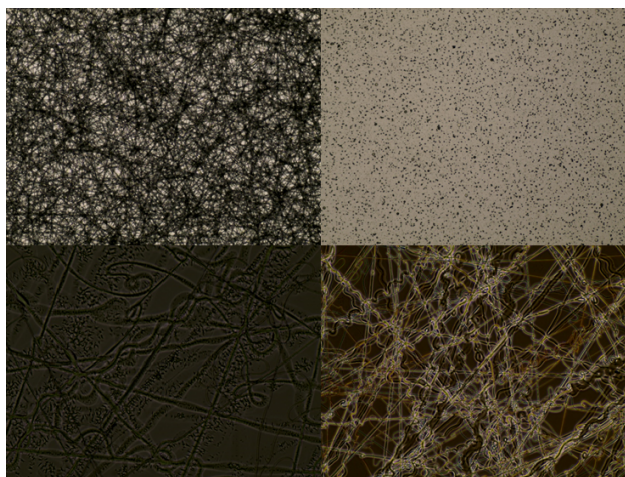


Fig1 – Examples of obtained structures at (A) under 39%, (B) 39-49% and (C&D) over 50%.

Annicsubmission.png

---

# Hydrogenization of fullerenes as a method of storage of hydrogen

---

Wednesday, 18th October - 13:30 - Poster Session - Hall & Room 3 - Poster - Abstract ID: 796

---

***Ms. Zhuldyz Otarbay<sup>1</sup>, Dr. Maratbek Gabdullin<sup>1</sup>, Mr. Yerassyl Yerlanuly<sup>1</sup>, Mr. Daniyar Ismailov<sup>1</sup>,  
Prof. Khabybulla Abdullyn<sup>1</sup>***

*1. National Nanotechnology Laboratory of the Open Type, Al-Farabi Kazakh National University*

## **Introduction**

Hydrogen is an ideal fuel with a high calorific value and a harmless combustion product - water vapor. Storage of hydrogen is one of the intermediate links in the life cycle of hydrogen from its production to consumption. The development of the most economical and efficient ways of storing hydrogen is one of the main technological problems of hydrogen energy.

## **Methods**

In the present work the method of catalytic hydrogenation of fullerenes is considered. At the moment, carbon nanomaterials are used to store hydrogen due to its low specific density and high specific surface area: activated carbon, graphene, multi-walled and single-walled carbon nanotubes, fullerenes, etc.

## **Results**

To determine the optimal regime for the hydrogenation of fullerenes at a hydrogen pressure of 12 MPa and a temperature in the range of 200-600°C, the mass of fullerite C60 is 0.501 g. First, vacuum conditions were created in the reactor, after which hydrogen was supplied to the reactor to pressure of 12.5 MPa and held for 4 hours. Then, the reactor temperature was raised to 200°C (at speed of 1° per minute) while the pressure in the reactor increased by 0.3 MPa (reaching 12.8 MPa). To stabilize the baro-temperature regime, the sample was kept for another 4 hours (T = 200°C, P = 12.8 MPa). At 480 minutes, the temperature rise in the reactor was continued from 200 to 600°C at rate of 0.125° per minute.

## **Discussion**

Increase in temperature can be explained by the decomposition of solvates formed during the crystallization of fullerite. It was found that the system reached its maximum interaction speed at 2150 minutes, which corresponded to temperature of 433°C. As a result, the temperature, at which the rate of interaction of hydrogen with the fullerene molecule is maximized, was clarified and the given value of temperature is in the range of 425-455°C, where the total hydrogen content is about 8.2% by weight. Further, the obtained hydrofullerites were studied using Raman microscopy. The results indicate that the obtained samples contain hydrogen atoms.

## Fiber optic sensor reduced by chemical etching for measuring refractive index of sucrose solutions

---

Wednesday, 18th October - 13:30 - Poster Session - Hall & Room 3 - Poster - Abstract ID: 812

---

***Dr. P. Zaca-Morán<sup>1</sup>, Dr. J. P. Padilla-Martínez<sup>1</sup>, Mr. J. M. Pérez-Corte<sup>2</sup>, Dr. J. G. Ortega-mendoza<sup>3</sup>, Dr. F. Chávez<sup>1</sup>, Dr. G. F. Pérez-sánchez<sup>1</sup>, Mr. N. Morales<sup>1</sup>***

*1. Benemérita Universidad Autónoma de Puebla, 2. Instituto Nacional de Astrofísica, Óptica y Electrónica, 3. Universidad Politécnica de Tulancingo*

In the present work, the reduction of single-mode optical fibers by chemical etching and its application as evanescent wave sensor for sucrose solutions was studied. The cladding of an optical fiber was completely removed using hydrofluoric acid at a concentration of 48-51% (obtaining a rate of etching of  $\sim 3.27 \mu\text{m}/\text{min}$ ) in order to leave the core uncovered. Using an infrared continuous wave radiation source at 1550 nm and an optical fiber with a reduced diameter of  $\sim 500 \text{ nm}$ , it was possible to characterize sucrose solutions at different concentrations [0% (water) to 65%] and their respective refractive indices [ $n=1.31$  to  $n=1.44$ , respectively]. The results obtained in this work suggest that the etched optical fiber could be used as a liquid refractive index sensor, which may play an important role in chemical applications. Furthermore, this sensing device shows potential application to measure glucose levels in blood.

---

# Unoccupied electronic states of few-layer graphene

---

Wednesday, 18th October - 13:30 - Poster Session - Hall & Room 3 - Poster - Abstract ID: 819

---

***Dr. pierfrancesco riccardi<sup>1</sup>, Dr. Antonio Sindona<sup>1</sup>***

*1. Dipartimento di fisica, Università della Calabria*

Two dimensional (2D) crystals are attracting interest in materials science as they can be the building blocks of more complex three dimensional (3D) hetero-structures with properties tailored to suit specific demands. On the other side, emerging facts and concepts about 2D materials can give new insight into the electronic properties of materials that have been widely investigated and applied, such as graphite. It is therefore an important issue, in both basic research and applications, to investigate if and how these peculiar properties of 2D crystals are reflected in 3D derived systems.

In this work, we present state of the art density functional theory (DFT) calculations [1] of the electronic band structure of graphene (1 to 3 layers) and graphite, focusing on the unoccupied energy levels up to 40 eV above the Fermi level. Particular attention is given to those one-electron states of graphene, below and above the continuum threshold, whose wavefunctions are less localized on the plane showing an extended tail into the vacuum: the so-called image potential states and the recently discovered scattering resonances [2,3].

We observe that the discrete states of graphene, below and above the vacuum level, are very sensitive to (and strongly interact with) the environment surrounding the plane. When different layers are assembled, these states hybridize, giving rise to more complex states, which evolve with increasing the number of layers. Such an evolution leads to highly dispersive states vs the one-electron out-of-plane wave-vector in graphite (,) *that are caught in Low energy electron diffraction and in electron emission experiments.*

1. M. Pisarra, P. Riccardi, A. Sindona, A. Cupolillo, N. Ligato, C. Giallombardo, L. S. Caputi Carbon 77 (2014) 796
2. V.U. Nazarov, E.E. Krasovskii, V.M. Silkin, Phys. Rev. B 87, 041405(R) (2013).
3. E. Kogan and V. U. Nazarov, Phys. Rev. B 85, 115418 (2012).

# Magnetron sputter deposition of thin VO<sub>2</sub> films onto polycrystalline substrate

Wednesday, 18th October - 13:30 - Poster Session - Hall & Room 3 - Poster - Abstract ID: 829

**Dr. Sergey Maklakov<sup>1</sup>, Prof. Sergey A. Maklakov<sup>1</sup>, Mr. Victor Polozov<sup>2</sup>, Mr. Alexey Mishin<sup>3</sup>, Prof. Ilya Ryzhikov<sup>1</sup>, Prof. Vladimir Kisel<sup>1</sup>**

*1. Institute for Theoretical and Applied Electromagnetics RAS, 2. Moscow Institute of Physics and Technology, 3. institute for the*

Vanadium dioxide is a crystalline compound which undergoes metal-insulator phase transition at 68°C. Grain boundaries in crystal structure of VO<sub>2</sub> decrease contrast of resistivity of VO<sub>2</sub> in metal state in comparison with insulator state. This is why growth of thin VO<sub>2</sub> films principally involves epitaxy.

We report on a reactive RF sputter deposition of polycrystalline VO<sub>2</sub> film onto polycrystalline non-oriented substrate of Al<sub>2</sub>O<sub>3</sub>. Appropriate sputtering conditions combined with relevant post-deposition annealing results in resistivity contrast of VO<sub>2</sub> of as much as R(30°C):R(90°C) ~ 1000 at the film thickness of 100 nm.

We found that temperature exposure in both steps, deposition and recrystallization, is necessary to form VO<sub>2</sub> film. On a deposition stage, high temperature of substrate enables VO<sub>2</sub> phase formation. In temperature range from 20°C to 400°C, the higher the temperature of the substrate, the easier VO<sub>2</sub> phase forms. Sputter conditions to be carefully matched in order to obtain V<sup>4+</sup> is composition of gas mixture and substrate bias. We show that exact combination of these parameters varies with a distance from target to substrate, pumping rate, pumping deceleration, and substrate temperature value.

As-deposited films show weak change in resistivity when heated from 30°C to 90°C. Post-deposition annealing causes recrystallization of the VO<sub>2</sub> film. We optimized annealing continuance, temperature, heating rate and cycling. We proposed that cyclic heating and cooling between 500°C and 750°C can improve effectiveness of recrystallization. This proposition is based on an existence of peritectic reaction  $V_6O_{13} \leftrightarrow VO_2 + \text{Liquid}$ , which occurs at ~700°C. However, this effect, if present, is negligible to the oxidation caused by insufficient grade of flowing inert gas during annealing. As a result of recrystallization, lateral crystallite size of VO<sub>2</sub> increases from 20 to 400 nm. Also, we found no texture formation of VO<sub>2</sub> crystals.

Thin films which are obtained via this procedure can be applied as electromagnetic interference shielding elements. When heated, these films change microwave transmittance coefficient by 1 dB in a range from 6 to 20 GHz.

This research was financially supported by the Russian foundation for basic research (RFBR project No. 16-33-01089).

---

## Rapid thermal process by RF heating of nano-graphene layer/silicon substrate structure: Heat explosion theory approach

---

Wednesday, 18th October - 13:30 - Poster Session - Hall & Room 3 - Poster - Abstract ID: 831

---

***Dr. Misha Sinder<sup>1</sup>, Prof. Joshua Pelleg<sup>1</sup>, Prof. Victor Meerovich<sup>1</sup>, Prof. Vladimir Sokolovsky<sup>1</sup>***

*1. Ben-Gurion University of the Negev*

**Introduction:** There are a number of investigations devoted to the induction heating (IH) of a conductor film/a silicon substrate structure in a radio-frequency (RF) magnetic field perpendicular to the substrate surface [1-2]. The heat explosion theory approach was used to describe the heating process. Results of the theory were successfully proved in the experiments with Ti and Ta-Ti-Si thin films deposited on Si (111) and Si (100) substrates [1-2]. One drawback of using these systems is pollution of silicon substrates due to the fast diffusion of metallic impurities.

**Methods:** A new rapid thermal process (RTP) is proposed which is based on IH of a nano-graphene layer deposited on back side of a silicon substrate in a RF magnetic field perpendicular to the layer surface. The characteristic property of the method is that no additional susceptor is required, despite the fact that thickness of the graphene layer/Si substrate structure is less than a skin depth. In contrast to metals, the diffusion of carbon in silicone is very slow. The novel RTP can be successfully applied in technological processes of fabrication of films and layers on silicon substrates as well as to study graphene transformations.

**Results and Discussion:** The heating kinetics is analyzed as a function of graphene layer thickness, sheet resistance of the graphene layer, specimen dimensions, thermal parameters, as well as the amplitude and frequency of the applied RF magnetic field. It is shown that two regimes of the heating can be realized. The first one is characterized by heating of the structure up to a finite temperature determined by equilibrium between dissipated power loss due to eddy-currents and heat transfer to environment. The second regime corresponds to a fast unlimited temperature increase (heat explosion). The criterion of realization of the regimes is obtained in analytical form. Based on this criterion, it is shown the possibility of the heat explosion regime for graphene layer/silicon substrate structure.

1. J. Pelleg, S. Rosenberg, and M. Sinder, *Acta Mater.*, Vol. 59, 4283–4290, 2011.

2. M. Sinder, J. Pelleg, V. Meerovich, and V. Sokolovsky, *PIERS Proceedings*, Stockholm, Sweden, Aug. 12–15, 1292-1296, 2013.

# Characterization and Comparison of Photocatalytic Activity Silver Ion doped on TiO<sub>2</sub>(TiO<sub>2</sub>/Ag<sup>+</sup>) and Silver Ion doped on Black TiO<sub>2</sub>(Black TiO<sub>2</sub>/Ag<sup>+</sup>)

Wednesday, 18th October - 13:30 - Poster Session - Hall & Room 3 - Poster - Abstract ID: 833

**Ms. Jin Yi Kim<sup>1</sup>, Mr. Ho Hyung Sim<sup>1</sup>, Mrs. SINAEE SONG<sup>2</sup>, Ms. Yeoung Ah Noh<sup>3</sup>, Mr. Hong Woon Lee<sup>4</sup>, Prof. Hee Taik Kim<sup>1</sup>**

*1. department of fusion chemical engineering, Hanyang University, 2. department of advanced material and science, 3. Department of Advanced Material and Science engineering, Hanyang University, 4. DAEGA POWDER SYSTEMS CO., LTD*

Titanium dioxide (TiO<sub>2</sub>) is one of the representative ceramic materials containing photocatalyst, optic and antibacterial activity. The hydroxyl radical in TiO<sub>2</sub> applies to the intensive oxidizing agent, hence TiO<sub>2</sub> is suitable to use photocatalytic materials. Black TiO<sub>2</sub> was prepared through reduction of amorphous TiO<sub>2</sub> conducting under H<sub>2</sub> which leads to color changes. Its black color is proven that absorbs 100% light across the whole-visible light, drawing enhancement of photocatalytic property. In this study, we aimed to compare the photocatalytic activity of silver ion doped on TiO<sub>2</sub>(TiO<sub>2</sub>/Ag<sup>+</sup>) and silver ion doped on black TiO<sub>2</sub>(black TiO<sub>2</sub>/Ag<sup>+</sup>) under visible light range. TiO<sub>2</sub>/Ag<sup>+</sup> was fabricated following steps. 1) TiO<sub>2</sub> was synthesized by a sol-gel method from Titanium tetra-isopropoxide (TTIP). 2) Then AgNO<sub>3</sub> was added during an aging process step for silver ion doping on the surface of TiO<sub>2</sub>. Moreover, Black TiO<sub>2</sub>/Ag<sup>+</sup> was obtained same as TiO<sub>2</sub>/Ag<sup>+</sup> except for calcination under H<sub>2</sub>. The samples were characterized X-ray diffraction (XRD), UV-visible reflectance (UV-vis DRS), and Methylene Blue degradation test. XRD analysis confirmed morphology of TiO<sub>2</sub>. The band gap of black TiO<sub>2</sub>/Ag<sup>+</sup> was confirmed (2.6 eV) through UV-vis DRS, which was lower than TiO<sub>2</sub>/Ag<sup>+</sup> (2.9 eV). The photocatalytic effect was conducted by methylene blue degradation test. It demonstrated that black TiO<sub>2</sub>/Ag<sup>+</sup> had a photocatalytic effect under UV light also visible light.

**Table 1. Doped TiO<sub>2</sub> particles size and bandgap.**

	Particle Size	Band gap
TiO <sub>2</sub> /Ag <sup>+</sup>	18 nm	2.9 eV
Black TiO <sub>2</sub> /Ag <sup>+</sup>	31 nm	2.6 eV

Table1.png

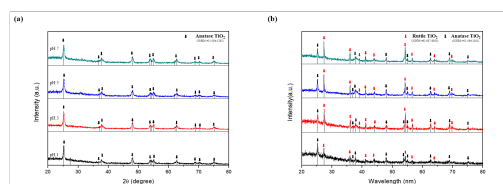


**Figure 1.** XRD analysis of Ag doped on TiO<sub>2</sub>; (a) calcined at 550 °C, and (b) 550 °C in H<sub>2</sub> atmosphere.

Fig1 xrd.png



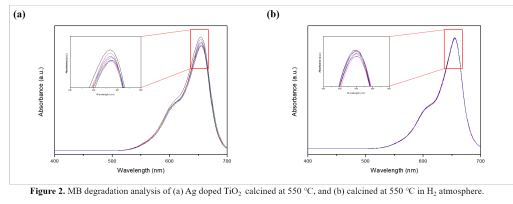


Figure 2. MB degradation analysis of (a) Ag doped TiO<sub>2</sub> calcined at 550 °C, and (b) calcined at 550 °C in H<sub>2</sub> atmosphere.

Fig2 uv-abs.png

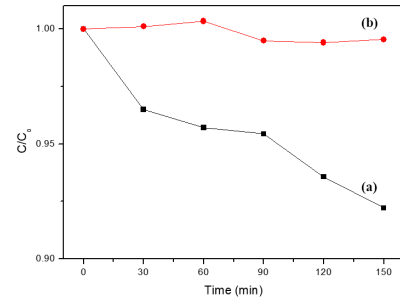


Figure 3. Comparison for MB(660 nm) concentration of (a) Ag doped TiO<sub>2</sub> calcined at 550 °C, and (b) calcined at 550 °C in H<sub>2</sub> atmosphere.

Fig3-1.png

# Structural, morphological and optical investigation of sol-gel Au-doped ZnO nanostructured thin films.

Wednesday, 18th October - 13:30 - Poster Session - Hall & Room 3 - Poster - Abstract ID: 65

**Ms. Lydia OUAREZ<sup>1</sup>, Prof. Azeddine CHELOUCHE<sup>1</sup>, Dr. Tahar TOUAM<sup>2</sup>, Dr. David BARBA<sup>3</sup>, Prof. Rachid MAHIOU<sup>4</sup>, Prof. Djamel DJOUADI<sup>1</sup>, Prof. Federico ROSEI<sup>3</sup>**

1. Laboratoire de Génie de l'Environnement, Faculté de Technologie, Université de Bejaia, 06000 Bejaia, Algeria, 2. Laboratoire des Semi-conducteurs, Université Badji Mokhtar-Annaba, BP 12, Annaba 23000, Algeria, 3. Institut National de la Recherche Scientifique Université du Québec 1650 Boulevard Lionel-Boulet Varennes, Québec J3X1S2, Canada, 4. Université Clermont Auvergne, Institut de Chimie de Clermont-Ferrand, UMR 6296 CNRS/UBP/Sigma Clermont, 63171 Aubière, France

Undoped and Au-doped ZnO thin films were prepared on glass substrates by sol-gel process and dip-coating technique. The effects of Au concentration (10-30 at.%) on the structural, morphological and optical properties of the ZnO films were studied using X-ray diffraction (XRD), field emission scanning electron microscopy (FE-SEM), atomic force microscopy (AFM), UV-Vis-NIR spectrometer and photoluminescence (PL) spectroscopy. XRD results showed that all films are well crystallized in a hexagonal wurtzite structure and highly c-axis oriented. Moreover, the crystal quality of the films was found to decrease with an increase in Au doping concentration and a weak diffraction peak related to Au cubic phase can also be observed at Au concentration higher than 10 at.%. FE-SEM micrographs and AFM images demonstrated that morphology and surface roughness were sensitive to Au doping concentration. UV-Vis-NIR optical spectra revealed that increasing Au doping content into ZnO films results to a significant enhancement in the transparency of the films. Photoluminescence measurements at room temperature put into evidence the presence of two intense bands at 373.6 and 385 nm in the UV spectra and four very weak emission bands in the visible region. All these emissions were found to be dependent upon the Au content.

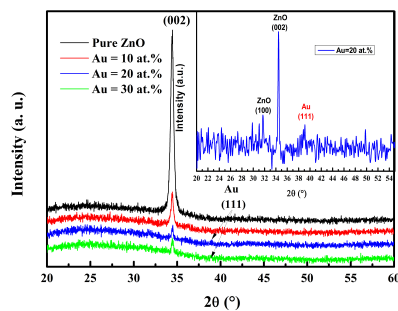


Fig.1- annic.jpg

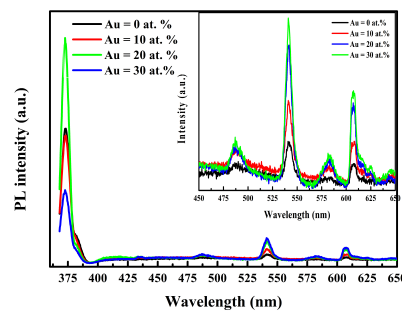


Fig.2- annic.jpg

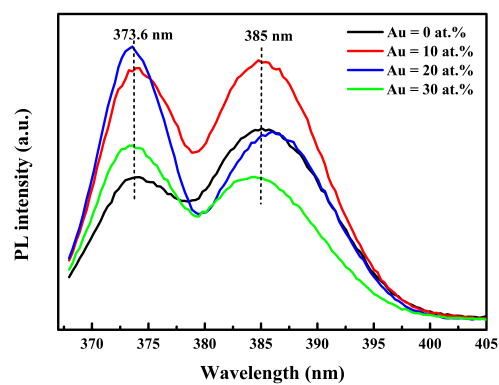


Fig.3- annic.jpg

# Feasibility of low-loss and high-speed plasmonic components and circuits

Wednesday, 18th October - 13:30 - Poster Session - Hall & Room 3 - Poster - Abstract ID: 70

**Prof. Mitsuo Fukuda<sup>1</sup>, Mr. Yuuta Tonooka<sup>1</sup>, Mr. Tomoaki Inoue<sup>1</sup>, Mr. Shinya Okahisa<sup>1</sup>, Dr. Yuya Ishii<sup>1</sup>**

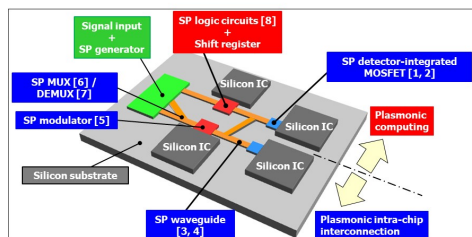
<sup>1</sup>

*1. Toyohashi University of Technology*

Plasmonic components and circuits have been researched and developed for various applications, especially for plasmonic integrated circuits (ICs). This paper clarifies the applicability of plasmonic devices in nano- and micro-scale circuits from the viewpoint of plasmonic signal transmission loss and speed.

In silicon ICs, wire delay and power consumption are serious problems. To solve these issues, optical interconnection techniques have been introduced to silicon ICs; however, this has caused other problems, namely a mismatch in size and of the materials between the optical and electronic components. Additionally, the optical components require complicated structures. These issues can be solved using plasmonic components. Therefore, we have developed various plasmonic components for ICs (see Fig. 1) in which surface plasmons are used as signal carriers transmitted at the speed of light. However, signal transmission loss is a growing concern in such plasmonic circuits and will determine the application range of plasmonic components.

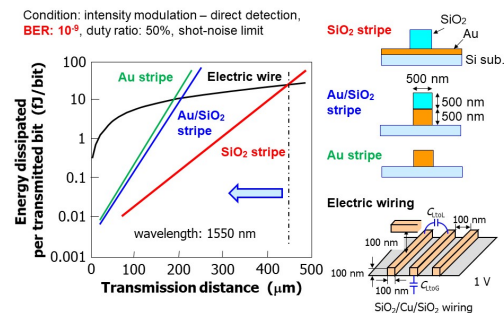
The signal transmission distance in plasmonic circuits is limited by ohmic and radiation loss. We have confirmed that low loss plasmonic component structures integrated on a silicon substrate can be fabricated by patterning a SiO<sub>2</sub> film on a metal film. For some waveguides, the energies required to detect plasmonic and electric signals after propagation were estimated at a bit error rate of 10<sup>-9</sup> according to Conway [Optics Exp., vol. 15, p. 4474, 2007.] and is shown in Fig. 2. The wavelength of the surface plasmons was set to 1550 nm. The energy dissipated per bit was lower in the plasmonic waveguide than in the electric wiring within a few hundred micrometers. The transmission speed of plasmonic signals was much higher than that of the electric signals, where the speed was limited with dispersion in plasmonic waveguides and capacitance in electric wiring. These results demonstrate that we can fabricate plasmonic components and circuits with lower losses and higher operating speeds than by using electric wires.



[1] T. Aihara, et al., IEEE Photon. J., vol. 5, 6800009, 2013. [2] H. Sakai, et al., Solid State Electron., vol. 125, p. 240, 2016. [3] M. Fukuhara, Appl. Phys. Lett., vol. 104, 081111, 2014. [4] M. Ota, et al., Opt. Lett., vol. 40, p. 2269, 2015. [5] S. Higuchi, et al., The 8th Int. Conf. Surface plasmon & Photon., Taiwan, May, 2017 (accepted). [6] A. Sumitani, IEEE Photon. Tech. Lett., vol. 28, p. 2419, 2016. [7] K. Nakayama, et al., The 8th Int. Conf. Surface plasmon & Photon., Taiwan, May, 2017 (accepted). [8] M. Ota, Sci. Rep., vol. 6, 24546, 2016.

TOYOHASHI  
UNIVERSITY OF TECHNOLOGY

Fig. 1 target plasmonic integrated circuits and components developed in our laboratory.jpg



TOYOHASHI  
UNIVERSITY OF TECHNOLOGY

Fig. 2 energy dissipation in plasmonic and electric wiring.jpg

---

## Influence of zinc oxide nanofillers on the mechanical properties of PDMS

---

Wednesday, 18th October - 13:30 - Poster Session - Hall & Room 3 - Poster - Abstract ID: 164

---

***Ms. Karina Jeronimo<sup>1</sup>, Prof. Vasileios Koutsos<sup>1</sup>, Dr. Enrico Mastropaolo<sup>1</sup>***

*1. University of Edinburgh*

Zinc oxide (ZnO) is a piezoelectric material, which can be used for sensors and actuators. The piezoelectric feature combined with the flexibility of a polymer offers novel opportunities to develop flexible force or pressure sensors for wearable health-care systems, electronic skins, and nanogenerators. In these applications, flexibility, high strain and robustness to repeated flexing and bending are crucial characteristics which can be enhanced by adding ZnO nanofillers to the flexible polymer. In this work, we analyse the mechanical properties of a nanocomposite formed of polydimethylsiloxane (PDMS), used as a polymer matrix, and ZnO piezoelectric nanofillers. PDMS nanocomposites were fabricated using two types of ZnO nanofillers: nanoparticles (NPs) and nanorods (NRs), in different concentrations (0.1 – 5 %w/w). The influence of shape and size of the nanofillers on the mechanical properties of the PDMS matrix is investigated. Tensile testing is carried out to determine the Young's modulus (E), ultimate tensile strength (UTS), elongation at break (%Eb) as function of particle concentration and after thermal ageing (24 hours at 200 °C).

E is found to decrease from  $1.42 \pm 0.21$  MPa to  $0.77 \pm 0.015$  MPa and  $1.13 \pm 0.02$  MPa when loading with high concentrations (5 %w/w) of NRs and NPs, respectively (Fig. 2a). In general, the nanocomposite showed an increased %Eb when compared to the unloaded PDMS. Thermal ageing resulted in an increase of E (Fig. 2b) and decrease of % Eb. Overall, the incorporation of ZnO nanofillers affects the crosslinked network with the filler's geometry influencing the mechanical properties of the nanocomposite. Dynamic mechanical analysis (DMA) of nanocomposites was performed to investigate the mechanical behaviour in a range of temperatures from -150 to 200° C. In this paper, we will present the details of the obtained results and in-depth analysis of the mechanical properties of the nanocomposites. The current results show that the nanocomposites retain a very good degree of flexibility regardless particle geometry, can possibly withstand microfabrication processing conditions and therefore are excellent materials for flexible sensor technology.

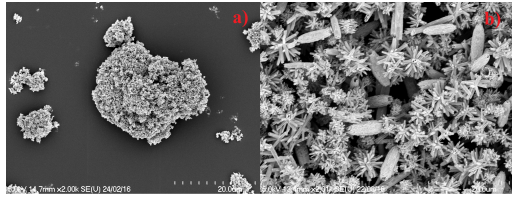


Fig 1. sem images of znO nps a and znO nws b .png

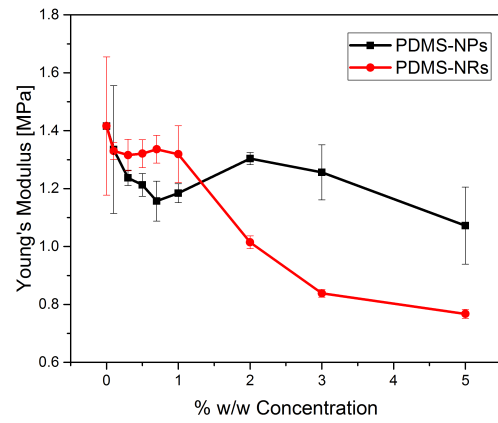


Fig 2. a young s modulus e of pdms-nps and pdms-nrs as a function of nanofiller concentrations ww .png

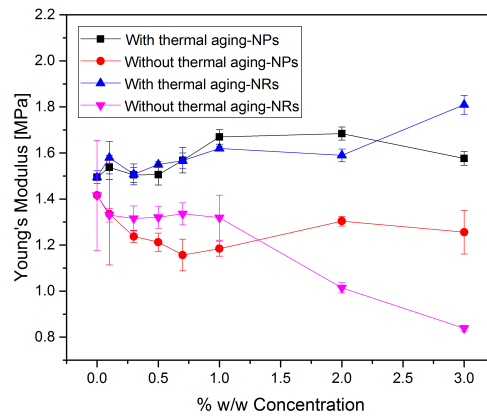


Fig 2. b e as a function of concentration before and after thermal ageing 24 hours at 200 c .png

# Pd surface functionalization of 3D electroformed Ni and Ni-Mo alloy metallic nanofoams for hydrogen production

Wednesday, 18th October - 13:30 - Poster Session - Hall & Room 3 - Poster - Abstract ID: 218

**Dr. Aurora PETICA<sup>1</sup>, Mr. Danut Balan<sup>1</sup>, Dr. Florentina Golgovici<sup>1</sup>, Prof. Marius Enachescu<sup>1</sup>, Dr. Liana Anicai<sup>1</sup>**

*1. University Politehnica of Bucharest, Center of Surface Science and Nanotechnology*

## Introduction

In the case of hydrogen production through water electrolysis, one of the main targets is to develop more active cathodic materials, in order to optimize the efficiency of hydrogen evolution reaction (HER) and, consequently, enhance the overall energy efficiency of electrolysis. Thus, to develop suitable HER electrocatalysts either an increase of the electrode active surface area or a design of a material having high intrinsic catalytic activity should be taken into consideration, both of them decreasing the HER overpotential.

The paper presents some experimental results regarding the functionalization of 3D electroformed Ni and Ni-Mo alloy nanofoams with Pd nanoclusters, as potential cathodic materials suitable for HER during water electrolysis.

## Methods

The electrodeposition from aqueous electrolytes containing  $\text{NiCl}_2$  and  $\text{NH}_4\text{Cl}$  has been applied to prepare the 3D Ni nanofoams. Ni-Mo (15-60 wt.% Mo) alloys have been electrodeposited involving either aqueous ammonium citrate type electrolytes or deep eutectic solvents based on choline chloride (DESS). Pd surface functionalization has been performed using both electroless and electrochemical procedures. To assess the HER efficiency against the Pd content characteristics, linear voltammetry, cyclic voltammetry and chronoamperometry techniques have been applied.

## Results and Discussion

The electroformed Ni nanofoams usually showed a porous structure having macropores of about 20-30  $\mu\text{m}$  and micropores of 3-5  $\mu\text{m}$ , with a nodular growth, leading to a cauliflower-like morphology. The use of DESS to electrodeposit porous Ni-Mo alloys facilitated the formation of a nanoporous structure associated with a cracks network as the molybdenum species content in the electrolyte increased. Depending on the applied procedure and the operation conditions, the content of the deposited Pd varied in the range of 0.35 – 3 wt.% (Fig.1). Depending on the porous structure characteristics of the metallic foams and Pd loading, Tafel slopes values between 65-150  $\text{mV.dec}^{-1}$  have been determined in natural sea water. A comparative analysis based on the determined Tafel slope values and hydrogen production rate vs. the applied current against the alloy deposit characteristics is presented, too.

**Acknowledgements:** The authors acknowledge Executive Agency for Higher Education, Research, Development and Innovation Funding, for the funding under NANOFOAM project 37/2016, M Era Net Program.

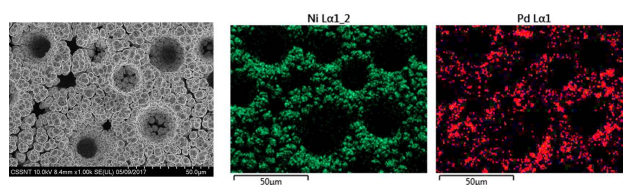


Fig 1 .jpg

---

## Nanofiber biomass carriers as effective tool for environmental monitoring and technical applications

---

Wednesday, 18th October - 13:30 - Poster Session - Hall & Room 3 - Poster - Abstract ID: 259

---

**Dr. Lukáš Dvořák<sup>1</sup>, Ms. Magda Nechanická<sup>1</sup>, Ms. Denisa Vlková<sup>1</sup>, Dr. Jan Dolina<sup>1</sup>, Mrs. Iva Dolinová<sup>1</sup>**

*1. Technical University of Liberec, Institute for Nanomaterials, Advanced Technologies and Innovation*

**Introduction:** Biomass carriers are widely used in various systems, e.g. to increase capability or efficiency. They are also used for biomass monitoring because proper sampling is crucial factor in understanding/controlling ongoing processes. Material features particularly determine the specific use of carriers. As nanomaterials exhibit very specific properties differing from bulk materials, they represent promising option for carrier's preparation. Main goal was, therefore, to develop new nanofiber biomass carriers which will be applicable in various systems: biomass monitoring, storage following biomass lyophilization and biofiltration of contaminated air.

**Material and methods:** Carriers were made of supporting thread coated by polyurethane nanofibers in various shapes and with different surface density. As blank, carriers without nanofibers were tested. Carriers were long-termly evaluated under laboratory conditions as well as at contaminated site (BTEX, chlorinated ethenes). To examine their applicability, particularly molecular-genetic methods as real-time PCR (16S rDNA and specific genes) were employed. Amplification of the region V4 of eubacterial 16S rRNA gene was performed with barcode primers 515F (5'–TGCCAGCMGCNGCGG–3') and 802R (5'–TACNVGGGTATCTAATCC–3') during NGS analysis.

**Results:** Long-term monitoring of carriers at contaminated sites showed fast colonization by autochthonous microorganisms. Nanofiber carries exhibited faster and more compact biofilm structure compared to ones without nanofibers. Biggest differences in microbial community were mainly in quantity of detected families than in composition of autochthonous microorganisms. As expected, families able to easily form biofilm were more common on carriers. Shape of carriers impacted the composition of present microorganisms only slightly. Moreover, more than one year lasting exposition at actual sites did not affected structure of nanofiber layers as evaluated through SEM. Results of lyophilization indicated that developed carries did not influence microorganisms, therefore, they can be used for storage. Carriers used in biofilter showed fast colonization and stable biomass growth even when feeding by mixture of air and toluene. Achieved results, thus, proved applicability of developed nanofiber carriers. Additionally, developed carriers are cheap and very easy to use without any samples preparation prior to analysis.

**Acknowledgment:** Project "Microbial colonization of the fiber surface for analytical and diagnostic practice and technical applications" (No. TA04021210) provided by TAČR CZ is gratefully acknowledged.



---

## Suppressing spontaneous polarization of p-GaN by graphene oxide passivation: enhanced light output of flexible UV-LED

---

Wednesday, 18th October - 13:30 - Poster Session - Hall & Room 3 - Poster - Abstract ID: 371

---

***Ms. Sooyeon JEONG<sup>1</sup>, Dr. Seung Yol Jeong<sup>1</sup>***

*1. Korea Electrotechnology Research Institute*

GaN-based ultraviolet (UV) LEDs are widely used in numerous applications, including white light pump sources, high-density optical data storage, medical equipment, and counterfeit bill detection. However, low hole injection rate in p-type region due to poorly activated holes and spontaneous polarization leads to insufficient light emission efficiency. Therefore, improving hole injection rate is a key step towards high performance UV-LEDs to expand their uses. Here, we report a new method for enhancing light output power of UV-LEDs by increasing hole injection rate in p-type region. This was achieved by simply passivating graphene oxide (GO) on top of the fully fabricated LED. The dipole field formed by the passivated GO and indium tin oxide (ITO) junction enhanced hole injection rate in p-type region and simultaneously increased hole concentration by about 60%. This not only improved the homogeneity of electroluminescence intensity in active layers but also enhanced light output power to about 60% in linear current region and almost twice in saturated current region due to the delayed hole saturation. Our simple approach of overcoming the limited carrier concentration of p-type GaN using GO passivation method disrupts the current state of the art technology and will be useful for high-efficiency and flexible UV-LED technology.

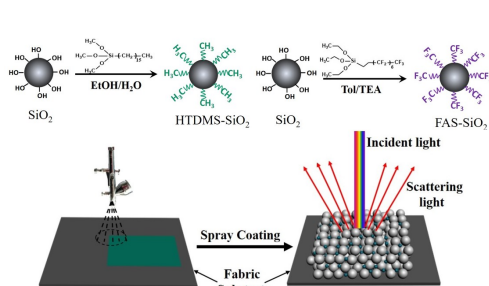
# Facile fabrication of non-iridescence structural colored films with high stability and superhydrophobic/oleophobic properties

Wednesday, 18th October - 13:30 - Poster Session - Hall & Room 3 - Poster - Abstract ID: 379

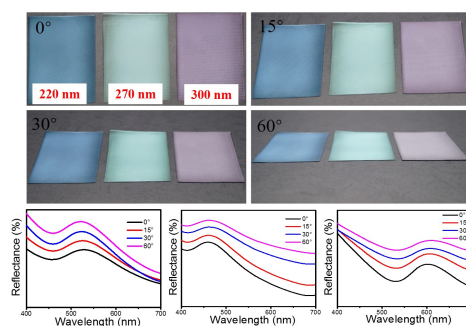
**Dr. Yichen Li<sup>1</sup>, Prof. Lan Zhou<sup>1</sup>, Dr. Guojin Liu<sup>1</sup>, Prof. Jianzhong Shao<sup>1</sup>**

**1. Zhejiang Sci-Tech University**

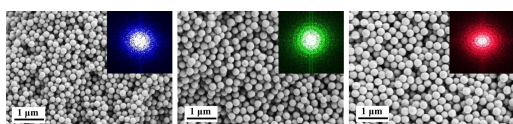
Non-iridescence structural colored films with both superhydrophobic and oleophobic properties as well as high structure stability were fabricated on fabric substrates by a composite of SiO<sub>2</sub> microspheres and Poly(methylmethacrylate-butylacrylate) [P(MMA-BA)] copolymer particles via a simple one-step spray-coating technology. With this strategy, the obtained films present short-ordered and amorphous structure array similar to the amorphous nanostructures of avian feathers. The structural colors of the films on fabric substrates display the same hue at different viewing angles and could be easily tuned by varying the diameters of the SiO<sub>2</sub> microspheres. The fabricated amorphous array were mechanically robust and strongly binding to the substrate because of the cementing effect caused by the soft P(MMA-BA) copolymer particles filling the interstices of the SiO<sub>2</sub> microspheres like cement filling the gap and tightly holding stones in a sturdy cement wall. Meanwhile, both superhydrophobic and oleophobic properties of the films were obtained owing to the alkyl and fluorosilane modification of silica microspheres. The as-prepared films could resist the destruction of external forces and the invasion of some solvents to retain their brilliant structural color unchanged, and this property is significant for their potential applications in textile structural coloration, full-color displays and colorimetric sensors etc.



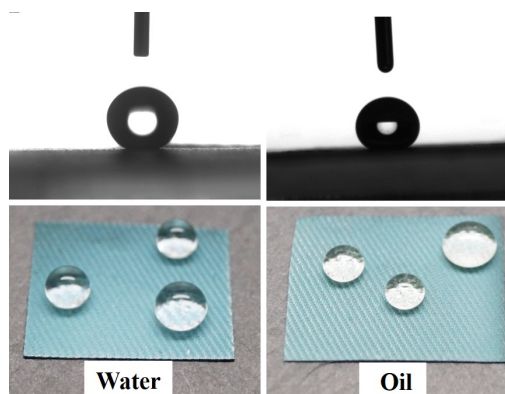
Schematic diagram.jpg



Non-iridescence.jpg



Amorphous array.jpg



Superhydrophobic oleophobic properties.jpg

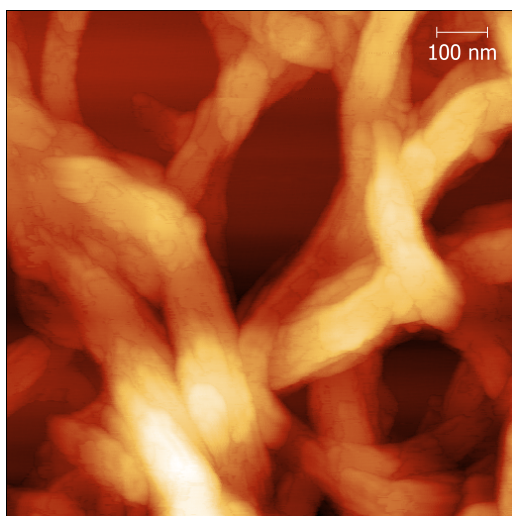
## Effects on the nanostructure of additive materials in complex solutions

Wednesday, 18th October - 13:30 - Poster Session - Hall & Room 3 - Poster - Abstract ID: 389

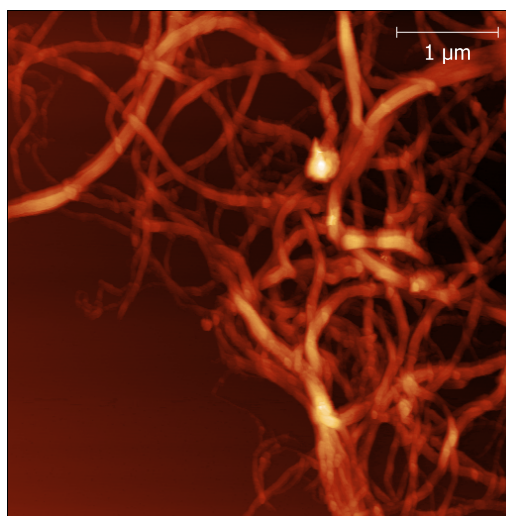
***Dr. Scott Jamieson***<sup>1</sup>

*1. CSGI, University of Florence*

In the development of both industrial and consumer solution-based products, maintaining or improving the physical attributes of the products while achieving a target cost can be achieved through the use of specific additives. Our research focuses on the effects and interactions of the additive materials with the target mixture in terms of the nanostructure (SAXS and AFM), crystal structure (XRD) and thermal analysis (DSC and TGA). This work forms part of a larger multi-faceted project working with a number of academic and industrial partners to select and modify naturally-sourced materials for large-scale rheological applications. We have observed that the packing structure and surface features of fibrous and crystalline materials have a unique effect on the total complex system, where chemical and physical modification of the additives does not necessarily show a clear relationship with the final rheology. Further investigation by small angle scattering and modelling of the system may provide key details on the variable characteristics of the additives and how we direct our future modifications.



Cp18 1um.png



Cp18 5um.png

# Design and Analysis of non-linear properties of photonic crystal fiber with Various Doping Concentration

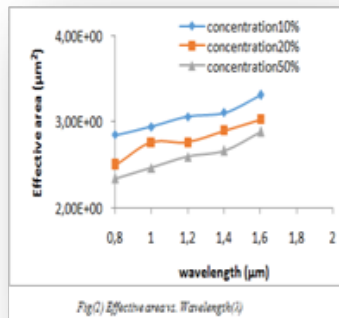
Wednesday, 18th October - 13:30 - Poster Session - Hall & Room 3 - Poster - Abstract ID: 498

***Dr. Mohamed Benhaddad<sup>1</sup>, Dr. Fouad Kerrou<sup>2</sup>, Prof. Ouanassa Benabbes<sup>2</sup>***

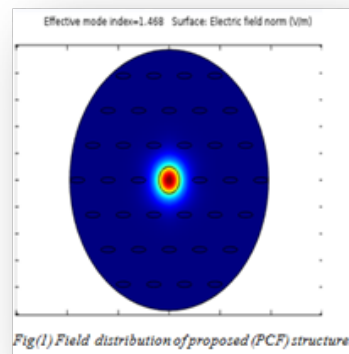
*1. University Brothers Mentouri of Constantine/, 2. University Brothers Mentouri of Constantine*

Photonic crystal fibers (PCFs) consisting of a central defect region surrounded by multiple air holes that run along the length of the fiber are attracting much attention in recent years because of unique properties which are not realized in conventional optical fibers[1,2]. In this work, a solid core photonic crystal fiber (PCF) is designed using Comsol Multiphysics software based on finite element method[3,4]. In our analysis the structure introduced is a structure formed by a doped core surrounded by a cladding which is composed by elliptical air holes in silica arranged in a hexagonal array. The important optical properties like effective area and nonlinear coefficient has been studied. Each characteristic has been investigated under different doping concentration within range of wavelength 800-1600 [nm]. The intensity and the shape of output light in two dimension is shown in figure (1).

Results show that effective area increases with increase of wavelength[5] and effective area decreases with increase of doping concentration as shown in figure (2).



Fig(2) Effective area vs. Wavelength(μ)



Fig(1) Field distribution of proposed (PCF) structure.

Nouvelle image 1 .png

Nouvelle image.png

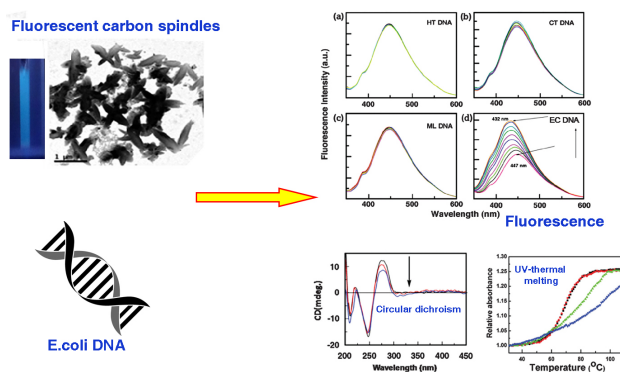
# Fluorescence Active Carbon Nano Spindles Used as a Probe for the Selective Detection of *Escherichia coli* DNA

Wednesday, 18th October - 13:30 - Poster Session - Hall & Room 3 - Poster - Abstract ID: 552

**Mr. sabyasachi Chatterjee<sup>1</sup>, Mr. Anurag Roy<sup>2</sup>, Mr. Srikrishna Pramanik<sup>2</sup>, Dr. Parukuttyamma Sujatha Devi<sup>2</sup>, Dr. Gopinatha Suresh Kumar<sup>1</sup>**

1. CSIR-Indian Institute of Chemical Biology, 2. CSIR-Central Glass and Ceramic Research Institute

The interaction of hydrophilic blue emitting carbon spindles (synthesized from commercially available glucose powder) with various deoxyribonucleic acids (DNA) having different base pair compositions, such as Herring testes (HT), calf thymus (CT), *Escherichia coli* (EC) and *Micrococcus lysodeikticus* (ML) DNA and also different synthetic DNA, was studied to develop nano materials based sensor devices and to understand the mode of interaction. Interestingly, the fluorescent carbon spindles selectively interacted with *E. coli* DNA, resulting in remarkable enhanced fluorescence of the former. Interaction of the same carbon with other DNAs exhibited insignificant changes in fluorescence. In addition, in the presence of EC DNA, the D band in the Raman spectrum attributed to the defect state completely disappeared, resulting in enhanced crystallinity. Electron microscopy images confirmed the wrapping of DNA on the carbon spindles leading to the assembly of spindles in the form of flowers. Both carbon and *E. coli* DNA exhibited negative charge with zeta values of -31.1 mV and -29.0 mV, respectively. The FT-IR spectra indicate the presence of hydrophilic functional groups such as -OH and COO- on the surface of the nanomaterials. Since both the systems have negative surface charge, electrostatic interaction with the phosphate backbone and carbon material cannot be the dominant factor of interaction. Circular dichroism spectra confirm that the carbon spindles are changing the *E. coli* DNA conformation. Dissociation of double-stranded DNA to single-stranded occurred upon interaction with carbon spindles, resulting in selective *E. coli* DNA interaction confirm by UV-thermal melting experiment. But in presence of same concentration (even higher) of carbon, the other DNA remains in double stranded conformation. The carbon spindles also exhibited a similar fluorescence enhancement upon treating with live *E. coli* bacteria and the fluorescence intensity was changes with time and getting saturated after 4 hr. These results confirm the possibility of low cost *E. coli* detection sensor in water and other liquid foods using such fluorescent carbon materials.



Abstract.jpg

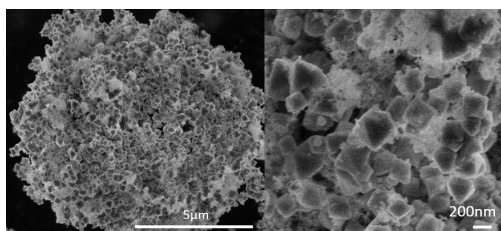
# Bi<sub>11</sub>VO<sub>19</sub>-VO<sub>2</sub> microstructure and its visible light driven photocatalytic performance in organic dye degradation

Wednesday, 18th October - 13:30 - Poster Session - Hall & Room 3 - Poster - Abstract ID: 602

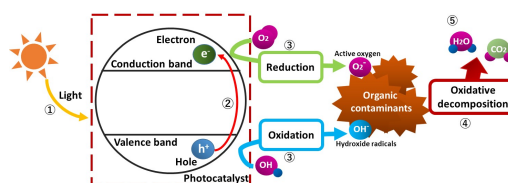
**Mrs. Arini Nuran Zulkifli<sup>1</sup>, Prof. Shinji Kimijima<sup>1</sup>, Prof. Jinhua Ye<sup>2</sup>**

**1. Shibaura Institute of Technology, 2. National Institute for Material Science**

A cubic Bi<sub>11</sub>VO<sub>19</sub>-VO<sub>2</sub> microstructure was successfully synthesized by a simple precipitation method at 65°C for 24 hours and calcination at 400°C for 6 hours. The crystal structure was investigated by X-ray powder diffraction (XRD) and characterized by scanning electron microscopy (SEM), energy dispersive X-ray spectroscopy (EDX), UV-vis spectroscopy, Raman and FTIR. The as-prepared samples have a light yellow color with a band-gap energy of 2.9 eV which indicates that it is suitable for photocatalytic degradation under visible light irradiation. The photocatalytic activity performance was evaluated by the photodegradation of the methylene blue (MB) as a cationic dye and methyl orange (MO) as the anionic dye under visible light irradiation ( $\lambda > 420$  nm). The results indicate that Bi<sub>11</sub>VO<sub>19</sub>-VO<sub>2</sub> has the potential to be used as a photocatalyst in the degradation of cationic dye, but not the anionic dye. The recyclability and active species were also studied via using the scavenger method for the cationic dye degradation.



Bi11vo19.jpg



Photocatalysis mechanism.jpg

---

## Development of NO<sub>2</sub> sensor by fungal-ZnFe<sub>2</sub>O<sub>4</sub> at room temperature

---

Wednesday, 18th October - 13:30 - Poster Session - Hall & Room 3 - Poster - Abstract ID: 622

---

***Mr. Goutham Solleti<sup>1</sup>, Ms. Kruthi Doriya<sup>2</sup>, Dr. Devarai Santhosh Kumar<sup>2</sup>, Prof. Kalagadda Venkateswara Rao<sup>1</sup>***

*1. Center for Nano Science and Technology, JNT University Hyderabad, 2. Department of Chemical Engineering, Indian Institute of Technology Hyderabad*

Hybrid nanomaterial (powdered fungi and ZnFe<sub>2</sub>O<sub>4</sub>) was developed and studied for gas sensing application, specifically for NO<sub>2</sub> gas detection. In this study, powdered Rhizopus species W3 and ZnFe<sub>2</sub>O<sub>4</sub> nano-powder were mixed at equal proportion to carryout sensing experiments. The conjugated material film was coated on the interdigitated electrodes (IDEs) by drop drying method, to determine the NO<sub>2</sub> gas sensing characteristics. It was found that the response of these hybrid material decrease resistance, thereby resembling to p-type semiconductor. The fungi W3- ZnFe<sub>2</sub>O<sub>4</sub> hybrid composite sensor showed better response, sensitivity, selectivity, stability and reproducibility at room temperature towards 30 ppm of NO<sub>2</sub>. N. Miura et al reported in 2002 ZnFe<sub>2</sub>O<sub>4</sub> shown good sensitivity for NO<sub>2</sub> (436 ppm) at 700°C operating temperature [1]. Therefore, In the present work effort was made to prepare novel hybrid material that is feasible, eco-friendly, flexible, cost-effective, low maintenance and light weight new device.

**Key words:** Fungi species, ZnFe<sub>2</sub>O<sub>4</sub>, NO<sub>2</sub>, gas sensor.

**Reference** [1] N. Miura, S. Zhuikov, T. Ono, M. Hasei, N. Yamazoe, Mixed potential type sensor using stabilized zirconia and ZnFe<sub>2</sub>O<sub>4</sub> sensing electrode for NO<sub>x</sub> detection at high temperature, Sensors and actuators B, 83 (2002) 222-229.



---

## Photoelectrochemical hydrogen production by decorated metal oxides

---

Wednesday, 18th October - 13:30 - Poster Session - Hall & Room 3 - Poster - Abstract ID: 698

---

***Mr. Nurlan Bakranov*<sup>1</sup>, *Dr. Sarkyt Kudaibergenov*<sup>1</sup>, *Prof. Niazbek Ibraev*<sup>2</sup>**

*1. KAZAKH NATIONAL RESEARCH TECHNICAL UNIVERSITY AFTER K. I. SATPAYEV, 2. Karaganda State Univ, Karaganda, Kazakhstan*

The study of solar energy conversion systems attracts tremendous attention due to growing demand of world community for electricity, heat, etc. Such, solar heat collectors and solar electricity panels have been developed, but until now they possess some difficulties associated with transportation and storage of converted energy. Therefore, the further development of solar energy converters is sought. A good alternative to available technologies may be the photoelectrochemical evolution of hydrogen from water. Hydrogen fuel production by photoelectrochemical water splitting is one of the most promising way to Sun energy conversion. Herein, the methods of PEC electrodes fabrication and characterisation are discussed. The basic photoactive materials, such as ZnO and TiO<sub>2</sub> were synthesized in different structures, such as rod and sheetlike by electrochemical and hydrothermal approaches. Further, obtained metal oxides were separately decorated with narrow bandgap semiconducting Fe<sub>2</sub>O<sub>3</sub> and CdS, and plasmonic Ag nanoparticles by simple spin- and dip-coating methods. Photoelectrochemical investigation of good photocatalysts for water decomposition were preceded by comparison of photocatalytic activity of obtained structures. Charge transport parameters of pristine and decorated metal oxides were studied by impedance technique. The structure and morphology of obtained samples were analyzed by XRD and SEM instruments respectively.



---

## Phase-Controlled Synthesis of Bismuth oxide Polymorphs towards Removal of Environmental Pollutants

---

Wednesday, 18th October - 13:30 - Poster Session - Hall & Room 3 - Poster - Abstract ID: 697

---

***Dr. Anandan Sambandam***<sup>1</sup>

*1. National Institute of Technology, Trichy, Tamil Nadu*

Up to now,  $\text{TiO}_2$  has been intensely used for environment application particularly in the removal of pollutants. However, in the past decade, bismuth-based compounds have been much involved for environmental applications. Bismuth oxide ( $\text{Bi}_2\text{O}_3$ ) is a p-type semiconductor with unique physicochemical properties in tremendous applications for photovoltaic, sensors, electrochromic and photocatalyst. In common,  $\text{Bi}_2\text{O}_3$  has six polymorphic forms. Among them,  $\alpha$ - $\text{Bi}_2\text{O}_3$  is a more stable monoclinic phase at room temperature whereas  $\delta$ - $\text{Bi}_2\text{O}_3$  (face centered cubic) is stable at high temperature. However  $\beta$  (tetragonal),  $\gamma$  (body centered cubic),  $\epsilon$  (tetragonal) and  $\omega$  (triclinic) phases are metastable in nature. In the past few years, several methods are followed regarding the synthesis of stable ( $\alpha$ - phase) and metastable ( $\beta$  - phase)  $\text{Bi}_2\text{O}_3$ . In this work, synthesis of stable and metastable  $\text{Bi}_2\text{O}_3$  ( $\alpha$  &  $\beta$  - phase) were considered via post-synthetic thermal decomposition process using bismutite as a precursor. As-synthesized samples are found in different phase which was confirmed by powder X-ray diffraction (XRD) and Raman spectroscopy. Moreover, the morphologies of samples were characterized by field emission scanning electron microscopy (FESEM) and high-resolution transmission electron microscopy (HRTEM). Further, the photocatalytic performance of as-synthesized samples will be explored under stimulated solar illumination.

---

# Effect of doping concentration of lanthanide nanoparticle on homeotropic liquid crystal alignment

---

Wednesday, 18th October - 13:30 - Poster Session - Hall & Room 3 - Poster - Abstract ID: 705

---

**Mr. Seok Gon Hwang<sup>1</sup>, Mr. Chan-woo Oh<sup>1</sup>, Mr. Eungon Park<sup>2</sup>, Prof. Hong-Gyu Park<sup>1</sup>**

*1. Changwon National University, 2. changwon*

Liquid crystal display (LCD) devices still have a lot of demand because of their simple structure, light weight and low power consumption. Various researches are continuously carried out to realize better performance. Recently, the combination of nanomaterials and nanotechnology into LCDs has attracted great attention in the scientific community due to their unique electro-optic properties [1-5]. Especially, many research groups have found the liquid crystal (LC)-nanoparticles mixtures show novel electro-optical (EO) properties such as memory effect [1,2], frequency modulation properties [3], low threshold voltage [4], and fast response time [5]. In this study, we demonstrated high performance EO properties of LC system via dispersive lanthanide oxide nanoparticles. Lanthanide oxides such as Dy<sub>2</sub>O<sub>3</sub>, Ho<sub>2</sub>O<sub>3</sub>, Gd<sub>2</sub>O<sub>3</sub>, Pr<sub>2</sub>O<sub>3</sub> and La<sub>2</sub>O<sub>3</sub> are widely used due to high dielectric constant, large band gaps and high thermal stability. Uniform LC alignments and regular pretilt angles were achieved as a function of nanoparticle concentrations. Also, this approach employed the conventional PI materials, the fabricate process, therefore, it could be adopted by the conventional LCD fabrication.

## References

- [1] A. Glushchenko, H. Kresse, V. Reshetnyak, Y. U. Reznikov, and O. Yaroshchuk, *Liq. Cryst.* **23**, 241 (1997).
- [2] D. Sikharulidze, *Appl. Phys. Lett.* **86**, 033507 (2005).
- [3] Y. Shiraishi, N. Toshima, K. Maeda, H. Yoshikawa, J. Xu, and S. Kobayashi, *Appl. Phys. Lett.* **81**, 2845 (2002).
- [4] W.-K. Lee, J.-H. Choi, H.-J. Na, J.-H. Lim, J.-M. Han, J.-Y. Hwang, and D.-S. Seo, *Opt. Lett.* **34**, 3653 (2009).
- [5] W. Lee, C.-Y. Wang, and Y.-C. Shih, *Appl. Phys. Lett.* **85**, 513 (2004).

---

# Relaxation dynamics of a multihierarchical polymer network based on Vicsek fractal and dendrimer

---

Wednesday, 18th October - 13:30 - Poster Session - Hall & Room 3 - Poster - Abstract ID: 752

---

***Dr. Aurel Jurjiu***<sup>1</sup>

*1. Babes-Bolyai University, Faculty of Physics*

A basic challenge in polymer physics is to understand how the underlying geometries of polymeric materials affect their dynamic behavior. Polymers, being intricate systems, demonstrate a wide range of dynamic features that cannot be fully understood without elucidating the connections between the topology of the structure and its reflection in the dynamics.

The present work enhances the scientific understanding of the relaxation dynamics of polymer networks by considering a new multihierarchical network which links in a regular way the Vicsek fractal with the regular dendrimer. Similar structures have been experimentally synthesized through the crosslinking of regular dendrimers.

The relaxation dynamics of our multihierarchical structure is investigated in the framework of the generalized Gaussian structure model employing both, Rouse and Zimm approaches. In the Rouse type-approach we develop an analytical method for the determining of the whole eigenvalue spectrum of the connectivity matrix. Based on the eigenvalues obtained in the iterative manner we are able to investigate the dynamics of the multihierarchical structure at very large generations, impossible to attain through numerical diagonalizations. In the Rouse type-approach, where the interactions are considered only between nearest neighbors monomers, the general picture that emerges is that the multihierarchical structure preserves the individual behaviors of its constituents. The intermediate time/frequency domain of the dynamical quantities divides into two regions, each region showing the typical behavior of a component of the multihierarchical structure.

Remarkably, the multihierarchical structure still holds the original individual relaxation behaviors of its components even with the hydrodynamic interactions taken into account. Although the Vicsek fractal was replicated in shape of a dendrimer and in the Zimm type-approach one allows to each monomer to interact with any other, not only with nearest neighbors, the intermediate domain of

the dynamical quantities still splits into two independent regions, each highlighting the individual dynamics of a constituent component of the multihierarchical structure.

We address the multihierarchical structure as possible theoretical models for the relaxation dynamics of different polymer systems such as physical polymer gels, associative polymer networks, supramolecular dendritic polymer networks, micelles networks, and dendronized polymers.

# Formation of various types of nanostructures on germanium surface by nanosecond laser pulses

Wednesday, 18th October - 13:30 - Poster Session - Hall & Room 3 - Poster - Abstract ID: 783

**Mr. Sergei Mikolutskiy<sup>1</sup>, Mr. Radmir Khasaya<sup>1</sup>, Mr. Yury Khomich<sup>1</sup>, Dr. Vladimir Yamshchikov<sup>1</sup>**

*1. Institute for Electrophysics and Electric Power RAS*

Nanostructures on semiconductor surfaces applied in microelectronics, super-high density storing of information, nanophotonics for development of light-emitting devices and for spectroscopy. Therefore it is of a great interest to develop new effective methods for obtaining surface structures with characteristic sizes less than 100 nm.

In this work the formation of nanoreliefs on germanium surface is carried out by one laser beam without any optional devices and masks. Such method is called the direct laser nanostructuring [1,2]. Figure 1 shows principle scheme of experimental setup for direct laser nanostructuring. The excimer ArF-laser with a wavelength of 193 nm is the main source of coherent radiation, which is strongly absorbed by most materials. After the necessary preparatory procedures germanium samples were irradiated by 20 nanosecond laser pulses transmitted through the optical system (figure 1).

The analysis of initial and irradiated sample surfaces is carried out by an atomic-force microscope (AFM). AFM-analysis shows the formation of various types of surface micro- and nanostructures in different parts of irradiation zone. For example, figure 2 represents nanostructures in the form of bulbs with rounded peaks with characteristic dimensions along the surface of 40-120 nm and a height of 40-70 nm. They are observed in peripheral low-intensity region of the laser spot and its size makes it possible to use such structures as quantum dots. Figure 3 shows hexa- and pentagonal cells with characteristic dimensions along the surface of 300-500 nm and the height of the edges between the cells of 20-25 nm in the region of "shallow" melt. Figure 4 represents wave-like microrelief in the zone of "deep" melt near the center of laser spot.

Considering experimental data, we propose a classification of surface reliefs, which includes five main types of reliefs characterized by the shape and size of the structures formed, their periodicity and the physical mechanism of the formation of structures in different regions of the irradiation spot.

References:

- [1] Mikolutskiy S.I., Khomich V.Yu., Shmakov V.A., Yamshchikov V.A., *Nanotechnologies in Russia*, 6 (2011) 733.
- [2] Ganin D.V., Mikolutskiy S.I., Tokarev V.N., Khomich V.Yu., Shmakov V.A., Yamshchikov V.A., *Quantum Electronics*, 44 (2014) 317.

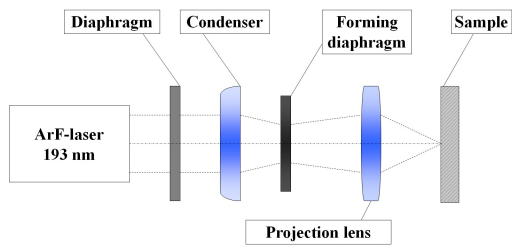


Figure 1. principal scheme of experimental setup.jpg

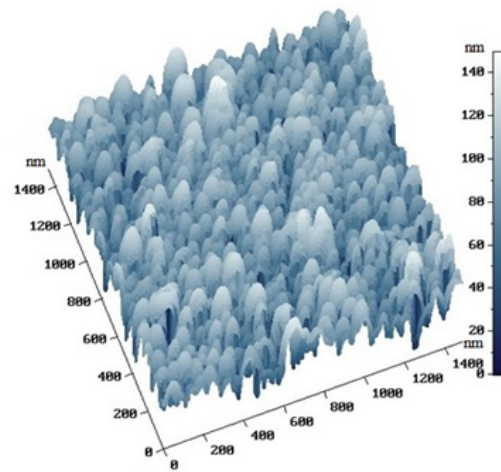


Figure 2. 3d afm image of irradiated germanium surface in low intensity region.jpg

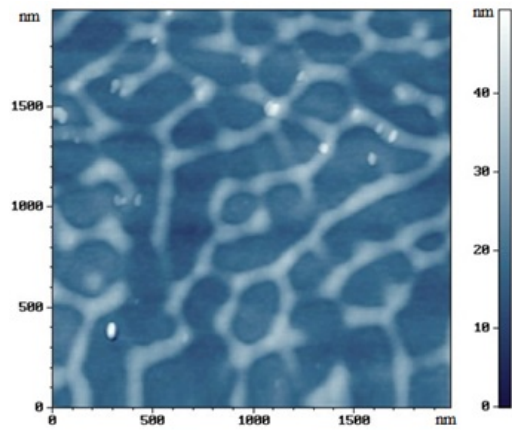


Figure 3. 2d afm image of irradiated germanium surface in the region of shallow melt.jpg

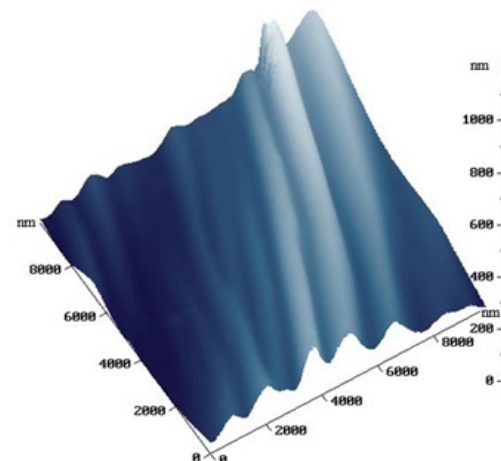


Figure 4. 3d afm image of irradiated germanium surface in the region of deep melt near the center of laser spot.jpg

# Highly efficient electrocatalysts by N-, S-doping of mesoporous carbons for enhanced oxygen reduction reaction

Wednesday, 18th October - 13:30 - Poster Session - Hall & Room 3 - Poster - Abstract ID: 795

**Mr. Riccardo Argurio<sup>1</sup>, Prof. Zheng Xiao Guo<sup>1</sup>, Dr. Yun Zong<sup>2</sup>**

**1. University College London, 2. Institute of Materials Research and Engineering (IMRE), A\*STAR, Singapore**

Synergistic catalytic effects of  $\text{MnO}_2$ , N,S-doping and curvature of carbon nanostructures are achieved from multi-component composites of  $\text{MnO}_2$ , Carbon Nanotubes and Graphene ( $\text{MnO}_2/\text{CNT}/\text{G}$ ) with carbonized l-cysteine/l-serine/melamine. These catalysts show much enhanced performance towards oxygen reduction reaction (ORR) in alkaline media, including low onset potentials and high current densities. The multi-component composites obtained after carbonization exhibit relatively high surface areas (BET) of  $306 \text{ m}^2 \text{ g}^{-1}$  and  $400 \text{ m}^2 \text{ g}^{-1}$ , for manganese-heteroatom doped carbons, N-S-C@MCG\_1000 and N-C@MCG\_1000, respectively. The  $\text{MnO}_2$  particles are well dispersed within the carbon support. The levels of nitrogen and sulphur (N-, S-) bonding formed at different carbonization temperatures strongly influence the ORR. The electron transfer numbers (4e-) show that these mesoporous catalysts can achieve an excellent stability and performance towards ORR. The Tafel slopes for ORR are comparable with that for Pt/C - with  $82.7 \text{ mV/dec}$  for N-S-C@MCG\_1000,  $88.9 \text{ mV/dec}$  for N-C@MCG\_1000 and  $92 \text{ mV/dec}$  for Pt/C, respectively.

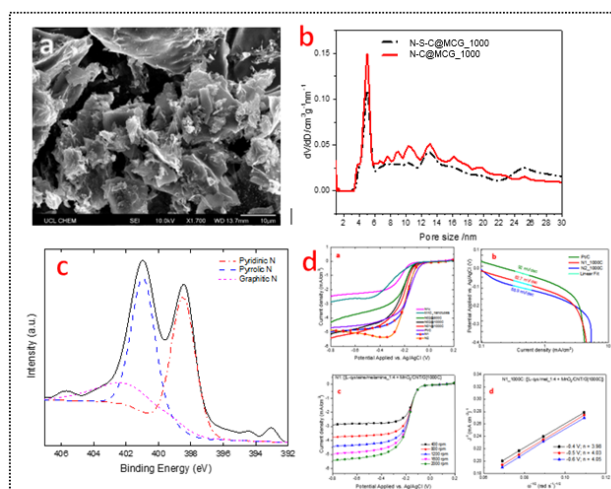


Figure 1: (a) SEM, (b) pore size distribution (PSD), (c) N(1s) XPS spectra showing pyridinic, pyrrolic, and graphitic N for N1 1000C, (d) electrochemical measurements for N-, S-doped mesoporous carbons.

Fig.1.png

---

## On low-dimensional models at NMR line shape analysis in nanomaterial systems

---

Wednesday, 18th October - 13:30 - Poster Session - Hall & Room 3 - Poster - Abstract ID: 809

---

***Prof. Mikhail Kuchero<sup>1</sup>, Dr. Oleg V. Falaleev<sup>2</sup>***

*1. Siberian Federal University, Institute of Space and Information Technology, 2. Siberian Division of the Russian Academy of Sciences, Krasnoyarsk*

Recently, considerable progress has been made in studies on many-spin mechanisms responsible for the wings of NMR absorption line [1]. Now we present a model of localized spin dynamics for the low-dimensional solid-state spin system, which contains small ensembles of magnetic nuclei ( $N \sim 20$ ). The standard spin Hamiltonian is the sum of the Zeeman term and the magnetic dipole interaction term. It is possible to truncate the interaction among the spins in a strong external magnetic field, keeping only the secular terms. The  $^{19}\text{F}$  spins in a single crystal of fluorapatite ( $\text{Ca}_5\text{F}(\text{PO}_4)_3$ ) at room temperature have often been used to approximate a one-dimensional spin system. The  $^{19}\text{F}$  NMR line in fluorapatite is split up into three lines if the constant external field is parallel to the  $c$  axis. In this crystal orientation, the 3D  $^{19}\text{F}$  system may be treated as a collection of many identical spin chains. Following direct-product formalism theory [2] we make the next approximation, namely, considering the longitudinal part of the secular term, we suggest that transverse component of a spin in a certain site rotates in a constant local magnetic field. This field changes if the spin jumps to another site. On return, this spin continues to rotate in the former field. Such a simplified description is necessary to obtain a computationally tractable model. We expand the density matrix in a set of eigenoperators of the Zeeman Hamiltonian. Then we obtain a system of coupled differential equations for the expansion coefficients. The system of equations is then solved by straightforward numerical methods, and the fluorine NMR line shapes of fluorapatite for different chain lengths are calculated. The structure in the resonances of one-dimensional ( $\text{Ca}_5\text{F}(\text{PO}_4)_3$ ) spin system is explained. The separation  $D$  between the satellites in fluorapatite was found 3.50 Oe in a good agreement with experiment [3] (the experimental value is  $3.64 \pm 0.20$  Oe). References: [1] V.E. Zobov, M.M. Kuchero, JETP 124, 151 (2017). [2] A. A. Nevzorov, J. H. Freed, J. Chem. Phys. 115, 2401 (2001). [3] W. Van der Lugt, W.J. Caspers, Physica (Amsterdam) 30, 1658 (1964)

# Hybrid epoxy nanocomposites reinforced with 1D & 2D carbon nanomaterials: Termomechanical and electrical properties.

Wednesday, 18th October - 13:30 - Poster Session - Hall & Room 3 - Poster - Abstract ID: 810

**Mr. Juventino López Barroso**<sup>1</sup>, **Dr. José Luis Rivera Armenta**<sup>1</sup>, **Dr. Ana Laura Martínez Hernández**<sup>2</sup>,  
**Dr. Armando Almendarez Camarillo**<sup>3</sup>, **Dr. Perla Elvia García Casillas**<sup>4</sup>, **Dr. Carlos Velasco Santos**<sup>5</sup>

*1. Instituto Tecnológico de Ciudad Madero. División de estudios de Posgrado e Investigación. Centro de Investigación en Petroquímica, Pról. Bahía De Aldair y Ave. de las Bahías, Parque de la pequeña y mediana industria, 89600 Altamira, Tamaulipas, 2. Tecnológico Nacional de México. Instituto Tecnológico de Querétaro. División de estudios de Posgrado e Investigación. Av. Tecnológico s/n, esq. Gral. Mariano Escobedo, Col. Centro Histórico, C.P. 76000, Santiago de Querétaro, Querétaro, México., 3. Tecnológico Nacional de México, Instituto Tecnológico de Celaya, Departamento de Ingeniería Química, Av. Tecnológico y Antonio García Cubas s/n, Col. Fovissste, C.P. 38010. Celaya, Guanajuato, 4. Universidad Autónoma de Ciudad Juárez, Av. del Charro # 450 Nte, col. Partido Romero, Cd. Juárez Chihuahua, CP 32310, 5. Tecnológico Nacional de México. Instituto Tecnológico de Querétaro. División de estudios de Posgrado e Investigación. Av. Tecnológico s/n, esq. Gral. Mariano Escobedo, Col. Centro Histórico, C.P. 76000, Santiago de Querétaro, Querétaro*

The effect of the incorporation of two types of carbon nanomaterials on Bisphenol-A di-glycidyl ether epoxy resin is studied in this research. The storage modulus ( $E'$ ) of hybrid nanocomposites show the synergetic effect of 1D as multi-wall carbon nanotubes and graphene derivatives as 2D carbon nanostructures. Consequently, an important increases on  $E'$  around 138% is obtained in the composite containing oxidized nanostructures in comparison with epoxy matrix. This synergetic effect can be related to the interaction of functional moieties that improves the dispersion of nanomaterials into the polymeric matrix and the co-supporting effect as an interconnected network of carbon nanomaterials. The possible formation of a 3D interconnected network allows modifications in the electrical properties of some nanocomposites, this is shown as an abrupt change in insulant nature of epoxy resin to semiconductor response on nanocomposites ( $3.7 \cdot 10^{-5} \text{ Sm}^{-1}$ ) containing multi-wall carbon nanotubes and reduced graphene oxide. TEM micrographs of thin slices of nanocomposites exhibit the interaction between 1D & 2D carbon nanomaterials and the possible creation of a network into the matrix. Finally, Raman spectroscopy results support the interaction of polymeric chains with their vicinities as different nanostructures are added and also their respective combinations.



# Indium-saving effect and physical properties of transparent conductive multilayers

Wednesday, 18th October - 13:30 - Poster Session - Hall & Room 3 - Poster - Abstract ID: 584

***Prof. Midori Kawamura<sup>1</sup>, Dr. Takayuki Kiba<sup>1</sup>, Prof. Yoshio Abe<sup>1</sup>, Dr. Kyung Ho Kim<sup>1</sup>***

*1. Kitami Institute of Technology*

Transparent conductive film is used as an essential component especially in display devices, such as organic light emitting diodes (OLEDs), and also in solar cells.

The most common material is indium tin oxide (ITO). On the other hand, indium is a rare metal, therefore, indium free or indium saving transparent conductive films are preferable. Recently, transparent conductive multilayers which consist of top and bottom metal oxide layers and thin metal (such as Ag) interlayer have been proposed. These multilayers can achieve a low sheet resistance due to the metal interlayer, therefore the use of indium can be also reduced, even if ITO is used.

We have reported a very high ( $68 \times 10^{-3} \Omega^{-1}$ ) figure of merit (FOM) of a multilayer consists of indium zinc oxide (IZO) and Ag interlayer (namely, IAI). An OLED where the IAI multilayer was applied showed an excellent device performance. In this study, a multilayer consists of top and bottom  $\text{MoO}_3$  layers and Ag interlayer is prepared on glass substrates by vacuum evaporation method. Transmittance and sheet resistance of the structures are evaluated and the optimum structure is found to be MAM (20/14/30 nm), showing the best FOM,  $6.2 \times 10^{-3} \Omega^{-1}$ , among the samples, though this value is much lower than that of the IAI multilayer. We also attempt to fabricate a multilayer consists of  $\text{MoO}_3$  layer, Ag interlayer, and IZO layer (namely, MAI). The obtained MAI (50/14/30 nm) multilayer shows higher FOM,  $32 \times 10^{-3} \Omega^{-1}$ , than MAM and a higher indium-saving feature than IAI.

Structures	FOM ( $\times 10^{-3} \Omega^{-1}$ )	Thickness of IZO layer (nm)
MAM(30/14/20)	6.2	0
MAI(50/14/30)	32	30
IAI(30/14/30)	68	60
IZO single film	2.3	70

Fom and indium usage of the multilayers.png

# Kinetics of the melting front movement in process of centrifugal induction surfacing of powder material with nanoscale modifiers

Wednesday, 18th October - 13:30 - Poster Session - Hall & Room 3 - Poster - Abstract ID: 31

***Mr. Ihor Sasnouski<sup>1</sup>, Mr. Artsiom Kurylionak<sup>1</sup>***

*1. Joint Institute of Mechanical Engineering of the National Academy of Sciences of Belarus*

For solving the problem of improving the powder coatings modified by nanostructure components obtained by induction surfacing method tribological characteristics it is necessary to study the kinetics of the powdered layer melting and define the minimum time of melting.

For powdered layer predetermined temperature maintenance at sintering mode stage it is required to determine the temperature difference through blank thickness of the for one hundred-day of the define the warm-up swing on of the stocking up by solving the thermal conductivity stationary problem for quill (hollow) cylinder with internal heat source. Herewith, since in practice thickness of the cylinder wall is much less then its diameter and the temperature difference is comparatively small, the thermal conductivity dependence upon the temperature can be treated as negligible.

As it was shown by our previous studies, in the induction heating process under powdered material centrifugal surfacing (i.e. before achieving the melting temperature) the temperature distribution in powdered layer thickness may be considered even. Hereinafter, considering the blank part induction heating process quasi-stationarity under Fo big values, it is possible to consider its internal surface heating as developing with constant velocity.

There is unlimited hollow cylinder at the temperature  $T_0 = T_m$  ( $T_m$  is a powder melting temperature). The cylinder external surface temperature increases linearly. Melted layer with thickness  $R - \eta = \xi$ , where  $\eta$  is a distance from axis of the cylinder to the layer boundary, is formed beginning from the cylinder surface.

1 – melted zone; 2 – not melted zone; 3 – blank.

Fig 1 – a boundary conditions under centrifugal induction surfacing.

As a result of development the melting front movement mathematical model in a powdered material with nanostructure modifiers the minimum surfacing time is defined. It allows to minimize negative impact of thermal influence on formation of applied coating structure, to raise productivity of the process, to lower power inputs and to ensure saving of nonferrous and high alloys by reducing the allowance for machining.

The difference of developed mathematical model of melting front movement from previously known is that the surface temperature from which the heat transfer occurs is a variable.

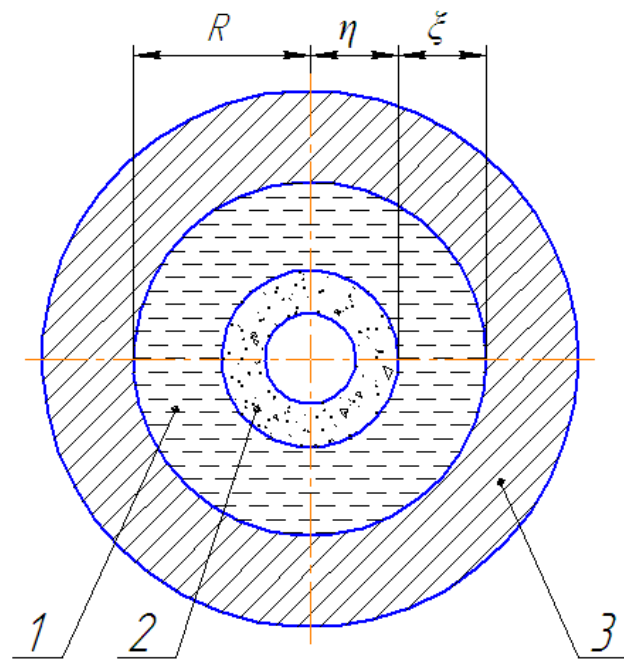


Fig 1.png

# Stretchable and flexible thermoelectric polymer composites

Wednesday, 18th October - 13:30 - Poster Session - Hall & Room 3 - Poster - Abstract ID: 313

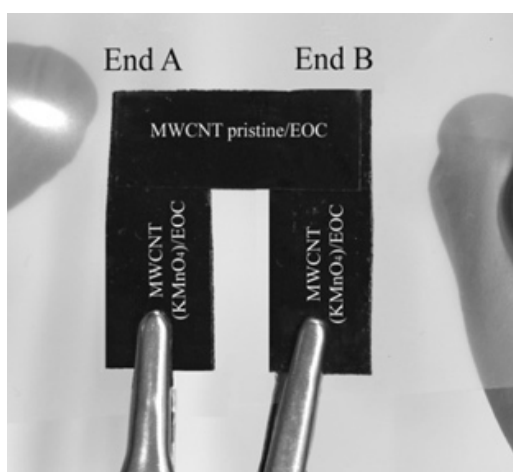
**Dr. Petr Slobodian<sup>1</sup>, Dr. Jiri Matyas<sup>1</sup>, Dr. Robert Olejnik<sup>1</sup>, Dr. Pavel Riha<sup>2</sup>**

1. Tomas Bata University in zlin, 2. Institute of Hydrodynamics, Academy of Sciences, Prague, Czech Republic

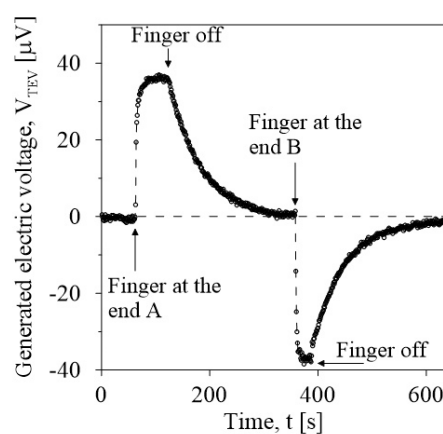
Thermoelectric devices generate an electrical current when there is a temperature gradient between the hot and cold junctions of two dissimilar conductive materials typically n-type and p-type semiconductors. Consequently, also the polymeric semiconductors filled by different forms of carbon nanotubes with proper structural hierarchy and thermoelectric properties may transfer temperature difference into electricity. In spite of their lower thermoelectric efficiency in terms of the figure of merit, the properties as stretchability, flexibility, light weight, low thermal conductivity, easy processing and low manufacturing cost are advantages in many technological and ecological applications.

Polyurethane based highly elastic composites filled by multiwalled carbon nanotubes (MWCTs) were prepared by sonication of nanotube dispersion in a polyurethane solution followed by their precipitation. The amounts of oxygenated functional groups attached on MWCNT surface, which constitute majority of p-type charge carriers, were further increased by  $\text{HNO}_3$  oxidation. P-type of charge carriers were further increased by doping with molecules of triphenylphosphine. For altering p-type MWCNTs into n-type ones, Ag nanoparticles were deposited on MWCNT surface and then doped by 7,7,8,8-tetracyanoquinodimethane. Both types of MWCNTs were used to manufacture thermoelectric module generating thermoelectric voltage, which proved also as a self-powered thermoelectric sensor for strain, stress and chemical vapor detection. It turned to advantage that the generation of thermoelectric power was significantly affected by the applied deformation or change of chemically monitored surroundings.

This work was supported by the Ministry of Education, Youth and Sports of the Czech Republic – Program NPU I (LO1504) and with the support of the Operational Program Research and Development for Innovations co-funded by the European Regional Development Fund (ERDF) and the national budget of the Czech Republic, within the framework of the project CPS-strengthening research capacity (reg. number: CZ.1.05/2.1.00/19.0409).



Organics thermoelectric device.jpg



Time-dependent generation of voltage after finger touching.jpg

# Synthesis and application of magnetic catalyst for hydrogenation reaction

Wednesday, 18th October - 13:30 - Poster Session - Hall & Room 3 - Poster - Abstract ID: 363

**Mr. Po-Wei Lan<sup>1</sup>, Prof. Chuh-yung Chen<sup>1</sup>, Prof. Cheng-Chien Wang<sup>2</sup>**

**1. National Cheng Kung University, 2. Southern Taiwan University of Science and Technology**

A novel method to growing Ni nanowires under a magnetic field was developed. Ni nanowires were formed with increasing of the magnetic field. XRD was employed to characteristic Ni crystal structure. The diameter of Ni nanowires was in the range of 100 nm to 150 nm from SEM observation. Interesting, the shape of Ni nanowire would be changed from the particles-assembled attachment to rod-like growth as the reduction rate was descended in low reductant concentration. Furthermore, in an unique and special magnetic field, nickel particles can be self-assembled to form balls shape. When those Ni balls was applied as the catalyst for the hydrogenation of carbon dioxide, over 90% of carbon dioxide could be converted to methane in this system. In addition, C1~C3 alkanes, which are the important fuel gases, would be formed from the hydrogenation of CO/CO<sub>2</sub> mixture gas, as the Ni balls were used as catalyst under atmospheric pressure and 170~200°C. Restated, high performance Ni catalyst, which can be applied on the simple carbon cycle, was developed by our laboratory. Those low energy consumption system maybe can solve the global warm problem in future.

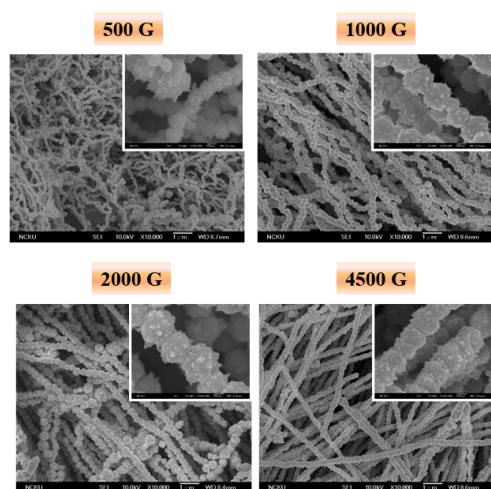


Image 1.png

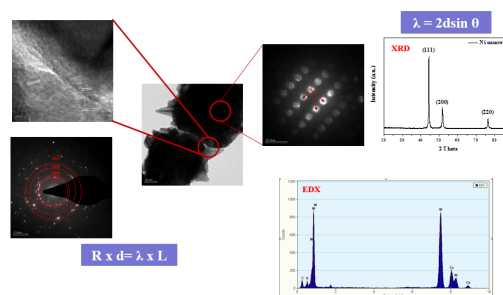


Image 2.png

---

## The effect of surface modification with silane coupling agent on blue-light curable inkjet printing of TiO<sub>2</sub> particles as white inks

---

Wednesday, 18th October - 13:30 - Poster Session - Hall & Room 3 - Poster - Abstract ID: 397

---

***Mr. Chenglong Wang<sup>1</sup>, Prof. Jianzhong Shao<sup>1</sup>, Mr. Yiding Meng<sup>1</sup>***

*1. Zhejiang Sci-Tech University*

A series of modified titanium dioxide (TiO<sub>2</sub>) particles was prepared by three kinds of silane coupling agent grafted on the surface of the TiO<sub>2</sub> particles. The modified TiO<sub>2</sub> particles were characterized by FT-IR, TGA, EDS and DLS. The modified TiO<sub>2</sub> particles were used in blue-light curable pigment inks as white pigment. The result confirmed that the three kinds of silane coupling agent had been successfully grafted onto the surface of the TiO<sub>2</sub> particles. The TGA and EDS also indicated that the TiO<sub>2</sub> particle surface had been grafted with the silane coupling agent. The TiO<sub>2</sub> particle size was decreased by the silanization modification. For the application of blue light curable pigment inks, the viscosity of the white ink is slightly reduced by the silanization modification, the photo-polymerization performance was obviously improved after modified with the 3-(Trimethoxysilyl)propyl methacrylate (KH570) and 3-Aminopropyltriethoxysilane (KH550), the dispersion stability of white ink was improved after modified with Hexadecyltrimethoxysilane (HDMTS) and KH570, the cured film prepared by KH570 modified TiO<sub>2</sub> had the best physical and mechanical properties

---

## Influence of gas flow ratio on formation of silicon nanocrystals in SiN<sub>x</sub>:H

---

Wednesday, 18th October - 13:30 - Poster Session - Hall & Room 3 - Poster - Abstract ID: 453

---

***Mrs. Faiza Tiour*<sup>1</sup>, *Dr. bedra Benyahia*<sup>2</sup>, *Dr. Noureddine Brihi*<sup>3</sup>, *Dr. Ali Sari*<sup>4</sup>, *Dr. Brahim Mahmoudi*<sup>5</sup>, *Mrs. Isa Menous*<sup>5</sup>**

*1. Research Center in Semiconductor Technology for Energy, 2. Research Center in Semiconductor Technology for Energy (crtse), 3. Faculty of Sciences, Jijel University, 4. Birine Nuclear Research Center, 5. Research Center in Semiconductor Technology for Energy(crtse)*

- Si-rich Silicon nitride SiN<sub>x</sub>: H films were grown on silicon substrates with LF-PECVD technique with a gas mixture of SiH<sub>4</sub> and NH<sub>3</sub> at flow ratios R from 0.25 up to 6. Thermal annealing at 1100 °C for 1 hour in the nitrogen ambient was applied to form the Si nanocrystals in the films that have been investigated by x-Ray diffraction, scanning electron microscopy and Raman scattering spectrum. Our experimental results reveal that the silicon nanoclusters can be precipitated from the hydrogenated silicon rich nitride films produced with lower ratio (R<2). It appears that the variation of NCs-Si size and crystalline fraction F<sub>c</sub> were intensively depended on the excess silicon content. A high crystalline volume fraction of 81% is obtained for a film deposited at R=0.25, and a dominance of silicon nanocrystallite having the sizes within the range 8–10 nm.

## Cytotoxicity of graphene oxide in human endothelial cells

Wednesday, 18th October - 13:30 - Poster Session - Hall & Room 3 - Poster - Abstract ID: 458

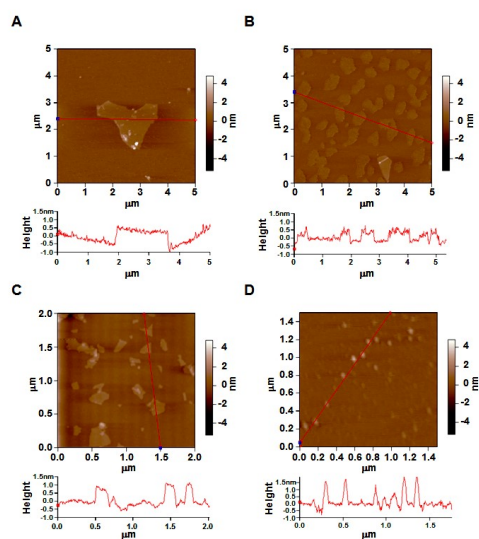
***Ms. Na Geum Lee<sup>1</sup>, Dr. Young-Lai Cho<sup>2</sup>, Dr. Jeong-ki Min<sup>2</sup>***

*1. Department of Biomolecular Science, University of Science & Technology, 2. Korea Research Institute of Bioscience and Biotechnology*

Despite the rapid expansion of the biomedical applications of graphene oxide (GO), safety issues related to GO, particularly with regard to its effects on vascular endothelial cells (ECs), have been poorly evaluated. To explore possible GO-mediated vasculature cytotoxicity and determine lateral GO size relevance, we constructed four types of GO: micrometer-sized GO (MGO;  $1089.9 \pm 135.3$  nm), submicrometer-sized GO (SGO;  $390.2 \pm 51.4$  nm), nanometer-sized GO (NGO;  $65.5 \pm 16.3$  nm), and graphene quantum dots (GQDs). All types but GQD showed a significant decrease in cellular viability in a dose-dependent manner. Notably, SGO or NGO, but not MGO, potently induced apoptosis while causing no detectable necrosis. Subsequently, SGO or NGO markedly induced autophagy through a process dependent on the c-Jun N-terminal kinase (JNK)-mediated phosphorylation of B-cell lymphoma 2 (Bcl-2), leading to the dissociation of Beclin-1 from the Beclin-1–Bcl-2 complex. Autophagy suppression attenuated the SGO- or NGO-induced apoptotic cell death of ECs, suggesting that SGO- or NGO-induced cytotoxicity is associated with autophagy. Moreover, SGO or NGO significantly induced increased intracellular calcium ion ( $\text{Ca}^{2+}$ ) levels. Intracellular  $\text{Ca}^{2+}$  chelation with BAPTA-AM significantly attenuated microtubule-associated protein 1A/1B-light chain 3-II accumulation and JNK phosphorylation, resulting in reduced autophagy. Furthermore, we found that SGO or NGO induced  $\text{Ca}^{2+}$  release from the endoplasmic reticulum through the  $\text{PLC}\beta 3/\text{IP}_3/\text{IP}_3\text{R}$  signaling axis. In this study, we presented experimental data regarding the differential size-related biological effects of GOs on ECs. Additionally, we demonstrated for the first time that GOs induce apoptotic death in ECs via autophagy activation. As presented in summary figure, SGOs or NGOs induce autophagic cell death through the  $\text{PLC}\beta 3/\text{IP}_3/\text{Ca}^{2+}/\text{JNK}$  signaling axis. Although further investigations are required before the current findings can be clinically applied, these data will provide a better understanding of the mechanism underlying GO size-dependent cytotoxicity in vasculature and facilitate the future development of safer biomedical applications of GOs. These results elucidate the mechanism underlying the size-dependent cytotoxicity of GOs in the vasculature and may facilitate the development of a safer biomedical application of GOs.



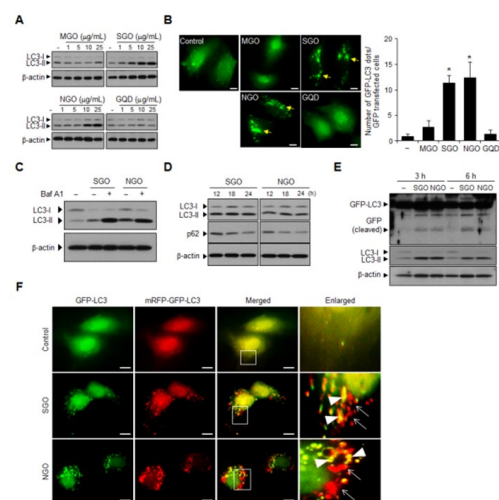
Figure 1



**Fig. 1.** Atomic force microscopy images and line profiles of four different forms of graphene oxide. (A) micrometer-sized graphene oxide (GO; MGO), (B) submicrometer-sized GO (SGO), (C) nanometer-sized (NGO), and (D) graphene quantum dots (GQDs).

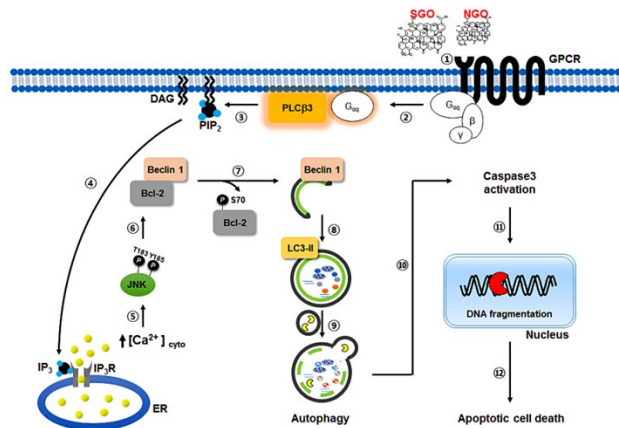
Figure 1.jpg

Figure 2



**Fig. 2.** Induction of autophagy in SGO- or NGO-treated ECs. (A) Western blot analysis of microtubule-associated protein 1A/1B-light chain 3 (LC3)-I to LC3-II conversion in HUVECs treated with GOs at the indicated concentrations for 24 h. (B) Representative images of green fluorescent protein (GFP)-LC3 punctae in HUVECs after treatment with GOs at 25  $\mu\text{g}/\text{mL}$  for 12 h (left panel). (C) Effect of a lysosomal inhibitor, Bafilomycin A1 (Baf A1), on SGO- or NGO-induced autophagy in HUVECs. (D) Western blot analysis of the LC3-I to LC3-II conversion and p62 protein levels in HUVECs treated with 25  $\mu\text{g}/\text{mL}$  GOs for the indicated times. (E) Western blot analysis of cleaved GFP fragments from GFP-LC3. (F) Representative images of mRFP-GFP-LC3 punctae. Colocalization of GFP and red fluorescent protein (RFP), indicated by yellow dots in the overlapped GFP and RFP images, is visible in autophagosomes (arrowhead), whereas only RFP fluorescence, indicated by red punctae, is observed in autolysosomes (arrow).

Figure 2.jpg

**Figure 3**

**Fig. 3.** Overview of GO-induced apoptotic cell death pathway in ECs. SGO and NGO bind to the cell membrane, leading to G protein-coupled receptor (GPCR) stimulation. Following the activation of GPCR, the Gq subunit induces PLC β3 activation, which hydrolyses phosphatidylinositol-4,5-bisphosphate (PIP<sub>2</sub>) to diacylglycerol (DAG) and inositol 1,4,5-trisphosphate (IP<sub>3</sub>). Subsequently, IP<sub>3</sub> binds the IP<sub>3</sub> receptor (IP<sub>3</sub>R) on the endoplasmic reticulum (ER) to induce Ca<sup>2+</sup> efflux from ER. Subsequently, the increased intracellular Ca<sup>2+</sup> level induced JNK phosphorylation, followed by Bcl-2 phosphorylation at serine 70 (S70) and dissociation of the Bcl-2–Beclin-1 complex. Following the dissociation of Beclin-1 from Bcl-2, activated Beclin-1 induces autophagy via LC3. As a result, autophagy induced by SGO or NGO induces apoptotic cell death via caspase-3 activation and DNA fragmentation.

Figure 3.jpg

# Anti-bacterial and anti-cancerous potential of medicinal plant mediated biofabricated nanoparticles: A question to its selective cytotoxicity?

Wednesday, 18th October - 13:30 - Poster Session - Hall & Room 3 - Poster - Abstract ID: 483

**Mr. Parth Sarthi Nayak<sup>1</sup>, Mr. Manish Sharma<sup>1</sup>, Dr. Suman Jha<sup>1</sup>**

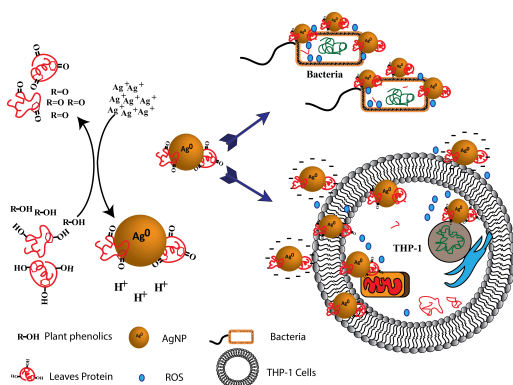
**1. National Institute of Technology, Rourkela**

**Introduction:** Physical, chemical and biological methods are the widely available approaches for nanoparticle synthesis. The common problems associated with nanoparticles assembly are control of crystal growth, stability, size, shape, and aggregation. Plants are the most exploited biological platform for safe, eco-friendly, precise morphology and large-scale production of nanoparticles. Nanoparticles fabricated using medicinal plant extract have advance potential in the area of nanomedicine. High surface to volume ratio of nanoparticle enhances the local active biomolecules concentration, leading to many folds increase in the medicinal potentials. Despite the remarkable development of nanotechnology, relatively little is known about the biomolecules characterized over nanoparticles in green synthesis and its fate inside the biological system.

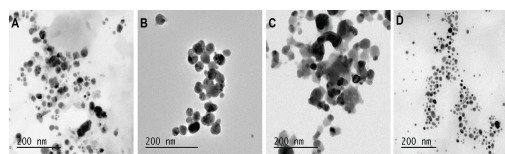
**Methods:** Hence, we fabricated the silver nanoparticles (AgNPs) using different indigenous medicinal plants of India, *Syzygium cumini*(1:1.5), *Azadirachta indica*(1:3), *Acorus calamus*(1:10)and *Pongamia pinnata*(1:10). The biofabricated AgNPs were purified through size exclusion chromatography using sodiumhexametaphosphate buffer. Biofabrication of AgNPs was characterized using different spectroscopic and microscopic techniques. The significant effect of biofabricated AgNPs was studied on the viability of prokaryotic and eukaryotic cells.

**Results:** Henceforth, the cytotoxic propensity of spherical biofabricated AgNP formulations were screened against Gram-positive (*Bacillus subtilis*), Gram-negative (*Escherichia coli*), cancerous (fibrosarcoma, HT1080) and non-cancerous (human embryonic kidney, HEK293) cell lines. The nanoparticle formulations showed relatively higher cytotoxic propensity against cancerous cell lines than non cancerous one.

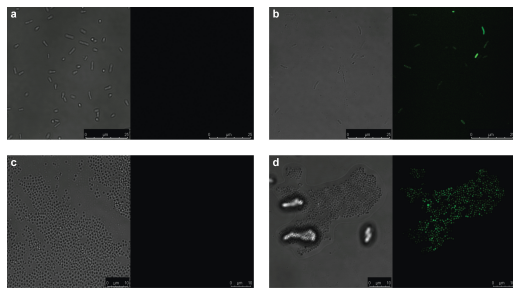
**Discussion:** The surface roughness and reactive oxygen species (ROS) measurements indicated that AgNP formulations modulate the cell viability predominantly by ROS-mediated change in cytoskeleton assembly and/or disruptive change in membrane morphology upon direct interaction with membrane. The internalization assay of biofabricated AgNPs shows the nuclear associated co-localization leads to its genotoxicity. Furthermore, the nanoparticle formulations obtained upon purification showed higher monodispersivity and enhanced selective cytotoxic propensity towards Gram-positive bacteria and cancerous cell lines. Hence, the overall study emphasizes the biofabrication of AgNP using medicinal plants with multifaceted biomedical application may find its significant role in nanomedicine.



Graphical abstract.jpg



Tem characterization.jpg



Internalization and colocalization.jpg

Before Size Exclusion chromatography											
Sample	Size (nm) ± S.D			Zeta (mV) ± S.D			$\lambda_{\text{Max}}$ (nm)		PDI		
<i>Azadirachta indica</i>	123.4 ± 42.3			-23.8 ± 6.45			433		0.283		
<i>Syzygium cumini</i>	128.8 ± 50.39			-27.3 ± 11			428		0.423		
<i>Acorus calamus</i>	124.3 ± 55.87			-35.2 ± 6.09			428		0.268		
After Size Exclusion chromatography											
Sample	Elution 1				Elution 2				Elution 3		
	Size (nm) ±S.D	Zeta (mV) ± S.D	$\lambda_{\text{Max}}$ (nm)	PDI	Size (nm) ± S.D	Zeta (mV)± S.D	$\lambda_{\text{Max}}$ (nm)	PDI	Size (nm) ±S.D	Zeta (mV) ± S.D	$\lambda_{\text{Max}}$ (nm)
<i>Azadirachta indica</i>	109 ± 33	-46.5 ± 8.77	432	0.37	109 ± 39.64	-45.8 ± 9.78	433	0.18	93.98 ± 31.98	-44 ± 9.64	422
<i>Syzygium cumini</i>	118 ± 36.07	-58.3 ± 5.92	424	0.35	98.26 ± 28.58	-41.3 ± 7.17	422	0.31	82.03 ± 19.79	-44.9 ± 6.9	419
<i>Acorus calamus</i>	113.1 ± 49.30	-45 ± 7.97	431	0.22	84.9 ± 27.14	-47.9 ± 5.17	425	0.32	62.79 ± 32.06	-45.2 ± 6.92	425

Zeta and dls tabulation.jpg

## Theoretical study on the origins of the gap bowing in $\text{Ca}_x\text{Mg}_{1-x}\text{S}$ alloys

---

Wednesday, 18th October - 13:30 - Poster Session - Hall & Room 3 - Poster - Abstract ID: 509

---

***Dr. Boutarfa Bariza***<sup>1</sup>

*1. Department of Materials Science, Guelma university*

The structural, electronic properties of three chalcogenide compounds MgS, CaS and their  $\text{Ca}_x\text{Mg}_{1-x}\text{S}$  ternary alloy in the rocksalt phase have been investigated by using the full-potential linearized augmented plane-wave method (FP-LAPW) within density functional theory (DFT). We employed the local density approximation (LDA) and generalized gradient approximation (GGA) for the calculation of exchange-correlation (XC) potential. The equilibrium lattice constants and the bulk modulus are in agreement with the values reported in the literature, their deviation from linearity has been examined and discussed. From the study of the electronic properties, we find that these binary compounds MgS and CaS, have indirect band gaps.

For ternary alloy  $\text{Ca}_x\text{Mg}_{1-x}\text{S}$  the study of these various properties are calculated, particularly the variation of structural and electronic parameters with concentration  $x$ . We focused our attention on the origins of bowing parameters corresponding to these physical properties.

In this study, we compare these predictions to the results already obtained experimentally as well as theoretical work in this regard.

## Large scale roll-to-roll coating process to enhance the optical and electrical properties for transparent conductive single-walled carbon nanotube /silver nanowire hybrid film

---

Wednesday, 18th October - 13:30 - Poster Session - Hall & Room 3 - Poster - Abstract ID: 628

---

***Prof. Kwan Han Yoon<sup>1</sup>, Prof. Young Sil Lee<sup>1</sup>***

*1. Kumoh National Institute of Technology*

For the application of the touch screen panel and transparent conductive electrode for the flexible display, highly transparent and electrically conductive film is required. To enhance the optical properties and the surface conductivity of carbon nanotube (CNT)/silver nanowire/polyethylene terephthalate (PET) hybrid film, inorganic overcoating has been applied by roll-to-roll coating processing. The maximum total transmittance of the hybrid film without washing and overcoating was less than 90%. The optimum thickness of the overcoating has been determined as 10 micrometer for the highest total transmittance, 92 %, while the sheet resistance of the hybrid film is 180 ohm/sq. For the further enhancement of the sheet resistance of the CNT/silver nanowire hybrid film to get less than 80 ohm/sq the thickness of the overcoating has been controlled as 30 micro meter, while the transmittance is more than 90%. The overcoating of nanoparticle can highly reduce the surface roughness of the CNT/silver nanowire hybrid film and enhance the optical clarity such as the total transmittance and the haze of the hybrid film. This work has been done using large scale roll-to-roll coating machine for the scalable product of the high performance flexible transparent conductive film.

# Fast and large-scale synthesis of 2D molybdenum trioxide (MoO<sub>3</sub>) nanosheets for ion-exchange battery applications

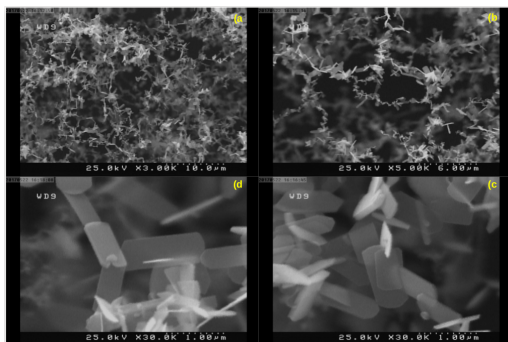
Wednesday, 18th October - 13:30 - Poster Session - Hall & Room 3 - Poster - Abstract ID: 444

***Mrs. Anousha Khamsavi<sup>1</sup>, Mr. Mahdi Sasar<sup>1</sup>, Dr. Yaser Abdi<sup>1</sup>***

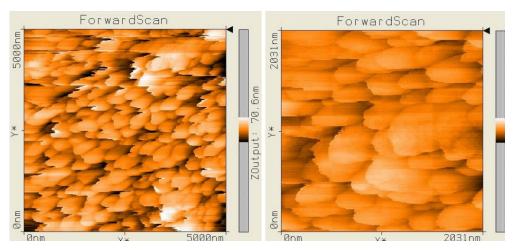
*1. University of Tehran*

A simple new method for synthesizing large-scale quantities of few layer MoO<sub>3</sub> nanosheets (thicknesses of 1.5 to 3 nm) is reported. It is shown that direct evaporation of pure molybdenum foil in low air pressures ( $\sim 10^{-1}$  to  $10^{-2}$  Torr), by applying high current, yields 2D few layer MoO<sub>3</sub> nanosheets in bulk quantities. Scanning electron microscope (SEM) and scanning tunneling microscope (STM) images of the as-prepared samples show that the nanosheets have uniform morphologies with areas in the order of  $1.5 \mu\text{m} \times 0.5 \mu\text{m}$ , and thicknesses of less than 3 nm.

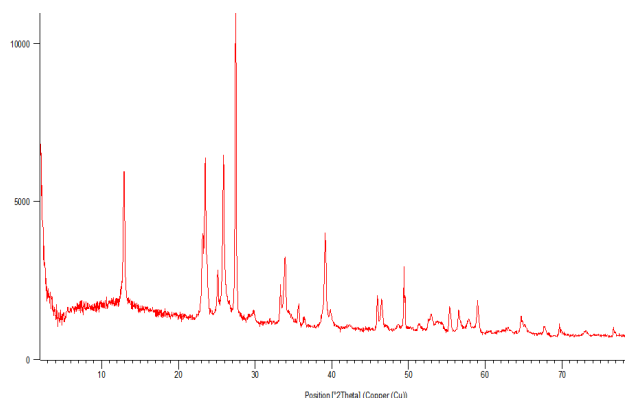
X-ray powder diffraction analysis and transmission electron microscope images show the single crystal structure of the nanosheets, which correspond to the known XRD peaks of MoO<sub>3</sub>. The fast synthesis method presented here could facilitate the commercial and industrial application of these nanosheets and their derivatives in high performance ion batteries and sensors.



Sem images of the as-prepared samples.png



Stm images of the as-prepared samples showing the uniform 2d morphologies.png



X-ray powder diffraction of the as-prepared samples showing corresponding peaks to molybdenum trioxide.png

# Epoxide-based organic inorganic nano-hybrid materials using surface modifier-free hybridization method toward highly effective filling of ZrO<sub>2</sub> nano-particles

Wednesday, 18th October - 13:30 - Poster Session - Hall & Room 3 - Poster - Abstract ID: 55

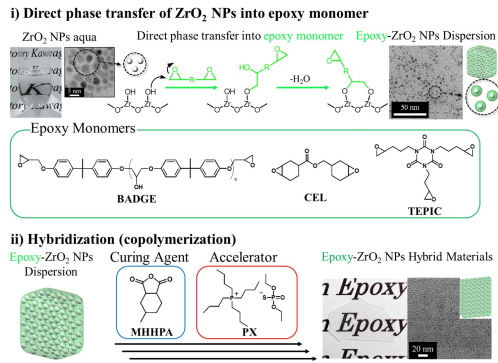
**Mr. Kazushi Enomoto<sup>1</sup>, Dr. Moriya Kikuchi<sup>2</sup>, Prof. Atsushi Narumi<sup>1</sup>, Prof. Seigou Kawaguchi<sup>1</sup>**

*1. Graduate school of Yamagata University, 2. Yamagata university*

A versatile and promising organic-inorganic nano-hybridization method is developed to fabricate epoxide-based transparent hybrid bulk materials containing crystalline ZrO<sub>2</sub> nanoparticles (NPs) with the number-averaged diameter of 3.1 nm. Two proposed key technologies are how to surface-treat, -hydrophobize, and -functionalize the ZrO<sub>2</sub> NPs originally dispersed in water, and how to nano-disperse them into polymer matrixes without any coagulations and/or agglomerations. Herein, a unique surface treatment method is demonstrated in which the hydrophobization and phase transfer of ZrO<sub>2</sub> NPs from water to organic solvent is simultaneously and gently conducted. We propose a new concept “*surface modifier-free hybridization method*” (**Figure 1**). In this method, bi-(or multi-) functional epoxy monomers are used as a surface modifier to give the monomer functionalized NPs directly dispersed in the monomers.

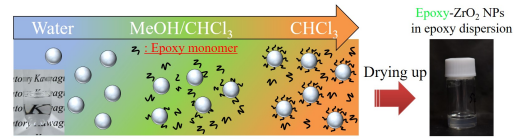
To demonstrate the versatility of this method, three types of epoxy monomers were examined for the preparation of epoxide-based hybrids. The direct phase transfer of ZrO<sub>2</sub> NPs was conducted by solvent exchange method to give transparent viscous monomer dispersions (**Figure 2**). These dispersions were cured by copolymerization with acid anhydride curing agent MHHPA and accelerator PX. **Figure 3** shows the optical images of the prepared three types of epoxide-based hybrids with several filling ratio of ZrO<sub>2</sub> NPs and TEM images of these ultrathin section. In all systems, highly transparent hybrids were successfully prepared regardless of high filling ratio ( $W_{\text{ZrO}_2} \geq 60$  wt%). **Figure 4** denotes the refractive indices ( $n_D$ ) and its wavelength dependence or  $n_D(\lambda)$  of the hybrids. The solid and dashed lines indicated the theoretical values calculated from the Lorentz-Lorenz theory. All experimental values were quantitatively described by the theory, in which the optical values of ZrO<sub>2</sub> monocrystal ( $n_D = 2.15$ ,  $n_D = 35$ ) were used. Generally, the functional surface modifier is often used to prevent the polymerization induced coagulations but it also decreases the optical performances. In remarkable contrast, the present surface modifier-free hybridization method allows one to fabricate the nano-hybrids composed of crystalline ZrO<sub>2</sub> NPs and epoxy resins. In the poster, we will also report in-depth characterizations of these hybrid systems using DLS, NMR, UV-vis spectroscopy, SAXS, and TGA.





**Figure 1.** Schematic illustration of the surface modifier-free hybridization which contains two steps; ie, i) direct phase transfer of  $\text{ZrO}_2$  NPs from water to epoxy monomer to give the monomer functionalized NPs dispersion, and ii) its copolymerization with MHHPA curing agent to achieve the hybridization of  $\text{ZrO}_2$  NPs and epoxy resin without any additional surface modifier.

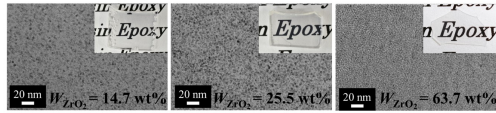
Figure 1.jpg



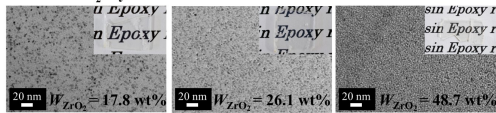
**Figure 2.** Schematic illustration of the solvent exchange method conducted by the dilution-concentration process using successive evaporations to give transparent viscous monomer dispersions.

Figure 2.jpg

#### ➤ BADGE- $\text{ZrO}_2$ Hybrid Materials



#### ➤ CEL- $\text{ZrO}_2$ Hybrid Materials



#### ➤ TEPIC- $\text{ZrO}_2$ Hybrid Materials

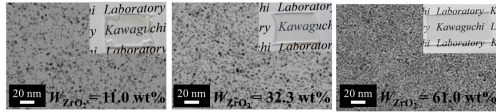


**Figure 3.** Optical images of the prepared three types of epoxide-based hybrids with several filling ratio of  $\text{ZrO}_2$  NPs and their TEM images of the ultrathin section sliced by ultramicrotome with 20 nm thickness.

Figure 3.jpg

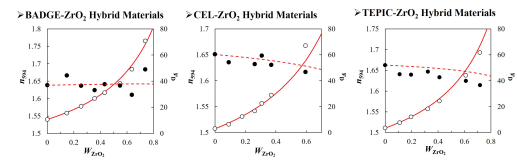


**Figure 4.** Refractive indices at 594 nm ( $\odot$ ) and abbe's numbers ( $\bullet$ ) of the prepared hybrid materials versus the weight fraction of  $\text{ZrO}_2$  NPs ( $W_{\text{ZrO}_2}$ ). The solid and broken lines are the theoretical curves predicted from the Lorentz-Lorenz theory.

Figure 4.jpg

# Comparison between layering NbSe<sub>2</sub> and rod characteristic of MgB<sub>2</sub> by investigation of elastic constants

Wednesday, 18th October - 13:30 - Poster Session - Hall & Room 3 - Poster - Abstract ID: 638

**Ms. Asiye Shokri<sup>1</sup>, Dr. Ahmad Yazdani<sup>2</sup>, Mr. behrad barakati<sup>1</sup>**

**1. Tarbiat Modares University, 2. Ta**

Although the delicate balancing of strong anisotropy, CDW- order " $T_{CDW}=33$  K" and finally emerging superconductivity at " $T_c= 7.2$  K" are the most intriguing question in characteristic behavior of NbSe<sub>2</sub>, but the original mechanism of MgB<sub>2</sub>old superconductor, which has unlike the *cuprates* a lower anisotropy and larger coherence length of the grain boundary to current flow is still unknown. Since the cause and the mechanism of band-effect of these two original layering- structures on bond- rupturing- atomic positions are unknown, here the stability of crystalline structure of interatomic potential through the elasticity-compressibility is investigated. The investigations are based on the presented different stiffness of two elements of the same column "Be" and "Mg" (table1). Whereas the direction of the semi-metallic bonding of "Be" is the cause of the quasi- two- dimension metallic surface state of Be, the MgB<sub>2</sub> could be formed as rod- and wiring- shape unlike the NbSe<sub>2</sub> which is to be layered. Relative to layering of low  $T_c=0.7$  of BeB<sub>2</sub>, as it's presented by others, high  $T_c=40$  of MgB<sub>2</sub> is decreased by external pressure, while, low  $T_c=7.2$  of NbSe<sub>2</sub> is increased up to critical pressure  $P_c=10$  (GPa) and then decrease. Therefore, the difference between layering character of NbSe<sub>2</sub> and rod-formation character of MgB<sub>2</sub> superconductors could be the intriguing question.

The directional bond formation or a strong anisotropy of different "B-B" length do to smaller- intro- layer to the inter-layer distance of "B-B" could be the cause where we are following characteristic behavior of MgB<sub>2</sub> for the cause of direction rod/wire character.

Insignificance of  $T_c=0.7$  in BeB<sub>2</sub> is surprisingly in a challenge which could be due to its layering- character- formation as its common feature with NbSe<sub>2</sub>. Consequently, in order to clear out the strong difference between the layering of NbSe<sub>2</sub> and domination of rod-character resulted to all about similarity consideration simultaneously the both stability of crystal structure through the cohesive energy  $c/a$ (fig1),  $c_{zz}$ (Fig2) and  $c_{33}$ (table2) are investigated. The proposed investigations are more evidence on different characteristic behavior of calculated parameters.

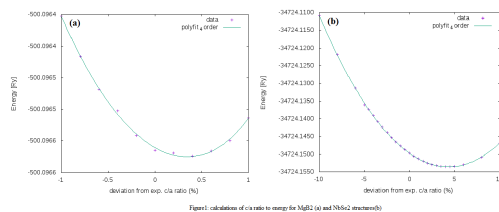


Fig1.png

Table1: Stiffness Constants(GPa) for Be and Mg metals

	$C_{11}$	$C_{12}$	$C_{13}$	$C_{33}$
Be	292	24	6	349
Mg	59.3	25.7	21.4	61.5

Table1.png

Table2: Stiffness Constants(GPa) of MgB<sub>2</sub> and NbSe<sub>2</sub>

	$C_{11}$	$C_{12}$	$C_{13}$	$C_{33}$	$C_{zz}$
MgB <sub>2</sub>	430.80	49.94	38.65	255.15	836.44
NbSe <sub>2</sub>	167.42	82.98	79.86	209.51	349.99

Table2.png

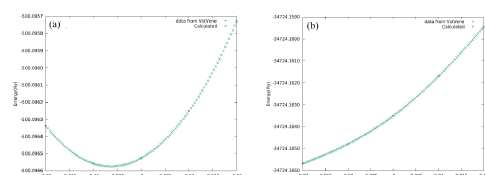


fig2. diagram of czz strain to energy for MgB2(a) and NbSe2(b)

Fig2.png

# Multifunctional graphene (RGO) wrapped Au plasmonic nanostructure: Giant enhanced photoluminescence, excellent visible-light assisted photodetection along with its application towards electrochemical non-enzymatic H<sub>2</sub>O<sub>2</sub> and AA biosensor

Wednesday, 18th October - 14:30 - Nanophotonics, optics and plasmonics - Room 1 - Oral - Abstract ID: 277

**Mr. Sumit Majumder<sup>1</sup>, Dr. Sanjay Kumar<sup>2</sup>, Prof. Sangam Banerjee<sup>3</sup>**

*1. Jadavpur University and Saha Institute of Nuclear Physics, 2. Jadavpur University, 3. Saha Institute of Nuclear Physics*

## Abstract:

We have synthesized bare GO (S1), RGO wrapped Au nanocomposite (S2) and characterized by FESEM and Raman. Electrochemical study shows that S2 exhibits very sensitive electrochemical sensing capability towards H<sub>2</sub>O<sub>2</sub> and AA due to presence of a large number of catalytic sites in the sample. Enhanced PL emission is due to combined influence of FRET and SPR effect for Au nanoparticles. Moreover, upon visible light illumination, S2 exhibits an enhanced current response of switching due to production of photocurrent through inter-band 6sp transition within Au.

## Introduction:

In the past few years nano/micro sized materials have gained considerable focus due to their large scale prospective applications. Hydrogen peroxide (H<sub>2</sub>O<sub>2</sub>) is extensively used in clinical, biopharmaceuticals, environmental and industrial fields. Ascorbic acid (AA) is a powerful antioxidant, naturally occurs in citrus fruits and vegetable products. Therefore, sensitive detection of a small quantity of H<sub>2</sub>O<sub>2</sub> or AA is of great scientific importance. We have studied PL, visible-light assisted photodetection and electrochemical sensing based on S2.

## Results and Discussion:

The FESEM images of both samples are depicted in Fig. 1(a) and 1(b), where RGO wrap a large no of Au nanoparticles (50-70 nm). Fig. 1(c) shows Raman spectra of S1 and S2, confirms the attachment of RGO with Au. Fig. 1(d) depicts that RGO-Au is more electroactive than bare GO. So, we have measured biosensing study (H<sub>2</sub>O<sub>2</sub> and AA) based on RGO-Au/ITO working electrode here. The value of the sensitivity obtained from the calibration curve (Fig. 2) are 280.28  $\mu\text{A}/\text{mM}\cdot\text{cm}^2$  (in a wide range from 1  $\mu\text{M}$  to 0.8 mM, correlation coefficient = 0.96681 and the lowest detection limit is estimated to be 6.80  $\mu\text{M}$  at S/N= 3) towards H<sub>2</sub>O<sub>2</sub> sensing and 314.07  $\mu\text{A}/\text{mM}\cdot\text{cm}^2$  (in a wide range from 25  $\mu\text{M}$  to 300  $\mu\text{M}$ , correlation coefficient = 0.97133 and the lowest detection limit is estimated to be 6.80  $\mu\text{M}$  at S/N= 3) towards AA sensing (Fig. 2). Moreover, S2 shows electrochemical switching under visible light, depicted in Figure 3.

## Conclusion:

So we can use RGO@Au for electrochemical H<sub>2</sub>O<sub>2</sub> and AA biosensor and visible light assisted photodetection applications purpose.

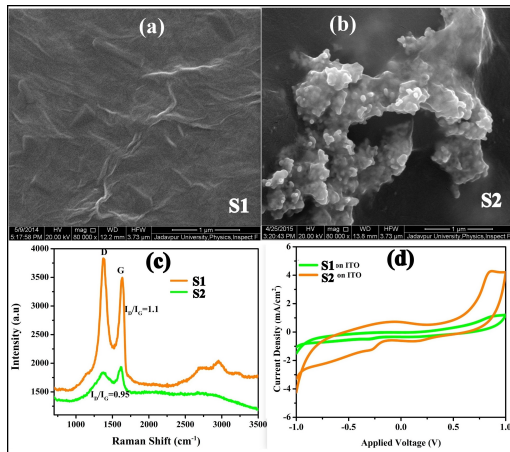


Figure 1.jpg

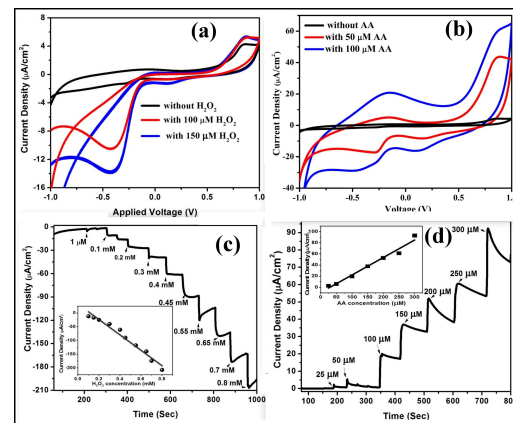


Figure 2.jpg

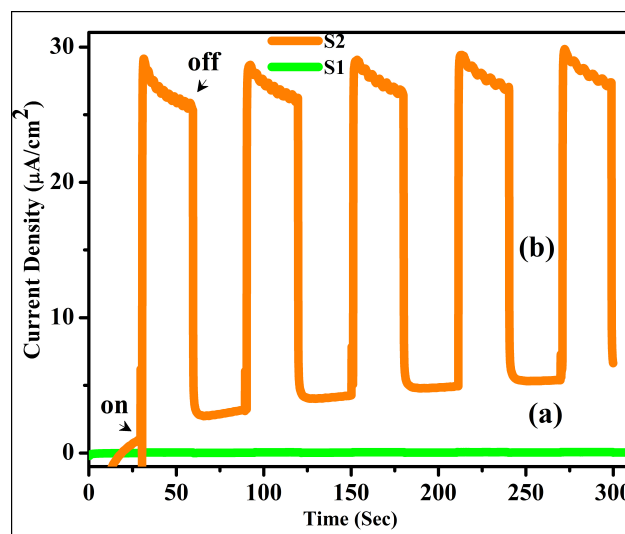


Figure 3.jpg

# Metamaterials based on mixture of Au and CdZnSe\ZnS nanoparticles for future sensorics

Wednesday, 18th October - 14:47 - Nanophotonics, optics and plasmonics - Room 1 - Oral - Abstract ID: 635

**Dr. Elena Ushakova<sup>1</sup>, Dr. Sergei Cherevkov<sup>1</sup>, Ms. Tatiana Kormilina<sup>1</sup>, Dr. Aliaksei Dubavik<sup>1</sup>, Mr. Mikhail Baranov<sup>1</sup>, Dr. Aleksandr Litvin<sup>1</sup>, Prof. Anatoly Fedorov<sup>1</sup>, Prof. Alexander Baranov<sup>1</sup>**

**1. ITMO University**

The design development and investigation of multicomponent nanostructured materials are the most promising research areas in modern Materials Science. Such materials combine and enhance the properties of each component, and also possess new properties. Therefore they are called metamaterials. In this paper we developed protocols for the formation of porous metamaterials based on mixtures of Au and CdZnSe\ZnS nanoparticles and investigated their optical properties.

Colloidal Au nanoparticles and semiconductor alloyed quantum dots (QDs) were synthesized by the organo-metallic method in colloidal solution. The developed protocols for the metamaterials formation are based on destabilization of colloidal solutions. (Fig. 1(a)). Hybrid complexes from Au particles and QDs were formed in the solution volume and fell onto the silicon substrate in the vial. Thus, porous structures with a shape varying from a spherical to flower-like were obtained. Figure 1 (b, c) shows SEM images obtained by electron microscopy (Merlin, Zeiss). The shape and size of the structures depend strongly on the method of colloidal solution destabilization.

The optical properties of the obtained metamaterials were studied using a laser scanning confocal microscope (LSM-710, Zeiss). Figure 2 shows a photoluminescent image of a sample containing flower-like superstructure. Spectral analysis showed that luminescent properties are changed as compared with those of structures formed by QDs only and for a QD colloidal solution (dashed lines). This can be explained by the interaction of Au nanoparticles and QDs in the superstructure.

The developed protocols for the formation of porous metamaterials with unique optical properties can be utilized for the development of the active materials for sensorics. The results on optical properties will expand the understanding of the interaction of components in hybrid nanostructured materials.

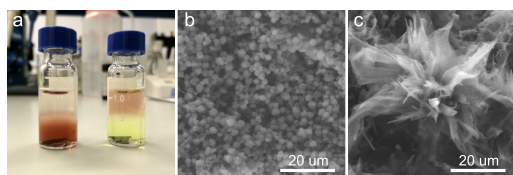


Fig.1. a - photo of colloidal mixtures of Au nanoparticles and QDs b and c - SEM images of metamaterials formed by different methods.png

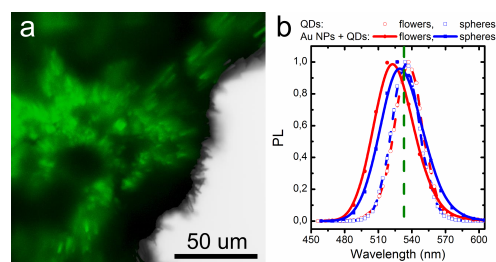


Fig.2. a - PL image of flower-like superstructure b - PL spectra from metamaterials solid lines superstructures from QDs only dashed lines and PL peak position for QD solution green dashed line.png

# Stabilization of silver nanoparticles with dyes for optical limiting

Wednesday, 18th October - 15:04 - Nanophotonics, optics and plasmonics - Room 1 - Oral - Abstract ID: 601

**Dr. Cordula Hege<sup>1</sup>, Dr. Olivier Muller<sup>1</sup>, Ms. Stefanie Dengler<sup>2</sup>, Dr. Bernd Eberle<sup>2</sup>, Mr. Lionel Merlat<sup>1</sup>**

**1. French-German Research Institute of Saint-Louis - ISL, 2. Fraunhofer IOSB, Institute of Optronics, System Technologies and Image Exploitation**

Lasers are getting more and more common, so also the risk for injury of the eyes or sensor due to laser radiation increases. Optical limiting is a method, which one can use to protect them. To use the method one can make filters with materials, which are nonlinear optical active. Optical limiting leads to an attenuation of their transmission above a certain laser intensity.

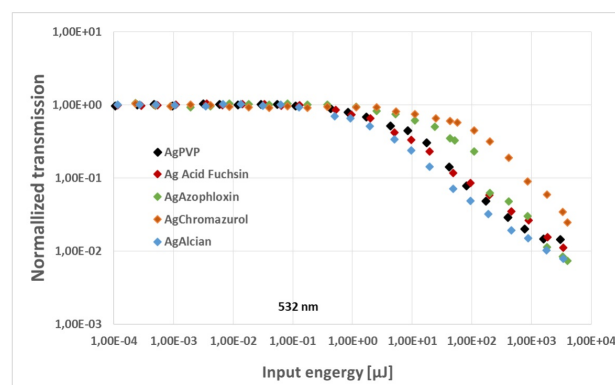
There are several materials like nanoparticles and dyes, which are nonlinear active. In case of metal nanoparticles, especially silver nanoparticles lead to good optical limiting.[1]

In our study we used dyes as stabilization agents for silver nanoparticles to produce hybrids out of dyes and nanoparticles. Different reduction technique were used like reduction with Sodium borohydride ( $\text{NaBH}_4$ ), and a variation of a polyol synthesis. In case of the polyol synthesis, dimethylacetamid (DMA) was used as solvent and pentaerythritol propoxylate was used as reduction agent. As stabilization agents in case of the  $\text{NaBH}_4$ -reduction Alcian Blue and acid fuchsin was used. Chromazurol and azophloxine were used for the polyol synthesis.

In case of the reduction with  $\text{NaBH}_4$ , one can see that the dyes normally lead to a better attenuation compared to the silver nanoparticles stabilized with polyvinylpyrrolidone (PVP). This is also the case with the silver nanoparticles stabilized with azophloxin, but there the threshold is higher.

Our results indicate that hybrids of silver nanoparticles and dyes are promising candidates for optical limiting.

[1] Muller, Olivier; Dengler, Stefanie; Ritt, Gunnar; Eberle, Bernd (2013): Size and shape effects on the nonlinear optical behavior of silver nanoparticles for power limiters. In: *Applied Optics* 52 (2), S. 139–149.



Optical-limiting-of-silver-hybrid-nanoparticles.jpg

---

## Tubular gold nanoparticle assemblies

---

Wednesday, 18th October - 15:21 - Nanophotonics, optics and plasmonics - Room 1 - Oral - Abstract ID: 325

---

***Mr. Priyadarshi Ranjan<sup>1</sup>, Dr. Ronit Popovitz-biro<sup>1</sup>, Dr. Iddo Pinkas<sup>1</sup>, Dr. Sidney Cohen<sup>1</sup>, Dr. Michal Lahav<sup>1</sup>, Prof. Reshef Tenne<sup>1</sup>, Prof. Milko van der Boom<sup>1</sup>***

*1. Weizmann Institute of Science*

Nanotubes of WS<sub>2</sub> (INT-WS<sub>2</sub>) have been uniformly decorated with 5 nm tetraoctyl ammonium bromide stabilized gold nanoparticles (AuNP). The interparticle distance of AuNP is 2 nm. This self-assembly process is likely to be driven by the lattice matching between the nanotube outer wall and AuNP and strengthened by the affinity of disulfide binding with Au. The optical band gap of INT-WS<sub>2</sub> can be varied from 1.82 eV for the bare nanotube to 1.75 eV for full AuNP coverage. AuNP decorated nanotubes are further functionalized with robust pyridine-based ruthenium complexes. The complexes adhere and link the surface-bound AuNPs through ligand exchange. The resulting network of AuNPs forms a coherent, tubular shell that persists even after complete removal of the underlying INT-WS<sub>2</sub> with hydrogen peroxide. The oxidation process is studied by electron microscopy and optical microscopy. Raman spectroscopic measurements of the single-walled AuNP tube shells depict the presence of the metal complex. The mechanical properties of the AuNP-tubes are studied by AFM-based nanoindentation. This study indicates that tubular structure is elastic in nature with stiffness dominated by interactions between the AuNPs.



# In situ synthesis of plasmonic and magnetic nanoparticles in polymer thin films under laser and solar irradiation

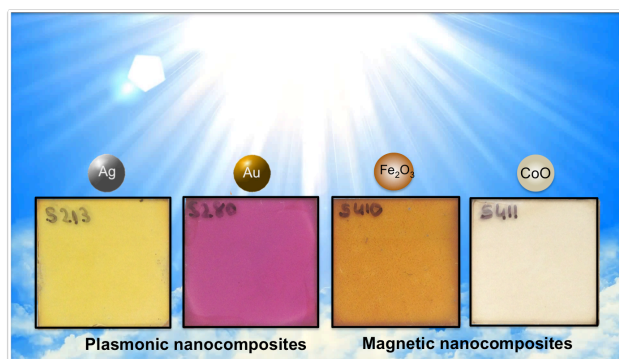
Wednesday, 18th October - 15:38 - Nanophotonics, optics and plasmonics - Room 1 - Oral - Abstract ID: 266

**Mr. Elie Nadal<sup>1</sup>, Mr. Laurent Peres<sup>2</sup>, Dr. Noémi Barros<sup>3</sup>, Prof. Marc Respaud<sup>2</sup>, Dr. Katerina Soulantica<sup>2</sup>, Prof. Hamid Kachkachi<sup>1</sup>**

**1. University of Perpignan Via Domitia (UPVD) / Laboratoire PROMES (PROcédés Matériaux et Energie Solaire) CNRS UPR8521,**

**2. Laboratoire de Physique et Chimie des Nano-Objects, UMR 5215 INSA/UPS/CNRS, 3. Université de Perpignan Via Domitia (UPVD)/ Laboratoire PROMES (PROcédés Matériaux et Energie Solaire) CNRS UPR8521**

Plasmonic and magnetic nanocomposite materials are of great interest in many applications such as photonics, photovoltaics, catalysis, medicine and biology. This field has been the subject of a large activity in the past decades. At the same time, chemists have demonstrated the versatility of wet synthesis approaches to fabricate nanoparticles with well-defined magnetic and optical properties. However, the insertion in matrices of such nanostructures on a large scale and at high concentrations in view of applications is still challenging. In order to address this issue, we propose two new approaches, based on the *in situ* synthesis of nanoparticles in polymer thin films under irradiation. In the first approach, our aim is to control the spatial organization of the nanoparticles within the polymer films by laser interferometry. We show that the plasmonic nanoparticle gratings thus formed present unusual diffractive properties that strongly depend on the plasmonic excitation of the system. In the second method, we study the *in situ* synthesis of nanoparticles in polymer thin films under concentrated solar irradiation. We show that this technique can be used as an efficient route for the fabrication of both plasmonic and magnetic nanocomposite thin films. In particular, we study for the first time the synthesis of magnetic nanoparticles under visible-light irradiation and without the use of chemical reducing agent to initiate the nanoparticle formation. This approach can be readily used for large-scale production and allows for the insertion of large metal filling fractions in the polymer films while keeping the nanoparticles from agglomeration. Moreover, in the case of plasmonic nanoparticles, we found that adjusting irradiation conditions, and especially the light flux, affects the size and morphology of the nanoparticles. Finally, we have successfully tested this approach by using biopolymer as matrices, thus meeting the requirements of green synthesis.



Nanocomposites synthesized under solar irradiation.png



# The dynamical and thermodynamic properties of the Pöschl-Teller oscillator in Quantum Engines.

Wednesday, 18th October - 15:55 - Nanophotonics, optics and plasmonics - Room 1 - Oral - Abstract ID: 558

**Dr. Enock Oluwale OLADIMEJI<sup>1</sup>, Prof. Rudoy Yuri G<sup>2</sup>**

1. Peoples' Friendship University of Russia, 2. Peoples' Friendship University of Russia

## Introduction.

Following the formulation of Pöschl-Teller [PT] model in our work [1], we continued with its dynamic and thermodynamic description [2,3] which has a relation with two well-known models –i.e., the free particle [FP] in the box and the quantum harmonic oscillator [QHO] which are frequently and effectively exploited in modern nanotechnology – e.g., in quantum dots and magnetic traps.

## Methods

In this work, dynamic and thermodynamic properties of [PT]-model are explored by constructing a quantum-mechanical analogue of the Joule-Brayton, Otto and Carnot cycles as shown [4]. The derived efficiency is compared to be analogous to those obtained for classical engines.

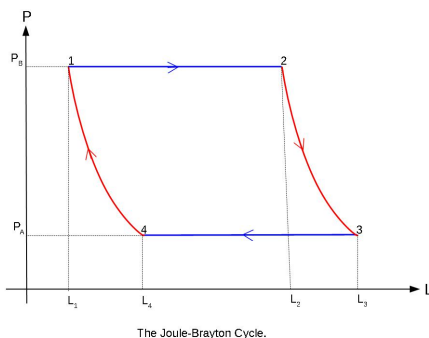
This construction is based on the formalism of a quantum engine that was proposed [5] for a single particle of mass *and confined to an infinite one-dimensional potential well of width*

## Results

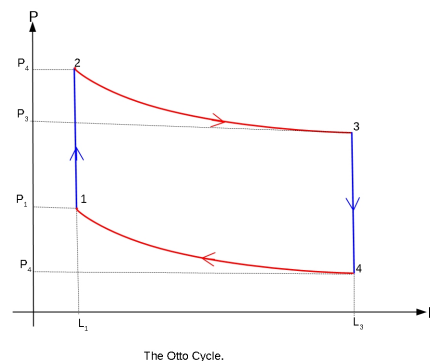
Our results are remarkable, the derived efficiencies of the quantum cycles, are analogous to the well-known efficiencies from classical thermodynamics. Also in comparism to [4] our efficiency is exactly the same when for free particle in the box [2].

## Discussion

- [1] Rudoy, Yu.G; Oladimeji E . 2017 Pressure Operator for the Pöschl–Teller Oscillator Rudn J. Math. Inf. Sci. Phys. **25** 276–82
- [2] Rudoy, Yu.G; Oladimeji E . 2017 About One Interesting and Important Model in Quantum Mechanics I. Dynamic Description Phys. High. Educ. **23** 20–33 [Russian]
- [3] Rudoy, Yu.G; Oladimeji E . 2017 About One Interesting and Important Model in Quantum Mechanics II. Thermodynamic Description Phys. High. Educ. **23** 11–23 [Russian]
- [4] Guzmán-Vargas L, Granados V, Mota R D and Guzman-Vargas L 2002 Efficiency of simple quantum engines: The Joule-Brayton and Otto cycles AIP Conf. Proc. **643**
- [5] Bender C, Brody D and Meisinger P N 2008 Quantum-Mechanical Carnot Engine Quantum **1**–10



Joule-brayton cycle wt arrows.jpg



The otto cycle wt arrows.jpg

# Electroactive Self-Assembled-Monolayer for Smart Functional Surfaces

Wednesday, 18th October - 14:30 - Nanoelectronic systems, components and devices - Room 2 - Oral - Abstract ID: 807

***Ms. Maria Serena Maglione<sup>1</sup>, Dr. Stefano Casalini<sup>1</sup>, Dr. Stamatis Georgakopoulos<sup>1</sup>, Dr. Nuria Crivillers<sup>1</sup>, Dr. Concepció Rovira<sup>1</sup>, Dr. Marianna Barbalinardo<sup>2</sup>, Mr. Vitaliy Parkula<sup>3</sup>, Dr. Pierpaolo Greco<sup>3</sup>, Dr. Marta Mas-Torrent<sup>1</sup>***

*1. ICMAB-CSIC, 2. CNR-ISMN, 3. Scriba Nanotecnologie*

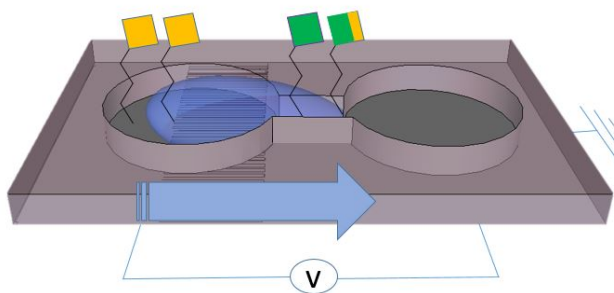
Self-assembled monolayers (SAMs) bearing a redox active terminal group on conducting surfaces can be interconverted between different states by the application of an external electrochemical stimulus. The high interest toward these systems is justified by the possibility to have a high control over the properties of the surface, that can be electrochemically tuned. For instance, the surface wettability strongly depends on the charge or the polarizability of the terminal groups.<sup>1</sup>

Here, a switchable ITO electrode coated with an anthraquinone-derivative (AQ) SAM is reported. A significant modulation of surface wettability yielded a change in surface contact angle as high as 25°. Furthermore, arrays of planar electrodes for droplets actuation were fabricated and integrated in a microfluidic device. We proved the possibility to induce directional movement of water droplets on the substrate to perform operations of mixing and separation on sub-nanoliter scale.

Compared with the typical configuration of electrowetting-on-dielectric (EWOD),<sup>2</sup> our system operates at very low voltages ( $\leq 2.8$  V) and, furthermore, it is biocompatible. Cells can be successfully transported on the surface without affecting its viability.

[1] a) N.L. Abbott and G.M. Whitesides, *Langmuir*, 1994, **10**, 1493-1497 b) C. Simao, M. Mas-Torrent, J. Veciana and C. Rovira, *Nanolett.*, 2011, **11**, 4382-4385 c) J. Casado Montenegro, M. Mas-Torrent, F. Oton, N. Crivillers, J. Veciana and C. Rovira, *Chem Commun*, 2013, **49**, 8084-8086 d) S. Casalini, M. Berto, C. A. Bortolotti, G. Foschi, A. Operamolla, M. Di Lauro, O. Hassan, A. Liscio, L. Pasquali, M. Montecchi, G. Farinola, M. Borsari *ACS Appl. Mater. Interfaces*, 2015, **7**, 3902-3909

[2] J. Lee, H. Moon, J. Fowler, T. Schollhammer and C. J. Kim, *Sens. Actuators A*, 2002, **95**, 259-268



Toc-abstract.jpg

# Magnetic, thermal and luminescence properties in room-temperature nanosecond electron-irradiated various metal oxide nanopowders

Wednesday, 18th October - 14:47 - Nanoelectronic systems, components and devices - Room 2 - Oral - Abstract ID: 95

***Prof. Sergey Sokovnin<sup>1</sup>, Dr. Vladislav Il'ves<sup>2</sup>, Mr. Michail Balezin<sup>2</sup>***

*1. Ural Federal University, 2. Institute of Electrophysics Ural Branch of Russian Academy of Sciences*

By method of pulsed electron beam evaporation in vacuum [1] of targets from non-magnetic in bulk state,  $\text{Al}_2\text{O}_3$ ,  $\text{SiO}_2$ ,  $\text{CeO}_2$  and YSZ ( $\text{Y}_2\text{O}_3$ -8%  $\text{Gd}_2\text{O}_3$ ) oxides, magnetic nanopowders with a high specific surface were produced. The nanopowders were irradiated in air in room-temperature by electrons with energy of 0.7 MeV with pulse FWHM of 100 ns, using a pulse-periodic accelerator URT-1 [2] for 15 and 30 minutes.

The magnetic, thermal, and cathodoluminescence characteristics of nanopowders were measured before and after irradiation. It was established that the electron irradiation non-monotonically changes the magnetization of the pristine samples. To the contrary, a clear correlation between the intensity of cathodoluminescence and their irradiation does is found in the most of the oxides. There was a decrease in the intensity of cathodoluminescence after irradiation. Thermal stability and phase transformations of unirradiated and irradiated  $\text{CeO}_2$  and YSZ oxides were analyzed by synchronous analysis using thermogravimetry and differential scanning calorimetry. Luminescent and thermal properties reflect the transformation of structural defects in NPs more strongly after the exposure to a pulsed electron beam in comparison with corresponding changes of the NP magnetic response.

Fig. 1 a) Dependences of the magnetization change in  $\text{Al}_2\text{O}_3$  NP magnetic field up to 12 kOe from the irradiation time (left) and b) PCL spectra not (1) and irradiated samples with doses 31.5 MGy (2) and 63 MGy (3).

Fig. 2 a) Dependences of the magnetization change in YSZ NP magnetic field up to 12 kOe from the irradiation time (left) and b) PCL spectra of not (1) and irradiated samples with doses 31.5 MGy (2) and 63 MGy (3).

## Reference

- [1] Sokovnin S.Yu., Il'ves V.G.. Production of nanopowders using pulsed electron beam / *Ferroelectrics*, V.436 (2012), I.1, 101 - 107. DOI:10.1080/10584587.2012.730951
- [2] Sokovnin S. Yu., Balezin M. E. and Shcherbinin S. V. A YPT-1M accelerator for radiation technologies. *Instr. and Exp. Tech.* V. 56 (2013), 4, 411-413. <http://dx.doi.org/10.1134/S002...>

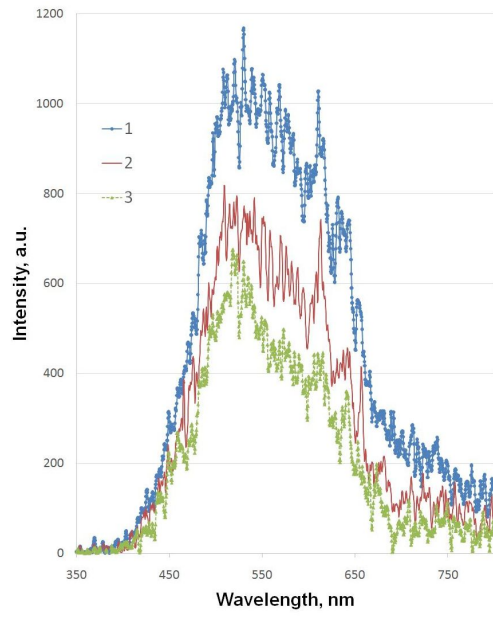


Fig 2b.jpg

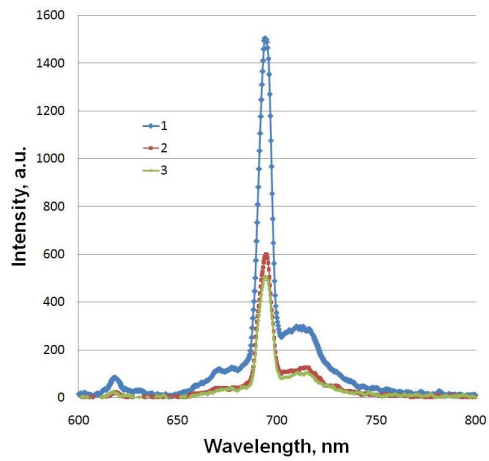


Fig 1b.jpg

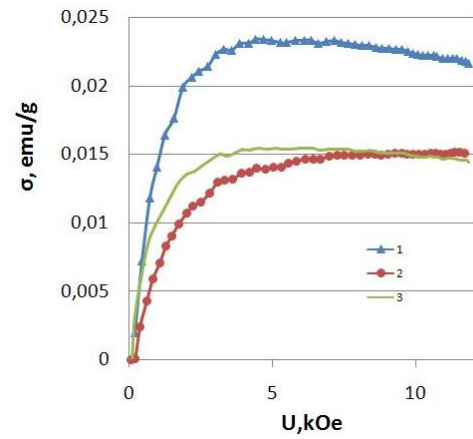


Fig 1a.jpg

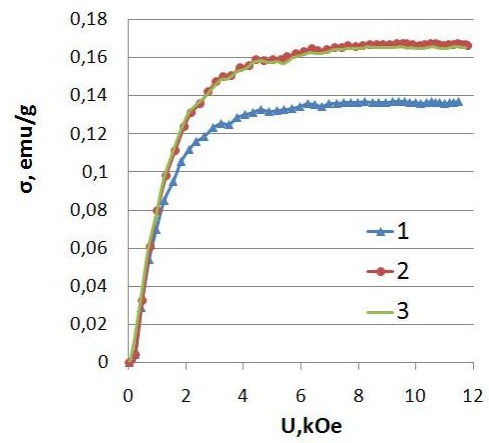


Fig 2.jpg

---

## High performance nanowire based field effect transistors for sensing applications

---

Wednesday, 18th October - 15:04 - Nanoelectronic systems, components and devices - Room 2 - Oral - Abstract ID: 633

---

***Dr. Camelia Florica<sup>1</sup>, Dr. Andreea Costas<sup>1</sup>, Dr. Nicoleta Preda<sup>1</sup>, Dr. Elena Matei<sup>1</sup>,  
Dr. Ionut Enculescu<sup>1</sup>***

*1. National Institute of Materials Physics*

Field effect transistors are omnipresent electronic devices with applications ranging from microprocessors to biosensors. New and improved architectures are sought with the aim in exploiting functionalities obtained from specific composition, morphology or working principles. The development in the field is further fueled by the need of developing devices which shall be used as platforms for smart sensors and exploiting the high surface to volume ratio of low dimensional structures represent a convenient approach.

Nanowires represent a particular case of nanostructures with high aspect ratio and were successfully used as building blocks for the fabrication of electronic devices, including here diodes and transistors.

In the present work we will describe our work regarding the fabrication of nanowire based field effect transistors. Several methods were employed for producing nanowires, wet methods such as electrochemical and chemical and thermal oxidation [1,2]. Each method we employed is low cost and had its own particularities both in terms of advantages and drawbacks. Further the nanowires are harvested and provided with electric contacts by lithographical methods, including here photolithography, electron beam lithography and ion beam induced metallization. When placed on Si/SiO<sub>2</sub> substrates one can use them as gate electrode/gate insulator and a field effect transistor is obtained. Electrical characterization was performed, source drain and gate characteristics being measured. Very high  $I_{on}/I_{off}$  ratios were measured.

Further functionalization of the nanowire channel field effect transistor leads to the fabrication of very effective sensors. By functionalization the selectivity of the devices can be optimized while the excellent electrical performances lead to increased sensitivity.

[1] C. Florica, A. Costas, A.G. Boni, R. Negrea, L. Ion, N. Preda, et al., Electrical properties of single CuO nanowires for device fabrication: Diodes and field effect transistors, 106 (2015). doi:10.1063/1.4921914.

[2] C. Florica, E. Matei, A. Costas, M.E.T. Molares, I. Enculescu, Field Effect Transistor with Electrodeposited ZnO Nanowire Channel, Electrochim. Acta. 137 (2014) 290–297. doi:10.1016/j.electacta.2014.05.124.

---

## Assessment on Lattice Thermal Transport Properties of Functionalized MXene Structures

---

Wednesday, 18th October - 15:21 - Nanoelectronic systems, components and devices - Room 2 - Oral - Abstract ID: 203

---

***Dr. Sevil Sarikurt<sup>1</sup>, Dr. Deniz Cakir<sup>2</sup>, Dr. Murat Keceli<sup>3</sup>, Dr. Cem Sevik<sup>4</sup>***

*1. Department of Physics, Faculty of Science, Dokuz Eylul University, Izmir, 2. Department of Physics and Astrophysics, University of North Dakota, Grand Forks, North Dakota, 3. Chemical Sciences and Engineering Division, Argonne National Laboratory, Argonne, Illinois, 4. Department of Mechanical Engineering, Faculty of Engineering, Anadolu University, Eskisehir*

The newest members of 2D transition metal carbides and nitrides, so-called MXenes, receive increasing attention due to their novel electronic and thermal properties that can be tuned for specific applications. Electronic properties and dynamical stabilities of various MXene structures have been investigated by different research groups, however, only a very few of them focused on thermoelectric performance of the semiconductor MXene materials. In this study, we investigated the lattice thermal conductivity and Seebeck coefficients of oxygen terminated  $M_2CO_2$  ( $M=Ti, Zr, Hf, Sc$ ) MXenes in two different configurations (MD-II, MD-III) using Density Functional Theory and the Phonon Boltzmann Transport Theory. Investigating the structural and compositional variety provides us additional degrees of freedom for modulating physical and chemical properties of MXenes. We found that within MD-III configurations, thermal conductivity can be lowered by a factor of three for  $Zr_2CO_2$  and by a factor of two for  $Ti_2CO_2$  and  $Hf_2CO_2$  in comparison to MD-II configurations. We also obtained that Seebeck coefficients are larger approximately by a factor of three for  $Ti_2CO_2$  and by a factor of 1.1 for  $Zr_2CO_2$  and  $Hf_2CO_2$  in the MD-III configurations compared to MD-II configurations. Our study demonstrated that  $Ti_2CO_2$  and  $Zr_2CO_2$  in MD-III configurations are promising candidates for next-generation thermoelectric applications thanks to their low thermal-conductivities and large Seebeck coefficients.

---

## Continuous production of monodisperse nanoparticles assemblies by an in-flow ligand desorption method.

---

Wednesday, 18th October - 15:38 - Nanoelectronic systems, components and devices - Room 2 - Oral - Abstract ID: 669

---

***Dr. Jenny Merlin<sup>1</sup>, Dr. Steven Ferguson<sup>1</sup>, Dr. Dermot F. Brougham<sup>1</sup>***

***1. University College Dublin***

Magnetic nanoparticles (NPs) present great potential in biomedical applications e.g. as contrast agents for magnetic resonance imaging, for hyperthermia therapy and for drug delivery, but their application is limited by the weak magnetic moment of single particles. This limitation can be addressed through the fabrication of clusters of NPs (NPCs). New processes for a large production of monodisperse NPCs with selectable size and surface chemistry are therefore required.

Our group have developed a novel technique for assembling stable monodisperse NPCs by competitive stabilizer desorption<sup>1</sup> to a liquid-liquid interface which allows fine control over the size of the formed NPCs, while retaining their monodispersity. The process is robust and reproducible; we will describe here how it can be adapted for continuous production of monodisperse suspensions of NPCs, and how these may be continuously collected using a bespoke liquid-liquid phase separator. Hence the production of NPCs is only limited by the initial quantity of the starting material available, while the final suspensions of NPCs remain monodisperse with size selectable through controllable experimental parameters.

[1] Stolarczyk JK, Swapankumar G and Brougham DF, *Angew. Chem. Int.Ed.* 2009, 48, 175178.

# Highly reliable controllability of quadruple-level-cell operation in HfO<sub>2</sub> based resistive switching device

Wednesday, 18th October - 15:55 - Nanoelectronic systems, components and devices - Room 2 - Oral - Abstract ID: 344

***Dr. Gun Hwan Kim<sup>1</sup>, Dr. Bo Keun Park<sup>1</sup>, Dr. Taek-mo Chung<sup>1</sup>, Dr. Young Kuk Lee<sup>1</sup>***

*1. Korea Research Institute of Chemical Technology*

Nowadays, semiconductor based electronic memory devices have been faced its physical limitations in further miniaturization for higher information storage capacity. Although vertical NAND FLASH memory, so-called V-NAND, was regarded as a permanent breakthrough for future memory technology which is independent from physical scaling limitation, several critical issues in its fabrication processes have been found, and some other solutions should be required. In this point of view, resistive switching random access memory (ReRAM) has been considered as a next-generation non-volatile memory device due to its high operation speed, scalability, and low energy consumption. However, stochastic nature in ReRAM operation hindered its commercialization because strict operational controllability is essential for not only good reliability but multi-level-cell operation (more than 1-bit ("0" and "1") operation) which is inevitable to achieve higher effective integration density. In spite of various related researches, obvious solution to control the randomness of ReRAM operation has not been appeared yet. Its main reason is difficulty of microscopic control of defects in resistive switching material. In fact, previous researches had been focused on passive methodologies, such as atomic element doping or scale-down of ReRAM device itself. However, it is time to solve the problem via active method.

The final ReRAM device structure used in this work is Au/Al<sub>2</sub>O<sub>3</sub>/HfO<sub>2</sub>/TiN stacked crossbar type device which has 10×10 μm<sup>2</sup> of junction area as shown in figure 1. Au and TiN layers play a role of top and bottom electrode, respectively, which was patterned by conventional photo-lithography and followed lift-off process. The blanket-type 6 nm-thick HfO<sub>2</sub> and 2 nm-thick Al<sub>2</sub>O<sub>3</sub> thin film layer was deposited by atomic layer deposition (ALD) method.

In this research, electrical control circuit algorithm was applied to ReRAM device, and highly reliable 4-bit (16 distinguishable resistance states in one cell) operation was achieved as shown in figure 2. It should be noted that the overlap probability between each state could be controlled even its stochastic nature as presented in figure 3. This work reports a critical step forward in the ReRAM field for its future adoption for data storage that can show higher competitiveness than the industry-standard NAND FLASH memory.



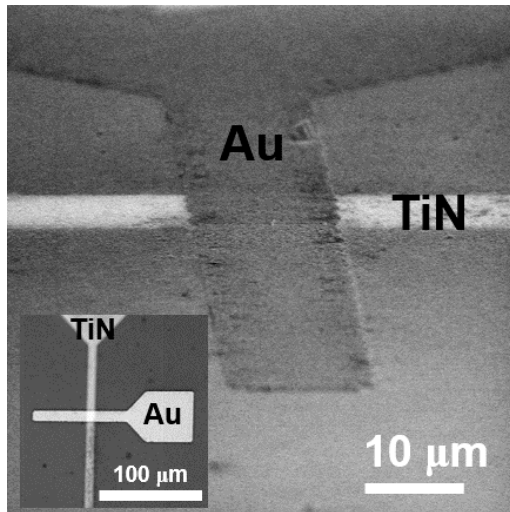


Figure 1.png

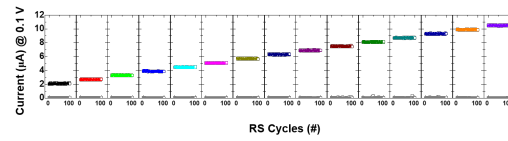


Figure 2.png

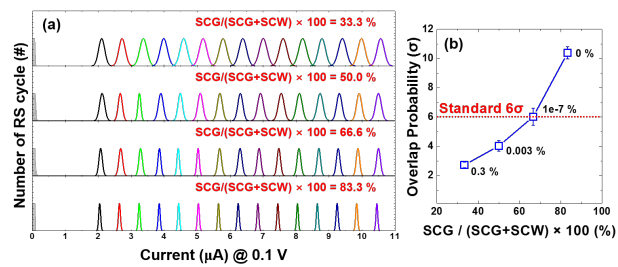


Figure 3.png

# Light-funnel arrays for photovoltaic applications: a novel approach toward absorption enhancement of the solar radiation

Wednesday, 18th October - 14:30 - Nanotechnology for environment and energy - Auditorium - Oral - Abstract ID: 448

***Dr. gil shalev<sup>1</sup>, Mr. Gilad Marko<sup>1</sup>, Mr. Tamir Gabay<sup>1</sup>, Mr. Yuval Nissan<sup>1</sup>***

*1. Ben-Gurion University of the Negev*

## Introduction

Light trapping is about capturing photons from an incident electromagnetic wave in order to generate heat or electric current. Surface decoration with arrays of subwavelength structures was demonstrated to provide increase in light trapping (exceeding the Yablonovitch limit) and, hence, light absorption enhancement. We recently introduced the light-funnel (LF) array as an absorption enhancement technique for photovoltaic applications that is bio-inspired by the properties of the *fovea centralis*<sup>1</sup>. The *fovea centralis* is a closely-packed vertical array of inverted-cone photoreceptor cells located in the retina that is responsible for high acuity binocular vision under well-lit conditions. In this manner the functionality of the *fovea centralis* resembles that of a photovoltaic cell: both trap light efficiently under bright light conditions.

## Methods

Fabrication of light-funnel arrays. Silicon wafers were patterned using nano-sphere lithography with Langmuir-Blodgett technique.

Numerical calculations. The optical and the electrical simulations were performed with Synopsys TCAD Sentaurus, Mountain View, CA, USA. The optical response of the system was calculated using finite-difference time-domain simulations. The Poisson and the Continuity equations were solved for each mesh vertex in conjunction with the respective carrier generation file. The modeling accounted for doping dependent Shockley-Read-Hall (SRH) recombination, Auger recombination, surface recombination, bandgap renormalization for degenerately doped silicon and doping dependent mobility.

## Results and discussion

Figure 2 presents a numerical evaluation of LF-based solar cells with an underlying substrate. The enhancement of the relative absorption of LF-arrays compared with undecorated thin film and an optimized nanopillar array is evident. LF-based solar cell exhibits a power conversion efficiency that is 45% higher than that of an optimized nanopillar-based cell. We suggest that the enhanced light absorption of the LF-arrays is due to the coupled effect of light trapping inside the arrays combined with light concentration of each one of the LFs in the array (a single LF is actually a light-cone, a known non-imaging light concentrator). Fabrication of silicon light-funnel arrays using low-cost processing techniques is also demonstrated.

## References

1. Shalev, G., Schmitt, S. W., Embrechts, H., Brönstrup, G. & Christiansen, S. Enhanced photovoltaics inspired by the *fovea centralis*. *Sci. Rep.* **5**, 8570 (2015).

**Figure1.** Light-funnel array. (a) Simulated LF array. (b) and (c) silicon LF arrays (from ref.<sup>1</sup>).

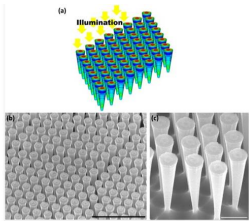
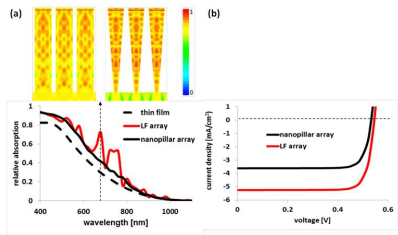


Figure 1.jpg



**Figure 2.** Absorption enhancement in LF-based photovoltaic cells. (a) Relative absorption of thin film, nanopillar array and LF array. The height is 2.2  $\mu\text{m}$  (including a 200 nm substrate). A 50 nm antireflection coating is considered. The array period is 500 nm. The diameter of the nanopillar is 400 nm. The top diameter of the LF is 400 nm and the bottom diameter is 100 nm. **Top:** Normalized absorbed photon density in nanopillar and LF arrays at wavelength 680 nm (marked in dashed arrow). (b) Simulated current-voltage curves under solar illumination (AM1.5 Global) for nanopillar and LF based solar cells. The curves correspond to the relative absorption in (a).

Figure 2.jpg

References

1. Shalev, G., Schmitt, S. W., Embrechts, H., Brönstrup, G. & Christiansen, S. Enhanced photovoltaics inspired by the fovea centralis. *Sci. Rep.* **5**, 8570 (2015).

Figure 3.jpg

## Point Defect-Passivated MoS<sub>2</sub> Nanosheet-Based High Performance Piezoelectric Nanogenerator

---

Wednesday, 18th October - 14:47 - Nanotechnology for environment and energy - Auditorium - Oral - Abstract  
ID: 329

---

***Dr. Sang A Han<sup>1</sup>, Prof. Sang-Woo Kim<sup>1</sup>***

*1. Sungkyunkwan University*

The piezoelectric characteristics of two-dimensional materials are of great interest for high-performance piezoelectric potential applications. The CVD-based large-area monolayer MoS<sub>2</sub> is essential for practical applications. However, the CVD-based MoS<sub>2</sub> has the intrinsic defect of sulfur vacancies during the growth process, and these defects play an important role in screening the piezoelectric potential. So only small piezoelectric potential induced power output has been observed from the CVD-grown MoS<sub>2</sub>. Here we demonstrate a high performance piezoelectric nanogenerator using CVD-based monolayer MoS<sub>2</sub> nanosheet by an additional sulfur treatment process during the MoS<sub>2</sub> growth process. The measured piezoelectric coefficient ( $d_{11}$ ) of the CVD-grown large-area monolayer MoS<sub>2</sub> nanosheet is 3.73 pm V<sup>-1</sup> using lateral PFM methods, and it generates a peak power density of 0.8 mW, which is 10 times higher than that of the pristine monolayer MoS<sub>2</sub> nanosheet.

---

# Electron Beam-Induced Transformation of Cesium Lead Halide Perovskite Nanocrystals

---

Wednesday, 18th October - 15:04 - Nanotechnology for environment and energy - Auditorium - Oral - Abstract ID: 806

---

***Dr. Zhiya Dang<sup>1</sup>, Mr. Javad Shamsi<sup>1</sup>, Mr. Muhammad Imran<sup>1</sup>, Mr. Quinten Akkerman<sup>1</sup>, Dr. Giovanni Bertoni<sup>1</sup>, Dr. Rosaria Brescia<sup>1</sup>, Prof. Liberato Manna<sup>1</sup>***

*1. Istituto Italiano di Tecnologia (IIT) - Genova*

## Introduction

Halide lead perovskites have received widespread attention due to their remarkable performances in photovoltaics and optoelectronics. We investigate the electron beam-induced transformations of perovskite NCs, when irradiated by high energy electron beam in a transmission electron microscope (TEM) (Z. Dang et al. ACS Nano, 11 (2), 2017; Z. Dang et al. ACS Omega, 2 (9), 2017).

## Methods

The electron beam irradiation experiments were carried out in a 80/200 keV microscope (JEOL JEM-2200FS) equipped with a spherical aberration corrector (CEOS) for the objective lens and an in-column image filter ( $\Omega$ -type). A Gatan cryotransfer holder with liquid nitrogen cooling equipped with a Model 900 Smartset cold stage controller was used for observing the electron beam-induced transformation at temperatures from -180 to 90 °C.

## Results and Discussion

Upon irradiation, Br desorption occurs. Br loss is more significant at an incident electron energy of 80 keV than at 200 keV, indicating a radiolysis dominant process. (Fig 1(a)) In parallel with the Br loss,  $\text{Pb}^{2+}$  ions are reduced to  $\text{Pb}^0$  atoms. When temperature (T) is high (above -40°C), the  $\text{Pb}^0$  atoms aggregate into Pb nanoparticles at a rate that depends on the temperature. (see Fig 1(b)) Meanwhile the locally Pb deficient perovskite structure becomes progressively amorphous, while the surrounding perovskite structure is maintained.

When T is below -40°C the  $\text{Pb}^0$  diffusion is drastically reduced, no Pb nanoparticles were visible; instead, the nanosheets turned porous. (Fig 2) The porous structure is composed of CsBr, CsPb, and  $\text{PbBr}_2$  domains. (Fig 3)  $\text{PbBr}_2$  and CsBr domains further lose Br upon irradiation, leading to a higher Br loss at lower temperatures (below -40°C) (see Fig 4).

These findings suggest that caution should be taken in the characterization of halide perovskites involving radiation sources. When dealing with halide perovskites characterization using electron microscopy, increasing the incident electron energy of the microscope can largely improve the stability of the sample. An appropriate temperature range needs to be chosen for the specimen in order to minimize both Pb nanoparticle formation and structure decomposition. For instance, for 200 keV electrons in typical TEM imaging conditions, the optimum temperature is -40 °C.

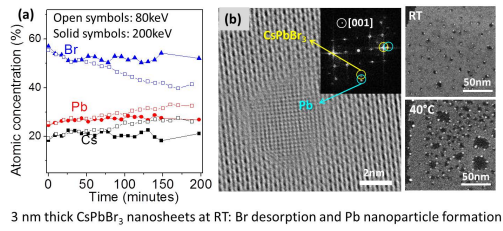


Fig 1.jpg

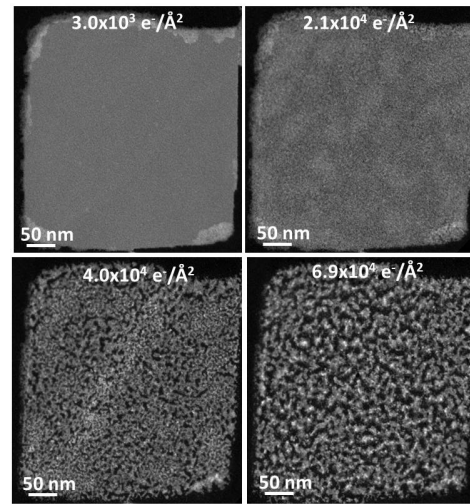


Fig 2.jpg

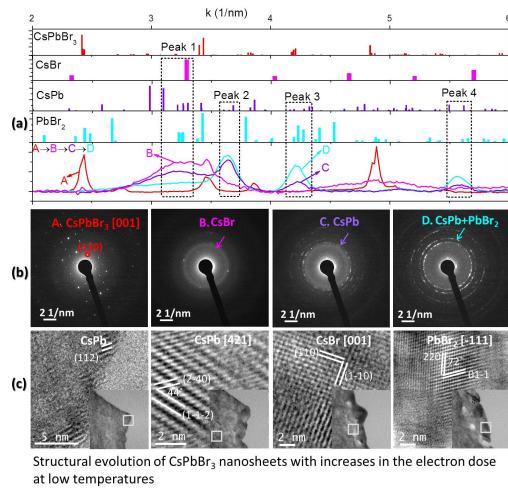


Fig 3.jpg

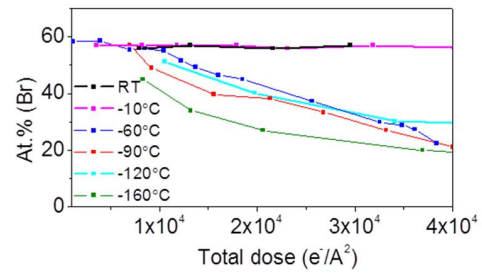


Fig 4.jpg

# Synthesis and characterization of Pd nanocatalyst at W based support for low temperature fuel cells application

Wednesday, 18th October - 15:21 - Nanotechnology for environment and energy - Auditorium - Oral - Abstract ID: 159

***Dr. Nevenka Elezovic<sup>1</sup>, Mrs. Mila Krstajic Pajic<sup>1</sup>, Dr. Piotr Zabinski<sup>2</sup>, Dr. Peter Ercius<sup>3</sup>, Prof. Velimir Radmilovic<sup>1</sup>, Prof. Nedeljko Krstajic<sup>1</sup>***

*1. University of Belgrade, 2. AGH University of Science and Technology, 3. LBNL University of California USA*

## Synthesis and characterization of Pd nanocatalyst at W based support for low temperature fuel cells application

N.R.Elezovic<sup>1</sup>, M.Krstajic Pajic<sup>2</sup>, P.Zabinski<sup>3</sup>, P. Ercius<sup>4</sup>, V.R.Radmilovic<sup>5,6</sup>, N.V. Krstajic<sup>6</sup>

<sup>1</sup>*Institute for Multidisciplinary Research, University of Belgrade, Kneza Viseslava 1, Belgrade, Serbia,*

<sup>2</sup>*Institute for Chemistry Technology and Metallurgy University of Belgrade, Serbia,*

<sup>3</sup>*AGH University of Science and Technology, Faculty of Non-Ferrous Metals, Al. Mickiewicza 30, 30-059 Krakow, Poland*

<sup>4</sup>*National Center for Electron Microscopy, LBNL University of California, Berkeley, CA, USA*

<sup>5</sup> *Serbian Academy of Sciences and Arts, Knez Mihailova 35, Belgrade, SERBIA*

<sup>6</sup>*Faculty of Technology and Metallurgy University of Belgrade*

### Introduction

Pt based nanoparticles supported on high surface area carbon (Vulcan XC 72 or Ketjen Black) are state of the art materials for low temperature fuel cells application. These catalysts have proper activity, however the stability is still a big challenge to overcome, to achieve durability and long life costs acceptable for practical purpose. The other big challenge is high oxygen reduction overpotential and slow kinetics, causing unacceptable power loss.

### Methods and Results

In this research we have synthesized novel Pd based nanocatalyst onto core-shell tungsten based support and characterized its activity and stability for oxygen reduction reaction. The support was prepared by polycondensation of resorcinol and formaldehyde from ammonium metatungstate in the presence cetyltrimethylammonium bromide surfactant. Pd nanocatalyst was synthesized by borohydride reduction. All materials were characterized by X-ray Diffraction, High Resolution Transmission Electron Microscopy, Electron Energy Loss Spectroscopy, X-ray Photoelectron Spectroscopy and electrochemical techniques: cyclic voltammetry and Accelerated Stability Testing (AST). The results confirmed high activity and stability of Pd nanocatalyst, compared to Pd/XC with the same noble metal loading. ORR activity expressed in terms of onset and half wave potential, as well as kinetic current density at 0.85 V vs RHE were comparable to Pt based catalysts. These results were assigned to the catalyst high surface area and consequently high noble metal utilization. AST proved high catalyst's durability, especially in alkaline electrolyte.

**Acknowledgements:** This work was supported by Ministry of Education, Science and Technological Development, Republic of Serbia, Contract No. 172054. The authors would like to acknowledge networking support by the COST Action MP1407.

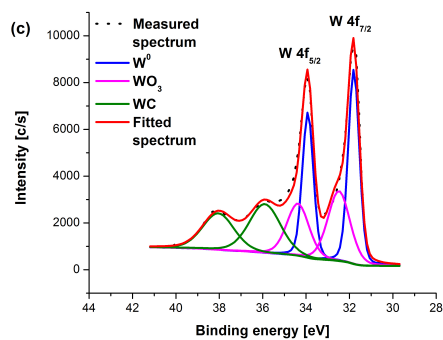


Fig.1.xps spectra of w wcwo3 w 4f line.jpg

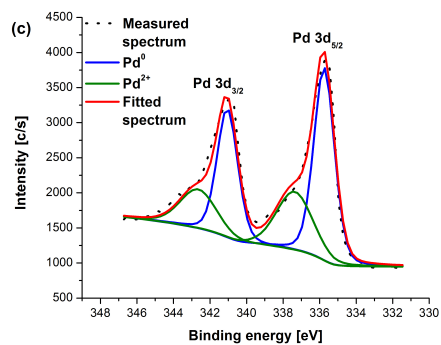


Fig.2.xps spectra of pdw wcwo3 pd 3d line.jpg

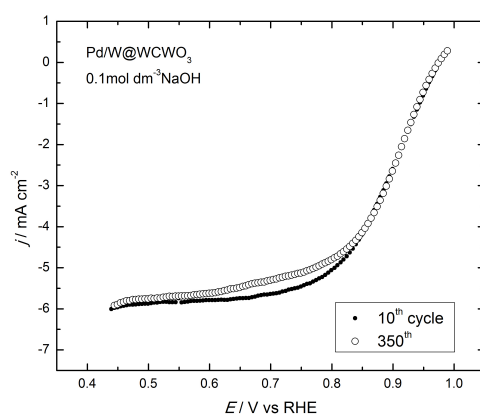


Fig.3polarization curves of pdw wcwo3 catalyst before and after asl test from 0 to 1.4 v vs rhe sweep rate 20 mv s-1 rotation rate 1600 rpm.jpg



# Effect of Mechanically-Induced Doping With 10 wt.% TiO<sub>2</sub> on the Hydrogen Uptake/Release Kinetics of Commercial MgH<sub>2</sub> Powders

Wednesday, 18th October - 15:38 - Nanotechnology for environment and energy - Auditorium - Oral - Abstract ID: 418

***Ms. shorouq ahmed*<sup>1</sup>**

*1. Kuwait Institute for Scientific Research (KISR)*

## INTRODUCTION

Hydrogen is an energy carrier holding tremendous promise as a clean energy option. In contrast to those traditional ways of storing hydrogen in gaseous and liquid states with their difficulties and unsafety issues, Mg and Mg-based systems have opened promising concept for storing hydrogen in a solid-state matter. However, MgH<sub>2</sub> system reveals serious drawbacks indexed by its slow hydrogenation / dehydrogenation kinetics and high thermal stability. The present work demonstrates has been addressed in part to improve the kinetics of hydrogen gas uptake/release for commercial MgH<sub>2</sub> powders by long term of reactive ball milling (RBM) time .

## EXPERIMENTAL

Sol-gel technique was used to prepare anatase phase of TiO<sub>2</sub> nanoparticles, used in the present work as catalytic agent for improving the hydrogenation / dehydrogenation kinetics of MgH<sub>2</sub> powders. For the purpose of the present study, certain amount (5g) of commercial-MgH<sub>2</sub> powders was balanced inside a helium gas atmosphere-glove box and then sealed together with forty hardened steel balls into a hardened steel vial . The vial was then filled with 50 bar of H<sub>2</sub> gas and mounted on a high-energy ball mill operated at 250rpm. The RBM process was halted after selected time to take samples for the vial inside the glove box. The as-ball milled MgH<sub>2</sub> powders obtained after 200h of RBM time was doped with 10 wt.% TiO<sub>2</sub> nanoparticles and then ball-milled for 50h under hydrogen gas atmosphere. samples were characterized by means of XRD, FE-HRTEM/STEM/EDS, and FE-SEM/EDS. The thermal stability were investigated by DSC at different heating rates.

## RESULTS AND DISCUSSION

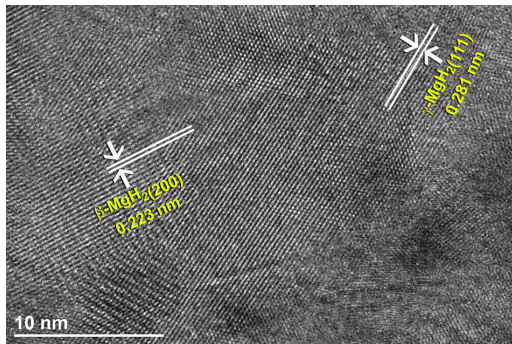
*Figures 1 presents the FE-HRTEM image of MgH<sub>2</sub> powders obtained after 200h of RBM.*

*Figure 2 displays the STEM (a) together with the EDS elemental mapping of Mg (b) and Ti(c) for MgH<sub>2</sub> powders milled for 200h and then ball milled with 10wt.% of TiO<sub>2</sub> nanopowders for 50h.*

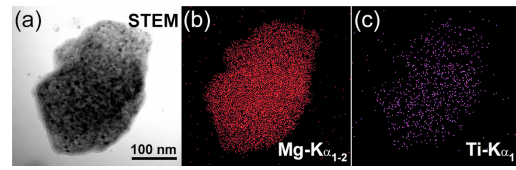
*Fig. 2(a) STEM of nanocomposite MgH<sub>2</sub>/10 wt. % TiO<sub>2</sub> powders obtained after 50h of RBM.*

*Fig. 3 Cycle-life-time examined at 275°C for nanocomposite MgH<sub>2</sub>/10wt.*

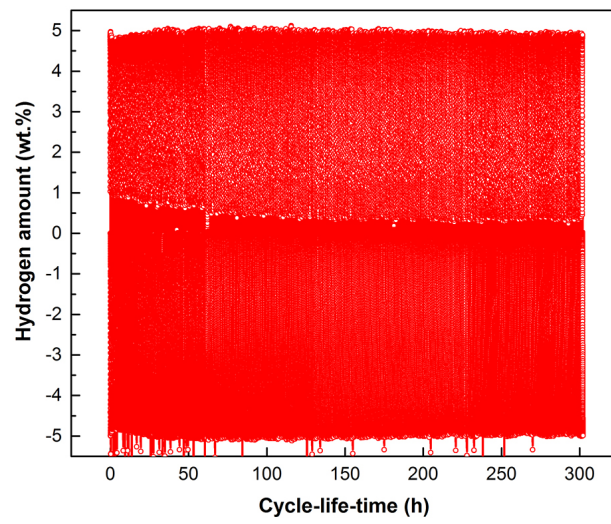
Nano composite MgH<sub>2</sub>/10 wt.% TiO<sub>2</sub> powders revealed excellent cycle-life- time extended up to 300h at moderate temperature (275°C) with hydrogen storage capacity of 5.17wt.% H<sub>2</sub>.



Nano technology 1.jpg



Nano technology2.jpg



Nano technology3.jpg

## Carbon nanofibers: A new adsorbent for Au (III)

Wednesday, 18th October - 15:55 - Nanotechnology for environment and energy - Auditorium - Oral - Abstract  
ID: 170

***Dr. Irene Garcia Diaz<sup>1</sup>, Dr. Felix Antonio Lopez<sup>2</sup>, Dr. Francisco José Alguacil<sup>2</sup>***

*1. CSIC, 2. National Center for Metallurgical Research, CSIC*

### Introduction:

The presence of metal in industrial effluent is one of the most crucial preoccupations nowadays due to the adverse environmental effect. Some of this metal could be considered valuables. So the effluent treatment before final discharge to recover and/or eliminate the metals is necessary [1].

Adsorption is a high efficiency, cost-effectiveness and easily handling method to recover metals from effluent liquids [2]. Currently are emerging new adsorbent nanomaterials. Among nanomaterials carbon nanofibers (CNF) show a great potential to be efficient adsorbents for the adsorption of all kinds of metal ions [3], especially heavy metals ions, such as gold, one of the most precious metals in the world.

The aim was to establish the adequate conditions for achieving gold adsorption by carbon nanofibers.

### Methods:

Batch adsorption and desorption experiments were carried out in a glass reactor provided or mechanical shaking. The gold was determined by AAS.

$$\%Au_{ad} = [(C_o - C_e)/C_e] \times 100$$

$C_e$  (mg Au L<sup>-1</sup>) in solution.

Adsorption parameters investigated were stirring speed, temperature, HCl, CNF and Au(III) concentration.

### Result and discussion:

Experimental result shows that it is possible to use CNF to recover Au(III) in effluent liquid at HCl medium. Figure 1 shows the effect of contact time on the gold adsorption, at 5 min over the 94% of total sorption has been occurred, and reach a maximum between 30-60 min, indicating that the sorption is a rapid process. The involved reaction could be:

#### a) Direct reduction



#### b) Reduction via $AuCl_2^-$



CNF is the electron donor

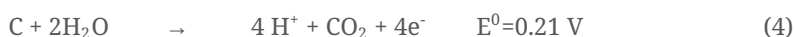


Figure 2 shows the gold particles.

#### Reference:

- 1.- D. de Agreda, I. García-Díaz, F.A. López, F.J Alguacil. (2011). Revista Metalurgia, 47(2), 146-168
- 2.- Y.C. Sharma, V. Srivastava, V.K. Singh, S.N. Kaul, C.H. Weng. (2009). Environmental Technology, 30 (6), 583-609
- 3.- X. Li, S. Chen, X. Fan, X. Quan, F. Tan, Y. Zhang, J. Gao. (2015). Journal of Colloid and Interface Science, 447,120-127

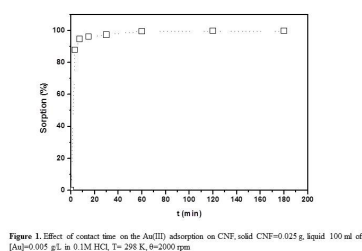


Figure 1.jpg

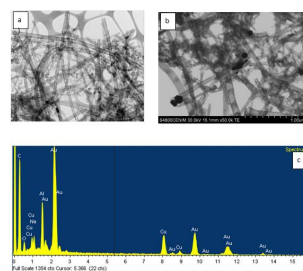


Figure 2.jpg

---

## On the interaction of TEMPO radicals with gold clusters

---

Wednesday, 18th October - 16:40 - Nanophotonics, optics and plasmonics - Room 1 - Oral - Abstract ID: 780

---

***Dr. Carolina Aliaga<sup>1</sup>, Dr. Marcos Rezende<sup>2</sup>, Ms. Camila Pastene<sup>2</sup>***

*1. Universidad de Santiago de Chile / Centro para el Desarrollo de la Nanociencia y la Nanotecnología, 2. Universidad de Santiago de Chile*

The effectiveness of radicals as fluorescence quenchers of nanostructures has been widely described. Gold nanoclusters (AuNCs) have shown to be highly fluorescent, photostable and versatile in their capping functional group employed to provide their bio-compatibility when compared to organic fluorescent dyes.

In an attempt to describe the interaction of a free radical with a nanoparticle, by using EPR such interaction was proposed as a “strong adsorption” when 4-aminoTEMPO radical was exposed to gold nanoparticles, suggesting that the radical adsorbs flat parallel to the metal surface<sup>1</sup>. In a more recent publication the quenching ability of AuNC by the 4-aminoTEMPO was confirmed with Stern-Volmer plots that were taken as indications of a direct binding between the nitroxyl radical and the metallic surface through the oxygen atom<sup>2</sup>. If this binding exists, it should occur for TEMPO itself, a fact which was not observed in another study on the interaction of nitroxide radicals with quantum dots.<sup>3</sup>

In the present study we employed a series of nitroxides among them 4-hydroxy- and 4-carboxyTEMPO radicals to quench the fluorescence of the AuNC and recorded their corresponding EPR spectra under the same quenching conditions. We observed that EPR signal intensities and shapes did not change. We also performed reactivity studies, confirming that when a hydrogen donor such as Trolox is exposed to AuNC-nitroxide, observing that the nitroxide moieties react with the same rate constant as in homogeneous phase.

SEM and TEM imagery, and microcalorimetry were also performed.

1 L. Zhang and E. Wang, *Nano Today*, 2014, **9**, 132–157.

2 C.-P. Liu, T.-H. Wu, C.-Y. Liu, H.-J. Cheng and S.-Y. Lin, *J. Mater. Chem. B*, 2015, **3**, 191–197.

3 J. C. Scaiano, M. Laferrière, R. E. Galian, V. Maurel and P. Billone, *Phys. Status Solidi Appl. Mater. Sci.*, 2006, **203**, 1337–1343.

# Fluorescence enhancement via excitation of bright and dark modes in 2D plasmonic nanostructures

Wednesday, 18th October - 16:57 - Nanophotonics, optics and plasmonics - Room 1 - Oral - Abstract ID: 600

**Mr. Alexey Shaymanov<sup>1</sup>, Mr. Igor Nechepurenko<sup>2</sup>, Mr. Alexander Baburin<sup>2</sup>, Mr. Kirill Khabarov<sup>1</sup>, Mr. Elena Ryzhova<sup>2</sup>, Mr. Alexander Dorofeenko<sup>1</sup>, Dr. Peter Tananaev<sup>1</sup>, Dr. George Yankovskij<sup>1</sup>, Dr. Ilya Rodionov<sup>2</sup>, Dr. Alexander Baryshev<sup>1</sup>**

*1. All-Russia Research Institute of Automatics, 2. Bauman Moscow State Technical University*

## Introduction

For the last decade, noble metal nanostructures are of the most studied ones, where light coupling to plasmonic modes of single nanoparticles and their periodic arrangement is under study. It is known that plasmonic lattices support so-called dark non-radiative modes of the higher Q-factor than that of the radiative (bright) modes. Indeed, such plasmonic structures are of interest for nanolasers [1,2] operating in the bright and dark modes' regimes.

## Methods

In this work, we experimentally studied 2D arrays of nanodisks having different periods embedded in a dye-doped polymer waveguiding layer (Rhodamin 101–Su8). The structural parameters of the samples were chosen so that to spectrally overlap the fluorescence spectrum with their optical resonances. For the fabricated dye-doped polymer waveguiding layer, the optical gain of 10–20 cm<sup>-1</sup> was measured by means of the variable stripe length method [3]. The samples have been studied for their optical responses, including measurement of the fluorescence lifetime, at excitation by pulse laser radiation.

## Results and Discussion

Our studies showed that the optical spectra of the samples exhibit three main features: a waveguide mode, grating localized plasmon resonance and non-radiative (dark) modes. By their intrinsic nature, the dark mode is not observed in transmission or reflection spectra of the samples. However, the fluorescence of Rhodamin 101 in the waveguiding layer led to excitation and visualization of the dark modes. Moreover, the fluorescence intensity for wavelengths corresponding to the dark modes was found to increase by one order of magnitude as compared with the intensity of the single dye-doped polymer layer at the same wavelengths. Note, also, that the enhancement due to the dark modes was larger than that of the waveguide mode and the mode associated with grating localized plasmon resonance. Studies on the fluorescence lifetimes showed that they became somewhat longer for the fluorescence at the dark modes' wavelengths. We believe that our results should prove useful for understanding and optimizing the nanolasers.

[1] Oulton R.F et al. (2009) Nature 461: 629–632.

[2] Hakala T.K. et al. (2017) Nature communications. T.8. C. 13687.

[3] Shaklee K.L., Leheny R.F. (1971) AppliedPhysicsLetters. T.18. №.11. C. 475-477.

# Plasmonic Enhanced Upconversion Nanostructure for Anti-counterfeit Devices

Wednesday, 18th October - 17:14 - Nanophotonics, optics and plasmonics - Room 1 - Oral - Abstract ID: 623

**Mrs. KISUN PARK<sup>1</sup>, Dr. Ho Seong Jang<sup>1</sup>, Dr. Il Ki Han<sup>1</sup>, Prof. Dongjin Byun<sup>2</sup>, Dr. Hyungduk Ko<sup>1</sup>**

**1. Korea Institute of Science and Technology, 2. Korea university**

Anti-counterfeit (AC) technologies developed and achieved with basing on information technology (IT), such as radio-frequency identification (RFID) chips, or Quick Response codes (QR-code). However, IT based AC technologies are essential to connect on communication system, and should accept the intrusion of privacy. Considering the growing demand for user-tailored and personalized security, we applied plasmonic enhanced upconversion(UC) nanostructure, pMUM(plasmonic Metal /UC nanoparticles/Metal film), to AC technologies.

The structure of pMUM with noble metal, Silver (Ag), shows great enhancement of UC luminescence (UCL), which emitting visible light via absorbing IR(980nm) ray, whereas UM (UC nanoparticles/Metal film) structure is deprived of luminescence from Ag film because of quenching effect. Taking advantages of the each characteristic of structure, we designed the AC system with pMUM structure which luminesce green light from UC particles while illuminating IR and when it destruct as UM structure, make it unable to find luminescence. The destruction and separation of pM from the nano-scaled structure could easily performed with scotch tape as Figure 1(a), and to avoid revert of AC system after tape detachment, the system made to flow in pollutant such as liquid PDMS to gap between detached tape and substrate. This AC system could alert the seal broken of cases or envelops and could be used as protection seal to obstruct the bottle abuse in such as counterfeit medications.

We adopted randomized Ag nanowires and Ag particles on pMUM structure as pM for the great enhancement of UCL, and several patterning steps are attempted to encode the real pattern to advance the security level. Luminescence enhanced with high security level of AC system will be reported on conference.

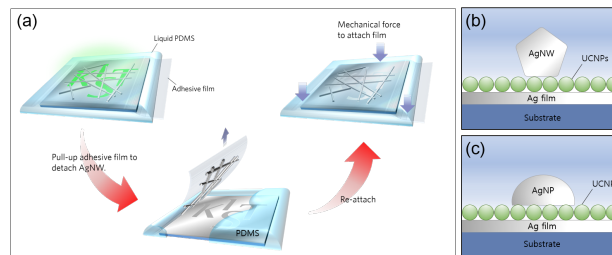


Figure.png

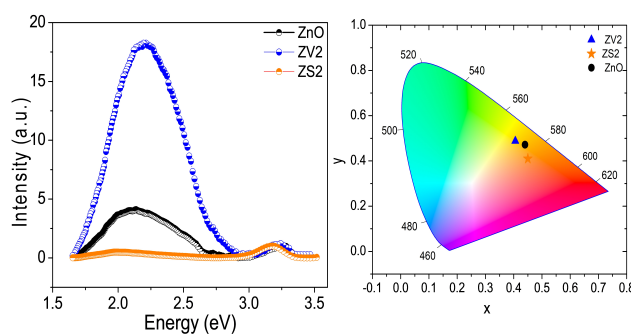
# Suppression and Enhancement of Deep Level Emission of ZnO on Si<sup>4+</sup> & V<sup>5+</sup> substitution

Wednesday, 18th October - 17:31 - Nanophotonics, optics and plasmonics - Room 1 - Oral - Abstract ID: 141

***Ms. Tulika Srivastava<sup>1</sup>, Mr. Gaurav Bajpai<sup>1</sup>, Dr. Somaditya Sen<sup>1</sup>***

*1. Indian Institute of Technology, Indore*

ZnO possess a wide range of tunable properties depending on the type and concentration of dopant. Defects in ZnO due to doped aliovalent ions can generate certain functionalities. Such defects in the lattice do not deteriorate the material properties but actually modifies the material towards infinite number of possibilities. Defects like oxygen vacancies play a significant role in photocatalytic and sensing applications. Depending upon the functionality, defect state of ZnO can be modified by suitable doping. Amount and nature of different dopant has different effect on defect state of ZnO. It depends upon the ionic radii, valence state, chemical stability etc. of the ion doped. Two samples with two different dopant i.e., silicon and vanadium, Zn<sub>1-x</sub>Si<sub>x</sub>O and Zn<sub>1-x</sub>V<sub>x</sub>O, for x=0 & 0.020, were synthesized using sol-gel method (a citric acid-glycerol route) followed by solid state sintering. A comparison of their optical properties, photoluminescence and Uv-Vis spectroscopy, with pure ZnO was studied at room temperature. Silicon doping drastically reduces whereas vanadium doping enhances the green emission as compared with pure ZnO. Suppression and enhancement of defect levels (DLE) is rationalized by the effects of extra charge present on Si<sup>4+</sup> & V<sup>5+</sup> (in comparison to Zn<sup>2+</sup>) and formation of new hybrid state (V3d O2p) within bandgap. Reduction of defects in Zn<sub>1-x</sub>Si<sub>x</sub>O makes it suitable material for opto-electronics application whereas enhancement in defects in Zn<sub>1-x</sub>V<sub>x</sub>O makes it suitable material for photocatalytic as well as gas sensing application.



Photoluminescence spectra and chromaticity diagram of zno zs2 and zv2.jpg



# On-chip Synthesis of Nanoporous Silver Microstructures (np-AgMSs) as Mesoporous Materials for SERS Substrate Application.

Wednesday, 18th October - 17:48 - Nanophotonics, optics and plasmonics - Room 1 - Oral - Abstract ID: 559

Ms. Duangtip Lawanstien<sup>1</sup>, Dr. Kanet Wongravee<sup>1</sup>, Dr. Mopichar Srisa-art<sup>1</sup>

1. Chulalongkorn university

Sensitivity and reproducibility of SERS detection were strongly related to the quality of hotspots. Mesoporous materials provide high quality hotspots compared to normal nano colloids because the size of hotspots is constant unlike dynamic hotspots that generated from electrostatic interaction of nano colloids. In this work nanoporous Ag microstructures (np-AgMSs) as mesoporous materials were synthesized using a template method in a microfluidic system. Using miniaturized flow-based system, mass and heat transfer are improved. Consequently, the growth of particles was fast and more reproducible compared to batch synthesis. A flow focusing microfluidic device composing of 3 inlets and 1 outlet was used. The synthesis started with fabrication of AgCl templates. A soluble complex of  $[\text{Ag}(\text{NH}_3)_2]^+$  was pre-prepared off-chip by mixing 0.1 M  $\text{AgNO}_3$  with 0.15 M  $\text{NH}_4\text{OH}$ . The  $[\text{Ag}(\text{NH}_3)_2]^+$  solution was pumped through the middle inlet or central flow, while 0.2 M  $\text{NaCl}$  solution was delivered through the side inlets or side flows (Fig.1). When both solutions were mixed,  $\text{Cl}^-$  induced precipitation of  $[\text{Ag}(\text{NH}_3)_2]^+$  was occurred. AgCl particles were instantly formed in the middle of microchannel (Fig.2). Effect of reactant concentration was studied by simply changing input reactant flow rates. The results showed that the concentration of reactants directly affected the morphology of AgCl templates. By changing the input flow rate of reactants systematically, four different morphologies of fabricated AgCl including cubic, tetrahedral, tripod and tetrapod were observed (Fig. 3). Particle size was in the range of 3-6  $\mu\text{m}$  which was easily observed under microscope. The obtained AgCl templates were subsequently reduced using  $\text{NaBH}_4$  to form np-AgMSs. The AgCl templates and np-AgMSs were characterized using SEM-EDS. After reduction with  $\text{NaBH}_4$ , structures of the parent AgCl could be retained (Fig. 4). SEM results showed that the interconnected grain size was found to be in the range of 40-65 nm. Finally, the np-AgMSs were tested as SERS substrates using p-aminothiophenol. It was found that each np-AgMS can be used as a highly sensitive single particle SERS substrate for the detection of p-aminothiophenol.

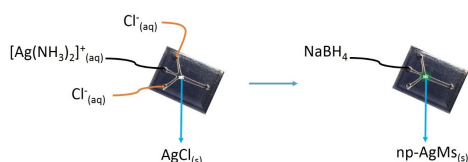


Fig. 1.jpg

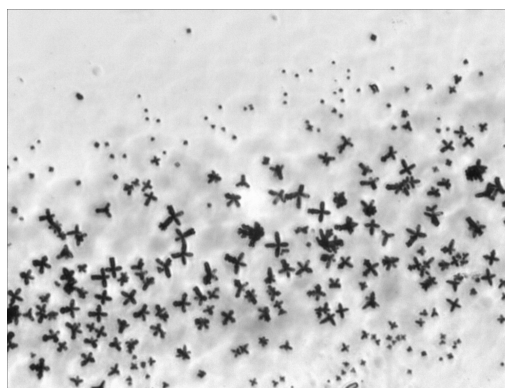


Fig. 2.jpg

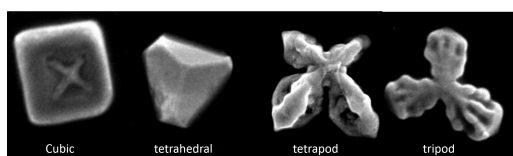


Fig. 3.jpg

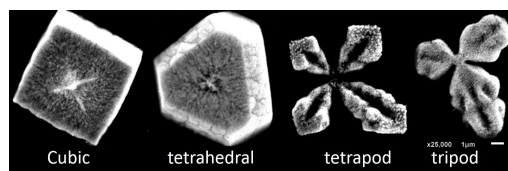


Fig. 4.jpg

---

## Conducting Polymer Nanospheres of High Electrochemical Activity – Synthesis and Sensor Applications

---

Wednesday, 18th October - 18:05 - Nanophotonics, optics and plasmonics - Room 1 - Oral - Abstract ID: 222

---

***Prof. Agata Michalska<sup>1</sup>, Prof. Krzysztof Maksymiuk<sup>1</sup>***

*1. University of Warsaw, Department of Chemistry*

Nanostructures of conducting polymers draw significant research attention, with a special emphasis on applications<sup>1</sup>. However, the methods for conducting polymer nanoparticle synthesis often require application of matrices. As a consequence the surface of resulting nanoparticles is compromised – the charge and/or ion exchange between nanoparticles and environment is hindered.

We propose a novel, alternative synthetic approach - template-free method, that yields nanoparticles of narrow size distribution and high electrochemical activity due to unblocked surface<sup>2</sup>. The method takes advantage of polymeric microparticles (e.g. polyacrylate or poly(vinyl chloride)) to deliver monomer of future conducting polymer to the polymerization reaction, oxidized – positively charged nanoparticles of polypyrrole or poly(3,4-ethylenedioxythiophene) form stable suspension in solution. The nanospheres synthesis conditions can be modified to functionalize particles e.g. by incorporation of fluorescent dyes.

The high electrochemical activity of obtained conducting polymer nanospheres: unblocked, reactive, surface and optionally presence of dyes opens novel possibilities of their application to improve existing or proposes novel electrochemical or optoelectronic devices and sensors. Conducting polymers can be used either as layers formed from nanoparticles e.g. by casting or spraying or in suspension. The source of analytical signal can be either change in electrochemical properties of the nanoparticles or change of the emission of dye embedded in the nanoparticles. To highlight the benefits of herein described method of conducting polymer nanoparticles synthesis, the following model systems have been tested:

(i) optical readout of conducting polymer oxidation state change: the change of solution redox potential or alteration of potential applied to the layer of nanoparticles can be observed as modulation of emission of fluorescent dye introduced to nanoparticles.

(ii) electrochemical sensors benefiting from high electrical conductivity of layers prepared from nanoparticles: e.g. ion-selective electrodes where nanoparticles have been used to obtain electrical leads and transducers, resulting in improved sensors.

### References

1. Yoon, H.; Choi, M.; Lee, K. J.; Jang, J. *Macromol.Res.*, **2008**, 16, 85
2. Kłucinska, K.; Jaworska, E.; Gryczan, P.; Maksymiuk, K.; Michalska A. *Chem.Comm.*, **2015**, 51, 12645

# Band edge corrections of semiconductor alloys for buffers nano-materials based solar cells

Wednesday, 18th October - 18:22 - Nanophotonics, optics and plasmonics - Room 1 - Oral - Abstract ID: 486

***Dr. OUARAB Nouredine***<sup>1</sup>

*1. Semiconductor Technology Research Center for Energetic-(CRTSE), 02, Bd Frantz Fanon Algiers, BP N° 140, Algeria*

Electronic and optical properties of  $\text{FeS}_{2-x}\text{A}_x$  alloys based on iron pyrite with (A=O, P, Cl and Se) are performed by using full potential linearized augmented plane wave method (FP-LAPW). Band gap energies have been calculated by using Tran Blaha modified Becke-Johnson (TB-mBJ) potentials in LDA approach<sup>[1]</sup>. The corrected positions related to valence band maximum (VBM) and conduction band minimum (CBM) have been evaluated by many-body perturbation theory in the GW approximation. The results given by using 3d eigen-energies performed from DFT+U are hopeful for GW quasi-particles approach to assess with great precision of the electron affinity and ionization potentials<sup>[2]</sup> of the studied alloys. The obtained values of internal physical parameters can help devices modeling to simulate the solar cell conversion efficiency<sup>[3]</sup>. Oxygen and phosphor alloyed  $\text{FeS}_2$  present p-type conductivity with variable electron affinities, which will be used as rear CZTS contact. The lattice parameters are further decreased with increase of O, P concentrations inducing that increase in band gap to 1.49 eV. However, chloride and selenium alloyed iron pyrite show n-type conductivity with important optical properties (absorption coefficients  $\sim 10^6 \text{ cm}^{-1}$ ). The band gap of specified alloys can increase to 1.25 eV, which is hopeful for their possible insertions as buffer nano-materials based solar cells with CZTS.

## References

- [1] N. Ouarab et al, EU-PVSEC Proceedings N° 31 (2015) 131–135, DOI: 10.4229/EUPVSEC20152015-1BV.6.12.
- [2] N. Ouarab, M. Boumaour, Current Applied Physics 17 (2017) 1169–1180.
- [3] M. Boumaour, S. Sali, A. Bahfir, S. Kermadi, L. Zougar, N. Ouarab, A. Larabi, Journal of Electronic Materials 45 (2016) 422.

# Carbon nanomaterials: Adsorbents for organic contaminants in wastewater

Wednesday, 18th October - 16:40 - Nanotechnology for environment and energy - Room 2 - Oral - Abstract ID: 153

*Mrs. Ana Lopez Fernandez<sup>1</sup>, Dr. Irene Garcia Diaz<sup>1</sup>, Dr. Lorena Alcaraz<sup>1</sup>, Prof. Miguel Angel Casermeiro<sup>2</sup>, Dr. Félix López<sup>1</sup>*

*1. CSIC, 2. UCM University, Faculty of Pharmacy*

## Introduction

The level of environmental pollution in the environment is increasing daily due to the rapid urbanization and the continuous population world increasing. [1]. There have been numerous reports of a great variety of organic compounds being detected at low concentrations ( $\text{ng L}^{-1}$ ) in liquid effluent (water, wastewater, groundwater or even drinking water). These compounds appears as a new class of organic pollutants environmental (emerging contaminants), coming from pharmaceutical, personal care products, herbicides, dyes and organics compounds [2]. This emerging contaminant, such as alkyl-phenols, analgesic, antibiotic, antidepressant, antineoplastic, beta blocker, hormones/steroids can cause adverse health effects in humans and/or organism. Therefore is important to the society to protect water supplies from acute contamination, so an effective method to eliminate this environmental pollutant must be developed.

Adsorption is a method simplest and effective to remove pollutants in liquid effluent or wastewater. Carbon nanomaterials present great adsorption capacities for a huge spectrum of organic and inorganic compounds [3, 4]. Different structures of carbon nanomaterials are considered: carbon nanotubes (single or multiwalled nanotubes), platelet, fishbone, ribbon, carbon nanofibers etc., being their capacity adsorption different. This research shows a preliminary characterization of different nanomaterials which will be used as organic adsorbent agent.

## Materials and methods

Raman spectroscopy, FTIR, SEM, TEM, Z potential and AFM were used to characterize carbon nanomaterials studied: carboxylic multiwalled carbon nanotubes (c-MWCNT); multiwalled carbon nanotubes (MWCNT); activated carbon (AC); carbon nanofibers (CNF) and graphene oxide.

## Result and discussion

Figure 1 shows the variation of potential Z as a function of pH, both in aqueous solution and in  $10^{-3}$  M KCl solution. Table 1 shows the values of the isoelectric point for each nanomaterial. The morphological aspects of the studied nanomaterials observed by TEM is showed in Figure 2.

## References

- [1] Bao C., Fang C.L. (2012). Water Resource Management 26, 531–552.
- [2] Saxena G., Chandra R., Bharagava R.N. (2017). Reviews of environmental contamination and toxicology 240, 31-69.
- [3] Kyzas G.Z., Matis K.A. (2015). Journal of Molecular Liquids, 203, 159-168.
- [4] Zyzas G.Z., Fu J., Lazaridis N.K., Bikiaris D.N., Matis K.A. (2015). Journal of Molecular Liquids, 209, 87-93.

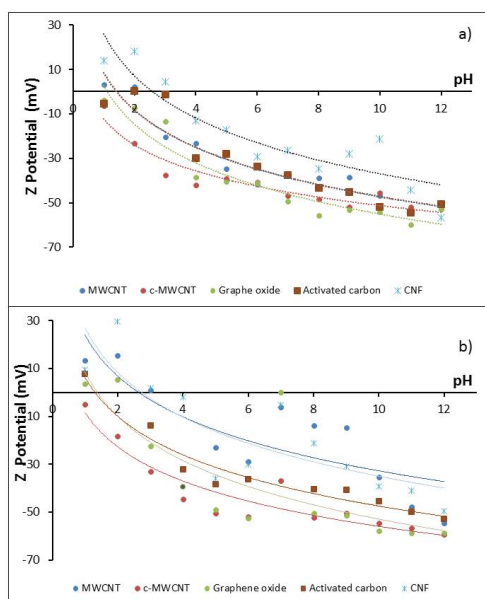


Figure 1.jpg

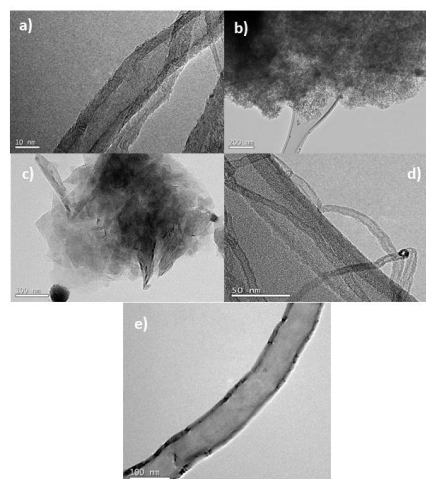


Figure 2.jpg

Nano-material	I <sub>H2O</sub>	I <sub>K10<sup>-3</sup> MKCl</sub>
c-MWCNT	0.30	0.67
Graphene oxide	1.16	1.38
MWCNT	1.40	2.65
AC	1.42	1.48
CNF	2.57	2.73

Table 1.png

---

## Determination of permeability of ultra-fine cupric oxide aerosol through military filters and protective filters

---

Wednesday, 18th October - 16:57 - Nanotechnology for environment and energy - Room 2 - Oral - Abstract ID: 620

---

***Ms. Eva Kellnerová<sup>1</sup>, Dr. Zbyněk Večeřa<sup>2</sup>, Prof. Josef Kellner<sup>1</sup>, Dr. Tomáš Zeman<sup>1</sup>, Dr. Josef Navrátil<sup>1</sup>***

*1. University of Defence Brno, 2. Institute of Analytical Chemistry of the Czech Academy of Sciences*

### Introduction

The paper evaluates the filtration and sorption efficiency of selected types of military combined filters and protective filters using the methodology and instrumentation introduced in the accredited laboratories of the Institute of Analytical Chemistry of the Czech Academy of Sciences.

### Methods

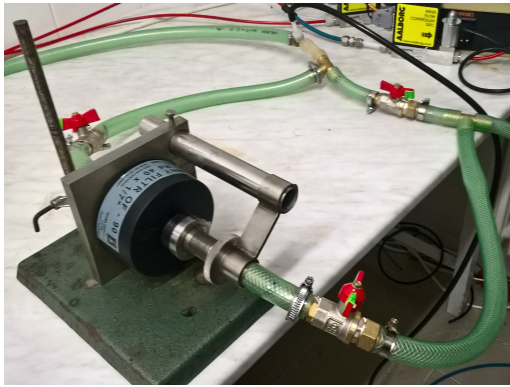
The testing was carried out with the use of ultra-fine aerosol containing cupric oxide nanoparticles ranging in size from 7.6 nm to 299.6 nm. Nanoparticles were generated in situ in a hot flow tubular reactor using the evaporation-oxidation-condensation technique. The resulting metal vapours were oxidised to cupric oxide after dilution with air. During the measurement, the aerosol flow rate was set to 96 l/min. The measurements of nanoparticles were carried out using a scanning mobility particle sizer before and after the passage through the filter and a specially developed sampling device at one level of concentration (total particle number concentration before entering the filters was approximately 750000 particles/cm<sup>3</sup>). Samples were obtained four times in five minute intervals (in 10,15,20 and 25 minutes).

### Results

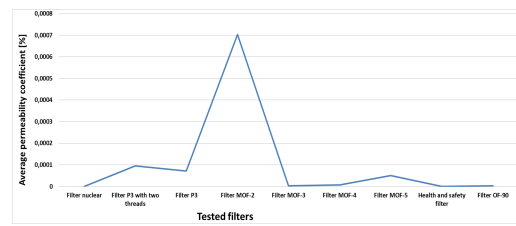
The basic parameters of permeability of ultra-fine aerosol passing through the tested material were evaluated, in particular particle size, mass and volume distribution, efficiency of nanoparticle capture by filter, nanoparticle penetration through filter and overall filtration efficiency.

### Discussion

The obtained measurement results have shown that the filtration efficiency over the entire measured range of nanoparticles was sufficient; however, it was different for particular particle sizes. The reason is probably the combination of surface and depth particle trapping mechanisms. The results of the total particle number concentration of the aerosol after the passage through the tested filters ranged from 0 to 6.59 particles/cm<sup>3</sup> (i.e. from 0 to 0.000871% of the original concentration). The results of the paper will be used for evaluating the quality of military protection filters used in the Armed Forces of the Czech Republic in military training and in the course of work of military formations at the specialized workplaces. The structure of filters used in the Fire Rescue Service is very similar to that of the military filters. The results, therefore, will also be used in the field of safety.



Sampling device.jpg



Average permeability coefficient of tested filters.png



# Enhancing the performance of water treatment polyethersulfone membranes using graphene materials

Wednesday, 18th October - 17:14 - Nanotechnology for environment and energy - Room 2 - Oral - Abstract ID: 598

***Prof. Ahmed Abdala***<sup>1</sup>

**1. Texas A&M University at Qatar**

Microfiltration and ultrafiltration polymeric membranes plays significant role in water treatment and water desalination pretreatment application. The performance of these membranes is measured by their flux, rejection of impurities such as hydrocarbon, microbial species, algae, ...etc, and resistance to inorganic, organic, and biofouling. In this presentation, we enhance the performance of polysulfone and ultrafiltration membranes by incorporation of small fractions (<1 wt.%) of using reduced graphene, graphene oxide, graphene-metal oxide nanocomposites, and amine functionalized graphene. Pure PES and PES mixed matrix membranes were fabricated by the phase inversion method. The surface of the developed membranes were characterized by contact angle measurement, AFM, SEM, and zeta potential measurements. The impact of the graphene material type and loading on porosity, pore size distribution, mechanical and thermal properties and is investigated. Moreover, the developed membranes are tested for removal of hydrocarbons and dyes from waste water and our results indicate that we can significantly enhance the performance of polymeric membranes using optimum loading of graphene based materials by simultaneously increasing flux, rejection, and fouling resistance.

Table 1: Effect of graphene loading on oil rejection of diesel from 100 ppm water diesel emulsion of PES MF membranes

Graphene Wt. %	Oil Rejection %	Residual Oil concentration ppm
0%	96.0%	4.0
0.10%	98.9%	1.1
0.25%	98.1%	1.9
0.50%	98.1%	1.9
1.00%	98.3%	1.7

Table 1 oil rejection.jpg

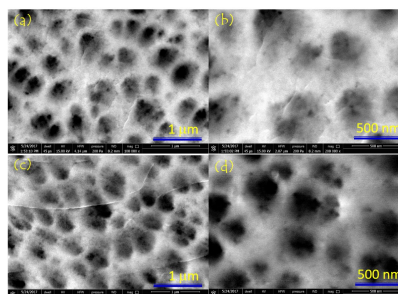


Figure 1: SEM images of PES microfiltration membrane with 0.25 wt.% of (a) and (b) graphene-TiO<sub>2</sub> nanocomposites and (c) and (d) amine-functionalized graphene.

Figure 1 sem images of pes graphene membranes.jpg

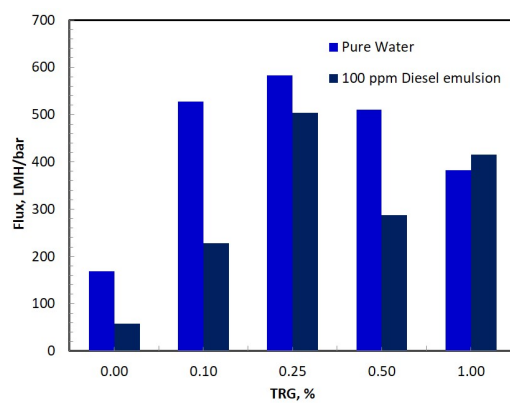


Figure 2: Pure water and diesel emulsion flux through PES with different loading of thermally reduced graphene

Figure 2 flux.jpg

# Controlling Hydrophilicity of Titanium Dioxide for Self-cleaning Surfaces

Wednesday, 18th October - 17:31 - Nanotechnology for environment and energy - Room 2 - Oral - Abstract ID: 199

***Mr. Abdullah Alkandary<sup>1</sup>, Dr. feras alzubi<sup>1</sup>***

*1. Kuwait Institute for Scientific Research*

## • Introduction

Titanium dioxide (TiO<sub>2</sub>) exhibits interesting properties when exposed to light. Since the 1960's, light-induced properties of TiO<sub>2</sub> were discovered and utilized such as electrochemical properties, photocatalytic purification, and hydrophilic properties. The prominence of TiO<sub>2</sub> as a hydrophilic coating is well established in different industries of which are fabrics, construction, windows, and solar panels. In this work, we apply a physical technique of nanofabrication that allows the controlling of the hydrophilicity of TiO<sub>2</sub>. The TiO<sub>2</sub> thin-films were deposited at different thicknesses using electron-beam physical vapor deposition (e-beam PVD) technique on quartz substrates. Surface topography of the TiO<sub>2</sub> thin-films were studied using atomic force microscopy (AFM) and investigation of hydrophilicity was conducted by water contact angle measurements. We have noticed a remarkable increase in surface hydrophilicity after applying thermal annealing on the as-deposited TiO<sub>2</sub> thin-film samples; with contact angle (CA) dropping from around 69° for as-deposited thin-films down to 20.2° for annealed thin-films.

## • Methods

Thin-films of TiO<sub>2</sub> were deposited using e-beam PVD in an ultra-high vacuum chamber (10<sup>-6</sup> torr) at thicknesses varying between 5nm and 60nm. The as-deposited samples were then thermally annealed to form nanostructures - in a thermal tube furnace at 800°C and under inert atmospheric pressure. The samples were characterized by AFM in contact mode to study surface topography of as-deposited thin-films and the annealed as well. In addition, deionized-water contact angle measurements were performed to evaluate surface hydrophilicity.

## • Results And Discussions

Figure 1 presents 2D and 3D topography images of the deposited 60nm TiO<sub>2</sub> thin-film. Figure 1 (a) and (b) show as-deposited, while Figure 1 (c) and (d) show the annealed samples; showing a slight change in the surface structure. The roughness value (RMS) decreased from (3.38 to 2.82 nm). The contact angle measurements illustrated in Figure 2 indicate a drastic decrease in average contact angle from 69.2° to 20.2°. Suggesting that the formation of TiO<sub>2</sub> nanostructures by thermal annealing of as-deposited TiO<sub>2</sub> thin-films result in a better hydrophilic surface. The other studied thicknesses followed a similar trend; and a thickness-dependent hydrophilicity behavior was noticed, allowing for the hydrophilicity of TiO<sub>2</sub> coated surfaces to be employed as desired.

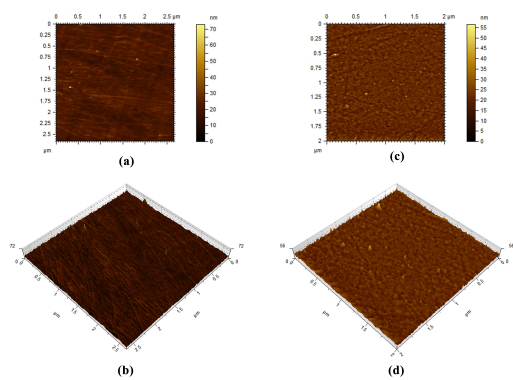


Figure 1 afm topography images of 60nm tio2 a as-deposited 2d b as-deposited 3d c annealed 2d d annealed 3d.jpg

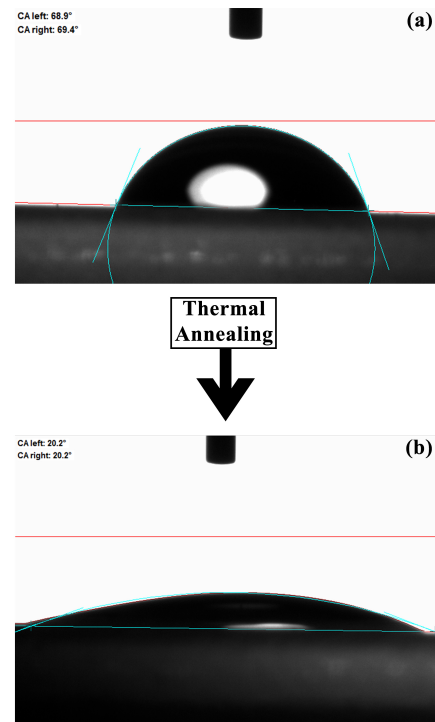


Figure 2 - contact angle measurements of tio2 60nm a as-deposited average ca 69.2 degrees and b after annealing average ca 20.2 degrees.jpg

---

# Synthesis, mechanistic studies and technological innovation of applying oxide nanomaterials in wastewater treatment by flotation

---

Wednesday, 18th October - 17:48 - Nanotechnology for environment and energy - Room 2 - Oral - Abstract ID: 813

---

***Prof. Cristina Covaliu<sup>1</sup>, Prof. Gigel Paraschiv<sup>1</sup>, Prof. Laura Toma<sup>2</sup>, Prof. Eugeniu Vasile<sup>3</sup>***

*1. University Politehnica of Bucharest, Faculty of Biotechnical Systems Engineering, 2. University politehnica of bucharest, 3. University Politehnica of Bucharest, Faculty of Applied Chemistry and Materials Science*

## **Introduction**

In the wastewater treatment by flotation technique, nanoparticles may act as surfactant molecules, being incorporated into surfactant-stabilised foams for several years.

The gas flotation process is divided in four main stages: generation of gas bubbles inside the liquid, occurrence of contact between gas bubbles and pollutants, adherence of pollutants to gas bubbles and the actual flotation of aggregates to the surface of the liquid where they form a foam that needs to be removed. A fifth stage can be added to this division, namely the use of surfactants to help the formation and stability foams formed by the gas-particle/oil aggregates. The paper is focused on the use of oxide nanoparticles as surfactants in the fifth stage of the flotation process to help the formation and stability of foams in wastewater treatments by air flotation.

## **Methods**

In this study, we investigate the application of nanomaterials as froth stabiliser in flotation and the experiments consisted in testing of two oxide nanomaterials for the removal of oil pollutant from wastewater.

Prior to the flotation experiments,  $\text{CuFe}_2\text{O}_4$  and  $\text{Fe}_3\text{O}_4$  nanomaterials were prepared by coprecipitation method. The experiments were done on a synthetic wastewater containing a concentration of oil of 25% in the presence and in the absence of  $\text{Fe}_3\text{O}_4$  and  $\text{CuFe}_2\text{O}_4$  nanomaterials. Dissolved air flotation system contained also 5% of anionic surfactants and 5 % of amphoteric surfactants.

## **Results and discussion**

Before testing their application in wastewater treatment by flotation, both oxides nanomaterials were structural and morphological characterized by XRD (Fig. 1a and b) and TEM analyses (Fig 2 a and b). In order to evaluate their potential of application in oil removal from wastewater by flotation were studied the following parameters such as: treatment efficiency [%] and the stability of froth.

The preliminary study of the influence of using  $\text{Fe}_3\text{O}_4$  or  $\text{CuFe}_2\text{O}_4$  nanomaterials in the wastewater treatment by flotation revealed that the main advantages were observed the increasing the stability of the foam containing the oil pollutant and the decreasing of the time needed for wastewater treatment.

For both ferrite nanoparicles ( $\text{CuFe}_2\text{O}_4$  and  $\text{Fe}_3\text{O}_4$ ) tested the wastewater treatment efficiency was 100 %.

---

## Structural and optical properties of SiC-SiO<sub>2</sub> nanocomposite thin films

---

Wednesday, 18th October - 18:05 - Nanotechnology for environment and energy - Room 2 - Oral - Abstract ID: 507

---

***Dr. isma bozetine<sup>1</sup>, Dr. Aissa Keffous<sup>2</sup>, Dr. Samira Kaci<sup>2</sup>, Mr. Menari Hamid<sup>3</sup>, Mr. Amar Manseri<sup>3</sup>***

***1. CRTSE, 2. CRTSE/CMSI, 3. CRTSE, 02 Bd Frantz Fanon B.P. 140 Alger 7 Merveilles, Algiers, Algérie***

This study deals with the deposition of thin films of a SiC-SiO<sub>2</sub> nanocomposite deposited on silicon and quartz substrates. The deposition is carried out by a co-sputtering RF magnetron 13.56 MHz, using two targets a polycrystalline 6H-SiC and sprigs of SiO<sub>2</sub>. In order to study the influence of the deposition time on the morphology, the structural and optical properties of the thin films produced, two series of samples were prepared, namely a series A with a 30 min deposition time and a series B of one hour duration. The samples were investigated using different characterization techniques such as Scanning Electron Microscope (SEM), X-ray Diffraction (DRX), Fourier Transform Infrared Spectroscopy (FTIR), Secondary Ion Mass Spectrometry (SIMS), X rays fluorescence (XRF) and Raman spectroscopy. The results obtained, reveal an optical gap varies between 1.4 and 2.4 eV depending on the thickness of the film; thus depending on the duration of deposition. The SIMS profile recorded the presence of oxygen (<sup>16</sup>O) on the surface, which the signal beneath the silicon signal (<sup>28</sup>Si) and carbon (<sup>12</sup>C) signals, which confirms that the oxide (SiO<sub>2</sub>) is the first material deposited at the interface film - substrate with an a-OSiC structure (Figs. 1a and 1b). The photoluminescence (PL) measurement exhibits two peaks, centred at 390 nm due to the oxide and at 416 nm due probably to the nanocrystals of SiC crystals, note that when the deposition time increases, the intensity of the PL drops drastically, result in agreement with dense and smooth film.

---

## N-DOPED TiO<sub>2</sub>/CdS NANOCOMPOSITE FILMS: SILAR SYNTHESIS, CHARACTERIZATION AND APPLICATION IN QUANTUM DOTS SOLAR CELL

---

Wednesday, 18th October - 18:22 - Nanotechnology for environment and energy - Room 2 - Oral - Abstract ID: 167

---

***Prof. Kristian Handoyo Sugiyarto<sup>1</sup>, Dr. Cahyorini Kusumawardani<sup>1</sup>, Prof. Anti Kolonial Prodjosantoso<sup>1</sup>***

*1. Yogyakarta State University*

The N-doped TiO<sub>2</sub>/CdS nanocomposite films have been prepared through a successive ionic layer adsorption and reaction (SILAR) method on the N-doped TiO<sub>2</sub> thin films with cadmium nitrate as Cd source and sodium sulphide as S precursor. The SILAR cycle was varied to study the CdS layer formation and its influence to the properties of resulted nanocomposite, i.e. 1, 5, 10, 20, and 50 cycles, respectively. The resulting materials were characterized using X-Ray Diffraction (XRD), UV/Vis Spectroscopy, FTIR Spectrophotometer, and Scanning Electron Microscopy (SEM). The result showed that the higher SILAR cycle resulted in a smaller CdS crystallite size and a higher band gap energy. The higher SILAR cycle was also provided the more intense response in visible light area. The prepared N-doped TiO<sub>2</sub>/CdS nanocomposite films were then applied in the quantum dots-sensitized solar cells (QDSSC) system. The solar cell performance test showed that there is an optimum cycle which results in a highest power conversion. The quantum dot solar cells based on N-doped TiO<sub>2</sub>/CdS nanocomposite prepared with 20 cycles provided the highest performance with overall efficiency of 8.3%. Thus, by varying the cycle number in the SILAR synthesis process, it is easy for tuning the nanocomposite properties that fulfill the requirements as sensitized-semiconductor material in the solar cell system.

**Keywords :** nanocomposite, SILAR method, quantum dots, N-doped TiO<sub>2</sub>, CdS, QDSSC

# Liposome-based Multifunctional glioblastoma-Targeted drug delivery

Wednesday, 18th October - 16:40 - Nanomedicine and nanobiotechnology - Auditorium - Oral - Abstract ID: 161

**Dr. Beatrice Formicola<sup>1</sup>, Dr. Lorena Passoni<sup>2</sup>, Prof. Michela Matteoli<sup>2</sup>, Dr. Maria Gregori<sup>1</sup>, Dr. Francesca Re<sup>1</sup>, Prof. Massimo Masserini<sup>1</sup>**

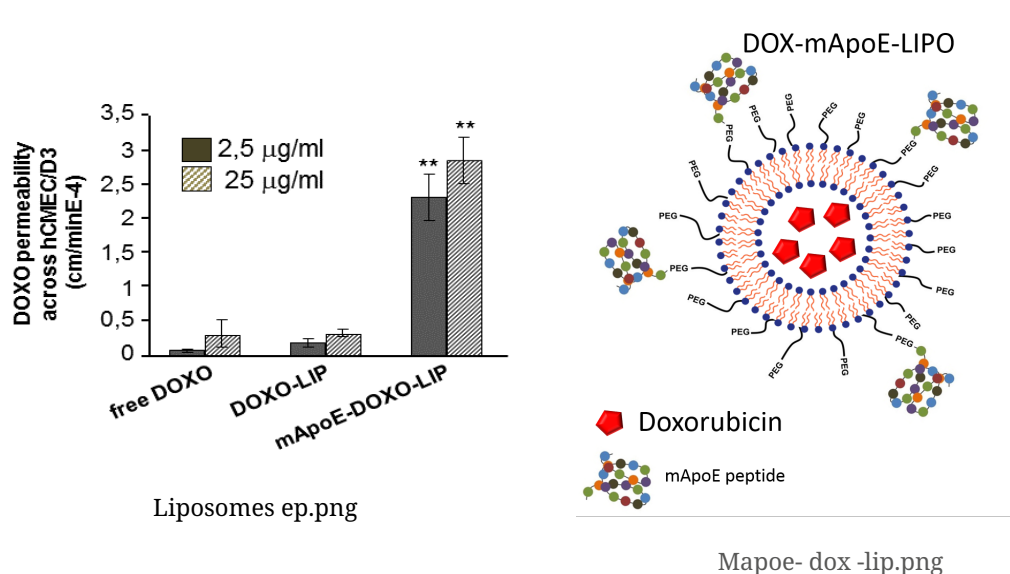
1. Università di Milano-Bicocca, 2. Istituto Clinico Humanitas

**Introduction:** Glioblastoma multiforme (GBM) is an aggressive and lethal brain tumor in humans with a median survival time of about 15 months after treatment. Doxorubicin (DOX) is a potent chemotherapeutic agent, but with severe side effects and inefficient blood-brain barrier (BBB) permeability. In this context, we developed multi-functionalized liposomes (LIP) for GBM therapy.

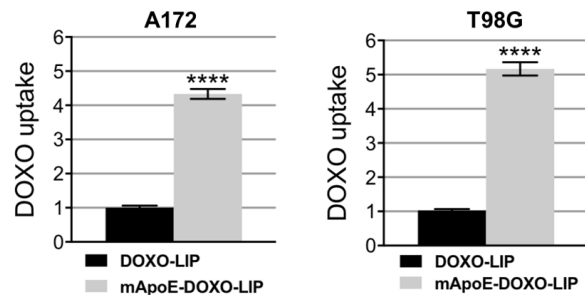
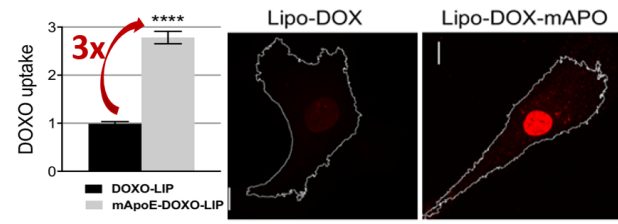
**METHODS:** LIP composed of Sphingomyelin, cholesterol (1:1, M/M) and 2.5mol% maleimide-PEG-lipid were prepared by extrusion procedure. DOX was incorporated in the LIP core by a transmembrane pH gradient. Free DOX was removed by gel filtration chromatography. To enhance the BBB permeability of DOX-LIP, a modified fragment of human Apolipoprotein E (mApoE, CWGLRKLRLRLR) was covalently attached on LIP surface by thiol-maleimide coupling. After characterization, the ability of mApoE-(DOX)-LIP to deliver DOX across the BBB was evaluated using an in vitro model made by hCMEC/D3 cells. Cytotoxicity of mApoE-(DOX)-LIP was evaluated by MTT test on hCMEC/D3 cells, GBM cell lines and GBM stem-like cells, alone or in co-culture with brain endothelial cells. In vivo biodistribution of mApoE-(DOX)-LIP and their co-localization with tumor cells were evaluated by radiochemical and fluorescent assays, respectively.

**RESULTS:** mApoE-(DOX)-LIP displayed a size of  $128 \pm 15$  nm, the DOX incorporation rate was  $95 \pm 3\%$ , the yield of mApoE coupling on LIP surface was  $91.48 \pm 2\%$ . The in vitro endothelial permeability of mApoE-(DOX)-LIP was 5-fold higher respect to DOXO-LIP. mApoE-(DOX)-LIP exerted their cytotoxicity on GBM cells, stem cells included, without affecting the endothelial cells viability. In vivo results showed that the DOX incorporation in mApoE-LIP reduces (-30%) liver and heart DOX accumulation, increases (4-fold) the amount of DOX in brain. Moreover, the in vivo co-localization between DOX and GBM cells was detected.

**DISCUSSION:** Our finding suggests that mApoE-(DOX)-LIP could be promising candidates GBM treatment.







Uptake gbm cells by confocal microscopy.png

# Alteration of temoporfin pharmacokinetics by $\beta$ -cyclodextrin derivatives

Wednesday, 18th October - 16:57 - Nanomedicine and nanobiotechnology - Auditorium - Oral - Abstract ID: 657

***Dr. Igor Yankovsky<sup>1</sup>, Mr. Ilya Yakavets<sup>2</sup>, Dr. Henri-Pierre Lassalle<sup>3</sup>, Dr. Lina Bezdetnaya<sup>3</sup>, Dr. Vladimir Zorin<sup>4</sup>***

*1. Department of Biophysics, Belarussian State University, 2. Department of Biophysics, Belarussian State University; Centre de Recherche en Automatique de Nancy, CNRS, Université de Lorraine; Institut de Cancérologie de Lorraine, 3. Centre de Recherche en Automatique de Nancy, CNRS, Université de Lorraine; Institut de Cancérologie de Lorraine, 4. Belarusian State University; International Sakharov Environmental Institute*

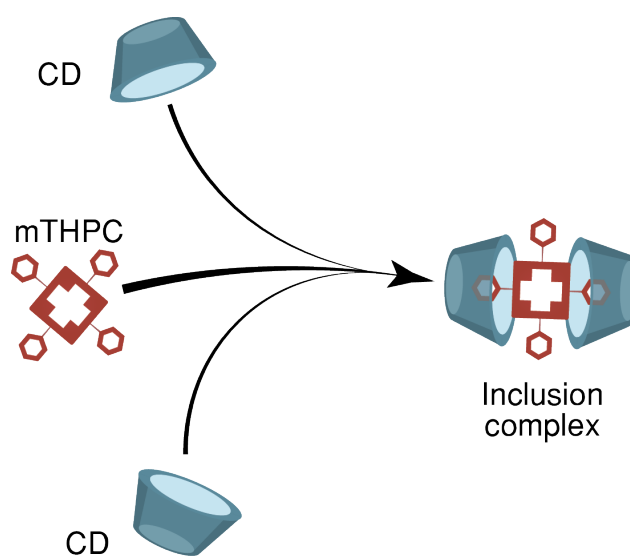
**Introduction.** The use of nanoscale delivery systems is the most promising way to improve the properties of new and already existing drugs. Due to their unique structure and properties  $\beta$ -cyclodextrin ( $\beta$ -CD) derivatives can be successfully used for nonpolar drug administration. Recently, in our laboratory it has been shown that  $\beta$ -CDs and meta-tetra(hydroxyphenyl)-chlorin (temoporfin, mTHPC) effectively form inclusion complexes [1-3]. It was demonstrated that the complexation of mTHPC with  $\beta$ -CDs results in a complete abolishment of mTHPC aggregation in aqueous solutions and significantly alters mTHPC distribution *in vitro* and *in vivo*. In the present study, we focused on the investigation of  $\beta$ -CDs influence on mTHPC pharmacokinetics in blood.

**Methods.** Inclusion complexes between  $\beta$ -CDs and mTHPC were formed using co-precipitation method. Effect of  $\beta$ -CDs on mTHPC interaction with blood was investigated by fluorescence spectroscopy, flow cytometry and fluorescence microscopy techniques.

**Results and Discussion.** Firstly, it was showed that  $\beta$ -CDs significantly accelerate mTHPC disaggregation in blood serum while co-administration of mTHPC with  $\beta$ -CDs completely abolishes photosensitizer aggregation. Secondly,  $\beta$ -CDs have a concentration-dependent effect on the processes of mTHPC distribution in blood. Thirdly,  $\beta$ -CDs increase diffusion movement of mTHPC molecules allowing to reach an equilibrium distribution much faster. Finally, flow cytometry data demonstrated that the presence of  $\beta$ -CDs significantly accelerate mTHPC accumulation in blood cells, especially in leukocytes. Thus,  $\beta$ -CDs can be successfully used to alter mTHPC behavior in the blood and these findings might have a potential relevance in the improvement of mTHPC-PDT.

**Acknowledgments:** This work was supported by the Institut de Cancérologie de Lorraine, French “Ligue Nationale contre le Cancer (CCIR-GE)”, Belarusian Republican Foundation for Fundamental Research (BRFFR) [grant numbers M16M-049 and M17MC-028]. We thank biolitec research GmbH (Jena, Germany) for providing us with mTHPC.

**References.** [1] Yankovsky, I., et al., 2016. European Journal of Pharmaceutical Sciences, 91, 172–182. [2] Yakavets, I., et al., V., 2017. Dyes and Pigments 137, 299–306. [3] Yakavets I., et al., 2017. International Journal of Pharmaceutics, 529, 568-575.



### **Inclusion complex formation**

Inclusion complex formation.png

---

# A Highly Promising Treatment Option for Glioblastoma Using Dual-Epitope Decorated Therapeutic Nanoparticles

---

Wednesday, 18th October - 17:14 - Nanomedicine and nanobiotechnology - Auditorium - Oral - Abstract ID: 805

---

***Dr. Sheikh Mohamed Mohamed<sup>1</sup>, Dr. Srivani Veerananarayanan<sup>1</sup>, Prof. Yasushi Sakamoto<sup>2</sup>, Prof. Toru Maekawa<sup>1</sup>, Prof. Sakthi Kumar D<sup>1</sup>***

*1. Toyo University, 2. Saitama Medical University*

## **Introduction:**

Brain tumors/cancer remains an unresolved challenge despite surgery, radio- and chemotherapy options, largely due to presence of physiological barriers, highly aggressive tumors, poor prognosis, and non-specific drug accumulation. Nanomedicine provides a window of hope with the promise of overcoming these hurdles by delivering the requisite therapeutic components to desired regions of brain, surpassing the physiological barrier, without causing any unwarranted side-effects.

## **Methods:**

Ribosome inactivating protein/quantum dots (QDs) loaded, hybrid solid-lipid nanoparticles (HSLNs) with dual, cancer and angiogenesis recognition ligands were developed for glioblastoma therapy and imaging. Intracranial glioma xenograft mice were used for intravenous administration of the nanoformulation and observations thereof.

## **Results:**

The nanoformulation exhibited excellent stability in aqueous suspension with a shelf life of more than a year. Drug loading efficacy was a commendable 66 % with a sustained release pattern. Nil toxicity was observed on intravenous administration to mice with the biochemical, hematological, histopathological, weight and behavioral parameters advocating the biocompatibility of HSLNs. The formulation exhibited extended blood circulation period and reduced hepatobiliary uptake. Dual-targeted QD-HSLNs successfully trespassed the blood brain barrier (BBB) and accumulated specifically in intracranial tumors, and were retained therein for approximately 72h. The HSLNs were found to diffuse across the fibrotic tissue and penetrated the deeper core of tumor. While mice in non-targeted and single targeted therapeutic versions succumbed to growing tumors within a month, the dual targeted nanoformulation exhibited complete tumor regression in 60 % of mice, extending their survival to nearly 7 months.

## **Discussion:**

Herein we present a pragmatic nanoformulation, based on highly biocompatible and FDA approved components for a precision-targeted anti-glioma therapy. ***So far, clinical use nanoformulations have shown to cure less than 50 % of subjects accompanied by severe side-effects. However, in our study, 60 % of test subjects were completely cured of tumors while the remaining 40 % presented a tumor regression of near to 90 %.*** We believe that extending the treatment, could further enhance the therapeutic outcome. These results are much superior to the present clinically approved formulations for treatment of various cancers. The resultant product is currently under discussion for technology transfer.

---

## Biodegradable multiliposomal carriers with controllable stability in water-salt media

---

Wednesday, 18th October - 17:31 - Nanomedicine and nanobiotechnology - Auditorium - Oral - Abstract ID: 155

---

***Dr. Olga Zaborova<sup>1</sup>, Dr. Andrey Sybachin<sup>1</sup>, Prof. Timothy Deming<sup>2</sup>, Prof. Alexander Yaroslavov<sup>1</sup>***

*1. M.V. Lomonosov Moscow State University, 2. University of California*

### Introduction

Liposomes represent an important category of nano-sized systems for biomedical applications. Due to unique structure, liposomes are used for encapsulation of different substances for improving their physical, chemical and operational characteristics. Liposomes immobilized on suitable surfaces could act as more capacious depots for pharmaceutical active compounds, and remain stable until they reach the target side. Previously [1] we suggested to use polypeptide vesicles formed from amphiphilic block-copolymers of poly(L-lysine)-b-poly(L-leucine) as carriers for anionic liposomes. This approach allowed one to create biodegradable and biocompatible multiliposomal carrier. Here we investigated the influence of cationic block nature on formation and physico-chemical properties of anionic liposomes-polypeptide vesicles complexes.

### Methods

Small unilamellar liposomes were prepared from mixtures of anionic and zwitterionic lipids using sonication technique. Cationic polypeptide vesicles (CPV) of two types: 1) CPV-R composed of poly(L-lysine)<sub>60</sub>-b-poly(L-leucine)<sub>20</sub> and 2) CPV-K composed of poly(L-arginine)<sub>60</sub>-b-poly(L-leucine)<sub>20</sub> were prepared as reported in [2]. To control the formation and physico-chemical properties of the complexes between anionic liposomes and CPVs, the multi-method approach was used including fluorescence spectroscopy, dynamic light scattering, laser microelectrophoresis, conductometry and isothermal titration calorimetry.

### Results and Discussion

It was demonstrated that both types of polypeptide vesicles effectively adsorb anionic liposomes on its surface and the liposomal structure remains intact after complexation. The vesicles could be effectively digested by proteolytic enzymes trypsin and  $\alpha$ -chymotrypsin even when their surface is covered by layer of liposomes. It was found that complexes of anionic liposomes with CPV-R are more stable towards dissociation in water-salt media than complexes with CPV-K. The latter can be attributed to different complexation mechanism for CPV-R and CPV-K as arginine is known to be able to form hydrogen bonds with choline head-groups of lipids.

### Acknowledgements

This work was supported by Russian Science Foundation (project 14-13-00255).

### References

1. A. A. Yaroslavov, O. V. Zaborova, A. V. Sybachin, I. V. Kalashnikova, E. Kesselman, J. Schmidt, Y. Talmon, A. R. Rodriguez and T. J. Deming, *RSC Adv.*, 2015, 5, 98687
2. E. P. Holowka, D. J. Pochan and T. J. Deming, *J. Am. Chem. Soc.*, 2005, 127, 12423

# Mechanical properties of nanoparticles affecting interactions with tumor cells

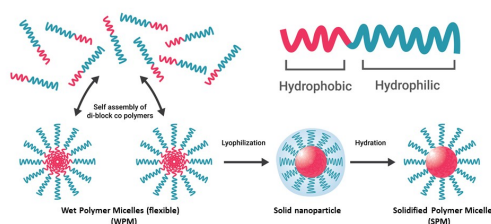
Wednesday, 18th October - 17:48 - Nanomedicine and nanobiotechnology - Auditorium - Oral - Abstract ID: 641

**Dr. Ofra Benny**<sup>1</sup>

*1. The Hebrew University of Jerusalem*

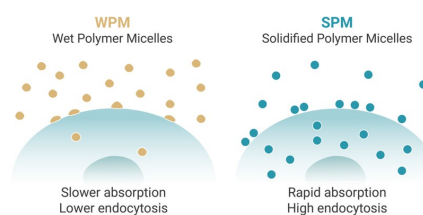
Controlling the interaction of drug delivery systems (DDS) with biological tissues is critical for the success of therapies. Specifically in cancer, due to the high density of the tumors, tissue penetration of DDS is critical and may be challenging. We showed that polymer nanoparticles can be used efficiently to deliver small molecule drugs into cancer cells and tissues. In our recent work we study the effect of mechanical cues of drug vehicle on their interactions with tumor cells and tissue-like 3D structures ex-vivo. Using polymer micelles we compared flexible “Wet Polymer Micelles” (WPM) to semi-solid “Solidified Polymer Micelles” (SPMs) for their physiochemical properties and their interactions with cancer cells. The composition of the polymer micelles, both flexible and rigid remained the same while the only difference was their mechanical properties. For that we have performed detailed characterization of SPM compared to WPM, including examinations of particle size, stability, drug release kinetics and cell transcytosis, in melanoma A-375 cells. Cell uptake measurements were done using FACS and microscopy imaging, showing enhanced abilities of SPMs to penetrate cells and tissues. A simple physical model is presented that well agrees with the experiments and provides insight about the role of particle rigidity in the engulfment mechanism. We conclude that particle rigidity can enhance cellular uptake and tissue penetration and that mechanical properties of DDS be used as a selective principle for drug uptake. We also introduced SPMs as a promising and effective, highly permeable DDS. Our findings can be important in future rational design of DDS for particle adjustment to specific tissues and pathology, and for personalized Nanomedicine.

## Tuning rigidity of nanoparticles

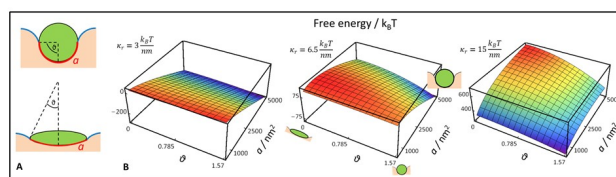


Revised spm figure.jpg

## Cell interaction with WPMs and SPMs



Revised spm figure2.jpg



Revised spm figure3.jpg

---

# Nanoclusters of self-assembled quantum dots driven by fluorine-fluorine interactions as delivery platform for enzymes

---

Wednesday, 18th October - 18:05 - Nanomedicine and nanobiotechnology - Auditorium - Oral - Abstract ID: 760

---

***Dr. Carolina Carrillo Carrion*<sup>1</sup>, *Dr. Mónica Carril*<sup>2</sup>, *Prof. Wolfgang Parak*<sup>3</sup>**

*1. Bioengineered Particles Group, CIC biomaGUNE, 2. Bioengineered Particles Group, CIC biomaGUNE AND Ikerbasque, Basque Foundation for Science, 3. Bioengineered Particles Group, CIC biomaGUNE AND Fachbereich Physik, Philipps Universität Marburg*

## Introduction

Self-assembled NPs are considered as one of the most promising nanosystems to deliver drugs and biological molecules such as enzymes for therapeutic applications. Non-covalent hydrophobic interactions play an important role in the formation of assemblies, and fluorine-fluorine interactions are particularly interesting because the unique hydrophobicity and lipophilicity of fluorine lead to stronger interactions. Herein, inspired by the role of fluorine in self-assembly and its favorable interaction with proteins, we report a novel delivery platform for enzymes based on self-assembled nanoclusters of fluorinated quantum dots (QD\_F).

## Methods

QD\_F were prepared by ligand-exchange of TOPO-capped QDs with a fluorinated ligand. The self-assembly process consisted simply in mixing the QD\_F dispersed in DMSO with water and stirring vigorously for 1 min. The encapsulation of the enzyme within the clusters involved two steps: i) enzyme incubation with QD\_F, and ii) formation of clusters (**Fig. 1**). TEM, <sup>1</sup>H and <sup>19</sup>F NMR, DLS, LDA, enzymatic activity assays, and BCA assay were used as characterization and analytical techniques.

## Results

The obtained nanoclusters with a size of ca. 44 nm and charge of -35 mV presented very good colloidal stability in the presence of diverse ions up to 500 μM, in a wide range of pH (from 5 to 9) and over the time. These clusters were able to encapsulate different enzymes (laccase and α-galactosidase) obtaining high loading efficiencies. Importantly, the encapsulated enzymes maintained their catalytic activity following a Michaelis-Menten kinetic, and presented higher K<sub>M</sub> and lower V<sub>max</sub> than their free forms, which was due to the modification of their microenvironment. Under acidic environment (as in endosomes/lysosomes), clusters were slowly disassembled allowing the release of enzymes. 50% of encapsulated enzyme was released within 24 h (**Fig. 2**). Importantly, enzymes retained their activity after release.

## Discussion

This is the first time that self-assembled fluorinated NPs are proposed as nanocarriers for drug delivery. The main achievements of this work are: (i) Proof of the potential of non-covalent fluorine-fluorine interactions as driving force for the self-assembly of NPs, and (ii) Demonstration of the ability of this system to carry and deliver enzymes in a controlled fashion.



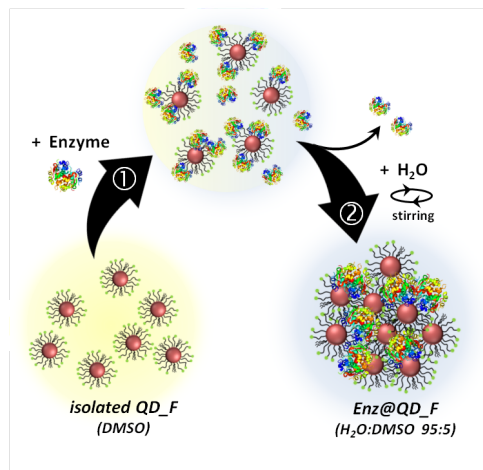


Figure 1.png

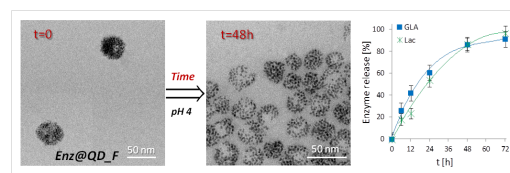


Figure 2.png

# Magnetically Targeted Delivery of Sorafenib to Liver Using Solid Lipid Nanoparticles for Treatment of Hepatocellular Carcinoma

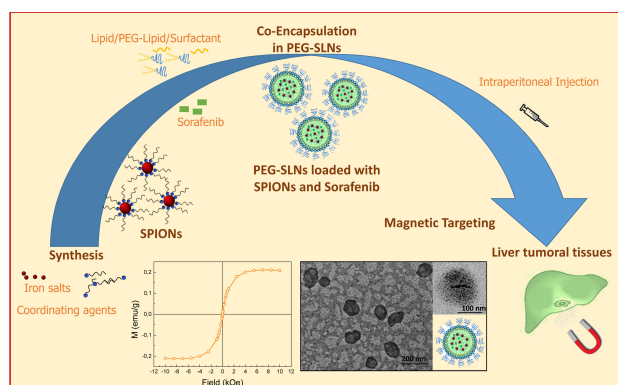
Wednesday, 18th October - 18:22 - Nanomedicine and nanobiotechnology - Auditorium - Oral - Abstract ID: 224

**Dr. Nicoletta Depalo<sup>1</sup>, Mr. Fabio Vischio<sup>1</sup>, Ms. Ilaria Arduino<sup>2</sup>, Ms. Silvia Villa<sup>3</sup>, Prof. Fabio Canepa<sup>3</sup>, Dr. Elisabetta Fanizza<sup>4</sup>, Prof. Byung Chul Lee<sup>5</sup>, Dr. Valentino Laquintana<sup>2</sup>, Prof. Angela Lopodota<sup>2</sup>, Dr. Annalisa Cutrignelli<sup>2</sup>, Dr. Maria Principia Scavo<sup>6</sup>, Dr. Marinella Striccoli<sup>1</sup>, Prof. Angela Agostiano<sup>4</sup>, Dr. M. Lucia Curri<sup>1</sup>, Dr. Nunzio Denora<sup>2</sup>**

**1.** Istituto per i Processi Chimico-Fisici-CNR SS Bari, **2.** Università degli Studi di Bari Aldo Moro, Dipartimento di Farmacia, Scienze del Farmaco, **3.** Dipartimento di Chimica e Chimica Industriale, Università di Genova, **4.** Università degli Studi di Bari Aldo Moro, Dipartimento di Chimica, **5.** Seoul National University College of Medicine, Seoul National University Bundang Hospital, Seongnam, **6.** Istituto Tumori IRCCS Giovanni Paolo II, Bari

Advanced hepatocellular carcinoma (HCC) is a clinical challenge with limited treatment options. The orally active multikinase inhibitor sorafenib is the only anticancer agent showing a survival benefit in these patients. As well as significant activity, sorafenib is characterized by severe toxic side effects limiting the possible therapeutic response (1). Nanoparticle (NP) based approaches offer a valuable alternative for cancer drug delivery, thus ensuring the accumulation of high concentrations of drug to the targeted cancer cell, with a concomitant reduced toxicity of normal tissue. Superparamagnetic iron oxide NPs (SPIONs) are very attractive for delivery of therapeutic agents as they have been reported to enhance the drug delivery to specific locations in the body through the application of an external magnetic field (2). Here, solid lipid NPs (SLNs) containing sorafenib and SPIONs have been prepared by a hot homogenization technique using cetyl palmitate as lipid matrix and polyethylene glycol modified phospholipids (PEG lipids), in order to achieve a PEG-based anti-fouling coating on SLN surface. These nanoformulations, thoroughly investigated by means of complementary techniques, have finally resulted effective drug delivery magnetic nanovectors with good stability in aqueous medium and high drug encapsulation efficiency. In addition, the relaxometric characterization has proven that the magnetic SLN loaded with sorafenib are also very efficient contrast agents, with a great potential in magnetic resonance imaging technique. The proposed magnetic SLNs loaded with sorafenib represent promising candidates for image guided and magnetic targeting of sorafenib to liver towards an efficacious treatment of HCC.

1. Villanueva A et al., *Gastroenterology* **2011**, 140, 1410-1426. 2. N. Depalo et al., *Nanoresearch* **2017** 5, 1909-1917.



Fabrication route of magnetic slns loaded with sorafenib.jpg

---

## Hybrid organic-inorganic materials as precursors for water splitting electrocatalysts

---

Thursday, 19th October - 09:00 - Plenary Speeches - Auditorium - Oral - Abstract ID: 842

---

**Mr. Rui Zhang<sup>1</sup>, Dr. Patricia Russo<sup>1</sup>, Prof. Nicola PINNA<sup>1</sup>**

*1. Humboldt University of Berlin*

Efficient water oxidation catalysts are required for the development of water splitting technologies. Herein, we report the synthesis of layered hybrid transition metal phosphonate compounds from metal acetylacetonate precursors and various phosphonic acid in benzyl alcohol. The hybrid particles are formed by inorganic layers of divalent transition metals (e.g. Fe, Co, Ni) in distorted octahedra environments separated by bilayers of the organic group.

These hybrid materials are used as precursors for water splitting electrocatalysts in two ways.

On the one hand, their direct use as anode materials, so as oxygen evolution catalyst, involves their gradual transformation to hydroxide nanosheets during operation. It is found that the hybrid particles template the formation *in situ* of transition metal hydroxide nanosheets of sizes between 5 and 25 nm and thicknesses between 3 and 10 nm.

X-ray absorption spectroscopy measurements suggest that the hybrid acts also as a template for the local structure of the metal sites in the active catalyst, which remain distorted after the transformation. Optimum electrocatalytic activity is achieved with the hybrid compound with a Fe content of 16 %. The combination of the synergistic effect between Ni and Fe with the structural properties of the hybrid results in an efficient catalyst that generates a current density of 10 mA cm<sup>-2</sup> at an overpotential of 240 mV, and also in a stable catalyst that operates continuously at low overpotentials for 160 h.

On the other hand, we report that nickel phosphides can be synthesized through thermal treatment of layered nickel phenyl- (NiPh) or methyl-phosphonates (NiMe) that act as single-source precursors. Ni<sub>12</sub>P<sub>5</sub>, Ni<sub>12</sub>P<sub>5</sub>-Ni<sub>2</sub>P and Ni<sub>2</sub>P nanoparticles with sizes of *ca.* 15-45 nm coated with a thin shell of carbonaceous material were produced. Thermogravimetric analysis coupled with mass spectrometry (TG-MS) showed that H<sub>2</sub>, H<sub>2</sub>O, P<sub>2</sub> and -C<sub>6</sub>H<sub>5</sub> are the main compounds formed during the transformation of the precursor under argon, while no hazard phosphorous-containing compounds are created, making this a simple and relatively safe route for fabricating nanostructured transition metal phosphides.

# Charge dynamics in composite systems for advanced applications

Thursday, 19th October - 09:40 - Plenary Speeches - Auditorium - Oral - Abstract ID: 77

***Prof. Alberto Vomiero***<sup>1</sup>

*1. Luleå University of Technology*

Charge dynamics (i.e. the processes of charge generation, dissociation and collection) plays a critical role in several advanced applications based on composite nanosystems, including solar energy, water splitting, nanothermometry.

In most of them, semiconducting nanocrystals exhibiting quantum confined effects (the so-called quantum dots, QDs) act as light absorbing materials, which are able to generate excitons as a consequence of photon absorption. Managing the photogenerated charges enables the exploitation of different physico-chemical processes, including charge separation and collection in photoelectrochemical systems for energy conversion or tuning photoluminescence properties in luminescent nanoprobes.

Key element for driving the processes to targeted applications is the modulation of composition and size of the nanomaterials, which determines the final electronic band structure of the composite systems and its functional properties.

We will illustrate different examples of composite systems, targeted for specific applications. (i) “Giant” composite core-shell QDs, in which modulation of core-to-shell interface induces a single- to double-color photoluminescence; (ii) Near-infrared QDs with increased Stokes shift due to suitable electronic structure of the core and shell, to be applied in luminescent solar concentrators; (iii) Composite TiO<sub>2</sub> mesoporous film sensitized by “giant” QDs with high charge injection from the photoexcited QD to the TiO<sub>2</sub> anode, for excitonic solar cells and water splitting.

We will discuss possible strategies to tailor the optical features of the different systems to optimize their functional properties, according to the specific application.

## Radical Properties in Functional Oxide Thin Films from Insulators to Superconductors

---

Thursday, 19th October - 10:45 - Plenary Speeches - Auditorium - Oral - Abstract ID: 37

---

***Prof. Judith Driscoll*** <sup>1</sup>

*1. University of Cambridge*

Since the discovery of high temperature superconductivity in perovskite oxides in 1986, the unearthing of a huge range of physical phenomena in transition metal oxides (TMOs) has been nothing short of remarkable, e.g. new magnetism, ferroelectrics, multiferroics, semiconductors, transparent conductors, calorics, plasmonics, catalysts, ionic conductors. Nearly **150,000** papers were published on the topic ‘oxide+thin film’ in the last 10 years, not far from the number published on graphene in this same period. However, there are few applications of complex oxide thin films today.

As stated in a recent perspective publication by the EU commission about emerging applications, “we have passed from the perception that materials are in the drawer to the realisation that materials are the bottleneck”. Addressing the oxide thin film bottleneck is long overdue. This talk will discuss new insight into and radical property enhancements in oxide thin films through nanostructuring the films. Hence, nanotechnology is merged with thin film science. Examples will be given of unprecedented functional property enhancements in systems such as ferroelectrics, ferromagnetics, superconductors and ionics.

## 2D Semiconductor nanostructures at atomic scale

Thursday, 19th October - 11:25 - Plenary Speeches - Auditorium - Oral - Abstract ID: 46

***Prof. Jordi Arbiol<sup>1</sup>***

*1. ICREA and Institut Català de Nanociència i Nanotecnologia (ICN2), CSIC & BIST*

Technology at the nanoscale has become one of the main challenges in science as new physical effects appear and can be modulated at will. Materials for spintronics, electronics, optoelectronics, chemical sensing, and new generations of functionalized materials are taking advantage of the low dimensionality, improving their properties and opening a new range of applications. As developments in materials science are pushing to the size limits of physics and chemistry, there is a critical need for understanding the origin of these unique physical properties (optical and electronic) and relate them to the changes originated at the atomic scale, e.g.: linked to changes in (electronic) structure of the material.

During the talk, I will show how atomic resolution high angle annular dark field (HAADF) scanning transmission electron microscopy (STEM) can help to understand the growth mechanisms of complex 2D nanostructures such as nanomembranes, nanoflakes or nanobelts.

The presentation will combine the visualization of 3D atomic models recreating the growth of these 2D nanostructures, as well as a direct correlation between their structure and chemical composition at the atomic scale, with their local properties at the nanoscale, electronic and photonic. In addition, I will show the in-situ dynamic reconstruction processes of monolayer grain boundaries in MoS<sub>2</sub> at atomic scale under the electron beam as well as the sulfurization evolution that drive the transformation of a MoO<sub>3</sub> nanomembrane to a MoS<sub>2</sub> nanoflake.

1. M. dela Mata, R. Leturcq, S. R. Plissard, C. Rolland, C. Magen, J. Arbiol,\* P.Caroff\*, Nano Letters, **16**, 825 (2016)
2. P.-Y.Tang, L.-J. Han, A. Genç, Y.-M. He, X. Zhang, L. Zhang, J. R. Galán-Mascarós, J.R. Morante, J. Arbiol, Nano Energy, **22**,189 (2016)
3. G.Tutuncuoglu, M. de la Mata, D. Deiana, H. Potts, F. Matteini, J. Arbiol, A.Fontcuberta i Morral, Nanoscale, **7**,19453 (2015).

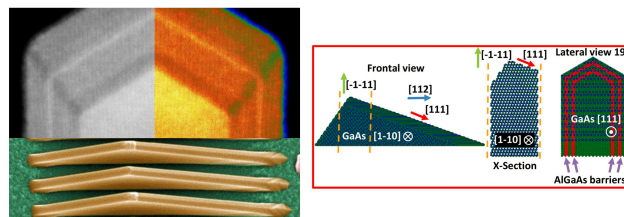


Figure 1.jpeg

---

## Design of screen-printed carbon electrodes on nanocellulose membranes

---

Thursday, 19th October - 13:30 - Poster Session - Hall & Room 3 - Poster - Abstract ID: 675

---

***Dr. Robson Silva<sup>1</sup>, Dr. Deivy Wilson<sup>1</sup>, Dr. Rafael R. Domenegueti<sup>2</sup>, Dr. Sidney J. L. Ribeiro<sup>2</sup>, Dr. Osvaldo N. Oliveira Jr.<sup>1</sup>***

*1. University of Sao Paulo/Physics Institute of Sao Carlos, 2. Institute of Chemistry, São Paulo State University, 14801-970, Araraquara-SP*

Bacterial nanocellulose (BNC) membranes are produced by some bacteria such as the specie *Gluconacetobacter xylinus* and commercially used as wound dressing. BC membranes have high crystalline 3D network composed by pure cellulosic fibers with diameters below 100 nm and lengths larger than 3  $\mu\text{m}$ . BNC membranes have good adherence to the wound, enable excellent water vapor permeability, and constitute physical barriers for microorganisms.

In particular, BC membranes have been poorly explored as substrate for biosensing materials based on sensors. Voltammetric sensors based on screen-printed carbon electrodes (SPCE's) built on BNC membranes may have an incredible potential to be used in biology-device interface. As a proof-of-concept, we evaluated the voltammetric behavior of well-known model analytes in SPCE's printed on BC membranes.

The SPCEs were home fabricated over dried BNC membranes substrate using a screen printer machine IMAH and appropriate stencil designs fabricated on polyester screens (150 meshes). First, a carbon layer was deposited on BC substrate using a pattern comprising the electrical contacts and the working and counter electrodes. They were obtained SPCEs with a working electrode area of  $0.09\text{ cm}^2$  and films thickness (determined by profilometry measurements,  $n=9$ ) of  $8.7\text{ }\mu\text{m}$  for Ag/AgCl and  $9.2\text{ }\mu\text{m}$  for carbon films.

By using BNC membrane as substrates for SPCE, we successfully detected uric acid, pyrogallol acid and ferrocyanide and ferricyanide ions model analytes dissolved in aqueous solutions at concentrations up to 60 ppm, 1 mM and 5 mM, respectively. We also evaluated the modification of SPCE working electrode with inkjet printed metallic nanoparticles and tyrosinase enzyme. Taking advantage of their remarkable biocompatibility, BNC membranes can be considered an excellent choice as an emergent biopolymer for the development of future implantable biosensors.

# Achieving higher sensitivity of CdS-based SAW sensor detecting visual light

Thursday, 19th October - 13:30 - Poster Session - Hall & Room 3 - Poster - Abstract ID: 666

**Mr. Byungmoon Lee<sup>1</sup>, Mr. Jin Woo Lee<sup>1</sup>, Mr. Jong Woo Kim<sup>1</sup>, Mr. Jinkee Hong<sup>2</sup>, Prof. Byeong-kwon Ju<sup>3</sup>**

*1. Korea university/Haesung DS, 2. Haesung DS, 3. Korea university*

**Introduction:** SAW sensors have been studied for various applications in mobile devices and achieving higher sensitivity has become a major issue. In this paper, CdS thin film with various thicknesses and areas were investigated and the proper design was proposed and we found that higher sensitivity could be achieved by changing thicknesses and areas of cadmium sulfide (CdS) thin films deposited on surface acoustic wave (SAW) sensors. **Methods:** We used 128° Y-X lithium niobate (LiNbO<sub>3</sub>) as a substrate. Aluminum was DC sputtered on cleaned substrate to fabricate inter-digitated transducers (IDTs). IDTs consist of 70 pairs of fingers with the width of 4 μm and the same spatial length. Thermal evaporation process was used to deposit CdS on prepared substrate. CdS thin films were deposited with different thickness of 140 nm and 190 nm to confirm the thickness effect. Roughness by thickness was characterized using atomic force microscope (AFM). To investigate the area dependency, SAW sensors were fabricated in two ways, one covered with CdS thin films in the whole IDT area, and the other covered in half of the IDT. The sensors were exposed under the light from 0 lux to 20,000 lux, in 2,000 lux increment, in the completely dark room. In each step, the sensors absorb the light for 10 seconds having 100 seconds of intervals. Resonant frequency responded to the intensity of light and was measured by network analyzer (Protek A333). **Results/Discussion:** The test comparing 140nm thin films with 190nm shows that thicker one results in higher sensitivity of the sensor. It was also confirmed, through area dependency test, that sensitivity grows higher as the area becomes larger. Using these two results, we can expect the design rules for developing CdS-based SAW sensors to be evaluated.

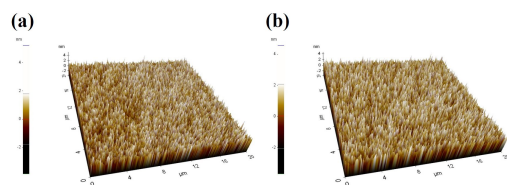


Fig. 1 afm images of thermally evaporated cds thin films a 140nm b 190nm.jpg

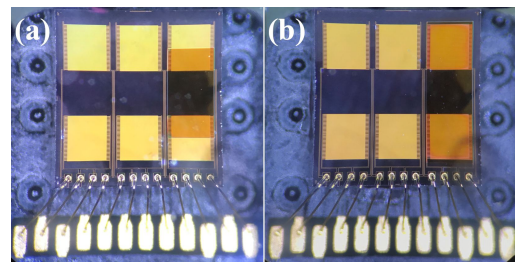


Fig. 2 microscope images of two types of sensitive films a half-covered b full-covered.jpg



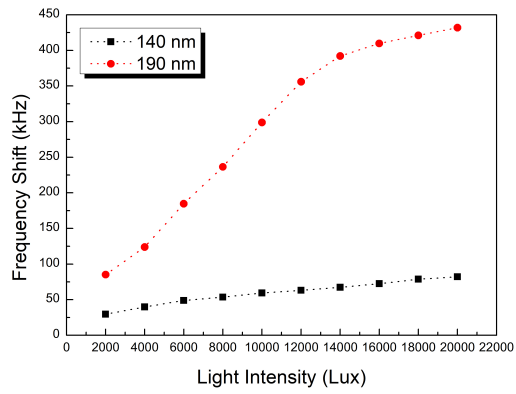


Fig. 3 resonant frequency responses with light intensity increases.jpg

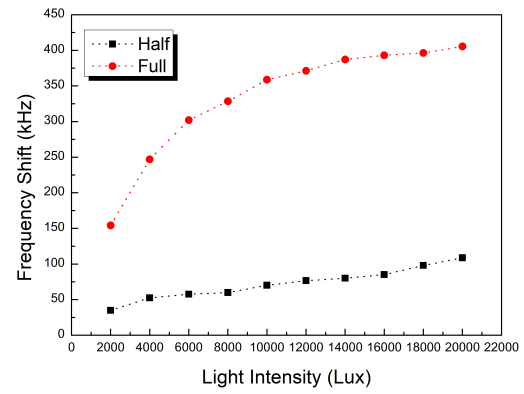


Fig. 4 resonant frequency responses with light intensity increases.jpg

# Investigation of etchant composition on the contact angle and morphology of the black silicon, formed by MACE with Ni

Thursday, 19th October - 13:30 - Poster Session - Hall & Room 3 - Poster - Abstract ID: 133

*Ms. Olga Volovlikova<sup>1</sup>, Mr. Sergey Gavrilov<sup>1</sup>, Mr. Gennady Silakov<sup>1</sup>, Mr. Artem Sysa<sup>1</sup>, Ms. Yana Grishina<sup>1</sup>, Ms. Yulia Shilyaeva<sup>1</sup>*

*1. National Research University of Electronic Technology*

In recent years, there has been much interest in the chemical formation of the silicon nanostructures by methods without electrical bias – metal-assisted chemical etching (MACE). Noble metals or its reaction products are used for MACE application remains on the etched Si surface. Recently shown, that Ni-assisted chemical etching leads to black silicon formation without contamination. There is a problem during MACE with Ni - hydrogen evolution. It prevents access reagents to surface. Addition of ethanol into solution leads to wetting of the Si and reduces  $H_2$  on the surface.

The goal of this work is investigation of the effect of  $C_2H_5OH$  and oxidizing agent  $H_2O_2$  on the morphology, etchant contact angle and roughness coefficient of the black silicon, formed by MACE. The etching of Si/Ni was carried out in a solution of  $HF/H_2O_2/C_2H_5OH/H_2O$  with different volume concentration (VC) of  $H_2O_2$  and  $C_2H_5OH$ . Contact angle was investigated in situ during 1 minute. Black silicon surface morphology was investigated after treatment during 40 minutes.

Increasing of ethanol VC promotes increasing of etchant wettability of Si/Ni and black silicon surface. Increasing of ethanol VC (0-12 vol.) leads to decreasing  $H_2O_2$  VC (0.12-0.2). The greatest value of the contact angle is  $32-33^\circ$ . It is observed in the case without ethanol in the solution, but the  $H_2O_2$  volume concentration is 0.14 and 0.2 (Fig.1). Further, with the addition of alcohol in solution or decreasing of  $H_2O_2$  VC to 0.12 and 0.17 the reduction of the contact angle to  $25$  and  $21^\circ$  is observed. It is due to the spreading solution over the surface.

Reduction of the contact angle to  $12 \pm 1^\circ$  and  $15 \pm 1^\circ$ , intensive gas evolution and darkening of the Si/Ni after 1 minute of treatment indicate black silicon formation by MACE. In the subsequent decrease the  $H_2O_2$  concentration leads to uniform and continuous black silicon formation (Fig.2).

This study was supported by the Russian Science Foundation, project no. 16-19-10625.

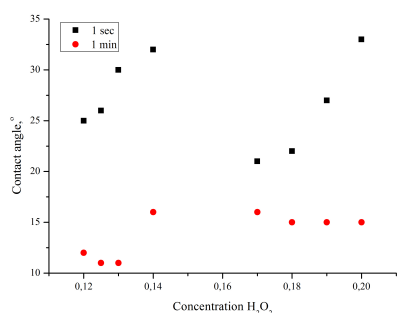


Figure 1 etchant contact angle on surface sini in the first second and first minute of treatment.jpg

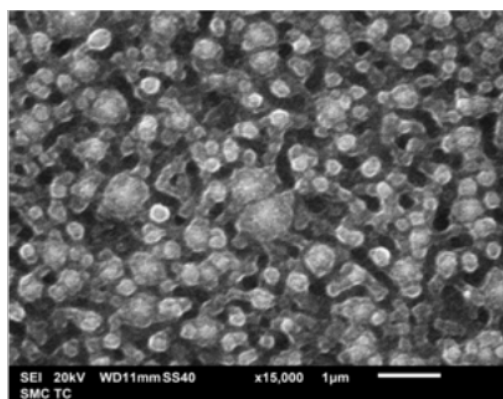


Fig.2a sem image of black silicon after treatment in solution hfh2o2h2o. concentration of h2o2 is 0.14.png

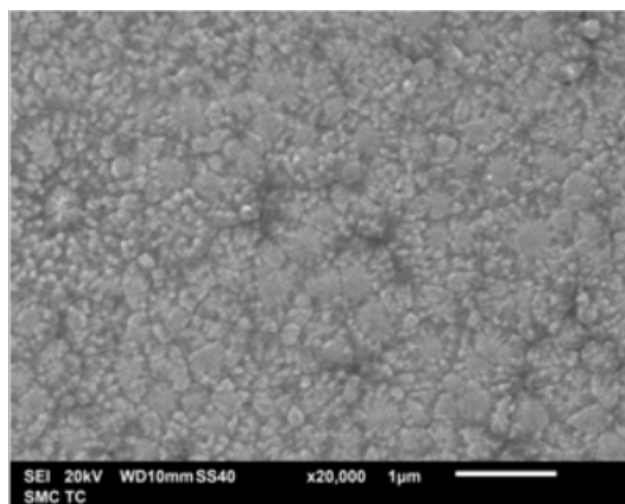


Fig.2b sem image of black silicon after treatment in solution  $\text{HfH}_2\text{O}_2\text{C}_2\text{H}_5\text{OH}$ . concentration of  $\text{H}_2\text{O}_2$  is 0.16.png

# Lateral epitaxial heterojunctions in single nanowires fabricated by masked cation exchange

Thursday, 19th October - 13:30 - Poster Session - Hall & Room 3 - Poster - Abstract ID: 147

**Dr. Sedat Dogan<sup>1</sup>, Dr. Stefan Kudera<sup>1</sup>, Dr. Zhiya Dang<sup>1</sup>, Dr. Francisco Palazon<sup>1</sup>, Dr. Urko Petralanda<sup>1</sup>, Dr. Sergey Artyukhin<sup>1</sup>, Dr. Luca De Trizio<sup>1</sup>, Prof. Liberato Manna<sup>1</sup>, Prof. Roman Krahne<sup>1</sup>**

<sup>1</sup>. Istituto Italiano di Tecnologia

Recently in our group it has been demonstrated that the cation exchange reaction can be exploited for fabrication of luminescent patterns and electrical circuits in chalcogenide NC films [1]. This approach, called masked cation exchange, combines the direct electron-beam exposure and the cation exchange reaction to create functional micro patterns. In this work we apply the masked cation exchange to fabricate heterojunction CdSe/Cu<sub>2</sub>Se nanowires using the cation exchange reaction from CdSe to Cu<sub>2</sub>Se. The formation of the heterojunction within a single nanowire is confirmed via high resolution TEM and energy-dispersive x-ray images (Fig.1). Interestingly, the CdSe and Cu<sub>2</sub>Se regions exhibit epitaxial relationships at the interface (Fig.1). Our experiments, supported by computational modeling, indicate that the cation exchange at the CdSe/Cu<sub>2</sub>Se interface is only possible if the displaced Cd<sup>2+</sup> ions can radially out-diffuse to the solution phase. For the irradiated section of the wire, this exit pathway is blocked and, therefore, the cation exchange cannot occur. Further electrical measurements are performed that probe the conductivity in such heterojunction CdSe/Cu<sub>2</sub>Se nanowires.

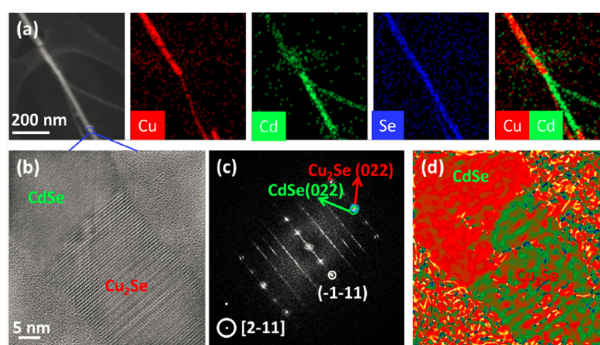


**Figure 1.** (a) HAADF-STEM image, and the corresponding STEM-EDS elemental maps, of a heterojunction CdSe/Cu<sub>2</sub>Se NW. (b) HRTEM image of the CdSe/Cu<sub>2</sub>Se interface found in the heterojunction's region marked with a box in panel (a), with the corresponding FFT showing the epitaxial relationship between CdSe and Cu<sub>2</sub>Se (c). (d) Mean dilation map calculated from the GPA analysis of the HRTEM image shown in panel

Picture1.png

# One-step synthesis of porous carbon nanosheets with controllable pore size and their dye adsorption performances

Thursday, 19th October - 13:30 - Poster Session - Hall & Room 3 - Poster - Abstract ID: 219

**Mrs. Jiyoung Lee<sup>1</sup>, Ms. Yeong A. Lee<sup>2</sup>, Dr. Chung-Yul Yoo<sup>3</sup>, Dr. Jung Joon Yoo<sup>3</sup>, Dr. Hana Yoon<sup>1</sup>, Prof. Bongsoo Kim<sup>1</sup>**

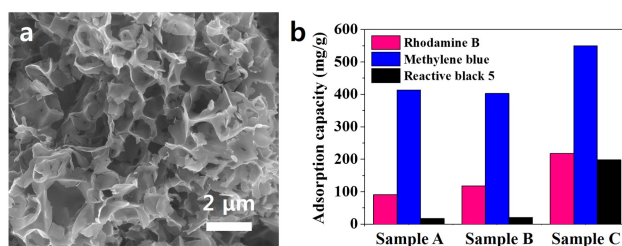
**1. Korea Advanced Institute of Science and Technology (KAIST), 2. Korea Institute of Energy Research (KIER), 3. Korea Institute of Energy Research (KIER)**

Porous carbons have received a great deal of attention because of their applicability for water purification, gas separation, catalyst supports, and electrode materials for supercapacitors and batteries. The performances of the porous carbons are determined by various characteristics like structure, pore size distribution, pore shape, electrical conductivity, and surface functionality. Among them, it is well-known that the pore size distribution of porous carbon determines performances including adsorption capacity. Furthermore, 3D interconnected nanosheet morphologies of the porous carbons are strongly recommended for various applications due to their short diffusion pathways, large specific surface area, and absence of self-restacking.

In this study, 3D interconnected porous carbon nanosheets with different pore size distributions are synthesized by direct carbonization of organic salts and their dye adsorption performances are analyzed. By controlling the type and ratio of organic salts used as precursors, we have synthesized porous carbon nanosheets with a controllable pore size distribution, ranging from microporous to mesoporous. The dye adsorption ability of porous carbon nanosheets are tested for rhodamine B, methylene blue, and reactive black 5 dyes. The dye adsorption capacities increase in the order of sample A (predominantly microporous carbon nanosheets) = sample B (hierarchical micro/mesoporous carbon nanosheets) < sample C (mostly mesoporous carbon nanosheets) for all three dyes. As-synthesized porous carbon nanosheets with different pore size distribution are expected to be widely applied as adsorbents for water purification, electrode materials for energy storage and conversion, and catalyst supports.

## Acknowledgement

This work was conducted under the framework of the Research and Development Program of the Korea Institute of Energy Research (KIER) (B7-2461-07) and the BK21 Plus-KAIST.



Annic 2017 abstract figure - jiyoung lee.jpg



---

## Silicon Nanowires for Water Splitting

---

Thursday, 19th October - 13:30 - Poster Session - Hall & Room 3 - Poster - Abstract ID: 280

---

***Dr. Vladislav Dřínek<sup>1</sup>, Dr. Pavel Dytrych<sup>1</sup>, Dr. Radek Fajgar<sup>1</sup>, Dr. Mariana Klementová<sup>2</sup>***

*1. Institute of Chemical Process Fundamentals of CAS, v.v.i., Czech Republic, 2. Institute of Physics of CAS, v.v.i., Czech Republic*

Nowadays a continual growing demand for green energy production, smart grids, energy storage, electric vehicles etc. boosts up a need for new technology approaches. One of the solutions is conversion of the solar energy into chemical bond energy.

As a first step an effort of researchers is focused to bring up a concept of a device – artificial leaf - producing a free hydrogen from water by absorbing and splitting the sunlight. Nevertheless, the concept of artificial leaf can be generalized; for example using CO<sub>2</sub> in combination with other common matter (water, hydrogen), the artificial leaf has a potential to produce a wide scale of products: formic acid, methanol, dimethylether, methane, alcohols and other various hydrocarbons [1,2]. The products can be divided into three groups: advanced materials, fine chemicals and fuels.

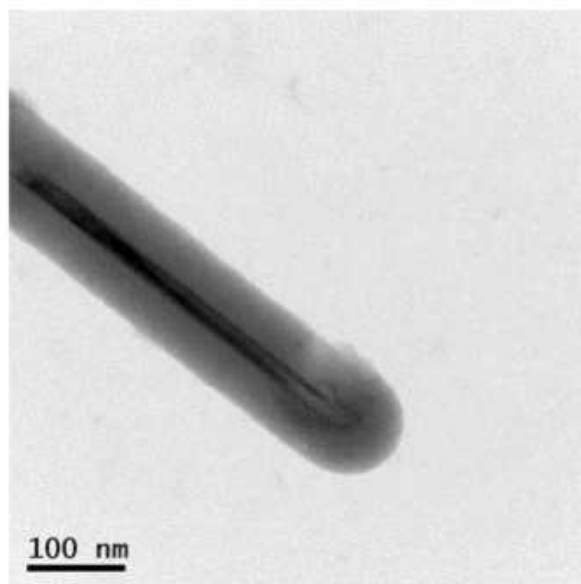
We have synthesized SiNWs by CVD of silane on molybdenum substrates [3]. Unlike other works when the SiNWs have been prepared mostly in crystalline form, our SiNWs possess more complex structure (Fig. 1): thin crystalline core covered by amorphous jacket. Absorptivity is more than 98 % in the whole range of visible radiation 400-800 nm. During photoelectrochemical experiments a strong evolution of bubbles was seen on SiNW deposit after irradiation of AM 1.5 G at 1 sunlight intensity. We suppose that the NWs are good candidates to substitute the standardly used tripple junction amorphous silicon (3jn-a-Si) layer system.

Fig. 1 - HRTEM image of a SiNW with clearly distinguished core-jacket structure

[1] R. Passalacqua, G. Centi, S. Perathoner, Oil & Gas Science and Technology 70 (2015) 799-815C

[2] Reece S. Y., Hamel J. A., Sung K., Jarvi T. D., Esswein A. J., Pijpers J. J. H., et al. Science 2011; 334: 645–8 I

[3] V. Drínek, M. Klementová, R. Fajgar, P. Dytrych, Materials Letters 160 (2015) 109–112



Sinw.jpg



# Magnetic thermometer: thermal effect on the dynamics of agglomeration of magnetite nanoparticles by magnetic field

Thursday, 19th October - 13:30 - Poster Session - Hall & Room 3 - Poster - Abstract ID: 530

***Prof. Hackjin Kim***<sup>1</sup>

*1. Chungnam National University*

We have investigated the dynamics of agglomeration of magnetite nanoparticles under magnetic field by measuring the magnetic weight. Round magnetite nanoparticles are synthesized and used in the experiments. Figure 1 shows the experimental setup.[1] The magnetic weight is monitored with a conventional electronic balance. Figure 2 shows a typical change of the magnetic weight. When the magnetite nanoparticle sample is placed under the magnetic field, the magnetic weight jumps instantaneously by the Neel and the Brown mechanism, and then increases slowly as the nanoparticles agglomerate. The temporal change of the magnetic weight fits well to the stretched exponential function,  $W(t) = W(\infty) + [W(0) - W(\infty)]\exp[-(t/\tau)^\beta]$  where  $\tau$  is the characteristic relaxation time and the exponent  $\beta$  is smaller than one.[2] The stretched exponential kinetics implies that the activation energy barrier involved in the dynamics has some distribution and that there are many different pathways for the agglomeration. The activation energy spectrum can be determined by the inverse Laplace transformation of the temporal change. Figure 3 shows the fluctuation of the magnetic weight when the laboratory temperature changes considerably in the winter season. Deviation from the stretched exponential function is attributed to thermal effect. Thermal motions of the nanoparticles destabilize the agglomerate of nanoparticles to reduce the magnetic weight. Figure 4 shows the difference of the measured and the fitted magnetic weight, and the laboratory temperature. The magnetic weight difference follows the temperature change exactly after the nanoparticles agglomerate. The fluctuation of the magnetic weight is explained well with the Boltzmann distribution,[3] which suggests that the magnetic weight of the agglomerate of magnetic nanoparticles works as a thermometer. Analysis with the Boltzmann distribution and the stretched exponential growth of the magnetic weight indicate that the agglomeration of magnetite nanoparticles by magnetic field is a complex process.

[1] D. Jin, H. Kim, *Bull. Korean Chem. Soc.* **2013**, 34, 1715.

[2] D. Jin, H. Kim, *Bull. Korean Chem. Soc.* **2015**, 36, 424.

[3] D. Jin, H. Kim, *Bull. Korean Chem. Soc.* **2016**, 37, 962.

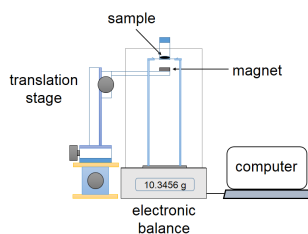


Figure 1 experimental setup.png

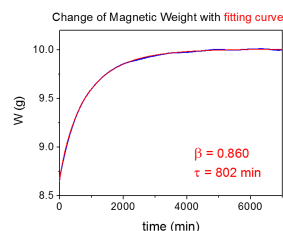


Figure 2 change of magnetic weight.png

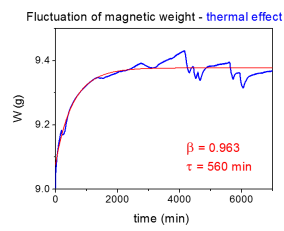


Figure 3 fluctuation of magnetic weight.png

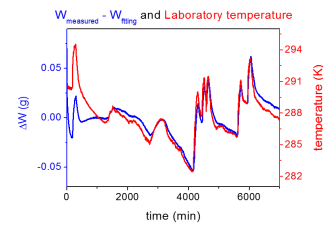


Figure 4 difference of magnetic weight and temperature.png

# Hydrogenation/ Dehydrogenation Kinetics Behaviors of MgH<sub>2</sub> Powders Doped With 10wt % ZnO Nanoparticles

Thursday, 19th October - 13:30 - Poster Session - Hall & Room 3 - Poster - Abstract ID: 426

*Ms. shorouq ahmed*<sup>1</sup>

1. Kuwait Institute for Scientific Research (KISR)

## Introduction

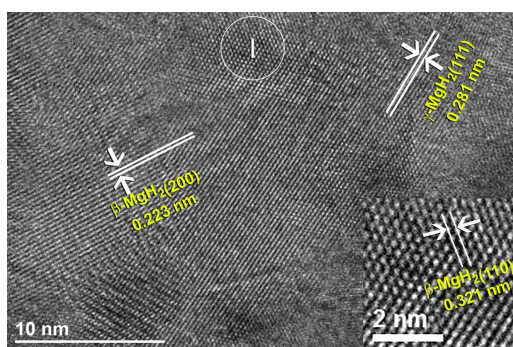
Hydrogen, which is enjoying a set of unique properties, offers the most potential solution to satisfying the global energy requirements for reducing carbon dioxide leading to improve the global energy security. Recent studies have shown that hydrogen fuel cost is reasonable and can be considered as an ideal candidate to replace fossil fuels. Number of obstacles must overcome before the hydrogen economy becomes a reality. One of the obstacles is, safe and efficient storage of hydrogen particularly for mobile/automotive applications.

## Method

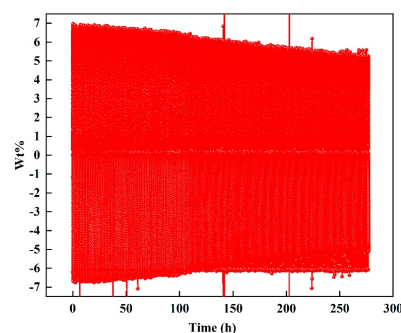
Nano crystalline MgH<sub>2</sub> powders were prepared by reactive ball milling (RBM) technique under a hydrogen pressure of 50bar, using high-energy planetary ball mills. In these experiments, 5g of as-received Mg powders were charged into a stainless steel vial and together with 50 stainless steel balls in a glove box under argon-gas atmosphere. The vial was then removed out from the glove box and charged with 50- 70 bar H<sub>2</sub> gas. The RBM process was started under the initial hydrogen pressure, planetary-type ball mill operated at a rotational speed of 250rpm. The nanocatalytic effect of metals oxide powders prepared by sol gel technique on the hydrogenation properties and stability of MgH<sub>2</sub> powders were investigated. X-ray diffraction (XRD),high resolution transmission electron microscope (HRTEM), scanning electron microscope (SEM), differential scanning calorimeter (DSC) and Sieverts machine were utilized for characterization the physical and chemical properties of the synthesized samples. Long RBM time was investigated to decrease the grain sizes of MgH<sub>2</sub> and improve the kinetics of hydrogen absorption/desorption and destabilizing of  $\mu$ -MgH<sub>2</sub> phase. In addition, it led to decreasing the activation energy of the system. Nanocomposite MgH<sub>2</sub>/10 wt. % TiO<sub>2</sub> powders showed pioneering hydrogenation properties, indexed by the high ability of absorbing hydrogen atoms at very low pressure.

## Conclusions

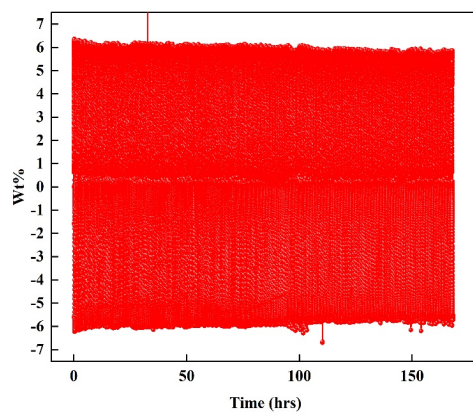
The catalytic effects of TM (ZnO) on the thermal stability represented (decomposition temperature) and hydrogenation properties,(absorption/desorption) of MgH<sub>2</sub> nanocrystalline powders, were investigated and found to be destabilizer additives of the MgH<sub>2</sub> phase. The particle size of the catalysts powders could play most vital role in improving the hydrogenation properties of MgH<sub>2</sub> and could lead to dramatic decrease on the decomposition temperature of the metal hydride phase.



Ga 1.png



Ga2.jpg



Ga3.jpg

# An investigation into the effect of thickness and annealing temperature on RF sputtered ZnO thin film properties for photonic applications

Thursday, 19th October - 13:30 - Poster Session - Hall & Room 3 - Poster - Abstract ID: 66

**Mr. Abderaouf NAMOUNE<sup>1</sup>, Dr. Tahar TOUAM<sup>1</sup>, Dr. Laid HAMMICHE<sup>2</sup>, Prof. Azeddine CHELOUCHE<sup>3</sup>, Prof. Djamel DJOUADI<sup>2</sup>**

**1.** Laboratoire des Semi-conducteurs, Université Badji Mokhtar-Annaba, BP 12, Annaba 23000, Algeria, **2.** Laboratoire de Génie de l'Environnement, Faculté de Technologie, Université de Bejaia, 06000 Bejaia, Algeria, **3.** Laboratoire de Génie de l'Environnement, Faculté de Technologie, Université de Bejaia, 06000 Bejaia

In this work, ZnO thin films were deposited on glass substrates by RF magnetron sputtering for 60 and 120 min, respectively. The as-grown films were annealed in air for one hour (1h) at various temperatures, ranging from 300 to 500 °C. Effects of film thickness and post-annealing on the structural, morphological, optical and waveguiding properties were investigated. X-ray diffraction (XRD) analyses showed that all ZnO films have a hexagonal wurtzite structure with higher *c*-axis preferred orientation, better crystallinity, larger crystallite size and lower compressive stress as film thickness and annealing temperature increase. Scanning electron microscopy (SEM) micrographs and atomic force microscopy (AFM) images revealed that the morphology and surface roughness of the ZnO samples depend on the film thickness and heat treatment temperature. The UV-Vis spectrophotometry characterization indicated that annealing enhanced the optical quality of the film regardless of the film thickness. M-lines spectroscopy (MLS) measurements at 632.8 nm wavelength put into evidence that the as-grown ZnO planar waveguides support single and multi-well confined guided modes for both transverse electric (TE) and transverse magnetic (TM) polarizations.

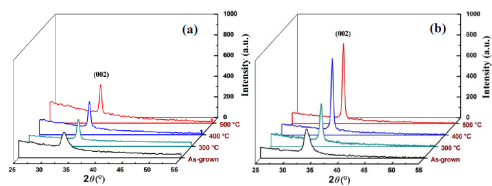


Fig. 1. XRD spectra of ZnO films deposited for (a) 60 min and (b) 120 min.

Fig.1.png

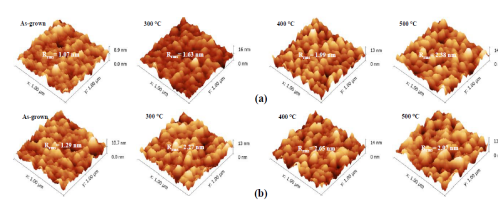


Fig. 2. AFM images of ZnO thin films deposited for (a) 60 min and (b) 120 min

Fig.2.png

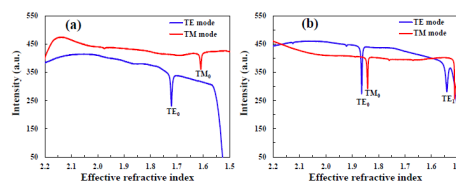


Fig. 3. TE and TM guided mode spectra of ZnO waveguides deposited for (a) 60 min and (b) 120 min.

Fig.3.png

# Effects of (Ce, Cu) co-doping on the structural and optical properties of ZnO aerogels synthesized in supercritical ethanol

Thursday, 19th October - 13:30 - Poster Session - Hall & Room 3 - Poster - Abstract ID: 79

**Prof. Djamel DJOUADI<sup>1</sup>, Mrs. Ouidette SLIMI<sup>1</sup>, Dr. Laid HAMMICHE<sup>2</sup>, Prof. Azeddine CHELOUCHE<sup>3</sup>, Dr. Tahar TOUAM<sup>4</sup>**

1. Laboratoire de Génie de l'Environnement, Faculté de Technologie, Université de Bejaia, 06000 Bejaia, Algeria, 2. Laboratoire de Génie de l'Environnement, Faculté de Technologie, Université de Bejaia, 06000 Bejaia, Al, 3. Laboratoire de Génie de l'Environnement, Faculté de Technologie, Université de Bejaia, 06000 Bejaia, 4. Laboratoire des Semi-conducteurs, Université Badji Mokhtar-Annaba, BP 12, Annaba 23000, Algeria

Undoped, Ce-doped, Cu-doped and (Ce,Cu) co-doped ZnO aerogels were synthesized by the sol-gel process in supercritical ethanol. [Cu]/[Zn] and [Ce]/[Zn] atomic ratios were fixed at 2%. The aerogels were investigated without any additional treatments by using X-ray diffraction (XRD), UV-visible spectrophotometry, scanning electron microscopy (SEM), Energy-dispersive X-ray spectroscopy (EDS), thermal gravimetric analysis (TGA), Fourier transforms infrared spectroscopy (FTIR) and photoluminescence spectroscopy (PL). XRD results revealed that all the samples are well crystallized in hexagonal wurtzite structure. TGA and EDS measurements showed that highly pure aerogels are prepared. SEM analysis indicated that the morphology of the samples is dependent on Cu and Ce dopants. From UV-visible spectroscopy analyses, it was shown that the absorption and the band gap of the aerogels are strongly affected by Ce and Cu dopants. FTIR spectra demonstrated that co-doping induces a shift of Zn-O bond vibration band toward low wavenumbers. The room temperature photoluminescence spectra put into evidence that the visible emission intensity is influenced by Ce and Cu doping. In particular, the co-doping leads to the appearance of a blue emission band at 443 nm.

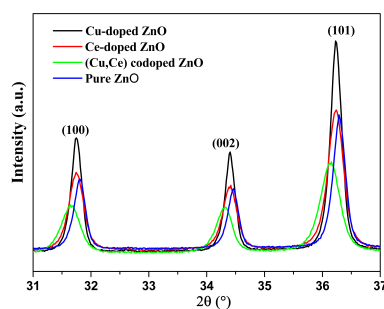


Fig. 1. Most pronounced XRD peaks of the aerogels

Fig.1.jpg

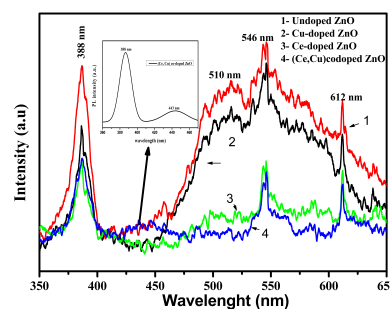


Fig. 2. Room temperature PL spectra of undoped, Ce-doped, Cu-doped and (Ce,Cu) co-doped ZnO aerogels.

Fig.2.jpg

---

## Simple morphological control over functional diversity of SERS materials

---

Thursday, 19th October - 13:30 - Poster Session - Hall & Room 3 - Poster - Abstract ID: 142

---

**Dr. Anna Semenova**<sup>1</sup>, **Dr. Alexander Barantchikov**<sup>2</sup>, **Prof. Vladimir Ivanov**<sup>2</sup>, **Prof. Eugene Goodilin**<sup>3</sup>

*1. Department of Materials Science, Lomonosov Moscow State University, 2. Kurnakov Institute of General and Inorganic Chemistry of the Russian Academy of Sciences, 3. Department of Materials Science and Department of Chemistry, Lomonosov Moscow State University; Kurnakov Institute of General and Inorganic Chemistry of the Russian Academy of Sciences*

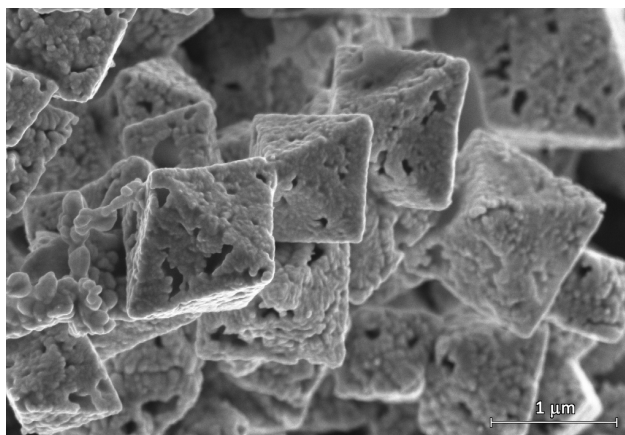
**Introduction.** Nowadays, surface-enhanced Raman spectroscopy (SERS) becomes a promising universal low-cost and real-time tool in biomedical applications, medical screening or forensic analysis allowing for detection of different molecules below nanomolar concentrations. Silver nanoparticles (AgNPs) and nanostructures (AgNSs) have proven to be a common choice for SERS measurements due to a tunable plasmon resonance, high stability and facile fabrication methods. However, a proper design of silver-based nanomaterials for highly sensitive SERS applications still remains a challenge. In this work, effective and simple preparation methods of various AgNSs is proposed and systematically developed using aqueous diamminesilver hydroxide as a precursor.

**Methods.** AgNPs and AgNSs were prepared using several novel routes based on transformation of  $[\text{Ag}(\text{NH}_3)_2]\text{OH}$  via formation of  $\text{Ag}_2\text{O}$  and pure silver under different conditions such as hydrolytic heating, aerosol pyrolysis or reduction by  $\text{H}_2\text{O}_2$ . The obtained AgNPs are comprehensively characterized by scanning and transmission electron microscopy; ultraviolet-visible, infrared and Raman spectroscopy; X-ray analysis; dynamic light scattering.

**Results.** The decomposition of aqueous diamminesilver hydroxide under heating or using aerosol spray pyrolysis results in formation of pure AgNPs and AgNSs with following morphologies: spheres, rings with hierarchical structures, porous spheroids, cuboids and more complex structures. The reduction of silver (I) oxide by hydrogen peroxide in the presence of polyvinylpyrrolidone leads to the formation of octahedral AgNSs with multiple hot spots. All described AgNPs and AgNSs demonstrate their high efficiency in SERS measurements with enhancement factors of about  $10^4$  -  $10^8$  and were used in a form of SERS active substrates for a study of different biomolecules and pollutants.

**Discussion.** The use of the aqueous diamminesilver hydroxide to prepare AgNSs gives a large benefit owing to the simplicity, promptness and low temperature conditions of the production process (typically lower than 250 °C). In particular, it demonstrates the formation of various nanoparticle morphologies highly suitable for different SERS measurements. It is shown that the best SERS active properties among the mentioned AgNSs are revealed for silver rings and octahedral silver skeleton particles.

*This research is supported by the Grant of the President of Russian Federation for the governmental support of young scientists (#MK-1146.2017.3).*



Sem image of a typical sample of nanostructured octahedral silver particles.jpg



## NFFA-Europe: enhancing European competitiveness in nanoscience research and innovation

---

Thursday, 19th October - 13:30 - Poster Session - Hall & Room 3 - Poster - Abstract ID: 330

---

***Dr. Flavio Carsughi***<sup>1</sup>

*1. NFFA*

**NFFA-Europe** is a European open-access resource for experimental & theoretical nanoscience that carries out comprehensive projects for multidisciplinary research at the nanoscale ranging from synthesis to nanocharacterization, to theory and numerical simulation. Advanced infrastructures specialized on growth, nano-lithography, nanocharacterization, theory and simulation and fine-analysis with Synchrotron, FEL and Neutron radiation sources are integrated into a multi-site combination to develop frontier research on methods for reproducible nanoscience research thus enabling European and international researchers from diverse disciplines to carry out advanced proposals impacting on science and innovation. **NFFA-Europe** coordinates access to infrastructures on different aspects of nanoscience research that are not currently available at single specialized sites without duplicating specific scopes. Internationally peer-reviewed approved user projects have access to the best suited instruments, competences and technical support for performing research, including access to analytical large scale facilities, theory and simulation and highperformance computing facilities. Access is offered free of charge to European users. Two researchers per user group are entitled to receive partial financial contribution towards the travel and subsistence costs incurred. The user access scheme includes at least two “installations” and is coordinated via a single entry point portal that activates an advanced user-infrastructure dialogue to build up a personalized access programme with an increasing return on science and innovation production. **NFFA-Europe**’s own research activity addresses key bottlenecks of nanoscience research: i.e. nanostructure traceability, protocol reproducibility, in-operando nano-manipulation and analysis, open data. ([www.nffa.eu](http://www.nffa.eu))

---

## The effect of Silicon Quantum Dots on Different Cell Types

---

Thursday, 19th October - 13:30 - Poster Session - Hall & Room 3 - Poster - Abstract ID: 808

---

**Ms. Tereza Belinova <sup>1</sup>, Dr. Iva Machová <sup>2</sup>, Ms. Lucie Vrabcová <sup>2</sup>, Dr. Anna Fucikova <sup>3</sup>, Prof. Jan Valenta <sup>3</sup>, Dr. Hiroshi Sugimoto <sup>4</sup>, Dr. Minoru Fujii <sup>4</sup>, Dr. Marie Hubalek Kalbacova <sup>5</sup>**

*1. Department of the Cell Biology, Faculty of Science, Charles University, Prague, 2. Biomedical Center, Faculty of Medicine in Pilsen, Charles University, Pilsen, 3. Department of Chemical Physics and Optics, Faculty of Mathematics and Physics, Prague, 4. Department of Electrical and Electronic Engineering, Graduate School of Engineering, Kobe, 5. Institute of Inherited Metabolic Disorders, 1st Faculty of Medicine, Charles University in Prague & Biomedical Centre, Faculty of Medicine in Pilsen, Charles University*

Silicon is an eligible material for biomedical studies due to its remarkable properties as biocompatibility and biodegradability.

Silicon nanoparticles (quantum dots) co-doped with boron and phosphorus, with diameter around 4 nanometres evincing fluorescence and dispersability in aqueous solutions were studied in respect to their impact on different human cells (osteoblasts and monocytes).

Their cytotoxicity in different types of human cells as well as their interactions with these cells were studied. Exposing cells to rising concentrations of quantum dots under different conditions and consecutive evaluation of their cytotoxicity brought an overview on cell specific reaction to their identical doses. Further, colocalization studies of nanoparticle signal and cell specific structures (organelles) of endocytic pathway were performed using fluorescence confocal microscopy.

Obtained results show significant importance of cultivation conditions (e.g. formation of protein corona on nanoparticles originating from media supplement) as well as significant impact of cell type (increased sensitivity of monocytes to studied quantum dots in comparison to other cell types). These results thus provide an insight on future directions of related research.

# Nanostructured zeolites for heavy metals removal from wastewater

Thursday, 19th October - 13:30 - Poster Session - Hall & Room 3 - Poster - Abstract ID: 823

**Prof. Cristina Covaliu<sup>1</sup>, Prof. Gigel Paraschiv<sup>1</sup>, Prof. Eugeniu Vasile<sup>2</sup>, Prof. Ecaterina Matei<sup>3</sup>**

**1.** University Politehnica of Bucharest, Faculty of Biotechnical Systems Engineering, **2.** Faculty of Applied Chemistry and Materials Science, University POLITEHNICA of Bucharest, **3.** University politehnica of bucharest

## Introduction

Zeolites used in wastewater treatment are efficient because of multiple reasons such as: ability to lose and gain water reversibly and to exchange some of their constituent elements without a major change of structure, high efficiency for retaining various compounds in their structure since will provide a high accessibility of them into the structure and at the active sites (adsorption), etc.

The purpose of this research was the study of ZSM-5 type zeolite for wastewater depollution by removal of two heavy metals ( $\text{Pb}^{2+}$  and  $\text{Cd}^{2+}$ ). After the synthesis, Na-ZSM-5 zeolites and its corresponding hybrid Na-ZSM-5-chit were characterized X-ray diffraction and transmission electron microscopy (TEM).

## Methods

The reagents used for the synthesis of Na-ZSM-5 and Na-ZSM-5chit were: sodium silicate (28%  $\text{SiO}_2$ , 8%  $\text{Na}_2\text{O}$  and 64%  $\text{H}_2\text{O}$ ), aluminium nitrate ( $\text{Al}(\text{NO}_3)_3 \cdot 9\text{H}_2\text{O}$ ), tetrapropyl-ammonium hydroxide (TPAOH), cetyltrimethyl-ammonium bromide (CTAB) and chitosan, obtained from Sigma Aldrich.

## Results and discussion

The XRD of the synthesized pristine powder depicted in Figure 1 reveal the presence of the MFI (mordenite framework inverted) structure that is typical for ZSM-5. The structure of ZSM-5 contains pentasil units bonded by bridges of oxygen forming pentasilchains which can be seen in Figure 2.

The morphology of the obtained zeolites materials was investigated by TEM analysis(Figure 3 a and b) show that the sample particles have elongated shape like plaques with an average size of 220 nm. The chitosan polymer looks as a shell on the Na-ZSM-5particles.

Adsorption studies were performed by mixing 0.1 g of each sample (Na-ZSM-5 and Na-ZSM-5-chit) with 100 mL mixed solution of Pb(II) and Cd(II),respectively at room temperature (21.5°C). The mixed solutions (100 mL) of Pb(II)and Cd(II) had the same concentrations: 10, 25, 50 and 100 mg/L of each metal.

Was observed that Na-ZSM-5 and Na-ZSM-5-chit are available to remove Pb(II) and Cd(II) from acidic wastewater (almost 50% efficiency), with the highest result in case Pb (over 55%), only after 15 minutes.

The removal efficiency for Pb(II) decrease as follows Na-ZSM-5 >Na-ZSM-5-chit. For Cd(II), the removal tendency is Na-ZSM-5-chit>Na-ZSM-5.

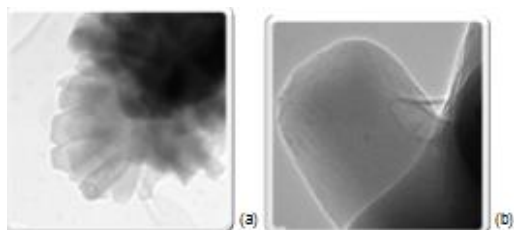


Fig.3 a and b.jpg

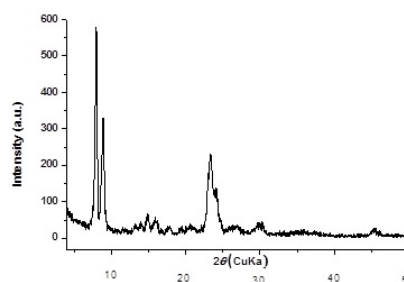


Fig.1.jpg



Fig.2.jpg

---

## High-contrast-resolution single nanoparticle spectroscopy with MEMS-scanning mirrors based polarization-interferometric laser microscope

---

Thursday, 19th October - 13:30 - Poster Session - Hall & Room 3 - Poster - Abstract ID: 109

---

***Prof. Chikara Egami<sup>1</sup>, Mr. Yuki Hata<sup>1</sup>***

*1. Shizuoka University*

Modern nanoparticle synthesis techniques have enable the development of nanoscale materials with unique optical properties for a wide range of applications, including cancer therapeutics and biomolecule detection. Particularly, nanoparticulate drug delivery systems (DDS) have attracted a lot of attention because of their size- and dopant-dependent characteristics. Nano formulations can be tailored to meet a wide range of product requirements dictated by disease condition, route of administration and considerations of cost, product stability, toxicity and efficacy. In addition, surface area to volume ratio in nanoparticles have a significant effect on the nanoparticles properties. Nanoparticles have a relative larger surface area when compared to the same volume of the material. Nanoparticles have a much greater surface area per unit volume compared with the larger particles. It leads to nanoparticles more chemically reactive. Single particle characterization is particularly important for the application of cancer therapeutics.

We have been focusing on spectroscopic analysis of a single polymer DDS nanoparticle with a polarization-interferometric nonlinear confocal microscope to analyze the nanoparticle at high CTF (Contrast Transfer Function) and high spatial resolution. The polarization-interferometric confocal microscopy is a label-free imaging technique allowing visualization of transparent single nanoparticle with CW (Continuous Wave) oscillators and simple optical elements. MEMS (Micro Electro Mechanical Systems) components included facilitate the control of the laser beam that is necessary to scan the sample in nanometer scale. We have demonstrated the nano region spectroscopy of a single 200-nm nanoparticle by vectorial polarization-interferometric technique that performs the electric field subtraction of the scattered light from tens-of-nanometer-scale target and the reference light. We have succeeded in evaluating surface condition of the DDS nanoparticle and dopant distribution in it. Also, polarization analysis estimated the molecular density, molecular orientation and refractive index difference between major and minor axes.

# Effect of thickness on physical and waveguiding properties of nanostructured AZO thin films by a sol-gel dip-coating method

Thursday, 19th October - 13:30 - Poster Session - Hall & Room 3 - Poster - Abstract ID: 86

**Mrs. Khamsa NECIB<sup>1</sup>, Dr. Tahar TOUAM<sup>2</sup>, Prof. Azeddine CHELOUCHE<sup>3</sup>, Ms. Lydia OUAREZ<sup>4</sup>, Prof. Djamal DJOUADI<sup>4</sup>, Dr. Laid HAMMICHE<sup>5</sup>**

**1.** Laboratoire des Semiconducteurs, Université Badji Mokhtar-Annaba, Algeria, **2.** Laboratoire des Semi-conducteurs, Université Badji Mokhtar-Annaba, BP 12, Annaba 23000, Algeria, **3.** Laboratoire de Génie de l'Environnement, Faculté de Technologie, Université de Bejaia, 06000 Bejaia, **4.** Laboratoire de Génie de l'Environnement, Faculté de Technologie, Université de Bejaia, 06000 Bejaia, Algeria, **5.** Laboratoire de Génie de l'Environnement, Faculté de Technologie, Université de Bejaia, 06000 Bejaia, Al

In the present work, 3.0 at. % aluminum doped zinc oxide (AZO) thin films were prepared at different number of coatings (6, 12, 18 and 24) on glass substrates by a sol-gel dip-coating process. The effect of film thickness on structural, morphological, optical and waveguiding properties of AZO thin films was studied through X-ray diffraction (XRD), scanning electron microscopy (SEM), atomic force microscopy (AFM), UV-Visible-NIR spectrophotometer and m-lines spectroscopy (MLS). XRD analysis showed that all the AZO films are polycrystalline and exhibit the hexagonal wurtzite crystal structure with a preferential growth orientation along the c-axis. The relative intensity of the (002) diffraction peak and crystallite size tend to increase with an increase in the number of layers indicating an improvement in the crystallinity of the films. SEM micrographs and AFM images revealed that the 6 layers AZO film exhibits very smooth surface consisted of small grain size particles, along with some pores over the film. In comparison, the surface of the films becomes denser and rougher with the grain size enlarged as the number of layers increases. Optical transmittance spectra showed that all of the multilayer films exhibited a high average transmittance (84-88%) in the visible region with the sharp absorption edge in the UV light region. It was also found that the band gap energy, calculated from the spectra of optical transmittance, show a significant dependence on the number of coatings. MLS measurements at 632.8 nm wavelength put into evidence that multilayer AZO planar waveguides support single and multi-well confined guided modes for both transverse electric (TE) and transverse magnetic (TM) polarizations. The film refractive index increase with thickness and reach a saturation value when the number of layers is higher than 12. Moreover, the 24 layers AZO planar waveguide shows propagation loss lower than 1 dB/cm for a wavelength of 632.8 nm.

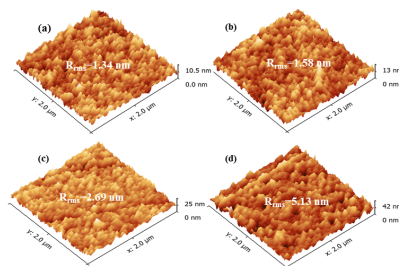


Fig. 1. 3D AFM images of multilayer AZO thin films: (a) 6 layers, (b) 12 layers, (c) 18 layers and (d) 24 layers.

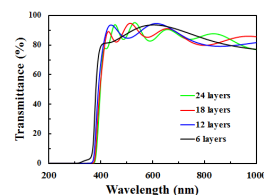


Fig. 2. Transmittance spectra of multilayer AZO thin films.

Fig.1..png

Fig.2.png

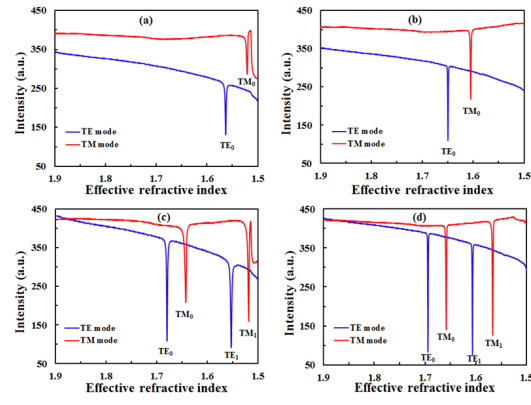


Fig. 3. TE and TM guided mode spectra of multilayer AZO thin films: (a) 6 layers, (b) 12 layers, (c) 18 layers and (d) 24 layers.

Fig.3.png

---

## Rapid Isolation and Diagnosis of Brain Injury Marker in Plasma by SERS Nanosensor

---

Thursday, 19th October - 13:30 - Poster Session - Hall & Room 3 - Poster - Abstract ID: 90

---

***Mr. Waleed Hassanain<sup>1</sup>, Dr. Sivanesan Arumugam<sup>1</sup>, Dr. Emad Kiriakous<sup>1</sup>, Prof. Godwin Ayoko<sup>1</sup>, Prof. Martin Sillence<sup>1</sup>***

*1. Queensland University of Technology*

### Introduction

S100B, calcium-binding protein, is an important biomarker for the clinical diagnosis for brain damage. It is also associated with neurodegenerative diseases like Alzheimer or other chronic neurological diseases. Due to its clinical value, it is critical to develop a rapid and sensitive methodology for its detection in biological fluids. This work presents a new nanosensor for the combined isolation and Raman detection of S100B in blood by handheld devices.

### Method

Extractor nanomaterial was fabricated by functionalising magnetic gold nanoparticles with monoclonal anti-S100B antibody thiol-ended fragments. To block the nanoparticle's remaining bare sites and eliminate nonspecific binding of foreign molecules, an alkanethiol was chemisorbed onto the gold surface of the nanoparticles. The functionalized nanoparticles were used for the selective capture of S100B from plasma within 15 minutes. After magnetic separation using a simple magnet, the protein-bound nanoparticles were washed and reconstituted in a releasing buffer to release the purified protein for detection. The released protein was scanned by surface enhanced Raman spectroscopy (SERS) using a nanostructured gold substrate and handheld device (fig.1).

### Results and Discussion

To synthesis target-specific extractor nanomaterial for S100, thiol-ended antibody fragments were developed by reducing the disulphide bonds of the antibody's hinge region and the formed free SH groups covalently bound to the nanoparticles gold surface in a highly oriented monolayer. Using this oriented immobilization strategy, the capture efficiency of the extractor nanoparticles was maximized. After selective capture of the protein from blood samples within 15 minutes, it was released from the extractor nanomaterial within 5 minutes by manipulating the pH of nanoparticles. The released protein was then loaded onto a nanostructured gold substrate and detected down to 1 pM by handheld device (fig.2). The wide optical field and the raster orbital scanning mode of the handheld Raman spectrometer allowed for reproducible and average SERS spectra of the protein to be acquired within 10 seconds. The method was cross validated against ELISA to confirm the determination of S100B in the samples. The new method has strong potential for the rapid and sensitive screening of protein biomarkers and environmental toxins in biomedical and environmental monitoring applications.



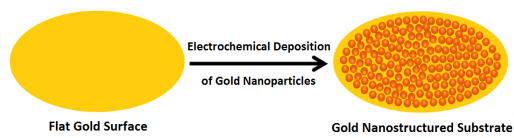
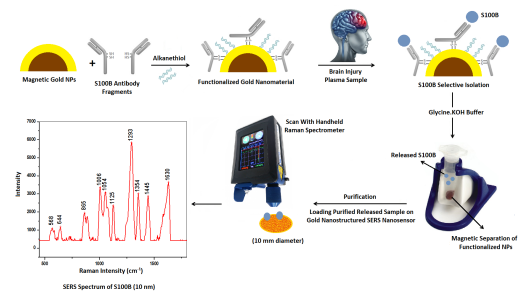


Fig 1. nanostructured sers nanosensor development by electrochemical deposition.png



---

# Glucose oxidase immobilization studies on boron doped CVD diamond coatings

---

Thursday, 19th October - 13:30 - Poster Session - Hall & Room 3 - Poster - Abstract ID: 91

---

***Prof. Rui Silva*<sup>1</sup>, *Dr. Miguel Neto*<sup>2</sup>, *Dr. Ana Piedade*<sup>3</sup>, *Dr. Filipe Oliveira*<sup>2</sup>**

***1. University of Aveiro, 2. Department of Materials and Ceramic Engineering, CICECO, University of Aveiro, 3. CEMMPRE - Mechanical Engineering Department, University of Coimbra, Rua Luís Reis Santos, 3030-788 Coimbra***

## INTRODUCTION

Boron-doped diamond (BDD) coatings obtained by chemical vapor deposition (CVD) are known to be intrinsically biocompatible [1], supporting cell adhesion and proliferation [2]. In this work we investigate the immobilization and activity of glucose oxidase (GOx) enzyme on different BDD coatings aiming their use as bio-platforms in devices for biosensing applications

## METHODS

BDD coatings were grown on sintered Si<sub>3</sub>N<sub>4</sub> disks, using an hot-filament chemical vapor deposition (HFCVD) equipment. Hydrogen and methane were used as the precursor gases for diamond growth and boron oxide diluted in ethanol and dragged by argon as the dopant. The coatings morphology (from nanocrystalline to microcrystalline) and p-type conductivity were varied by changing the CH<sub>4</sub>/H<sub>2</sub> ratio and system pressure (e.g. sample 25/2 means grown at 25mbar for a CH<sub>4</sub> flow of 2sccm).

The covalent immobilization of glucose oxidase (GOx) to the diamond coatings was made through the carboxyl-to-amine crosslinking using carbodiimine. The enzymatic activity of the free and covalent bond GOx was performed by spectrophotometric evaluation the amount of H<sub>2</sub>O<sub>2</sub> produced.

## RESULTS

Data presented in Table 1 and surface morphologies depicted in Figure 1 show that the surface density of immobilized enzyme is not the same in all samples. Plots in Figure 2 illustrate the enzyme activity of GOx over the course of four weeks as a function of the main CVD growth parameters: total pressure and CH<sub>4</sub> flow.

## DISCUSSION

These preliminar results show that there is no clear correlation between surface morphology and GOx immobilization efficiency. However, the coatings with the longest GOx activity (30% still active after week four) were obtained at 50mbar with the highest methane flow (6sccm and 8sccm, respectively for samples 50/6 and 50/8). This indicates more favorable and stable chemical environment for the attachment of GOx on these coatings.

## ACKNOWLEDGMENTS

This work was developed within the project CICECO-Aveiro Institute of Materials, POCI-01-0145-FEDER-007679 (FCT Ref. UID /CTM /50011/2013), financed through the FCT/MEC and co-financed by FEDER under the PT2020 Partnership Agreement.

## REFERENCES

- [1] A. Kromka, L. Grausova, L. Bacakova, et al (2010) Diam. Relat. Mater. 19:190-95.
- [2] M. A. Neto, C.M.F. Gomes, E.L. Silva, et al (2012) Procedia Chemistry 6:117-124.

Sample	Immobilized GOx. (mg/dm <sup>2</sup> )
Si <sub>3</sub> N <sub>4</sub> substrate	91.4
25/2	68.3
25/4	110.9
25/6	210.4
25/8	140.8
50/2	175.8
50/4	117.7
50/6	134.7
50/8	51.8
100/2	112.1
100/4	147.2
100/6	152.6
100/8	91.4

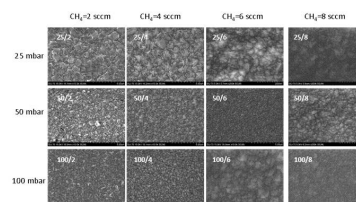


Figure 1.jpg

Table 1.jpg

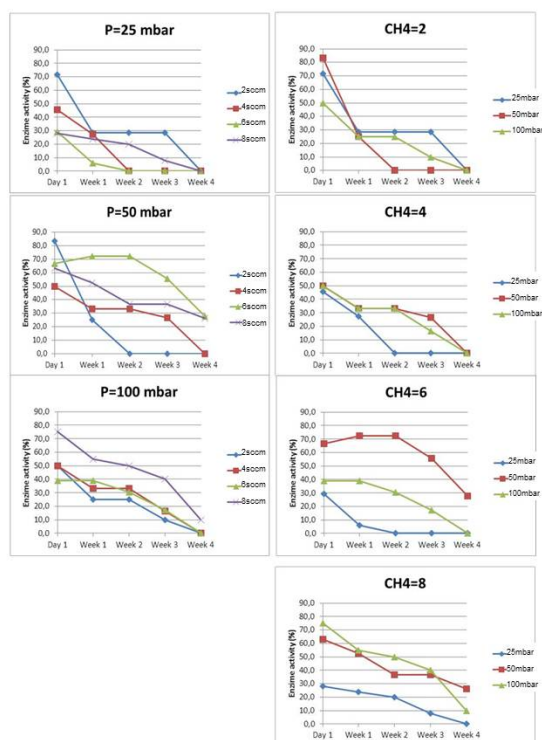


Figure 2.jpg

---

## Surface Modification of Porous Silicon Carbide by formation of a Functionalized Polymer

---

Thursday, 19th October - 13:30 - Poster Session - Hall & Room 3 - Poster - Abstract ID: 173

---

***Mrs. Lamia TALBI*<sup>1</sup>**

***1. USTHB/CRTSE/CMSI***

In recent years, the functionalization of porous silicon carbide surfaces by macromolecules constitutes an attractive approach for designing novel microsystems for numerous applications; such as electrochromic devices, rechargeable batteries, electromagnetic interference shielding, and sensors for detection of toxic gases. The advantages of these polymeric / silicon carbide nanostructures are their ease of fabrication, a high sensitivity and the most important is their room temperature operation. The characterization of polymer chains onto porous silicon carbide has received increasing attention mainly due to the possibility of controlling and modifying the properties of the porous material.

In this work, we explain the electrodeposition of PANI doped with two acids on porous silicon carbide. The nanostructured porous silicon carbide layers were formed by the electrochemical etch in appropriate ratio of components in the HF/H<sub>2</sub>O/H<sub>2</sub>O<sub>2</sub> solution, under a current constant source.

The deposited polymeric films on the porous silicon surface were confirmed by Fourier transform infrared spectroscopy (FTIR), which displayed the principal characteristic peaks attributed to the different functional groups. In addition, scanning electron microscopy (SEM) was used to characterize the surface morphology of the material. The structure has been used for ammoniac (NH<sub>3</sub>) vapor detection. The results show that the synthesized film exhibits a nanofibrous texture with a good sensitivity against NH<sub>3</sub> vapor with a good response time as 9 s and a recovery time 2 s for a low NH<sub>3</sub> concentration.

---

## Characterization of local atomic structure in Co/Zn based ZIFs by XAFS

---

Thursday, 19th October - 13:30 - Poster Session - Hall & Room 3 - Poster - Abstract ID: 175

---

**Ms. Yulia Podkovyrina<sup>1</sup>, Ms. Vera Butova<sup>1</sup>, Ms. Elena Bulanova<sup>1</sup>, Dr. Andriy Budnik<sup>1</sup>, Prof. Alexander Soldatov<sup>1</sup>, Prof. Carlo Lamberti<sup>2</sup>**

*1. International Research Center "Smart Materials", Southern Federal University, 2. Department of Chemistry, University of Turin, Italy*

Due to unique structural properties, high porosity, surface area and unexpected thermal and chemical stability zeolitic imidazolate frameworks (ZIFs) could be applied in catalysis, gas separation and storage [1]. For example, ZIF-8 could be effectively applied for iodine isotopes, which are a by-product of nuclear fuel cycle [2]. Most of ZIFs structures studied during the last decades are based on single metals and their properties mainly depend on metal species. Therefore, construction of mixed ZIFs would be an interesting option for tuning or introducing new properties in ZIFs.

In this study  $\text{Co}_x\text{Zn}_{1-x}$ -ZIF-8 ( $x=5, 25, 75\%$ ) frameworks we synthesized using microwave radiation [3]. The experimental Co K-edge (7709 eV) and Zn-K edge (9659 eV) XANES spectra were measured using in-house X-ray spectrometer Rigaku R-XAS Looper. The crystal structure of  $\text{Co}_x\text{Zn}_{1-x}$ -ZIF8 samples were characterized with powder X-ray diffraction (PXRD). Additionally, for the characterization of the samples XRF, TEM techniques were used.

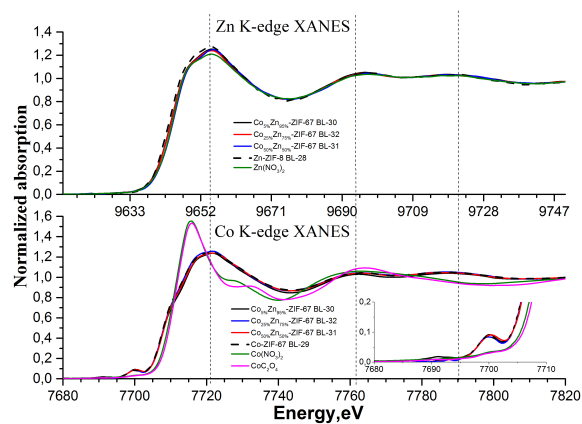
XRD patterns of synthesized samples suggests that the bimetallic ZIFs have the same crystalline structure as that of Zn-ZIF-8. A well-resolved pre-edge feature on the Co-K-edge XANES spectra ( $\sim 7,700$  eV) is characterized by an  $1s \rightarrow 3d$  electronic transition and clearly indicates that the local environment of cobalt atoms is not centrally symmetric and confirms the tetrahedral symmetry. The position of the absorption edge and the white line ( $\sim 7708$  eV) on the XANES spectra for the Co-ZIF-67 sample and the bimetallic  $\text{Co}_x\text{Zn}_{1-x}$ -ZIF-8 zeolites coincide, which means that the bimetallic ZIFs as well as the original Co-ZIF-67 material contain divalent cobalt ions, which is consistent with the data of X-ray diffraction.

This work was supported by the Government of the Russian Federation (Mega-grant no. 14.Y26.31.0001).

1. Tulchinsky, Y., et al., *Reversible Capture and Release of  $\text{Cl}_2$  and  $\text{Br}_2$  with a Redox-Active Metal–Organic Framework*. J. Am. Chem. Soc., 2017. **139**: p. 5992-5997.

2. Sava, D.F., et al., *Capture of Volatile Iodine, a Gaseous Fission Product, by Zeolitic Imidazolate Framework-8*. J. American Chem. Soc., 2011. **133**: p. 12398-12401.

3. Butova, V.V., et al., *New microwave-assisted synthesis of ZIF-8*. Mendeleev Commun., 2016. **26**: p. 43-44.



Xanes.jpg

# Highly controlled nanoporous Ag electrode by vaporization control of 2-Ethoxyethanol for a flexible supercapacitor application

Thursday, 19th October - 13:30 - Poster Session - Hall & Room 3 - Poster - Abstract ID: 176

**Mr. Jinwoo Lee<sup>1</sup>, Mr. Jinhyeong Kwon<sup>1</sup>, Mr. Habeom Lee<sup>1</sup>, Prof. Seung Hwan Ko<sup>1</sup>**

<sup>1</sup>. Seoul National University

Fine-tuning the surface morphology of the electrode on the nanoscale has attracted much attention in various fields, because the surface morphology of a material allows the functionalization in diverse areas of studies. In this study, we report a simple and cost-effective process to control the surface morphology and fabricate controlled nanopores on the silver electrode by employing 2-ethoxyethanol and two successive heat treatments. Varying a couple parameters, concentration of 2-ethoxyethanol in Ag organometallic ink and annealing temperature, serves to control the size, depth and morphology of nanopores. As a proof-of-concept, a high-performance supercapacitor was fabricated based on nanoporous silver electrode by electrodepositing MnO<sub>2</sub>.

To analyze the surface morphology, we utilized SEM and AFM characterization, and XRD confirmed the absence of oxidation in nanoporous silver. After electrodepositing MnO<sub>2</sub> on NPS, various electrochemical examinations such as cyclic voltammetry, galvanostatic charge-discharge measurement, and electro-chemical impedance spectroscopy were conducted to investigate the practicality of device. High electrical conductivity and mechanical robustness of nanoporous silver, which were examined with four-point probe test and bending test respectively, substantiate its prospect to be utilized in a variety of applications demanding a certain extent of flexibility. A supercapacitor was fabricated to illustrate the potential practicality of the silver nanoporous electrode herein. The energy density and specific capacitance of supercapacitor based upon the silver nanoporous electrode was measured to be 19.8Wh/kg and 327F/kg respectively at scan rate of 1mV/s. This value was almost three times higher than that of supercapacitor without any pore.

The results demonstrate a simple and economical method to highly control the surface morphology and create nanopores on the Ag electrode. This method is expected to be employed not only in energy storage device but also in other fields by developing a certain surface morphology suitable for each electronic application.

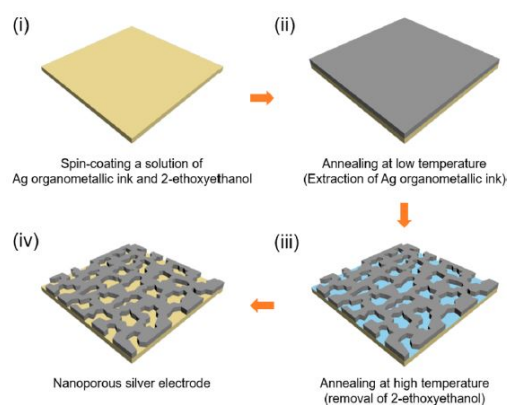


**Figure 1.** Schematic illustration of the fabrication process of NPS by two successive heat treatments.

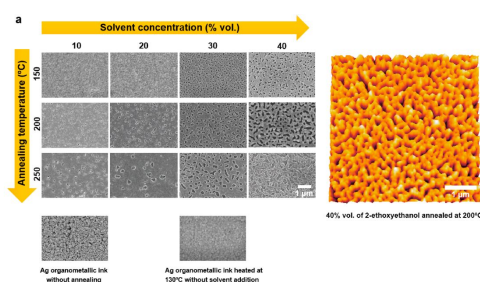


**Figure 2.** SEM image of nanoporous Ag electrode fabricated by varying the concentration of 2-ethoxyethanol and postannealing temperature. AFM profile of the representative image is shown on the right.

2.jpg

1.jpg

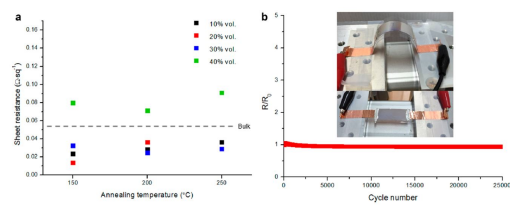


Figure 3 (a) sheet resistance measurement by varying the concentration of 3-ethoxyethanol and post annealing temperature in comparison with sheet resistance of thin film silver (b) cyclic bending test of NPS recording the change in resistance using a linear stage.

3.jpg

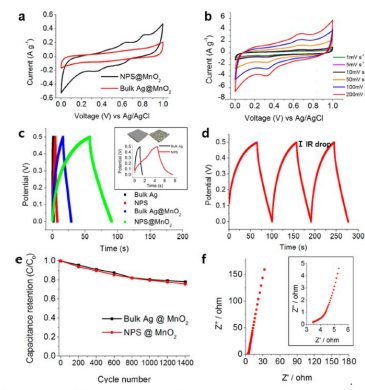


Figure 4. (a) Cyclic voltammetry of NPS@MnO<sub>2</sub> and Bulk Ag@MnO<sub>2</sub> at scan rate of 5 mV s<sup>-1</sup>. (b) Cyclic voltammetry at different scan rates. (c) Galvanostatic charge/discharge measurement (1 A/g) of Ag smooth thin film and NPS loaded with MnO<sub>2</sub>. Ag smooth thin film was prepared by heating Ag organometallic ink at 130 °C. Inset includes the charge/discharge curve of Ag smooth thin film and NPS. (d) Galvanostatic charge/discharge measurement of NPS@MnO<sub>2</sub> at current density of 1 A/g. (e) Cyclic retention of NPS@MnO<sub>2</sub> and Ag film. (f) Nyquist plot of NPS@MnO<sub>2</sub>. Inset shows the electrical impedance behavior at high-frequency region.

4.jpg



## Adherence of amino acids functionalized iron oxide nanoparticles on bacterial models *E. coli* and *B. subtilis*

Thursday, 19th October - 13:30 - Poster Session - Hall & Room 3 - Poster - Abstract ID: 193

**Dr. Wiliam Trujillo<sup>1</sup>, Ms. jacquelyne zarria romero<sup>2</sup>, Dr. J. Pino Gaviño<sup>2</sup>, Ms. Lucila Menacho<sup>1</sup>, Dr. M. Coca Calderón<sup>2</sup>, Dr. Angel Bustamante<sup>1</sup>**

*1. Laboratorio de Cerámicos y Nanomateriales, Facultad de Ciencias Físicas, Universidad Nacional Mayor de San Marcos, 2. Laboratorio de Reproducción y Biología del Desarrollo, Facultad de Ciencias Biológicas, Universidad Nacional Mayor de San Marcos*

Magnetic iron oxides nanoparticles (NPs) functionalized with lysine (Lys) and arginine (Arg) was obtained by following chemical co-precipitation route in basic medium. The synthesis was performed by mixing ferrous chloride ( $\text{FeCl}_2 \cdot 4\text{H}_2\text{O}$ ), ferric chloride ( $\text{FeCl}_3 \cdot 6\text{H}_2\text{O}$ ) and the specific amino acid in a molar ratio of 1: 2: 0.5, respectively. High pH sample was washed several times with distilled water to reach a pH similar to distilled water (pH=7) after the synthesis process, part of the NPs obtained was dried. The dried samples were characterized by X-ray diffraction (XRD), Mössbauer spectroscopy (MS), infrared Fourier transform spectroscopy (F-TIR) and zeta potential ( $\zeta$ ). Of the measurements of XRD and MS was obtained that the samples are magnetic nanoparticles (core-shell) of magnetite and maghemite of about 9 nm in diameter. Of the F-TIR and zeta potential measures was obtained that the amino acids Lys and Arg were correctly functionalized at magnetic nanoparticles, referred to herein as M@Lys and M@Arg.

In order to demonstrate the capture and adhesion of the nanoparticles to the bacteria, scanning electron microscopy (SEM) was performed. The obtained visualizations of both bacteria show that they are coated by the magnetic particles. In addition, M@Lys (*B. subtilis*) were cultured to verify the inhibition of growth measured by colony forming units (CFU), the concentrations of M@Lys used were  $1.75 \times 10^2$  g/mL and  $0.875 \times 10^2$  g/mL, After the confrontation obtained efficiencies of 75.63% and 98.75% respectively for the third dilution. While for the fourth dilution efficiencies were 90% and 98.57% respectively were obtained for each concentration of nanoparticles. Hinting that a high efficiency of bacterial capture at very low concentrations of NPs, which gives us a tool to capture nanobiotechnology bacteria in liquid cultures with application to capture them in wastewater. Based on our results we concluded that NPs functionalized with the amino acids Lys and Arg adhere to the bacteria efficiently in low concentrations.

**Keywords:** iron oxides, nanoparticles, maghemite, *E. coli*, *B. subtilis*, functionalization, SEM, UFC.

# Dynamic Consolidation and Investigation of Nanostructural W-Cu / W-Y Cylindrical Billets

Thursday, 19th October - 13:30 - Poster Session - Hall & Room 3 - Poster - Abstract ID: 256

***Dr. Bagrat Godibadze*<sup>1</sup>, *Dr. Akaki Peikrishvili*<sup>2</sup>, *Dr. Elguja Chagelishvili*<sup>3</sup>, *Mr. Avtandil Dgebuadze*<sup>1</sup>,  
*Dr. Grigor Mamniashvili*<sup>4</sup>**

*1. G. Tsulukidze Mining Institute, 2. F. Tavadze Institute of Metallurgy and Materials Science, 3. G. Tsulukidze Mining Institute, 4. E. Andronikashvili Institute of Physics. Ivane Javakhishvili Tbilisi State University.*

The main purpose of presented work is to obtain W-Cu&W-Y cylindrical bulk nanostructured billets by explosive consolidation technology in hot condition, near to theoretical densities and improved physical/mechanical properties.

The first stage investigation were carried out for explosive consolidation of powders at room temperatures to obtain billets with increased density without cracks and activated surfaces of consolidated particles. The second stage investigation were carried out for the same billets, but consolidation were conducted in hot conditions, after heating of samples in between 940-1100<sup>0</sup>C, the intensity of loading was equal to 10GPa.

Consolidated different type of W-Cu composition containing 10-40% of nanoscale W, during investigation showed that the combination of high temperatures (above 940°C) and two-stage shock wave compression was beneficial to the consolidation of the incompatible pair W-Cu composites, resulting in high densities, good integrity and good electronic properties.

It was established that in comparison with W-Cu composites with coarse tungsten the application of nanoscale W precursors and depending of content of W gives different result.

Tungsten is a prime material candidate for the first wall of a future fusion reactor. In this study, the microstructure and microhardness of tungsten-yttrium (W-Y) composites were investigated as a function of Y doping content (0.5÷2wt.%). It was found that the crystallite sizes and the powder particle sizes were increased as a result of the increase of Y content. Nearly fully dense materials were obtained for W-Y alloys when the Y content was higher than 0.5wt.%. Investigation revealed that the Y rich phases were complex (W-Y) oxides formed during the sintering process. Also very interesting to use doping chromium with yttrium-containing alloys. e.g. (W-10÷12Cr-0.5÷2Y)wt.%. The extent up to which yttrium acts as an active element improving the adherence and stability of the protective Cr<sub>2</sub>O<sub>3</sub> layer formed during oxidation is assessed.

The processing of the precursors and the fabrication of nanostructured composites together with the detail description of explosive consolidation technique in hot condition and other features of structure-property relationship will be presented and discussed.

## Acknowledgements

The authors gratefully acknowledge the financial support of the Shota Rustaveli National Science Foundation (SRNSF Grant Agreement № YS15\_2.2.10\_101).

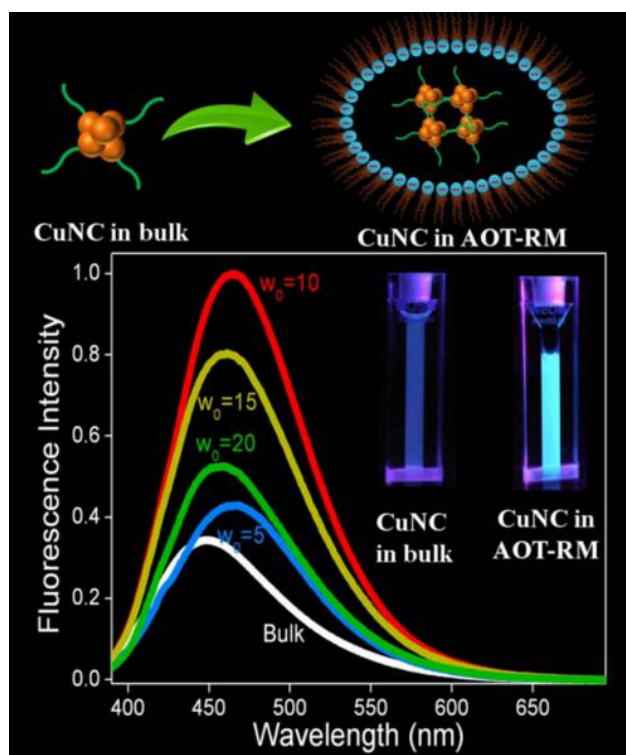
# Unraveling the ultrafast fluorescence properties of copper nanoclusters synthesized within the nanopool of reverse micelles

Thursday, 19th October - 13:30 - Poster Session - Hall & Room 3 - Poster - Abstract ID: 278

***Mr. Raj Kumar Koninti<sup>1</sup>, Mr. Partha Hazra<sup>1</sup>***

*1. Indian Institute of Science Education and Research, Pune*

We reported a new design strategy for the preparation of highly stable and ultrabright fluorescent copper nanoclusters (CuNCs) with L-cysteine (Cys) as a protecting ligand within the water nanopool of reverse micelles (RMs). Present work has been under taken to address the mysterious origins of excitation-dependent fluorescence spectral shift of CuNCs and investigate its ultrafast fluorescence dynamics using steady-state and femto-second fluorescence upconversion techniques. From our experiments, we elucidate that the broad fluorescence from CuNCs in RM consists of two spectral overlapped bands corresponding to the metal-core and surface states of CuCN-Cys, respectively. The intrinsic emission of CuNCs distributed in shorter wavelength regions (<470 nm) mainly originates from metal-core. This intrinsic emission band obeys the Jellium model<sup>1</sup> and the spectral broadening of this intrinsic emission band mainly originates from the effective electron-electron scattering.<sup>2</sup> On the other hand, extrinsic fluorescence band (above 470 nm) is caused by surface states. The extrinsic emission band has a much broader emission due to the presence of numerous surface states. The trapping of excited electrons in the various surface states leads to emission in the longer wavelength regions as well as excitation dependent emission of CuNCs in RM. Femto-second fluorescence upconversion and TCPSC decays of CuNCs in RMs comprise of an ultrafast sub-pico second (~700 fs), a fast pico second (~30 ps), a nano-second (~1 ns) component and a ultra-slow (~5 ns) components. The fast component of ~700 fs and 30 ps are attributed to the relaxation of excited state electron within the core states of CuNCs nano-clusters/trapped in surface states and electron-acoustic phonon scattering, respectively. The slowest component (~1 ns) is originated due to the recombination of electrons and holes from the metal core states. The ultra-slow (~5 ns) component may be arises due to recombination of electrons trapped in the surface states.



Toc.jpg

# Graphene/styrene-isoprene-styrene copolymer composite thin film as a flexible microstrip antenna for heptane vapors detection

Thursday, 19th October - 13:30 - Poster Session - Hall & Room 3 - Poster - Abstract ID: 314

**Dr. Robert Olejnik<sup>1</sup>, Dr. Jiri Matyas<sup>1</sup>, Dr. Petr Slobodian<sup>1</sup>, Dr. Pavel Riha<sup>2</sup>**

*1. Tomas Bata University in zlin, 2. Institute of Hydrodynamics, Academy of Sciences, Prague, Czech Republic*

The electronic devices use mainly copper based microstrip antenna for communication between each portable device in a network. In many fields of science, graphene is one of the most promising material. Gradually, there are increasing possibilities for the use of graphene in electronics. The main reasons for employing this material are its characteristics, which are, for instance, the good electrical conductivity or great potential for miniaturization.

This contribution is focused on the use of polymer composite containing graphene as a filler for the application materialized in a passive antenna. This device consists of a layer of particular graphene/styrene-isoprene-styrene copolymer composite deposited on PET foil substrate. To make the antenna, the graphene/styrene-isoprene-styrene copolymer dispersion was prepared by sonication of the polymer toluene solution and after that dip-coated on the PET foil substrate (25 % by wt. of graphene particles). The thickness of electrically conductive composite film active layer was 0.58 mm while of the PET foil 0.21 mm. The prepared microstrip antenna (width 10, length 25 mm) operates at frequency 1.8 GHz (-40.02 dB). The measurement set up is schematically demonstrated in Fig. 1. The main advantage of the antenna is its low weight and flexibility. This antenna was finally exposed to saturated vapors of heptane at 25°C. Heptane is a solvent for the styrene-isoprene-styrene copolymer leading to the composite film swelling. The swelling caused volume changes of the polymer layer as well as a change of its macroscopic electrical resistance. Consequently, also the antenna parameters were changed such as the gain in decibels and the shift of resonant frequency. It suggests, that the made polymer composite based thin film flexible microstrip antenna can be used for heptane vapor detection.

This work was supported by the Ministry of Education, Youth and Sports of the Czech Republic – Program NPU I (LO1504) and with the support of the Operational Program Research and Development for Innovations co-funded by the European Regional Development Fund (ERDF) and the national budget of the Czech Republic, within the framework of the project CPS-strengthening research capacity (reg. number: CZ.1.05/2.1.00/19.0409).

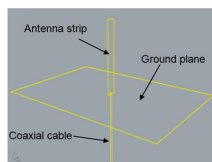


Fig. 1 Schematic illustration of the antenna set up with the antenna composite/PET foil strip connected to the ground plane made of FR-4 copper substrate of the size 65 × 75 mm and the coaxial cable.

Antenna set up.jpg

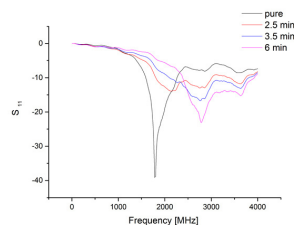


Fig. 2 Frequency dependence of antenna gain for the pure composite and after exposition to heptane saturated vapour during different time of exposure.

Detection of heptane by antenna.jpg

# Understanding of two distinct and independent mechanisms of apoptosis and autophagy-mediated necrosis in human endothelial cells to determine size allowance of silica nanoparticles for biomedical application

Thursday, 19th October - 13:30 - Poster Session - Hall & Room 3 - Poster - Abstract ID: 456

**Dr. Young-Lai Cho<sup>1</sup>, Ms. Na Geum Lee<sup>2</sup>, Dr. Kwang-hee Bae<sup>1</sup>**

**1. Korea Research Institute of Bioscience and Biotechnology, 2. Department of Biomolecular Science, University of Science & Technology**

Nanotechnology has brought a rapid progress in the field of pharmacology and medicine. In particular, nanoparticles (NPs) have been extensively applied for targeted delivery system of contrast agents and drugs to fulfil more successful diagnosis and therapy of diseases. Many nanoparticles have been developed using various organic, inorganic and hybrid materials, and among them silica is one of attractive base materials in engineered nanoparticles. Silica nanoparticles (SiNPs) have been found considerable biomedical science, for such fields as biosensor, medical diagnostics, drug delivery, and cancer therapy. Although recent advances in potentials and risk assessment of SiNPs have been reported, the corresponding guideline to appropriate size and the toxic mechanisms of SiNPs have not been fully defined. To explore possible SiNPs-mediated cytotoxicity and determine size relevance, we fabricated SiNPs which enable facile control of their sizes: ‘seed’ SiNPs (20nm SiNPs; 22.98±0.66 nm) and ‘regrowth’ SiNPs (30,40,and 50nm SiNPs; 30.22±1.97, 40.91±2.88, and 48.84±1.22 nm. In a relative low range (< 25 µg/ml), even only 20nm SiNPs showed a significant decrease in cellular viability in a dose-dependent manner. Notably, they potently induced both apoptosis and necrosis, which was distinct mechanisms independently. First, exposure of the trace SiNPs increased ROS production at short time, and it was leading to direct influence on ER stress induction, supporting that the ROS-mediated ER stress is a crucial signaling in mitochondrial apoptosis pathway. Moreover, ROS significantly triggered increases in intracellular calcium ion (Ca<sup>2+</sup>) levels on ECs. Subsequently, 20nm SiNPs markedly induced autophagy through **PI3K/Akt/eNOS** signaling axis, and then autophagy induction triggered necrotic cell death of ECs, indicating that SiNPs-induced cytotoxicity is associated with autophagy-mediated necrosis. In this study, we presented experimental data regarding the differential size-related biological effects of SiNPs on ECs. Although further investigations are required before the current findings can be clinically applied, these data will provide a better understanding of the mechanism underlying SiNPs size-dependent cytotoxicity in vasculature and facilitate the future development of safer biomedical applications of SiNPs

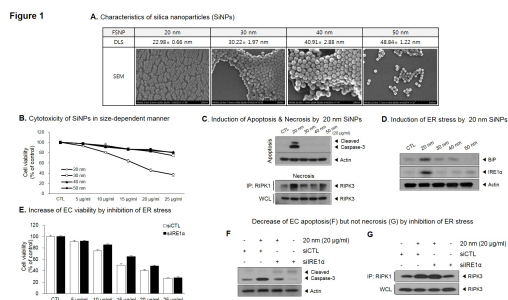


Fig.1.jpg

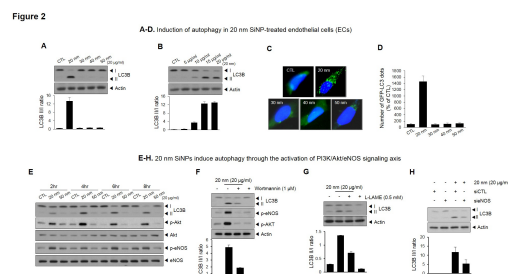


Fig.2.jpg

Figure 3

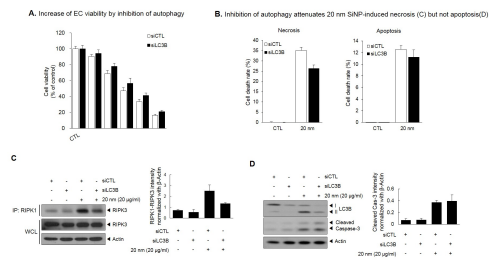


Fig.3.jpg

Figure 4

**A-C.** 20 nm SNPs induce both ER stress-mediated apoptosis and autophagy-mediated necrosis, independently

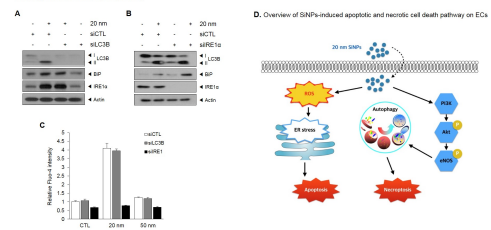


Fig.4.jpg

---

# Wireless electronic manometer based on nanomaterials

---

Thursday, 19th October - 13:30 - Poster Session - Hall & Room 3 - Poster - Abstract ID: 803

---

***Ms. Zhuldyz Otarbay<sup>1</sup>, Ms. Dilyara Abay<sup>1</sup>, Ms. Madengul Token<sup>1</sup>, Dr. Mukhit Muratov<sup>1</sup>, Mr. Daniyar Ismailov<sup>1</sup>, Mr. Nazim Guseinov<sup>1</sup>, Dr. Maratbek Gabdullin<sup>1</sup>***

*1. National Nanotechnology Laboratory of the Open Type, Al-Farabi Kazakh National University*

## Introduction

Currently, nanomaterials are widely used in all fields of activity. They have unique properties due to small size, structure, chemical composition and large surface area. This article examines the use of electronic sensors based on nanomaterials. Manometer-instrument for measuring of excess pressure in liquid and gaseous media. Manometric devices have a variety of applications: industry, transport, household appliances, scientific researches etc.

## Methods

The main method of obtaining the CNM was the CVD method. This method is relevant, in connection with the frequency of output. The essence of the method is the pyrolytic decomposition of a gas containing carbon and the synthesis of CNTs on catalyst particles that are in the form of a thin film on a substrate or a powder in a stationary or mobile (pseudo-boiling) layer.

## Results

Initially, Si substrates were used which were previously deposited by spraying the film with Ni catalysts, for the further growth of CNTs. The process of synthesis, growth of CNTs passed in a tube furnace with a gradual heating up to 750<sup>0</sup> C, and also with a constant supply of hydrogen. After the temperature of the preset bar 750<sup>0</sup> C was set, the alcohol itself was supplied directly for 15-20 minutes, the carbon carrier, which when decomposed into the oven and deposited on the film, formed CNTs with Ni catalysts on the film, the average tube diameter reached 80 nm, and the structure was a felt of a long order of 1.5 μm.

## Discussion

In this work, an experiment was carried out with Ni catalysts at a temperature of 750 ° C for 15-20 min, and CNTs with a diameter of 80 nm were formed on the film, and the structure was 1.5 μm. The resulting nanotubes were used in manometers with a possible remote control system. Next, a hardware part was created that was a set of mounted PCBs and a software part with output to wireless interfaces. The wireless electronic manometer reduces operational costs, improves security and provides continuous access to data through a wireless device via Bluetooth or Wi-Fi.



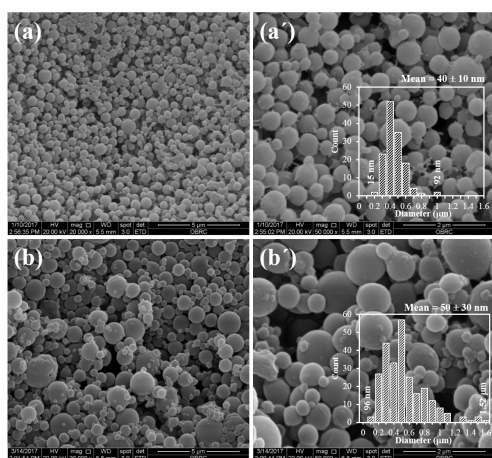
# Antibiotic-Encapsulated Poly(lactic acid) Particles integrated in Porous Gelatin Scaffolds for Tissue Engineering Applications

Thursday, 19th October - 13:30 - Poster Session - Hall & Room 3 - Poster - Abstract ID: 532

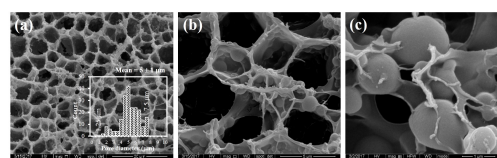
**Dr. Patcharakamon Nooeaid<sup>1</sup>, Dr. Piyachat Chuysinuan<sup>2</sup>, Dr. Chalanan Pengsuk<sup>1</sup>, Dr. Decha Dechtrirat<sup>3</sup>, Prof. Supanna Techasakul<sup>2</sup>**

1. Srinakharinwirot University, 2. Chulabhorn Research Institute, 3. kasetsart University

Loss and damage of tissues generally arise from chronic diseases and traumatic lesions. For instance, infections, inflammatory diseases, severe burns and deep wounds are needed a promising strategy to reconstruct new tissue with showing normal functions. Due to complexity and diversity of specific tissues, three-dimensional scaffolds showing microporous structure and optical physico-chemical properties with an addition of therapeutic drugs have gained high interests with the basis of tissue engineering. Therefore, tetracycline hydrochloride-encapsulated poly(lactic acid) (TCH-PLA) particles were fabricated by the method of double emulsion/solvent evaporation and were incorporated into gelatin foams, forming three-dimensional TCH-PLA/Gel porous scaffolds. Morphology, encapsulation efficiency and chemical composition of the fabricated particles were investigated. The results demonstrated that drug-free PLA- and TCH-PLA particles were in submicron-sized spherical shape (up to 0.5 micrometers). Their size distribution was heterogeneous when the drug was encapsulated and the encapsulation efficiency was found at around 77%. In addition, TCH-PLA particles were incorporated in porous gelatin foams fabricated by lyophilization method followed by chemical crosslinking. FTIR analysis was used to confirm the existence of both PLA and gelatin. In vitro release study showed that the TCH-PLA particles exhibited TCH release in an initial burst release reaching around 55% after 72 h of immersion in phosphate buffered saline solution, followed by a sustain release (up to 60%) at longer time. Meanwhile, the TCH-PLA/Gel scaffolds released lower amount of drug compared to the TCH-PLA particles at the same time. Antibacterial test was performed to confirm the antibacterial activity of TCH-PLA/Gel scaffolds against *S. aureus* and *E. coli*, indicated by the reduction of bacteria after incubation for 1, 3 and 7 days. From the results, TCH-PLA/Gel scaffolds with drug releasing function are able to be used in tissue engineering.



Sem.jpg



Sem-scaffold.jpg

# Microstructure Characterization of Mechanically-Induced Synthesizing of Zinc Metatitanate

Thursday, 19th October - 13:30 - Poster Session - Hall & Room 3 - Poster - Abstract ID: 597

**Dr. Latifah Alhajji<sup>1</sup>**

**1. Kuwait Institute for Scientific Research (KISR)**

Recently, extensive research focus was directed toward zinc titanates. Considerable interest had been revealed for their importance in various applications due to their low cost and being environmentally friendly. Zinc titanates exist in three multiphases resulted from the reaction of  $\text{TiO}_2$  and  $\text{ZnO}$ . The metatitanate phase ( $\text{ZnTiO}_3$ ) is distinct amongst analogous zinc titanates by its significance to development of dielectric materials for microwave frequencies and hence, significance in satellite communication systems industry. Pure product synthesis of  $\text{ZnTiO}_3$  was reported elsewhere to be hard, and additives and/or heat treatments were required, which will add cost.

The present investigation was focused on the preparation of  $\text{ZnTiO}_3$  via solid-state reaction in an equimolar loose powder mixture of  $\alpha\text{-TiO}_2$  and  $\text{ZnO}$ . The reaction was conducted at room temperature by utilization of high mechanical force induced by ball milling at different time intervals up to 9 hrs, and without the need of additives or high temperature treatment of either reactants or product. The milled powders were characterized by XRD, SEM, HR-TEM and UV-vis reflectance spectroscopy. Accordingly, XRD results (Fig. 1) revealed the commence of the solid state reaction between the two metal oxides after 3 hrs of milling recorded by the evolution of tiny peak at  $2\theta = 29.9$ , which continued to increase as milling time increased. After 9 hrs, the dominant product was  $\text{ZnTiO}_3$ .  $\text{Zn}_2\text{Ti}_3\text{O}_8$  existed as a minor product. Its existence was confirmed by HR-TEM (Fig.2). The minimum and maximum bandgap energy values of 3.14 eV and 3.29 eV were observed in  $\alpha\text{-TiO}_2/\text{ZnO}$  nanocomposite before milling and after milling for 9 hrs, respectively.

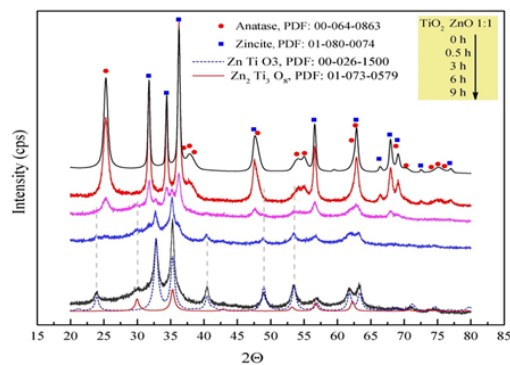


Figure 1 xrd patterns for 1-1 tio2 zno after ball milling for 0 0.5 3 6 and 9 hrs.png

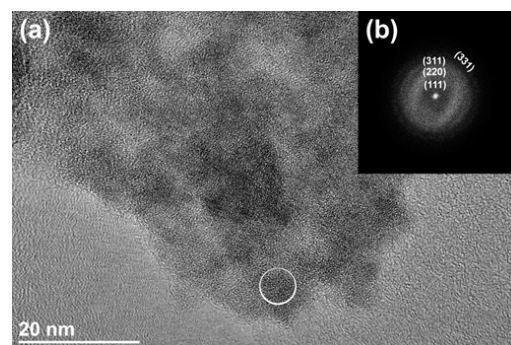


Figure 2 hrtem image and the corresponding sadp.png

---

## Cytochrome P450 genes expression in HepG2 cells after treatment with nanostructures of different allotropic forms of carbon

---

Thursday, 19th October - 13:30 - Poster Session - Hall & Room 3 - Poster - Abstract ID: 634

---

**Ms. Barbara Strojny<sup>1</sup>, Dr. Marta Grodzik<sup>1</sup>, Ms. Malwina Sosnowska<sup>1</sup>, Mr. Jarosław Szczepaniak<sup>1</sup>, Dr. Marta Kutwin<sup>1</sup>, Dr. Sławomir Jaworski<sup>1</sup>, Ms. Natalia Kurantowicz<sup>1</sup>, Dr. Mateusz Wierzbicki<sup>2</sup>, Dr. Anna Hotowy<sup>1</sup>, Prof. Ewa Sawosz<sup>1</sup>**

*1. Faculty of Animal Science, Warsaw University of Life Sciences, 2. Faculty of Animal Science, Warsaw University of Life Science*

### Introduction

Carbon nanomaterials, such as diamond nanoparticles (DN), graphene oxide (GO) or graphite (GR) nanoplatelet-shave been recently studied for several biomedical applications, what results from their unique properties at nanoscale and high biocompatibility. The safety of their application depends not only on the lack of systemic toxic effects, but also on the possibility of metabolism alteration of co-administrated xenobiotics. The mechanism of carbon nanoparticles metabolism within liver, where nanoparticles are relocated after *in vivo* administration, is also still unknown. Thereby, effects of DN, GO and GR on expression of genes responsible mainly for drug metabolism in liver were studied on HepG2 *in vitro* model of liver cells.

### Methods

Morphology of DN, GO and GR was assessed using transmission electron microscopy. Cytotoxic effect of DN, GO and GR against HepG2 cells was determined by MTT viability assay in doses ranging from 3,125 to 100 µg/mL. Gene expression on mRNA level was quantified using real-time PCR with ddC<sub>T</sub> relative method, using β-actin as a calibrator. Following genes were studied: AhR, CAR, PXR receptors and CYP1A2, CYP2B6, CYP2D6, CYP2E1, CYP3A4 cytochrome P450 genes.

### Results

DN did not affect the HepG2 cells viability, whereas GO and GR induced cytotoxic effect in dose-dependent manner. All used nanomaterials decreased expression of genes for receptors CAR, AhR and PXR, as well as for CYP2D6 and CYP3A4, inducing at the same time over-expression of CYP1A2 and CYP2B6. CYP2E1 expression increased in DN and GR groups, and decreased in GO group.

### Discussion

Obtained results confirmed that out of the three examined nanostructures, DN are characterized by the highest biocompatibility. It is in accordance with the previous results, where toxicity of DN, GO and GR were studied on rat model during the 12-week long experiment. Alterations of indices such as glutathione and MDA levels in rat livers suggested relocation of nanoparticles into the liver. Analysis of gene expression for cytochrome P450 enzymes and regulatory receptors on *in vitro* liver model showed that all three carbon materials induced similar response, what may be first step toward understanding the mechanism of carbon nanoparticles metabolism.

# Anti-inflammatory properties of new hybrid biomaterials based on silver nanoparticles and polyphenols from European elderberry fruits

Thursday, 19th October - 13:30 - Poster Session - Hall & Room 3 - Poster - Abstract ID: 670

**Prof. Luminita David<sup>1</sup>, Dr. Bianca Moldovan<sup>1</sup>, Mrs. Nicoleta Decea<sup>2</sup>, Prof. Gabriela Adriana Filip<sup>2</sup>**

**1.** Faculty of Chemistry and Chemical Engineering, Babes-Bolyai – University, **2.** Iuliu Hatieganu University of Medicine and Pharmacy

**Introduction:** In recent years, silver nanoparticles have been intensively studied, due to their diverse applications in medicine, such as antiviral, antimicrobial, anticancer, antiangiogenic and antioxidant agents. The phytomediated synthesis of silver nanoparticles, using plants or fruits extracts, gained lately much popularity, offering an effective, safe and free of side effects therapeutic alternative for a wide variety of diseases. The aim of our study was the green synthesis of silver nanoparticles using European elderberry fruit extract and the investigation of their anti-inflammatory effects.

**Methods:** The green synthesis of silver nanoparticles has been achieved by reducing silver ions from silver nitrate solution with European elderberry fruit extract, at different nitrate:extract ratios, at room temperature. The anti-inflammatory effect of the obtained nanoparticles was studied *in vivo* on acute inflammation model in Wistar rats in comparison with Indomethacin (a widely used non-steroidal anti-inflammatory drug), by measuring the pro-inflammatory cytokine tumor necrosis factor alpha (TNF $\alpha$ ) levels at 2, 24 and 48 hours after carrageenan induced inflammation.

**Results and Discussion:** The optimum ratio nitrate:extract for the synthesis of new hybrid biomaterial using biologically active compounds from European elderberry fruit extract was found to be 7:3. The obtained silver nanoparticles were characterized using different techniques such as UV-VIS spectroscopy, transmission electron microscopy (TEM), X-ray diffraction technique (XRD) and differential scanning calorimetry (DSC) and have been stable for more than 60 days. Treatment with silver nanoparticles significantly decreased the TNF $\alpha$  levels at all the investigated time intervals after carrageenan administration compared to indomethacin.

**Conclusion:** An eco-friendly, rapid and cost effective method for the biosynthesis of silver nanoparticles using the European elderberry fruits extract was developed. Investigation of their anti-inflammatory properties revealed a better activity compared to indomethacin, suggesting their great potential as ingredients of new therapeutic agents for treatment of inflammatory diseases.



European elderberry fruits.jpg

---

# Microstructure analysis of differently shaped nanocrystalline (Fe,Y)3O4

---

Thursday, 19th October - 13:30 - Poster Session - Hall & Room 3 - Poster - Abstract ID: 678

---

***Dr. Bratislav Antic***<sup>1</sup>

*1. University of Belgrade*

## Introduction

One of possibilities to tailor the physical/chemical properties of magnetite (Fe<sub>3</sub>O<sub>4</sub>) is a partial substitution of iron by 3d and 4f elements. The rare earth (4f) ions are larger than the hosts, hence they often create structural distortions and have significant influence on the crystallite size, strain and morphology. The main aim of the research was to analyze effects of partial substitution of Fe<sup>3+</sup> by Y<sup>3+</sup> in nanocrystalline magnetite, Fe<sub>3</sub>O<sub>4</sub>. Possibilities for arsenic III and arsenic V removal from water by synthesized materials were tested.

## Methods

Nanocrystalline Fe<sub>3-x</sub>Y<sub>x</sub>O<sub>4</sub> (x=0.00, 0.05, 0.10) were prepared by use of two-stage procedure, co-precipitation at room temperature accompanied by hydrothermal treatment at 200 °C. Transmission electron micrographs and selected-area diffraction patterns were collected with a Jeol JEM 2100. X-ray powder diffraction data (XRPD) were collected on a PANalytical X'pert PRO MPD diffractometer.

## Results

Introducing yttrium in spinel lattice of magnetite has led to the formation of nanorods and spherical nano particles with spinel structure. Results of X-ray line broadening analysis show that addition of Y<sup>3+</sup> provokes increase of apparent strain and crystallite size values in all directions. Largest average apparent crystallite size is down [110] for all compositions. With Y<sup>3+</sup> concentration increase average apparent crystallite size along [110] becomes 2-3 times a larger than along [100] and [111] direction. For Fe<sub>3</sub>O<sub>4</sub>, the largest average strain was found in [100] direction, and the lowest in [111] direction. By TEM it was determined that the direction of growth of the spinel nanorods is down [110]. Materials characteristics toward arsenic (III) and (V) adsorption were investigated. It was found that increase of Y<sup>3+</sup> concentration was followed with decrease of As (III) removal efficiency and increase in As (V) removal characteristics.

## Discussion

To our best knowledge this is the first report on investigation the impact of yttrium ions on the morphology of (Fe,Y)<sub>3</sub>O<sub>4</sub>. The influence of partial Fe<sup>3+</sup> substitution by Y<sup>3+</sup> in nanocrystalline magnetite on sample morphology and on arsenic adsorption was shown. Arsenic (III) and (V) removal tests show that introducing yttrium in magnetite, with controllable synthesis procedure, can be crucial for physical/chemical properties of studied materials.



---

## Material Science and Nanotechnology Application in Biomedical Practice.

---

Thursday, 19th October - 13:30 - Poster Session - Hall & Room 3 - Poster - Abstract ID: 763

---

**Dr. Sidorenko Evgeny <sup>1</sup>, Dr. Musina Alvina <sup>2</sup>**

1. Russian State Medical University, 2. Russian State Institute of Eye and Plastic Surgery

*Polymer materials are widely used in medicine, due to their low price and the tendency of single-use application. But the wide use of polymers has resulted in a variety of diseases associated with microorganisms of the biofilm formed on the polymer surface. The process of the biofilm formation is due to the loose friable porous structure of polymer materials, which is a nutrient medium for microorganisms. There exists a class of “diseases caused by the biofilm pathogens”, a separate class of severe diseases. Sometimes they are not amenable to conventional treatment. Considering the fact that the microorganisms have the ability to synthesize proteins from inorganic compounds, it enhances the harmfulness of biofilm agents and the danger of new, stronger and more resistant strains. The aforementioned reasons either require using more expensive materials than polymers or the application the modification of the polymer material surface.*

*The research explores the treating of container polymer surface for storage of different alloplants, artificial substitutes, preventing any danger of biofilm formation when contacting with biological environment and providing the guaranty for aseptic and prolonged storage conditions. The application of nanotechnology is aimed at the modification of the physical-chemical surface characteristics: the relief, chemical element composition, atomic structure, charge on the surface, which can assist the adhesion features or impart the repelling of a certain element, biochemical compounds, proteins, cells from the interface. The creation of active functional groups of composite NSS (nano structured surface) gives a new quality of material with the certain NSS features.*

*Carbon is chemical element with one of the smallest size allows obtaining an unlimited number of chemical compounds or gas mixtures for surface treatment, to obtain a wide range of surface characteristics with any desired properties. The use of carbon\carbyne-containing films treatment by means of of surface nanostructuration and following nanomodification technology for protecting polymer surface is a solution to the problem of biofilm formation, aseptical condition and ensuring the biocompatibility of the treated surface with the contacting living tissues. It's as a small step in the study of a complex and currently not well-studied Biorganic structure creation or self-reproduction.*

---

# Luminescent Dye-Doped Polymer Nanofibers Produced by Electrospinning Technique

---

Thursday, 19th October - 13:30 - Poster Session - Hall & Room 3 - Poster - Abstract ID: 837

---

**Dr. Monica Enculescu <sup>1</sup>, Mr. Alex Evanghelidis <sup>1</sup>, Dr. Ionut Enculescu <sup>1</sup>**

*1. National Institute of Materials Physics*

Among numerous methods for obtaining polymer nanofibers, electrospinning technique distinguishes itself due to the more growing interest induced by its proved utility. Production of doped polymeric nanofibers was intensively studied lately because of the increased interest for the obtaining of functional nanofibers.

Electrospinning is a facile method for producing polymer nanofibers with diameters from nanometrical to micrometrical sizes that are cheap, flexible, scalable, functional and biocompatible. Besides the multiple applications in medicine, electrospun polymeric nanofibers permit manipulation of light at nanometric dimensions when doped with organic dyes or different nanoparticles. The technique uses an electrical field to draw fine nanofibers from solutions and does not require complicated devices or high temperatures. Different morphologies of the nanofibers are obtained for the same polymeric host when different process parameters are used. Consequently, optical properties of the nanofibers can be tuned (e.g. changing the emission peak's wavelength) by varying the electrospinning parameters.

We focus on obtaining doped polymer nanofibers with enhanced optical properties using the electrospinning technique. The aim of the paper is to produce dye-doped polymer nanofibers' mats incorporating uniformly dispersed dyes. Transmission and fluorescence of the fibers will be evaluated by spectroscopy methods. The morphological properties of the dye-doped polymer fibers will be evaluated using scanning electron microscopy (SEM). We will tailor the luminescent properties by doping the polymer (polyvinylpyrrolidone or polymethylmetacrilate) with different dyes (coumarins, rhodamines and sulforhodamines). The luminescent properties of electrospun polymeric nanofibers that are doped with different dyes can be changed by using different electrospinning parameters (electric voltage, distance between electrodes, flow rate of the solution, etc.). Furthermore, we can evaluate the dye concentration's influence on the emissive properties of dye-doped polymer nanofibers. The advantages offered by the electrospinning technique when producing polymeric fibers are given by the simplicity of the method, the tuneability of the morphology allowed by the possibility of controlling all the process parameters (temperature, viscosity of polymeric solution, applied voltage, distance between electrodes, etc.), and by the absence of harsh and supplementary chemicals.

Acknowledgments: The authors acknowledge the financial support received through IFA CEA Project No. C5-08/2016.

---

## Poly (lactic acid) (PLA) electrospun nanofibers containing rice extracts for biomedical applications

---

Thursday, 19th October - 13:30 - Poster Session - Hall & Room 3 - Poster - Abstract ID: 531

---

***Dr. Piyachat Chuysinuan<sup>1</sup>, Mr. Nitirat Chimnoi<sup>1</sup>, Mrs. Lalita Pattani<sup>1</sup>, Mrs. Panita Khlaychan<sup>1</sup>, Dr. Patcharakamon Nooeaid<sup>2</sup>, Prof. Supanna Techasakul<sup>1</sup>***

*1. Chulabhorn Research Institute, 2. Srinakharinwirot University*

Poly(lactic acid) (PLA) is one of the most promising biodegradable polymers for biomedical applications because of good biocompatibility, tunable mechanical properties and ease of fabrication into ultra-fine fibers using electrospinning. This study aimed to fabricate electrospun poly(lactic acid)(PLA) fiber mats containing 3 kinds of rice extract (rice bran, riceberry and LeumPhum rice extracts) by using electrospinning process. Rice is a main cereal crop in Thailand. The rice extract has been reported to exhibit antioxidant activities. As-prepared electrospun PLA nanofibers showed smooth and uniform fibers without the formation of beads and possessed average diameters ranging from 498-668 nm. The SEM observations found that the electrospinning process conditions were appropriate for the fabrication of smooth, uniform, and randomly-oriented fibers (Figure 1). Release characteristics of the rice extract-loaded electrospun PLA fiber mats were investigated using total immersion methods. The release of rice extracts showed a burst release at the initial stage of approximately 25-30 %, followed by slower release that maintained at 26-33 %. At 300 min, the cumulative amount of Rice bran, Rice berry, and LeumPhum was about 22 %, 23 %, and 24 %. At the longest submersion time (@2880 min), the value increased slightly to 26 %, 26 %, and 33 %, respectively (Figure 2). The scavenging ability of LeumPhum rice extract-loaded electrospun fibers showed superior scavenging activity as determined using the DPPH radical scavenging method. The antioxidant capacity of as-released rice bran ranged between 28.45 and 34.58 %, while those of Riceberry and LeumPhum ranged between 32.73 and 32.60 % and 37.58 and 38.54 %, respectively. The physical properties such as swelling and weight loss behavior, and tensile strength were investigated to evaluate the usefulness of electrospun nanofibers to wound dressing. Furthermore, the potential use of these rice extract-loaded PLA electrospun fibers were further assessed in terms of the indirect cytotoxicity, *in vitro* attachment and proliferation of dermal human fibroblasts (HDFa). Therefore, the results suggest that rice extract-loaded PLA electrospun fibers have the antioxidant capacity for potential application as wound dressings.



# Observation of partial relaxation mechanisms via anisotropic strain relief on epitaxial islands using semiconductor nanomembranes

Thursday, 19th October - 13:30 - Poster Session - Hall & Room 3 - Poster - Abstract ID: 582

**Ms. Bárbara Rosa<sup>1</sup>, Ms. Lucas Marçal<sup>1</sup>, Dr. Rodrigo Andrade<sup>1</sup>, Dr. Luciana Dornelas<sup>2</sup>, Prof. Wagner N Rodrigues<sup>1</sup>, Prof. Patricia Lustoza<sup>2</sup>, Prof. Maurício Pires<sup>2</sup>, Prof. Ricardo W Nunes<sup>1</sup>, Prof. Ângelo Malachias<sup>1</sup>**

*1. Federal University of Minas Gerais, 2. Pontifical Catholic University of Rio de Janeiro*

In this work we attempt to directly observe anisotropic partial relaxation of epitaxial InAs islands using transmission electron microscopy and synchrotron x-ray diffraction on a 10 nm thick InAs:GaAs nanomembrane. Figure 1 and 2 show TEM and x-ray diffraction measurements of the heterostructure explored in this paper. We show that under such conditions TEM provides improved real-space statistics, allowing the observation of partial relaxation processes that were not previously detected by other techniques or by usual TEM cross section images. These results can be seen in Figure 3. Besides the fully coherent and fully relaxed islands that are known to exist above previously established critical thickness, we prove the existence of partially relaxed islands, where incomplete 60° half-loop misfit dislocations lead to a lattice relaxation along one of the  $\langle 110 \rangle$  directions, keeping a strained lattice in the perpendicular direction. These growing processes are sketched in Figure 4. Although individual defects cannot be directly observed, their implications to the resulting island registry are identified and discussed within the frame of half-loops propagations.

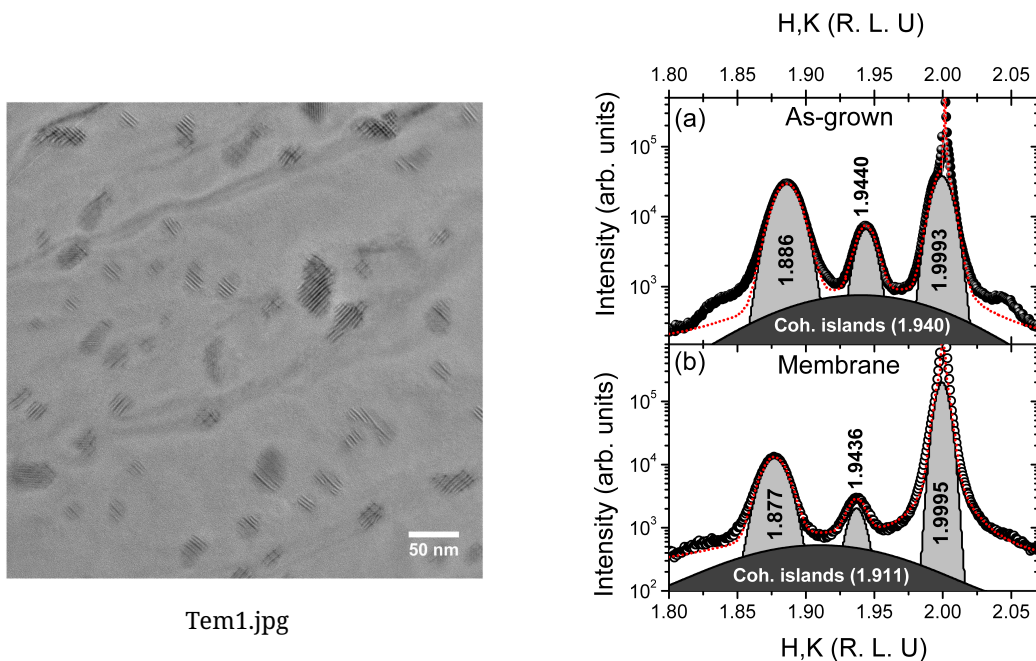
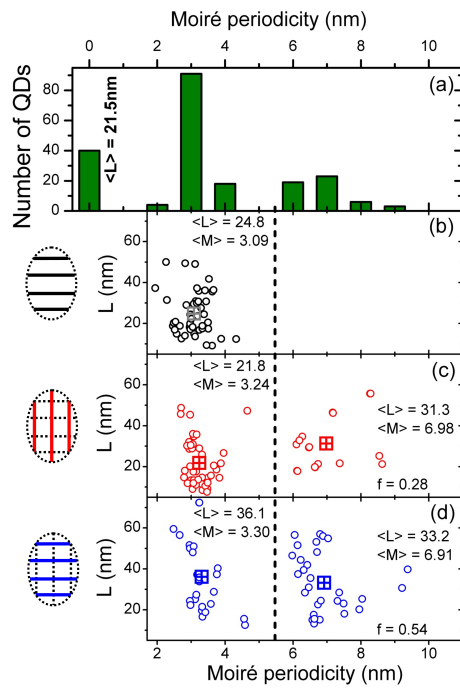
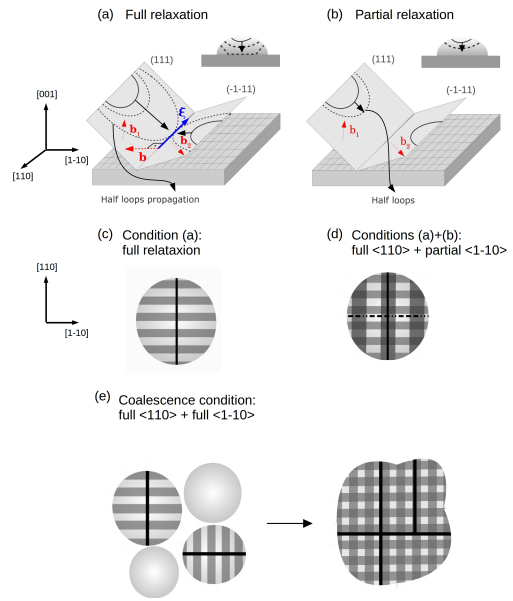


Fig2 ab.jpg



Allstats fig4 final.jpg



Full partial relaxation final3.jpg

# The effects of biofunctionalized silver nanoparticles with polyphenols from *Cornus Mas* in experimental inflammation

Thursday, 19th October - 13:30 - Poster Session - Hall & Room 3 - Poster - Abstract ID: 611

**Prof. Gabriela Adriana Filip<sup>1</sup>, Prof. Simona Clichici<sup>1</sup>, Mrs. Nicoleta Decea<sup>1</sup>, Dr. Ioana Baldea<sup>1</sup>, Dr. Diana Olteanu<sup>1</sup>, Dr. Ramona Suharoschi<sup>2</sup>, Dr. Ioana Scrobota<sup>3</sup>, Dr. Mihai Cenariu<sup>4</sup>, Dr. Bianca Moldovan<sup>5</sup>, Prof. Luminita David<sup>6</sup>**

**1.** Iuliu Hatieganu University of Medicine and Pharmacy, **2.** University of Agricultural Sciences and Veterinary Medicine, **3.** Department of Dental Medicine, Faculty of Medicine and Pharmacy, University of Oradea, **4.** University of Agricultural Sciences and Veterinary Medicine, Department of Biochemistry, **5.** Faculty of Chemistry and Chemical Engineering, Babes-Bolyai – University, **6.** Faculty of Chemistry

**Introduction:** Silver nanoparticles (AgNPs), especially due to their properties, have gained in recent years a growing popularity in the field of nanotechnology applied in medicine, including in carcinogenesis. The interactions between AgNPs and tissues are complex, therefore careful evaluation of real efficacy and safety is a prerequisite for the development of a specific chemopreventive product.

**Methods:** The present study aims to investigate the biological activity of silver nanoparticles functionalized with polyphenols from *Cornus mas* fruits (0.3 mg/kg b.w. AgNPs-CM) on experimental model of acute inflammation (100 µl 1% carrageenan injected in paw tissue). The antioxidant and modulatory effect on inflammation and cell death were studied in comparison with the extract (15 mg/kg b.w. CM), indomethacin (5 mg/kg) and saline solution. All the substances were orally administered, during 4 days, before carrageenan injection. At 2h, 24h and 48h after induction of inflammation, the plantar tissue samples were taken for oxidative stress, inflammation and apoptosis rate investigations.

**Results and Discussion:** AgNPs-CM reduced significantly interleukin (IL)-1α, IL-6, monocyte chemotactic protein (MCP)-1 levels and cell death ( $p < 0.001$ ) at 2h after carrageenan administration. The effect was maintained at 24h for IL-1α in parallel with an increased activity of GPx. At 48 h the rate of apoptosis and ERK ½ activation increased significantly while the GSH-GSSG ratio diminished.

**Conclusion:** Our results suggest that bioconjugates prepared from silver nanoparticles and natural extracts from *Cornus mas* have dual effect on inflammation: reduced the secretion of proinflammatory cytokines in early stage of inflammation while at 48h increased the apoptosis and induced ERK ½ activation in parallel with reduction of antioxidant defense. This behavior suggests a possible role of AgNPs-CM as chemopreventive agent.

# Magnetic and Structural Properties of the Maghemite Core-Shell Nanoparticles at Elevated Temperatures

Thursday, 19th October - 13:30 - Poster Session - Hall & Room 3 - Poster - Abstract ID: 645

**Mr. Ihor Syvorotka**<sup>1</sup>, **Mr. Stepan Hurskyy**<sup>2</sup>, **Prof. Sergii Ubizskii**<sup>2</sup>, **Prof. Leonid Vasylechko**<sup>2</sup>

1. Scientific Research Company "Carat"/ Lviv Polytechnic National University, 2. Lviv Polytechnic National University

Iron oxide-based nanoparticles are of great interest for various biomedical applications, such as targeted drug delivery, magnetic resonance imaging, magnetic separation, hyperthermia treatment etc. due to their small size, non-toxicity and biocompatibility. The most common structural modifications of iron oxide are maghemite ( $\gamma\text{-Fe}_2\text{O}_3$ ), magnetite ( $\text{Fe}_3\text{O}_4$ ), hematite ( $\alpha\text{-Fe}_2\text{O}_3$ ), wuestite ( $\text{FeO}$ ),  $\beta\text{-Fe}_2\text{O}_3$  and  $\varepsilon\text{-Fe}_2\text{O}_3$ . At high temperature structural transformations between these phases are possible that change in part their magnetic properties. Such transformations in nanosized particles can be different from those of bulk material. The aim of this study was to identify the main features of changes of magnetic and structural properties of core-shell maghemite nanoparticles at elevated temperature.

Composite nanoparticles («magnetic core – polymer shell») grown by homogeneous nucleation with average core diameter of  $\sim 8$  nm [1] were used for investigation. Temperature dependence of magnetization during heating and cooling in air in the range from RT to  $650^\circ\text{C}$  was measured by vibrating sample magnetometer. The phase composition and structure parameters of the nanoparticles' core were studied in temperature range from RT to  $910^\circ\text{C}$  using synchrotron X-ray diffraction.

**Fig.1.** Thermal behaviour of nanoparticles' core unit cell at the first heating (a) and temperature dependence of sample's magnetization in external magnetic field  $H = 3940$  Oe (b).

The studied nanoparticles possess superparamagnetic properties at room temperature and undergo irreversible changes of magnetic properties while being heated to  $\sim 250^\circ\text{C}$ . According to diffraction data maghemite cores contained before heating up to 20 w.% of ammonium chloride as a impurity from fabrication process. At temperature about  $\sim 250^\circ\text{C}$  atypical structural phase transition from maghemite to magnetite was identified. After heating to  $\sim 700^\circ\text{C}$  sample undergoes the second-order phase transition from magnetite to wuestite. It is supposed that these irreversible transformations occur due to reducing action of impurity and/or polymer shell presence in composite nanoparticles at elevated temperatures.

*This work is supported by project DB/KMON of Ministry of Education and Science of Ukraine. Authors are grateful to Dr. O.S. Zaichenko and Dr. N.Ye. Mitina for synthesis of maghemite core-shell nanoparticles.*

[1] P. Demchenko, N. Nedelko, N. Mitina et al., J. Magn. Mat. 379 (2015) 28-38.

---

## Development of a thermo-reversible *in situ* forming implant associated with Nanostructured Lipid Carriers (NLC) as sustained delivery system for estradiol valerate.

---

Thursday, 19th October - 13:30 - Poster Session - Hall & Room 3 - Poster - Abstract ID: 673

---

***Mrs. María Teresa Pineda Hernández<sup>1</sup>, Dr. Flora Adriana Ganem Rondero<sup>1</sup>***

*1. Facultad de Estudios Superiores Cuautitlán, Universidad Nacional Autónoma de México*

**Introduction:** Estradiol Valerate (EV), an estrogen, has been used in the post-menopausal hormone replacement therapy. Decreased levels of estradiol after menopause, results in different symptoms such as hot flashes, night sweats, insomnia, increased fatigue, irritability, depression, cardiovascular disease and osteoporosis. NLC are composed by a mixture of solid and liquid lipids, resulting in a little-ordered crystal lattice, attaining high drug encapsulation.

Thermo-reversible *in situ* forming implants of Poloxamer 407 (P-407) consist of low viscosity transparent solutions, capable of being transformed into solid gels, once they reach the corporal temperature. This feature allows the formation of a sustained release reservoir.

The aim of this work was to develop EV loaded NLC, included in a thermo-reversible implant of *in situ* formation, capable of achieving the sustained release of EV.

**Methods:** NLC were prepared by the hot high pressure homogenization technique and were characterized by average particle size (PS), polydispersity index (PDI), zeta potential (ZP) by dynamic light scattering, and entrapment efficiency (EE) using a centrifugation method to separate the free drug from that encapsulated in the NLC.

P-407 gels were prepared by the cold method, with or without NLC. The sol-gel temperature was determined using the tube inversion method and by viscosity measurements, performed by placing gels on a digital viscometer plate in a temperature range of 10 to 40°C, at 50 rpm using no. 1 circular spindle.

**Results and Discussion:** NLC with an average PS of 242.73 nm, and PDI of 0.307, were obtained. A ZP of -10.3 mV translates into a system with good physical stability. The EE was 92.72%, attaining high drug encapsulation. Below 37 °C the P-407 system was fluid enough to be injected, occurring the sol-gel transition at 37 °C, ensuring the *in situ* formation of an implant, and consequently the sustained release of EV.

**Conclusions:** NLC with good characteristics of PS, PDI and ZP were obtained, with high EE. Incorporation of NLC into a P-407 gel had the proper conditions to form a sustained delivery system for EV.

**Acknowledgement:** To PAPIIT/UNAM (Ref. IN216016).

---

# Shock Assisted Liquid Phase Consolidation of Nanostructured W-Ag Composites

---

Thursday, 19th October - 13:30 - Poster Session - Hall & Room 3 - Poster - Abstract ID: 235

---

***Dr. Akaki Peikrishvili<sup>1</sup>, Dr. George Tavadze<sup>1</sup>, Dr. Bagrat Godibadze<sup>2</sup>, Dr. Elguja Chagelishvili<sup>2</sup>, Mr. Avtandil Dgebuadze<sup>3</sup>***

*1. F. Tavadze Institute of Metallurgy and Materials Science, 2. G. Tsulukidze Mining Institute, 3. G. Tsulukidze Mining Institute*

In order to fabricate and to consolidate different compositions within the W-Ag powder systems and to obtain bulk nanostructured billets near to theoretical densities, nanoscale tungsten precursors we used, with grain sizes under 100nm. Conventional silver powders with grain size around 5 $\mu$  were then added to the W matrices. The temperature of heating and loading during the processing ranged from below to above the melting point of silver and up to 1000<sup>o</sup>C. The intensity of loading was under 10GPa. Using Hot Explosive consolidation technology several compositions of nanostructured mixtures of W-Ag blended powders were consolidated to near the theoretical density. These investigations showed that the application of nanostructured W-Ag blends of powders, followed by their explosive consolidation at near to the melting point of silver preserved the nanoscale of the grains of W and enabled the fabrication of cylindrical billets with density near to the theoretical values without visible coarsening. The consolidated samples were characterized with good integrity and improved physical and mechanical properties. The structure and characteristics of the obtained samples depends on the phase content, distribution of phases and processing parameters during explosive synthesis and consolidation. Additionally, we observed that the electrical properties (resistance and dependence of the susceptibility) of the consolidated W-Ag composites were dependent upon the phase content and the density of the consolidated samples. It also observed that the CTE of the nanostructured W-Ag composites was improved and that the microstructures showed better stability in comparison with existing W-Cu and AlSiC materials. In this paper we present and discuss the processing of the precursors and the fabrication of W-Ag nanostructured composites together with the detail description of HEC technique.

---

# Graphene-based nanocomposites decorated with silver nanoparticles as antibacterial agent

---

Thursday, 19th October - 13:30 - Poster Session - Hall & Room 3 - Poster - Abstract ID: 637

---

**Dr. Sławomir Jaworski<sup>1</sup>, Dr. Mateusz Wierzbicki<sup>1</sup>, Prof. Ewa Sawosz<sup>2</sup>, Dr. Marta Kutwin<sup>2</sup>, Ms. Barbara Strojny<sup>1</sup>, Ms. Natalia Kurantowicz<sup>2</sup>, Dr. Marta Grodzik<sup>2</sup>**

1. Faculty of Animal Science, Warsaw University of Life Science, 2. Faculty of Animal Science, Warsaw University of Life Sciences

## Introduction

The development of antibiotics has played a significant role in controlling the number of bacterial infections. However, the improper use and the overuse of antibiotics led to the development of multidrug resistance in many bacteria species. Some strains have become resistant to practically all of the commonly available agents: beta-lactams, tetracycline, aminoglycosides.

One of the promising method against drug-resistant bacteria can be surface modified materials with biocidal nanoparticles and nanocomposites. Herein, we present a nanocomposite with silver nanoparticles (Ag-NPs) on the surface of graphene oxide (GO), as a novel multifunctional antibacterial and antifungal material.

## Methods

Ultrasonic technologies has been used as an effective method of coating polyurethane foils. Toxicity on Gram-negative bacteria (*Escherichia coli*), Gram-positive bacteria (*Staphylococcus aureus* and *Staphylococcus epidermidis*) and pathogenic yeast (*Candida albicans*) was evaluated by analysis of cell morphology, assessment of cell viability by Presto Blue assay, analysis of cell membrane integrity by LDH assay and reactive oxygen species production.

## Results

Ag-NPs, GO and Ag-GO nanocomposites showed antibacterial activity that is stronger against Gram-negative bacteria (*E. coli*) than against Gram-positive bacteria, (*S. aureus* and *S. epidermidis*) and yeast (*C. albicans*). A disruption of membrane functionality from an interaction between released Ag nanoparticles/Ag<sup>+</sup> ions and the cell membrane and extensive cell membrane damage caused by the formation of ROS ultimately causing damage to the cell due to oxidative stress. The synergistic effect between GO and Ag-NPs has reduced the Ag content without compromising the antibacterial performance.

## Discussion

Silver nanoparticles can cause direct damage to the bacterial cell membrane. Bacteria may be killed by the combined bactericidal effects of the released Ag ions and Ag nanoparticles. Many studies have sought to establish a mechanism of action of antibacterial activity exhibited by silver in both its colloidal and ionic form. A disruption of membrane functionality from an interaction between released Ag<sup>+</sup> ions and the cell membrane and extensive cell membrane damage caused by the formation of reactive oxygen species (ROS) ultimately causing damage to the cell due to oxidative stress. Foils coated with Ag-NPs and GO-Ag increased the ROS production of all tested microorganisms compared with the control group.

## Thermophysical properties of nanofluids containing nanodiamonds/graphite mixture with various ash fractions

---

Thursday, 19th October - 13:30 - Poster Session - Hall & Room 3 - Poster - Abstract ID: 81

---

***Dr. Gawel Żyła<sup>1</sup>, Mr. Jacek Fal<sup>1</sup>, Dr. Patrice Estellé<sup>2</sup>***

*1. Department of Physics and Medical Engineering, Rzeszow University of Technology, 2. Materials and Thermo-Rheology team at LGCGM, Universite Rennes 1*

The influence of ash content on thermophysical properties of nanofluids containing nanodiamonds/graphite mixture was investigated. Rheological behaviour, thermal and electrical conductivity of this materials were measured. Two types of samples with various ash content were prepared. Each type of nanofluid was investigated with various volume fraction of nanoparticles from 0.004 to 0.023. All measurements were performed in constant temperature of 298.15 K. It was presented that ash content in this kind of nanofluids changes significantly its rheological properties. While the variation in ash content does not affect thermal conductivity of nanofluids, a big impact on electrical conductivity is reported [1].

[1] G. Żyła, J. Fal, P. Estellé, The influence of ash content on thermophysical properties of ethylene glycol based graphite/diamonds mixture nanofluids, *Diamond & Related Materials*, in press, DOI: 10.1016/j.diamond.2017.02.008 (2017)



---

## Water purification via traditional pottery impregnated with silver nanoparticles

---

Thursday, 19th October - 13:30 - Poster Session - Hall & Room 3 - Poster - Abstract ID: 192

---

**Dr. Heli Piedra-gil<sup>1</sup>, Dr. Juan Antonio Hoyoz-guzman<sup>1</sup>, Dr. Lesli Ortega-arroyo<sup>1</sup>, Dr. Jorge Humberto Vargas-aparicio<sup>1</sup>, Dr. Maria Sanchez-góngora<sup>2</sup>, Dr. Teresita Cardona-juárez<sup>3</sup>, Dr. Eduardo San Martín<sup>4</sup>, Dr. Luz Perez-rea<sup>5</sup>, Dr. Fabio Vengoechea<sup>6</sup>, Dr. Victor M Castaño<sup>7</sup>**

*1. School of Mechanical and Electrical Engineering, ESIME-IPN Azcapotzalco, 2. School of Mechanical and Electrical Engineering, Zacantenco, IPN., 3. Center for Research and Technological Innovation of the National Polytechnic Institute, IPN, 4. Laboratory of Biotechnology, Center for Research in Applied Science and Advanced Technology, IPN, 5. Faculty of Engineering, Universidad Autónoma de Querétaro, 6. Avi-Mex Laboratory, 7. Center of Applied Physics and Advanced Technology, National Autonomous University of Mexico*

The quality of drinking water was investigated in order to ensure provision for the protection of public health ceramic filters, which are impregnated with Nanoparticles (NPs) Silver (Ag). A number of parameters such as pH, hardness (CaCO<sub>3</sub>), Chloride (Cl<sup>-1</sup>) and determination of Total Coliforms, was carried out. The river water was filtered from Tomatal region in Guerrero, a state of Mexico, and 14 ceramic were evaluated using the Response Surface Methodology. Water filtration was conducted during the period from January to August. The obtained values of each parameter were compared with standard values set by NOM-127-SSA1-1994, which are local regulations. It was found that the values of each parameter are into safety limits established

---

## Electrodeposition of Sn-rGO composites involving choline chloride – ethylene glycol ionic liquids with applications in electronics

---

Thursday, 19th October - 13:30 - Poster Session - Hall & Room 3 - Poster - Abstract ID: 231

---

**Mrs. Stefania Costovici<sup>1</sup>, Mr. Dan Balan<sup>2</sup>, Ms. Oana Brincoveanu<sup>3</sup>, Prof. Teodor Visan<sup>4</sup>, Dr. Liana Anicai<sup>3</sup>, Prof. Marius Enachescu<sup>5</sup>**

*1. S.C. Mibatron SRL, 2. Center of Surface Science and Nanotechnology, University Politehnica of Bucharest, 3. Center of Surface Science and Nanotechnology, University Politehnica of Bucharest,, 4. Department of Inorganic Chemistry, Physical Chemistry and Electrochemistry, University Politehnica of Bucharest, 5. University Politehnica of Bucharest, Center of Surface Science and Nanotechnology*

The paper presents some experimental results regarding the electrodeposition of tin - reduced graphene oxide (Sn-rGO) composite coatings using choline chloride-ethylene glycol eutectic mixtures (denoted ILEG), also known as deep eutectic solvents, DESs.

The influence of graphene oxide addition during electrodeposition of Sn from ILEG based electrolyte has been investigated, in order to suppress whiskers growth and to reinforce Sn alloys as lead-free solders.

The Sn-rGO film was electrodeposited on copper substrate from ILEG system containing 0.7M SnCl<sub>2</sub> and 20mL L<sup>-1</sup>N-doped graphene oxide (1mg.mL<sup>-1</sup>, dispersion in H<sub>2</sub>O), at various applied current densities in the range of 5-30 mAcm<sup>-2</sup> and a temperature of 70°C, under magnetic stirring. Adherent and uniform coatings were obtained. The characterization of deposits was performed using cyclic voltammetry, current - time transients, scanning electron microscopy (SEM), X-ray diffraction (XRD) and Raman spectroscopy.

The SEM micrographs showed that the presence of rGO in the deposit (see Fig.1). Moreover, current densities higher than 15 mA cm<sup>-2</sup> are required for an efficient insertion.

The Raman spectra of the electrodeposited Sn-rGO evidence the presence of both G and D bands (at 1584 and 1352 cm<sup>-1</sup>, respectively); however, with an increased D/G intensity ratio compared to that in GO. This change suggests that GO is electrochemically reduced (see Fig.2).

**Acknowledgements:** The work was supported by Romanian Ministry of Education and by Executive Agency for Higher Education, Research, Development and Innovation Funding, under NOVTINALBEST project 38/2016, M Era Net Program.

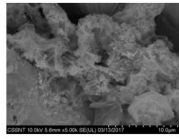


Fig.1- SEM image of Sn-rGO composite coating electrodeposited from ILEG based electrolyte containing 0.7M  $\text{SnCl}_2$  and 20mM  $\text{L-Ascorbic acid}$  at 15  $\text{mA cm}^{-2}$

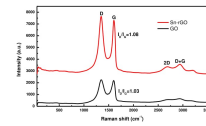


Fig.2 The Raman spectra of GO (black) and Sn-rGO electrodeposited from ILEG based electrolyte containing 0.7M  $\text{SnCl}_2$  and 20mM  $\text{L-Ascorbic acid}$  at 15  $\text{mA cm}^{-2}$  (red)

Fig 1.jpg

Fig 2.jpg

# Niobium oxide nanocolumns formed via anodic alumina with modulated pore diameters

Thursday, 19th October - 13:30 - Poster Session - Hall & Room 3 - Poster - Abstract ID: 348

**Dr. Andrei Pligovka<sup>1</sup>, Ms. Anna Zakhlebayaeva<sup>1</sup>, Mr. Andrei Lazavenka<sup>1</sup>**

*1. Belarusian State University of Informatics and Radioelectronics*

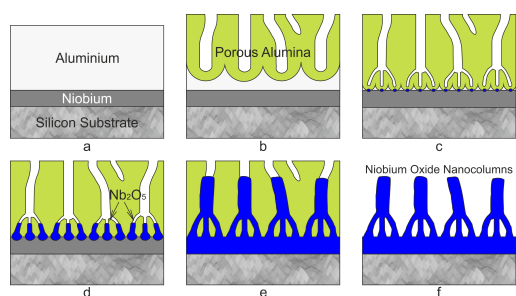
Porous anodic alumina matrixes (AAM) are characterized by uniform cylindrical pores which can be used for templated synthesis of arrays of various nanostructures. Manipulation of the size, position and regularity of the pores AAM allow forming conceptually new structures on its base with wide range of applications.

This paper presents the results of forming of metal oxide nanocolumns with variable diameters by high-voltage reanodization via AAM with modulated pore diameters. The main stages of film growth, with the relation between the film layers thick, are depicted in Fig. 1.

Single silicon wafer with magnetron-sputtered layers of 300 nm Nb and 1200 nm Al was used as substrate (Fig. 1, a). Regular AAM with modulated pore diameters was formed by sequential anodization of the Al in  $0.2 \text{ mol} \cdot \text{d}^{-3} \text{ C}_4\text{H}_6\text{O}_6$  at 180 V and in  $0.4 \text{ mol} \cdot \text{d}^{-3} \text{ H}_2\text{C}_2\text{O}_4$  at 37 V (Fig. 1, b, c). Array of niobium oxide nanocolumns was formed by high-voltage reanodization of the Nb layer via AAM in the mixed solution of  $0.5 \text{ mol} \cdot \text{d}^{-3} \text{ H}_3\text{BO}_3$  and  $0.05 \text{ mol} \cdot \text{d}^{-3} \text{ Na}_2\text{B}_4\text{O}_7$  in potentiodynamic mode at 400 V (Fig. 1, d, e). Further AAM was selective dissolved in 50 %  $\text{H}_3\text{PO}_4$  (Fig. 1, f). As a result, array of  $\text{Nb}_2\text{O}_5$  nanocolumns high 800 nm was formed on the solid layer  $\text{NbO}_2$  thin 450 nm on Si-substrate (Fig. 2).

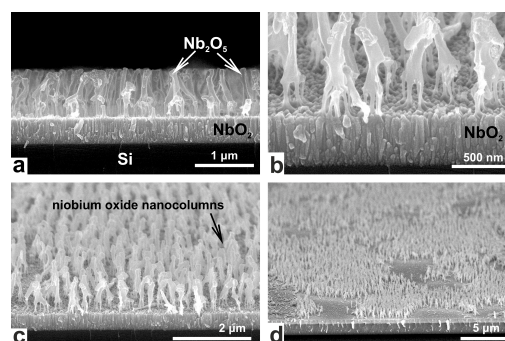
The nanocolumns consist of upper layer high 630 nm and diameter 100 nm in the base of which are located 4-7 columns high 170 nm and diameter 25 nm. Nanocolumns have an unordered structure because anodization of aluminum was carried out in one step without preliminary structuring of the surface. The additional ordering of the Al layer by the two-step anodization will make possible to form regular AAM and produce high-ordered nanocolumns on their basis.

So, the developed technique based on the combination of the methods of formation of porous anodic alumina with modulated pore diameters and high-voltage reanodization of Nb underlayer via the AAM. The formed structures can be used as photonic crystals, autoemission elements and functional applications of promising devices of nano- and optoelectronics.



(a) sputter-deposition of Nb-Al bilayer on  $\text{SiO}_2/\text{Si}$  substrate, (b) growth of porous alumina film, (c) anodization of the Nb underlayer through the alumina nanopores, (d) growth of thin niobium oxide nanocolumns in the alumina pores, (e) growth of thick niobium oxide nanocolumns in the alumina pores, (f) dissolution of the alumina ("alumina-free" sample).

**Fig. 1 the main phases of the films formation process .jpg**



Samples formed by sequential anodization at 180 V in  $\text{C}_4\text{H}_6\text{O}_6$  and at 37 V in  $\text{H}_2\text{C}_2\text{O}_4$ , then reanodization at 400 V in  $\text{H}_3\text{BO}_3$ . All images of the nanostructures were obtained after dissolution of the alumina ("alumina-free" samples).

**Fig. 2 scanning electron microscope images of arrays of niobium oxide nanocolumns on si-substrate .jpg**

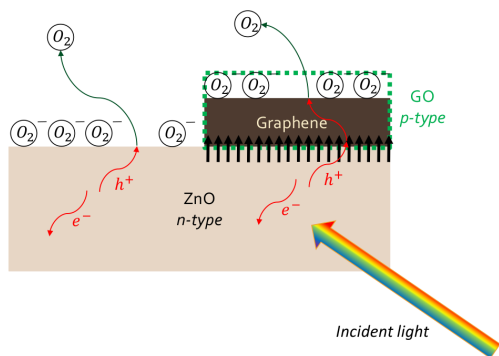
# Light-induced oxygen sensing using a ZnO/GO based oxygen sensor

Thursday, 19th October - 13:30 - Poster Session - Hall & Room 3 - Poster - Abstract ID: 446

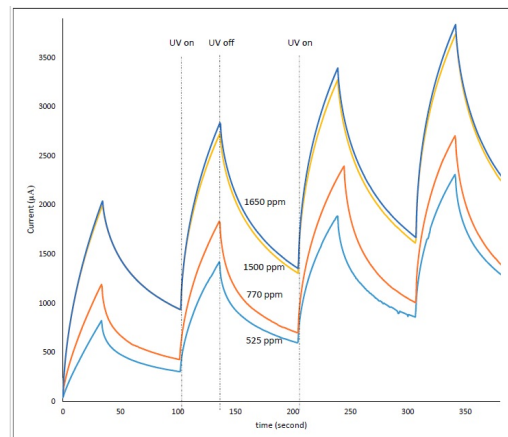
**Mr. Mahdi Sasar<sup>1</sup>, Mrs. Anousha Khamsavi<sup>1</sup>, Mr. Yusef Khosravi<sup>1</sup>, Dr. Yaser Abdi<sup>1</sup>**

**1. University of Tehran**

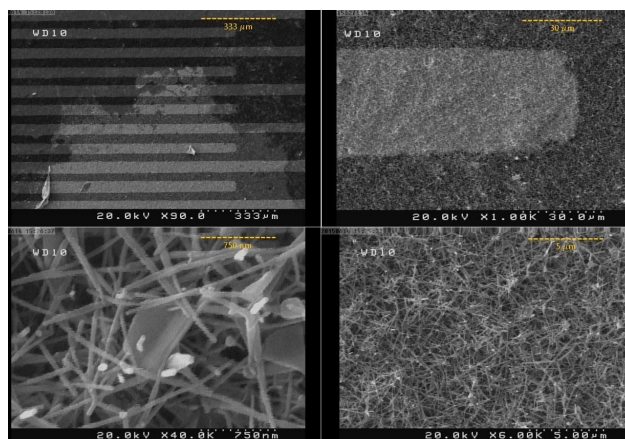
We report the fabrication of a novel room temperature oxygen sensor using ZnO nanowires and reduced graphene oxide (GO) sheet, which operates based on the photocurrent response of this hybrid structure and the photocatalytic reduction of GO. ZnO nanowires were deposited on interdigitated Au electrodes and the GO sheet was deposited on the ZnO nanowires by dip coating. Under UV light illumination, the fabricated device shows an enhanced sensitivity to different concentrations of oxygen gas. Oxygen adsorption/desorption on the surface of the ZnO nanowires and on the exposed surface of the GO sheet contribute to the decay and the growth of the photocurrent. We analyze the transient photocurrents using stretched exponential functions, showing that the specific times and the exponents of these fits are excellent candidates for distinguishing different ppm of oxygen gas in the medium. Furthermore, because of oxygen vacancies and other defects in the ZnO nanowires, the sample is seen to show response to visible light. We study the case of visible light and show that once again the sample shows clear sensitivity to different concentrations of oxygen gas.



Schematics of the mechanisms of the sensor.png



Current vs. time for the sample under uv illumination in the presence of different oxygen concentrations.jpg



Sem images of the prepared sample showing the znO nanowires and the graphene oxide sheet.jpg

## Growth of a highly c-axis oriented AlN thin films

Thursday, 19th October - 13:30 - Poster Session - Hall & Room 3 - Poster - Abstract ID: 485

***Dr. Nabila Redjda*<sup>1</sup>, *Prof. Mouhamed Azzaz*<sup>2</sup>, *Dr. Nouredine Gabouze*<sup>3</sup>, *Dr. Olivier Tottereau*<sup>4</sup>, *Mr. Hamid Menari*<sup>5</sup>, *Dr. Bendiba Guedouar*<sup>6</sup>**

*1. Centre de Recherche en Technologie des Semi-conducteurs pour l'Energétique- Faculté de Génie Mécanique et Génie des procédés, USTHB- Algeria, 2. Faculté de Génie Mécanique et Génie des procédés, USTHB- Algeria, 3. Centre de Recherche en Technologie des Semi-conducteurs pour l'Energétique, Algiers, Algeria, 4. Centre de Recherches Hétéroépitaxie Et Applications, Rue Bernard Grégory- Valbonne- France, 5. Centre de Recherche en Technologie des Semi-conducteurs pour l'Energétique, Algiers,, 6. Centre de développement des technologies Avancée, Cité 20 août 1956 Baba Hassen- Algeria*

The realization of AlN thin films, mainly oriented along (002) direction, is an important achievement for their integration in piezoelectric devices. This work reports structural properties of predominantly c-axis oriented AlN thin films. The studied films were grown on semiconductor seed layer using sputtering DC magnetron method.

After the growth process, film crystallinity quality of the resulting products was probed by X-ray Diffraction (XRD), Scanning Electron Microscopy (SEM), Raman spectroscopy (HORIBA JobinYvonLabRAM) with a He-Ne laser excitation wavelength of 633. A surface morphology and roughness were studied by atomic force microscopy (AFM). In addition, the optical properties of the AlN films were studied using a Varian Cary-500 spectrophotometer.

Microscopy analysis showed that the DC magnetron films displayed a uniform surface without any micro-cracks. The cross-section SEM images revealed that the AlN films consist of oriented columnar grains that are perpendicular to the surface of the Si substrates. The XRD patterns showed the formation of the polycrystalline phase of AlN where (100), (002) and (101) peaks appears. Besides, it was noted that the addition of seed layer boost the growth on a (002) direction. The experimental values of the Raman frequencies allowed in backscattering measurements and their lines widths confirm the high crystalline quality of the Wurtzite AlN.

Our research results shows that the texture of the elaborated AlN thin films is influenced by the use of the semiconductor seed layer surface.

## Synthesis of nanocrystalline $\alpha$ -Fe<sub>2</sub>O<sub>3</sub> by using thermal Oxidation of Fe Films

Thursday, 19th October - 13:30 - Poster Session - Hall & Room 3 - Poster - Abstract ID: 546

**Ms. Ghania Fortas<sup>1</sup>, Dr. Nouredine Gabouze<sup>2</sup>, Prof. Nacereddine Haine<sup>1</sup>, Mr. Amar Manseri<sup>3</sup>, Prof. Mourad Zergoug<sup>4</sup>, Mr. Menari Hamid<sup>3</sup>, Dr. Sam Sabrina<sup>5</sup>, Mr. Hocine Cheraga<sup>2</sup>, Dr. isma bozetine<sup>6</sup>**

**1.** Université des Sciences et de la Technologie Houari Boumediene, Faculté de physique, BP 32 El Alia 16111 Bab Ezzouar Alger, Algérie, **2.** Centre de Recherche en Technologie des Semi-conducteurs pour l'Energétique, Bd. 2 Frantz Fanon, les sept merveilles B.P.140, Alger, Algérie., **3.** Centre de Recherche en Technologie des Semi-conducteurs pour l'Energétique, Bd. 2 Frantz Fanon, les sept merveilles B.P.140, Alger, Algérie, **4.** Centre de Recherche en technologie Industrielles, Route de Dely Ibrahim, BP 64 16002, Cheraga, Algérie, **5.** Centre de Recherche en Technologie des Semi-conducteurs pour l'Energétique, Algiers, Algeria, **6.** CRTSE, 02 Bd Frantz Fanon B.P. 140 Alger 7 Merveilles, Algiers, Algérie

Iron oxides have received considerable attention due to their interesting electrical, magnetic and optical properties. Its potential applications extend on several fields: spin electronics, catalysis, photocatalysis and especially in the fields of biology and of biomedical. In this work,  $\alpha$ -Fe<sub>2</sub>O<sub>3</sub> hematite films were prepared by thermal oxidation from Fe films electroplated on silicon. Electrodeposition of Fe thin films was carried out from a sulfate bath containing an ammonium chloride complexing agent. The electrochemical study was performed by cyclic voltammetry. The SEM analysis of the films obtained at a -1.3 V constant polarization shows dendritic grains in the form of islands. The DRX spectra exhibit characteristic iron peaks according to the center-face cubic structure. These samples were annealed. At a temperature of 650 ° C, a single iron oxide phase was well formed, with the hematite structure. The SEM photos show a well-assembled columnar structure with formation of nano-wires at the surface of the deposit. The transmittance and reflectance spectra reveal an absorption in the ultraviolet range.

**Keywords:**  $\alpha$ -Fe<sub>2</sub>O<sub>3</sub> hematite, silicon, thermal oxidation, electrodeposition.



# Polyamide/Polyethylene/ Oxidized Graphite Nanocomposites With Functional Compatibilizers: Caracterization By Physico-Mechanical Tests And Atr-Ftir Spectrometry

Thursday, 19th October - 13:30 - Poster Session - Hall & Room 3 - Poster - Abstract ID: 200

**Dr. Alexandrescu Laurentia<sup>1</sup>, Mr. Mihai Georgescu<sup>1</sup>, Dr. Maria Sonmez<sup>1</sup>, Dr. Anton Ficai<sup>2</sup>, Dr. Denisa Ficai<sup>2</sup>, Mr. Ligian Tudoroiu<sup>3</sup>, Dr. Roxana Trusca<sup>2</sup>**

*1. National Research and Development Institute for Textile and Leather - Division Leather and Footwear Research Institute - INCDTP-ICPI, 2. Faculty of Applied Chemistry and Materials Science, University POLITEHNICA of Bucharest, 3. SC RONERA RUBBER SA*

Compounding polymers is widely used for the preparation of new materials. The disadvantage of this research is that the polymers are usually not compatible and the preparation of compounds with suitable (mainly processing and physico-mechanical) properties is not performant [1]. Polyamide/polyethylene (PA/PE) composites are interesting because both components are relatively cheap, with advantageous properties, and are processable by melting [2]. The compatibilisation of binary polymer compounds can be made by the addition of graft copolymer, segments of which have physical or chemical affinity with two immiscible homopolymers [3]. In this case, polyethylene grafted with maleic anhydride (PE-g-MA) it was used. Polymer nanocomposites containing graphite have been considered as a new generation of composites materials due to their expected unique properties attributed to the high aspect ratio of the inorganic pellets [4,5]. Combined effects of graphite treatment and compatibilizer polymers (PE-g-MA) on the structure and properties of PA/PE/PE-g-MA/oxidized graphite composites were studied. The optimum formulation was used to prepare a series of nanocomposites under different technological conditions. Also, a correlation between their physico-mechanical properties and IR spectra (ATR technique) was proposed.

## ACKNOWLEDGEMENTS

This research was financed through **PN-III-P2-2.1-PTE-2016**, project: **“New nanostructured polymeric composites for centre pivot liners, centre plate and other components for the railway industry - RONER-ANANOSTRUCT”** supported by UEFISCDI Romania.

## References

1. Bhattacharya, M. Polymer Nanocomposites—A Comparison between Carbon Nanotubes, Graphene, and Clay as Nanofillers. *Materials* 2016, 9, 262-297.
2. Lee, C.; Wei, X.; Kysar, J.W.; Hone, J. Measurement of the Elastic Properties and Intrinsic Strength of Monolayer Graphene. *Science* 2008, 321, 385–388.
3. Geim, A.K.; Novoselov, K.S. The rise of graphene. *Nat. Mater.* 2007, 6, 183–191.
4. Balandin, A.A.; Ghosh, S.; Bao, W.; Calizo, I.; Teweldebrhan, D.; Miao, F.; Lau, C.N. Superior Thermal Conductivity of Single-Layer Graphene. *Nano Lett.* 2008, 8, 902–907.
5. Bunch, J.S.; Alden, J.S.; Zand, A.M.; Parpia, J.M.; Craighead, H.G.; McEuen, P.L. Impermeable Atomic Membranes from Graphene Sheets. *Nano Lett.* 2008, 8, 2458–2462

## Composite Material Polystyrene activated carbon for Water Purification

---

Thursday, 19th October - 13:30 - Poster Session - Hall & Room 3 - Poster - Abstract ID: 647

---

***Dr. Abdelhak Maghchiche***<sup>1</sup>

*1. 1Département de pharmacie, faculté de médecine, université Batna 2 - Algeria*

The use of activated carbon as an organic molecules adsorbent have many regeneration problems, the most recent research works tend to combine activated carbon with a material possessing original physical properties in order to obtain multifunctional composite materials, our work consists in the design of a unique process multifunctional, for fine and hyper fine separation and improvement of the adsorption and discoloration of pollute solution in the presence of composite material, the results suggest the development of economic and effective water purification system.

This process is designed from the following elements: inert carrier porous, a cartridge type PP105M (5 micron) in which it incorporates in its structure polystyrene and active carbon.

This work highlighted also the improvement of the phenomena of adsorption, and discoloration of pollute solution in the presence of the composite material.

# Electrical properties of thin films deposited from TMS/O<sub>2</sub> in Microwave Multipolar Plasma reactor

Thursday, 19th October - 13:30 - Poster Session - Hall & Room 3 - Poster - Abstract ID: 727

**Mr. Kihel Mouloud<sup>1</sup>, Prof. Salah Sahli<sup>2</sup>, Prof. Patrice Raynaud<sup>3</sup>, Dr. Mohamed Benhaddad<sup>4</sup>, Dr. Fermi Youcef<sup>2</sup>**

1. Frères Mentouri Constantine, 2. Frères Mentouri Constantine1, 3. LAPLACE, CNRS, Université Paul Sabatier Toulouse, 4. University Brothers Mentouri of Constantine/

Thin films have been deposited from Tetramethylsilane or a mixture of Tetramethylsilane and oxygen (TMS/O<sub>2</sub>). The plasma discharge power and the working pressure in the reactor were kept constant and equal to 400 W and 1 mTorr, respectively. It has been observed that the oxygen proportion addition in the plasma mixture lead to the change of the structure films from organic character to inorganic character close to SiO<sub>x</sub>-like structure [1].

The current voltage characteristics I (V) study of Metal-Insulating-Metal structures for organic and inorganic films structure suggest that the carrier transport in the deposited films is limited by a space charge conduction mechanism. Moreover, it has been revealed that the electrical current of inorganic films decrease compared to the organic films, which is probably due to the decrease of the defects in the elaborated films. On the other hand, C-V characteristics exhibit deltaV shift towards negative values for organic films. The area of delta-V shift as we can see in figure 1 decrease with the increase of the oxygen ratio until disappear for inorganic films (deposited with high oxygen ratio). This behavior indicated the presence of defects in the organic films and the decrease of these defects according to the change of films structure from organic to inorganic character, this result is in good agreement with I(V) study. Therefore, the formation of more inorganic groups improve the electrical properties films.

[1] M. Kihel, S. Sahli, A. Zenasni, P. Raynaud, Y. Segui, "Dielectric properties of SiO<sub>x</sub> like films deposited from TMS/O<sub>2</sub> mixture in low pressure microwave plasma", Vacuum 107 (2014), pp264-268.

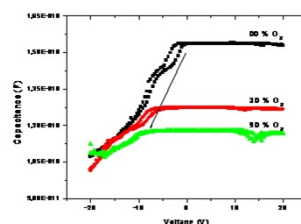


Figure 1.jpg

# Magneto-thermal competition on interface effect of urea-nano size magnetite formation

Thursday, 19th October - 13:30 - Poster Session - Hall & Room 3 - Poster - Abstract ID: 642

**Dr. Ahmad Yazdani<sup>1</sup>, Ms. samira sharifi<sup>1</sup>**

**1. Tarbiat Modares University, Jallal-Al-Ahmad Ave., Tehran, Iran, p.o.box 14115-111**

Since urea is one of the most effective factors in the chemical fertilizer for the plant growth, we considered its various effects on the magnetic structure of the nano-sized particle  $\text{Fe}_3\text{O}_4$  (magnetite) during its chemical coprecipitation synthesis through the effect of stirring ammonia on the various ratios of ferrous and ferric salts. The effects are supposed to be related to the thermal activation of the urea blow down as well as the rate of precipitation reaction of ammonia, through a competition between environment temperature  $T_m$  and magnetic exchange temperature  $T_B$ . Whereas the thermal magnetic stability process is a consequence of relaxation time of nano-magnetite  $\text{Fe}_3\text{O}_4$  particles' formation, which is related to the translocation and accumulation of soil ground water of agricultural environment. Thus, the effect is related to the exchange heat due to the conversion of heat exchange and magnetic character that results to the thermo-magnetic size stability process of the hysteresis loop. In this agri-ingestion, it is imperative to have an agri-compatible solvent at controlled optimum "pH" in natural local environment temperature range during ingestion of plant growth, which is supposed to be in the range of "0-3 °C" (winter) to "25-27°C" (spring). The experimental results of XRD, SEM, FTIR, and magnetization VSM at room temperature are investigated.

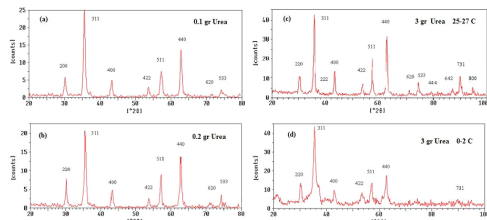


Figure 1 (a, b, and c) shows XRD patterns  $\text{Fe}_3\text{O}_4$  particles synthesized with three amounts of urea (0.1, 0.2, and 3 gr).

Fig1.png

Table 1: Magnetic saturation and coercivity for nanoparticles with different Iron salts at 300 K

Iron Salts	Magnetic Saturation ( $\text{emu gr}^{-1}$ )	Coersivity (Oe)
Ferrous Sulfate and Ferric sulfate	86.6	66.0
Ferrous Sulfate and Iron chloride	46.7	8.8
Ferric sulfate and Iron chloride	55.4	9.8

Table1.png

Table 2: Grain sizes, crystallite sizes, lattice constants and experimental lattice constants of  $\text{Fe}_3\text{O}_4$  at different temperature of 25-27°C and 0-2°C with 3g urea.

Temperature of reaction	25-27(°C)	0-2(°C)
Grain Sizes (SEM) (nm)	40-50	35-45
Crystalline sizes (XRD) (nm)	26.9	10.5
Experimental lattice constant (Å)	8.3420	8.3705
Lattice constant (Å)*	8.3740	8.3740

Table2.png

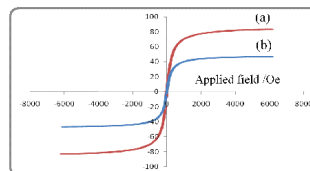


Figure 5 hysteresis loops of the measurements on the prepared sample

Fig 5.png

# Poly(3,4-ethylenedioxythiophene)-Single Walled Carbon Nanohorns Composite Coatings for Neural Sensing and Stimulation

Thursday, 19th October - 14:30 - Polymer, carbon and graphene nanostructures - Room 1 - Oral - Abstract ID: 575

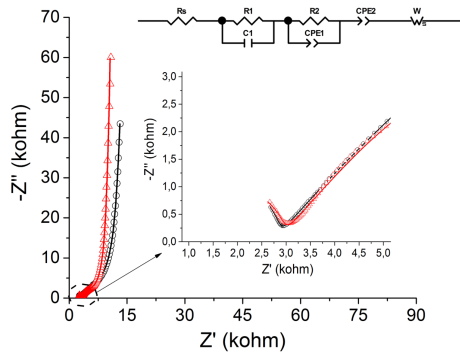
**Dr. stefano carli<sup>1</sup>, Mrs. Linda Lambertini<sup>1</sup>, Dr. Elena Zucchini<sup>1</sup>, Dr. Francesca Ciarpella<sup>1</sup>, Dr. Alice Scarpellini<sup>2</sup>, Dr. Mirko Prato<sup>3</sup>, Dr. Elisa Castagnola<sup>4</sup>, Dr. Davide Ricci<sup>1</sup>, Prof. Luciano Fadiga<sup>1</sup>**

*1. Center for Translational Neurophysiology of Speech and Communication, Istituto Italiano di Tecnologia, 2. Electron Microscopy Facility, Istituto Italiano di Tecnologia, 3. Materials Characterization Facility, Istituto Italiano di Tecnologia, 4. MEMS Research Lab., Department of Mechanical Engineering, College of Engineering*

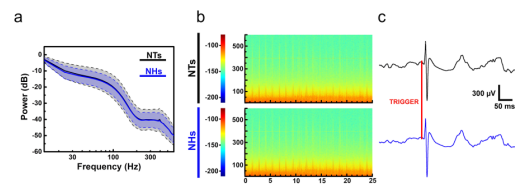
Typical neural electrodes are fabricated with noble metals and alloys but recently other new materials, including glassy carbon based microelectrode arrays, have emerged. For neural stimulation, these electrodes should be capable of injecting relatively large currents while minimizing electrode degradation due to faradaic effects, requirements generally satisfied by increasing the electrode size.

To improve electrochemical properties and stability of microelectrode arrays, conductive polymers (CPs), such as poly(3,4-ethylenedioxythiophene) (PEDOT), are often electrodeposited onto the metal underlayer in order to significantly reduce total impedance as well as to increase the total charge that can be accumulated, leading to higher S/N ratios, higher charge injection limits and less heat generated at the interface during stimulation.

Here, for the first time, (PEDOT) was electrodeposited in conjunction with oxidized single walled carbon nanohorns (ox-SWCNHs) onto gold microelectrode arrays in the framework of brain activity recordings and stimulation. The electrochemical, morphological and stability properties of coatings, as well as the ability of coated microelectrodes to record neural activity were investigated. Ox-SWCNHs based coatings have shown very promising properties in terms of charge injection limit, stability to pulsed electrical stimulus, neural sensing and biocompatibility. PEDOT/ox-SWCNHs composites were compared with films prepared with one of the most notorious carbonaceous material, multi-walled Carbon Nanotubes (MWCNTs). Our findings furnished comparable results for PEDOT/ox-SWCNHs and PEDOT/ox-SWCNHs coatings, in terms of surface characterization (SEM and XPS), electrochemical characterization (electrochemical impedance, cyclic voltammetry) and stability under fast pulsed charge stimulation. PEDOT/ox-SWCNHs and MWCNTs were found to be able to acquire the same neural signal information from the rat cortex with the best results in a relevant ECoG signal frequencies interval, from delta to high gamma bands, for brain-computer interfaces applications. More importantly, our preliminary results suggest that PEDOT/ox-SWCNHs material are very promising in terms of higher biocompatibility. Thanks to their extremely porous structure PEDOT/ox-SWCNHs films exhibited a higher charge storage capacity, with respect to PEDOT/MWCNTs, leading to an improved charge injection dynamic, with lower voltage excursion during electrochemical stimulation, which is very important in order to reduce, for instance, dramatic faradaic processes at the interface electrode/neural tissue.



Nyquist plot for nhs and nts.png



Signal psd spectrogram and traces of neural activity.png

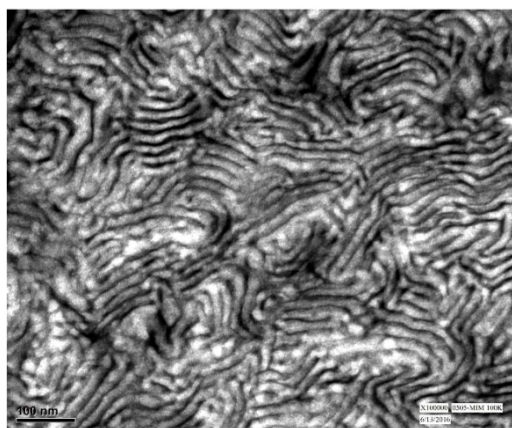
# Synthesis ABA Triblock Copolymers by Complex Living Free Radical Polymerization

Thursday, 19th October - 14:47 - Polymer, carbon and graphene nanostructures - Room 1 - Oral - Abstract ID: 398

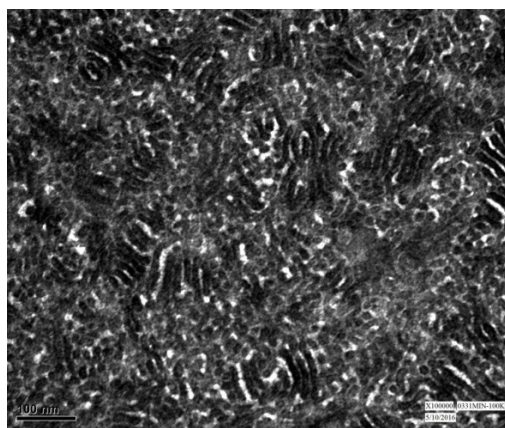
***Mrs. PIN-CHEN LEE<sup>1</sup>, Prof. Chuh-yung Chen<sup>1</sup>, Prof. Cheng-Chien Wang<sup>2</sup>***

*1. Department of Chemical Engineering, National Cheng Kung University, 2. Department of Chemical and Materials Engineering, Southern Taiwan University Science and Technology*

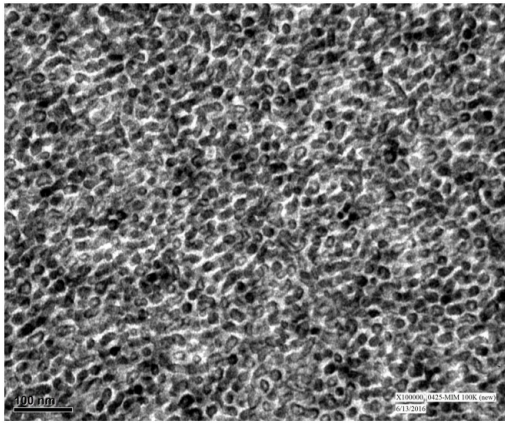
Triblock copolymers, methyl methacrylate-isoprene-methyl methacrylate (MIM), was successfully synthesized via anionic living polymerization (ALP) following the novel mercaptan/ $\epsilon$ -caprolactam living polymerization (MLP) at low reaction temperature. The MLP overcame that the severe polymerization conditions of acrylate monomer is needed in anionic living polymerization. Molecular weight of each segment in MIM was identified by using GPC and  $^1\text{H-NMR}$  instrument, respectively. Mw of isoprene and methyl methacrylate segments of MIM are in the range of 10,000~20,000 and 60,000~140,000, respectively. PDI of isoprene segment and MIM are located at 1.10 and 1.20~1.80, respectively. Two glass transition temperature ( $T_g$ ), -60~ $^{\circ}\text{C}$ ~ -8.5 $^{\circ}\text{C}$  for isoprene domain and 115 $^{\circ}\text{C}$  for methyl methacrylate domain, of MIM was clearly presented on the DSC curve, which reveals the completely immiscible between PI and PMMA domains. This result also can be confirmed by TEM micrographs. In TEM pictures, regularly phase domain pattern was formed via self-assembled of polymer chains without annealing treatment. This phase diagram of MIM material has highly potential applied on biomaterial research in future.



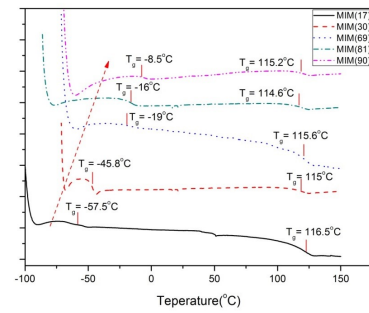
Mim 18 .jpg



Mim 69 .jpg



Mim 90 .jpg

Dsc curves of the different vinyl group of pi block  
in mim.jpg



# Nanofibrous Waterproof Breathable Protective Clothing

Thursday, 19th October - 15:04 - Polymer, carbon and graphene nanostructures - Room 1 - Oral - Abstract ID: 262

**Mr. Fouad J. Maksoud<sup>1</sup>, Mr. Mohammad Lameh<sup>1</sup>, Mr. Sary Fayyad<sup>1</sup>, Dr. Nagham Ismail<sup>1</sup>,  
Dr. Ali Tehrani<sup>1</sup>, Prof. Nesreen Ghaddar<sup>1</sup>, Prof. Kamel Ghali<sup>1</sup>**

*1. American University of Beirut*

Waterproof breathable membranes allow water vapor to pass through and prevent liquid water from penetration. They have a wide range of applications (e.g., skiwear, sleeping bag, water purification, wound healing, gas diffusion, etc.). In this study, several nanofibrous membranes were electrospun by changing different effective parameters (e.g., polymeric concentration, voltage, feed flow, etc.). The physical-chemical properties of the membranes (i.e., average fiber diameters, thickness, areal density, porosity, contact angle, waterproofness, air permeability, water vapor transmittance and aerosol filtration) were studied based on the standard test methods.

The beads-free webs with average fiber diameter as small as 200 nm were achieved from electrospinning of 10wt.% polyurethane in dimethylformamide, at feed rate of 0.5 ml/h, applied voltage of 25kV, and tip to collector distance of 15 cm (Figure 1). The thickness and areal density of the membranes increased linearly by time of electrospinning (Figure 2). By optimization of the electrospinning parameters, a web with high level of waterproofness, high air permeability (AP), and high water vapor transmission rate (WVTR) was obtained (Figure 3). A linear empirical equation was found for the estimation of AP and WVTR based on the average pore size diameter, the membrane thickness, and the porosity with very high regression coefficients ( $R^2 > 0.97$ ).

The selected membrane, with thickness=60  $\mu\text{m}$ , and average pore size diameter=3mm, showed very good air permeability of 9 mm/s, hydrostatic pressure resistance of 155 cm  $\text{H}_2\text{O}$ , and WVTR of 42.5  $\text{g/m}^2/\text{h}$ . This membrane could remove the particles larger than 0.6  $\mu\text{m}$  completely (100%) from the air stream while it efficiently reduced the concentration of the smaller particles by minimum 92% (Figure 4).

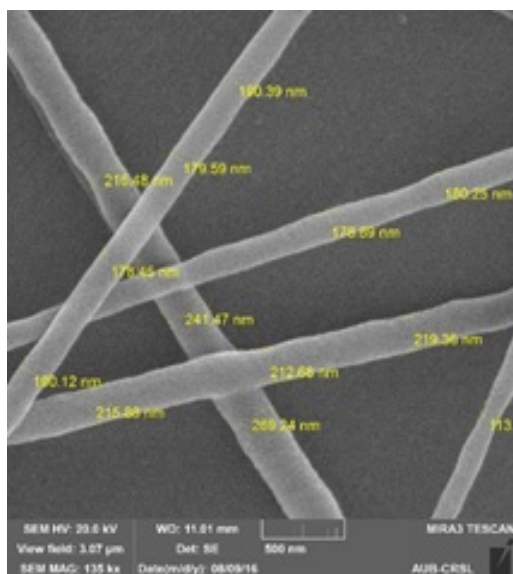


Figure 1.jpg

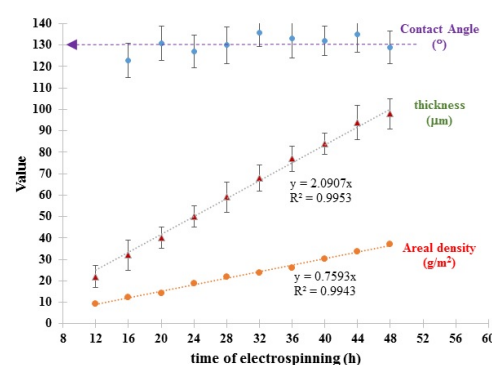


Figure 2.jpg

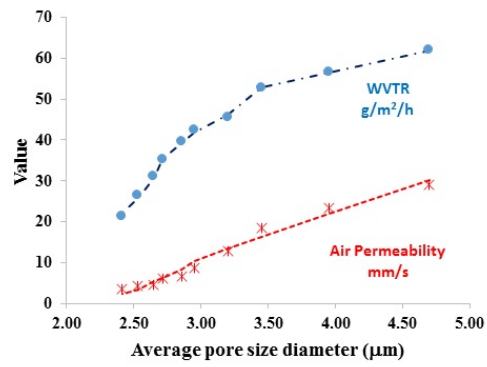


Figure 3.jpg

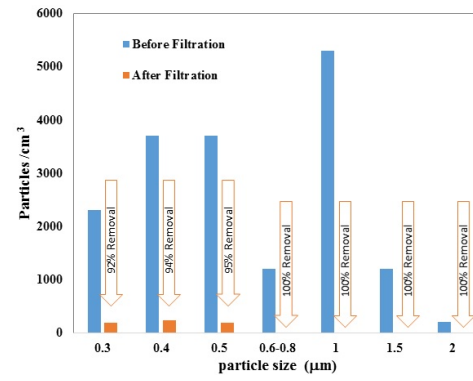


Figure 4.jpg

# Concepts of Novel Infrared Photodetectors Based on van der Waals/Graphene Heterostructures

Thursday, 19th October - 15:21 - Polymer, carbon and graphene nanostructures - Room 1 - Oral - Abstract ID: 630

**Dr. Maxim Ryzhii<sup>1</sup>, Prof. Victor Ryzhii<sup>2</sup>, Prof. Taiichi Otsuji<sup>2</sup>, Prof. Michael Shur<sup>3</sup>**

**1. University of Aizu, 2. RIEC, Tohoku University, 3. Rensselaer Polytechnic Institute**

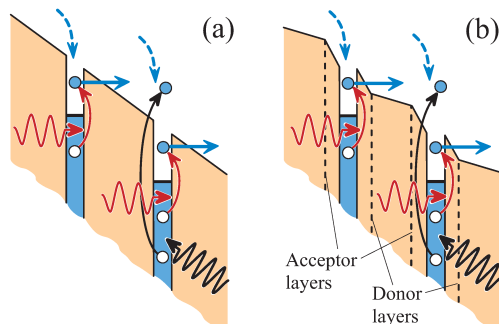
Creation of the heterostructures based on the van der Waals (vdW) materials [1] with graphene layers (GLs) opens up prospects in implementation of novel optoelectronics devices. Contrary to the traditional epitaxially grown heterostructures, in the vdW heterostructures the layers with different lattice constants can be stacked together because of weak inter-layer bonding. As a result, a wide family of the vdW materials could form heterostructures with required properties. In this report, we analyze the concept and consider the characteristics of the recently proposed infrared photodetectors based on the vertical heterostructures with the vdW material's barrier layers, GLs, and n-type emitter and collector contacts [2]. The vdW/GL infrared photodetectors in question can be made using a single or multiple GLs sandwiched between the vdW material barrier layers (hBN, WS<sub>2</sub>, WSe<sub>2</sub>, and similar materials).

Using the developed analytical device model we calculate the vdW/GL infrared photodetector responsivity and dark current detectivity as functions of the energy of incident infrared photons and the structural parameters. The doping engineering can be used for the optimization of vdW/GL infrared photodetectors operating in different radiation spectrum ranges.

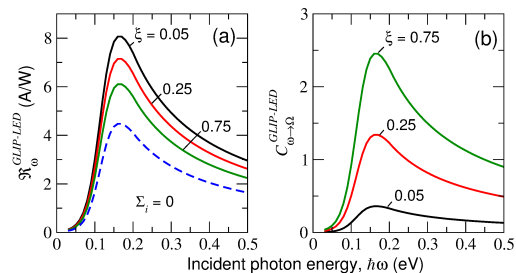
We compare the responsivity, detectivity, and performance of the vertical vdW/GL infrared photodetectors with other photodetectors based on the lateral single- and multiple-GL heterostructures with p-i-n junctions [3] and with the vertical single- and multiple-quantum-well infrared photodetectors (QWIPs) using the intersubband transitions. As shown, the proposed vertical vdW/GL infrared photodetectors might exhibit the following advantages: (i) sensitivity to the normally incident infrared radiation due to the use of the interband transitions in the gapless GLs, (ii) a higher probability of the electron photoexcitation from the GLs, (iii) a lower probability of the capture of the electrons propagating above the barriers in into the GLs, and (iv) a weaker dark current promoting higher detectivity values.

## References

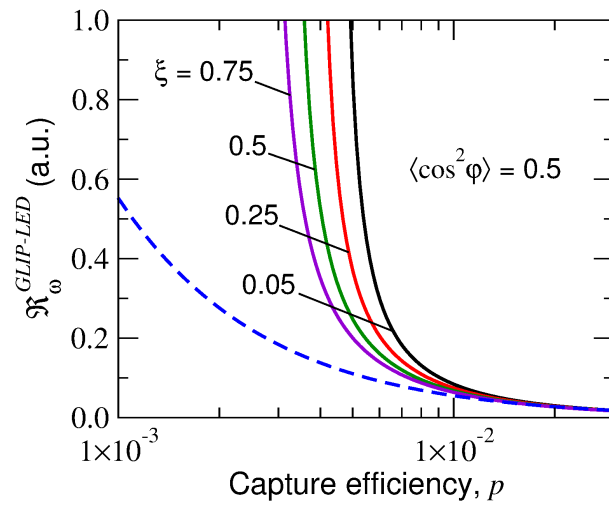
- [1] A. K. Geim and I. V. Grigoreva, Nature 499, 419 (2013).
- [2] V. Ryzhii, et al., Infrared Phys. Technol. (2017), in press.
- [3] V. Ryzhii, et al., J. Appl. Phys. 107, 054512 (2010).



Fragments of band diagrams.png



Responsivity1.png



Responsivity2.png

# Nonlinear behavior of fluid conveying single-walled carbon nanotubes with a geometrical imperfection

Thursday, 19th October - 15:38 - Polymer, carbon and graphene nanostructures - Room 1 - Oral - Abstract ID: 480

***Ms. Liu Chenxin<sup>1</sup>, Prof. Ni Qiao<sup>1</sup>***

*1. Huazhong University of Science and Technology*

## Abstract

There are many previous papers simulate the CNT conveying fluid which assume the longitudinal shape of the nanotube is entirely straight. However, the photos taken by transmission electron microscopes show that the CNT usually present curvature along their length, which influences their dynamical behavior efficiently. Motivated by the lack of study on the imperfection CNT, we will investigate the nonlinear dynamics of geometrical imperfect CNT.

In this research, we focus on transverse vibration of a single-walled carbon nanotube conveying fluid with supported ends based on the nonlocal elasticity theory and Timoshenko model. This CNT is assumed to be embedded in a Pasternak foundation and have a slight curvature initially as geometrical imperfection. Hamilton's principle is applied to get the governing equation in this case, which considers stretching, large deformation and imperfection nonlinearities. Then, the Galerkin method is adopted to discretize the nonlinear governing equation. Eventually, the numerical results are obtained by Runge-Kutta algorithm. Stability, bifurcation, vibration frequencies and response behavior of the nanotube are obtained by analytical solutions.

The obtained results reveal that at high flow velocities, nonlinearity of the model become more important, especially for a slightly curved nanotube. Moreover, the existence of the geometrical imperfection and the surrounding elastic medium causes the natural frequency to increase while under the same flow velocity, which implies the rise of critical velocity. It is also demonstrated that the nonlocal parameter decrease the buckling natural frequency and critical velocity. According to the bifurcation diagram, the results show that the local parameter and geometrical imperfection have significant impact on the maximum amplitude of the oscillation. As the local parameter and initial curvature increase, the maximum amplitude increase.

Keywords: nanotube conveying fluid; nonlinear model; nonlocal elasticity theory; Timoshenko beam; natural frequency; imperfection

---

## A new biochemical approach for controlled release of dexamethasone from functionalized PEDOT coatings for neural applications.

---

Thursday, 19th October - 15:55 - Polymer, carbon and graphene nanostructures - Room 1 - Oral - Abstract ID: 571

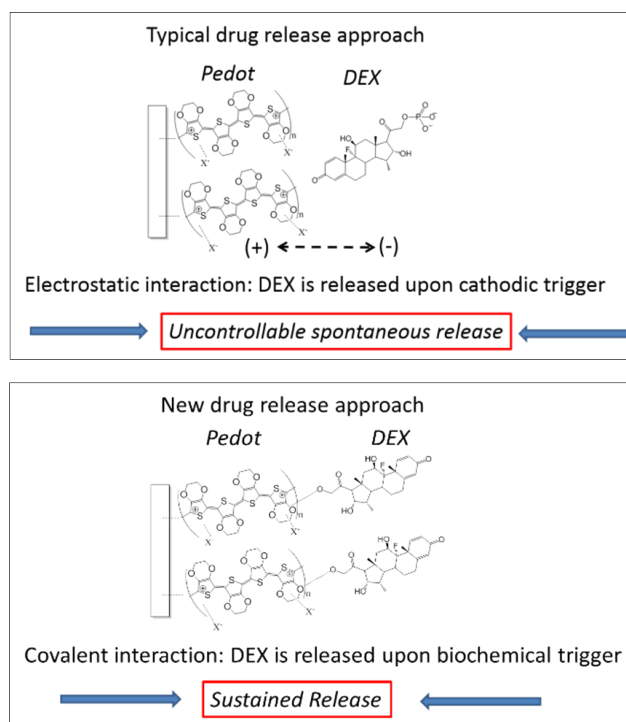
---

***Dr. stefano carli*<sup>1</sup>, *Prof. Claudio Trapella*<sup>2</sup>, *Mrs. Linda Lambertini*<sup>1</sup>, *Dr. Anna Fantinati*<sup>2</sup>, *Dr. Elisa Castagnola*<sup>3</sup>, *Ms. Claudia Cea*<sup>3</sup>, *Ms. Surabhi Nimbalkar*<sup>3</sup>, *Dr. Alice Scarpellini*<sup>4</sup>, *Dr. Mirko Prato*<sup>5</sup>, *Prof. Sam Kassegne*<sup>3</sup>, *Dr. Davide Ricci*<sup>1</sup>, *Prof. Luciano Fadiga*<sup>1</sup>**

*1. Center for Translational Neurophysiology of Speech and Communication, Istituto Italiano di Tecnologia, 2. University of Ferrara/Dept. of Chemical and Pharmaceutical Sciences, 3. MEMS Research Lab., Department of Mechanical Engineering, College of Engineering, 4. Electron Microscopy Facility, Istituto Italiano di Tecnologia, 5. Materials Characterization Facility, Istituto Italiano di Tecnologia*

Neural interfaces represent an important tool for enabling better fundamental understanding of the central and peripheral nervous systems, as well as for restoring damaged or lost sensorimotor functions. Conductive polymers, including poly(3,4-ethylenedioxythiophene (PEDOT), are typically electrodeposited onto microelectrodes to reduce the total impedance as well as improving the charge storage capacity, necessary for the goal of neural stimulation, for instance. In order to prevent the inflammation of the tissue surrounding the device and the subsequent glial scar formation, which eventually leads to the encapsulation of the implant and device failure, an interesting approach consists in the integration of a PEDOT matrix with anti-inflammatory glucocorticoid such as dexamethasone (DEX). We discuss on the possibility of controlling the drug release from the PEDOT coating via 1) electrochemical stimulus or 2) biochemical trigger.

*Method 1.* DEX was used as counter ion to counterbalance the positively charged PEDOT chain during electrodeposition. This approach enables an electrochemically controlled drug release system. The typical approach consists on the use of the anionic dexamethasone-phosphate to counterbalance the positively charged PEDOT chain. In such a way the drug is released from the PEDOT film by an electrochemical trigger that can be achieved via pulsed electrical stimuli or cyclic voltammetry in order to reach the neutral reduced state of the conductive polymer matrix, and the subsequent drug release. This approach has two main drawbacks: 1) the need of inducing current-voltage stimulus 2) uncontrollable drug release due to spontaneous ion exchange and subsequent drug diffusion into the bulk solution. *Method 2.* In order to circumvent these disadvantages, a new DEX functionalized EDOT monomer was prepared and used to prepare electrodeposited PEDOT coatings in which the drug is chemically linked to the polymer backbone, enabling a biochemically triggered drug release system. The new PEDOT-DEX composite films were electrodeposited onto Glassy carbon electrodes in order to optimize the deposition method as well as to collect a preliminary evaluation of the stored/released drug.



Pedot-dex drug release approaches.png

# Microfluidic synthesis of multifunctional liposomes for targeted drug delivery

Thursday, 19th October - 14:30 - Nanomedicine and nanobiotechnology - Room 2 - Oral - Abstract ID: 540

**Mr. Rui Ran**<sup>1</sup>

<sup>1</sup>. Australian Institute for Bioengineering and Nanotechnology, The university of Queensland

## Introduction:

Multifunctional liposome is a promising nano-system for various applications, such as cancer drug delivery, vaccine delivery, etc. However, more functionality requires more complex synthesis processes, resulting in poor reproducibility, low yield, and high production cost, hence difficulties in clinical translation. Therefore, it is imperative to develop simple approaches for making multifunctional liposomes.

## Methods:

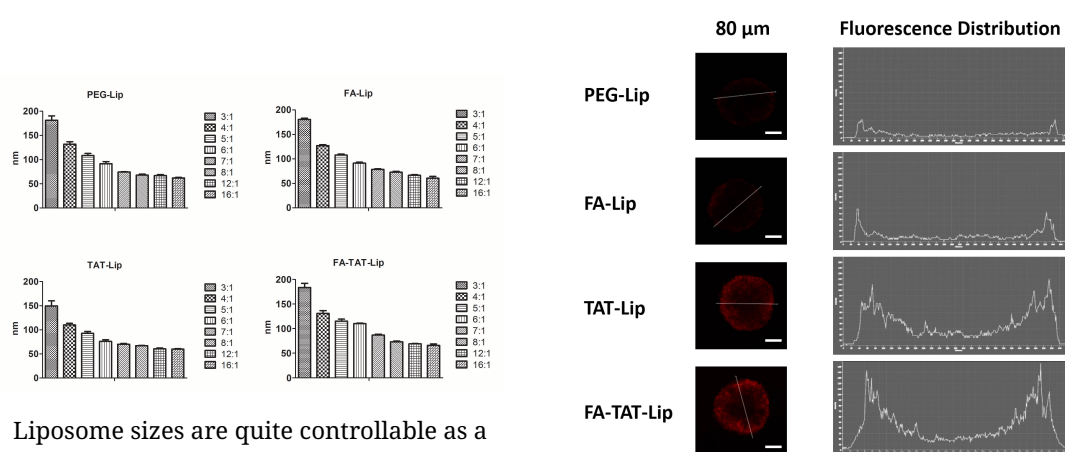
A hydrodynamic flow-focusing (HFF) microfluidic method has been developed to make a library of multifunctional liposomes with systematically varied properties, including PEGylated liposomes (PEG-Lip); single ligand folic acid (FA) modified liposomes (FA-Lip); single ligand cell penetrating peptide TAT modified liposomes (TAT-Lip) and dual-ligand liposomes (FA-TAT-Lip).

## Results:

The size of the liposomes with different formulations can be precisely controlled by tuning the microfluidic operation conditions (device design, flow rate ratio, etc) ranging from as low as 50 nm to about 200 nm. The FA-targeted liposomes demonstrated enhanced cellular uptake by the receptor positive cells, but limited tumour penetration capability. While combining the targeting ligand FA and the TAT peptide showed a synergistic targeting and tumour penetration effect.

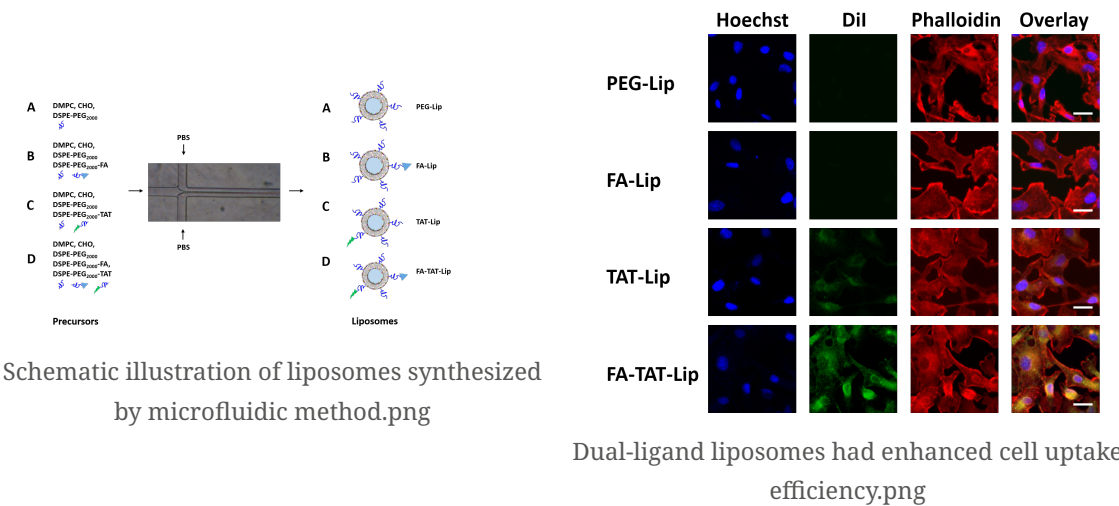
## Discussion:

The microfluidic HFF approach represents a new and very effective way in synthesizing multifunctional liposomes with controllable size and surface properties and superior biological functions, and it will serve as a promising platform for producing multifunctional liposomes for practical applications.



Dual ligand liposome also had enhanced tumor penetrating capability.jpg





## Potential environmental risk of $^{223}\text{Ra}$ -labelled hydroxyapatite nanoparticles.

Thursday, 19th October - 14:47 - Nanomedicine and nanobiotechnology - Room 2 - Oral - Abstract ID: 496

**Prof. Stanislav Smrcek**<sup>1</sup>, **Mr. Pavel Nykl**<sup>2</sup>, **Ms. Tereza Krmelová**<sup>1</sup>, **Dr. Martin Vlk**<sup>2</sup>, **Prof. Ján Kozempel**

<sup>2</sup>

1. Faculty of Science, Charles University, 2. Faculty of Nuclear Sciences and Physical Engineering, Czech technical University in Prague

**Introduction:** Nanoparticles have been used in many technological and consumer products worldwide. One of the new attractive field is their use in radionuclide therapy. Radium-223 labelled hydroxyapatites seem to be prospective carrier of Radium intended for the treatment of cancer after proper targeting. After medical use the applied nanoparticles are excreted by usual ways into the ecosystem. Thus they can attack water and soil and can enter into plants which are common source of animal and human food. The investigation of possible contamination of plants is therefore needed because the adverse effects of nanoparticles and radioactivity on human and animal health are reported.

**Methods:** The uptake and translocation of nanoparticles was tested using *in vitro* sterile cultivated plants *Zea mays* and *Avena sativa* at cultivation with tap water enriched with Ra-223 labelled hydroxyapatite nanoparticles (ca. 1 kBq, 0,3 mg) for three weeks. Then the uptake and translocation of the radioactivity was evaluated by electronic autoradiography and scintillation counting.

**Results:** Experiments with *Zea mays* plants showed the uptake of 36 % of applied radioactivity into plant tissues of which 88 % was localized in root and 12 % in shoot parts, respectively. In *Avena sativa* plants the total activity uptake was 53 %, of which 88 % was present in roots and 12 % in shoots.

**Discussion:** From the results it is clear that Radium is extracted into plant tissues. The simplest explanation is to consider the entry of nanoparticles through the pores of the root membrane. Then the extraction efficiency would be limited by the pore size (e.g. 6 nm in diameter at *Zea mays*). On the other hand, the penetration of even larger nanoparticles than the pore size is known from the literature, but the mechanism of the process is not clear yet. It is also possible that soluble Radium ions are formed and then translocated. Regardless of the mechanism, it can be concluded that the Radium and/or radioactive nanoparticles uptake by plants is possible. Therefore there is a real risk of ecosystem contamination and on the other hand, the technological possibility of removing radioactive contaminants using plant biotechnology.

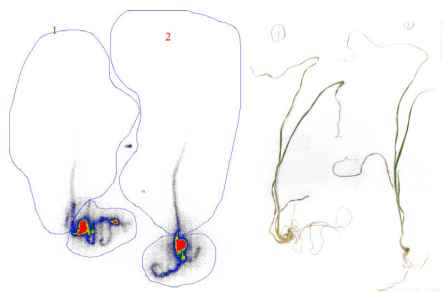


Fig. 1 Radioactivity distribution (kBq) in *avena sativa* plants (right).

Smrcek fig1.png

# Antibacterial nanosilver: defeating resistance, prolonged effects, mechanisms, and potential applications

Thursday, 19th October - 15:04 - Nanomedicine and nanobiotechnology - Room 2 - Oral - Abstract ID: 640

**Ms. Dina Mosselhy**<sup>1</sup>, **Ms. Henrika Granbhom**<sup>2</sup>, **Dr. Ulla Hynönen**<sup>3</sup>, **Dr. Yanling Ge**<sup>2</sup>, **Prof. Airi Palva**<sup>3</sup>,  
**Prof. Katrina Nordström**<sup>1</sup>, **Prof. Simo-Pekka Hannula**<sup>2</sup>

1. Department of Bioproducts and Biosystems, School of Chemical Engineering, Aalto University, 02150 Espoo, Finland, 2. Aalto University, Department of Chemistry and Materials Science, School of Chemical Engineering, 3. Department of Veterinary Biosciences, Division of Veterinary Microbiology and Epidemiology, University of Helsinki, P.O. Box 66, 00014 Helsinki, Finland

Antibiotics have traditionally been used to fight bacterial infections until the emergence of antibiotic-resistant bacteria. Methicillin-resistant *Staphylococcus aureus* (MRSA) is a challenging stated infection, not only in hospital environments [1,2] but also in the community reservoir [3,4], causing deaths [5,6]. This resistance dilemma has made it compelling to apply alternative antibacterial agents. Silver (Ag) is an alternative arsenal used in medical applications, such as wound dressings, to fight the antibiotic-resistant bacteria. Despite the tremendous interest in commercial antibacterial applications of Ag, there has been little agreement on the exact mechanism of antibacterial action of Ag NPs. On the other hand, Ag NPs might easily be aggregated, losing their antibacterial properties. Therefore, docking Ag NPs on carriers, forming composites can bridge the aggregation problem. Moreover, immobilization can endow Ag NPs intriguing antibacterial applications owing to the prolonged Ag release. Consequently, I will demonstrate our approach of immobilizing Ag NPs onto silica, allowing for the prolonged Ag release and antibacterial properties [7]. The defeat of MRSA and *Escherichia coli* by the immobilized Ag NPs will also be presented, in light of our results, along with a comparative applicable example for the prolonged antibacterial properties of a gauze-impregnated with the immobilized Ag NPs and a commercial Ag-containing dressing [7]. I will further unveil the mechanisms of antibacterial effects of the immobilized Ag NPs, using transmission electron microscope (TEM) and scanning TEM (STEM). We foresee the promising prolonged antibacterial properties of the immobilized Ag NPs for wound dressing applications [7].

## References

- [1] Church, D. et al. *Clin. Microbiol. Rev.* **2006**, *19*, 403–434.
- [2] Strohal, R. et al. *J. Hosp. Infect.* **2005**, *60*, 226–230.
- [3] Chambers, H. F. *Emerging Infect. Dis.* **2001**, *7*, 178–182.
- [4] Okuma, K. et al. *J. Clin. Microbiol.* **2002**, *40*, 4289–4294.
- [5] Leaper, D. J. *Int. Wound J.* **2006**, *3*, 282–294.
- [6] Centers for Disease Control and Prevention (CDC). *MMWR Morb. Mortal. Wkly. Rep.* **1999**, *48*, 707–710.
- [7] Mosselhy, D. A. et al. *Nanomaterials* **2017**, *7*, 261.

---

## Proteins immobilized on nanoparticles – determination of the surface coverage

---

Thursday, 19th October - 15:21 - Nanomedicine and nanobiotechnology - Room 2 - Oral - Abstract ID: 516

---

***Dr. Jaroslaw Grobelny<sup>1</sup>, Dr. Katarzyna Ranoszek-Soliwoda<sup>1</sup>, Ms. Ewa Czechowska<sup>1</sup>, Dr. Emilia Tomaszewska<sup>1</sup>, Dr. Grzegorz Celichowski<sup>1</sup>, Prof. Janusz Szemraj<sup>2</sup>***

*1. University of Lodz, 2. Medical University of Lodz*

### Introduction

Proteins can be immobilised on the surface of nanoparticles (NPs) by two main roads: covalent bounding or via adsorption process. Regardless the method, the immobilisation of proteins on NPs allows to design a protein-particle hybrid system which may exhibit a new properties that result from synergistic effect of combination of its components (NPs and protein). Hence, the precise characterization of NPs and proteins, as well as the determination of the amount of proteins on NPs, is crucial. There are several methods available to characterize NPs and proteins separately, but the quantification of the amount of protein on the single NP surface is still challenging. In this work a simple, reproducible and highly sensitive analytical method to determine the amount of protein adsorbed on a single NP will be presented.

### Methods

Metallic nanoparticles (mNPs) synthesized via chemical reduction method were modified with proteins (catalase-CAT) by incubation. Dynamic Light Scattering was used to monitor the agglomeration state of colloids before and after the immobilisation of CAT as well as to investigate the hydrodynamic size of mNPs modified with CAT. Morphological studies of the mNPs before and after modification were performed by S-TEM. Determination of CAT adsorption was carried out with different electrophoresis protocols to find the optimal conditions for quantification of the surface coverage of mNPs by catalase.

### Results

It was found that the modification process with CAT did not disturb the stability of NPs. Particles were colloidally stable after the modification without any aggregates or agglomerates. The hydrodynamic size of protein-modified ANPs increased compared to non-modified which confirmed the successful modification process. The determination of the surface coverage of NPs with CAT was performed based on the native-PAGE for which the most sensitive conditions were found.

### Discussion

The presented method allowed for the identification and quantification of the amount of CAT adsorbed on the surface of NPs in a colloidal state. The obtained results prove that the method is effective and versatile and can be successfully used for the identification and quantification of proteins adsorbed on the surface of different types of colloidal NPs.

NSC of Poland 2013/09/B/NZ7/01019

# Nanomedicines as photodynamic therapy for cancer

Thursday, 19th October - 15:38 - Nanomedicine and nanobiotechnology - Room 2 - Oral - Abstract ID: 169

**Dr. Swati Biswas<sup>1</sup>, Ms. Preeti Jha<sup>1</sup>, Dr. Balaram Ghosh<sup>1</sup>, Dr. Vladimir Zorin<sup>2</sup>**

**1. Birla Institute of Technology and Science-Pilani, Hyderabad, 2. Belarusian State University**

Photodynamic therapy (PDT) is an emerging treatment modality for cancer, especially for the treatment of superficial tumors, including melanoma, oesophagus and head and neck cancers. This is a low traumatic method for the treatment of oncological patients compared to surgery, which is gaining high recognition due to the moderate cost, absence of serious complications, and comparative selectivity of anticancer activity. PDT utilizes chemical photosensitizers (PSs), which produces reactive oxygen species (ROS) upon light irradiation at specific wavelengths, which kills target tumor tissues. Although PSs are highly effective in inducing apoptosis, and relatively non-toxic without irradiation, the poor hydrophobicity limits its therapeutic application. Therefore, effective delivery system for PSs is highly sought.

In our study, we have developed a nanomedicine, where a photosensitizer chlorin e6 (Ce6) had been loaded in a polymeric micellar system, poly(ethylene glycol)-poly(D,L-Lactide) (mPEG-PLA). After physico-chemical characterization, the cellular uptake and phototoxicity of Ce6-mPEG-PLA were evaluated compared to free Ce6 in Human lung adenocarcinoma cells (A549) in monolayer and in spheroid tumor model.

The micellar system was efficient in loading Ce6 in the hydrophobic core as indicated by physico-chemical studies. Ce6-mPEG-PLA micelles showed high solubility and fluorescence intensity in aqueous media compared to free Ce6. Moreover, the ability of Ce6-mPEG-PLA to produce singlet oxygen, the primary inducer of apoptosis, was assessed in aqueous media. Ce6-loaded mPEG-PLA micelles showed enhanced cellular uptake in A549 cells, decreased cell viability, and improved cellular internalization of the PS resulting in higher growth inhibition in avascular A549 spheroids compared to free drug.

In conclusion, Ce6 loaded mPEG-PLA micelles demonstrated significant cell killing ability in both monolayer and spheroid cultures compared to free Ce6. Considering that the mPEG-PLA nanocarrier is biocompatible, and biodegradable, this newly developed nano-formulation could have a great potential as clinical PDT for cancer.

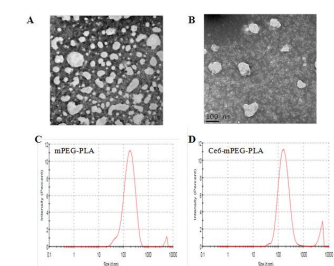


Figure 1. TEM images and DLS graphs of (A), (C) for mPEG-PLA; (B and D) for Ce6-mPEG-PLA

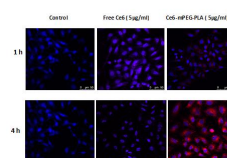


Figure 2. Confocal micrographs of A549 cells treated with Ce6 and Ce6-mPEG-PLA at the cell concentration of 7.5 µg/mL at 1 and 4 h post-treatment (Red and blue colors are representative of Ce6 and DAPI fluorescence, respectively).

Figure 2.jpg

Figure 1.jpg

---

# Stability enhancement in organic photovoltaics: in-situ structural/morphological monitoring approach applied to plasmonic devices

---

Thursday, 19th October - 14:30 - Nanophotonics, optics and plasmonics - Auditorium - Oral - Abstract ID: 774

---

**Dr. Barbara Paci<sup>1</sup>, Dr. Amanda Generosi<sup>1</sup>, Dr. George Kakavelakis<sup>2</sup>, Mr. Marco Guaragno<sup>1</sup>, Dr. Valerio Rossi Albertini<sup>1</sup>, Dr. Emmanuel Stratakis<sup>3</sup>, Prof. Emmanuel Kymakis<sup>4</sup>**

*1. Istituto di Struttura della Materia/CNR, Via del Fosso del Cavaliere 100, 00133 Roma, 2. Center of Materials Technology and Photonics, TEI, Heraklion, GR-710 04, Crete, Greece, 3. Institute of Electronic Structure and Laser (IESL) Foundation for Research and Technology-Hellas (FORTH), Heraklion, GR-711 10, Crete., 4. Center of Materials Technology and Photonics, TEI, Heraklion, GR-710 04, Crete*

## Introduction

Recent results in bulk heterojunction (BHJ) organic photovoltaic (OPV) devices incorporating metallic nanoparticles (NPs) in the photoactive layer are discussed. Our research focuses on two key aspects: rising the efficiency and the long-term stability of such low environmental impact, flexible and low cost devices. We take advantage of the ability of metallic NPs to raise the BHJ optical absorption by the excitation of localized surface plasmon resonance to address the efficiency issue. At the same time, in-situ time-resolved characterization is applied for understanding the NPs role in inhibiting the chemical/physical mechanisms driving device degradation.

## Methods

Plasmonic devices are studied by an unconventional approach based on time-resolved Energy Dispersive X-ray Reflectivity /Diffraction (EDXR/EDXD) techniques, applied jointly with in-situ atomic force microscopy.

## Results and Discussion

We found that the polymer conformational properties are stabilized when the BHJ is doped with NPs, also preserving the donor-acceptor network nanoscale morphology. Furthermore, Au NPs doping results in stabilizing the cathode buried interface, a fact ascribed to a NP-mediated mitigation of photo-oxidation effects. As a result, we obtain an increase in the device performance (by 40%) and a significant enhancement in lifetime (by 3 times) with respect to reference undoped devices. These investigations, also demonstrating the great potential of the structural/morphological cross-monitoring approach in directly observing the nanoscale modifications of the bulk/interface properties, pave the way towards OPVs with improved efficiency and stability.

Figure 1: Time-resolved EDXR and AFM analysis of OPV device incorporating metal NPs, demonstrating a NPs mediated mitigation of the aging effects.

## References:

[1] B. Paci, G. Kakavelakis, A. Generosi, J. Wright, C. Ferrero, E. Stratakis, E. Kymakis, *Solar Energy Materials & Solar Cells*, **159**, 617–624, 2017.

- [2] B. Paci, D. Bailo, V. Rossi Albertini, J. Wright, C. Ferrero, G. D. Spyropoulos, E. Stratakis, E. Kymakis, *Adv. Mater.*, **25**, 4760-4765, 2013.
- [3] B. Paci, A. Generosi, V. Rossi Albertini, G. Spyropoulos, E. Stratakis, E.; Kymakis, *Nanoscale*, **4** (23), 7452 – 7459, 2012.
- [4] B. Paci, A. Generosi, D. Bailo, V. Rossi Albertini, G. Spyropoulos, E. Stratakis, E. Kymakis, *Adv. Funct. Mater.*, **21**, 3578-3582, 2011.

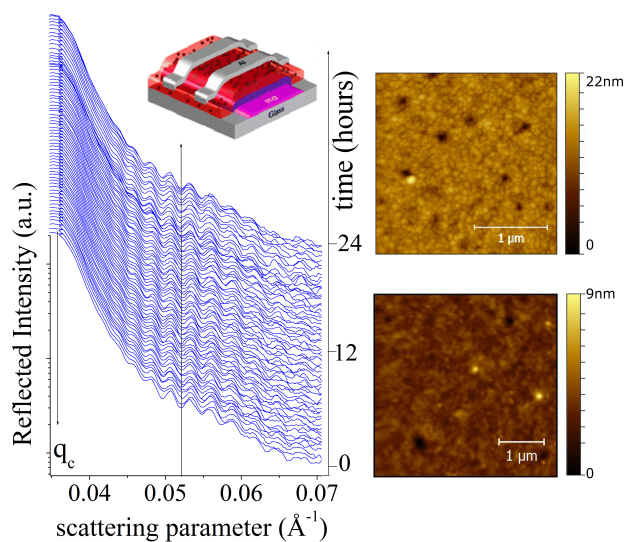


Figure 1.jpg

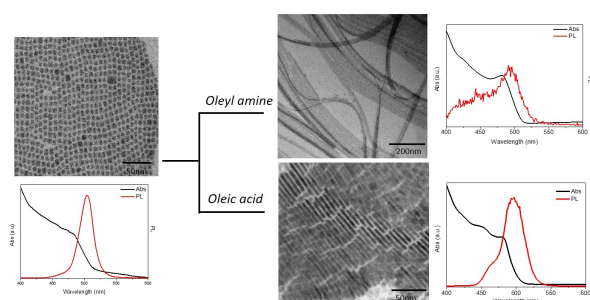
# Ligand Induced Shape Control of Cesium Lead Bromide Nanocrystals by Post Synthetic Treatments

Thursday, 19th October - 14:47 - Nanophotonics, optics and plasmonics - Auditorium - Oral - Abstract ID: 225

**Dr. Elisabetta Fanizza**<sup>1</sup>, **Ms. Francesca Cascella**<sup>1</sup>, **Dr. Annamaria Panniello**<sup>2</sup>, **Dr. Leonardo Triggiani**<sup>1</sup>, **Dr. Nicoletta Depalo**<sup>2</sup>, **Dr. Cinzia Giannini**<sup>3</sup>, **Dr. Davide Altamura**<sup>3</sup>, **Prof. Angela Agostiano**<sup>1</sup>, **Dr. M. Lucia Curri**<sup>2</sup>, **Dr. Marinella Striccoli**<sup>2</sup>

**1.** Università degli Studi di Bari "Aldo Moro", **2.** CNR IPCF-Istituto per i Processi Chimico Fisici, **3.** CNR IC- Istituto di Cristallografia

All-inorganic lead halide perovskite materials have attracted significant attention in the context of photovoltaic and optoelectronic applications, and recently, efforts have been devoted to the fabrication of colloidal stable versions of these materials. Cesium Lead Halide Bromide (CsPbBr<sub>3</sub>) colloidal nanocrystals (NCs), in particular, exhibit bright, size and shape-tunable photoluminescence in the blue-green region of the visible spectrum, that is usually not easily accessible with conventional quantum dots. It is worth to note that surfactants assist the shape and size regulation during the synthetic step, provide the better stability and help to maintain the optical properties of the final colloidal forms, but the role of ligands in post-synthetic treatments at room temperature is still a critical issue towards the application of this class of material for devices fabrication. The ionic nature of the CsPbBr<sub>3</sub> NCs and dynamic interaction of the ligands with the colloidal NC surface suggest a crucial role of surface chemistry of the as prepared NCs. In this regards this work investigates the shape regulation, structural changes and, thus modification of the optical properties, of as synthesized CsPbBr<sub>3</sub> NCs induced by post synthetic ligand treatments, based on addition of freshly oleylamine and oleic acid. The morphological, optical and structural characterization will shed light on the colloidal stability of this appealing new class of material, and also predict its transformation and properties in multicomponent complex systems for optoelectronic device fabrication.



Ligand mediated synthesis of cspbbr3.jpg



---

## Size and temperature effect on the photoluminescent properties of Europium-doped silica nanoparticles

---

Thursday, 19th October - 15:04 - Nanophotonics, optics and plasmonics - Auditorium - Oral - Abstract ID: 804

---

**Mr. Hussein Fneich<sup>1</sup>, Dr. Nathalie Gaumer<sup>2</sup>, Prof. Stephane Chaussedent<sup>2</sup>, Mr. Manuel Vermillac<sup>3</sup>,  
Dr. Wilfried Blanc<sup>3</sup>, Prof. Ahmad Mehdi<sup>1</sup>**

*1. University of Montpellier, ICGM, CNRS UMR 5253, 34095 Montpellier Cedex 5, France, 2. University of Angers, LPhiA, UPRES EA 4464, 49045 Angers Cedex 01, France, 3. University of Côte d'Azur, InPhyNi, CNRS UMR 7010, 06108 Nice Cedex 2, France*

Optical fibers containing rare-earth (RE) doped nanoparticles are investigated to develop new devices such as fiber lasers or amplifiers [1,2]. Thanks to this route, alteration of the spectroscopic properties of RE ions have been already reported [2,3]. However, the broad size distribution of vitreous nanoparticles does not allow discriminating between the role of their composition and their size on the luminescent properties. In this context, we take advantage of the sol-gel process to prepare nanoparticles with controlled sizes and to study their luminescent properties before and after annealing at 900°C.

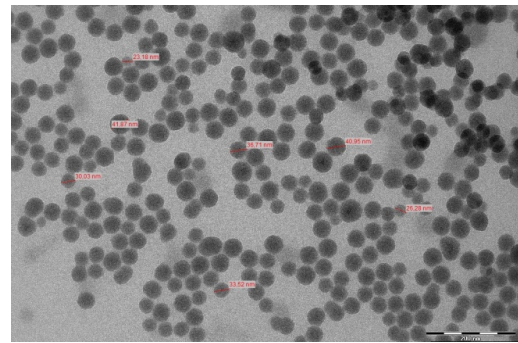
The classic sol-gel process remains one of the most important approach for the preparation of such nanoparticles with diameter larger than 50 nm using the Stöber method [4]. Smaller ones (around 10 nm) can be obtained by Sol-Gel in reverse micro emulsion method (water in oil) [5, 6]. In this case, the hydrolysis and the polycondensation take place in the hydrophilic micelles that play the role of nanoreactors.

For this study, silica nanoparticles with several molar contents of europium (0.2, 0.5 and 1%) were prepared in one step.

All nanoparticles were characterized by Transmission Electron Microscopy (TEM) and Inductively Coupled Plasma Mass Spectrometry (ICP-MS). The effects of the size of the nanoparticles and their Eu content as well as the temperature effect on their photoluminescent properties have been investigated. These results will be presented and discussed.

### References:

- [1] W. Blanc, *Applied Optics*, 48, 31 (2009).
- [2] M. Vermillac, *Optical Materials* 68, 24-28 (2017)
- [3] F. d'Acapito, *Journal of Non-Crystalline Solids*, 401, 50-53 (2014).
- [4] W. Stöber, *Journal of Colloid and Interface Science*, 26, 62-69 (1968).
- [5] J.H. Schulman, *The Journal of Physical Chemistry*, 63, 1677-1680 (1959).
- [6] W. Yang, *Analytica Chimica Acta*, 503, 163-169 (2004).



Tem image of silica nanoparticles with around 10 nm diameter.png

Tem image of silica nanoparticles with around 50 nm diameter.jpg

# Broadband Nonlinear Optical Response of Colloidal Carbon Nanohorns

Thursday, 19th October - 15:21 - Nanophotonics, optics and plasmonics - Auditorium - Oral - Abstract ID: 337

**Ms. Stefanie Dengler<sup>1</sup>, Dr. Olivier Muller<sup>2</sup>, Dr. Cordula Hege<sup>2</sup>, Dr. Bernd Eberle<sup>1</sup>**

**1. Fraunhofer IOSB, Institute of Optronics, System Technologies and Image Exploitation, 2. French-German Research Institute of Saint-Louis - ISL**

Carbon-based nanomaterials, like single- or multiwalled carbon nanotubes (CNT), fullerenes or graphene, were intensively studied by many different groups during the last decades. They show excellent electrical, thermal and mechanical properties, which make them suitable for a wide variety of applications. Many of these materials have been found to show also a strong nonlinear optical (NLO) behavior.

Carbon nanohorns (CNH) are a relatively unknown subclass of carbon-based nanomaterials. They consist of single-walled carbonic tubes with a conical end and typically assemble to spherical aggregates of 50 – 100 nm in diameter and larger agglomerates up to several micrometers (Fig. 1).

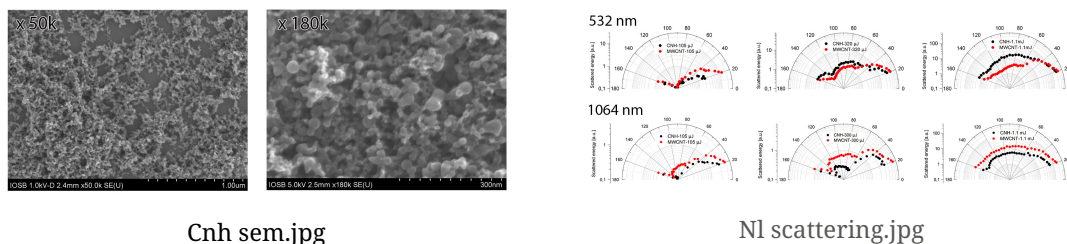
*Fig. 1: SEM-images of CNH at different magnifications.*

In this work, a comparative study on the NLO response of suspended CNH and MWCNT is presented. Nonlinear (NL) transmittance and scattering phenomena were investigated using nanosecond laser pulses at 532 nm and 1064 nm. The NLO properties of MWCNT suspensions are well studied and it is generally believed that NL scattering dominates their NLO characteristics.

Our investigations reveal a strong NLO effect in CNH suspensions, much stronger than in the benchmark material MWCNT (Fig. 2). To ascertain the contribution of NL scattering within the NL attenuation process, angle dependent measurements of the scattered light at different energy levels were performed (Fig. 3). It turned out that the NL behavior of CNH suspensions at 532 nm near the NL onset can be attributed to NL absorption, since only a weak scattering signal was observed. Towards higher energy levels, absorption-induced scattering increases strongly. In contrast to that, at 1064 nm the NL performance is dominated by NL absorption in the complete NL range. NL scattering plays only a minor role even at high input energies. Our results indicated CNH as a promising candidate for optoelectronic devices, such as optical limiting applications.

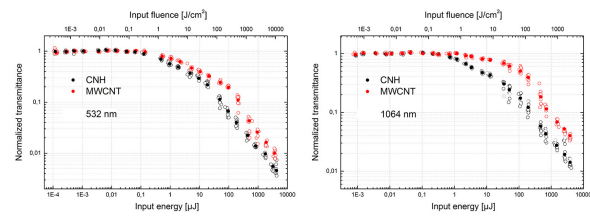
**Fig. 2: Nonlinear transmittance as a function of the input laser energy and input fluence of suspended CNH and MWCNT at 532 nm (left) and 1064 nm (right).**

**Fig. 3: Nonlinear scattering of suspended CNH and MWCNT at 532 nm (top) and 1064 nm (bottom) at three different energy levels.**



Cnh sem.jpg

Nl scattering.jpg



Nl transmittance.jpg

---

# Influence of aggregation on magnetic and optical properties of CoFe<sub>2</sub>O<sub>4</sub> superparamagnetic nanoparticles

---

Thursday, 19th October - 15:38 - Nanophotonics, optics and plasmonics - Auditorium - Oral - Abstract ID: 667

---

***Dr. Yulia Gromova*<sup>1</sup>, *Prof. Vladimir Maslov*<sup>1</sup>, *Mr. Mikhail Baranov*<sup>1</sup>, *Dr. Raquel Serano*<sup>2</sup>, *Mrs. Vera Kuznetsova*<sup>2</sup>, *Dr. Finn Purcell-milton*<sup>2</sup>, *Prof. Yurii Gun'ko*<sup>2</sup>, *Prof. Alexander Baranov*<sup>1</sup>, *Prof. Anatoly Fedorov*<sup>1</sup>**

*1. ITMO University, 2. School of Chemistry, Trinity College Dublin*

Magnetic nanoparticles (MNP) attract persist attention due to their unique magnetic, electrical, catalytic and optical properties, which in the most cases differ from the properties of the bulk material [1]. Superparamagnetism is one of extremely important MNP property for their application in biomedicine. The absence of remanence after elimination of the external magnetic field decrease probability of MNP aggregation that makes superparamagnetic MNPs a perfect candidate for drug delivery using blood flows without dangerous of obstruction of vessels. The drawback of using MNPs is that isolated MNPs are weakly magnetized, in contrast to the aggregated MNPs. Therefore control of MNP aggregation with keeping their superparamagnetic properties is an emerging challenge in drug delivery area [2].

In present work, we investigated magnetic and optical properties of both isolated and aggregated superparamagnetic CoFe<sub>2</sub>O<sub>4</sub> nanoparticles synthesized by the co-precipitation method and coated by chiral ligands. We applied magnetic circular dichroism (MCD) spectroscopy to probe the magnetic, optical and structural properties of MNPs. Analysis of transitions in the MCD spectra of single MNPs shows that Co<sup>2+</sup> ions occupied both tetrahedral and octahedral sites. Also it was found that all MCD band intensities dependence on applied magnetic field is proportional to MNP magnetization curve. MNP aggregation leads to changing MCD signal intensity as well. Correlation between MCD band intensity and MNP magnetization allowed making assumptions about an influence of aggregation on MNP magnetic properties.

[1] Owens, F. J., Physics of magnetic nanostructures. John Wiley & Sons: 2015.

[2] Amiri, S.; Shokrollahi, H., The role of cobalt ferrite magnetic nanoparticles in medical science. Materials Science and Engineering: C 2013, 33 (1), 1-8.

# Nanocrystals of GeSn alloys in oxide matrix for optoelectronic applications

Thursday, 19th October - 15:55 - Nanophotonics, optics and plasmonics - Auditorium - Oral - Abstract ID: 581

**Dr. Ionel STAVARACHE<sup>1</sup>, Dr. Adrian SLAV<sup>1</sup>, Dr. Mariana BRAIC<sup>2</sup>, Dr. Valentin Serban TEODORESCU<sup>1</sup>, Dr. Petronela PREPELITA<sup>3</sup>, Dr. Catalin PALADE<sup>1</sup>, Dr. Ana-Maria LEPADATU<sup>1</sup>, Dr. Sorina LAZANU<sup>1</sup>, Dr. Magdalena Lidia CIUREA<sup>1</sup>, Ms. Daniela STANGE<sup>4</sup>, Dr. Dan Mihai BUCU<sup>4</sup>, Dr. Toma STOICA<sup>1</sup>**

**1. National Institute of Materials Physics, 2. National Institute for Optoelectronics, 3. National Institute for Laser, Plasma and Radiation Physics, 4. Peter Grünberg Institut 9 and JARA Fundamentals of Future Information Technologies**

Obtaining direct bandgap in semiconductor alloys of the group IV elements is highly desired for photonic applications. GeSn alloys show a transition from Ge indirect to direct bandgap GeSn for compositions higher than 8% Sn [D. Stange et al. ACS Photon. 3, 1279 (2016)]. Additionally, alloying Ge with Sn features the possibility of tuning the bandgap of Ge to lower energies [P. Moontragoon, et al. Semicond. Sci. Technol. 22, 742 (2007)]. Challenges in obtaining direct bandgap GeSn is related to the low miscibility of Ge and Sn (less than 1%), as well as to the compressive strain in GeSn layers epitaxially grown on substrates as Si and Ge. However, metastable direct bandgap GeSn layers with up to 14%-16% Sn have been obtained and even the lasing effect was demonstrated [S. Wirths et al. Nat. Photonics 9, 88–92 (2015)].

We have investigated the properties of GeSn nanocrystals embedded in SiO<sub>2</sub> matrix. (Ge<sub>1-x</sub>Sn<sub>x</sub>)<sub>1-y</sub>(SiO<sub>2</sub>)<sub>y</sub> alloy layers were obtained by magnetron sputtering co-deposition on c-Si and fused quartz substrates. The Sn composition was varied between 9% and 16%, while the SiO<sub>2</sub> composition lies within a range of 0-17%. The as-deposited amorphous layers were subject to rapid thermal annealing resulting in segregation of GeSn and formation of nanocrystals at temperatures in the range of 350 °C-450 °C depending on the film composition. In Fig.1, X-Ray diffraction curves for two annealing temperatures at 400 °C and 450 °C (x=9%; y=9%) are shown. The formation of GeSn crystals with the Ge network structure but higher lattice constant of 5.58 Å is evidenced. At 450 °C, a segregation of metallic beta Sn is observed. The size of the nanocrystals of 3-7 nm was evaluated from HRTEM imaging and XRD measurements. Optical transmittance and reflectance in VIS-IR range have been measured to study the optical absorption and optical bandgap for different compositions and annealing temperatures. In general, two bandgap values E<sub>g1</sub> and E<sub>g2</sub> are found (Fig.2). The obtained data dependence demonstrates the tunability of the optical bandgap of GeSn nanocrystals in oxide matrix as function of Sn composition, offering great potential for optoelectronic applications in MIR range.

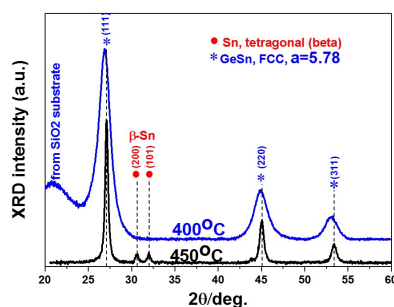


Fig.1 – XRD curves for two annealing temperatures.

Fig1.jpg

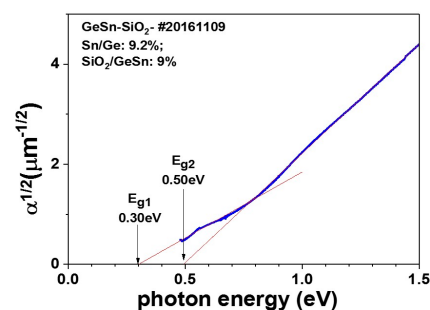


Fig.2 – Absorption coefficient of an as-deposited GeSn-SiO<sub>2</sub> layer.

Fig2.jpg

# Water stable nanofibrous tubes from hyaluronan derivative and nanocrystalline cellulose

Thursday, 19th October - 16:50 - Nanofabrication, nanoprocessing and nanomanufacturing - Room 1 - Oral - Abstract ID: 207

***Dr. Adela Kotzianova<sup>1</sup>, Mr. Jan Klemes<sup>1</sup>, Mr. Ondrej Zidek<sup>1</sup>, Dr. Marek Pokorny<sup>1</sup>, Dr. Gloria Huerta-Angeles<sup>1</sup>, Dr. Vladimir Velebny<sup>1</sup>***

*1. Contipro a.s.*

The field of nanotechnology has undergone unprecedented development in the recent decades and nanofibrous structures are still in the focus of attention. One of the current topics in this field is a preparation of the vascular grafts by the electrospinning method. This method enables easy preparation of grafts with diameter smaller than 6 mm, which could be used e.g. as coronary arteries grafts. In most cases, electrospun grafts are made of a synthetic polymer (PCL, PLA) as it provides sufficient mechanical properties, but their slow degradation rates limit cell infiltration. Synthetic polymers are thus often combined with a natural polymer (e.g. chitosan), which are hydrophilic and have faster degradation rates, but suffer from insufficient mechanical properties. This work aims to describe preparation and characterization of nanofibrous tubes made of a natural polymer - a hyaluronic acid, respectively its 3-(2-furyl)acrylic acid derivative (HA-FU). Using the classic process of electrospinning we were able to prepare nanofibrous tubes, from water solutions only, with a diameter of 3 mm and length up to 15 cm. The UV-crosslinkable hyaluronan enabled us to prepare water stable nanofibrous tubes (Fig.1 left) that could be used e.g. as a top layer of the synthetic grafts and thus enhance its bio properties. To enhance mechanical properties of the HA-FU tubes and made them more durable, a non-toxic, natural and biocompatible nanocrystalline cellulose (NCC) was used as an additive. The presence of NCC in tube structure after 7-day water immersion was confirmed by the confocal microscopy (Fig.2). Mechanical tests showed significant enhancement when 5% of NCC was added (Fig.3). The viability of 3T3 fibroblast was determined to show a non-toxic behaviour of prepared tubes. The viability was not significantly affected by the samples. Based on these results we do not suppose any cytotoxic effect of the HA-FU and HA-FU+NCC nanofibers. The NCC addition does not affect material toxicity. To demonstrate it possible application within a nanofibrous graft from a synthetic polymer, a composite tube made of PCL:HA-FU tube was prepared. The tube kept its shape after immersion and formed a gel HA-FU layer on its top (Fig.1 right).

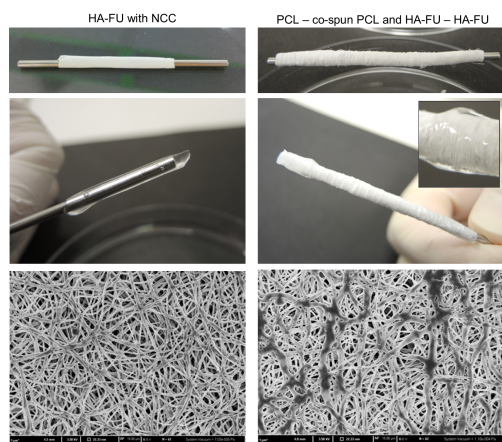


Fig. 1: Images of nanofibrous tubes from HA-FU with NCC additive (left) and PCL tube with HA-FU top layer (right) before and 7 days after immersing into distilled water and related SEM before immersing.

Fig1.png

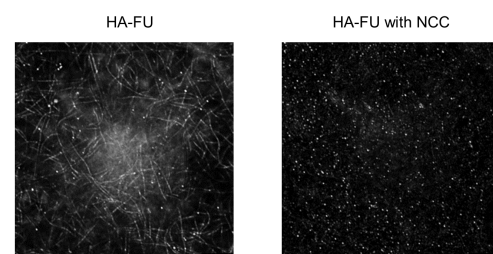


Fig. 2: Confocal images showing presence of nanocrystalline cellulose after water immersion.

Fig2.png



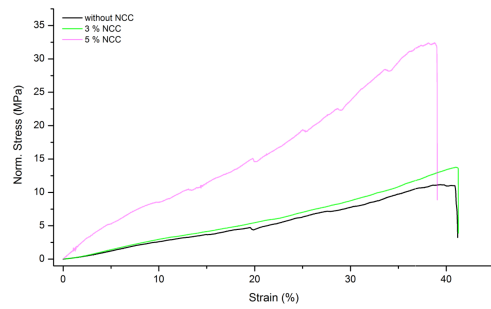


Fig. 3. Stress-strain curves showing enhancement of mechanical properties due to NCC addition into HA-FU.

This research has received funding from the European Community's Seventh Framework Programme (FP7-NMP-2013-SME-7) under grant agreement no 604450 (NEURIMP "Novel combination of biopolymers and manufacturing technologies for production of a peripheral nerve implant-containing an internal aligned channels array").

Funding information.png

Fig3.png



---

## Preparation of Hollow Cationic-Poly(cyclodextrin) Nanoparticles through Colloidal Templating

---

Thursday, 19th October - 17:07 - Nanofabrication, nanoprocessing and nanomanufacturing - Room 1 - Oral -  
Abstract ID: 149

---

***Dr. Sabrina Belbekhouche<sup>1</sup>, Ms. Imane El Joukhar<sup>1</sup>, Prof. Benjamin Carbonnier<sup>1</sup>***

***1. Université Paris Est (UPEC) / East Paris Institute of chemistry and Materials Science (ICMPE)***

Recent progress in supramolecular chemistry leads to unrivalled control over the composition and shape factor of colloidal systems. In this context, we propose to combine two concepts, i.e. the design of nanometer-sized capsules and the assembly via host-guest, in the aim of merging new tailor-made system in the field of supramolecular chemistry. We design biocompatible hollow capsules combining several favorable features as both unique biological functions of polysaccharide, transport properties of the multilayer shell and as a hydrophobic drug carrier, including host-guest complexation in the shell. These capsules were generated via colloid-templated layer-by-layer electrostatic assembly of cationic-poly(cyclodextrin) and alginate onto gold nanoparticles. A model of hydrophobic drug was loaded inside the cyclodextrin cavity present in the particle shell via host-guest interaction. Successful removal of the gold core is evidenced by time-dependence monitoring of the gold spectroscopic signature leading to colloidally stable capsule. The implemented strategy allows easy and fast design of well-ordered multilayer films allowing the elaboration of ultra-low size particle containing cyclodextrin derivative.

---

# Biodistribution and quantitation of metal oxide nanoparticle at the subcellular level using confocal Raman microscopy

---

Thursday, 19th October - 17:24 - Nanofabrication, nanoprocessing and nanomanufacturing - Room 1 - Oral -  
Abstract ID: 570

---

***Dr. Vincenzo Calcagno<sup>1</sup>, Mrs. Carolin Merker<sup>1</sup>, Dr. Jana Fleddermann<sup>1</sup>, Dr. José Barzola Quiquia<sup>1</sup>,  
Mr. Thomas Meyer<sup>1</sup>, Prof. Jan Meijer<sup>1</sup>, Dr. Irina Estrela-lopis<sup>1</sup>***

*1. University of Leipzig*

## *Introduction*

Health impact of nanomaterials is getting more relevance, since they are increasingly finding applications in many industrial and biomedical fields. To evaluate the toxicological response of NMs, and in particular of metal oxide nanoparticle (NPs), their quantification in biological matrixes and distribution pattern are essential. With current technologies locating and quantifying metal oxide NPs in cells and organs is still complicated, expansive and time consuming. Here we demonstrate that Confocal Raman Microscopy (CRM) – a non-invasive, non-destructive and label-free technique – can be used not only for the visualization and detection of NMs within biological systems, but also for their simultaneous quantification.

## *Methods*

Nanostructured composite films containing cerium dioxide nanoparticles (CeO<sub>2</sub> NPs) have been fabricated exploiting the layer-by-layer (LbL) technique (Figure 1). We used such nano-composite films as standards to calibrate CRM device by using Ion Beam Microscopy (IBM) techniques as dosimetric reference tool.

## *Results*

Nano-composite films with homogeneous distribution and controlled amounts of CeO<sub>2</sub> NPs have been built up and well characterized (Figure 1). A good correlation between the absolute amount of Ce, determined with IBM techniques, and the CRM response is obtained. The method has been validated with a biological matrix, by using the CRM for the simultaneous imaging, detection and quantification of CeO<sub>2</sub> NPs in lung tissue (Figure 2).

## *Discussion*

CRM combines confocal optics features with the ability of Raman spectroscopy to determine the chemical composition of the materials. Consequently, it can be used for the 3D co-localization of metal oxide NPs with cell compartments. Results demonstrate that this novel approach can be further used for the simultaneous imaging and quantification of metal oxide NPs within biological systems. This label-free, non-destructive and fast approach overcomes the limitations of other technologies currently applied in nano-toxicology for NPs dosimetry.

## *Images*

*Figure 1: Nano-composite film of CeO<sub>2</sub> NPs on a silicon substrate: SEM and confocal Raman images overlapped.*

*Figure 2: Bright-field image and 3D Raman Image reconstruction of a macrophage in vicinity of alveola from lung tissue section.*

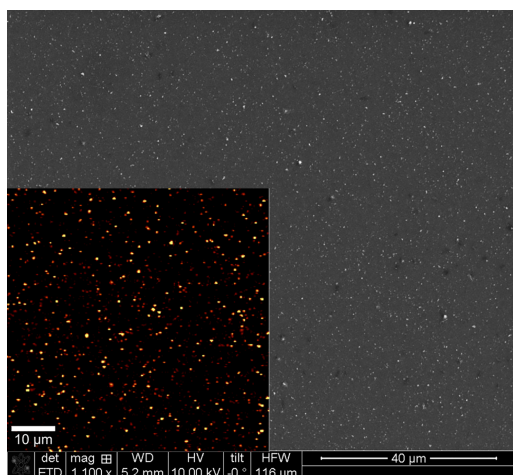


Figure 1.jpg

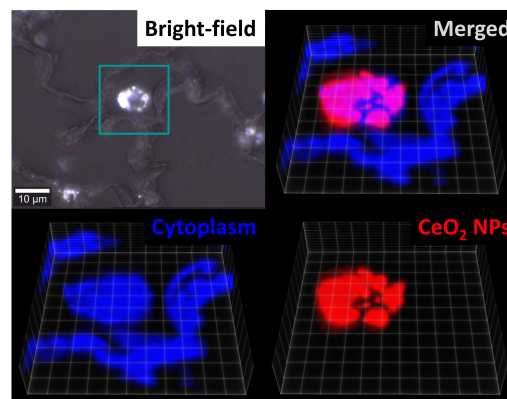


Figure 2.jpg

# Rediscovering mechanochemistry: new opportunities in the synthesis of nanocomposites by High Energy Ball Milling

Thursday, 19th October - 17:41 - Nanofabrication, nanoprocessing and nanomanufacturing - Room 1 - Oral - Abstract ID: 229

**Dr. Alessandra Scano<sup>1</sup>, Dr. Martina Pilloni<sup>1</sup>, Dr. Valentina Cabras<sup>1</sup>, Mr. Federico Ebau<sup>1</sup>, Dr. Maria Letizia Manca<sup>2</sup>, Prof. Anna Maria Fadda<sup>2</sup>, Prof. Guido Ennas<sup>1</sup>**

1. Chemical and Geological Science Dept., University of Cagliari, Cittadella Universitaria di Monserrato, SS554 Bivio per Sestu, 09042 Monserrato (Cagliari), 2. Life and Environment Science Dept., Section of Drug Sciences, CNBS, University of Cagliari, Via Ospedale 72, 09124 Cagliari

## 1. Introduction

High Energy Ball Milling (HEBM) is a top-down synthesis approach developed in the 70s as an industrial process to produce alloys and composites<sup>[1]</sup>. Recently, it has shown to be versatile and successfully also for the production of several novel materials by chemical transformations that are accessible with difficulty or not at all in solution. Moreover, HEBM has the advantage to avoid the use of solvents demonstrating to be a green, energy efficient, inexpensive, fast and easy to scale-up synthesis method.

This work presents an assortment of novel nanocomposites (NCs) for biomedical applications prepared by HEBM synthesis approach at University of Cagliari: *Superparamagnetic Magnetite-Silica NCs* ( $Fe_3O_4/SiO_2$ ); *Caffeine-Silica NCs* ( $CAF/SiO_2$ ); *Natural Extract-Silica NCs* ( $NE/SiO_2$ )<sup>[2-4]</sup>.

## 2. Methods

$Fe_3O_4/SiO_2$ . In a typical synthesis  $Fe_2O_3$  and Si mixture was sealed in a stainless steel vial with steel balls. Ball milling experiments were performed in a vibratory mill apparatus.

$CAF/SiO_2$  and  $NE/SiO_2$ . A mixture of anhydrous caffeine or a natural extract (*Vitis Vinifera* and *Centella Asiatica*) with fumed  $SiO_2$  was milled in an agate vial together with agate balls using a planetary mill.

The effect of milling was monitored by X-Ray Powder Diffraction, Infrared Spectroscopy, Transmission and Scanning Electron Microscopy performed on small portions of the powder samples at different milling time.

## 3. Results and discussions

$Fe_3O_4/SiO_2$ . The milling process produced NCs with an average size ranging from 100 to 200nm, where  $Fe_3O_4$  nanoparticles (4-6nm size) are homogeneously dispersed into the amorphous  $SiO_2$  matrix.

$CAF/SiO_2$ . After milling process, caffeine was nanosized and embedded in the  $SiO_2$  matrix in core-shell and multilayered structures. The inclusion of the caffeine in the  $SiO_2$  matrix reduced drug molecule diffusion through the matrix and then the drug release.

$NE/SiO_2$ . NCs with high antioxidant activity were obtained by the milling process, showing an enhanced agglomeration increasing the milling time and the NE amount.

## References

- [1] Kong et al., Progress in Materials Science 2008, 53, 207-322.
- [2] Scano et al., Materials Research Express (Volume 4) 2017.
- [3] Pilloni et al., International Journal of Pharmaceutics 2010, 401, 103-112.
- [4] Pilloni et al., Pharmaceutical Development and Technology 2013, 18(3), 626-33

# Nanoparticles of copper salts by in-situ surface modification and their effectiveness in antibacterial activity

Thursday, 19th October - 17:58 - Nanofabrication, nanoprocessing and nanomanufacturing - Room 1 - Oral - Abstract ID: 158

**Dr. Esin Akarsu<sup>1</sup>, Dr. Ömer Kesmez<sup>1</sup>**

**1. Akdeniz University**

Diseases caused by microorganism increasingly lead to mortality in humans and high costs of health care system. The microbial resistance to existing active substances is another source of problems related to providing hygienic conditions at hospitals. Although silver nanoparticles show promising results in providing high antimicrobial property, it is expensive. Another metal with high antimicrobial activity is Cu and its low price makes it a considerable candidate for new materials.

In this study, the particles of Cu salts of  $\text{CuSO}_4 \cdot \text{Cu}(\text{OH})_2$  and  $\text{CuCO}_3 \cdot \text{Cu}(\text{OH})_2$  were produced by the reaction of Cu ions with proper anions in the presence of sodium lignosulfonate (LS) as a in-situ surface modifier. The obtained Cu salt-particles were analyzed by AAS and characterized by DLS, FT-IR, XRD and TEM methods. The minimum inhibitory concentration (MIC) method was used to investigate their antibacterial activity.

As the ratio of Cu to LS in a solution with the Cu concentration of 3 weight percentage for  $\text{CuSO}_4 \cdot \text{Cu}(\text{OH})_2$  synthesis is increased to from 0 to 3 stepwise, the particle size goes from 1-2 micrometer down to 100 nm. When the Cu concentration at the ratio of C to LS of 3 is lowered to 1 percentage, particles with the size of around 30 nm are obtained and are spherical (Figure 1). In the  $\text{CuCO}_3 \cdot \text{Cu}(\text{OH})_2$  synthesis, nanoparticles are produced without the use of in-situ surface modifier although the obtained nanoparticles are highly agglomerated in the range of micrometer. As LS is added to the solution at the increasing ratio, nanoparticles become agglomerate-free, their size goes down to 30 nm and have rod-like shape (Figure 2). The minimum inhibitory concentration (MIC) of the synthesized samples of Cu salts are tested against E. Coli and the solutions of the sources of Cu ions are served as reference. MIC values of samples with smallest sizes of Cu salt particles are lowest (0.55  $\mu\text{g/mL}$  and 0.25  $\mu\text{g/mL}$  for  $\text{CuSO}_4 \cdot \text{Cu}(\text{OH})_2$  and  $\text{CuCO}_3 \cdot \text{Cu}(\text{OH})_2$  respectively), which are 5 to 12 folds lower than of solution containing the same amount of Cu ions. With an increase in the amount of LS, the MIC values within the same type of Cu salt-particles diminish.

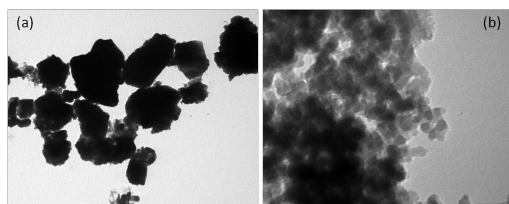


Figure 1. TEM images of  $\text{CuSO}_4 \cdot \text{Cu}(\text{OH})_2$  particles from the solution (a) without LS containing 3 percentage of Cu ions (b) with the ratio of Cu to LS of 3 containing 1 percentage of Cu ions.

Figure 1.png

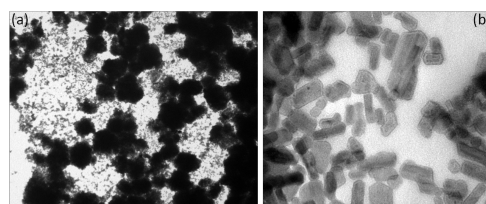


Figure 2. TEM images of  $\text{CuCO}_3 \cdot \text{Cu}(\text{OH})_2$  particles from the solution (a) without LS containing 3 percentage of Cu ions (b) with the ratio of Cu to LS of 3 containing 3 percentage of Cu ions.

Figure 2.png

---

## Highly versatile metal-organic frameworks

---

Thursday, 19th October - 18:15 - Nanofabrication, nanoprocessing and nanomanufacturing - Room 1 - Oral -  
Abstract ID: 534

---

***Dr. Maria Chiara di Gregorio<sup>1</sup>, Dr. Linda J. W. Shimon<sup>1</sup>, Dr. Lothar Houben<sup>1</sup>, Dr. Vlad Brumfeld<sup>1</sup>, Dr. Michal Lahav<sup>1</sup>, Prof. Milko van der Boom<sup>1</sup>***

*1. Weizmann Institute of Science*

Control over size and shape of nano-micro objects is a pivotal point in modern colloid chemistry both for the investigation of fundamental aspects and for the material design. The synthetic tools to achieve such a control are well established for different classes of inorganic and organic materials and they have led to the enlargement of material properties and applications. However size and shape control is still largely unexplored in the field of metal organic frameworks (MOFs) where hitherto major efforts aimed at the design of the crystallographic structure. In general MOFs produced by free modulator synthesis exhibit a non-homogeneous shape or simple polyhedral morphologies, usually reflecting the underlying geometry of the crystallographic structure. In our work we report on a straightforward, bottom-up approach that results in a tremendous variability of MOF morphologies as consequence of small parameter variation involving just the building blocks. No external templates or modulators are introduced. The set of MOFs that was obtained included rare polyhedral shapes, hollow structures and unique morphologies not classifiable according to the conventional rules for crystalline habit description. Moreover, we show that such shaping ability, beyond the MOF field interests, can also be exploited to address the fundamental question about the relationship between chiralities among different size hierarchies. In particular we prepared a MOF-based system in which the chirality of the crystal structure and morphology were coupled with an unprecedented level of complexity. Unlike most of the examples of organic and inorganic systems used for such studies, in our case at both hierarchies the chirality was not induced by chiral properties of the building blocks or by external chiral agents, strongly suggesting a direct mutual influence between the two levels. The high versatility and the degree of controlling the shaping process proved in this work, suggest new scenario for MOFs, commending them not just as molecular frameworks but also as 3D objects for fundamental studies and nanotechnological applications.

# The electrospinning of xanthan gum: from solution to nanofiber formation

Thursday, 19th October - 18:32 - Nanofabrication, nanoprocessing and nanomanufacturing - Room 1 - Oral - Abstract ID: 632

**Ms. Elhamalsadat Shekarforoush<sup>1</sup>, Dr. Ana Carina Loureiro Mendes<sup>1</sup>, Prof. Ioannis S. Chronakis<sup>1</sup>**

**1. Technical University of Denmark**

The interest on electrospinning of individual polysaccharides has been growing in the last years. Xanthan gum, an extracellular heteropolysaccharide produced by the bacterium *Xanthomonas campestris*, has been largely used and investigated in areas such as food, pharmaceutical, cosmetics, biomedical and tissue engineering industries. However the electrospinning of xanthan gum to produce nanofibers has never been reported.

In the present study we report for the first time the formation of electrospun xanthan nanofibers using formic acid as a solvent. The correlation between the concentration and the rheological properties of xanthan solutions, with the spinability (production of uniform nanofibers) of the nanofibers was investigated (Figure 1). Morphological studies by scanning electron microscopy show that uniform fibers with average diameters ranging from  $128 \pm 36.7$  to  $240 \pm 80.7$  nm are formed depending on the polysaccharide concentration (0.5 to 2.5 wt/vol%) The typical “weak gel-like” and thixotropic properties known for aqueous xanthan solutions, are not observed for the xanthan solutions in formic acid. The Fourier transform infrared spectroscopic and circular dichroism studies verify that an esterification reaction takes place, where formic acid reacts with the pyruvic acid groups of xanthan. Moreover, the results obtained from size-exclusion chromatography reveal a small difference in the molecular weight of the polysaccharide when dissolved in distilled water or in formic acid. We are currently investigating the utilisation of these electrospun xanthan nanofibers as a carrier for the encapsulation of bioactive compounds. Moreover due to the low cost, biocompatibility of xanthan nanofiber mats, we expect that a broad range of other applications within life sciences will benefit from the use of these novel nanofibers.

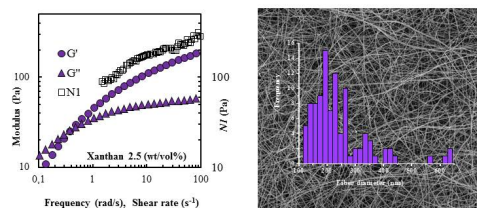


Figure 1. The correlation between the rheological properties of xanthan solutions, with the spinability (production of uniform nanofibers) of the nanofibers (Shekarforoush et al. 2017).

Annic 2017 conference.jpg



# Engineering of the highly active low-temperature oxidation ceria based catalyst – surface structures and bulk doping.

Thursday, 19th October - 16:50 - Nanocatalysis - Auditorium - Oral - Abstract ID: 688

***Dr. Roman Gulyaev*<sup>1</sup>, *Dr. Sergey Malykhin*<sup>2</sup>, *Dr. Arcady Ishchenko*<sup>2</sup>, *Dr. Tatyana Kardash*<sup>2</sup>, *Dr. Alexandra Ivanova*<sup>2</sup>**

*1. NIOST LLC; Boreskov Institute of Catalysis, 2. Boreskov Institute of Catalysis*

The interaction of palladium and ceria with formation of ionic palladium species is considered to be a main reason of high activity of Pd/CeO<sub>2</sub> catalysts in CO and methane oxidation at low-temperatures (below ambient temperature for CO and less than 300°C for methane). The formation of solid solutions Pd<sub>x</sub>Ce<sub>1-x</sub>O<sub>2-xδ</sub> in Pd/CeO<sub>2</sub> catalysts have been proposed in literature, and the near-square-planar local environment of Pd<sup>2+</sup> ion in ceria lattice was established experimentally in our work [1]. The bifunctional role of palladium in Pd/CeO<sub>2</sub> catalysts is proposed in literature; surface Pd<sup>2+</sup> ions provide the substrate activation, while the bulk Pd<sup>2+</sup> ions, serving as a dopants, increase the O<sup>2-</sup> ions non-stoichiometry and mobility in parent ceria phase [2].

In this work we present a new evidence of Pd<sup>2+</sup> ions incorporation into ceria lattice with the new superstructure formation. This structure was formed via the calcination of ultrasonically mixed nanodispersions of metallic palladium and highly defective ceria obtained via laser ablation technique which was accompanied by a sharp rise of the catalyst activity. Thus the formation of such structures gives grounds to suppose the crucial role of Pd<sup>2+</sup> ions superstructures in the high catalyst activity rather than single Pd<sup>2+</sup> ions in good agreement with the literature [3,4].

Fig.1. Pd<sub>6</sub>Ce<sub>26</sub>O<sub>58</sub> superstructure discovered in the laser ablated Pd-CeO<sub>2</sub> sample calcined at 600°C and CO oxidation activity of the sample calcined at different temperatures.

We also made a successful attempt to generate surface structures by way of calcination of diluted solid solutions of Pd in ceria lattice which led to segregation of Pd<sup>2+</sup> to subsurface layers and local enrichment. Moreover, additional doping of ceria with Ni<sup>2+</sup> ions led to increase the PdNi/CeO<sub>2</sub> catalyst activity and thermal stability due to Ni<sup>2+</sup> ions took the part of Pd<sup>2+</sup> ions functions as activators of oxygen non-stoichiometry of ceria lattice. Literature.

1. Gulyaev R.V., et.al, PCCP, 2014, 16, 13523-13539
2. M. S. Hegde et. al, Catalysis Today, 2015, **253**, 40-50.
3. S. Colussi et. al, Angewandte Chemie International Edition, 2009, **48**, 8481-8484.
4. P. Senftle et. al, ACS Catalysis, 2015, **5**, 6187-6199.

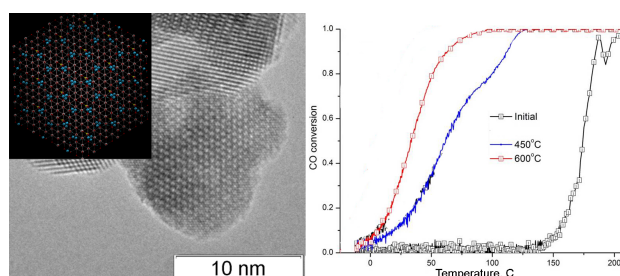


Fig.1.jpg



# Direct access to primary amines and particle morphology control in nanoporous CO<sub>2</sub> sorbents

Thursday, 19th October - 17:07 - Nanocatalysis - Auditorium - Oral - Abstract ID: 102

**Ms. Nesibe A Dogan<sup>1</sup>, Dr. Ercan Ozdemir<sup>1</sup>, Dr. Cafer T Yavuz<sup>1</sup>**

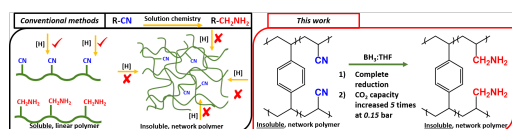
*1. Korea Advanced Institute of Science and Technology*

**Introduction**-Chemical tuning of nanoporous, solid sorbents for an ideal CO<sub>2</sub> binding requires unhindered amine functional groups on the pore walls. Although common for soluble organics, post-synthetic reduction of nitriles in porous networks often fail due to the insufficient and irreversible metal hydride penetration. Here, we synthesized a nanoporous network with pendant nitrile groups, microsphere morphology and in large scale. The hollow microspheres were easily decorated with primary amines through in situ reduction by widely available boranes. CO<sub>2</sub> capture capacity of the modified sorbent was increased up to four times of the starting nanoporous network with a high heat of adsorption (98 kJ/mol). Surface area can be easily tuned between 1 and 354 m<sup>2</sup>/g. Average particle size (~50 µm) is also quite suitable for CO<sub>2</sub> capture applications where processes like fluidized bed require spheres of micron sizes.

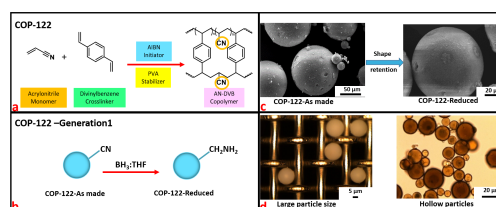
**Methods**-Polymer beads were synthesized by suspension polymerization. The solution containing monomers and porogen was sonicated and the mixture was introduced to the aqueous phase. The polymer is referred to as Covalent Organic Polymer 122 (COP-122). Nitrile functional groups were reduced by 1.0 M BH<sub>3</sub> in THF under N<sub>2</sub> atmosphere, resulting in complete conversion which is indexed as (COP-122-G1).

**Results**-Chemisorption of CO<sub>2</sub> by amine groups is evident in COP-122-G1 from the hysteretic isotherm that rapidly increases at low partial pressures. The original COP-122 is mainly a physisorptive solid, hence low capacity with negligible hysteresis. Conversion of the nitrile groups clearly increases the binding, leading to a dominant chemisorptive mode.

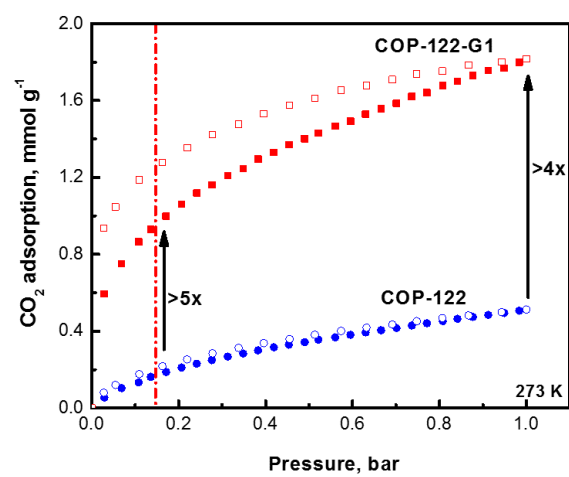
**Discussion**-In summary, acrylonitrile-divinylbenzene copolymers with nanoporous nature have been designed and synthesized for effective and cheap post-combustion CO<sub>2</sub> capture. Surface area and pore volumes can be altered by employing different types of porogens, while highest observed surface area was 354 m<sup>2</sup>/g. The hollow core inside of each single particle shows potential for acting as a carrier for various cargos, such as drugs. Amine functionalization of COP-122 particles make them promising candidates for CO<sub>2</sub> capture operations. Furthermore, this material is easy to handle because of its large particle size and non-corrosive nature, providing low attrition potential.



Nanoporous polymers for co2 capture.png



Network polymers synthesis.png



Capture capacity increases 4 times.png

## Preparation of Ceria Nanoparticles by Precipitation Method and Investigation of their Defect Characteristics

---

Thursday, 19th October - 17:24 - Nanocatalysis - Auditorium - Oral - Abstract ID: 442

---

**Mr. Zhao Liu**<sup>1</sup>

*1. University of New South Wales*

Ceria nanoparticles were synthesised by the simple precipitation method without any additional heat treatment at high temperatures. The synthesis involved initially the formation of cerium hydroxide by precipitation of cerium nitrate with sodium hydroxide. The effect of parameters such as the reaction temperature, time of reactions, and the volume of the solutions were studied. The reaction temperature was varied from 30°C to 90°C and the volume of the reaction solution was varied from 20 mL to 80 mL. X-ray diffraction (XRD) and high resolution transmission electron microscopy (HR-TEM) were used to analyse the crystallinity and morphology of the samples. The average size of the particles was ~ 5 nm and the particles were of a mixed morphology (octahedral and rod shapes). Laser Raman spectroscopy and X-ray photoelectron spectroscopy (XPS) were conducted to determine the characteristics and volumes of the defect sites on the surface of the particles.

# Nanocrystalline TiC Powers For Improving The Hydrogenation/Dehydrogenation Behaviors of MgH<sub>2</sub>

Thursday, 19th October - 17:41 - Nanocatalysis - Auditorium - Oral - Abstract ID: 419

***Ms. shorouq ahmed*<sup>1</sup>**

*1. Kuwait Institute for Scientific Research (KISR)*

## INTRODUCTION

Owing to the dramatic growing global demands for energy and the huge consumption of the finite resources of fossil fuels, coupled with drastic global environmental changes caused by the carbon dioxide emissions, developing alternate and renewable energy sources become necessary for a sustainable future. Hydrogen is an energy carrier, which holds tremendous promise as a new renewable and clean energy option. However, hydrogen can be stored in its gaseous or liquids states, the real applications of these methods have shown many technical difficulties due to the high cost and safety issues. The worldwide interest in MgH<sub>2</sub> storage system is attributed to its pioneering coupling a light weight and a high storage capacity, cost effective, reversibility, and cyclability of Mg metal.

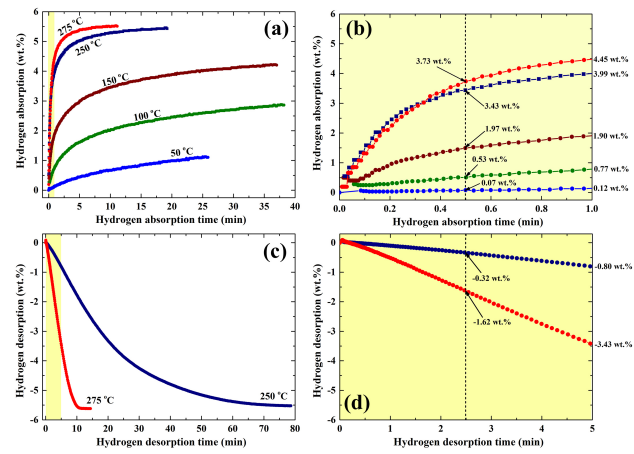
## EXPERIMENTAL

Certain amount (5 g) of hcp-Mg the powder was balanced inside a helium gas atmosphere-glove box and then sealed together with forty hardened steel balls into a hardened steel vial. The vial was then filled with 50 bar of H<sub>2</sub> gas and mounted on a high-energy ball mill operated at 250 rpm. The as-synthesized MgH<sub>2</sub> powders obtained after 200 h of milling time was then doped with 5 wt.% TiC nanocrystalline powders and then ball-milled for 50 h under hydrogen gas atmosphere. The samples obtained after selected ball milling time were characterized by means of XRD, FE-HRTEM/STEM, and FE-SEM. The thermal stability of the milled powders were investigated by DSC with different heating rates.

## RESULTS AND DISCUSSION

*Figures 1(a) and 1(b) displays the temperature effect on the hydrogenation absorption for nanocomposite MgH<sub>2</sub>/5wt.% TiC powders obtained after 50h of milling time.*

The synthesized nanocomposite powders showed excellent absorbing kinetics with short time at temperature ranging from 50°C up to 275°C as shown in Fig. 1(a). The maximum H<sub>2</sub> contents and the corresponding absorption time of the samples examined at 275, 250 and 150°C were 5.50wt.%/6.95 min, 5.28wt.%/ 19 min, and 4.18 wt.%/37.17 min, respectively. (a). The desorption behaviors at 275°C showed fast kinetics, indexed by the short time (10 min) required to release about 5.50 wt.% of hydrogen, as shown in Fig.1(c).



Nano technology 4.jpg

# Tailoring Cu nanoparticles using the spinning disc reactor for methanol synthesis

Thursday, 19th October - 17:58 - Nanocatalysis - Auditorium - Oral - Abstract ID: 554

**Mr. Christian Ahoba-Sam<sup>1</sup>, Dr. Kamelia V.K. Boodhoo<sup>2</sup>, Prof. Unni Olsbye<sup>3</sup>, Prof. Klaus-joachim Jens<sup>1</sup>**

*1. University College of Southeast Norway, 2. Newcastle University, 3. University of Oslo*

Synthesis of Cu nanoparticles (NP) has attracted much attention over some time now due to their unique applications in optics, conduction and catalysis [1]. One such catalytic application is in producing methanol from synthetic gas ( $\text{CO} + \text{H}_2$ ) at 100 °C and 20 bar. Methanol yield, for example, was observed to decrease with increasing Cu NP size from 7 to 21 nm [2]. Several synthetic techniques for making NP have been explored in literature. A promising technique is the use of a Spinning Disc Reactor (SDR). SDR is a process intensification technique, which enhances production efficiency, safety and minimizes cost. Liquid introduced into the SDR forms a thin film due to centrifugal acceleration created by rotation of the disc, resulting in uniform micro-mixing which is critical in nucleation and crystal growth in precipitation reaction [3].

Our aim therefore is to study how the SDR operating parameters affect Cu nanoparticles sizes and its application in methanol synthesis. The Cu NP was obtained by borohydride reduction using aqueous  $\text{Cu}(\text{NO}_3)_2$  solution in one stream and  $\text{NaBH}_4$  solution in a second stream and products collected in 2 % w/v starch solution to minimize agglomeration. Particle sizes were analysed using dynamic light scattering, XRD and TEM.

Our results show that variation of parameters such as flow ratio, flow rate, SDR rotation speed, reactants mole ratio and temperature affected Cu NP size distribution. Typically, Cu NP ranging from 3 to 100 nm were made depending on the parameter at play. For example faster SDR rotation led to narrower particle size distribution (Fig. 1) as adequate mass and heat transfer is enhanced for efficient micro mixing during both nucleation and crystal growth. Furthermore, the Cu NP were tested to be active for methanol synthesis.

## References

- [1] M.B. Gawande, A. Goswami, F.-X. Felpin, T. Asefa, X. Huang, R. Silva, X. Zou, R. Zboril, R.S. Varma, Cu and Cu-Based Nanoparticles: Synthesis and Applications in Catalysis, Chem. Rev., 116 (2016) 3722-3811.
- [2] C. Ahoba-Sam, U. Olsbye, K.-J. Jens, Low temperature methanol synthesis catalyzed by copper nanoparticles, Catal. Today, (2017).
- [3] S. Mohammadi, A. Harvey, K.V.K. Boodhoo, Chem. Eng. Journal, 258 (2014) 171-184.

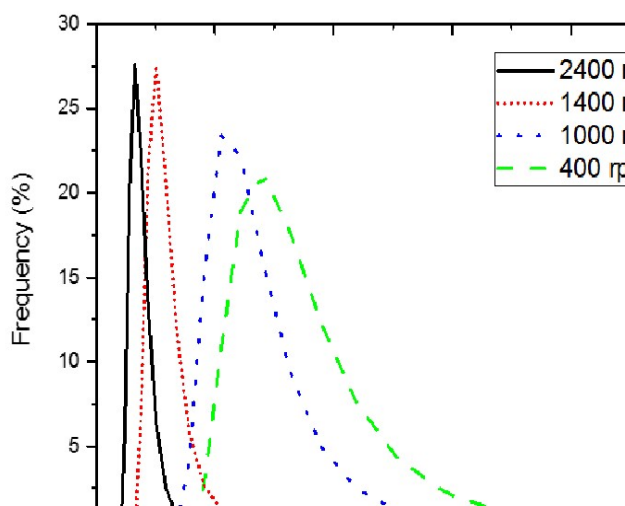


Figure 1.jpg

---

## Self-assembled transient networks of surfactant based nano-worms

---

Thursday, 19th October - 18:15 - Nanocatalysis - Auditorium - Oral - Abstract ID: 499

---

***Dr. Vyacheslav Molchanov<sup>1</sup>, Mr. Alexander Kwiatkowski<sup>1</sup>, Prof. Olga Philippova<sup>1</sup>***

*1. Lomonosov Moscow State University*

Surfactant molecules possess an amphiphilic structure leading to aggregation in aqueous medium even in polymer-like nano-worms, so-called wormlike micelles. So it is known that the wormlike micelles are enormously long flexible cylindrical micelles of a surfactant, which may be self-assembly formed by long tail surfactant molecules due to balance of hydrophobic interactions of the tails and electrostatic interactions of the heads. Similarly to polymer chains in semidilute regime these long entangled self-assembled micellar chains forming transient network impact viscoelastic properties into a solution up to gel-like state. The wormlike micelles are widely used as thickening agents in food, paints, cosmetics, oilfield industry.

In contrast to polymer chains such micellar chains incessantly break and recombine as result of weak hydrophobic interaction. They reorganize easily and can transform into droplets of microemulsions if the hydrocarbons were added, then the network of the entangled chains broken. This is one of the numerous specific highly responsive properties. Thus the other general issue is interactions and self-assembly in surfactant/polymer systems.

Polymer and surfactant self-assembly in aqueous solution attract interest due to influence of the components on a shape and a conformation of each other. In the case of addition of nonsoluble polymer the micellar chains can be transformed into more compact polymer/surfactant complex as we suggest on base of macroscopic rheological investigations, where gel-like state – liquid like state transition was observed. According to literature addition of nonsoluble polymers in a wormlike micelles solution may lead to phase separation or their transformation into short rodlike or spherical micelles.

Effect of nonsoluble polymer on the morphology of micellar chains was obtained. The results shown flexible cylindrical shape of the objects at saturated conditions, that indicates on wormlike micelles covered by polymer chains instead globule-like collapsed polymer chains stabilized by surfactant shell as might be proposed. Thus surfactant based nano-worms containing trapped nonsoluble polymer was observed.

Acknowledgement: the financial support of Russian Science Foundation (project №15-13-00114).

---

## PDMS membranes loaded with TiO<sub>2</sub>NPs for antibacterial activity

---

Thursday, 19th October - 18:32 - Nanocatalysis - Auditorium - Oral - Abstract ID: 243

---

**Dr. Valentina Caratto**<sup>1</sup>, **Dr. Stefano Alberti**<sup>1</sup>, **Prof. Silvia Vicini**<sup>2</sup>, **Prof. Maila Castellano**<sup>2</sup>, **Dr. Marco Mauri**<sup>1</sup>, **Prof. Maurizio Ferretti**<sup>1</sup>

1. Department of Chemistry and Industrial Chemistry, University of Genoa, Genoa 16146, 2. Department of Chemistry and Industrial Chemistry, University of Genoa, Genoa 16146, Italy

Poly (dimethyl siloxane) “PDMS” is a highly hydrophobic, thermally and mechanically stable polymer whose features are attributable to its Si-O bonds, which have higher bond strengths and larger bond lengths than average C-C bonds. Therefore, PDMS is widely used in different fields, such as sealants, separating membranes and biomedical devices. In order to fit the PDMS synthesis to the electrospinning, a sol-gel route was used to synthesize PDMS elastomer. PDMS hydroxyl terminated prepolymers with two different molecular weights and therefore viscosities (20.000 e 50.000 cSt), TEOS (tetraethyl orthosilicate) as multifunctional cross-linking agent, THF as solvent and HNO<sub>3</sub> as acid catalyst were used. The sol-gel route is essential for the electrospinning process, which guarantees a fibrous structure with microscale to nanoscale dimensions (fig. 1). In order to obtain the cross-linked PDMS membranes coupled with TiO<sub>2</sub>, a Sn-based catalyst was used. Bare TiO<sub>2</sub> was synthesized using titanium tetraisopropoxide, 2-propanol and water (1:2:5, V/V) while N and Fe dopings were achieved using an NH<sub>3</sub> solution and Fe<sub>3</sub>O<sub>4</sub> NPs. An amorphous gel was obtained and it was then subjected to two different thermal treatments, that are a solid-state and a hydrothermal synthesis, to get crystalline anatase TiO<sub>2</sub>. This coupled system allows to have membrane sheets loaded with NPs TiO<sub>2</sub>, combining the high adsorbent capacity and the macroscopic handling of the membrane with the photocatalytic antibacterial features of TiO<sub>2</sub>. The photocatalytic activity of this system can be activated by a solar light source, whose photons have an energy at least equal to the doped TiO<sub>2</sub> energy gap which is lower than the bare TiO<sub>2</sub> energy gap. For this work, different synthetic conditions were investigated, varying the PDMS prepolymers ratio, the temperature and the time of the polymer synthesis and the electrospinning conditions (voltage, flow, distance from the electrodes). Two different amounts of the three investigated TiO<sub>2</sub> were loaded (5% and 10% w/w) inside the membranes, by suspending the powders or the sol in a THF solution and then electrospaying together with the PDMS membrane. The synthesized samples were characterized by means of rheological measurements and FE-SEM, while the antibacterial activity was evaluated on E.Coli abatement.



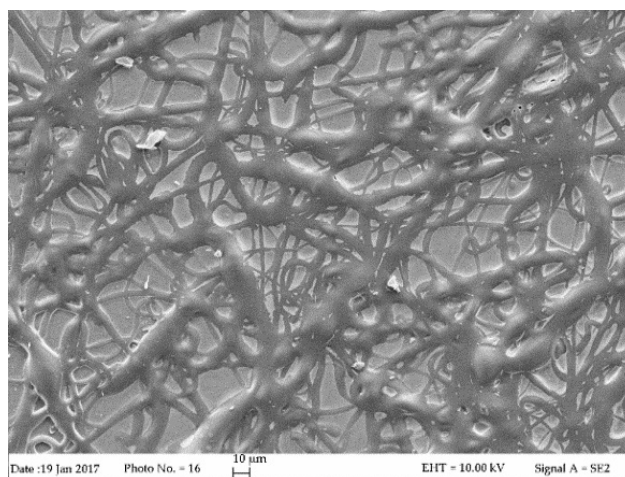


Fig.1 fe-sem .jpg

# Flexible, stretchable and healable electronics

Friday, 20th October - 09:00 - Plenary Speeches - Auditorium - Workshop - Abstract ID: 791

***Prof. Fabio Cicoira***<sup>1</sup>

*1. Polytechnique Montréal*

Organic electronics, based on semiconducting and conducting polymers, have been extensively investigated in the past two decades and have found commercial applications in lighting panels, smartphone screens, and TV screens using organic light emitting diodes technology. Many other applications are foreseen to reach the commercial maturity in future in areas such as transistors, sensors and photovoltaics.

Organic electronic devices, apart from consumer applications, are paving the path for key applications at the interface between electronics and biology. In such applications, organic polymers are very attractive candidates, due to their distinct properties of mechanical flexibility, self-healing and mixed conduction, i.e the ability to transport both electron/holes and ionic species.

My group investigated the processing conditions leading to high electrical conductivity, long-term stability in aqueous media as well as robust mechanical properties of the conducting polymer poly(3,4-ethylenedioxythiophene) doped with polystyrenesulfonate (PEDOT:PSS), on rigid, flexible and stretchable substrates [1-3]. We have demonstrated that stretchable PEDOT:PSS films can be achieved by adding a fluorosurfactant to the film processing mixture and by pre-stretching the substrate during film deposition. We have achieved patterning of organic materials on a wide range of substrates, using orthogonal lithography, parylene patterning and pattern transfer (Figure 1) [4-5]. Recently we have discovered that PEDOT:PSS films can be rapidly healed with water drops after being damaged with a sharp blade (Figure 2)[6].

My talk will deal with processing, characterization and patterning of conducting polymer films and devices for flexible, stretchable and healable electronics. I will particularly focus on the strategies to achieve films with optimized electrical conductivity and mechanical properties, on unconventional micro patterning on flexible and stretchable substrates, on the different routes to achieve films stretchability and self-healing.

- F. Cicoira et al. *APL Mat.* 3, 014911, 2015.
- F. Cicoira et al. *Appl. Phys. Lett.* 107, 053303, 2015.
- F. Cicoira, et al. *Appl. Phys. Lett.*, in press (APL17-AR-02492R1).
- F. Cicoira et al. *Chem. Mater.* 29, 3126-3132, 2017.
- F. Cicoira et al. *J. Mater. Chem. C* 4, 1382-85, 2016.
- F. Cicoira et al. *Adv. Mater.*, in press (adma201703098).

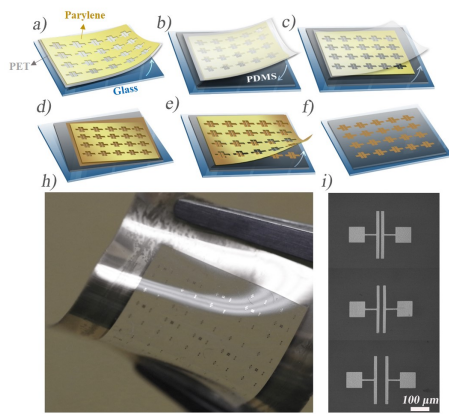


Figure 1.jpg

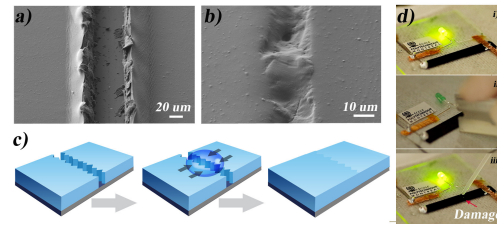


Figure 2.jpg

## Novel Broadpectrum Antivirals

---

Friday, 20th October - 09:40 - Plenary Speeches - Auditorium - Oral - Abstract ID: 846

---

***Prof. Francesco Stellacci***<sup>1</sup>

*1. EPFL*

Coming soon

# **Engineered nanomaterial interactions with biological exudates – do we need to redesign standard testing approaches for nanomaterials?**

---

Friday, 20th October - 10:45 - Plenary Speeches - Auditorium - Oral - Abstract ID: 847

---

**Prof. Iseult Lynch**<sup>1</sup>

**1.** *University of Birmingham*

Coming soon

---

## Labs, Cells and Organs on Chip.

---

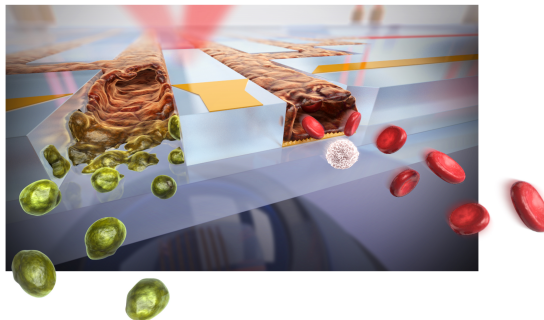
Friday, 20th October - 11:25 - Plenary Speeches - Auditorium - Oral - Abstract ID: 42

---

***Prof. albert van den berg***<sup>1</sup>

**1.** MESA+ and MIRA Institute, University of Twente

*The recent rapid developments in microfluidics technologies has enabled the realization of miniaturized laboratories. These Labs-on-a-Chip will play an important role in future medicine, both in point-of-care devices for drug or biomarker monitoring, as well as in early diagnostic devices. We developed a pre-filled ready-to-use capillary electrophoresis platform for measuring ions in blood. It is used to monitor lithium in finger-prick blood of manic-depressive patients, but can also be used for measuring calcium in blood for prevention of milk fever, or for measuring creatinine in blood or sodium in urine for early detection of ESRD. Microfluidics can also be exploited to manipulate and experiment with cells on chip. We have developed a microsystem for sperm analysis and selection for artificial insemination, where we can electrically detect and sort healthy sperm cells. Using microdevices we have been able to electroporate and transfect genes into individual cells, and a microdroplet platform was used for encapsulation of single cells in microdroplets, ordering of these microdroplets and 1:1 fusion of these droplets to form hybridomas. We believe this is a very powerful new tool that can be used for high-throughput single cell experimentation. Apart from diagnostic and cell manipulation devices, microfluidic devices are increasingly used to realise advance disease and organ-models, as illustrated by the blood-brain barrier chip and a blood vessel on a chip to study atherosclerosis.*



Vessel illustratie extension.jpg

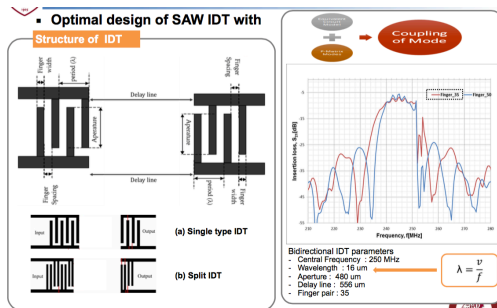
# SAW sensor based on ZnO thin film for ultraviolet light measurement

Friday, 20th October - 13:30 - Poster Session - Hall & Room 3 - Poster - Abstract ID: 668

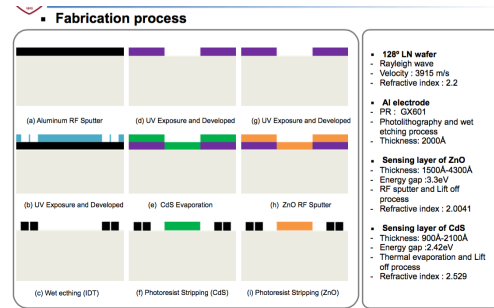
**Mr. seawhan choi<sup>1</sup>, Mr. Kunnyun Kim<sup>2</sup>, Ms. Yeon Hwa Kwak<sup>2</sup>, Prof. Byeong-kwon Ju<sup>3</sup>**

**1. Korea university / Korea Electronics Technology Institute, 2. Korea Electronics Technology Institute, 3. Korea university**

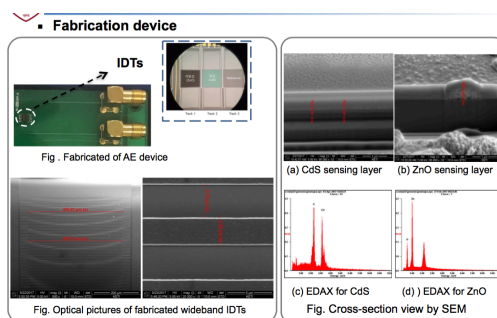
This research is focusing on SAW (Surface Acoustic Wave) Sensor based on ZnO (Zinc oxide) thin film for ultraviolet light sensing. ZnO is a semiconductor and has a characteristic of wide-bandgap. ZnO material is used as an optical sensor for measuring the intensity of ultraviolet light [1]. A mechanical stress generates propagating mechanical waves on SAW sensor as an electric field is applied on piezoelectric substrate. SAW sensor is composed of a sensing area in the middle, called the delay line, of the wave propagation. When an electrical conductivity is changed in the sensing film, Propagated saw speed changes and is measured as a frequency change [2]. In this study, a SAW based ultraviolet light sensor using ZnO thin film as a sensing film was researched and a change of frequency were measured according to the thickness of the sensing area. ZnO, which is a sensing area in the delay line, was deposited at a thickness of 50 to 430 nm by RF(Radio Frequency) sputter. The RF sputter conditions are T:26°, 100W, 10mTorr, and Ar:O<sub>2</sub> = 10:2 of gas ratio. When ZnO thin film thickness was 100nm, the linear characteristics were observed up to 1.94 mw/cm<sup>2</sup> light intensity and the sensitivity was 4.8x10<sup>-5</sup>/mW. ZnO was used as a material to detect the intensity of light, and the sensor showed a linear characteristic up to 1.9426 mw/cm<sup>2</sup> on the SAW sensor. As this ultraviolet light sensor is expected to be a notable technology in smart phone that can replace sensor of photodiode type which has been various researched.



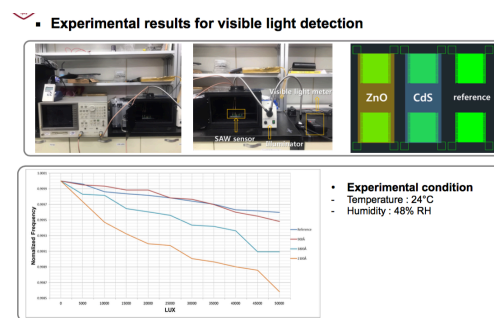
Attachment 1.png



Attachment 2.png



Attachment 3.png



Attachment 4.png

# Optical Absorption Caused by Periodic Antenna Array-induced Surface Plasmons in the Mid-infrared Range

Friday, 20th October - 13:30 - Poster Session - Hall & Room 3 - Poster - Abstract ID: 212

**Dr. Kenichi Kasahara**<sup>1</sup>

<sup>1</sup>. Ritsumeikan University

It is known that resonant excitation of surface plasmon polaritons (SPPs) manifests itself in the specular reflection on the surface of an antenna array. Ohmic loss of SPPs on the surface of a metallic film becomes small in the mid-infrared range compared to the visible region. In addition, attenuation depth of the SPP, at which the electric field of SPP decreases to  $1/e$  of the intensity at a metal-material interface, also increases as wavelength, for example, being as deep as  $\sim 0.5 \mu\text{m}$  at  $10 \mu\text{m}$  in the case of Au/n-GaAs. Thus, SPPs can be utilized as a low-loss optical spectral filter detecting at different mid-infrared wavelengths. SPP characteristics appearing in an antenna array in the mid-infrared have been reported primarily for semiconductor materials. However, very little experimental work is currently available based on this viewpoint. Here, we prepared two kinds of devices with  $10 \times 10$  circular slot antennas formed on the top of SiC and n-GaAs (doping concentration:  $2 \times 10^{18} \text{ cm}^{-3}$ ) substrates with different absorption coefficients. Figure 1 shows the measured reflectivity of SiC having openings with a diameter of  $6 \mu\text{m}$  and three different spacings. The results considering different filling factors are shown in Fig. 2. Reflectivity decreases at  $940$  and  $980 \text{ cm}^{-1}$  corresponded to signals arising from surface-phonon polariton and the resonance of one circular slot antenna, following a Fabry-Perot condition. It should be noted that the reflectivity for the sample with a separation of  $9 \mu\text{m}$  decreased slightly at  $1020 \text{ cm}^{-1}$ . This was ascribed to SPP generation at the interface of metal/SiC, whose wavelengths were in agreement with the calculated results. Figure 3 shows both reflectivities for n-GaAs (diameter:  $1.4 \mu\text{m}$ ; spacing:  $2.5, 2.9$ , and  $3.9 \mu\text{m}$ ). Antenna resonance for  $1.4 \mu\text{m}$ -diameter was calculated to be  $\sim 1640 \text{ cm}^{-1}$ , and much different from the measured SPP wavenumbers when compared to SiC samples. However, reflection dips, caused by SPPs, were clearly observed because of free carrier absorption in this case. Experimental results confirmed that SPPs excited resonantly from the periodic antenna array act as a tailored optical filter rather than loss generation in the mid-infrared region.

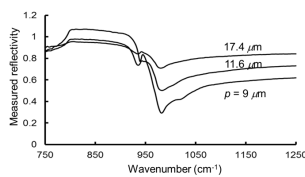


Figure 1 Measured reflectivity for SiC devices with a diameter of  $6 \mu\text{m}$  having three different separations,  $p$ , of  $9, 11.6$  and  $17.4 \mu\text{m}$ . Circular openings were arranged in a triangular lattice.

Figure 1.png

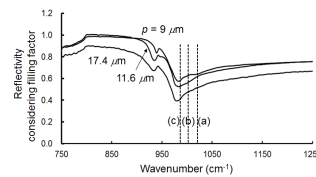


Figure 2 Reflectivity considering the filling factor (the ratio of whole opening area to an aperture size of FTIR) corresponding to the results shown in Fig. 1. (a), (b), and (c) indicate the wavenumber calculated from the SPP generation condition between the Au-SiC interface for  $(m, n) = (1, 0), (1, 1),$  and  $(2, 1)$ , respectively.  $m$  and  $n$  are integers related to the reciprocal lattice vectors for the triangular lattice.

Figure 2.png



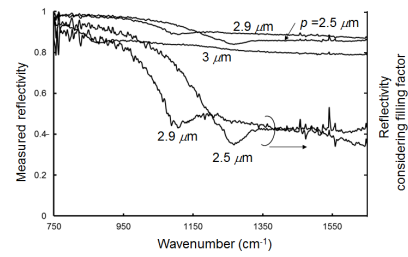


Figure 3 Measured and filling factor-considered reflectivities for n-GaAs devices. Reflection dips originated from SPPs shifted towards short wavenumbers as increasing the separation.

Figure 3.png

---

# Investigation of the phase formation from nickel-modified nanostructured silicon

---

Friday, 20th October - 13:30 - Poster Session - Hall & Room 3 - Poster - Abstract ID: 217

---

***Ms. Olga Volovlikova<sup>1</sup>, Ms. Yulia Shilyaeva<sup>1</sup>, Ms. Alexandra Berezkina<sup>1</sup>, Mr. Sergey Gavrilov<sup>1</sup>***

*1. National Research University of Electronic Technology*

## **Introduction**

The nickel-modified nanostructured silicon allows to implement a number of different applications. It is known as promising material for use in devices of silicon microelectronics, for gas sensing and for active layers of betavoltaic batteries. Moreover, the nanostructured nickel silicides, which can be obtained during the solid-phase interaction between the Si and Ni, come into use in recent years. Nevertheless, it should be taken into account that the solid-phase reactions in nanocomposites can occur at the interfaces at relatively low temperatures non-typical for similar processes in macrosystems. In this regard, the problem of estimating and predicting the thermal properties of such materials is of primer importance. The present work focuses on the influence of the interphase boundary “nanostructured Si – Ni” on phase formation during heating.

## **Methods**

In this paper, Si/Ni nanocomposite samples were formed by electrochemical etching of p-type silicon and subsequent cathodic electrodeposition of nickel. The obtained samples were characterized by means of scanning electron microscopy and phase X-ray diffraction analysis before and after heat treatment. The thermal behavior of Si/Ni nanocomposites was investigated by means of differential scanning calorimetry (DSC).

## **Results and Discussion**

The results of the X-ray phase analysis reflect the differences in phase composition of Si/Ni nanocomposites from the reference Si/Ni sample based on monocrystalline Si. The diffraction pattern of the sample before the heat treatment shows the signals from the nickel nanosized crystallites. The silicide phases are missing. After heat treatment in argon atmosphere for 20 minutes at 500 °C, the nickel crystallites have aggregated, and the NiSi crystalline phase has formed. In order to investigate solid phase interactions by DSC there were obtained Si/Ni nanocomposite samples on the basis of Si membrane. DSC data showing almost equal behaviour of the nanostructured Si/Ni samples during heating at the temperature range from 25 to 500 °C. To accurately define the temperature characteristics the DSC curves were computer processed with modelling thermal effects using a normal distribution.

*The reported study was funded by RFBR according to the research project No. 16-33-00712 мол\_a.*

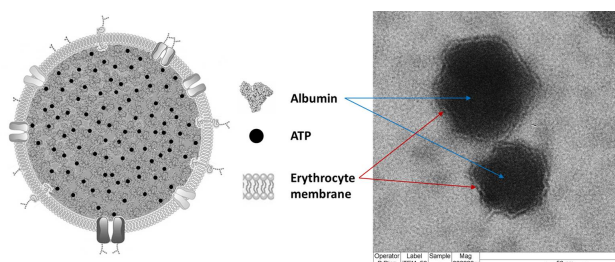
# Development of long-circulating nanoparticles for ATP delivery

Friday, 20th October - 13:30 - Poster Session - Hall & Room 3 - Poster - Abstract ID: 220

***Dr. Patricia Diaz<sup>1</sup>, Dr. Juan Huidobro-Toro<sup>1</sup>***

*1. Universidad de Santiago de Chile / Centro para el Desarrollo de la Nanociencia y la Nanotecnología*

The antitumoral effect of ATP requires its interaction with membrane receptors in target cells, but due to its short lifetime it is necessary to be kept in high concentrations in the extracellular space. We propose the use of albumin nanoparticles (ANs) coated with erythrocytes membranes (EMs) to allow extending the time of drug circulation. Our aim was to synthesize and characterize long-circulating ANs, coated with EMs and loaded with ATP. ANs were synthesized by the desolvation method, determining the optimal values of pH (8-10), albumin concentration (10, 20 or 40 mg/ml) and ethanol volume as precipitating agent ( $2.33 \pm 0.04$  ml). EMs were derived from erythrocyte lysates and used to coat ANs using an extruder. Size was determined by transmission electron microscopy (ANs =  $91.9 \pm 4.3$  nm and AN-EMs =  $98.3 \pm 5.1$  nm), while hydrodynamic size (AN =  $180.5 \pm 6.8$  nm and AN-EMs =  $197.8 \pm 3.2$  nm) and Z potential (AN =  $+17.8 \pm 3.5$  mV and AN-EMs =  $-13.7 \pm 2.9$  mV) was determined by dynamic light scattering. The coating of the ANs with the EMs was verified by TEM and confocal microscopy, via the colocalization of hydrophobic (DiI for AN-EMs) and hydrophilic fluorophores (Fluorescein for ANs). The cell uptake of nanoparticles was analyzed by confocal microscopy using HeLa cell cultures treated with nanoparticles stained with the same fluorophores. A smaller number of internalized AN-EMs compared to non-coated ANs was observed. Our current results show that it is possible to obtain nanoparticles from highly biocompatible, biodegradable materials, and that their coating with EMs allows regulating the internalization process in order to promote longer circulation times. These nanoparticles will be used to assess the release of ATP in *in vitro* and *in vivo* cancer models.



Albumin nanoparticles coated with erythrocytes membranes.jpg

# Colloidal synthesis of metastable AuCuS phase nanocrystals and in-situ TEM heating study of their transformation

Friday, 20th October - 13:30 - Poster Session - Hall & Room 3 - Poster - Abstract ID: 315

***Mr. Muhammad Imran<sup>1</sup>, Prof. Liberato Manna<sup>1</sup>, Dr. Rosaria Brescia<sup>1</sup>***

*1. Istituto Italiano di Tecnologia*

## Introduction:

Post-synthetic transformation of as synthesized nanocrystals leads to the novel nanoscale heterostructures that contain multiple distinct material domains coupled together through well-defined solid–solid interfaces which are inaccessible by conventional synthesis methods. Herein we report a novel, metastable ternary phase, with composition AuCuS, resulting from a colloidal synthesis protocol. Au<sup>+</sup> ions from solution diffuse into stoichiometric Cu<sub>2</sub>S (high chalcocite) disk-shaped nanocrystals obtained by formerly reported procedures (Figure 1a) [1]. Inward diffusion of Au<sup>+</sup> ions is accompanied by outward migration of an equal number of Cu<sup>+</sup> ions, resulting in a sort of cation exchange reaction [2]. Independent of the Au concentration in solution, the resulting particles are preferentially Janus-type structures, with the novel phase domain and the remaining Cu<sub>2</sub>S one separated by sharp interfaces (Figure 1b). Only in few cases, the nanocrystals evolve entirely into the ternary phase, in which case the energetically favored structure is composed by multiple domains. In addition, the thermal stability of the AuCuS phase has been examined by in-situ heating TEM experiments, during which outwards diffusion of Au and metallic Au domain formation was observed at about 150°C. This is due to the high diffusivity of Au through the Cu<sub>2</sub>S template structure, eventually leading to Au-decorated Cu<sub>2-x</sub>S nanocrystals (Figure 1c). The initial ternary phase, the mechanisms leading to it starting from the parent high chalcocite phase and its thermal stability will be discussed in detail in this contribution.

## References

1. F. Wang et al., J. Am. Chem. Soc. 137 (2015) 12006–12012.
2. D. H. Son et al., Science 306 (2004) 1009-1012.
3. We acknowledge funding from the European Union under grant agreement n. 614897 (ERC Grant TRANS-NANO).

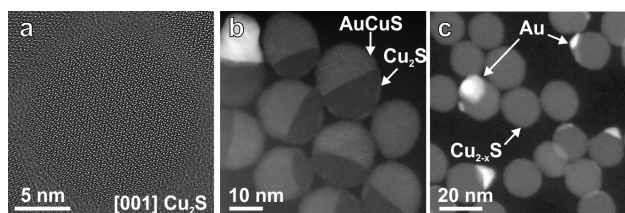


Figure1.png

# Collagen/hydroxyapatite nanostructured layers with controlled release of different antimicrobial agents: the release kinetics, antimicrobial activity and cytocompatibility

Friday, 20th October - 13:30 - Poster Session - Hall & Room 3 - Poster - Abstract ID: 347

**Dr. Tomas Suchy<sup>1</sup>, Dr. Monika Supova<sup>2</sup>, Dr. Eva Klapkova<sup>3</sup>, Dr. Vaclava Adamkova<sup>4</sup>, Dr. Rastislav Ballay<sup>5</sup>, Dr. Frantisek Denk<sup>2</sup>, Dr. Marek Pokorny<sup>6</sup>, Dr. Pavla Sauerova<sup>7</sup>, Dr. Marie Hubalek Kalbacova<sup>7</sup>**

*1. Department of Composites and Carbon Materials, Institute of Rock Structure and Mechanics, Academy of Sciences of the Czech Republic, Prague & Faculty of Mechanical Engineering, Czech Technical University in Prague, Prague, 2. Department of Composites and Carbon Materials, Institute of Rock Structure and Mechanics, Academy of Sciences of the Czech Republic, 3. Department of Medical Chemistry and Clinical Biochemistry, Charles University, 2nd Medical School and University Hospital Motol, 4. Clinical microbiology and ATB centre, Institute of Medical Biochemistry and Laboratory Diagnostics, 1st Faculty of Medicine, Charles University in Prague and Motol University Hospital, 5. 1st Department of Orthopaedics, 1st Faculty of Medicine, Charles University in Prague and Motol University Hospital, 6. Contipro a.s., 7. Institute of Inherited Metabolic Disorders, 1st Faculty of Medicine, Charles University in Prague & Biomedical Centre, Faculty of Medicine in Pilsen, Charles University*

## Introduction

The infection of implanted endoprostheses represents a serious problem with respect to orthopaedic and trauma surgery. One of the ways in which to increase the efficacy of therapy consists of the application of a local antibiotic delivery system. The local delivery of antibiotics maximises target tissue concentration while minimising the risk of systemic toxicity. The aim of this study is to compare the release kinetics, antimicrobial activity and cytocompatibility of collagen/hydroxyapatite (COL-CaP) nanostructured carriers loaded by three different antibiotics.

## Methods

Nanostructured layers based on collagen (type I, VUP Medical, CZ) and 0, 5 or 15wt% of hydroxyapatite (HA) nanoparticles (avg. 150nm, Sigma Aldrich) were prepared employing electrospinning and subsequently cross-linked by EDC/NHS (Sigma Aldrich). Cross-linked electrospun mats were subsequently impregnated with i) 10wt% of vancomycin (Mylan S.A.S), ii) gentamicin (Sigma Aldrich) or iii) combination of vancomycin/gentamicin (1/1, w/w) respectively. The *in vitro* release rates of antibiotics were characterized by HPLC. The antimicrobial effects of the layers were determined using agar diffusion testing against four different clinical isolates. The *in vitro* biological evaluation was conducted using SAOS-2 cells in direct contact with the layers or 24h infusions (MTS/LDH tests).

## Results

The maximum concentration of the released antibiotics was assessed for COL-CaP-VANCOMYCIN layers 700mg/l immediately after 3hours, for COL-CaP-GENTAMICIN layers 1020mg/l after 96hours, and for COL-CaP-VANCOMYCIN/GENTAMICIN layers 250mg/l of vancomycin after 96hours and 340mg/l of gentamicin immediately after 3 hours (see Figure 1). Concentrations exceeded the minimum inhibitory concentrations for three weeks. The effect of different amount of HA wasn't statistically significant. Agar diffusion tests revealed that COL-CaP-VANCOMYCIN layers exhibited the highest antimicrobial activity. Biological evaluation demonstrated that gentamicin impregnated layers dramatically reduced cell metabolic activity and cell amounts and vancomycin impregnated layers were markedly less cytotoxic. The positive effect of HA content on cells was demonstrated, HA induced reduction of cytotoxicity of all antibiotics-impregnated layers.

## Discussion

Our results suggest that the local application of high-dose vancomycin via drug delivery carriers provides a safe therapeutic osteomyelitis treatment method that prevents the development of bacterial resistance.

## Acknowledgments

This study was supported by the Technology Agency of the Czech Republic (project no. TA04010330).

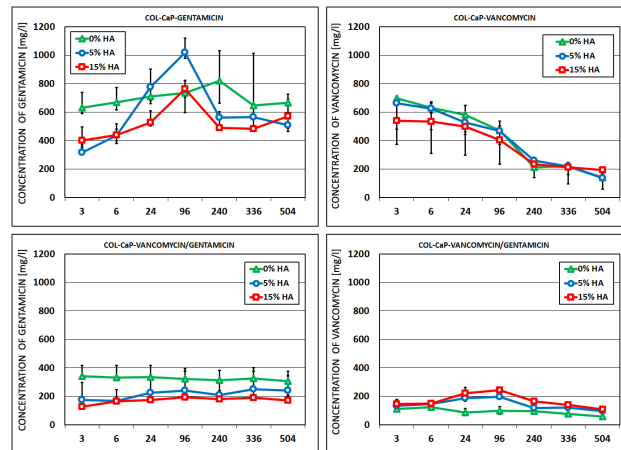


Figure 1- comparison of release kinetics.jpg

# Thermoluminescent and dosimetric properties of Mn-doped YAP nanoceramics

Friday, 20th October - 13:30 - Poster Session - Hall & Room 3 - Poster - Abstract ID: 536

**Dr. Nataliya Martynyuk<sup>1</sup>, Dr. Yaroslav Zhydachevskyy<sup>2</sup>, Dr. Anatolii Popov<sup>3</sup>, Dr. Dmytro Sugak<sup>1</sup>, Dr. Pawel Bilski<sup>4</sup>, Prof. Sergii Ubizskii<sup>1</sup>, Prof. Marek Berkowski<sup>5</sup>, Prof. Andrzej Suchocki<sup>5</sup>**

*1. Lviv Polytechnic National University, 2. Lviv Polytechnic National University / Institute of Physics, Polish Academy of Sciences, 3. Institute of Solid State Physics, University of Latvia, 4. Institute of Nuclear Physics, Polish Academy of Sciences, 5. Institute of Physics, Polish Academy of Sciences*

Application potential of Mn<sup>2+</sup>-doped YAlO<sub>3</sub> (YAP) for thermoluminescent (TL) dosimetry of ionizing radiation has been shown previously (see [1] and references therein). For this purpose, one of two types of detectors can be used. The first type produces green emission near 530 nm (caused by Mn<sup>2+</sup> ions) in the main TL peak at 200 °C, whereas the second type produces an orange emission around 640 nm in the TL peak near 350 °C.

Main features of the single crystalline YAlO<sub>3</sub>:Mn<sup>2+</sup> detectors are as following: high thermochemical and time stability, high resistance to radiation damage, high sensitivity to ionizing radiation, extremely wide range of linearity (from few mGy up to few kGy), high effective atomic number ( $Z_{eff} = 31.4$ ) and consequently high energy response, low thermal fading of single crystalline detectors. In such a way the material is a good candidate for wide-range dose measurements, especially when tissue equivalence is not required, as well as for a purpose of the radiation quality determination if used alongside with other low-Z materials.

The Mn-doped YAP mainly in the form of single crystals grown by the Czochralski method has been studied previously. However, an easy, cheap and practical method is preferred for synthesis of an efficient material applicable for TL dosimetry. The solution combustion synthesis is an appropriate method for obtaining of the Mn<sup>2+</sup>-doped YAP nanoceramic detectors which have thermoluminescent properties comparable with the corresponding single crystalline material [2].

Therefore, the purpose of the present work was to study in details thermoluminescent and main dosimetric properties of YAP:Mn detectors in the form of ceramics prepared from the nanocrystalline material synthesized by the solution combustion method using urea as a fuel. TL response and sensitivity of the studied nanoceramic detectors to various kinds of radiations (gamma, beta and alpha radiation) as well as thermally induced fading of the detectors have been measured and analyzed in comparison with the single crystalline detectors studied previously. The observed differences in thermoluminescent and dosimetric properties of nanoceramic and single crystalline detectors are discussed in terms of peculiarities of the nanoceramic material (optical opacity, grain boundaries etc.).

---

# Spin injection from a semiconductor to a 3D topological insulator: a pathway for hybrid opto-spintronics

---

Friday, 20th October - 13:30 - Poster Session - Hall & Room 3 - Poster - Abstract ID: 562

---

**Mr. Y.Q. Huang<sup>1</sup>, Dr. Y.X. Song<sup>2</sup>, Prof. S.M. Wang<sup>2</sup>, Prof. I.A. Buyanova<sup>1</sup>, Prof. Weimin M. Chen<sup>1</sup>**

*1. Linköping University, 2. Shanghai Institute of Microsystem and Information Technology*

A critical step towards spin functionalized electronics and optoelectronics is to generate and manipulate spin current in a desirable way. In 3D topological insulators (TIs), a strong spin-orbit interaction and the time-reversal symmetry result in spin-momentum locking of the surface electrons, which leads to a unique surface spin texture and the prospect of generating directional and dissipationless spin current running across the surface that is promising for spintronic applications. However, the metallic nature that is often found to be common in many 3D TIs due to residual defects has unfortunately imposed a severe obstacle to controlling surface spin current. As a result, very little experimental work has been done so far on this issue. Moreover, the contribution of the out-of-plane spin texture to the photocurrent remains elusive so far. In this work, we show that, with circular polarized light, helicity driven photocurrent is obtained in 3D TI Bi<sub>2</sub>Te<sub>3</sub> that exhibits a strong hexagonal warping effect. We find the helicity-dependent photocurrent to be sensitive to the incident angle of the light, which could be explained within the framework of the circular photo-galvanic effect (CPGE) by taking into account the spin texture of the topological surface state. By correlating the light incident angle and probing surface current directions, we are able to identify photocurrent components associated with the in-plane and out-of-plane spin texture of the TI and thereby directly uncover the impact of the out-of-plane spin texture on surface spin current promoted by the strong hexagonal warping effect. By exploring the out-of-plane spin texture, we demonstrate spin injection from GaAs to TI and its significant contribution to the surface current [1]. We further show that the spin current of TI can be manipulated by the precession of injected electron spins in an external magnetic field. These discoveries pave the way to not only intriguing new physics but also enriched spin functionalities by integrating TI with conventional semiconductors, such that spin-enabled optoelectronic devices may be fabricated in such hybrid structures.

[1] Y. Q. Huang, Y. X. Song, S. M. Wang, I.A. Buyanova, W.M. Chen, Nat. Commun. 8, 15401 (2017).



# Magnetically guided viral transduction of gene-based sensitization for localized photodynamic therapy to overcome multi drug resistance in breast cancer cells

Friday, 20th October - 13:30 - Poster Session - Hall & Room 3 - Poster - Abstract ID: 587

**Prof. Zi-Xian Liao<sup>1</sup>**

*1. Institute of Medical Science and Technology, National Sun Yat-sen University*

Chemotherapy represents a conventional treatment for many cancers at different stages either solely prescribed or concomitant to surgery and/or radiotherapy. However, treatment is tempered in instances of acquired drug resistance in response to either chemo- or targeted-therapy, leading to therapeutic failure. To overcome this challenge, many studies focus on how cancer cells manipulate their genomes and metabolism to prevent drug influx and/or facilitate efflux of accumulated chemo drugs. We previously developed 'controllable' virus' for either recombinant adeno-associated virus serotype 2 (AAV2) via chemical conjugation with iron oxide nanoparticles that could be directed with magnetic fields. Furthermore, a gene of the photosensitive protein was introduced into the AAV2 genome to enable photo-dynamic therapy (PDT). In the case of PDT, irradiation with a specific light bandwidth generates reactive oxygen species leading to irreversible DNA damage and cell killing via an apoptotic pathway (Figure 1); offering additional options in cancer treatment. Here, we present an improvement to this previous work that promotes viral transduction in chemo drug resistant-MCF-7 (<sup>CDR</sup>MCF-7) cells under magnetic field, and express the KillerRed (KR) protein in transduced cells for light-triggered virotherapy (AAV2-KR) (Figure 2). We have demonstrated highly efficient photosensitization with the gene-based KillerRed photosensitizer. Loco-regional specificity was achieved for viral transduction via utility of a magnetic field and conjugation of magnetic nanoparticles to the virus. This demonstrated successful anti-proliferation of chemotherapy drug resistant cancer cells. Such a technological model with improved virotherapy loco-regional specificity could be harnessed to overcome drug resistant cancer cells.

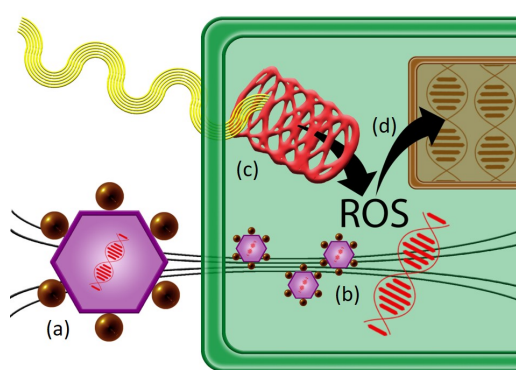


Figure 1.jpg

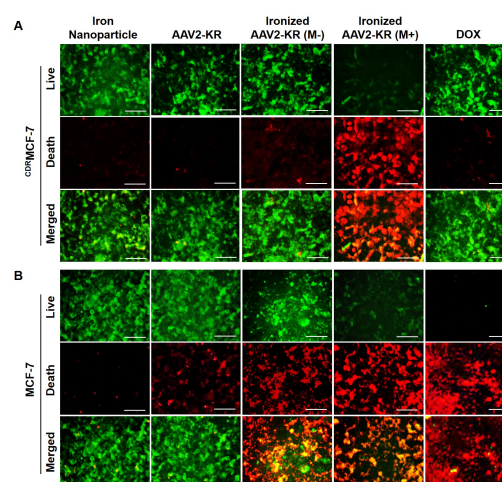


Figure 2.jpg

# Plasmonic Nanostructures for IR Photodetectors

Friday, 20th October - 13:30 - Poster Session - Hall & Room 3 - Poster - Abstract ID: 646

**Dr. Dana Cristea<sup>1</sup>, Dr. Paula Obreja<sup>1</sup>, Dr. Adrian Dinescu<sup>1</sup>, Dr. Roxana Tomescu<sup>1</sup>**

*1. National Institute for R&D in Microtechnologies, IMT Bucharest*

Plasmonic nanostructures have been used in the last years to improve the photocurrent generation in detectors and solar cells by plasmonic light trapping or electromagnetic field local enhancement due to the excitation of localized surface plasmons (SPPs). These plasmonic devices combine a metallic nanostructures that supports SPPs with photonic detection using electron-hole pair photogeneration or internal photoemission effect (IPE). The paper presents simple and low cost processes for fabrication of IR plasmonic photodetectors. We used Ag nanoparticles (NPs) to improve the light absorption in PbS quantum dots (QDs) photoconductors and in silicon Schottky IPE based photodetectors. The NPs have been obtained using either chemical reaction of AgNO<sub>3</sub> and oleylamine solution at 180°C, or vacuum deposition of very thin layers followed by thermal annealing.

Ag NPs obtained by chemical synthesized were mixed with PbS QDs (1.5 nm diameter) in different concentrations and deposited on pre-patterned electrodes (oxidized Si substrate) using the layer-by-layer approach to obtain PbS QDs-Ag NPs based photodetectors. The second approach was used to obtain Ag islandized layers on Si Schottky or MSM photodetectors to improve the efficiency of IPE. The Ag NPs were characterized using SEM, AFM. The size can be tuned by modifying the process parameters. Fig. 1 shows examples SEM images of the obtained Ag NPs in different conditions. Absorption spectra in IR were characterised with FT-IR spectrometer VERTEX 80/80v. The I-V characteristics in dark and under illumination were measured using a Semiconductor Characterization System Keithley 4200-SCS with shielded probe station and monochromatic light sources (laser diodes and LEDs).

The paper presents the influence of NPs size, concentration, device lay-out on the photoresponse and the spectral characteristics. In fig. 2 and 3 two examples of measurement results are presented. The measurements indicate that Ag NPs can improve the responsivity in IR of the PbS QD-based photodetectors, and of the Si Schottky diodes based on IPE as well. Higher responsivities compared with those recently reported in literature for IPE photodetectors were obtained: up to 11mA/W at 1550 nm.

Acknowledgements: The work was supported by the Romanian National Research Programme PN III, project PN-III-P2-2.1-PED-2016-0307 TemptSys.

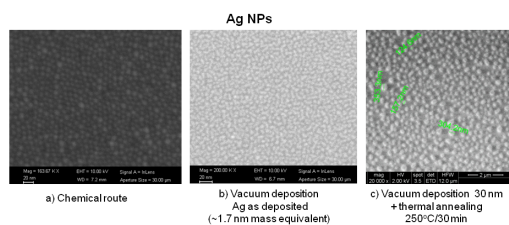


Fig. 1. sem images of ag nps.png

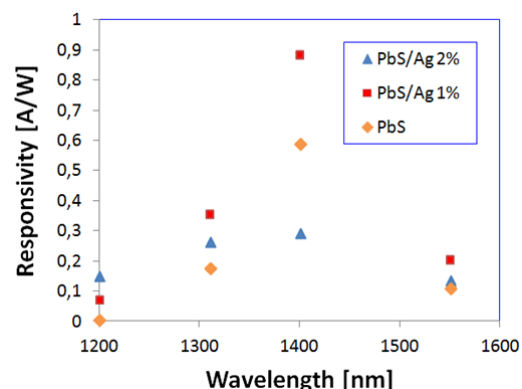


Fig. 2. spectral responsivity of pbs qds-ag nps based ir photodetector.png

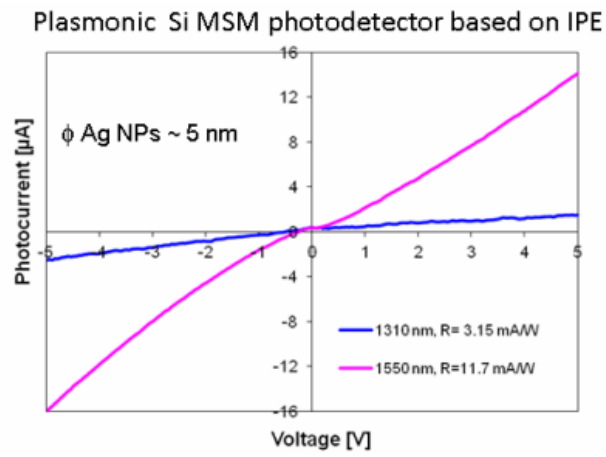


Fig. 3 photocurrent vs. applied voltage for a plasmonic si ipe photodetector.png

---

## Fabrication of composite cathodes by electrodeposition for solid oxide fuel cells

---

Friday, 20th October - 13:30 - Poster Session - Hall & Room 3 - Poster - Abstract ID: 656

---

***Mr. Saeed ur Rehman<sup>1</sup>, Dr. Rak-hyun Song<sup>1</sup>, Dr. Seok-joo Park<sup>1</sup>, Dr. Tak-hyung Lim<sup>1</sup>, Dr. Jong-eun Hong<sup>1</sup>, Dr. Jon-won Lee<sup>1</sup>, Dr. Seung-bok Lee<sup>1</sup>***

*1. Korea university of science and technology Daejeon (UST), Korea Institute of Energy Research (KIER)*

Cobaltite-based perovskites (CBPs) such as LSC, SSC, LSCF and BSCF have been studied as promising cathode materials for intermediate temperature solid oxide fuel cells (SOFCs) due to their high mixed ionic and electronic conductivity and high activity for oxygen reduction reaction. However, CBPs form insulating phases with YSZ during conventional high temperature sintering. To avoid the high sintering temperatures, the CBPs are usually infiltrated into a back bone of YSZ. But the infiltration is a tedious process as many infiltration cycles might be required to achieve a desired perovskite loading. Another technique that can be used to fabricate nanostructured cathodes for SOFCs is electrodeposition. Electrodeposition gives significant advantage over the infiltration technique as a higher catalyst loading can be achieved in a single step.

In this work a new process is being developed to fabricate high surface area electrodes for SOFCs by electrodeposition onto carbon nanofibers template that had been grown onto a porous ion conducting scaffold (ICS). Anode supported half cells (NiO-YSZ|NiO-SSZ|SSZ) were fabricated by uniaxial pressing and pre-sintering of NiO-YSZ powders, followed by dip-coating of NiO-SSZ anode functional layer and SSZ electrolyte layer and finally sintering at 1400 °C. Porous ICSs were fabricated onto the dense SSZ electrolyte by screen printing and sintering of an ink containing SSZ, GDC and PMMA powders. The carbon nanofibers were grown onto the ICS by thermal chemical vapor deposition of carbon atoms by using C<sub>2</sub>H<sub>4</sub> as a source of carbon. The images taken by a scanning electron microscope (SEM) revealed the formation of carbon nanofibers grown randomly onto the porous ICS. Moreover, LaCoO<sub>3</sub> (LCO) was successfully electrodeposited onto the carbon deposited ICS. The morphology of LCO deposition was observed to be similar to that of carbon nanofibers template. Energy dispersive X-ray spectroscopy (EDS) showed an average of 25 weight percent of LCO deposited throughout the cross section of porous ICS. Also, the elemental composition of lanthanum and cobalt was found to be stoichiometric for the formation of a pure LCO perovskite phase.

---

## Formation of crystal nuclei in small volumes near critical supercooling

---

Friday, 20th October - 13:30 - Poster Session - Hall & Room 3 - Poster - Abstract ID: 665

---

***Dr. Zdeněk Kožíšek<sup>1</sup>, Prof. Pavel Demo<sup>1</sup>***

*1. Institute of Physics CAS, Prague, Czech Republic*

Phase transition starts via formation of small nanoparticles called nuclei. Formation of nuclei plays the crucial role as this process predetermines structure and the physical properties of the new forming material. Up to this time, we do not fully understand this process. Molecular simulations (MS) enable to determine the structure of newly forming clusters. However, the timescale in MS is too short (about nanoseconds).

The beginning of the phase transition process is often detected via thermal analysis or light scattering techniques when critical supercooling (or supersaturation) is detected. However, it is not clear how many particles of various sizes formed at the critical supersaturation.

We numerically solved kinetic equations to determine the size distribution of nuclei as a function of time and size near critical supercooling, when the first particles are created [1]. We have determined the maximum size of nuclei  $r_{\max}$  and also the growth rate  $v=dr_{\max}/dt$ . In sufficiently large volumes of the parent phase, the growth rate after reaching of certain minimum increases with time to the flat interface limit. However, in small volumes depletion of the parent plays an important role and the growth rate of particles after reaching some maximum decreases in time.

*This work was supported by the Project no. LD1504 of the Ministry of Education, Youth and Sports of the Czech Republic (COST Action CM1402).*

[1] Z. Kožíšek, P. Demo: J. Cryst. Growth 475 (2017) 247.

---

## Zein-phosphatidylcoline mixed nanoparticles as a hydrophobic drug carrier

---

Friday, 20th October - 13:30 - Poster Session - Hall & Room 3 - Poster - Abstract ID: 749

---

***Dr. Soon-seok Hong<sup>1</sup>, Prof. Soo-jeong Lim<sup>1</sup>***

*1. Sejong University/Drug Delivery System/Department of Bioscience and Biotechnology*

**Introduction:** Zein is an amphiphilic and hydrophobic protein obtained from corn. Its use in the fields of food science and biomedicine have brought widespread interest due to its FDA “GRAS” status and ease of fabrication into spherical colloidal particles. The present study was undertaken to develop zein-phosphatidylcholine mixed nanoparticles (Z/PC-NPs) in order to combine the beneficial features of both zein nanoparticles and liposomes as a hydrophobic drug carrier.

**Methods:** Formation of Z/PC-NPs was investigated by differential scanning calorimetry and Fourier transform infrared spectroscopy analysis. Size and morphology of various nanoparticles were determined by dynamic light scattering method and negative staining transmission electron microscopy. Drug concentration loaded in various nanoparticles were determined by HPLC (paclitaxel, docetaxel and celecoxib) and fluorescence spectroscopy (curcumin). Stability of various nanoparticles during storage or after lyophilization was assessed by the changes in the mean particle size and retained drug content. Drug release profile of various nanoparticles was assessed in physiologically relevant conditions by using docetaxel as a loaded model drug.

**Results:** Formation of Z/PC-NPs were confirmed by the lowered phase transition temperature of PC by DSC analysis and the appearance of weakened but clear amide bond of zein by FTIR analysis. Z/PC-NPs were spherical particles with <200 nm mean particle size. Compared to Z-NPs and PC-NPs, Z/PC-NPs exhibited the higher drug-loading capacity in cases of all four hydrophobic drugs and the highest stability during storage and after lyophilization. The time-dependent release of docetaxel was the fastest in case of Z-PC, followed by Z/PC-NPs and the slowest in case of PC-NPs. Lyophilization-induced changes in terms of particle size and retained docetaxel content was the smallest in Z/PC-NPs regardless of cryoprotectant supplementation.

**Discussion:** Z/PC-NPs exhibited improved hydrophobic drug-loading capacity and colloidal stability compared to PC-NPs and Z-NPs, while exhibiting the drug release rate in the middle of PC-NPs and Z-NPs. Taken together, Z/PC-NPs has a promising potential as an effective hydrophobic drug platform dosage form.

---

## Dynamics of a Sierpinski-dendrimer type polymer network

---

Friday, 20th October - 13:30 - Poster Session - Hall & Room 3 - Poster - Abstract ID: 755

---

***Dr. Flaviu Turcu<sup>1</sup>, Dr. Aurel Jurjiu<sup>1</sup>, Mr. Teodor Biter<sup>2</sup>***

*1. Babes-Bolyai University, Faculty of Physics, 2. Babes-Bolyai, Faculty of Physics*

Fractals are of particular relevance in many fields of science. In physics and chemistry the concept of fractals is widely used for describing the disordered systems, growth phenomena, chemical reactions controlled by diffusion, and relaxation dynamics of polymer networks.

Because of their shape and topology dendrimers are very interesting macromolecules both to pure science and everyday life. Most of the properties of dendrimers are related to the nature of their numerous terminal groups that may be varied at will to fulfil the desired properties. Dendrimers have potential applications in different fields, such as in biosensors, catalysis, nanomedicine for drug delivery and gene therapy.

The present work extends the theoretical studies on relaxation dynamics of polymers with complex architectures by considering a new multihierarchical polymer network which is built through the replication of the dual Sierpinski gasket in the form of a regular dendrimer.

The relaxation dynamics of the multihierarchical structure is investigated in the framework of generalized Gaussian structure model which represents the extensions of the Rouse and Zimm models, developed for linear polymer chains, to polymer systems with arbitrary topologies and which highlight both the connectivity of the molecules under investigation, as well as the influence of hydrodynamic interactions.

In the Rouse model, taking the advantage that the main relaxation patterns depend only on the eigenvalues, we have developed a method whereby the whole eigenvalue spectrum of the connectivity matrix of the multihierarchical structure can be determined iteratively. Based on the eigenvalues obtained in the iterative manner we are able to investigate the dynamics of the multihierarchical structure at very large generations, impossible to attain through numerical diagonalizations.

Remarkably, the general picture that emerges from both approaches, even though we have a mixed growth algorithm and the monomers interactions are taken into account specifically to the adopted approach, is that the multihierarchical structure preserves the individual relaxation behaviors of its constituent components. Our theoretical findings with respect to the splitting of the intermediate domain of the relaxation quantities are well supported by mechanical experiments performed on associative polymer networks, micelles networks, physical polymer gels, and supramolecular dendritic polymer network.

# Magnetic and magneto-optical properties of $\text{Co}_{1-x}\text{Dy}_x\text{Fe}_2\text{O}_4$ nanoparticles and thin films synthesized by co-precipitation

Friday, 20th October - 13:30 - Poster Session - Hall & Room 3 - Poster - Abstract ID: 767

*Ms. maryam karimi*<sup>1</sup>

1. ISLAMIC AZAD UNIVERSITY

The modification and optimization of the magnetic and magneto-optical properties of cobalt ferrite are of great importance result in their various applications in well-known scientific and industrial categories. In the present work the effect of adding  $\text{Dy}^{3+}$  to the cobalt ferrite composition,  $\text{Co}_{1-x}\text{Dy}_x\text{Fe}_2\text{O}_4$  ( $0 \leq x \leq 0.1$ ) ceramic nanoparticles were synthesized by the co-precipitation method and then their microstructure and magnetism were investigated through x-ray diffractometry, TEM micrography, IR spectroscopy and VSM magnetometry. The polar magneto-optical Kerr effect of the thin film specimens was also studied. The results reveal that the doping of  $\text{Dy}^{3+}$  ions could effectively alter the inversion degree of the spinel structure and the following magnetic and magneto-optical features (Fig.1). The ferrite coercivity was enhanced by 150% after adding Dy ( table1). The perceptible shifts of peak rotations were observed in the Kerr spectra for the Dy-doped  $\text{CoFe}_2\text{O}_4$  films (Fig.2). Furthermore, TC had a descending trend with the addition of Dy from 440 °C to 420 °C for  $\text{Co}_{0.95}\text{Dy}_{0.05}\text{Fe}_2\text{O}_4$ .

Fig.1. Polar Kerr hysteresis loops measured at room temperature for 650 nm wavelength

Fig.2. The Kerr spectra of the samples under a fixed 5 kOe magnetic field in the range of 400–800 nm.

Table. 1. Saturation magnetization (MS), coercive field (HC), remanent magnetization (Mr), theoretical saturation magnetization (MS Th) and Curie temperature (TC).

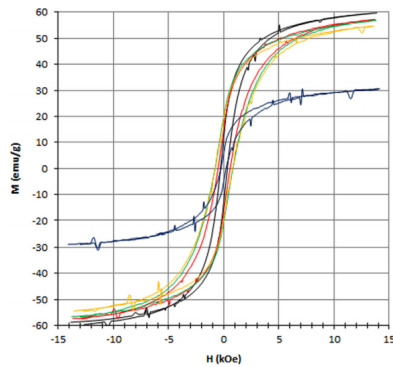


Fig.1.png

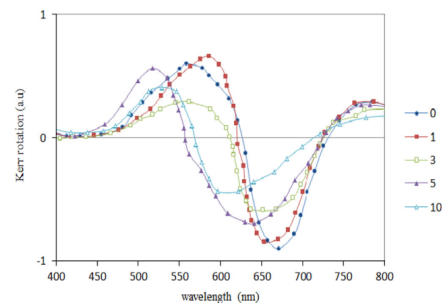


Fig.2.png

Dy content	$M_s \pm 0.01$ (emu/g)	$M_s$ th (emu/g)	$H_c \pm 0.01$ (Oe)	$M_r \pm 0.01$ (emu/g)	$\mu_B$	$S$ (kOe emu/g)	$K \times 10^3$ (erg/g)	$T_C \pm 1$ (°C)
0.00	59.74	81.45	306.90	12.68	2.51	25.3	19.10	440
0.01	57.02	80.10	546.96	15.93	2.41	41.6	32.49	423
0.03	56.79	77.51	785.13	19.60	2.42	49.2	46.45	427
0.05	54.67	75.30	793.99	19.46	2.35	48.3	45.22	417
0.10	30.60	70.09	229.49	5.33	1.34	15.6	07.31	240

Table.1.png



# Design and Simulation of SAW sensor for Photo Sensing

Friday, 20th October - 13:30 - Poster Session - Hall & Room 3 - Poster - Abstract ID: 679

**Mr. Jong Woo Kim<sup>1</sup>, Mr. Jin Woo Lee<sup>1</sup>, Mr. Byungmoon Lee<sup>1</sup>, Mr. Jinkee Hong<sup>2</sup>, Prof. Byeong-kwon Ju<sup>3</sup>**

1. Korea university/Haesungds, 2. Haesungds, 3. Korea university

Surface acoustic wave (SAW) devices based on various types of acoustic waves such as Rayleigh wave, Shear-SAW, Love wave, acoustic plate mode (APM) and flexural plate wave (FPM) have been explored for sensors, actuators and telecommunication applications.

The velocities of waves depend on density and elasticity material properties and are very sensitive on change of surface layer mechanical parameters. This sensitivity is why SAW devices are as popular as sensor devices.

The SAW can be generated in piezoelectric material using interdigital transducer (IDT). It is basically comb-like structure with fingers connected to electric terminals. The width and spacing of fingers affect the center frequency of IDT. The number of IDTs affects the length of impulse characteristics and filter band-width. The length of IDT fingers affects primarily the input admittance of IDT and defines the width of wave-beam, what is important when considering the diffraction effects.

This paper reports on fast and high resolution photo detectors based on SAW sensor. In this device deals with Design and Simulation of SAW sensor using various methods such as equivalent circuit model, coupling of modes methods.

SAW sensor is made from optical grade application of LiNbO<sub>3</sub> substrate. And IDT make of aluminum material. We analyzed the sensitive device designed by simulating the electrical characteristics changes of the saw device according to the aperture and delay lines.

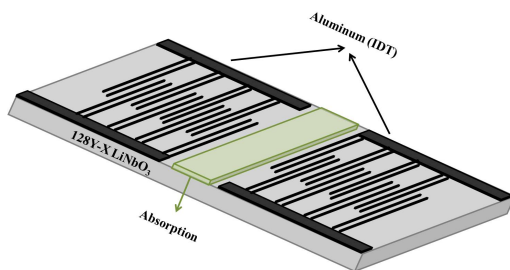


Figure 1 design of saw sensor.jpg

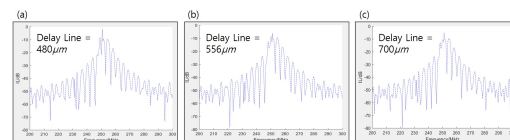


Figure 2 characteristics of delay line dependency.jpg

# Graphene like ZnO 2D structure from semiconductor to conductor behavior by doping F

Friday, 20th October - 13:30 - Poster Session - Hall & Room 3 - Poster - Abstract ID: 682

**Dr. Ahmad Yazdani <sup>1</sup>, Mr. behrad barakati <sup>1</sup>, Mrs. Asiye Shokri <sup>1</sup>**

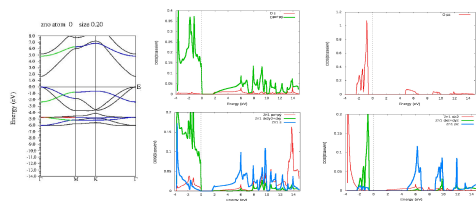
*1. Tarbiat Modares University*

2D ZnO honeycomb structure was recently fabricated. This new semiconductor material with band gap about 1.7 eV is great for applications which needs this gap and such dimension. This material has a great electronic structure which was investigated in this article. Due to this especial electronic structure here we found that this material could be change its behavior to metal material with doping F elements on the surface.

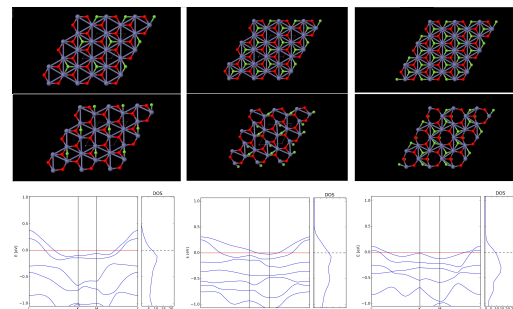
For achieving to our suggestion we use Density Functional Theory (DFT) method by using WIEN2K and FHI-aims packages. All structure was relaxed and the structure stability was checked out.

At first the electronic structure of single ZnO layer was investigated. As could be seen in the DOS results (see picture 1) the band gap is 1.67 eV which is have great agreement with experimental result. On the other hand as could be seen we have 2 different type of hybridization in this material 1) in the XY plane and 2) due to Z direction. Which the second type band is located in the middle of the first band due to the energy and located in out of XY plane in the Z direction due to the space. The Zn-O bond length in this structure was obtained 1.90 Å.

So because of this electronic structure by doping hole in the second type orbitals (the orbitals which are located out of XY plane) metallic characteristic behavior could be induced to this material. In this situation we doping F elements to the surface of ZnO sheet by different concentration (One, two and three F elements for each three ZnO hexagon). The results show all of the structures could be metallic (see figure 2). This three structures have different Fermi surface which could be used for different applications.



Picture 1.jpg



Picture 2.jpg

---

# SYNTHESIS AND CHARACTERIZATION OF PEPTIDE LOADED NANOPARTICLES FOR USE IN NEW GENERATION VACCINE SYSTEMS

---

Friday, 20th October - 13:30 - Poster Session - Hall & Room 3 - Poster - Abstract ID: 466

---

**Ms. Elif F. Yilmaz<sup>1</sup>, Ms. Pelin Pelit Arayıcı<sup>1</sup>, Dr. Mesut Karahan<sup>2</sup>, Dr. Zeynep Mustafaeva<sup>1</sup>**

**1.** Yildiz Technical University, Bioengineering Department, **2.** Üsküdar University, Faculty of Engineering and Natural Sciences, Department of Bioengineering

**Introduction:** Recent studies with polymeric carriers have gained importance as they provide advantages to synthetic peptides that are frequently used in vaccine technology such as higher immunity, longer survival in biological system and more stability against destructive factors. Among these developed carriers, nanoparticles are extremely popular in recent years, especially with their cellular dimensions, controlled release possibilities, high biocompatibilities.

**Methods:** In our studies, antigenic peptide epitopes of a current disease are encapsulated to albumin, PLGA or PLA etc. nanoparticles. Synthesized nanoparticles were characterized by methods of ZetaSizer, scanning electron microscopy (SEM) and Fourier transform infrared (FTIR) spectroscopy. Loading and encapsulations yields were calculated, bio-release experimentations were performed.

**Results:** As a result of the obtained data, it was seen that highly efficient, biodegradable and biocompatible nanostructured vaccine prototypes have been successfully prepared.

**Discussion:** Within the scope of our studies, it is expected that the systems in which synthetic peptides with antigenic properties are encapsulated in nanoparticles will increase the biocompatibility of the peptides and increase the immunogenic properties in the result of controlled release and decrease the side effects caused.

**Keywords:** Nanoparticles, synthetic peptides, vaccine prototypes

**References:**

- Yilmaz, E. F., Pelit-Arayıcı, P., Maharramov, A. M., Mustafaeva, Z. (2016). The Approaches to Designing of New Generation Vaccines Against The Sheep Pox Disease, *Biotechnologia Acta*, 9 (6), 7-15.
- Karahan M., Tuğlu S., Mustafaeva Z. (2012). Synthesis of microwave assisted poly methyl vinyl ether co maleic anhydride bovine serum albumin bioconjugates, *Artificial Cells, Blood Substitutes, and Biotechnology*, 40 (6).
- Karahan, M., Mustafaeva, Z., Ozeroglu, C. (2014). The Formation of Polycomplexes of Poly (Methyl Vinyl Ether-Co-Maleic Anhydride) and Bovine Serum Albumin in the Presence of Copper Ions, *Polish Journal of Chemical Technology*, 16(3), 97-105.

---

# Study of Spectroscopic Properties of Nanosized Particles of Core-shell Morphology

---

Friday, 20th October - 13:30 - Poster Session - Hall & Room 3 - Poster - Abstract ID: 128

---

***Dr. Tamar Bzhalava<sup>1</sup>, Prof. Paata Kervalishvili<sup>1</sup>***

*1. Georgian Technical University*

Nanosized organic, inorganic or hybrid particles of different origin of core-shell morphology are targets of interest of material science, nanomedicine, nanotechnology. Fundamentally new properties and functions of nanoscaled materials are widely applied in medical diagnostic, drug delivery and nanosensory systems. Study of spectroscopic properties of bio or non-bioparticles, determination of resonance wavelength range, specific and unique “spectral” signatures is important in sensing and identification of nanobioparticles, viruses. Method of studying is based on the concept, which considers the viruses as physical objects characterized by the set of electro-geometric parameters. Elaboration of relevant models of viruses, estimation of spectral response on interaction of electromagnetic (EM) field and viral nanoparticle is the goal of proposed methodology. Core-shell model of virion, the extracellular infective form of a virus, is used as the first approximation of shape-structure of virion. Theoretical solution is based on Maxwell’s EM theory, separation of variables method for solving Helmholtz’s equation. Rigorous theoretical solution of EM wave scattering problem on spherical core-shell particle is applied to nanosized virus-like particles (VLPs) of icosahedral morphology for determination of EM fields in the areas of core, shell and surrounding medium of VLP, as well as scattering or absorption characteristics. Theoretical and numerical results are demonstrated for estimation of “spectra” of bacteriophage T7 obtained by computer simulation, based on MatLab software. Analysis shows: expected spectral response is observable on far-field characterizations; spectroscopic characteristics strongly depend on core-shell related electric and geometric parameters of VLP in resonance wavelengths range (Ultra-Violet for VLP-T7); resonance wavelengths could be associated with the values corresponding to the maximums of scattering cross ( $\sigma$ ) sections - total and forward or backward, respective to wave propagation directions. Proposed method should be applied for investigation, appreciation and modelling of spectral properties of nano/micro particles of core-shell structure, including un-enveloped viruses. Obtained analytical EM field expressions, modelling technique in complement with experimental spectroscopic methods should be the way of providing the virus spectral signatures, important in nanobioparticles characterization. Findings are applicable in nanobio-science, nanomaterials engineering, aerosol spectroscopic studies as well. The work was supported by Shota Rustaveli National Science Foundation (SRNSF), project no.FR/430/3-250/13.

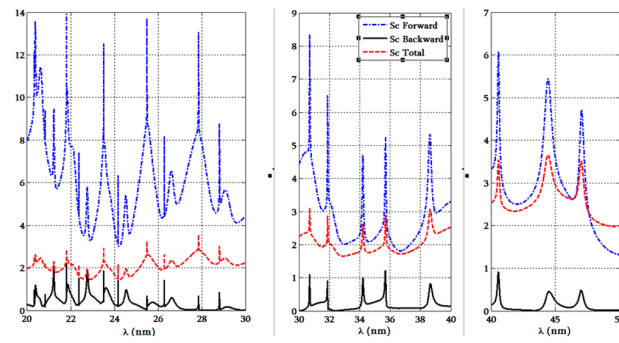


**Figure 1.** "Spectra" of T7 virus. Scattering cross section ( $\sigma/d_2^2$ ) vs excitation wave length ( $\lambda$ ). Parameters of core-shell model: diameters of core -  $d_1 = 42.6$  nm, shell -  $d_2 = 56.6$  nm, dielectric permittivity of core -  $\epsilon_1 = 6.3$ , shell -  $\epsilon_2 = 3.5$ , surrounding medium -  $\epsilon_3 = 1$ .

Spectra of t7 virus.png

# A new peptide-based fluorescent probe selective for mercury(II)

Friday, 20th October - 13:30 - Poster Session - Hall & Room 3 - Poster - Abstract ID: 125

**Dr. Giuliana Donadio<sup>1</sup>, Dr. Rosario Oliva<sup>1</sup>, Dr. Marialuisa Siepi<sup>1</sup>, Prof. Pompea Del Vecchio<sup>1</sup>, Prof. Luigi Petraccone<sup>1</sup>, Prof. Ezio Ricca<sup>2</sup>, Prof. Rachele Isticato<sup>2</sup>, Ms. Mariamichela Lanzilli<sup>1</sup>, Prof. Eugenio Notomista<sup>1</sup>**

1. University of Naples Federico II, 2. Università degli studi di Napoli Federico II

## Introduction

Mercury is a hazardous environmental contaminant, highly toxic even at low concentrations. We have previously developed a fluorescent peptidyl sensor named dH3w(dansyl-HPHGHW-NH<sub>2</sub>) based on an internal repeat of human histidine rich glycoprotein (Donadio *et al.* 2016 J. Mater. Chem. B, 4, 6979). dH3w showed a turn on response to Zn<sup>2+</sup> and a turn off response to Cu<sup>2+</sup>. Other heavy metals (Mn<sup>2+</sup>, Fe<sup>2+</sup>, Ni<sup>2+</sup>, Co<sup>2+</sup>, Pb<sup>2+</sup> and Cd<sup>2+</sup>) did not interfere with the detection of Zn<sup>2+</sup> and Cu<sup>2+</sup>. Here we report that dH3w has an affinity for Hg<sup>2+</sup> considerably higher than those for Zn<sup>2+</sup> and Cu<sup>2+</sup>, thus it could be used as a fluorescent probe for Hg<sup>2+</sup>.

## Methods

Steady-state fluorescence measurements were performed in 20 mM MOPS pH 7.0 with the peptide at a fixed concentration (7 μM). The dansyl fluorophore was excited at 340 nm. Emission spectra were recorded in the range 450–630 nm. In the displacement experiments Zn<sup>2+</sup> and dH3w were kept at fixed concentrations (100 or 200 μM and 7 μM, respectively) whereas the concentration of Hg was gradually increased up to 100 μM.

## Results

The addition of Hg<sup>2+</sup> to dH3w at concentrations lower than 10 μM induced a reduction of the emission without changes to the spectrum features. However at concentrations higher than 15 μM Hg<sup>2+</sup> induced a noteworthy blue-shift of the λ<sub>max</sub>, from 560 to 510 nm (Fig. 1) and an increase of the fluorescence intensity. Very interestingly Hg<sup>2+</sup> was able to displace Zn<sup>2+</sup> (Fig. 2) and Cu<sup>2+</sup> even when these metals were present in large excess. Also in the presence of Zn<sup>2+</sup>, low Hg<sup>2+</sup> concentrations induced a reduction of the fluorescence intensity, whereas at higher concentrations a blue-shift in the λ<sub>max</sub> was observed.

## Discussion

This behaviour strongly suggests that at least two complexes form at different Hg<sup>2+</sup>/dH3w ratios, possibly with different stoichiometries and/or geometries. The significant blue-shift of the maximum emission could be tentatively attributed to the deprotonation of the dansyl-sulfonamide moiety upon binding to the strongly electrophilic Hg<sup>2+</sup> ion. The determination of the nature of the two Hg<sup>2+</sup>/dH3w complexes will require further investigations.

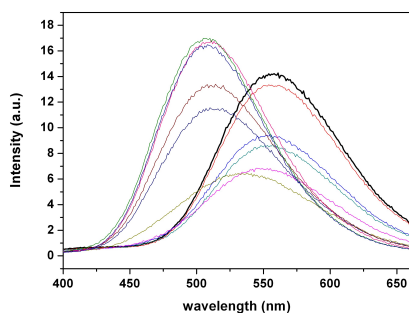


Fig.1.jpg

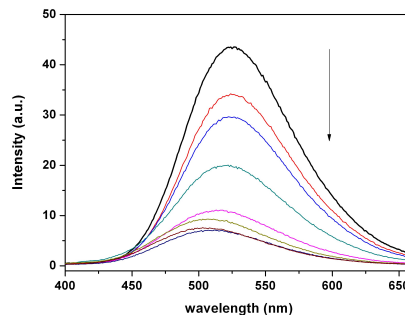


Fig.2.jpg

# Biodegradable Ultrafine Nanoparticles of Poly(Methyl Methacrylate-co- Methacrylic Acid) Prepared via Semicontinuous Heterophase Polymerization

Friday, 20th October - 13:30 - Poster Session - Hall & Room 3 - Poster - Abstract ID: 88

**Mrs. Hened Saade<sup>1</sup>, Dr. R. Guillermo López<sup>1</sup>**

*1. Centro de Investigación en Química Aplicada*

## Introduction

The biodegradable copolymer methyl methacrylate (MMA)-co-methacrylic acid (MAA) 2/1 (mol/mol), under the commercial name of Eudragit S-100 (ES-100), is used for the elaboration of drug-loaded pills because its solubility at pH > 7.<sup>1</sup> Nanoparticles of this material were prepared by *semicontinuous heterophase polymerization at monomer starved conditions*. As far as we know this is the first report on the preparation of ultrafine nanoparticles of this copolymer.

## Experimental Part

For polymerization at 70°C, a micellar solution containing the initiator was prepared in a 150 mL glass reactor. Then the monomers mixture was dosed on this solution. Conversions and surface tension of samples taken along the polymerization were determined. Additionally, these samples were analyzed by QLS, STEM, DSC and GPC.

## Results and Discussion

Kinetics corresponds to that typical of a polymerization at monomer starved conditions.<sup>2</sup> Surface tension measurements indicate the absence of micelles in the final latex. Mean particle diameter decreases as polymerization evolves (Fig. 1) as a result of the diminution in the polymerization rate within the particles, attaining a value  $\approx 10$  nm. Glass transition temperature indicates that a copolymer with a composition similar to that of the feed one was obtained. In accordance with the average molecular weights obtained, bimolecular reaction is probably the dominant mode of chain growing termination. The slight increase in molecular weights with  $X$  was probably due to a decrease in termination rate, resulting from a decrease in the radicals to nanoparticles ratio.

**Conclusions** A latex containing P(MMA-co-MAA) nanoparticles with  $\approx 10$  nm in mean diameter and  $\approx 10$  % in solid content was prepared. Furthermore, the copolymer composition was similar to that of the feed one.

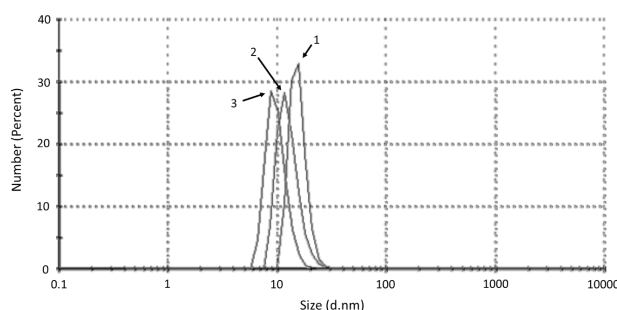


Fig resumen annic 2017.png

# Computational study on the structure, stability, and growth of supported gold nanoparticles

Friday, 20th October - 13:30 - Poster Session - Hall & Room 3 - Poster - Abstract ID: 146

***Dr. Julien Engel<sup>1</sup>, Ms. Samantha Francis<sup>1</sup>, Dr. Alberto Roldan<sup>1</sup>***

*1. Cardiff University*

Supported nanoparticles play a key role in a wide-ranging implications in health, information, energy, and many other fields where there is a major economic benefit in the commercialization of new technologies.<sup>[1,2]</sup> The activity and selectivity of the catalysts are highly dependent on the size and shape of the metal nanoparticles. However, the catalysts are deactivated under reaction conditions, mainly due to the sintering process leading to the formation of larger and less active particles. The major mechanism for the particles' sintering is *Ostwald ripening* (Fig 1a), which is the merging of small clusters or single adatoms with larger clusters, and the *migration and coalescence* (Fig 1b) of larger clusters. Especially, the loss of very small and often highly active clusters at the early stage of the sintering process is mainly caused by Ostwald ripening.<sup>[3]</sup>

In the presented study, we use dispersion-corrected density functional theory to evaluate the structure and growth of gold nanoparticles on different supports from first principles. Using the Vienna ab initio simulation package (VASP), the structures of Au<sub>n</sub> clusters (n = 1-20) on MgO (001), CeO<sub>2</sub> (111), and graphite (001) model surfaces were investigated. Moreover, the mobility of gold adatoms and their coalescence with larger clusters according to the Ostwald ripening mechanism was studied. Hence, the presented results give a comprehensive insight into the influence of the support material on the structure, mobility and growth of supported gold clusters.

References:

- [1] J. A. Anderson, J. A. Anderson, M. Fernández-García, *Supported Metals in Catalysis*, Imperial College Press, **2005**.
- [2] A. Wieckowski, E. R. Savinova, C. G. Vayenas, *Catalysis and electrocatalysis at nanoparticle surfaces*, CRC Press, **2003**.
- [3] T. W. Hansen, A. T. DeLaRiva, S. R. Challa, A. K. Datye, *Acc. Chem. Res.* **2013**, *46*, 1720–1730.

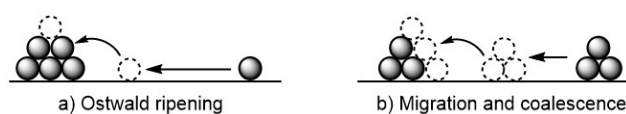


Figure 1.jpg



# Temperature-dependent Emission Properties of CdSe/CdS/CdTe Core/Crown Nanoplatelets

Friday, 20th October - 13:30 - Poster Session - Hall & Room 3 - Poster - Abstract ID: 307

**Mrs. palvasha ijaz<sup>1</sup>, Dr. Ilaria Angeloni<sup>1</sup>, Dr. Guillaume Bertrand<sup>1</sup>, Dr. Iwan Moreels<sup>1</sup>**

*1. Istituto Italiano di Tecnologia (IIT) - Genova*

**Introduction.** Colloidal 2D nanoplatelets (NPLs) demonstrate remarkable optoelectronic properties. In particular, they have a narrow and –at room temperature- homogeneously broadened emission linewidth, fast exciton recombination and high fluorescence quantum efficiency. These advantageous properties can be further tuned in heterostructures, where in the case of 2D materials a second semiconductor can be grown either on top or bottom facets (core/shell nanoplatelets), or on the lateral facets of the nanoplatelet (core/crown nanoplatelets). Here, we present results on a ternary architecture, CdSe/CdS/CdTe core/crown nanoplatelets. Due to the peculiar band alignment of the three semiconductors, the CdS layer acts as a hole tunneling barrier, while electron relaxation from the CdTe crown into the CdSe remains possible.

**Methods.** CdSe/CdS/CdTe core/crown nanoplatelets were synthesized following literature protocols (Tessier et al., Nano Lett. 2014, 14, 207–213; Pedetti et al. J. Am. Chem. Soc. 2014, 136, 16430–16438) and drop cast on a sapphire substrate to form a close-packed thin film. We loaded the samples in a close-cycle cryostat and cooled them to 4K to investigate the temperature dependent emission properties. We excited the samples with a 405 nm pulsed laser and collected the fluorescence spectra and time-resolved fluorescence decay.

**Results and discussion.** Due to the staggered band offset between CdSe and CdTe, we observed emission from an indirect transition around 650 nm. As CdS forms a barrier for hole relaxation between crown and core regions, the CdSe/CdS/CdTe yielded an additional emission peak from the CdSe core, in contrast with CdSe/CdTe core/crown nanoplatelets without a barrier. The resulting dual emission was investigated as a function of temperature. The different nature of both emission peaks (direct in CdSe vs. indirect across the CdSe/CdTe interface) yielded a spectrally and temporally stable indirect transition as a function of temperature, while the emission rate of the CdSe emission increased at lower temperatures, and the spectral position shifted to shorter wavelengths. We finally explored the possibility of using the dual emission as a ratiometric sensor.

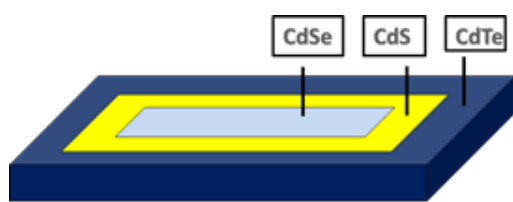


Figure 1. CdSe/CdS/CdTe core/crown nanoplatelets

Npls.png

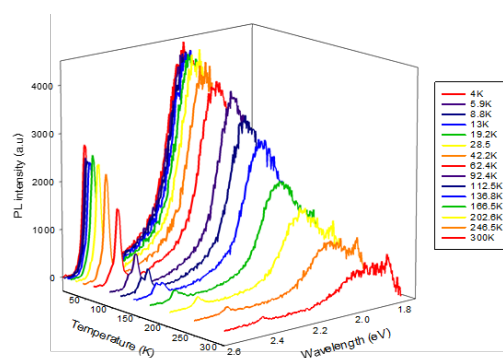


Figure 2. Evolution of the PL spectra with temperature in a range 4K-300K for typical CdSe/CdS/CdTe nanoplatelets.

Pl spectra.png

# Influence of Au nanoparticles for enhanced performance of quantum dot light-emitting diodes

Friday, 20th October - 13:30 - Poster Session - Hall & Room 3 - Poster - Abstract ID: 357

**Prof. Jiwan Kim<sup>1</sup>**

*1. Kyonggi University*

## 1. INTRODUCTION

Colloidal quantum dots (QDs) emit vivid light with narrow full width half maximum and their wavelength is tunable due to quantum confinement effect. From these unique optical/electrical properties, various display applications using QDs, therefore, have been spotlighted as a post OLED display technology. One of advantages of quantum dot light-emitting diodes (QLEDs) is a low fabrication cost, because it is based on a solution process. However, the lower current efficiency compared to OLED is still a weakness. Many researchers have been constantly tried various materials for efficient charge transport within device, at last, they came to agreement the use of inorganic nanoparticles (NPs) as an electron transport layer to improve the performance of QLEDs.

## 2. METHODS

The blended PEDOT:PSS:Au NPs were spin-coated on the cleaned ITO substrate. To observe the effect of the Au NPs density, the density of the Au NPs in blended solution was increased up to 0.01, 0.02, 0.03 mg/ml respectively. TFB dissolved in chlorobenzene was spin-coated on the blended PEDOT:PSS:Au NPs layer. For the light emission layer, QDs were dispersed in Heptane and spin-coated on the TFB layer. Then, ZnO NPs was spin-coated as an ETL. After finishing solution process, the Al cathode was deposited by thermal evaporation on the ZnO NPs layer.

## 3. RESULTS AND DISCUSSION

The light extraction technology is one of the well-known technologies to increase the optical efficiency of the light emitting devices. Among them, localized surface plasmon resonance (LSPR) is a technology that can improve the luminance by controlling refraction and scattering of light using metal NPs in the device. Here, we investigated the LSPR effect on the device performance by dispersing the Au NPs in the hole transport layer (HTL) and hole injection layer (HIL) (Figure 1). The result indicates that the optical enhancement of the QLEDs is attributed to strong resonance coupling between excitons in the QDs and LSP in the Au NPs in the HIL. Further optimization using Au NPs will help make highly efficient QLEDs for future display application.

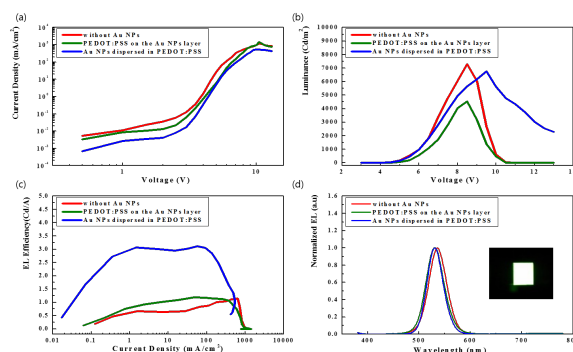


Figure . (a) Current density-Voltage (b) Luminance-Voltage (c) EL efficiency-Current density and (d) Normalized EL peaks of QLEDs with/without Au NPs in PEDOT:PSS

Figure.png

# Fluorescent triazolyl-coumarin carbon spheres synthesized from waste tyres for Fe<sup>3+</sup> detection

Friday, 20th October - 13:30 - Poster Session - Hall & Room 3 - Poster - Abstract ID: 475

**Ms. Jacolien Du Plessis<sup>1</sup>, Dr. Neliswa Mama<sup>1</sup>, Prof. Vincent Nyamori<sup>2</sup>**

**1. Nelson Mandela University, 2. University of KwaZulu-Natal**

The recycling and re-use of waste tyres is an important area for global research to find ways in alleviating the hazardous impact of these hardy materials on the environment. The use of recycled waste tyres as carbon source to synthesize fluorescent chemosensing carbon spheres for the detection of harmful chemicals in water is proposed in this work. Three key problems are addressed at once: *i*) re-using waste tyre products *ii*) synthesis of low-cost carbon nanomaterial *iii*) detection of harmful compounds within environment systems. The carbon spheres were synthesized from waste tyre pyrolysis oil using chemical vapour deposition (CVD) at 950 °C with ferrocene as catalyst. Characterization of the carbon spheres were done using TEM, SEM, Raman, TGA and XRD. The two-unit triazolyl-coumarin was synthesized through a multi-step procedure with the “click-reaction” as one of the steps. The carbon spheres were functionalized with the triazolyl-coumarin units through Steglich esterification to yield fluorescent carbon spheres. Functionalization was confirmed using XPS, FT-IR and TGA. Complexation studies were done using UV/Vis and fluorescence with a wide range of elements; Ag<sup>+</sup>, Al<sup>3+</sup>, Co<sup>2+</sup>, Cr<sup>3+</sup>, Cu<sup>2+</sup>, Fe<sup>3+</sup>, Hg<sup>2+</sup>, Li<sup>+</sup>, Ni<sup>2+</sup>, Pb<sup>2+</sup> and Zn<sup>2+</sup>. The triazolyl-coumarin carbon spheres showed reasonable sensitivity and selectivity towards Fe<sup>3+</sup> in water with a quenching effect in fluorescence. It was shown that the 1,2,3-triazole is a possible binding site for Fe<sup>3+</sup> on the triazolyl-coumarin carbon sphere, determined through the comparison of emission responses of the fluorescent carbon spheres, starting carbon sphere and a reference compound. Titration studies with Fe<sup>3+</sup> were also done with results indicating an exponential decay of quenching in the fluorescence up to 70%. Ferric ion (Fe<sup>3+</sup>) is a crucial element used in the maintenance of biochemical processes within living systems. Detection of Fe<sup>3+</sup> is therefore crucial for monitoring the limits within the environment and living systems.

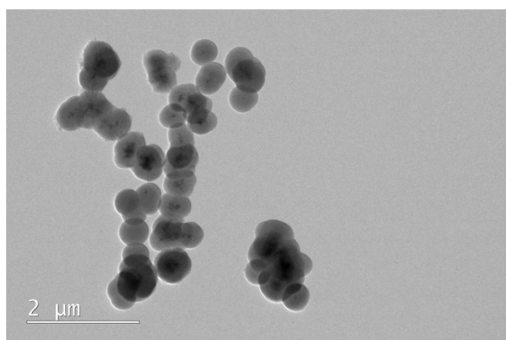


Figure 1: TEM imaging of carbon spheres synthesized from waste tyre pyrolysis oil using CVD at 950 °C with ferrocene as catalyst.

Carbon spheres.png

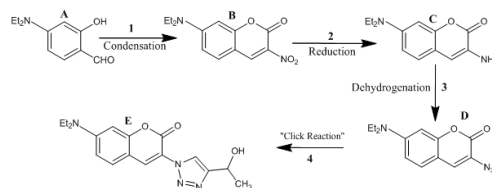


Figure 2: Scheme for the multi-step synthesis of the triazolyl-coumarin units

Triazolyl coumarin synthesis scheme.png

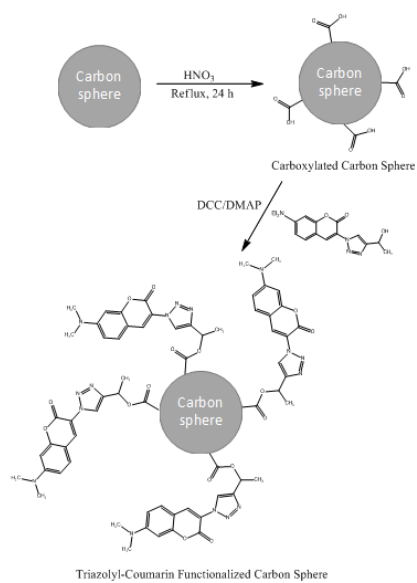
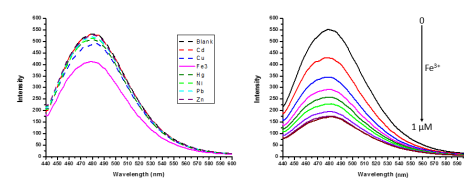


Figure 3: Scheme for the functionalization of the carbon spheres with triazolyl-coumarin units

Carbon sphere functionalization.png



Emission spectra.png

# Advanced nanocomposite materials for Oil & Gas production

Friday, 20th October - 13:30 - Poster Session - Hall & Room 3 - Poster - Abstract ID: 528

**Ms. Chinyere Okolo<sup>1</sup>, Dr. Fawad Inam<sup>1</sup>**

*1. Northumbria University*

**INTRODUCTION:** The search for novel materials has continued to dominate industries like automotive, power, aerospace and energy where maintaining a competitive edge is necessary for increasing industry market share. For subsea applications, where high pressures and temperatures are the norm, using reinforced composites have potential as the next generation solution.

This presentation investigates the influence of micro/nano fillers on mechanical properties of lightweight polymeric materials employed in thermoplastic risers and hoses for subsea applications and the challenge of incorporating such novel materials for potential up-scaling.

To obtain commercially viable microstructures, a two-step processing routes was selected and its influence on final polymer nanocomposite morphology has been studied.

**METHODOLOGY:** The polymer nanocomposite used in this study consists of carbon nanotubes and HDPE purchased from Nanocyl SA. The pellets were fed into a Brabender single screw laboratory extruder with conditions selected to optimize dispersion and distribution. Filler orientation by shear flow extrusion was achieved by using a rectangular shaped die with unique design and area.

Tensile samples were prepared by punching out dog-shaped dumbbells with die cutter sized-ISO 527-2 5A. Morphology of the fractured surfaces were obtained from the tensile samples examined via FE-SEM (TESCAN MIRA 3; 5KV) after sputter coating (Q150T Turbo-Pumped Sputter Coater) with platinum.

**RESULTS:** Figure 1 attached compares the Tensile Strength and Young's Moduli of the different concentrations (0%-3%) of carbon nano-tubes in HDPE.

Figure 2 attached shows the micro-graphs of well dispersed 1 wt% CNT in HDPE.

**DISCUSSION:** By adding approximately 1% by weight (wt%) of carbon nano-tubes, we found the nano-composite to have a Young's modulus of  $1.462 \pm 0.263$  GPa, an increase of about 15% compared to the pure matrix.

Increasing the filler loading to 2% resulted in improved modulus and tensile strength properties without good dispersion. The CNTs can be seen to be bridging cracks in the matrix. The degree of improved dispersion at 1% wt which is demonstrated in FE-SEM images, translated into an improved composite reinforcement.

In summary, the study showed improvements in mechanical properties can be achieved using a two-step processing route. Further studies to develop practical quality control methods are being considered.

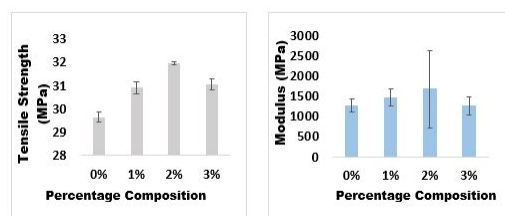


Fig 1. comparison of tensile strength and youngs moduli of 0 -3 carbon nanotubes in hdpe.jpg

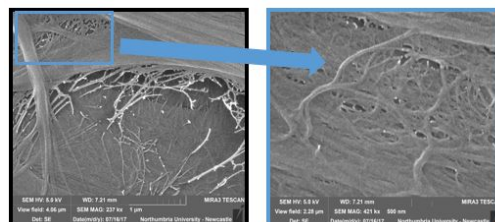


Fig 2. micrographs of 1 wt carbon nanotubes in hdpe.jpg

---

## Biocompatible and functionalized electrospun fibers

---

Friday, 20th October - 13:30 - Poster Session - Hall & Room 3 - Poster - Abstract ID: 672

---

***Dr. Elena Matei<sup>1</sup>, Mrs. Mihaela Oancea<sup>1</sup>, Mr. Alexandru Evanghelidis<sup>1</sup>, Dr. Ionut Enculescu<sup>1</sup>***

*1. National Institute of Materials Physics*

Electrospinning represent a “classic” technique to obtain micrometer and sub micrometer fibers for a wide range of applications. The technique is relatively simple and allows the preparation of industrial amounts of material with low cost. A polymer solution droplet is exposed to an intense electric field which leads to the formation of a jet and further to a very thin fiber of the polymer.

Functionalization represents a step which can tremendously increase the range of applications of these thin fibers. Therefore our aim was to test several paths towards new and more complex architectures. In the present report we will describe our work regarding functionalized biocompatible fiber arrays based on a set of preparation methods which start with electrospinning. In order to achieve the desired functionality sputtering of a thin metal layer leads to conductive fibers. We used these as working electrodes for electrochemical deposition and the fibers were covered with polymers such as polyaniline[1,2] or with ZnO. The sequence of steps enabled us to obtain mats with either electroactive properties or with photocatalytic activity. Both these properties are very interesting for applications ranging from artificial muscles to substrates with antimicrobial activity. The straightforward, scalable methods of fabrication make the approach a very interesting one for lucrative applications.

[1] M. Beregoi, C. Busuioc, A. Evanghelidis, E. Matei, F. Iordache, M. Radu, et al., Electrochromic properties of polyaniline-coated fiber webs for tissue engineering applications, *Int. J. Pharm.* (2015). doi:10.1016/j.ijpharm.2015.11.055.

[2] M. Beregoi, A. Evanghelidis, E. Matei, I. Enculescu, Polyaniline based microtubes as building-blocks for artificial muscle applications, *Sensors Actuators, B Chem.* 253 (2017). doi:10.1016/j.snb.2017.06.128.

## Catalytic activity of bimetallic AuPd alloys supported MgO and MnO<sub>2</sub> nanostructures and their role in selective aerobic oxidation of alcohols

---

Friday, 20th October - 13:30 - Poster Session - Hall & Room 3 - Poster - Abstract ID: 49

---

***Dr. Hamed Alshammari*<sup>1</sup>**

*1. university of Hail*

The use of metal oxides as supports for gold and palladium (Au-Pd) nanoalloys constitutes new horizons to improve new active catalysts in very important reactions. From the literatures, Pd-based bimetallic nanostructures have great properties and active catalytic performance. In this study, nanostructures of Magnesium oxide (MgO) and nano Manganese dioxide (MnO<sub>2</sub>) were synthesised and utilized as supports for Au-Pd nanoparticles catalysts. Gold and palladium were deposited on these supports using sol-immobilisation method. The MgO and MnO<sub>2</sub> supported Au-Pd catalysts were evaluated for the oxidation of benzyl alcohol, aliphatic, aromatic alcohols and 1-octanol, respectively. This catalyst was found to be selective, active and reusable than the corresponding monometallic Au and Pd catalysts. The outcomes of this work shed light on the selective aerobic oxidation of alcohols using bimetallic Au-Pd nanoalloys and pave the way to a complete investigation of more basic metal oxides for various aliphatic alcohols

---

# Colloidal Synthesis of Bipolar Off-Stoichiometric Gallium Iron Oxide Spinel-Type Nanocrystals with Near-IR Plasmon Resonance

---

Friday, 20th October - 13:30 - Poster Session - Hall & Room 3 - Poster - Abstract ID: 117

---

**Dr. Carmine Urso<sup>1</sup>, Dr. Mariam Barawi<sup>1</sup>, Dr. Roberto Gaspari<sup>1</sup>, Dr. Gianluca Sirigu<sup>2</sup>, Dr. Ilka Kriegel<sup>2</sup>, Dr. Margherita Zavelani-rossi<sup>2</sup>, Dr. Francesco Scotognella<sup>2</sup>, Dr. Michele Manca<sup>1</sup>, Dr. Mirko Prato<sup>1</sup>, Dr. Luca De Trizio<sup>1</sup>, Prof. Liberato Manna<sup>1</sup>**

*1. Istituto Italiano di Tecnologia, 2. Politecnico di Milano*

We report the colloidal synthesis of ~5.5nm inverse spinel-type oxide Ga<sub>2</sub>FeO<sub>4</sub> (GFO) nanocrystals (NCs) with control over the gallium and iron content. As recently theoretically predicted, some classes of spinel-type oxide materials can be intrinsically doped by means of structural disorder and/or change in stoichiometry. Here we show that, indeed, while stoichiometric Ga<sub>2</sub>FeO<sub>4</sub>NCs are intrinsic small bandgap semiconductors, off-stoichiometric GFO NCs, produced under either Fe-rich or Ga-rich conditions, behave as degenerately doped semiconductors. As a consequence of the generation of free carriers, both Fe-rich and Ga-rich GFO NCs exhibit a localized surface plasmon resonance in the near-infrared at ~1000nm, as confirmed by our pump-probe absorption measurements. Noteworthy, the photo-electrochemical characterization of our GFO NCs reveal that the majority carriers are holes in Fe-rich samples, and electrons in Ga-rich ones, highlighting the bipolar nature of this material. The behavior of such off-stoichiometric NCs was explained by our density functional theory calculations as follow: the substitution of Ga<sup>3+</sup> by Fe<sup>2+</sup> ions, occurring in Fe-rich conditions, can generate free holes (p-type doping), while the replacement of Fe<sup>2+</sup> by Ga<sup>3+</sup> cations, taking place in Ga-rich samples, produces free electrons (n-type doping). These findings underscore the potential relevance of spinel-type oxides as p-type transparent conductive oxides and as plasmonic semiconductors.



---

## Local atomic and electronic structure of Cu (I,II) binding site in amyloid beta peptide: theoretical HERFD XANES study

---

Friday, 20th October - 13:30 - Poster Session - Hall & Room 3 - Poster - Abstract ID: 187

---

**Mrs. Maria Kremennaya<sup>1</sup>, Dr. Mikhail Soldatov<sup>1</sup>, Ms. Yulia Podkovyrina<sup>2</sup>, Mrs. Irina Dadasheva<sup>1</sup>**

**1. Southern Federal University, IRC "Smart Materials", 2. International Research Center "Smart Materials", Southern Federal University**

Copper is an essential trace element. Being a part of many enzymes and proteins, it is involved in their life cycle [1]. However, copper can be toxic if its homeostasis is not controlled. Some known pathologies associated with the abnormal copper homeostasis are Wilson and Menkes diseases and neurodegenerative disorders such as Alzheimer's or Prion diseases [2]. Currently, Alzheimer's disease is considered one of the most common progressive neurodegenerative disorders. It is known that Alzheimer's disease brain is characterized by elevated levels of oxidative stress and high levels of redox active transition metals such as Cu and Fe [3].

Atomic structure of copper (I,II) binding site in A $\beta$  peptide was studied by means of combination techniques of quantum chemical calculations and advanced theoretical XANES analysis. Theoretical models of copper Cu (I, II) binding site in A $\beta$  peptide were calculated in ADF (Amsterdam Density Functional) package [4]. The calculation of theoretical X-ray absorption spectra was carried out in an accelerated version FDMNES code [5]. Acceleration software for FDMNES code was developed in International Research Center "Smart materials".

In addition, for obtained models high energy resolution fluorescence detected X-ray absorption near edge structure (HERFD XANES) spectra calculations was carried out. Information obtained from HERFD XANES spectra gives more detailed information on local atomic and electronic structure of protein samples compared traditional XANES spectra.

The main structural parameters such as interatomic distances and bond angles for both copper (I, II) binding site configurations of amyloid beta were obtained.

This study was supported by the Russian Foundation for Basic Research, project № 16-32-00568.

[1] H. Tapiero, D. M. Townsend, and K. D. Tew, *Biomedicine & Pharmacotherapy* 57 (2003) 386.

[2] C. Hureau, H. Eury, R. Guillot et. *Al Chem. Eur. J.* 2011, 17, 10151 – 10160

[3] C. Schoneich, *Journal of Pharmaceutical and Biomedical Analysis*, 2000. Vol. 21. PP. 1093-1097.

[4] G. Te Velde, et al, *Journal of Computational Chemistry*, 2001. Vol. 22. P. 931.

[5] S. A. Guda, A. A. Guda, M. A. Soldatov, et al. *Journal of Chemical Theory and Computation*. 2015. Vol.11, P.4512.

# Effects of the compliance current on the resistive switching behavior of arsenic telluride thin films

Friday, 20th October - 13:30 - Poster Session - Hall & Room 3 - Poster - Abstract ID: 246

**Prof. Taeho Kim<sup>1</sup>, Prof. hyunchul Sohn<sup>1</sup>, Mr. Jinyeol Lee<sup>1</sup>, Ms. Dayoon Lee<sup>1</sup>, Mr. Jaeyeon Kim<sup>1</sup>**

<sup>1</sup>. Yonsei University/Semiconductor Memory Lab/Materials Science & Engineering

## Introduction

3D X-point array structure has attracted increasing attention for high-density resistive memory devices, but 3D X-point array structure with a purely linear resistive switching element suffers from sneak current paths. To suppress the leakage current, a two-terminal selection device, series connected with each resistive element in a one selector one resistive element (1S1R) memory cell configuration has been proposed. Recently, phase change random access memory (PRAM) has been intensively investigated for the application to cross-point array structure material because of their favorable features such as the low cost, non-volatility, simple structure etc. And selection devices which are based on chalcogenide material are interested as a 1S1R structure by intel-micron (2016).

## Method

In this study, Arsenic telluride binary chalcogenide compounds were used for memory switching and threshold switching material. Arsenic telluride amorphous thin films were deposited by RF magnetron co-sputter using As<sub>2</sub>Te target and Te target. The thicknesses of the Arsenic telluride thin films were 40 nm for all compositions, which was confirmed by Transmittance electron microscopy (TEM). Crystallinity of Arsenic telluride thin films as a function of annealing temperature and Te compositions was investigated by X-ray diffraction (XRD) and transmission electron microscopy (TEM). Crystallization temperature was analyzed by Differential scanning calorimeter (DSC) and analysis of the chemical bonding states with varying post annealing temperature of As-Te thin films by Raman spectroscopy.

## Result

OTS behavior with As<sub>x</sub>Te<sub>1-x</sub> film thickness, device area and annealing temperatures were investigated. OTS behavior with As<sub>x</sub>Te<sub>1-x</sub> film thickness, device area and annealing temperatures were investigated. We observed two types of changeable resistance switching effects in a arsenic telluride film, memory type resistive switching at high compliance current and threshold switching type at low compliance current.

## Discussion

The result shows that memory and threshold switching is occurred by control of compliance current, films of thermal stability and concentration of Te composition in Arsenic telluride binary thin film devices.

Compliance Current	300uA	500uA	800uA	1mA	2mA	3mA	4mA	5mA
Switching characteristics	As <sub>47</sub> Te <sub>53</sub>	OTS	OTS	OTS	Memory	Memory	Memory	Memory
	As <sub>41</sub> Te <sub>59</sub>	OTS	OTS	OTS	OTS	OTS	Memory	Memory
	As <sub>33</sub> Te <sub>67</sub>	OTS	OTS	OTS	OTS	OTS	OTS	OTS

Table. 1. Restive Switching Characteristics change with composition and compliance current.

Table1.png

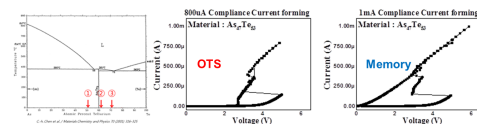


Fig. 3. I-V Characteristics of Arsenic Telluride Thin film with increase Compliance Current.

Fig3.png

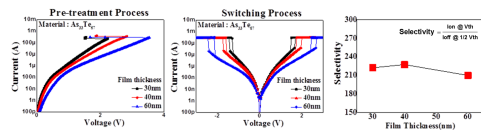


Fig. 2. I-V Characteristics of  $As_{23}Te_{67}$  Thin film with increase thickness.

Fig2.png

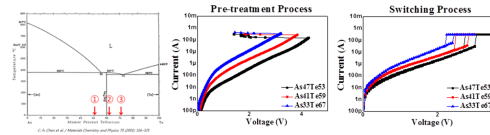


Fig. 1. I-V Characteristics of Arsenic Telluride Thin films with increase Te concentration.

Fig1.png

# Characterization of Polycaprolactone and Rice Husk Silica Composite (PCL-SiO<sub>2</sub>) by E-Spinning to Apply Supporter for Drug Release

Friday, 20th October - 13:30 - Poster Session - Hall & Room 3 - Poster - Abstract ID: 284

**Mrs. SINA E SONG<sup>1</sup>, Ms. Yeoung Ah Noh<sup>1</sup>, Ms. Jin Yi Kim<sup>2</sup>, Prof. Hee Taik Kim<sup>2</sup>**

**1.** Department of Advanced Material and Science engineering, Hanyang University, **2.** department of fusion chemical engineering, Hanyang University

Polycaprolactone (PCL) is an interesting material to apply biomedical field owing to its biodegradability and biocompatibility which is suitable for a specific site with longer healing times. Blending the polymer with other materials has degradation property improved with the effective and economic method.

This study was conducted to fabricate supporter based on Polycaprolactone and Rice husk silica (PCL-SiO<sub>2</sub>) by using electrospinning, which was loaded Rhodamine B (RhB) alternative drug for modeling of drug release. Nanoporous silica in the composite was synthesized from rice husk having properties of economic, eco-friendly and high surface area. It drew to enhance the amount of drug loading in the carrier. Electrospinning technique is used to fabricate fibrous component by optimization condition obtained from previous mechanical properties experiments. Release experiment was carried out by the degree of dye absorbance at 544nm by ultraviolet-visible spectroscopy, the RhB in PCL-SiO<sub>2</sub> was released for 1hr ~ 15days at 37°C in phosphate buffer. Furthermore, the Mechanical property was confirmed by DSC, DMA, and TG. Morphology and degree of biodegradation were shown as SEM images and EDS.



Figure 1. image of rice husk on each step

Figure 1.png

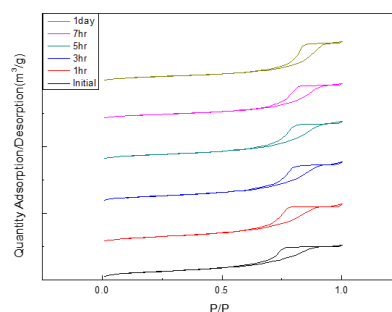


Figure 2. Nitrogen adsorption-desorption isotherm of the samples calculated from the adsorption branch of the isotherm using BJH method.

Figure 2.png

Table1. Experimental measured values for Surface Area( $S_{BET}$ ) with condition of 300mg rice husk ash, pH 4 on each aging time .

Samples	$S_{BET}$ ( $m^2/g$ )	$V_{total}$ ( $cm^3/g$ )	Pore size (nm)
Initial	417.50	0.81	7.53
1hr	454.84	0.97	8.32
3hr	415.47	0.97	9.08
5hr	397.12	0.94	9.32
7hr	343.85	0.87	9.87
1day	332.47	0.97	11.36

Table 1.png

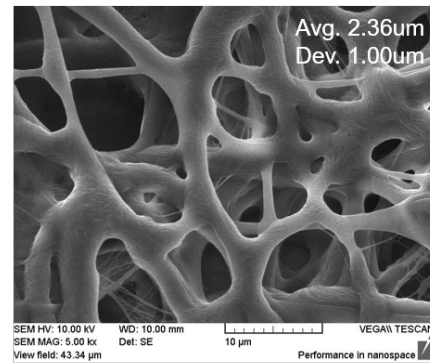


Figure 3. FE-SEM image of PCL fiber with optimized condition; 13kV, 1ml/h, 23G and 40min.

Figure 3.png

# Analysis of Ge/GaAs heterojunction-based PN junction tunneling field-effect transistor with dual-metal-gate structure for high-performance and low-power applications

Friday, 20th October - 13:30 - Poster Session - Hall & Room 3 - Poster - Abstract ID: 311

**Mr. Jae Hwa Seo<sup>1</sup>, Mr. Young Jun Yoon<sup>1</sup>, Mr. Min Su Cho<sup>1</sup>, Prof. In Man Kang<sup>1</sup>**

*1. Kyungpook National University*

Tunneling field-effect transistors (TFETs) have been studied as a prospective low-power (LP) device because TFETs can achieve a low off-state current ( $I_{\text{off}}$ ) and a small subthreshold swing ( $S$ ) under 60 mV/dec by using the band-to-band tunneling (BTBT) mechanism. However, a low on-state current ( $I_{\text{on}}$ ) is caused by the BTBT mechanism. And,  $I_{\text{on}}$  and LP performance of TFETs is degraded by the graded doping profile. To reduce of a high tunneling resistance and the impact of the doping profile on tunneling current, it is essential to design a novel device structure. In this paper, a Ge/GaAs heterojunction-based PN junction TFET with a dual-metal-gate structure have been proposed for application of high-performance (HP) and LP device. And, we executed a design optimization for a source-side gate length ( $L_{\text{S-Gate}}$ ) in the dual-metal-gate structure to improve LP performance as well as  $I_{\text{on}}$ . Figure 1 shows schematics of the proposed device. The proposed device is composed of a nanowire structure based on Ge/GaAs heterojunction. A radius ( $R$ ) in nanowire structure is 10 nm. Doping concentrations of Ge and GaAs layers are  $p^+ 5 \times 10^{19} \text{ cm}^{-3}$  and  $n^+ 5 \times 10^{18} \text{ cm}^{-3}$ , respectively. A total gate length ( $L_G$ ) is 50 nm and the gate dielectric is used as a high- $k$  dielectric  $\text{HfO}_2$  with a thickness ( $T_{\text{ox}}$ ) of 3 nm. We carried out a simulation work to investigate the performance of the proposed TFET. To obtain an accurate simulation result, various physical models such as Shockley-Read-Hall (SRH) recombination, trap-assisted tunneling (TAT), BTBT, and concentration-dependent mobility models are used in device simulation. Figure 2 shows transfer characteristics of the proposed TFET with different  $L_{\text{S-Gate}}$ . The  $I_{\text{on}}$  and  $S$  of the dual-metal-gate TFET is largely influenced by a change in the  $L_{\text{S-Gate}}$  in the dual-metal-gate. We confirmed that the proposed TFET with a  $L_{\text{S-Gate}}$  of 10 nm exhibited a higher  $I_{\text{on}}$  of 275.6  $\mu\text{A}/\mu\text{m}$  and a smaller  $S$  of 25.4 mV/dec owing to effective tunneling operation. Consequentially, by applying the steep PN junction and dual-metal-gate structure, the proposed TFET simultaneously achieved superior a high  $I_{\text{on}}$  and LP performance.

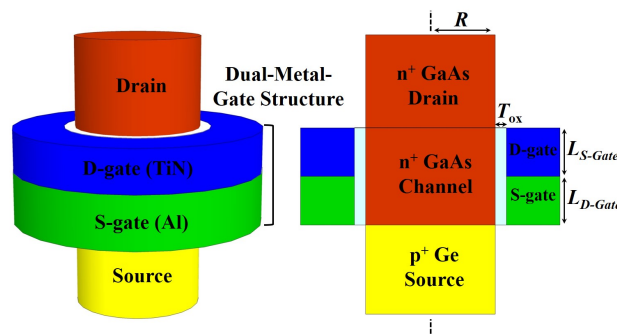


Figure 1. schematics of the proposed device.jpg

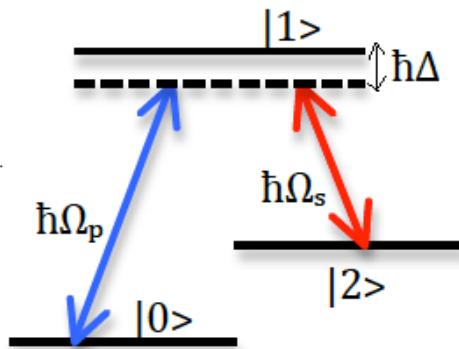
# All Optical Programmable Logic Array (PLA)

Friday, 20th October - 13:30 - Poster Session - Hall & Room 3 - Poster - Abstract ID: 506

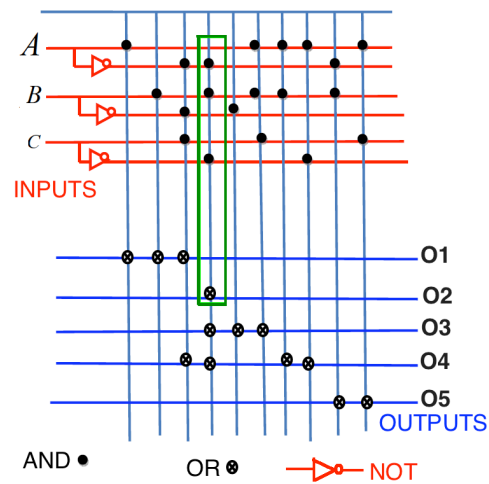
***Dr. Dawit Hailu***<sup>1</sup>

*1. Ben-Gurion University of the Negev*

A programmable logic array (PLA) is an integrated circuit (IC) logic device that can be reconfigured to implement various kinds of combinational logic circuits. The device has a number of AND and OR gates which are linked together to give output or further combined with more gates or logic circuits. This work presents the realization of PLAs via the physics of a three level system interacting with light. By studying the dynamics of three level atom perturbed by laser in the adiabatic limit and studying the response of the system after and before the interaction with the laser, we here implement a PLA. A programmable logic array is designed such that a number of different logical functions can be combined as a sum-of-product or product-of-sum form. We present an all optical PLAs with the aid of laser light and observables of quantum systems, where encoded information can be considered as memory chip. The dynamics of the physical system is investigated using Lie algebra approach.



30level.png



Pla.png

# Detection of organic vapors on sputtered and annealed thin Au films

Friday, 20th October - 13:30 - Poster Session - Hall & Room 3 - Poster - Abstract ID: 591

**Dr. Ondrej Kvitek<sup>1</sup>, Mr. Vojtech Kopacek<sup>1</sup>, Dr. Alena Reznickova<sup>1</sup>, Prof. Vaclav Svorcik<sup>1</sup>**

*1. Department of Solid State Engineering, University of Chemistry and Technology, Prague*

## Introduction

Thanks to a high ratio of free volume the atoms forming thin films are susceptible to surface diffusion over substrates and the films undergo a structural change after annealing at relatively low temperatures. This transformation process called solid state dewetting leads to evolution of an island-like structure. Isolated metal islands show interesting properties, namely localised surface plasmon resonance (LSPR), which is observed as a distinct absorption band in UV-Vis spectrum, which is highly influenced by refractive index of surrounding medium. This phenomenon can be used for construction of sensitive devices for detection of gases in the atmosphere around the metal nanostructure.

## Methods

Au films of 2-60 nm thickness were prepared by cathode sputtering at 20 mA for 10-300 s on glass slips. Annealing of the thin Au films was performed in FED 23 oven at 300 °C for 1 h. Surface structure was observed by atomic force microscopy (AFM, CP II Bruker, tapping mode), optical properties were determined by UV-Vis spectroscopy (Lambda 25, Perkin Elmer). The prepared Au nanostructures were tested for their optical response to introduction of vapors of acetone, water, ethanol and toluene in an experimental arrangement (Fig. 1).

## Results

AFM measurements showed dramatic structural change occurring after annealing of the thin Au films. The as prepared continuous films are transformed into structure of separated Au nanoislands. This phenomenon is readily observable on the thicker Au layers (Fig. 2). Impact of the structural change on optical properties of the material is expressed in the UV-Vis spectra as evolution of strong absorption bands associated with LSPR of the fine metal nanostructure (Fig. 3). Measurements of response of the nanostructure to organic vapors showed the highest sensitivity in the case of 4 nm thick films and the highest response was found to be to acetone vapors (Fig. 4).

## Discussion

The optical properties of the Au nanostructures were found to be definitively dependent on the presence of organic vapors. However, selectivity of such a simple sensitive system is low. This problem could, however, be solved in further research by e.g. addition of a polymer layer with affinity to specific analyte.

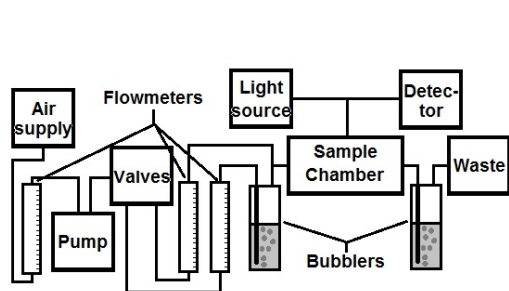


Fig. 1 - schematic of the experimental detection device layout.jpg

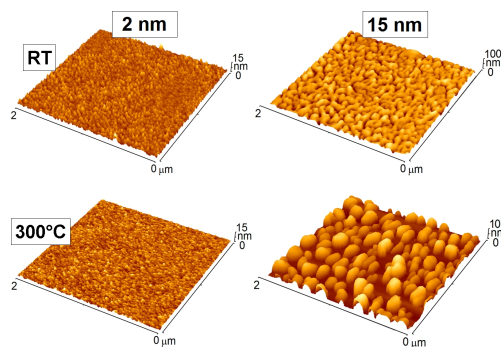


Fig. 2 - afm images of as sputtered and subsequently annealed thin au films.jpg



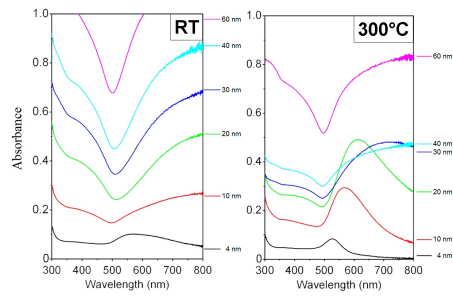


Fig. 3 - uv-vis spectra of as sputtered and annealed thin au films of various thickness.jpg

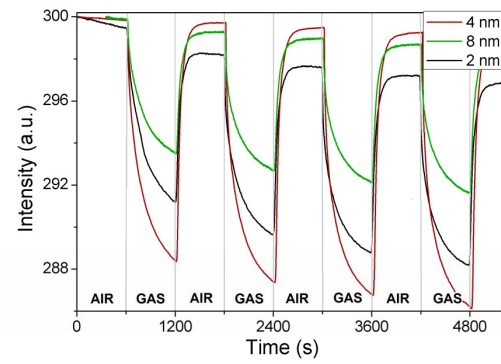


Fig. 4 - sensorgrams of optical response of annealed thin au films on acetone vapors.jpg

# Investigation on Nonlinear Optical Properties of MoS<sub>2</sub> Nanoflake, Grown on Silicon and Quartz Substrates

Friday, 20th October - 13:30 - Poster Session - Hall & Room 3 - Poster - Abstract ID: 609

*Mrs. samaneh bayesteh*<sup>1</sup>, *Dr. Seyedeh Zahra Mortazavi*<sup>1</sup>, *Dr. Ali Reyhani*<sup>1</sup>

*1. Imam Khomeini international university*

Two-dimensional (2D) materials like molybdenum disulfide (MoS<sub>2</sub>) are attracting substantial interest because of having optical and electronic properties and unique nonlinear optical response. Bulk or multilayer MoS<sub>2</sub> is a semiconductor with an indirect band gap of 1/2 eV. However, single-layer MoS<sub>2</sub> shows a direct band gap of 1/9 eV. This decreasing of the layers has been attracted attention of optics community like saturable absorption, nonlinear absorption, nonlinear scattering and nonlinear refraction. In this study, MoS<sub>2</sub> was directly synthesized by chemical vapor deposition (CVD), on different substrates including Si/SiO<sub>2</sub> and quartz, using MoO<sub>3</sub> and sulfide powders as precursor. The X-Ray diffraction patterns demonstrate the high crystallinity of MoS<sub>2</sub> on Si/SiO<sub>2</sub> and quartz substrates as seen in Fig 1. Scanning electron microscopy confirmed the formation of MoS<sub>2</sub> grown on both substrates as seen in Fig 2. According to line width and frequency difference between the E<sub>2g</sub><sup>1</sup> and A<sub>1g</sub> in Raman spectroscopy, it is inferred that the MoS<sub>2</sub> grown on Si/SiO<sub>2</sub> substrate is monolayer (frequency difference between two peaks: 20 Cm<sup>-1</sup>) and the MoS<sub>2</sub> grown on quartz substrate is multilayer (frequency difference between two peaks: 25 Cm<sup>-1</sup>) as seen in Fig 3. Moreover, by assessment of MoS<sub>2</sub> nanoflake band gap via UV-visible analysis, it verified the formation of few layer structures. In addition, the open-aperture and close-aperture Z-scan techniques were employed to study the nonlinear optical properties including nonlinear absorption and nonlinear refraction of the synthesized MoS<sub>2</sub>. All experiments were performed using a diode laser with a wavelength of 532 nm as light source. The monolayer MoS<sub>2</sub> synthesized on Si/SiO<sub>2</sub>, display considerable two-photon absorption. However, the multilayer MoS<sub>2</sub> synthesized on quartz displayed saturable absorption (SA) as seen in Fig 4. It is noticeable that both samples demonstrate obvious self-defocusing behavior. In general, few layered MoS<sub>2</sub> would be useful for the development of nanophotonic devices like optical limiters, optical switchers, etc.

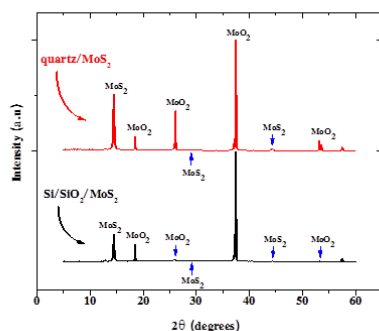


Figure 1.png

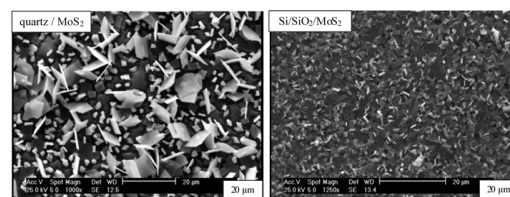


Figure 2.png

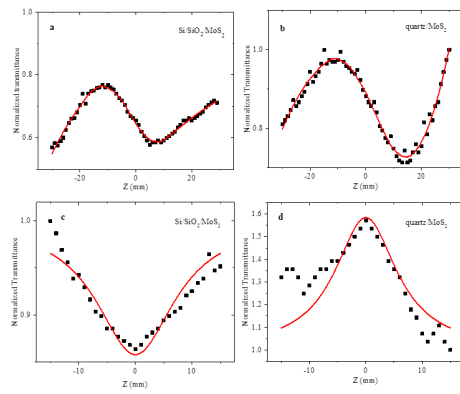


Figure 4.png

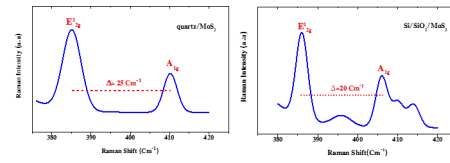


Figure 3.png

# Pegylated and amphiphilic Chitosan coated manganese ferrite nanoparticles for pH-sensitive delivery of methotrexate: synthesis and characterization

Friday, 20th October - 13:30 - Poster Session - Hall & Room 3 - Poster - Abstract ID: 770

**Mrs. leila karimi**<sup>1</sup>

<sup>1</sup>. Department of Materials Engineering, Islamic Azad University, Ahvaz, Iran

Magnetic nanoparticles (MNPs) are the major class of nanoparticles (NPs) with specific functional properties that make them good candidates for biomedical applications. Due to their response to the magnetic field, they can be used in targeted drug delivery systems. In current research, the MNPs were synthesized with the general formula of  $\text{Fe}_{1-x}\text{Mn}_x\text{Fe}_2\text{O}_4$  by the co-precipitation technique. First, the effect of the  $\text{Fe}^{2+}$  ions in the system was investigated. Succinic anhydride was used as the first stabilizer to prepare surface for binding two types of polymer, including Polyethylene glycol (PEG) and palmitoylated polyethylene glycol-grafted Chitosan (Cs-PEG-PA) were introduced as a polymeric shell. The composition, size, structure and magnetic properties of NPs were determined by the particle size analysis (PSA), X-ray diffractometry (XRD), Fourier transform infrared spectroscopy (FTIR) and vibrating sample magnetometer (VSM). Determining the well-defined properties of MNPs, methotrexate (MTX), as a common anticancer drug, was encapsulated into the coated MNPs. The drug encapsulation efficiency was as high as 92.8 % (Table 1) with the magnetization value of 19.7 emu/g (Fig 1). The in-vitro release pattern was studied, showing only 6% of the drug release in pH= 7.4 (as a model of the physiological environment) and 25% in pH= 5.4 (as a model of the tumor tissue environment) after 72 h (Fig 2). Based on these results, we may be able to introduce this specific system as a novel pH sensitive MNP system for MTX targeting to tumor tissues in cancer chemotherapy.

Fig 1. The Hysteresis loops of the NPs samples,  $\text{S-Fe}_{0.3}\text{Mn}_{0.7}\text{Fe}_2\text{O}_4$ ,  $\text{S-Fe}_{0.3}\text{Mn}_{0.7}\text{Fe}_2\text{O}_4\text{-PEG-PA-MTX}$  and  $\text{S-Fe}_{0.3}\text{Mn}_{0.7}\text{Fe}_2\text{O}_4\text{-Cs-PEG-PA-MTX}$  samples at room temperature.

Fig 2. The drug release pattern of the Cs-PEG-PA-coated MNP at the 1:1 weight ratio of the coating materials to MNPs in pH=7.4 and pH=5.4.

Table 4. Drug loading percentage and drug retention percentage in PEG-OH-coated and Cs-PEG-PAcoated MNPs.

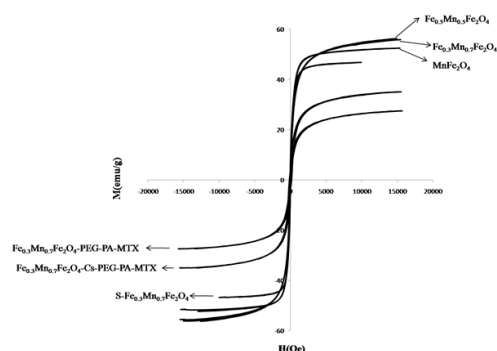


Fig 1.png

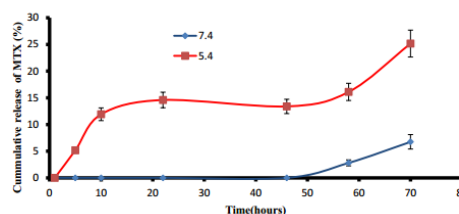


Fig 2.png

Sample	Nanoparticles: Polymer percentage	Drug Loading percentage	Drug retention percentage
S-Fe <sub>0.3</sub> Mn <sub>0.7</sub> Fe <sub>2</sub> O <sub>4</sub> PEG-MTX-	1:01	40.20%	81.10%
	01:00.5	38.40%	76.90%
	01:00.3	32.40%	64.80%
S-Fe <sub>0.3</sub> Mn <sub>0.7</sub> Fe <sub>2</sub> O <sub>4</sub> CS-PEG-PA-MTX-	1:01	48.20%	92.80%
	01:00.5	44.20%	88.40%
	01:00.3	40.50%	80.10%

Table 1.png

# UV-spectroscopy Method for Detecting the Chitosan Nanoparticles Formation

Friday, 20th October - 13:30 - Poster Session - Hall & Room 3 - Poster - Abstract ID: 69

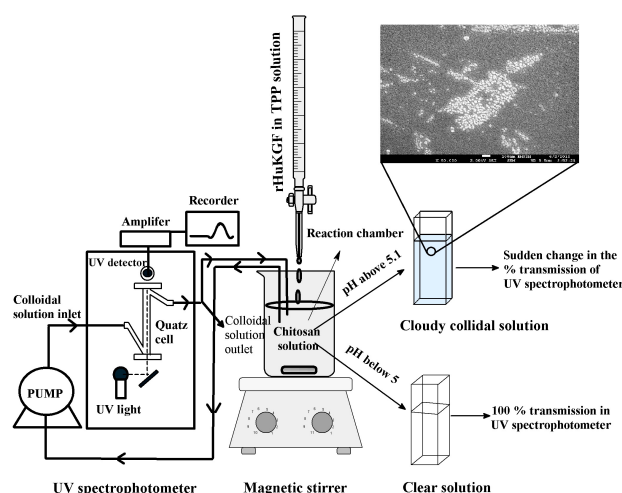
**Dr. Palanirajan Vijayaraj Kumar<sup>1</sup>, Mr. Marwan Abdelmahmoud Abdelkarim Maki<sup>1</sup>, Dr. Lee Ming Tatt<sup>1</sup>, Dr. Yeong Siew Wei<sup>1</sup>, Prof. Abu Bakar Bin Abdul Majeed<sup>2</sup>**

1. UCSI University, Faculty of Pharmaceutical Sciences, No. 1, Jalan Menara Gading, Taman Connaught, Cheras 56000, Kuala Lumpur., 2. Universiti Teknologi MARA, Faculty of Pharmacy, Research Management Institute, Shah Alam.

This research work reviews the UV spectroscopic technique developed for the detection of formation low molecular weight (LMW) chitosan mucoadhesive nanoparticles loaded by recombinant human keratinocyte growth factor (rHuKGF). These nanoparticles were prepared by the ionic gelation method. This method is one of the most widely accepted protocols for chitosan nanoparticles synthesis and it produces colourless and cloudy polydisperse chitosan nanoparticles. In the research work, the rHuKGF in tripolyphosphate (TPP) solution was added in drops to produce rHuKGF loaded LMW chitosan nanoparticles. The ionic gelating agent TPP will react with LWM chitosan at above pH5.2 and form the nanoparticles. During the formation of LWM chitosan nanoparticles, the rHuKGF will be entrapped in the nanoparticles. The main issue is that of maximizing the loading capacity of rHuKGF in LWM chitosan nanoparticles and avoiding its wastage. It depends on how much amount of rHuKGF in TPP solution was added to convert all the chitosan molecules in the solution to form as nanoparticles. A possible method for detecting the formation of these rHuKGF loaded chitosan nanoparticles is done by observing their light scattering property. In this study formation of nanoparticles was accurately detected by using UV-spectrophotometer at 231 nm and avoided the excessive addition of rHuKGF.

## ACKNOWLEDGMENT:

This project (Ref: FRGS/2/2014/SKK02/UCSI/02/1) is supported by Department of Higher Education, Ministry of Education Malaysia, under the Fundamental Research Grant Scheme (FRGS) Malaysia.



Schematic diagram showing the uv-spectroscopy method for detecting the formation of human keratinocyte growth factor loaded chitosan nanoparticles.jpg

---

## SYNTHESIS OF A NEW SPIRONUCLEOSIDE: SULFAHYDANTOCIDINE

---

Friday, 20th October - 13:30 - Poster Session - Hall & Room 3 - Poster - Abstract ID: 76

---

***Dr. Fatma-Zohra SMAINE<sup>1</sup>, Dr. Jean-yves Winum<sup>2</sup>***

***1. 1Laboratory of ecocompatible asymmetric catalysis. Departement of Chemistry, Faculty of Sciences, Annaba-Badji- Mokhtar University, BP12 Annaba, Algeria., 2. Institut des Biomolécules Max Mousseron (IBMM) UMR 5247 CNRS-ENSCM-Université de Montpellier***

The chemistry of spironucleosides, a type of nucleoside in which the anomeric carbon belongs simultaneously to the sugar ring and to the nitrogenated heterocyclic moiety, has received a considerable development in the last decade especially from the isolation of (+)-hydantocidin, the first natural spironucleoside<sup>1</sup>, which shows low toxicity for mammals and has herbicidal and plant growth-regulatory activities<sup>2</sup>. Glucopyranose analogue of hydantocidin was discovered in 1995 has a significant inhibition for glycogen phosphorylase<sup>3</sup>, an enzyme that catalyzes the regulation of glycogen degradation.

In this communication, we report the preparation of new spironucleoside the Sulfahydantocidine, starting from the D (+)-Ribolactone, using chlorosulfonylisocyanate to incorporate the sulfamoyl moiety.

1- Haruyama, H.; Takayanna, T.; Kinoshita, T.; Kondo, M.; Nakajima, M.; Haneishi, T. *J.Chem. Soc. Perkin Trans.1*, **1991**, 1637-1640.

2- Poland, B. W.; Lee, S. F.; Subramanian, M. V.; Siehl, D. L.; Andersen, R. J.; Fromm, H. J.; Honzatko, R. B. *Biochemistry***1996**, 35, 15753-15759.

3- Gyémant, G.; Kandra, L.; Nagy, V.; Somsak, L. *Biochem.Biophys. Res.Comm.***2003**, 313, 334-339.

# Fabrication and characterization of Rice Husk Aerogel-Polydimethylsiloxane (PDMS) Insulation Film

Friday, 20th October - 13:30 - Poster Session - Hall & Room 3 - Poster - Abstract ID: 288

**Ms. Yeoung Ah Noh<sup>1</sup>, Mrs. SINAEE SONG<sup>2</sup>, Ms. Jin Yi Kim<sup>3</sup>, Prof. Hee Taik Kim<sup>3</sup>**

**1. Department of Advanced Material and Science engineering, Hanyang University, 2. department of advanced material and science, 3. department of fusion chemical engineering, Hanyang University**

The windows have a large impact on the space heating demand and the indoor environment is affected by climate or daylight. Hence, aerogel has generally used as a film to reduce the coefficient of the window in the building. Silica aerogel is a suitable material to apply for insulation material with lower thermal conductivity than that of air to save interior energy. However expensive precursor and drying process were the main issue of the silica aerogel synthesis and practical usage.

We attempt to fabricate aerogel insulation film on glass for energy saving through the economic process under ambient pressure. Silica aerogel was synthesized from rice husk ash, which was an agricultural waste to be able to recycle. Taguchi design was used to optimize the parameters controlling the surface area of silica aerogel. The silica aerogel is prepared by sol-gel processing through acidic treatment and aging. The silica aerogel was obtained by modification of silica hydrogel surface and dry at ambient pressure. Finally, aerogel insulation film was fabricated by the different content of aerogel in polydimethylsiloxane (PDMS). Particle size, surface area and pore size of silica aerogel were respectively confirmed 21~24nm, 832.26 m<sup>2</sup>/g and 3.30nm by Scanning Electron Microscopy (SEM), Brunauer Emmett Teller (BET). Then thermal conductivity ( $\lambda$ ) of the aerogel insulation film was analyzed 0.002 W/mK by thermal wave system. This study demonstrates an eco-friendly and low-cost route to synthesize silica aerogel via rice husk and aerogel insulation film was obtained with low thermal conductivity similar to property of a commercial product.

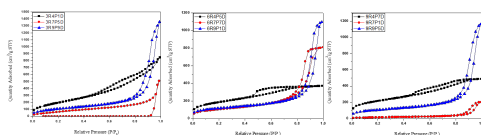


Figure1 n 2 adsorption and desorption isotherms obtained in this study.png

Sample name	Surface Area (m <sup>2</sup> /g)	Pore Volume (cm <sup>3</sup> /g)	Pore Size (nm)	S/N ratio
3R4P1D	803.2134	1.302576	5.5066	58.10
3R7P5D	252.7870	1.705966	2.30199	48.05
3R9P7D	404.6793	1.984050	16.7239	52.14
6R4P5D	648.9354	0.611904	3.5343	56.24
6R7P7D	225.8407	0.908649	17.8232	47.08
6R9P1D	380.4050	1.296178	11.5926	51.60
9R4P7D	656.6611	0.696341	4.0696	56.35
9R7P1D	348.4073	1.941976	20.7929	50.84
9R9P5D	357.9130	1.711594	18.9157	51.08

Table1 surface area average pore diameter and pore volume of aerogels obtained in this study..png

	PDMS	PDMS+ 0.1% silica aerogel	PDMS+ 0.2% silica aerogel	PDMS+ 0.4% silica aerogel
Thermal conductivity(W/mK)	0.15	0.065	0.048	0.002

Table2 thermal conductivity of silica aerogel pdms insulation film.png



# A built-in sensor with carbon nanotubes coated by Ag clusters for deformation monitoring of glass fiber/epoxy composites

Friday, 20th October - 13:30 - Poster Session - Hall & Room 3 - Poster - Abstract ID: 312

**Dr. Petr Slobodian<sup>1</sup>, Dr. Pavel Riha<sup>2</sup>, Dr. Robert Olejnik<sup>1</sup>, Dr. Jiri Matyas<sup>1</sup>, Ms. Silvia Pertegas<sup>3</sup>, Prof. Ralf Schledjewski<sup>3</sup>**

1. Tomas Bata University in Zlin, 2. Institute of Hydrodynamics, Academy of Sciences, Prague, Czech Republic, 3. Christian Doppler Laboratory for High Efficient Composite processing, Department of Polymer Engineering and Science, Montanuniversitaet Leoben, Leoben, Austria

Strain sensing composite materials have attracted considerable attention for their unique characteristics exceeding conventionally applied materials. Between different solutions and various types of transducers available for these applications, piezo-resistive strain sensors are among the most investigated ones usually based on conductive polymer composites prepared by embedding of electrically conductive fillers as carbon nanotubes into a polymeric matrix. This principle can be used for monitoring of deformation or stress stimulus in elongation or compression. The responses are sensitive and reversible with sufficient durability in the dynamic loadings measured by a macroscopic electrical resistance change.

In our contribution we introduce a strain sensing composite material composed of electrically conductive entangled network of Ag decorated multiwalled carbon nanotubes (MWCNTs) integrated into the glass fiber/epoxy composite. A vacuum infusion technique was used for the composite fabrication. The experimental results revealed that an integrated strain sensing exhibit long term electromechanical stability which was linked to the level of strain in the host glass fiber/epoxy structure. It has been proven that modification of pristine MWCNTs with Ag nanoparticles increase the sensitivity to applied strain. Simultaneously pre-strain stimulation was also applied to further enhance detection ability. The resistance sensitivity, quantified by a gauge factor, increased more than hundredfold for a pre-strained sensor with Ag decorated nanotubes in comparison with the value of about 5 for sensor with pristine nanotubes. This is a substantial increase which ranks this new material among strain gauges with the highest electromechanical sensitivity. The obtained data indicated also a reasonable stability of the measurement with no effect of load alterations on the sensor resistance changes.

This work was supported by the Ministry of Education, Youth and Sports of the Czech Republic, under the project Czech-Austrian mobility (program KONTAKT II) project-7AMB16AT033 and by the OeAD, the Austrian Agency for International Mobility and Cooperation in Education Research in collaboration of the Thomas Bata University (TBU) in Zlin and Montanuniversitaet in Leoben (MUL). This work was also supported by the Ministry of Education, Youth and Sports of the Czech Republic – Program NPU I (LO1504).

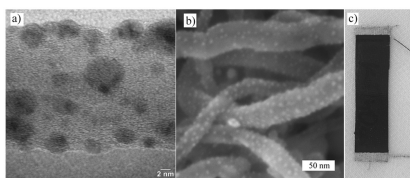


Fig. 1 a) HRTEM detailed view of the structure of individual MWCNT with deposited Ag nanoparticles; b) SEM micrographs of the surface of entangled MWCNT network made of nanotubes decorated by Ag; c) The inbuilt MWCNT layer with attached silver electrodes and Cu wiring into epoxy glass fibre composite.

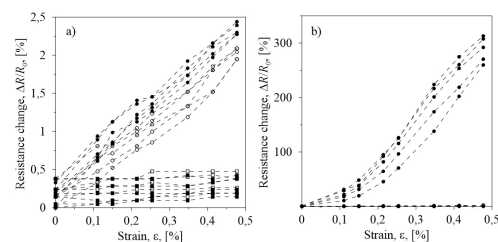


Fig. 2 The resistance change of the sensor integrated into the glass fiber/epoxy composite during its elongation and relaxation course denoted by circles and squares, respectively. The symbols for not pre-strained sensor are open and for the pre-strained sensor by 0.94 % strain

Tem and sem analysis of mwcnt.jpg

Resistance change on strain.jpg

# The effect of processing variables on the morphology of electrospun nanofibers

Friday, 20th October - 13:30 - Poster Session - Hall & Room 3 - Poster - Abstract ID: 323

**Dr. Muhammad Ali Zulfikar<sup>1</sup>, Mrs. Irlin Afrianingsih<sup>1</sup>, Dr. Muhamad Nasir<sup>2</sup>, Dr. Anita Alni<sup>1</sup>**

*1. Institut Teknologi Bandung, 2. Indonesian Institute of Sciences*

The electrospinning is a straightforward way to produce ultrafine fibrous membranes from polymer solutions or melts under a high electric voltage. In the electrospinning process, some parameters such as polymer concentration, feeding rate of the polymer solution, additives, humidity, viscosity, surface tension, applied voltage, and nozzle-to ground collector distance will affect the fiber diameter and morphology. The aim of present work is to investigate the effects of processing parameters including the spinning voltage and solution concentration on the morphology of the fibers formed. The solutions used in the electrospinning experiments were prepared using Poly(vinylidene fluoride) (PVDF). This material was dissolved in N,N-dimethylformamide (DMF) to make solutions with concentrations ranging from 16 to 20 wt%. These solutions were spun from a 5 ml plastic syringe connected to a nozzle using a plastic hose (2 mm in diameter) then clamped to a ring stand that was 15 cm above a grounded metal screen and using voltages ranging from 16.0-20.0 kV. Optical micrographs of electrospun fiber mats produced were taken with a Nikon Eclips E400. Effects of PVDF/DMF concentrations on morphology of the nanofibers formed are shown in Fig. 1. These images demonstrate that formation of the fiber depends on the polymer concentration. The increase in the polymer concentration caused beads on the string disappeared and morphology of the fibers produced becomes more uniform and continuous.

The effect of applied voltage on morphology of the nanofibers formed can be seen at Fig. 2. As voltage is increased, the electrospun fibers produced have essentially a cylindrical morphology, but there is a distinct decrease in number of bead defects present in the fiber mat. At 20.0 kV, the morphology of the fibers produced becomes more uniform, the bead defects are lost and the fibers are continuous.

Increasing the applied voltage increased the force that overcomes the surface tension of the polymer solution. This will also increase the amount of polymer sprayed during the ESD process.

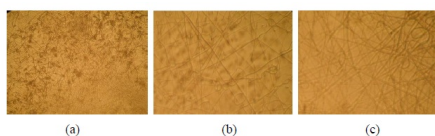


Fig. 1. Optical micrographs of nanofiber by electrospinning from PVDF solution at different concentrations (a) 16% wt (b) 18% wt and (c) 20% wt.

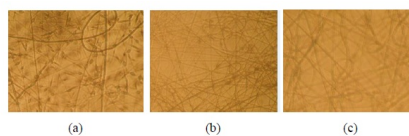


Fig. 2. Optical micrographs of nanofiber by electrospinning from PVDF solution at different voltage applied (a) 16 kV (b) 18 kV and (c) 20 kV.

Fig. 1.jpg

Fig. 2.jpg

# In a SiNx-based membrane for EUV pellicle, Evaluation of Stress Variation and Mechanical Strength According to Film Deposition Process Conditions

Friday, 20th October - 13:30 - Poster Session - Hall & Room 3 - Poster - Abstract ID: 543

**Mr. Gi-sung Lee<sup>1</sup>, Mr. Kwang-hee Kim<sup>1</sup>, Mr. Dong-wook Lee<sup>1</sup>, Mr. Hae-chul Hwang<sup>1</sup>, Mr. Nam-soo Park<sup>1</sup>, Mr. Hee-oh Kang<sup>1</sup>, Mrs. Kyung-jin Park<sup>1</sup>, Mr. Changho Seo<sup>1</sup>**

**1. National Nanofab Center**

During the EUV exposure process, EUV pellicles are needed to protect the EUV mask from defects and contamination that occur in the EUV lithography process. The EUV pellicle must be made of a thin film membrane for high EUV wavelength transmittance. Moreover, since the inside of the EUV exposure tool is in a high vacuum environment, the EUV pellicle gives stress to the membrane thin film. Therefore, the EUV pellicle can be easily deformed during the exposure process. It is very important to ensure mechanical safety to withstand such environments. In this paper, SiNx thin film was deposited by LPCVD method. The residual stress of the thin film was varied by changing the composition ratio of the gas (three conditions were evaluated). As the Si component becomes richer, the refractive index of the SiNx thin film increases and the etching rate of the KOH chemical increases. It can be confirmed that this is due to the change of stress of SiNx thin film. As a result, when the SiH<sub>2</sub>Cl<sub>2</sub>/NH<sub>3</sub> gas composition ratio is 2.5: 1, the SiNx thin film has a tensile strength of less than 50 MPa. It was confirmed that it is a very ideal condition without wrinkle phenomenon in membrane fabrication. The mechanical strength of the SiNx thin film was evaluated by changing the stress of the thin film. The evaluation method is bulge test, which is a method to confirm the deflection of the thin film and burst pressure by applying a pressure difference across the thin film. As a result of the bulge test, SiNx thin film deposition conditions of SiH<sub>2</sub>Cl<sub>2</sub>/NH<sub>3</sub> gas composition ratio of 2.5: 1 showed higher burst pressure and longer time than other conditions. (SiH<sub>2</sub>Cl<sub>2</sub>/NH<sub>3</sub> = 4: 1 condition is caused by wrinkle phenomenon where deflection is large). As a result, it was confirmed that the stress of the SiNx thin film could be improved by changing the SiNx thin film deposition conditions, and this result showed that the mechanical strength of the thin film could be improved.

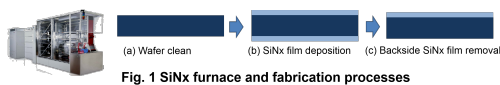


Fig. 1 SiNx furnace and fabrication processes

Sinx fabrication.png

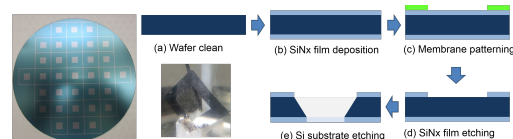


Fig. 2 Fabrication processes for SiNx membrane

Sinx membrane fabrication.png

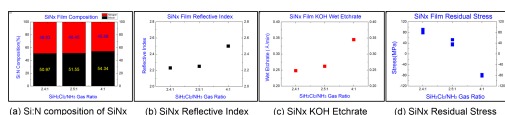


Fig. 3 Characteristics of SiNx film by deposition conditions

Sinx characteristics.png

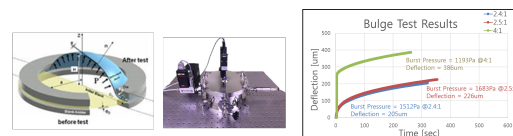


Fig.4 Bulge test result

Bulge test result.png

## Angle aligned electrospun metal fibers and its potential for stretchable electrodes for wearable electronics.

Friday, 20th October - 13:30 - Poster Session - Hall & Room 3 - Poster - Abstract ID: 590

**Dr. doo-hyeb youn<sup>1</sup>, Dr. Changbong Yeon<sup>1</sup>, Dr. Sun Jin Yun<sup>2</sup>**

**1. ETRI, 2. 1Laboratory of ecocompatible asymmetric catalysis. Departement of Chemistry, Faculty of Sciences, Annaba-Badji-Mokhtar University, BP12 Annaba, Algeria.**

Figure 1 demonstrate the conventional parallel fiber align using two parallel bars. Where align bar is composed of aluminum. Figure 1 illustrates the schematic setup used to align fiber using the specially designed jig. It is essentially the same as the conventional electrospinning configuration except for the use of an align-jig put on the surface of collector. The parallel aligned and diagonal aligned arrays of the metal fibers were fabricated on stretchable rubber substrates using the alignment jig. After clamping those aligned fibers by two fixtures connected to the current-voltage measurement system, they were stretched in specific elongation directions and lengths using a mechanical apparatus. When the parallel aligned metal lines (formed using the parallel-type collector) were stretched parallel to their alignment direction up to 10 %, these metal lines were broken due to the applied tensile force. However, diagonal aligned fibers can avoid this parallel alignment between the metal fibers and this misalignment can dissipate the applied tensile force. For example, the sample of diagonal alignment could be stretched up to ~ 90 % in strain with an increase in resistance of ~ 40% (figure 2). This mechanical stretchability of the metal fiber was superior to that of ITO, which can be cracked by applying a tensile strain of 1%. The locally broken parts of the parallel aligned fibers that resulted from stretching them into their alignment direction with a 10% strain. After stretching further, the metal fiber with the cracked lines became nonconductive.

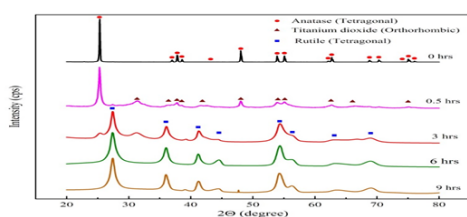
# Investigation on the Effect of Preparation Techniques of Anatase on its Structural and Optical Properties

Friday, 20th October - 13:30 - Poster Session - Hall & Room 3 - Poster - Abstract ID: 618

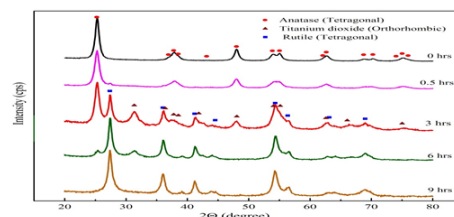
**Mrs. Zakiya Rashid<sup>1</sup>, Ms. Faten Almutawa<sup>1</sup>, Dr. Latifah Alhajji<sup>2</sup>**

**1. Kuwait Institute for Scientific Research (KISR), 2. Kuwait Institute for Scientific Research**

The structural transformations of anatase-TiO<sub>2</sub> (a-TiO<sub>2</sub>) nanopowders have been explored upon its synthesis via different routes. Mechanically-induced synthesis was conducting by subjecting vibratory ball milling on microscale a-TiO<sub>2</sub> for different time intervals at ambient temperature. On the other hand, nano-scale a-TiO<sub>2</sub> was prepared by sol-gel method via the hydrolysis of titanium tetrachloride (TiCl<sub>4</sub>) followed by ball milling. The synthesized nano-powders were characterized by XRD, SEM, HR-TEM and UV-vis reflectance spectroscopy. Band gap was calculated by applying Kubelka-Munk equation on the UV-visible diffuse reflectance spectra. This study showed that the mechanical ball milling stimulates TiO<sub>2</sub> (Fig. 1) to undergo phase transformations from a-TiO<sub>2</sub> (tetragonal) to srilankite (s-TiO<sub>2</sub>-orthorhombic) then to rutile (r-TiO<sub>2</sub>-tetragonal). Within 0.5 hrs of milling, s-TiO<sub>2</sub> peak evolved in the bulk powder then completely transformed to rutile after 6 hrs. On the other hand, TiO<sub>2</sub> nanoparticles (Fig. 2), which were prepared via sol-gel method followed by mechanical treatment, had shown to be more resistance towards phase transformation. The phase transformation was slower. It took 9 hrs of milling to completely transform into rutile phase. Both synthesized nano powders experienced a shift in band gap towards visible region by 0.28 and 0.23 eV, respectively after 9 hrs of milling.



Ball-milled tio2.png



Sol-gel tio2.png

# Facile photocatalyst sedimentation: Utilizing isoelectric point for immediate TiO<sub>2</sub> nanoparticles separation.

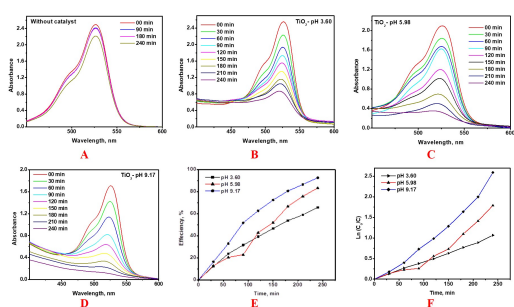
Friday, 20th October - 13:30 - Poster Session - Hall & Room 3 - Poster - Abstract ID: 709

**Dr. Entesar Al-Hetlani<sup>1</sup>, Mr. Mohamed O. Amin<sup>1</sup>, Dr. Metwally Madkour<sup>1</sup>**

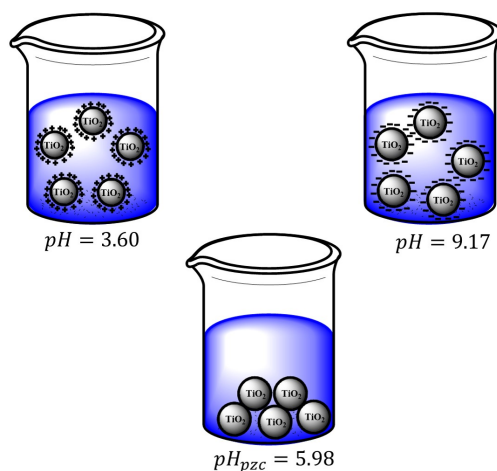
<sup>1</sup>. Kuwait University

TiO<sub>2</sub> photocatalysis is commonly utilized in diverse applications such as environmental waste management, biomedical and energy fields. The present study demonstrates the effect of temperature on the characteristics of TiO<sub>2</sub> nanoparticles (NPs) using XRD, UV-Vis, N<sub>2</sub> sorpometry and TEM techniques. The optimum surface area of the photocatalyst was obtained at 60°C.

Afterwards, rapid photodegradation of Rhodamine 6G dye (R6G) with efficiency of 92.5% at pH= 9.17 was accomplished using the optimized NPs. The main focus of this study is to establish a new avenue that can be used to separate the photocatalyst from the reaction medium after the photodegradation experiment is completed. In this study, the photocatalyst was completely detached from the reaction medium in 3 minutes without utilization of coagulant agents or magnetic NPs. This was lucratively accomplished by adjusting the pH of the medium to match the isoelectric point (pH<sub>PZC</sub>) of the photocatalyst and annulling its surface charge, hence rapid sedimentation was observed by means of turbidimetry. This new method has proven to be simple, rapid, and applicable to all types of photocatalysts on the industrial scale.



a-d uv-vis spectra of photocatalytic degradation of r6g dye e plots of ln coc vs. time for photodegradation of r6g and f percent r6g degradation vs. time.jpg



A schematic representation of annulling the surface charge of tio2 nps and its sedimentation..jpg

# Thermal and non-thermal explosion in metals ablation by femtosecond laser pulse: classical approach of the Two Temperature Model

---

Friday, 20th October - 13:30 - Poster Session - Hall & Room 3 - Poster - Abstract ID: 735

---

**Mr. Ahmed Abdelmalek<sup>1</sup>, Dr. Zeyneb Bedrane<sup>1</sup>**

*1. Tlemcen University, Theoretical Physics laboratory, Physics Dpt., Sciences Faculty*

It has been experimentally demonstrated that metal ablation by ultrashort laser pulses at femtosecond regime is very different from that due to short laser pulses owing to the difference between the corresponding physical mechanisms that take place. In literature, there is no great differences between the theoretical models applied for the both regimes.

In this work we propose a classical approach with a two Temperature Model TTMc to study a copper target irradiated by single laser pulse with 120 fs at 800 nm in air room. In our modeling we consider the metal film during the irradiation as an ideal plasma. Our numerical result are compared to those obtained by the existing TTM and also with the experimental data.

It is well known that the metal ablation mechanism by short laser pulses mainly occurs by phase explosion (thermal explosion), then our purpose is to bring an answer to the rising question: what is the physical mechanism responsible for the ablation of metals by ultrashort laser pulse?

Our results show that, successively, a thermal and non-thermal explosion occurs in metal ablation by ultrashort laser pulse.



# Local electronic interaction effects on Dynamical and static spin susceptibilities of doped gapped graphene nanoribbon

Friday, 20th October - 13:30 - Poster Session - Hall & Room 3 - Poster - Abstract ID: 738

***Dr. Hamed Rezania***<sup>1</sup>

*1. Razi University*

We present the behaviors of both dynamical and static spin susceptibilities of doped gapped armchair graphene nanoribbon using the Green's function approach in the context of Hubbard model Hamiltonian.

Specially, the effects of spin polarization and gap parameter on the spin excitation modes of armchair graphene nanoribbon are investigated via calculating correlation function of spin density operators.

The electron density dependence of static charge structure factor of armchair graphene nanoribbon is studied. The effects of both gap parameter and magnetic ordering on the static structure factor are discussed in details.

In experimental viewpoint, the spin excitation plasmonic modes of electron gas in graphene nanoribbon or the other systems have been obtained by neutron scattering. Because neutrons have been coupled with electrons via spin degrees of freedom, the plasmonic spin excitation spectrum has been manifested.

In this theoretical work, the dynamical spin susceptibility components have been calculated by quantum many particle method.

The imaginary part of dynamical spin susceptibilities is proportional to inelastic cross section of neutron beam. Thus the main research goal of this work is the study of plasmonic spectrum of graphene nanoribbon in the presence of electron electron interaction via theoretical calculation of dynamical susceptibility. The frequency position of sharp peaks in dynamical spin susceptibility presents the magnetic plasmonic excitation spectrum of graphene nanoribbon.

The frequency position of sharp peak in dynamical spin susceptibility introduces the plasmonic oscillations of the mentioned nano structure. The effects of magnetic ordering on the behavior of static and dynamical charge susceptibilities have been focused.

Figure captions:

Fig1: Transverse dynamical spin susceptibility of undoped gapped graphene nanoribbon versus normalized frequency for different values of gap parameter and for zero magnetization at zero temperature

Fig2: Transverse dynamical



spin susceptibility of doped gapped  
graphene nanoribbon versus normalized frequency  
for different values of normalized chemical potential and for full spin polarization at  
zero temperature.

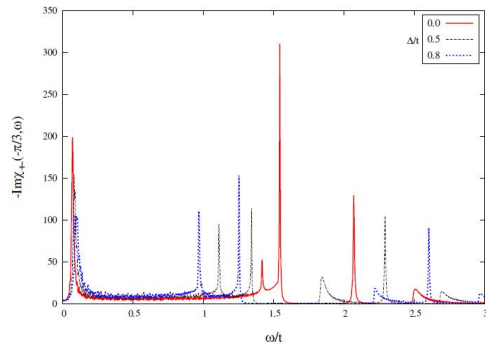


Fig1.jpg

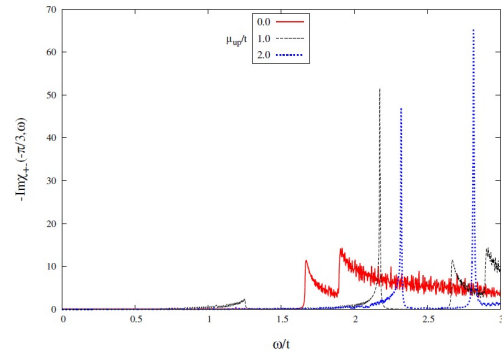


Fig2.jpg

# The method of synthesizing of superhydrophobic surfaces by PECVD

Friday, 20th October - 13:30 - Poster Session - Hall & Room 3 - Poster - Abstract ID: 798

**Ms. Zhuldyz Otarbay<sup>1</sup>, Dr. Sagi Orazbayev<sup>1</sup>, Dr. Maratbek Gabdullin<sup>1</sup>, Dr. Merlan Dosbolayev<sup>1</sup>, Prof. Tlekkabul Ramazanov<sup>2</sup>, Mr. Askar Zhunisbekov<sup>2</sup>, Mr. Dulat Omirbekov<sup>1</sup>**

*1. National Nanotechnology Laboratory of the Open Type, Al-Farabi Kazakh National University, 2. Scientific and Research Institute of Experimental and Theoretical Physics, Al-Farabi Kazakh National University*

Nowadays the wettability of solid surfaces is a decisive factor in many applications. Control of the hydrophobic or hydrophilic property is a key aspect for microelectronics, antifouling coatings, anti-ice, light industry, etc. The wettability of the surface generally depends on two factors: surface chemistry and surface roughness. If both parameters are used properly, it is possible to develop superhydrophobic surfaces with a contact angle close to 180°, with very small grazing angle (lotus effect). There are different methods of obtaining hydrophobic surfaces, such as phase separation, CVD, electrochemical deposition, plasma method, crystallization control, wet chemical reaction, sol-gel processing and so on.

In this work, firstly, we got superhydrophobic surfaces using a simple one-step process, based on polymerizing carbonaceous nanoparticles in plasma and deposition on silicon wafer. Nanoparticles arising in plasma polymerization process are typical example of plasma polymers, i.e. materials, which in difference to conventional structured polymers, do not consist of repeating units. In addition, we researched how wetting characteristics were changing when processed in different plasma environments. We focused on the process of growth of nanoparticles and their subsequent deposition. Specific feature of this process is the negative charge of the nanoparticles. Once the particles reach a size of several nanometers, they quickly collect a negative charge (due to the high mobility of the electrons in the plasma). As a result, the particles are held in positive plasma potential, i.e. they are levitating in the discharge, where they continue to grow due to the accumulation of neutral radicals and positive ions. After the plasma turns off, particles lose the negative charge and fall down to the lower electrode. Every time plasma is turned off a certain amount of nanoparticles will fall onto the substrate, which is located on the lower electrode. The SEM image shows that the synthesized materials have a rough surface with contact angles of from 100° to 165°, depending on the plasma parameters. Experimentally it has been found, that the number of particles on a silicon substrate depends on the number of cycles, i.e. the film's hydrophobic feature (contact angle) increases with the number of cycles.

# Shift of semimetal-semiconductor bond direction on “0 1 1” to “1 1 1” Bismuth quasi-two- dimension system

Friday, 20th October - 13:30 - Poster Session - Hall & Room 3 - Poster - Abstract ID: 593

**Dr. Ahmad Yazdani<sup>1</sup>, Mr. Sajad Hamreh<sup>1</sup>**

*1. Tarbiat Modares University*

## Abstract

The electronic structure of the nanocrystallines and quasi-two-dimensional systems strongly impressed by the thermodynamic-behavior mainly due to excess of hidden surface free- energy. Therefore, the stability of crystalline structure's change could be related to band-offset of bond rupturing of atomic displacements. Although “Be” has been found to be one of the metallic surface states characterized by semimetal character, its atomic-orbitals are closed and its diboride composition  $\text{BeB}_2$  is surprisingly emerged as a superconductor with too much low-value of  $T_c=0.7$ . The character of topological insulator Bi which is more expressed and quickly oxidizing could be an intriguing question. Besides all of the characters behave spatial like strong sensitive oxidation and electronic structure in the absence of Oxygen. This effect on the electronic-structure of “Bi” is supposed to be the cause of strong-correlated electron system emerging on the competition of super-double exchange with strong spin-orbit coupling resulted to the bond-exchange on direction of redistribution of surface chemical bond formation before any reconstructive structure. Where

- The metallic direction of electronic structure “0 1 1” is changed to “1 1 1” semiconductor direction(fig1). Where the effect of L.S is not observable around the fermi surface (fig1.b). This effect is more evident on the local density of state. The effect could be consequence of sliding deformation which is the cause of privation in formation mechanism of quasi-two dimension in “0 1 1” direction resulted to bond rupturing atomic displacement of semi metallic character of “1 1 1”.
- Strong effect of spin-orbit interaction on splitting of the valance to nearly conduction band (fig2). The effect of the L.S is strongly evident around the fermi surface (fig2.b).

Which could be a question whether the Bychkov-rashba SOI in the conduction band resulted from the electric field in the valence band or the dynamical Landau-ginzburg-broken symmetry could be the cause, which is the main goal of this article.

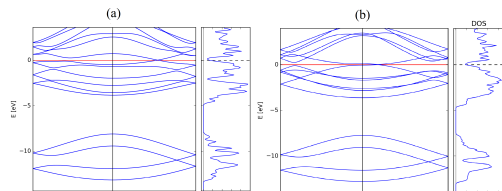


Fig1.png

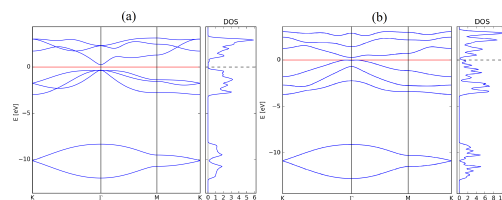


Fig2.png

# Metal nanolayer deposited highly stable Ag thin films and their optical properties

Friday, 20th October - 13:30 - Poster Session - Hall & Room 3 - Poster - Abstract ID: 438

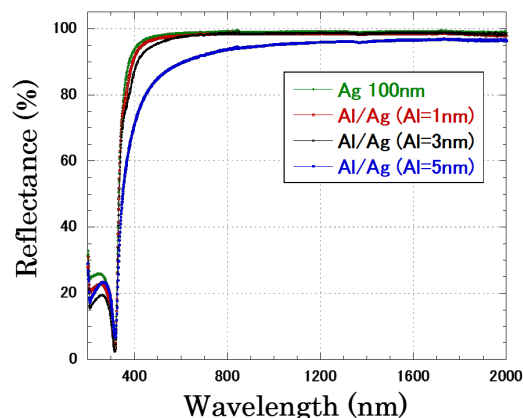
**Prof. Midori Kawamura<sup>1</sup>, Dr. Takayuki Kiba<sup>1</sup>, Prof. Yoshio Abe<sup>1</sup>, Dr. Kyung Ho Kim<sup>1</sup>, Prof. Hiroshi Murotani<sup>2</sup>**

1. Kitami Institute of Technology, 2. Tokai University

Silver (Ag) is a material with excellent electrical, optical and thermal properties. However, Ag thin films readily agglomerate and become rough or even discontinuous films by heat treatment, because of the easy migration of Ag atoms. We have developed thermally stable Ag thin film structures where Ag film is sandwiched with surface and interface metal nanolayers, for example, Al/Ag/Al structure. The deposited Al metal nanolayer becomes Al oxide nanolayer by natural oxidation. This is a simple and convenient method to prepare oxide nanolayer, which can avoid any damage to surface of the Ag film.

In the present study, we investigated optical properties of the multilayers. It is known that Al film shows lower reflectance than Ag film except ultraviolet region. On the other hand, Al oxide is transparent, which may give no influence on reflectance. Therefore, objective of the study is to investigate influence of the Al surface layer on reflectance. We compared the properties of same multilayer structures by different deposition methods.

We prepared multilayers consisting of Al surface layer and Ag thin film by rf sputtering (SP) and vacuum evaporation (EV). The films were deposited on glass substrates. The obtained films were characterized using XRD, AFM, and the optical reflectance spectra were measured by a spectrophotometer. As an influence of Al nanolayer on the specular reflectance, the reflectance of Al/Ag multilayer were almost the same as Ag films where Al thickness was 1 nm (SP) and 1 and 3 nm (EV). It is considered that Al surface layer was fully oxidized where the thickness was 1 nm, but Al remains in metal state where the thickness was further increased. In conclusion, we confirmed that metal nanolayer deposited Ag films which possess high thermal stability, also achieve high optical reflectance.



Reflectance.png

## Phisico-chemical properties of zinc coating with modified detonation nano diamonds additives

---

Friday, 20th October - 13:30 - Poster Session - Hall & Room 3 - Poster - Abstract ID: 848

---

***Ms. Elvina Osmanova<sup>1</sup>, Ms. Ksenia Svir<sup>1</sup>***

*1. St. Petersburg State Technological Institute*

Despite the widespread of industrial coverings (about 40% of all galvanic coverings fall at galvanization process), there are few studies about the application of nanocarbonic additives in this process.

Zinc is associated with a combination of resistance to the environment and low prices of inorganic zinc compounds. Its standard capacity is 0, 76 V in a significant negative potential of iron is 0, 40 V. Thus, being the anode against it, zinc performs an electrochemical protection.

Rising requirements to such settings have led to the creation of composite electrochemical coverings.

In this research we used A-1DM (by “Chemeta” company). This addition increases the cathodic polarization, changing the polarization curves towards negative potentials.

One of the rapidly developing ways for improving physical and chemical qualities of coverings is the use of dispersible materials. The addition of heterogenic particles to the electrolytic settings helps to create a composite electrochemical covering (CEC).

Nano diamonds are the composite additives of a new generation. They are much better than previous supplements and haven't got any drawbacks. They are easily regenerated, evaluated and are environmentally friendly.

The main functional of zinc coating quality is the corrosion resistance, which increases when getting dense cryptocrystalline layers, which are usually got by a strong polarization changing to negative potentials. The introduction of nanodiamonds greatly helps to such shift and getting cryptocrystalline coverings.

---

# Fabrication Techniques for Platelet-Functionalized Nanofibers

---

Friday, 20th October - 13:30 - Poster Session - Hall & Room 3 - Poster - Abstract ID: 849

---

***Ms. Karolina Vocetkova<sup>1</sup>, Mr. Matej Buzgo<sup>2</sup>, Ms. Vera Sovkova<sup>1</sup>, Prof. Evzen Amler<sup>3</sup>***

*1. Institute of Experimental Medicine Czech Academy of Sciences, 2. University Centre for Energy Efficient Buildings, 3. Institute of Biophysics 2nd Faculty of Medicine, Charles University*

Wound healing is a complex biological process. Disruption of the interplay of various signal molecules, cells and extracellular matrix may lead to chronic wounds. Chronic wound care is becoming a worldwide issue and thus, novel wound dressings are needed. Electrospun polymeric nanofibrous mats can serve as such dressing. They mimic extracellular matrix and can be functionalized with bioactive substances. Suitable source of bioactive substances are platelets, as they contain broad spectrum of growth factors in physiological ratio. The aim of this work was to develop and characterize platelet-functionalized polymer nanofiber to promote keratinocyte metabolic activity and proliferation.

Polymeric polycaprolactone (PCL) nanofibers were prepared using the needleless electrospinning technique. Firstly, the PCL was functionalized by plain adhesion of platelets to the surface of nanofibers. Secondly, to improve the release characteristics of the composite scaffold, the platelets were embedded into PCL/polyvinyl alcohol (PVA) coaxial nanofibers, using the coaxial needleless electrospinning technique. The composite scaffolds were then seeded with keratinocytes and the influence of released growth factors on behavior of the keratinocytes was investigated.

The data showed that PCL scaffolds functionalized with platelets significantly promoted the initial adhesion, proliferation and metabolic activity of the seeded keratinocytes in comparison to the plain PCL control. The results indicate that such composite scaffolds are very promising in the field of regenerative medicine.

The study was supported by the Ministry of Education, Youth and Sports of the Czech Republic within National Sustainability Program I: projects No. LO1605, LO1508, LO1309 and the Internal Grant Agency of the Ministry of Health of the Czech Republic project No. 17-32285A.

---

# Testing the Biocompatibility of Fully Porous Ceramics for Bone Tissue Engineering

---

Friday, 20th October - 13:30 - Poster Session - Hall & Room 3 - Poster - Abstract ID: 850

---

***Ms. Vera Lukasova<sup>1</sup>, Mr. Premysl Stastny<sup>2</sup>, Mr. Martin Trunec<sup>2</sup>***

*1. 1 University Centre for Energy Efficient Buildings, Czech Technical University 2 Laboratory of Tissue Engineering, Institute of Experimental Medicine, Czech Academy of Sciences, 2. CEITEC - Central European Institute of Technology Brno University of Technology*

A suitable cell-free scaffold for use in bone tissue engineering should promote cell migration into the site of the defect and should further support cell adhesion. The ceramic scaffolds consisting of hydroxyapatite (HA) or tricalcium phosphate (TCP) are biocompatible with hard tissues, offer osteoconductivity and bioactivity and, moreover, are not cytotoxic. Controlled degradation of ceramic scaffolds offers sufficient support until the new bone is formed. Furthermore, hydroxyapatite scaffolds are materials widely used in regeneration of bone. HA enhances the bioactivity of the scaffold as it provides a source of calcium and phosphate ions that are important for the process of bone mineralization. The present study focuses on comparison of four differently composed ceramic scaffolds and their effect on human mesenchymal stem cells (hMSC) adhesion, proliferation and metabolic activity.

Ceramic scaffolds were seeded with hMSC and cultured for 14 days in growth medium. The metabolic activity of cells was determined using the MTS assay, cell proliferation was measured by the PicoGreen assay, adhesion and proliferation was further monitored by confocal microscopy and scanning electron microscopy. According to the obtained data, all of the tested materials are biocompatible. However, the HA/TCP scaffold showed to be the most promising in hMSC stimulation. The topic will be further investigated.

Acknowledgement: This study has been supported by the Internal Grant Agency of the Ministry of Health of the Czech Republic (MZ-VES project no. 17-31276A) and the Ministry of Education, Youth, and Sports of the Czech Republic (Research Program NPU I:LO1309 and LO1508).

# Collagen type I based foamed scaffold for bone defects therapy

Friday, 20th October - 13:30 - Poster Session - Hall & Room 3 - Poster - Abstract ID: 851

***Ms. Veronika Blahnova<sup>1</sup>, Dr. Eva Filova<sup>2</sup>, Ms. Veronika Svachova<sup>3</sup>, Mr. Martin Trunec<sup>3</sup>, Dr. Lucy Vojtova<sup>4</sup>, Prof. Evzen Amler<sup>5</sup>***

*1. Institute of Biophysics 2nd Faculty of Medicine, Charles University, Institute of Experimental Medicine of Czech Academy of Sciences, University Centre for Energy Efficient Buildings, 2. Institute of Biophysics 2nd Faculty of Medicine, Charles University, Institute of Experimental Medicine of Czech Academy of Sciences, 3. Central European Institute of Technology, 4. Central European Institute of Technology, Sciteg, a.s., 5. Institute of Biophysics 2nd Faculty of Medicine, Charles University, University Centre for Energy Efficient Buildings*

Bone defects as results of an illness or an accident belong among those with frequent healing complications. One of bad healing wounds are so called critical size bone defects. Such a defect has low capacity to regenerate and also a bad prognosis of tissue function restoration.[1] Implantation of a biocompatible non-cellular collagen type I scaffold with addition of specific inorganic substances naturally occurring naturally in bone extracellular matrix could work as a chanceful alternative therapy approach of these injuries. In this study we examined osteogenic potential of porous scaffolds made from the material Lyopor (Sciteg, a.s.) containing collagen type I, tricalcium phosphate and calcium phosphate in various modifications. Size of pores was measured by scanning electron microscopy. For determination of the level of cellular metabolism an MTS assay based on reduction of substrate by mitochondrial enzymes was used. We also performed rt-PCR in order to quantify relative mRNA expression of osteogenic markers RunX2 and collagen type I. For visualization of bone extracellular protein osteocalcin an immunohistochemical staining was used. Samples were observed using confocal microscopy. After 21, respectively 35 days of cultivation we showed, that any of tested scaffolds does not have a cytotoxic effect on the human mesenchymal stem cells originating from bone marrow. According to the data obtained from rt-PCR we assume the most suitable for osteogenic proteins mRNA expression scaffold composed from collagen type I with hydroxyapatite addition. This carrier also supported proliferation of the cells, which means that its 3D structure was sufficient for mechanical stimulation and support. Strong osteocalcin synthesis was observed on scaffolds containing hydroxyapatite both calcined and non-calcined.

Reference:

[1] Amini, A. R., Laurencin, C. T. & Nukavarapu, S. P. Bone tissue engineering: recent advances and challenges. Crit. Rev. Biomed. Eng. 40, 363–408 (2012).

Acknowledgement: This study was supported by the Ministry of Education Youth and Sports: RP NPU I:LO1309, RP NPU I:LO1508, LQ1601, by the Czech Science Foundation Grant No. 15-15697S, the Ministry of Health: VES 16-28637A and The Internal Grant Agency of the Ministry of Health of the Czech Republic 17-32285A.



---

## Investigation on the piezoelectrical properties of single layered MoS<sub>2</sub> at various conditions

---

Friday, 20th October - 14:30 - Nanotechnology for environment and energy - Room 1 - Oral - Abstract ID: 328

---

***Dr. Ahrum Sohn<sup>1</sup>, Mr. Seung Choi<sup>1</sup>, Mr. Tae-Ho Kim<sup>1</sup>, Dr. Sang A Han<sup>1</sup>, Prof. Sang-Woo Kim<sup>1</sup>***

*1. Sungkyunkwan University*

Single layered MoS<sub>2</sub> has been actively studied as a next-generation material to replace Si. Because Single layered MoS<sub>2</sub> is a semiconductor unlike graphene and it has the tunable bandgap as decreasing its thickness. Besides, single layered MoS<sub>2</sub> has a charge mobility of 217 cm<sup>2</sup>/V•S comparable to Si thin film or graphene nanoribbons and its on / off ratio is around 10<sup>8</sup> with abrupt electrical switching.[1] Also, several researchers reported that single layered MoS<sub>2</sub> had unchanging electrical properties during or after mechanical bending. These papers make MoS<sub>2</sub> a candidate material of the flexible device. However, Wu *et al.* observed that when odd layered MoS<sub>2</sub> was under the strain, its transport behavior showed a strong piezoelectrical characteristics due to strain-induced lattice distortion and the associated ion charge polarization.[2] Also, Jena *et al.* reported calculated results of the piezoelectric stress and the strain coefficient change under the strain.[3] Therefore, the transport behavior change of single layered MoS<sub>2</sub> during strain is still under debate. In this study, we investigated the electrical properties of single layered MoS<sub>2</sub> grown by CVD method while varying strains. First of all, we checked the temperature dependent resistance change of our MoS<sub>2</sub>. As previous other groups reported, we was confirmed that our single layered MoS<sub>2</sub> also followed the variable-range hopping model. After transferring MoS<sub>2</sub> to the flexible substrate, we measured Schottky barrier height of the MoS<sub>2</sub> while varying the strain. Also, we investigated the piezoelectrical property of MoS<sub>2</sub> while sample temperature changed from 6°C to room temperature.

# Novel magnetic nanoadsorbents for wastewater remediation

Friday, 20th October - 14:47 - Nanotechnology for environment and energy - Room 1 - Oral - Abstract ID: 96

***Dr. Alex Fabiano Campos<sup>1</sup>, Ms. Helena Augusta Lisboa de Oliveira<sup>1</sup>, Mr. Paulo H. M. Brito<sup>1</sup>, Dr. Renata Aquino<sup>1</sup>, Dr. Franciscarlos G. da Silva<sup>1</sup>, Dr. Jerome Depeyrot<sup>1</sup>***

*1. Universidade de Brasília*

The tannery, petrochemical and dye manufacturing industries produce large quantities of liquid effluents with heavy metals, dangerous dyes, pigments and hazardous organic compounds. The unappropriated discharge of these wastewaters poses serious threats to the environment due to the adverse effects of their pollutants. The magnetically assisted chemical separation technology have proven to be a very promising tool to remove pollutants from industry effluents because it is efficient, economical, and fast [1]. This work addresses the removal of Remazol Brilliant Blue R (RBBR), Direct Yellow 12 (DY12) and hexavalent chromium (Cr(VI)) from aqueous solutions using magnetic nanoadsorbents based on ferrite nanoparticles (NP) modified with cetyltrimethylammonium bromide (CTAB). The nanoadsorbents were synthesized using the hydrothermal coprecipitation method in alkaline medium followed by a surface treatment with  $\text{Fe}(\text{NO}_3)_3$ . Controlling the pH of the medium (NaOH or  $\text{CH}_3\text{NH}_2$ ), samples composed by nanoparticles of two different mean sizes were produced (7.2 nm and 14.0 nm). The surface modification was carried out by mixing the NP and CTAB in aqueous solution at an appropriate pH with sonication for 15 min leading to  $\text{CoFe}_2\text{O}_4@\gamma\text{-Fe}_2\text{O}_3@\text{CTAB}$  nanoparticles. The influence of pH, contact time and initial pollutant concentration were evaluated from batch studies using 0.7 g/L of the nanoadsorbent. After adsorption, the NP were separated using a hand-held magnet and the final concentration of the pollutants in decanted solution (Fig.1) was determined. The results of the batch studies were analyzed in the framework of Langmuir and Freundlich models to evaluate the maximum adsorption capacity and the extent of affinity. The maximum adsorption of RBBR, DY12 and Cr(VI) occurred at pH 3.0, 5.0 and 2.5 respectively leading to almost 100% of pollutant removal. The pollutants adsorption onto the magnetic adsorbents well followed the pseudo-second-order rate indicating that the rate-limiting step involves electrostatic forces between pollutants and nanoadsorbents. It was evidenced that the maximum adsorption capacity was nearly 50% higher for the nanosorbents of the smaller mean size due to its higher surface area.

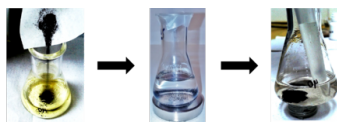


Fig.1 – Pollutant adsorption followed by magnetically assisted chemical separation.

Figure 1.png

## Enhancing the Pozzolanicity of Jordanian Volcanic Tuffs using Calcium Carbonate Nanoparticles

---

Friday, 20th October - 15:04 - Nanotechnology for environment and energy - Room 1 - Oral - Abstract ID: 388

---

***Dr. Ayman Ababneh<sup>1</sup>, Prof. Borhan Aldeen Albiss<sup>1</sup>, Ms. Tasneem Laft<sup>1</sup>***

*1. Jordan University of Science & Technology*

The effect of nano-CaCO<sub>3</sub> on the fresh and mechanical properties of mortar containing high volume of Jordanian natural Pozzolan HVNP was investigated. The fresh properties included the workability and the setting time where the mechanical properties included the compressive and flexural strength. The nano-CaCO<sub>3</sub> particles were prepared in the first part, the second part determined the optimum contents of nano-CaCO<sub>3</sub> (NC) based on compressive strength development of ordinary Portland cement (OPC) mortar. The optimum content that achieved the highest compressive strength was used in the third part of this study to evaluate the effect of nano-CaCO<sub>3</sub> on the properties of HVNP mortars containing 40% and 60% natural Pozzolan as partial replacement of cement. The results show that 1% nano-CaCO<sub>3</sub> is the optimum content which increases the compressive and flexural strength, the results also show that nano-CaCO<sub>3</sub> shortened the setting time and reduced the workability. The X-Ray Diffraction (XRD) and the Scanning Electron Microscopy (SEM) analysis support the results.

# Effect of Metallic Thin-films' Type on Sessile Droplet Contact Angle

Friday, 20th October - 15:21 - Nanotechnology for environment and energy - Room 1 - Oral - Abstract ID: 238

*Dr. feras alzubi<sup>1</sup>, Mr. Abdullah Alkandary<sup>1</sup>*

*1. Kuwait Institute for Scientific Research*

## Introduction

The area of wetting plays a major role in many engineering processes, such as oil recovery, printing, and coating. During the last decade, research work has been increasing to study wetting properties of metallic materials, due to their major impact in applications like self-cleaning and nanofluids. Determination of hydrophobicity and hydrophilicity of surfaces involves the measurement of contact angle when a coated surface and liquid interact. This contact angle is affected by several parameters such as liquid's surface energy, roughness of the surface, type of material of the surface, etc.

This work investigates the change in contact angle of droplet of deionized water (DIW) when interact with different metallic surfaces (Fe, Ni, Au, Pd, and Cr) fabricated at the nanoscale (Figure 1). Moreover, the surfaces will be exposed to thermal environment to study its effect on the contact angle for the studied materials.

## Experimental

Thin films of Fe, Ni, Au, Pd, and Cr were deposited on Si substrates by electron-beam physical vapor deposition (e-beam PVD) technique under low pressure  $< 10^{-6}$  Torr. Deposited film thickness of all studied materials was 4 nm. Experimental measurements of the contact angle of DIW droplets dispensed on the deposited metallic thin films on silicon substrate was carried out by Optical Contact Angle system (OCA 100 Dataphysics).

## Results and Analysis

Results show that the contact angle depends strongly on the type deposited material. 4 nm gold surface has revealed the highest contact angle  $97.6^\circ$  closer to be hydrophobic surface as shown in Figure 2. On the other hand, the iron 4 nm surface has shown a contact angle of  $70.2^\circ$  which is considered a hydrophilic surface. Moreover, contact angle values of DIW with Ni, Pd, and Cr surfaces are falling in between gold and iron values, which are considered to be hydrophilic surfaces (Figure 3). These findings contribute to understanding the role of metallic thin films of different types on surface wettability.

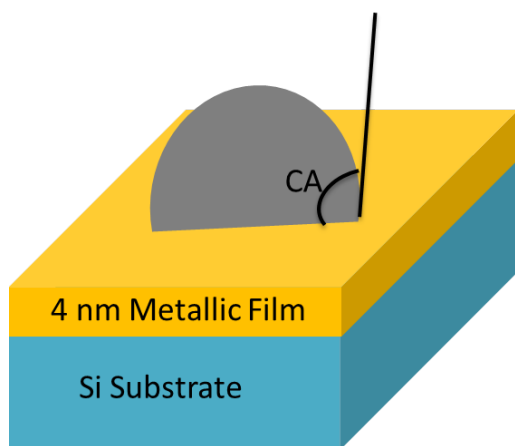


Figure 1 schematic diagram of the tested samples with diw droplet on surface to measure contact angle ca .png

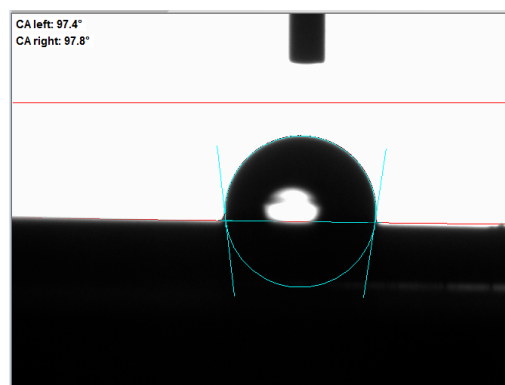


Figure 2 optical image of the diw droplet on 4 nm gold au surface with displayed ca measurement.png

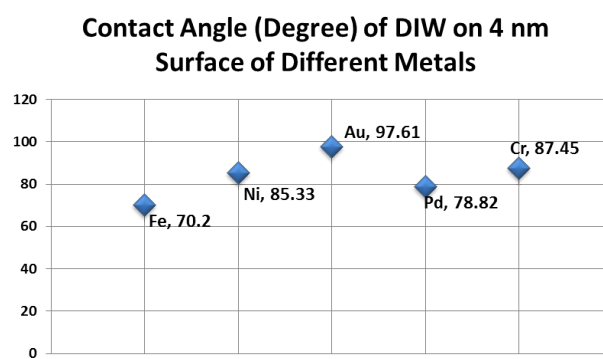


Figure 3 contact angle of diw on 4 nm surfaces of different metals.png

---

## A Sustainable Green Biosynthesis of Silver Nanoparticles Using Plant Leaves Extracts

---

Friday, 20th October - 15:38 - Nanotechnology for environment and energy - Room 1 - Oral - Abstract ID: 319

---

***Prof. Muna AbuDalo*<sup>1</sup>, *Mr. Ismaeel Al-mheidat*<sup>1</sup>, *Mrs. Alham Al-shurafat*<sup>2</sup>, *Mrs. Colleen Grinham*<sup>3</sup>,  
*Mrs. Vinka Oyanedel-Craver*<sup>3</sup>**

*1. Jordan University of Science & Technology, 2. Jordan University of Science and Technology, 3. University of Rhode Island*

Silver Nanoparticles (AgNPs) are well known for their extraordinary antibacterial activity along with other valuable chemical and physical properties. Such trait led to numerous biomedical, health and water purification applications. In light of rapid advances in silver nanoparticles production, sustainability protruded as design criterion in the synthesis. Green chemistry has evolved as the bestead synthesis framework toward sustainability and environment protection for nanoparticles production.

As an endeavour within this trend, an eco-friendly rapid bioreduction of Tollens reagent  $\text{Ag}(\text{NH}_3)_2^+$  (aq) into silver nanoparticles (AgNPs) utilizing plant leaves extracts of olive (OLE) and rosemary (RLE) was successfully achieved. The synthesis had been optimized employing UV-Vis spectroscopy, Scanning Electron Microscopy (SEM) and Dynamic Light Scattering (DLS) analysis to obtain smaller AgNP core size, approximate spherical shape and higher monodispersed. Effect of various experimental parameters on the particle size and stability of nanoparticles were studied and controlled. The manufactured AgNPs showed significant antibacterial effect against *Escherichia coli*, *Salmonella enterica*, and *Staphylococcus aureus* indicating their potential use in pharmaceuticals and water treatment applications.

**Keywords:** Silver nanoparticles (AgNPs); Tollens method; Olive leaves extract (PLE) and Rosemary leaves extract (RLE).

---

## Relevance of LiPF<sub>6</sub> as Etching Agent of LiMnPO<sub>4</sub> Colloidal Nanocrystals for High Rate Performing Li-ion Battery Cathodes

---

Friday, 20th October - 15:55 - Nanotechnology for environment and energy - Room 1 - Oral - Abstract ID: 392

---

***Ms. Lin Chen*<sup>1</sup>, *Dr. Enrico Dilella*<sup>2</sup>, *Dr. Andrea Paolella*<sup>3</sup>, *Dr. Giovanni Bertoni*<sup>2</sup>, *Dr. Alberto Ansaldo*<sup>2</sup>, *Dr. Massimo Colombo*<sup>2</sup>, *Mr. Sergio Marras*<sup>2</sup>, *Prof. Bruno Scrosati*<sup>2</sup>, *Prof. Liberato Manna*<sup>2</sup>, *Dr. Simone Monaco*<sup>2</sup>**

*1. Istituto Italiano di Tecnologia, Università degli Studi di Genova, 2. Istituto Italiano di Tecnologia, 3. McGill University*

LiMnPO<sub>4</sub> is an attractive cathode material for the next-generation high power Li-ion batteries, due to its high theoretical specific capacity (170 mAh g<sup>-1</sup>) and working voltage (4.1 V vs Li<sup>+</sup>/Li). However, two main drawbacks prevent the practical use of LiMnPO<sub>4</sub>: its low electronic conductivity and the limited lithium diffusion rate, which are responsible for the poor rate capability of the cathode. The electronic resistance is usually lowered by coating the particles with carbon, while the use of nanosize particles can alleviate the issues associated with poor ionic conductivity. It is therefore of primary importance to develop a synthetic route to LiMnPO<sub>4</sub> nanocrystals (NCs) with controlled size and coated with a highly conductive carbon layer. We report here the combination of a new colloidal approach to LiMnPO<sub>4</sub> NCs and an effective surface etching process (using LiPF<sub>6</sub>) that makes the NCs miscible in the aqueous glucose solution used as carbon source for the carbon coating step. Also, it is likely that the improved exposure of the NC surface to glucose facilitates the formation of a conductive carbon layer that is in intimate contact with the inorganic core, resulting in a high electronic conductivity of the electrode, as observed by us. The carbon coated etched LiMnPO<sub>4</sub>-based electrode exhibited a specific capacity of 118 mAh g<sup>-1</sup> at 1C, with a stable cycling performance and a capacity retention of 92% after 120 cycles at different C-rates. The delivered capacities were higher than those of electrodes based on not etched carbon coated NCs, which never exceeded 30 mAh g<sup>-1</sup>. The rate capability here reported for the carbon coated etched LiMnPO<sub>4</sub> nanocrystals represents an important result, taking into account that in the electrode formulation 80 % wt. is made of the active material and the adopted charge protocol is based on reasonable fast charge times.

## The new investigation on CTAB synthesis of vanadium oxide nanorods

---

Friday, 20th October - 14:30 - Nanofabrication, nanoprocessing and nanomanufacturing - Room 2 - Oral -  
Abstract ID: 744

---

***Mr. Alireza Behfar<sup>1</sup>, Prof. Theodore Betley<sup>2</sup>, Prof. Cynthia Friend<sup>3</sup>***

*1. Young Researchers and Elite Club, Najafabad Branch, Islamic Azad University, Najafabad, Iran, 2. Professor of Chemistry and Chemical Biology, Harvard university, 3. Professor of Chemistry and Professor of Materials Science, Harvard university*

In this paper, structural and morphological properties of vanadium oxides ( $V_2O_5$ ) nanoparticles have been studied.  $V_2O_5$  nanoparticles were synthesized using a simple chemical method by sodium metavanadate as precursor and Cetyl trimethylammonium bromide (CTAB) as surfactant. The samples were characterized by high resolution transmission electron microscopy (HRTEM), field effect scanning electron microscopy (FESEM) and X-ray diffraction (XRD). As there are many forms of vanadium oxides produced during this process, x-ray diffraction (XRD) technique was used to identify  $V_2O_5$  phase. particles was around 5 nm as estimated by HRTEM technique and average diameter of annealed nanorods was around 9 nm as estimated by XRD technique and direct FESEM observation. The surface morphological studies from SEM depicted that nanorods were appeared after annealing process. The effect of CTAB surfactant on the particle morphology was also studied and the results show that the CTAB can reduce the particle size of nanorods to less than 10 nm.



# Magnetic and electrical performance of atomic layer deposited nanolaminates

Friday, 20th October - 14:47 - Nanofabrication, nanoprocessing and nanomanufacturing - Room 2 - Oral -  
Abstract ID: 655

**Dr. Aile Tamm**<sup>1</sup>, **Mr. Kristjan Kalam**<sup>1</sup>, **Mr. Mats Mikkor**<sup>1</sup>, **Ms. Helina Seemen**<sup>1</sup>, **Dr. Mihkel Rähn**<sup>1</sup>,  
**Prof. Kaupo Kukli**<sup>1</sup>, **Mr. Joosep Link**<sup>2</sup>, **Dr. Raivo Stern**<sup>2</sup>, **Dr. Helena Castán**<sup>3</sup>, **Prof. Salvador Dueñas**<sup>3</sup>

**1.** University of Tartu, **2.** National Institute of Chemical Physics and Biophysics, **3.** University of Valladolid

The synthesis of multiferroic materials is of relevance while developing the next generation electronic and spintronic devices [1]. Theoretically, several materials could demonstrate saturating and remnant polarization in both electric and magnetic fields, but it is challenging to actually synthesize thin films which demonstrate multiferroic behaviour, because the physical performance of the materials may considerably depend on their synthesis routes. In this study the nanolaminate films consisting of high-permittivity oxides ( $\text{ZrO}_2$ ,  $\text{Er}_2\text{O}_3$ ) and magnetic materials, ( $\text{Fe}_2\text{O}_3$ ,  $\text{Co}_3\text{O}_4$ ) were grown by atomic layer deposition (ALD) on silicon and titanium nitride substrates at 300, 350 and 375 °C using erbium diketonate, ferrocene, zirconium chloride, tris(2,4-pentanedionato)cobalt and ozone precursors. Laminated ALD films could be uniformly deposited into three dimensional stacked substrates using the same cycle times otherwise suited to the uniform coverage of planar substrates (Fig. 1 d). Morphology, crystalline phases and composition of  $\text{Fe}_2\text{O}_3$ - $\text{Er}_2\text{O}_3$  (Fig. 1),  $\text{Co}_3\text{O}_4$ - $\text{ZrO}_2$  (Fig. 2) and  $\text{Fe}_2\text{O}_3$ - $\text{ZrO}_2$  [2] stacked oxides were described. The multilayered structures promoted both charge polarization and saturative magnetisation compared to these phenomena in the more homogeneously mixed films (Fig. 1 d, e). Promising results in terms of the simultaneous appearance of the internal magnetization and certain electrical charge polarization were demonstrated in planar laminated structures. Further electrical and magnetic modelling and analysis will be needed in order to elaborate the phenomenon and optimize the material structure for the magnetoelectric performance.

## Acknowledgements

This work was funded by the European Regional Development Fund the project TK134 “Emerging orders in quantum and nanomaterials”, Estonian Research Agency (IUT2-24), Estonian Academy of Sciences (SLT-FYUPROF), and Spanish Ministry of Economy and Competitiveness through the project TEC2014-52152-C3-3-R with support of Feder funds.

## References

- [1] R. Thomas *et. al.*, “Multiferroic thin-film integration onto semiconductor devices”, J. Phys. Condens. Matter, 2010.
- [2] K.Kalam *et. al.*, “Atomic layer deposition of  $\text{ZrO}_2$ - $\text{Fe}_2\text{O}_3$  thin films”, Beilstein J. Nanotechnol., 2017 *submitted*.

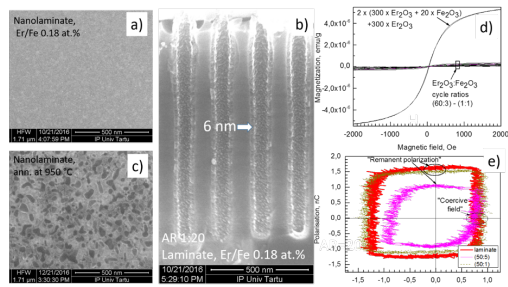


Figure 1. Bird-eye scanning electron microscope images of  $Er_2O_3-Fe_2O_3$  nanolaminated films as-deposited (a) and annealed at 950 °C (c) and a film grown on a three-dimensionally trenched substrate (stack) with an aspect ratio of 1:20 (b). Representative magnetic moment vs external magnetic field strength curves measured from all  $Er_2O_3-Fe_2O_3$  films deposited (d) and polarization charge against voltage applied to capacitive elements in Sawyer-Tower circuit for  $Er_2O_3-Fe_2O_3$  films (e) with cycle ratios denoted by labels.

Figure 1.png

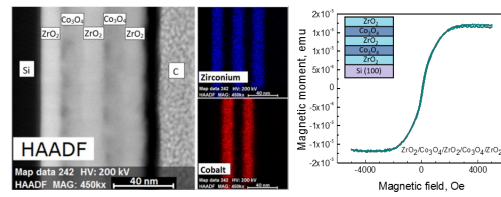


Figure 2. Cross-sectional EDX composition profiling (left) and magnetic moment vs. external magnetic field curve (right) of the multilayer object.

Figure 2.png

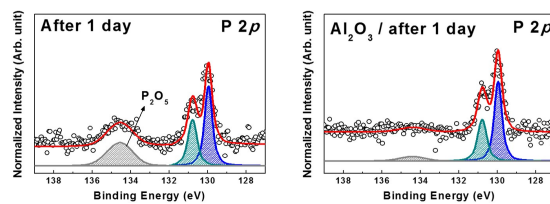
# Interfacial self-reaction during atomic layer deposition of Al<sub>2</sub>O<sub>3</sub> on oxidized black phosphorus and improved electrical properties by stable surface chemical structure

Friday, 20th October - 15:04 - Nanofabrication, nanoprocessing and nanomanufacturing - Room 2 - Oral - Abstract ID: 720

Mr. Dae-Kyoung KIM<sup>1</sup>, Mr. Jimin CHAE<sup>1</sup>, Mr. Hanbum PARK<sup>1</sup>, Prof. Mann-Ho CHO<sup>1</sup>

<sup>1</sup>. Yonsei University/Division of physics

We investigated the interfacial reaction of the between high-k dielectric grown by the atomic layer deposition (ALD) process and exfoliated black phosphorus (BP) as a function of air exposure time. The change in chemical state and structure analysis on oxidized phosphorus species before and after ALD process were investigated using x-ray photoelectron spectroscopy (XPS), scanning electron microscope (SEM), Atomic force microscopy (AFM), first-principles DFT calculations, and characteristics of a field-effect transistor (FET) based on BP. We observed that oxidized phosphorus species (PO<sub>x</sub>) were significantly reduced during the ALD-Al<sub>2</sub>O<sub>3</sub> process. In particular, field effect characteristic of Al<sub>2</sub>O<sub>3</sub> on oxidized black phosphorus showed that the enhancing electrical properties (mobilities of  $\sim 253 \text{ cm}^2 \text{V}^{-1} \text{s}^{-1}$  and on-off ratios of  $\sim 10^5$ ) at the 1 day of exposure time in BP sample. These results of self-reaction between the ALD-Al<sub>2</sub>O<sub>3</sub> process and oxidized BP provide an reduction of oxidized phosphorus species by the ALD reaction process and *enhancing electrical* characteristics of the oxidized BP FET, even in the air exposure environment.



Al<sub>2</sub>O<sub>3</sub> oxidized black phosphorus.jpg

---

## Fabrication of Self-Organized Precisely Tunable Plasmonic SERS Substrates via Glancing Angle Deposition

---

Friday, 20th October - 15:21 - Nanofabrication, nanoprocessing and nanomanufacturing - Room 2 - Oral - Abstract ID: 300

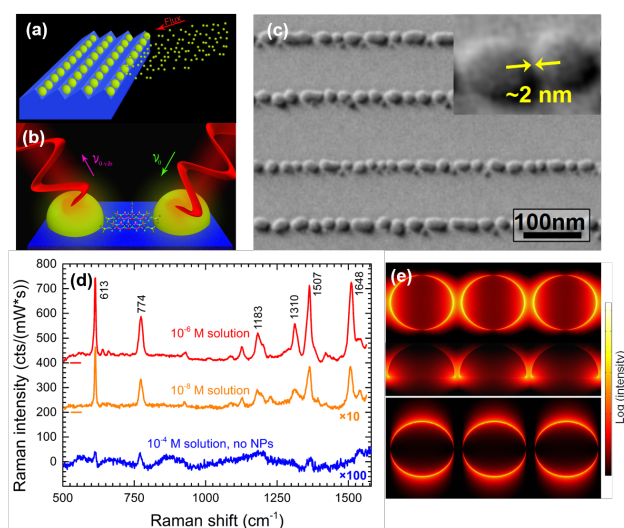
---

***Dr. Oral Ualibek<sup>1</sup>, Dr. Ehsan Rezvani<sup>2</sup>, Dr. Brendan Bulfin<sup>3</sup>, Prof. Igor Shvets<sup>4</sup>, Dr. Gulnar Sugurbekova<sup>1</sup>***

*1. National Laboratory Astana, Nazarbayev University, 2. Department of Materials Science and Engineering, Sharif University of Technology, 3. German Aerospace Center, 4. School of Physics, Trinity College Dublin*

Plasmonic nanostructures offer great enhancement of the Raman signal due to the strong confinement of the electromagnetic field. Thus, they are considered as suitable candidates for surface enhanced Raman spectroscopy (SERS). In this work, we present an alternative fabrication route, called the glancing angle deposition (GLAD), for tunable fabrication of plasmonic self-organized Ag nanoparticle arrays aimed at SERS. Using the GLAD technique, the inter-particle distance within the arrays can be made as small as 1 nm. Moreover, the plasmonic resonance can be precisely tuned over the whole visible range. The GLAD method can be up-scaled; and when a transparent substrate is used, it enables various measurement geometries. The enhancement factor for the employed probe molecule in this study, rhodamine 6G, is estimated to be in the order of  $\sim 10^8$ . It is noted that the nature of the GLAD-made substrates leads to the polarization dependence of the signal enhancement. The polarization studies show a stronger enhancement along the nanoparticles chain. Finally the experimental results were compared with finite element calculations for quantitative and qualitative analysis, confirming the effect of the small NP gaps on the enhancement factor and importance of the small inter-particle gap for use of NP arrays as SERS substrates.

This work has been supported by the Ministry of Education and Science of Kazakhstan under the NU- Berkeley No. 0115PK03029 and Parasat financial support.



(a) A schematic view of the GLAD technique: a flux of collimated adatoms is sent toward the stepped template surface at a glancing angle. In this way one can grow asymmetric NP arrays. (b) Schematic view of the SERS measurement, where the highest electric field occurs between the coupled NPs at the "hotspots". (c) Scanning electron microscope (SEM) image of Ag NP-arrays grown on  $\text{Al}_2\text{O}_3$  stepped templates. (d) Raman spectra of R6G adsorbed on Ag NP substrates after exposure to different concentrated R6G aqueous solutions and a reference measurement. (e) Simulated electric field maps for Ag NP chains subjected to light which is polarized parallel (top panel) and perpendicular (bottom panel) to the NP chains.

Abstract image oral ualibek.png

# Preparation of Novel Nanocomposites Modified with Hybrid Nano-Reinforcements

Friday, 20th October - 14:30 - Polymer, carbon and graphene nanostructures - Auditorium - Oral - Abstract ID: 270

**Mr. Ayad Mahuof<sup>1</sup>, Dr. George Kotsikos<sup>1</sup>, Prof. Geoff Gibson<sup>1</sup>**

**1. Newcastle University**

In this study, graphene nanoplatelets (GNP) and cup-stacked carbon nanotubes (CSCNT) were used to enhance the mechanical properties of carbon fibre epoxy composites. The principal challenge was to accomplish homogenous dispersion and full exfoliation of the nanoparticles in the matrix. The combined techniques of sonication and ball milling were used to disperse the two types of nano-reinforcements into the epoxy matrix at various weight concentrations, ranging from 0 to 7wt.%. Characterisation of the nanocomposites was performed via mechanical testing on three types of epoxy nanocomposites: a) GNP/epoxy, b) CSCNT/epoxy, c) hybrid GNP-CSCNT/epoxy. The results showed that optimum mechanical strength was achieved after adding 5wt. % of GNP, 6wt. % of CSCNT and 4wt. % of hybrid nanofillers to the epoxy matrix; thus, the weight ratio of the hybrid nanofillers was equalised. The optimum weight concentration for each type of nanocomposites was subsequently used to improve the mechanical properties of carbon fibre reinforced composites. Three types of woven roving carbon fibre composite laminates using the abovementioned nanofilled epoxy formulations were produced via the impregnation route using the hand lay-up method with the following formulations: a) GNP/CF/epoxy, b) CSCNT/CF/epoxy, and c) hybrid GNP-CSCNT/CF/ epoxy. Flexural strength and interlaminar fracture toughness (mode I) tests were conducted on the laminates produced. The results revealed that the flexural strength and propagation energy toughness increased by approximately 20% and 15% in the GNP/CF/ epoxy respectively, and 25% and 104% in the CSCNT/CF/epoxy respectively (see Fig 1 & Table 1). In addition, there was a significant improvement of approximately 18% and 73% respectively in the hybrid GNP-CSCNT/CF/epoxy composite laminates. Transmission Electron Microscopy (TEM) and Scanning Electron Microscopy (SEMs) were used to evaluate the dispersion of the nano-reinforcements into the epoxy matrix and the fracture mechanism of the epoxy composites (see Fig 2). The microstructural details demonstrated a uniform dispersion and optimum exfoliation of the nanoparticles, and strong bond between the nanofilled epoxy matrix and the carbon fibre reinforcement network

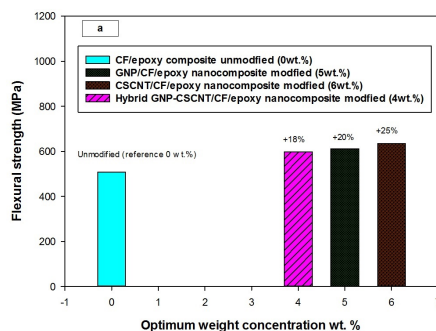


Figure 1 flexural strength.jpg

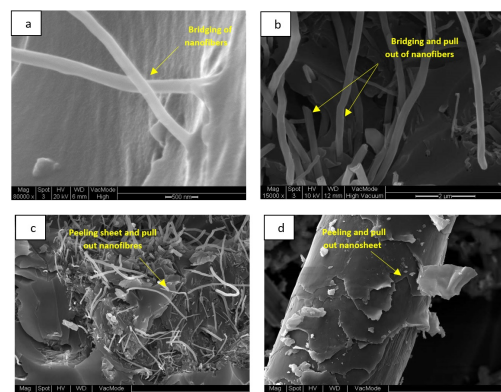


Figure 2 the sems images illustrate the fracture behaviour systems in hybrid composites a bridging of nanotubes b c d combination of fracture mechanisms.jpg

Sample	Weight concentration %wt	Initial propagation toughness (KJ.m <sup>-2</sup> )						Propagation toughness (KJ.m <sup>-2</sup> )	Inc.%
		Non-linear NL	Inc.%	Visual onset VIS	Inc.%	Offset 5% MAX	Inc.%		
CF/epoxy composite	Base (0)	0.31425±0.0877	-	0.3013±0.094	-	0.32123±0.078	-	0.40505±0.056	-
GNP/CF/epoxy nanocomposites	5	0.3245±0.0394	+3.26	0.3996±0.09	+32.04	0.3376±0.067	+5.09	0.4655±0.0838	+14.92
CSCNT/CF/epoxy nanocomposites	6	0.57994±0.1748	+84.54	0.5677±0.163	+88.41	0.59118±0.1651	+84.03	0.82626±0.1827	+103.98
Hybrid GNP-CSCNT/CF/epoxy nanocomposites	4	0.3141±0.065	-0.047	0.2851±0.0197	-5.3	0.3583±0.104	+11.54	0.700±0.1339	+72.818

Table 1 comparison and evaluation of fracture toughness energy mode I for three formulations of hybrid composites modified with gnp cscnt and hybrid gnp-cscnt nanofillers at optimum weight concentration.jpg

## Development of super repellent nano-composite coatings based on functionalised nano-silica.

Friday, 20th October - 14:47 - Polymer, carbon and graphene nanostructures - Auditorium - Oral - Abstract ID: 346

***Prof. Geraldine Durand<sup>1</sup>, Prof. Alan Taylor<sup>2</sup>, Ms. Marta Alvarez<sup>2</sup>, Ms. Nadia Sid<sup>2</sup>, Ms. Maria Linzoain<sup>2</sup>, Dr. Anna Wojdyla-cieslak<sup>2</sup>, Mr. Angelo La Rosa<sup>1</sup>***

*1. London south Bank University, 2. TWI Ltd*

Highly repellent surfaces are needed in a large number of industrial sectors, where the accumulation of unwanted contamination (ice, debris, insects etc...) can have a significant impact on the operational performance of affect parts. Ice formation on wind turbines, insect accretion on aircraft and dust build-up on solar panel all introduce major costs to industry and are an ongoing cause of failure. Current mitigation technologies rely on active processes such as electrical heating, application of de-icing chemicals, manual cleaning etc. These can be expensive, time consuming, inefficient and sometime damaging to the environment. Emerging technologies for nanostructured coatings have significant potential for the development of very high performance surfaces. However, the lack of retention of functional performance is widely recognised as the primary barrier to industrial adoption.

The aim of this work is to develop novel durable highly repellent coatings that can be customised depending on: the application, the contamination and the operational environment. A materials-by-design approach has been developed where nanoscale silica nanoparticles are being designed to provide reinforcement to conventional coatings or composite materials and also to allow surface roughness. The introduction of multiple functionalities onto the surface of nanoscale silica is a key enabler for the development of a mechanically durable and highly repellent material. These nanoparticles are designed to allow high loading into the resin matrix without affecting its viscosity and homogeneity. The surface chemistry of the nanoparticles can be adjusted to allow crosslinking with the polymer matrix and the full integration of the nanoparticle within the network and thereby creating a more durable resin without the associated brittleness. Moreover, at the surface, the nanoparticles are expected to both improve erosion resistance and, by use of suitable surface chemistry provide significantly enhanced non-wetting characteristics leading to a new route to durable, repellent materials. This development will have far-reaching impact across a wide range of sectors, including aviation and energy generation.



---

## Far-Red Fluorescent carbon nano-onions for high-resolution cellular imaging

---

Friday, 20th October - 15:04 - Polymer, carbon and graphene nanostructures - Auditorium - Oral - Abstract ID: 318

---

**Mr. Adalberto Camisasca<sup>1</sup>, Dr. Stefania Lettieri<sup>1</sup>, Dr. Marta D'amora<sup>1</sup>, Prof. Silvia Giordani<sup>1</sup>**

**1. Istituto Italiano di Tecnologia**

The development of novel fluorescent systems for bio-imaging applications is a research field of increasing interest and many efforts have been made for the implementation of imaging agents for the biologically relevant near-infra red (NIR) region, where tissues exhibit minimal absorbance. Carbon nano-onions (CNOs) are an emerging class of nanoparticles which showed great potential in a variety of different applications [1]. The functionalization of CNOs with different functional groups increases the ability to penetrate into the cells [2] and allows for the conjugation of different diagnostic and therapeutic agents, opening new avenues in theranostic applications [3].

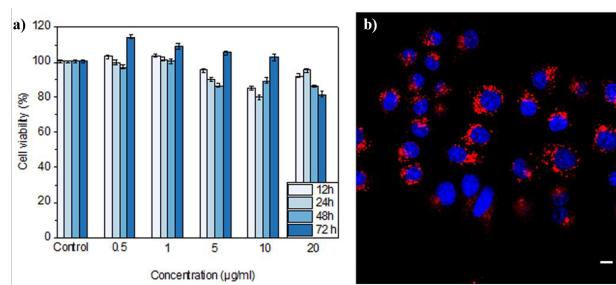
Our recent reports showed that fluorescently labelled CNOs exhibit weak inflammatory potential and a low cytotoxicity [4] and are readily internalized by cancer cells and deposited in the lysosomes [5]. Moreover, *in vivo* studies on zebrafish larvae (*Danio Rerio*) during the development shown their biocompatibility and homogeneous distribution in a vertebrate model system [6].

Here we report the development of a novel class of fluorescent nanoprobes with enhanced solubility in biological media and bright photoluminescence. The fluorescent CNOs (fluo-CNOs) have been characterized by different analytical techniques such as spectroscopy (Raman, x-ray photoelectron, fluorescence), thermogravimetric analysis (TGA), dynamic light scattering (DLS), zeta potential as well as microscopy.

The internalization and cytotoxicity of fluo-CNOs have been analyzed in human cervical carcinoma (HeLa) and human breast cancer (MCF-7) cells, showing any significant toxic effect on cell morphology and cell viability in both cell lines (Figure 1a). Moreover, the functionalized CNOs showed high fluorescence intensity even at very low concentration with partially localization in the lysosomes (Figure 1b) [7]. Our findings confirmed the excellent potentialities of these functionalized carbon nanomaterials as biocompatible platform for high-resolution cellular imaging.

### References

- [1] Bartelmess, J. et al. *Beilstein J. Nanotechnol.* **2014**, 5, 1980
- [2] Frasconi, M. et al. *Methods Appl. Fluoresc.* **2015**, 3, 044005
- [3] Frasconi, M. et al. *Chem. Eur. J.* **2015**, 21, 19071
- [4] Yang, M. et al. *Small* **2013**, 9, 4194
- [5] Bartelmess, J. *Nanoscale* 2014, 6, 13761
- [6] d'Amora, M. et al. *Sci. Rep.* **2016**, 6, 33923
- [7] Lettieri, S. et al. *RSC Adv.* **2017**, 7, 45676



Cellular viability and confocal image of mcf7 cells treated with fluo-cnOs.png

# Biomimetic design, fabrication and development of nano-microstructured layered urine bladder scaffolds for bladder tissue engineering

Friday, 20th October - 15:21 - Polymer, carbon and graphene nanostructures - Auditorium - Oral - Abstract ID: 671

***Dr. Fatemeh Ajalloueian***<sup>1</sup>

*1. Technical University of Denmark*

## Introduction

Tissue engineering of the urinary bladder has evolved as an attractive alternative method (compared to applying vascularized intestinal grafts) for treating bladder anomalies<sup>1-3</sup>. Scaffold, one of the key aspects of tissue engineering, has recently attracted more attention. 3D scaffolds mimicking the natural extracellular matrix of the native tissue, are considered as a structural template to support cell adhesion, migration, proliferation and differentiation. Right selection of biopolymers and fabrication methods are expected to improve regeneration of a target tissue<sup>4</sup>. In this study, we have tried to look at morphology of main layers of bladder to mimic their structure for a functional bladder wall regeneration.

## Materials and methods

To look at the morphology of bladder main layers in a porcine sample, the bladder was opened, fixed on a plate, and urothelium was separated manually from detrusor. Both layers were examined by scanning electron microscopy (SEM). Specimens were fixed in 10% formalin, washed with distilled water, and passed through a graded ethanol series to remove water, and immersed in hexa- methylsilazane. Samples were then air-dried, mounted on stubs, sputter-coated with gold, and examined on a digital scanning electron microscope. Two different biopolyemrs and fabrication techniques were selected based on the SEM observations to make the final scaffold for tissue engineering studies.

## Results and discussions

According to macroscopic and SEM observations, urothelium was found as a thin layer with nanofibrous structure, compared to detrusor with higher thickness and containing combination of microfilaments and nanoscale fibers. In this regard, we applied silk fibroin knitted fabric as a microfilament substrate replicating the detrusor. Collagen was selected as the optimum biomaterial for regeneration of urothelium, and the fabrication technique was compression of collagen hydrogel into the knitted fabric. Consequently, an integrated layered structure resembling the native bladder wall was fabricated. Our tissue-seeding studies into this construct have shown successful regeneration of multilayerd urothelium, and 3D regeneration of smooth muscle cells in a silk-collagen micro-nanostructured substrate similar to detrusor.

1. Atala, A. *Br. Med. Bull.* (2011)
2. Atala, A., et al *Lancet* (2006)
3. Atala, A. *BJU Int.* (2001)
4. Ajalloueian, F., et al. *Biomaterials* (2014)

# Scanning tunneling spectroscopy investigation of van der Waals based metal/semiconductor interfaces

Friday, 20th October - 15:38 - Polymer, carbon and graphene nanostructures - Auditorium - Oral - Abstract ID: 332

***Dr. toai le quang<sup>1</sup>, Dr. Vladimir Cerchez<sup>1</sup>, Dr. Karol Nogajewski<sup>1</sup>, Prof. Marek Potemski<sup>1</sup>, Dr. Minh Tuan Dau<sup>2</sup>, Prof. Matthieu Jamet<sup>2</sup>, Prof. Pierre Mallet<sup>3</sup>, Prof. Jean-yves Veuillen<sup>3</sup>***

*1. CNRS, Université Grenoble Alpes, 2. CEA-INAC, 3. CNRS*

We study van der Waals (vdW) based heterostructures, combining graphene and few-layer semiconducting Transition Metal Dichalcogenides (TMDs) films, by using cryogenic scanning tunneling microscopy (STM) in ultra-high vacuum. The fabrication of vdW structures is done either by exfoliating and transferring WSe<sub>2</sub> flakes on epitaxial graphene (Gr) on SiC(0001), or by growing by molecular beam epitaxy (MBE) monolayer (1L) either MoSe<sub>2</sub> or WSe<sub>2</sub> flakes on similar substrates (Fig. 1a). We then locally probe the local density of states of the TMD flakes using scanning tunneling spectroscopy (STS). STS provides a direct access to the band onsets and the electronic band-gap of the TMD (Fig. 1b) [1,2].

A noteworthy result is presented in Fig.1b : The dI/dV spectra that we measure on 1L-MoSe<sub>2</sub> are strongly impacted by the number of graphene layers below the TMD flake. As shown in the figure, the spectra are rigidly shifted towards negative biases by 130 mV when going from bilayer (BLG) to single-layer graphene (SLG). This shift is observed either for 1L-MoSe<sub>2</sub> or 1L-WSe<sub>2</sub> flakes, and is still present with the same order of magnitude for 3L-WSe<sub>2</sub>. Additionally, this effect does not depend on the TMD preparation method. As it will be detailed in the contribution [3], we interpret our experimental data within the framework of semiconductor/metal (SC/M) interfaces, where graphene (either SLG or BLG) acts as the metal part of the junction (this is justified because SLG or BLG on SiC are both heavily n-doped). We will show that all our measurements reflect an unconventional behavior of the SC/M junction (namely the absence of Fermi level pinning), which was recently predicted for junctions made of two-dimensional materials coupled with vdW interactions [4]

1. M. Ugeda *et al.*, *Nat.Mater.*, **13**, (2014), 1091.
2. A. Bradley, *et al.*, *Nano.Lett.*, **15**, (2015), 2594.
3. T. Le Quang, *et al.*, submitted to *2D Mater.*
4. Y. Liu *et al.*, *Sci.Adv.*, **2**, (2016), e1600069.

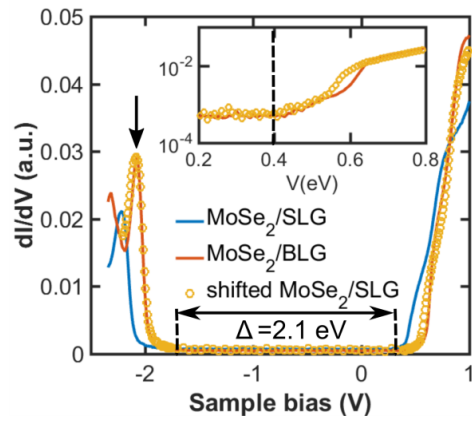


Figure 1b.png

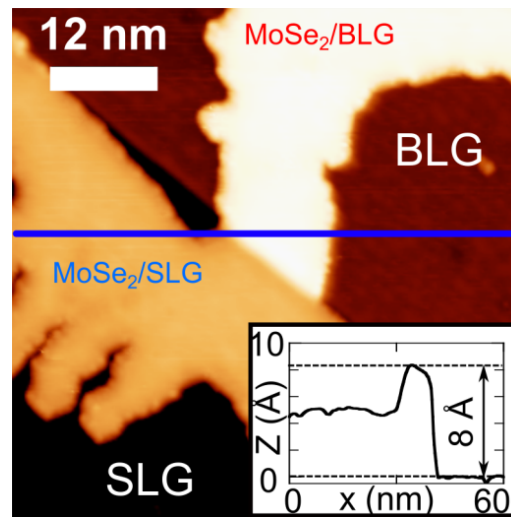


Figure 1a.png

# Nonlinear behavior and buckling of double-carbon nanotubes systems conveying fluid

Friday, 20th October - 15:55 - Polymer, carbon and graphene nanostructures - Auditorium - Oral - Abstract ID: 478

***Dr. Kun Zhou<sup>1</sup>, Prof. Ni Qiao<sup>1</sup>***

*1. Huazhong University of Science and Technology*

## Abstract

In the past years, the works on nanostructures are mainly related to investigations of a single nanotube/nanobeam. Recently, some scientists have done some research on complex beam systems, the systems are commonly encountered in mechanical, construction, and aeronautical industry. Motivated by this, we will investigate the nonlinear behavior of the double-carbon nanotubes system (DCNTS).

The system is composed of two single-walled carbon nanotubes, and the two carbon nanotubes are assumed to be connected by an elastic spring medium. Using the theory of nonlocal elasticity, a nonlocal Euler-Bernoulli elastic beam model is developed. And it has to be emphasized that the geometric nonlinearity associated with the mid-plane stretching of the nanotubes is also taking into account. The equations of motion of the double-carbon nanotubes system are derived using the Hamilton's principle. Then, the two coupled nonlinear partial differential equations, discretized using the Galerkin method, are solved by a fourth-order Runge-Kutta integration algorithm. The nonlocal effect and the geometric nonlinearity effect on the in-phase (synchronous) and out-of-phase (asynchronous) vibration of fluid-conveying DCNTS are discussed.

According to the numerical results, it is demonstrated that an increase in the nonlocal parameter has an obvious reducing effect on the critical-flow velocity, but the buckled static displacement of the nanotubes are increased with increasing values of nonlocal parameter. And it is also found that the geometric nonlinearity term has no effect on the critical-flow velocity, but the geometric nonlinearity term can effect the buckled static displacement of the nanotubes. For the case of out-of-phase vibration, results shows the connection stiffness has a significant effect on critical-flow velocity and the buckled static displacement of the nanotubes, it will reduce the nonlocal effect.

**Keywords:** nonlocal elasticity theory; nonlinear dynamics; double-carbon nanotubes systems; buckling.

# Facile synthesis of MoS<sub>2</sub>-flakes/amorphous-carbon composite as anode for lithium-ion batteries

Friday, 20th October - 16:40 - Multi-Topic - Auditorium - Oral - Abstract ID: 748

**Mr. Duc Anh Dinh**<sup>1</sup>

<sup>1</sup>. Istituto Italiano di Tecnologia

Today, lithium-ion batteries (LIBs)<sup>1</sup> are dominating the ever-increasing market for portable electronic devices. Commercial LIBs are based on graphite anode and LiCoO<sub>2</sub> cathode, exhibiting specific capacity of 372 mAh g<sup>-1</sup> and energy densities of 120–150 Wh kg<sup>-1</sup>,<sup>1</sup> thus being unable to meet the requirement of high energy applications. In order to increase the energy/power density of current LIBs, tremendous efforts have been made in the quest of alternative anode materials. Amongst them, molybdenum disulfide (MoS<sub>2</sub>), having a theoretical specific capacity of 670 mAh g<sup>-1</sup> and a large spacing layer (0.62 nm)<sup>2</sup> compared to graphite (0.34 nm),<sup>3</sup> has attracted great attention as a promising LIB anode material. However, MoS<sub>2</sub> as stand-alone anode is limited by its low electrical conductivity and pulverization upon lithiation/delithiation.<sup>3</sup> Here, we propose the use of MoS<sub>2</sub> flakes/carbon (MoS<sub>2</sub>/C) composites as active materials for LIB anode. The MoS<sub>2</sub> flakes are obtained by liquid phase exfoliation of bulk MoS<sub>2</sub> in 2-propanol, with average lateral size of ~90 nm and inter-layer spacing (0.64 nm), see Fig. 1a,b, favorable for Li<sup>+</sup> diffusion. The thermal decomposition of polyacrylic acid is exploited for the MoS<sub>2</sub>/C composites realization. The MoS<sub>2</sub>/C with three different C ratios (10%, 16% and 30%) are deposited onto copper substrate as anode and tested in half-cell configuration. The MoS<sub>2</sub>/C composite anode with carbon content of 16% exhibits the reversible specific capacity of 521 mAh g<sup>-1</sup> at 100 mA g<sup>-1</sup> after 100 cycles, with a coulombic efficiency of 99.7%, see Fig. 2. Moreover, this electrode exhibits a low value of charge transfer resistance (26 Ω) with respect to the one of pristine MoS<sub>2</sub> electrode (170 Ω) after 100 cycles, see Fig. 3. Thus, the carbon network has a double function: (i) buffers volume expansion, (ii) enhances the electrical conductivity of the active material during lithiation/de-lithiation. Our study demonstrates the optimization of the electrochemical properties of MoS<sub>2</sub>/C electrode for LIB by exploiting a facile process, which is promising for an environmentally friendly, low-cost and large-scale production process.

1. Hassoun, J.; et al. *Nano Lett.* **2014**, 14, 4901

2. Du, G.; et al. *Chem Commun.* **2010**, 46, 1106

3. Stephenson, T.; et al. *Energ Environ Sci* **2014**, 7, 209

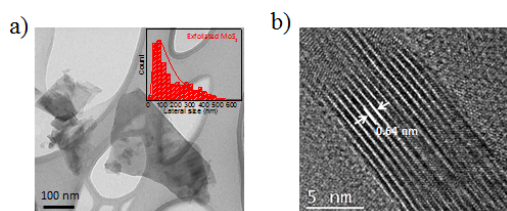


Fig. 1.png

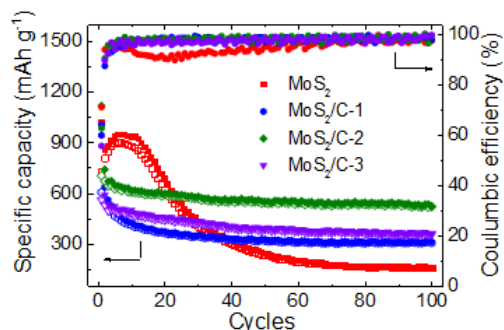


Fig. 2.png

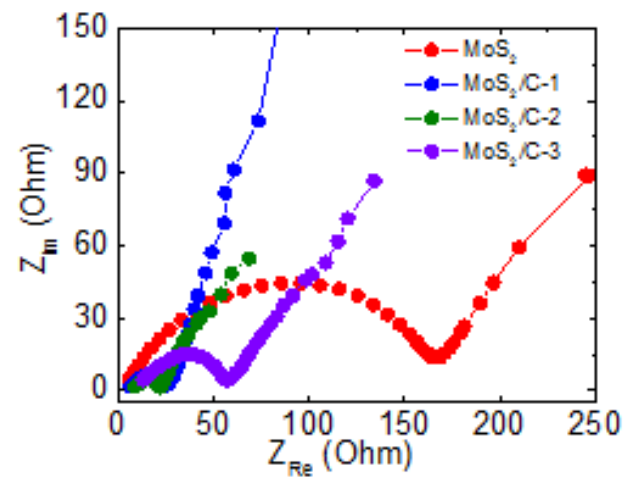


Fig. 3.png



---

# Printing Three-dimensional Conducting Polymer Structures Using Scanned Nanopipettes with Submicron Resolution

---

Friday, 20th October - 16:57 - Multi-Topic - Auditorium - Oral - Abstract ID: 427

---

***Mr. Alex Wibawa<sup>1</sup>, Dr. Pavel Novak<sup>1</sup>***

*1. Queen Mary University of London*

**INTRODUCTION:** Conducting polymers (CP) are organic polymers that have a capability to conduct electrical current, while keeping the other properties of polymers such as elasticity. The unique combination of electrical and mechanical properties of CPs makes them a promising material for wide range of new applications such as printable flexible electronic circuits, biosensors or electroactive scaffolds for tissue engineering. A number of different strategies for printing of CPs or creating scaffolds containing CPs have been developed over the years, however controlled assembly of three-dimensional CP-based structures with submicron resolution remains challenging. Here we explore the use of glass nanopipettes and principles of scanning ion conductance microscopy (SICM) for printing CP structures.

**METHODS:** SICM is a non-contact type of scanning probe microscopy utilising tapered glass nanopipette filled with electrolyte. In this work, we used nanopipettes with tip diameter in the range of 100 - 300 nm filled with 0.1 M pyrrole dissolved in 0.1 M H<sub>2</sub>SO<sub>4</sub> mounted on z-axis piezoactuator of the SICM scanner above a conductive substrate. The nanopipette position was controlled based on the current flowing between the substrate acting as a working electrode and the Ag/AgCl reference electrode immersed in the monomer solution in the nanopipette (Figure 1A).

**RESULTS:** We have implemented a software module for SICM scanner capable of executing complex 3D movements of the nanopipette at controlled velocity and defined nanopipette voltage. Using the velocity control of the module, we were able to control the thickness of vertically printed polypyrrole rods in the range of 500 nm – 2 µm, demonstrating the submicron resolution of the setup (Figure 1B). Lateral movement of the nanopipette created approximately 300 nm high layer of the polymer allowing printing more complex 3D structures with submicron resolution using layer-by-layer approach as illustrated in Figure 1C.

**DISCUSSION:** According to our knowledge, this is first successful attempt to create conductive polypyrrole structures of substantial complexity using submicron sized nanopipettes. This technological advancement opens possibilities for designing custom shaped interfaces between man-made electronics and submicron sized membrane structures such as neuronal dendrites.

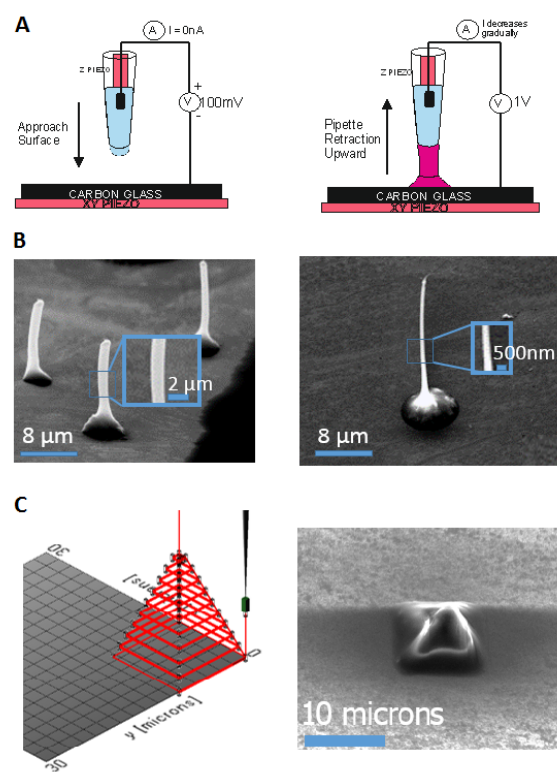


Figure1.png

---

# Controlling Charge Transport in Molecular Electronics by Tuning the Molecular Conformation of Floppy Molecules Self-Assembled in Monolayers Adsorbed on Electrodes

---

Friday, 20th October - 17:14 - Multi-Topic - Auditorium - Oral - Abstract ID: 585

---

***Dr. Ioan Baldea***<sup>1</sup>

*1. Heidelberg University*

In the present work I will present results [1] demonstrating a surprising way to control the charge transport in molecular electronic devices based on floppy molecules forming self-assembled monolayers (SAMs) adsorbed on electrodes. To be specific, I will consider two benchmark molecules often used to fabricate molecular junctions: 4-methyl-4'-mercaptobiphenyl ( $\text{CH}_3\text{-(C}_6\text{H}_4)_2\text{-SH}$ , BPMT) and 4,4'-dithiol-1,1'-biphenyl ( $\text{HS-(C}_6\text{H}_4)_2\text{-SH}$ , BPDT) [2] adsorbed on Au(111). Their most salient structural feature is the twisting angle  $\phi$  between the two phenyl rings that can easily rotate relative to each other.

Changing  $\phi$  in molecules of this kind is important *e.g.* for molecular switches because the low bias conductance  $G$  scales as  $\cos^2\phi$  but the question is how can one substantially modify the twisting angle. Adding fractional electronic charge  $q$  represents a possibility; still, significant  $\phi$ -variations require transferring of average charge fractions  $q \sim 80\%$  [3], which is much more than presently achieved ( $q \leq 10\%$ ) in experiments on molecular junctions.

Results obtained *via* DFT calculations demonstrate that the SAM coverage can have a strong impact on the torsional angle  $\phi$  [1]. While the  $\phi$ -values at low coverages do not significantly differ from the values  $\phi \approx 36^\circ$  characteristic for the isolated molecular species, they substantially change in cases of high coverages. To illustrate with a situation typical for the second case, I refer to SAMs with herringbone arrangements. The supercell corresponding to herringbone ordering comprises two crystallographically nonequivalent molecules. Calculations yield values  $\phi_{1,2} \approx 76^\circ$  (*cf.* Tables 1 and 2) for the slightly different twisting angles  $\phi_{1,2}$  of the two molecules [1]. This translates into a reduction in conductance by a factor  $\sim 10$ .

So, a SAM herringbone arrangement appears to suppress conduction in junctions based on molecules of the type considered. In fact, for 2BDT junctions this ordering could be ruled out in a recent joint experimental-theoretical study [4].

1. I. Bâldea, Faraday Disc. 2017, DOI 10.1039/C7FD00101K.

2. Z. Xie, I. Bâldea, C. Smith, Y. Wu, and C. D. Frisbie, ACS Nano 2015, 9, 8022.

3. I. Bâldea, RSC Adv. 2016, 6, 111903.

5. Z. Xie, I. Bâldea, A. T. Demissie, C. E. Smith, Y. Wu, G. Haugstad, and C. D. Frisbie, JACS 2017, 139, 5696.

Method, BPDT	$\varphi_1$	$\theta_1$	$d_1^{(1)}$	$d_1^{(2)}$	$d_1^{(3)}$	$L_1$	$z_1$	$Z_1$
0.02	75.036	10.006	2.6287	2.7851	2.8833	10.7074	2.1973	12.8746
DZP-TZP	71.881	9.990	2.6248	2.7842	2.8824	10.7071	2.1947	12.8733
VDW-DRSLL	74.760	9.819	2.6976	2.8951	3.0177	10.7465	2.3182	13.0660
0.01	75.152	10.018	2.6313	2.78293	2.8719	10.7074	2.1939	12.8655
0.005	73.562	10.034	2.6276	2.7844	2.8706	10.7040	2.1922	12.8636
CABCAB	74.672	10.277	2.6240	2.7827	2.8882	10.7041	2.1956	12.7280
CAB-R	74.457	11.424	—	—	—	10.6903	—	—
CABCAB-R	74.541	11.605	—	—	—	10.6784	—	—

Method, BPDT	$\varphi_2$	$\theta_2$	$d_2^{(1)}$	$d_2^{(2)}$	$d_2^{(3)}$	$L_2$	$z_2$	$Z_2$
0.02	75.561	10.344	2.6185	2.7865	2.8827	10.7056	2.1925	12.8533
DZP-TZP	71.891	10.236	2.6151	2.7838	2.8814	10.7059	2.1892	12.8517
VDW-DRSLL	71.583	9.933	2.7069	2.8957	2.9996	10.7472	2.3197	13.0580
0.01	75.322	10.227	2.6194	2.7784	2.8847	10.7093	2.1903	12.8472
0.005	73.779	10.270	2.6177	2.7900	2.8798	10.7105	2.1925	12.8508
CABCAB	74.535	10.050	2.6355	2.7828	2.8854	10.7063	2.2005	12.7426
CAB-R	74.769	11.382	—	—	—	10.6789	—	—
CABCAB-R	74.851	11.603	—	—	—	10.6698	—	—

Method, BPDT	$\alpha_s$	$\alpha_f$	$SS_s$	$SS_f$	$HH_{ss}$	$HH_{sf}$	$HH_{ss}$	$HH_{sf}$
0.02	74.070	72.510	4.9710	5.7271	2.8833	2.9055	2.9227	3.3043
DZP-TZP	75.221	71.801	4.9706	5.7265	2.884	2.9082	2.9257	3.3054
VDW-DRSLL	76.439	72.953	5.0242	5.6716	2.9256	2.9084	2.9159	3.2629
0.01	74.418	71.066	4.9615	5.7349	2.8750	2.9170	2.9523	3.3215
0.005	74.335	72.760	4.9566	5.7366	2.8836	2.9326	2.9793	3.3506
CABCAB	73.972	72.420	4.9697	5.7236	2.8831	2.9076	2.9261	3.3044
CAB-R	74.580	70.779	4.9320	5.8431	2.8807	2.9444	3.0133	3.4369
CABCAB-R	74.371	70.764	4.9361	5.6901	2.8813	2.9315	2.9907	3.3956

**Table 2** Results for SAMs of BPDT forming a regular herringbone superstructure on an fcc Au(111) surface. Lengths in angstrom, angles in degrees. Results reproduced from ref. 1 where more details can be found.

Bild1.png

Method, BPMT	$\varphi_1$	$\theta_1$	$d_1^{(1)}$	$d_1^{(2)}$	$d_1^{(3)}$	$L_1$	$z_1$	$Z_1$
0.02	75.916	5.697	2.6564	2.6852	2.7880	8.9714	2.1430	12.1772
DZP-TZP	76.024	5.699	2.6701	2.6842	2.7916	8.9708	2.1420	12.1759
VDW-DRSLL	74.077	5.720	2.7552	2.7774	2.8779	9.0038	2.2526	12.3167
CABCAB	73.856	5.745	2.6632	2.6903	2.7833	8.9700	2.1385	12.1703
CAB-R	74.626	6.725	—	—	—	8.9559	—	—
CABCAB-R	74.936	7.933	—	—	—	8.9080	—	—

Method, BPMT	$\varphi_2$	$\theta_2$	$d_2^{(1)}$	$d_2^{(2)}$	$d_2^{(3)}$	$L_2$	$z_2$	$Z_2$
0.02	75.935	5.670	2.6698	2.6860	2.7928	8.9721	2.1348	12.1700
DZP-TZP	75.987	5.676	2.6570	2.6845	2.7872	8.9710	2.1345	12.1670
VDW-DRSLL	77.179	5.745	2.7845	2.7700	2.8767	9.0011	2.2531	12.3141
CABCAB	77.992	5.765	2.6757	2.6902	2.7882	8.9698	2.1459	12.1788
CAB-R	78.294	6.945	—	—	—	8.9494	—	—
CABCAB-R	78.422	8.213	—	—	—	8.9162	—	—

Method, BPMT	$\alpha_s$	$\alpha_f$	$CC_s$	$SS_s$	$HH_{ss}$	$HH_{sf}$	$HH_{ss}$	$HH_{sf}$
0.02	74.994	76.422	4.9670	4.9574	2.9802	2.9891	2.9943	2.9951
DZP-TZP	75.660	76.456	4.9673	4.9603	2.9814	2.9907	2.9946	2.9958
VDW-DRSLL	74.681	74.681	4.9700	4.9672	2.9770	2.9871	3.0206	3.0301
CABCAB	75.042	75.042	4.9680	4.9607	2.9795	2.9899	2.9916	2.9941
CAB-R	75.356	75.356	4.7935	4.9692	2.9653	2.9867	3.0204	2.9978
CABCAB-R	75.205	75.205	4.2600	4.9714	2.9677	3.0044	3.0106	2.9924

**Table 1** Results for SAMs of BPMT forming a regular herringbone superstructure on an fcc Au(111) surface. Lengths in angstrom, angles in degrees. Results reproduced from ref. 1 where more details can be found.

Bild2.png

# Optical fiber meta-tips

Friday, 20th October - 17:31 - Multi-Topic - Auditorium - Oral - Abstract ID: 335

**Dr. Maria Principe<sup>1</sup>, Prof. Marco Consales<sup>1</sup>, Dr. Alberto Micco<sup>1</sup>, Dr. Alessio Crescitelli<sup>2</sup>, Dr. Giuseppe Castaldi<sup>1</sup>, Dr. Emanuela Esposito<sup>3</sup>, Dr. Vera La Ferrara<sup>4</sup>, Prof. Antonello Cutolo<sup>1</sup>, Prof. Vincenzo Galdi<sup>1</sup>, Prof. Andrea Cusano<sup>1</sup>**

*1. University of Sannio, 2. Institute for Microelectronics and Microsystems, National Research Council, 3. Institute of Nanotechnology – CNR, 4. UTPP-MDB, Materials and devices, ENEA — Portici Research Center*

We present the first experimental demonstration of an optical-fiber “meta-tip” (OFMT). OFMTs are the result of the integration of a metasurface on the tip of an optical fiber (Figure 1a). Metasurfaces (MSs) are 2D implementations of metamaterials and are able to impress abrupt phase and amplitude variations in an impinging light wavefront so to allow local light manipulation for a large variety of applications. MSs are much easier to fabricate with respect to their bulk (3D) counterpart and compatible with on-chip photonics. We use plasmonic metasurfaces, based on an array of rotated rectangular aperture (Figure 1c) nanoantennas milled in a thin gold film deposited on the tip of an optical fiber. The antennas present a suitable spatial-modulation of the element sizes so as to implement a linear phase (or a constant phase gradient) trend (Figure 2). Such a MS will impress abrupt phase variations in the impinging field wavefront. We fabricated (Figure 3) and characterized in the far-field (Figure 4) several near-infrared prototypes implementing generalized forms of the Snell’s transmission/reflection laws, in terms of beam steering, with various angles  $\theta_t$  (Figure 1b). The measured steering angles are in fairly good agreement with the theory for all fabricated samples. As limit case we realized an OFMT exciting surface waves in transmission, i.e. with steering angle exceeding  $90^\circ$ , and explore its capability to work as a sensor. OFMT’s sensitivity to refractive index variations has been tested and compared to a gradient-free plasmonic benchmark array: the sensitivity of the OFMT overwhelms that of the benchmark by a factor of 1.7. Our results set the stage for the integration of metasurfaces, and their exceptional light-manipulation capabilities, in fiber-optics technological platforms, within the emerging “lab-on-fiber” paradigm. By leveraging the versatility and ubiquity of fiber-optics technology, this may constitute a key step towards the widespread use of optical metasurfaces in real-world applications to communications, signal processing, imaging and sensing.

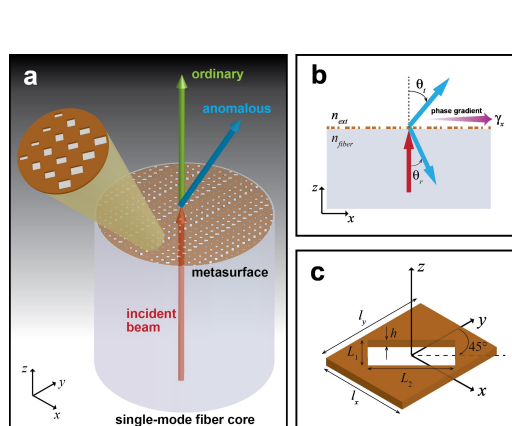


Figure 1.jpg

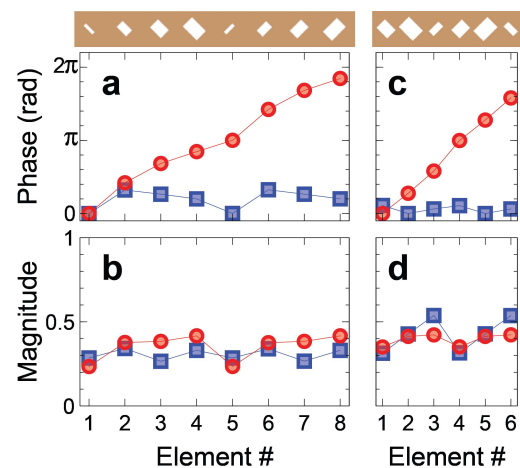


Figure 2.jpg

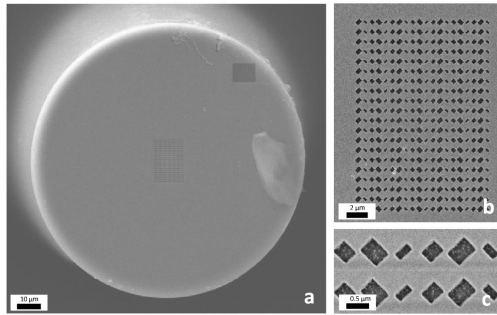


Figure 3.jpg

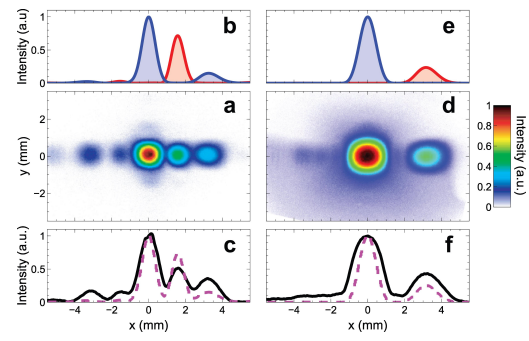


Figure 4.jpg

---

## Staphylococcus aureus Exotoxin Detection Using Potentiometric Nanobiosensor(MIP) based on Microbial Electrode Approach with Effects of pH and Temperature

---

Friday, 20th October - 20:00 - Video Presentation - Online - Video - Abstract ID: 377

---

**Dr. HAMED AHARI<sup>1</sup>, Dr. Mehdi Hedayati<sup>2</sup>, Dr. Amirali Anvar<sup>3</sup>, Dr. Behrouz Akbari-adergani<sup>4</sup>, Prof. Hedayat Hosseini<sup>5</sup>, Dr. Shapour Kakoolaki<sup>6</sup>**

*1. Department of Food Science and Technology, Science and Research Branch, Islamic Azad University, 2. Cellular and Molecular Endocrine Research Center, Research Institute for Endocrine Sciences, Shahid Beheshti University of Medical Sciences., 3. Hygiene department of Science and Research Branch, Islamic Azad University, 4. Food and Drug Laboratory Research Center, Food and Drug Organization, Ministry of Health and Medical Education, 5. Department of Food Sciences & Technology, National Nutrition and Food Technology Research Institute, Faculty of Nutrition Sciences and Food Technology, Shahid Beheshti University of Medical Sciences, 6. Agricultural Research, Education and Extension Organization (AREEO), Iranian Fisheries Science Research Institute*

Considering the ever-increasing population and trends in industrialization, it is difficult to detect the toxins produced in food products using traditional techniques. In this study, the potentiometric nanobiosensor technique using selective patterns for *Staphylococcus aureus* exotoxin was thoroughly considered. A molecular framework with polymer was produced using methacrylic acid (MAA) monomers, which formed covalent bonds between MAA monomers to produce a white polymer. In addition, hydrogen bonds formed between the amino acids of the exotoxin and the MAA functional groups, which functioned as selective sites for the polymer. To evaluate the effect of pH on the *S. aureus* exotoxin nanobiosensor, diluted solutions of NaOH and HNO<sub>3</sub> were applied for the upper and lower pH levels, respectively. The effect of temperature was adjusted by incubating the exotoxin solutions in an incubator. The results showed that the molecular framework polymer (MFP) in the designed biosensor was able to detect an exotoxin density up to the detectable limit (10<sup>-3</sup>M) at 68 nm of synthesized molecularly imprinted polymer (MIP) during the first 32 days of the experiment (from a total of 56 days). The potential differences remained constants at an optimum pH range of 5.0–8.5 and at an optimum temperature range of 15°C–25°C. Therefore, we concluded that the pH and temperature can affect the precision of a potentiometric nanobiosensor for detecting *S. aureus* exotoxin.

# Authors Index

Ababneh, A.	319	Anicai, L.	35, 190
Abay, D.	172	Ansaldo, A.	323
Abdala, A.	109	Antic, B.	177
Abdelmahmoud Abdelkarim Maki, M.	298	Anvar, A.	347
Abdelmalek, A.	307	Aquino, R.	318
Abdi, Y.	67, 193	Arbiol, J.	130
Abdullyn, K.	23	Arduino, I.	126
Abe, Y.	53, 312	Argurio, R.	50
Abu Dalo, M.	322	Artyukhin, S.	136
Adamkova, V.	257	Arumugam, S.	156
Afrianingsih, I.	302	Ayoko, G.	156
Agostiano, A.	126, 220	Aznar Gimeno, E.	14
Ahari, H.	347	Azzaz, M.	195
Ahmed, s.	93, 143, 240		
Ahoba Sam, C.	242	Baburin, A.	98
Ajalloueian, F.	335	Bae, K.	170
Akarsu, E.	233	Bajpai, G.	100
Akbari Adergani, B.	347	Bakranov, N.	44
Akkerman, Q.	89	Balan, D.	35, 190
Al Hetlani, E.	306	Baldea, I.	183, 343
Al Mheidat, I.	322	Balezin, M.	79
Al Shurafat, A.	322	Ballay, R.	257
Alberti, S.	244	Banerjee, S.	71
Albiss, B.	319	Barakati, b.	70, 270
Alcaraz, L.	105	Baranov, A.	73, 225
Alguacil, F.	95	Baranov, M.	73, 225
Alhajji, L.	174, 305	Barantchikov, A.	147
Aliaga, C.	97	Barawi, M.	284
Alkandary, A.	111, 320	Barba, D.	30
Almendarez Camarillo, A.	52	Barbalinardo, M.	78
Almutawa, F.	305	Barbosa Sabanero, G.	20
Alni, A.	302	Bariza, B.	65
Alshammari, H.	283	Barros, N.	76
Altamura, D.	220	Baryshev, A.	98
Alvarado Caudillo, Y.	20	Barzola Quiquia, J.	230
Alvarez, M.	332	Bayesteh, s.	294
Alvina, M.	178	Bedrane, Z.	307
Alzubi, f.	111, 320	Behfar, A.	324
Amin, M.	306	Belbekhouche, S.	229
Amler, E.	314, 316	Belinova, T.	150
Andrade, R.	181	Benabbes, O.	40
Angeloni, I.	277	Benhaddad, M.	40, 199



Benny, O.	122	Carrillo Carrion, C.	124
Benyahia, b.	59	Carsughi, F.	149
Berezkina, A.	254	Casalini, S.	78
Berkowski, M.	259	Cascella, F.	220
Bertoni, G.	89, 323	Casermeiro, M.	105
Bertrand, G.	277	Castagnola, E.	201, 210
Betley, T.	324	Castaldi, G.	345
Bezdetnaya, L.	118	Castaña, V.	189
Bianconi, A.	4	Castellano, M.	244
Bilski, P.	259	Castán, H.	325
Bin Abdul Majeed, A.	298	Cea, C.	210
Biswas, S.	217	Celichowski, G.	216
Biter, T.	267	Cenariu, M.	183
Blahnova, V.	316	Cerchez, V.	336
Blanc, W.	221	Chae, J.	327
Boodhoo, K.	242	Chagelishvili, E.	166, 186
Bozetine, i.	114, 196	Chatterjee, s.	41
Braic, M.	226	Chaussedent, S.	221
Brescia, R.	89, 256	Chelouche, A.	30, 145, 146, 154
Brihi, N.	59	Chen, C.	57, 203
Brincoveanu, O.	190	Chen, L.	323
Brito, P.	318	Chen, W.	260
Brougham, D.	83	Chenxin, L.	209
Brumfeld, V.	234	Cheraga, H.	196
Buca, D.	226	Cherevkov, S.	73
Budnik, A.	161	Chimnoi, N.	180
Bulanova, E.	161	Cho, M.	290, 327
Bulfin, B.	328	Cho, Y.	60, 170
Bustamante, A.	165	Choi, S.	317
Butova, V.	161	Choi, s.	251
Buyanova, I.	260	Chronakis, I.	235
Buzgo, M.	314	Chung, T.	84
Bystronova, J.	6	Chuysinuan, P.	10, 173, 180
Byun, D.	99	Chávez, F.	24
Bzhalava, T.	272	Ciarpella, F.	201
		Cicoira, F.	246
Cabras, V.	232	Ciurea, M.	226
Cakir, D.	82	Clichici, S.	183
Calcagno, V.	230	Coca Calderón, M.	165
Camisasca, A.	333	Cogoi, S.	138
Campos, A.	318	Cohen, S.	75
Canepa, F.	126	Colombo, M.	323
Caratto, V.	244	Consales, M.	345
Carbonnier, B.	229	Costas, A.	81
Cardona Juárez, T.	189	Costovici, S.	190
Carli, s.	201, 210	Covaliu, C.	113, 151
Carril, M.	124	Crescitelli, A.	345
Carriles, R.	20		

---

Cristea, D.	262	Durand, G.	332
Crivillers, N.	78	Dvořák, L.	36
Cuenca Bustos, A.	14	Dytrych, P.	139
Curri, M.	126, 220	Dřínek, V.	139
Cusano, A.	345	Ebau, F.	232
Cutolo, A.	345	Eberle, B.	74, 223
Cutrignelli, A.	126	Egami, C.	153
Czechowska, E.	216	El Joukhar, I.	229
D Amora, M.	333	Elezovic, N.	91
D, S.	120	Enachescu, M.	35, 190
Dadasheva, I.	285	Enculescu, I.	81, 179, 282
Dang, Z.	89, 136	Enculescu, M.	179
Darbyshire, A.	21	Engel, J.	276
Dau, M.	336	Ennas, G.	232
David, L.	176, 183	Enomoto, K.	68
De Trizio, L.	136, 284	Ercius, P.	91
Decea, N.	176, 183	Esposito, E.	345
Dechtrirat, D.	10, 173	Estellé, P.	188
Del Vecchio, P.	274	Estrela Lopis, I.	230
Deming, T.	121	Evanghelidis, A.	179, 282
Demo, P.	265	Evgeny, S.	178
Dengler, S.	74, 223	Fadda, A.	232
Denk, F.	257	Fadiga, L.	201, 210
Denora, N.	126	Fajgar, R.	8, 139
Depalo, N.	126, 220	Fal, J.	188
Depeyrot, J.	318	Falaleev, O.	51
Devi, P.	41	Fan, X.	5
Dgebuadze, A.	166, 186	Fanizza, E.	126, 220
Di Gregorio, M.	234	Fantinati, A.	210
Diaz, P.	255	Fayyad, S.	205
Dilena, E.	323	Fedorov, A.	73, 225
Dinescu, A.	262	Ferguson, S.	83
Dinh, D.	339	Ferretti, M.	244
Djouadi, D.	30, 145, 146, 154	Ficai, A.	197
Dogan, N.	237	Ficai, D.	197
Dogan, S.	136	Filip, G.	176, 183
Dolina, J.	36	Filova, E.	316
Dolinová, I.	36	Fleddermann, J.	230
Donadio, G.	274	Florica, C.	81
Doriya, K.	43	Fneich, H.	221
Dornelas, L.	181	Formicola, B.	116
Dorofeenko, A.	98	Fortas, G.	196
Dosbolayev, M.	310	Francis, S.	276
Driscoll, J.	129	Friend, C.	324
Du Plessis, J.	279	Fucikova, A.	150
Dubavik, A.	73	Fujii, M.	150
Dueñas, S.	325		

---

Fukuda, M.	32	Hannula, S.	215
Gabay, T.	86	Hassanain, W.	156
Gabdullin, M.	23, 172, 310	Hata, Y.	153
Gabouze, N.	195, 196	Hazra, P.	167
Galdi, V.	345	Hedayati, M.	347
Ganem Rondero, F.	185	Hege, C.	74, 223
Garcia Diaz, I.	95, 105	Helmig, R.	12
García Casillas, P.	52	Henke, P.	15
Gaspari, R.	284	Hong, J.	132, 264, 269
Gaumer, N.	221	Hong, S.	266
Gavrilov, S.	134, 254	Hosseini, H.	347
Ge, Y.	215	Hotowy, A.	175
Generosi, A.	218	Houben, L.	234
Georgakopoulos, S.	78	Hoyoz Guzman, J.	189
Georgescu, M.	197	Huang, Y.	12, 18, 260
Ghaddar, N.	205	Hubalek Kalbacova, M.	150, 257
Ghali, K.	205	Huerta Angeles, G.	227
Ghosh, B.	217	Huidobro Toro, J.	255
Giannini, C.	220	Hurskyy, S.	184
Gibson, G.	330	Hwang, H.	303
Giordani, S.	333	Hwang, S.	46
Godibadze, B.	166, 186	Hynönen, U.	215
Golgovici, F.	35	Ibraev, N.	44
Goodilin, E.	147	Ijaz, p.	277
Granbhom, H.	215	Il'ves, V.	79
Graup, V.	21	Imran, M.	89, 256
Greco, P.	78	Inam, F.	281
Gregori, M.	116	Inoue, T.	32
Grinham, C.	322	Ishchenko, A.	236
Grishina, Y.	134	Ishii, Y.	32
Grobelny, J.	216	Ismail, N.	205
Grodzik, M.	175, 187	Ismailov, D.	23, 172
Gromova, Y.	225	Isticato, R.	274
Guaragno, M.	218	Ivanov, V.	147
Guedouar, B.	195	Ivanova, A.	236
Gulyaev, R.	236		
Gun'ko, Y.	225	J. L. Ribeiro, S.	131
Guo, Z.	50	J. W. Shimon, L.	234
Guseinov, N.	172	Jakobsen, U.	138
		Jamet, M.	336
Hailu, D.	291	Jamieson, S.	39
Haine, N.	196	Jandová, V.	8
Hamid, M.	114, 196	Jang, H.	99
Hamliche, L.	145, 146, 154	Jaworski, S.	175, 187
Hamreh, S.	311	Jens, K.	242
Han, I.	99	Jeong, S.	37
Han, S.	88, 317	Jeronimo, K.	33

Jha, P.	217	Klemes, J.	6, 227
Jha, S.	63	Ko, H.	99
Ju, B.	132, 251, 269	Ko, S.	163
Jurjiu, A.	47, 267	Koninti, R.	167
Kachkachi, H.	76	Kopacek, V.	292
Kaci, S.	114	Kormilina, T.	73
Kakavelakis, G.	218	Kotsikos, G.	330
Kakoolaki, S.	347	Kotzianova, A.	6, 227
Kalam, K.	325	Koutsos, V.	33
Kang, H.	303	Kozempel, J.	214
Kang, I.	290	Koštejn, M.	8
Karahan, M.	271	Kožíšek, Z.	265
Kardash, T.	236	Krahne, R.	136
Karimi, I.	296	Kremennaya, M.	285
Karimi, m.	268	Kriegel, I.	284
Kasahara, K.	252	Krmelová, T.	214
Kassegne, S.	210	Krstajic Pajic, M.	91
Kawaguchi, S.	68	Krstajic, N.	91
Kawamura, M.	53, 312	Kubát, P.	15
Keceli, M.	82	Kuchеров, M.	51
Keffous, A.	114	Kudaibergenov, S.	44
Kellner, J.	107	Kudera, S.	136
Kellnerová, E.	107	Kukli, K.	325
Kerrou, F.	40	Kumar, G.	41
Kervailishvili, P.	272	Kunar, S.	71
Kesmez, Ö.	233	Kurantowicz, N.	175, 187
Khabarov, K.	98	Kurylionak, A.	54
Khamsavi, A.	67, 193	Kusumawardani, C.	115
Khasaya, R.	48	Kutwin, M.	175, 187
Khlaychan, P.	180	Kuznetsova, V.	225
Khomich, Y.	48	Kvitek, O.	292
Khosravi, Y.	193	Kwak, Y.	251
Kiba, T.	53, 312	Kwiatkowski, A.	243
Kikuchi, M.	68	Kwon, G.	11
Kim, B.	137	Kwon, J.	163
Kim, D.	327	Kymakis, E.	218
Kim, G.	84	La Ferrara, V.	345
Kim, H.	11, 28, 141, 288, 300	La Rosa, A.	332
Kim, J.	28, 132, 269, 278, 286, 288, 300	Lafi, T.	319
Kim, K.	53, 251, 303, 312	Lahav, M.	75, 234
Kim, S.	1, 88, 317	Lamberti, C.	161
Kim, T.	286, 317	Lambertini, L.	201, 210
Kimijima, S.	42	Lameh, M.	205
Kiriakous, E.	156	Lan, P.	57
Kisel, V.	26	Lanzilli, M.	274
Klapkova, E.	257	Laquintana, V.	126
Klementová, M.	139	Lassalle, H.	118

---

Laurentia, A.	197	Mahiou, R.	30
Lawanstien, D.	101	Mahmoudi, B.	59
Lazanu, S.	226	Mahuof, A.	330
Lazavenka, A.	192	Majumder, S.	71
Le Quang, t.	336	Maklakov, S.	26
Lee, B.	126, 132, 269	Maksoud, F.	205
Lee, D.	286, 303	Maksymiuk, K.	103
Lee, G.	303	Malachias, Â.	181
Lee, H.	28, 163	Mallet, P.	336
Lee, J.	132, 137, 163, 264, 269, 286	Malykhin, S.	236
Lee, N.	60, 170	Mama, N.	279
Lee, P.	203	Mamniashvili, G.	166
Lee, S.	264	Manca, M.	232, 284
Lee, Y.	66, 84, 137	Manna, L.	89, 136, 256, 284, 323
Lepadatu, A.	226	Manseri, A.	114, 196
Lesniewski, A.	16	Manzanares, A.	20
Lettieri, S.	333	Marcos Martinez, M.	14
Li, Y.	38	Marko, G.	86
Liao, Z.	261	Marras, S.	323
Lim, S.	266	Martynyuk, N.	259
Lim, T.	264	Martínez Antonio, A.	20
Link, J.	325	Martínez Hernández, A.	52
Linzoain, M.	332	Marçal, L.	181
Lisboa De Oliveira, H.	318	Mas Torrent, M.	78
Litvin, A.	73	Maslov, V.	225
Liu, G.	38	Masserini, M.	116
Liu, J.	5	Mastropaolo, E.	33
Liu, Z.	239	Matei, E.	81, 151, 282
Lopedota, A.	126	Matteoli, M.	116
Lopez Fernandez, A.	105	Matyas, J.	56, 169, 301
Lopez Tendero, M.	14	Matyjewicz, J.	16
Lopez, F.	95	Mauri, M.	244
Loureiro Mendes, A.	235	Meerovich, V.	27
Lukasova, V.	315	Mehdi, A.	221
Lund, G.	20	Meijer, J.	230
Lustoza, P.	181	Menacho, L.	165
Lv, R.	12	Menari, H.	195
Lynch, I.	249	Meng, Y.	18, 58
Lyutakov, O.	8	Menous, I.	59
López Barroso, J.	52	Merker, C.	230
López, F.	105	Merlat, L.	74
López, R.	275	Merlin, J.	83
Machová, I.	150	Meyer, T.	230
Madkour, M.	306	Micco, A.	345
Maekawa, T.	120	Michalska, A.	103
Maghchiche, A.	198	Mikkor, M.	325
Maglione, M.	78	Mikolutskiy, S.	48

---

Min, J.	60	Okolo, C.	281
Ming Tatt, L.	298	Oladimeji, E.	77
Mishin, A.	26	Olejniak, R.	56, 169, 301
Mohamed, S.	120	Oliva, R.	274
Molchanov, V.	243	Oliveira, F.	158
Moldovan, B.	176, 183	Olsbye, U.	242
Monaco, S.	323	Olteanu, D.	183
Morales, N.	24	Omirebekov, D.	310
Moreels, I.	277	Orazbayev, S.	310
Mortazavi, S.	294	Ortega Arroyo, L.	189
Mosinger, J.	15	Ortega Mendoza, J.	24
Mosselhy, D.	215	Osmanova, E.	313
Mouloud, K.	199	Otarbay, Z.	23, 172, 310
Muller, O.	74, 223	Otsuji, T.	207
Muratov, M.	172	Ouarez, L.	30, 154
Murotani, H.	312	Oyanedel Craver, V.	322
Mustafaeva, Z.	271	Ozdemir, E.	237
N. Oliveira Jr., O.	131	Paci, B.	218
Nadal, E.	76	Padilla Martínez, J.	24
Namoune, A.	145	Palade, C.	226
Narumi, A.	68	Palazon, F.	136
Nasir, M.	302	Palermo, V.	2
Navratil, J.	107	Palva, A.	215
Nayak, P.	63	Pananon, P.	10
Nechanická, M.	36	Panniello, A.	220
Nechepurenko, I.	98	Paolella, A.	323
Necib, K.	154	Parak, W.	124
Neto, M.	158	Paraschiv, G.	113, 151
Niedziolka Jonsson, J.	16	Park, B.	84
Nimbalkar, S.	210	Park, E.	46
Nissan, Y.	86	Park, H.	46, 327
Nogajewski, K.	336	Park, K.	99, 303
Noh, Y.	28, 288, 300	Park, N.	303
Nooeaid, P.	173, 180	Park, S.	264
Nordström, K.	215	Parkula, V.	78
Notomista, E.	274	Passoni, L.	116
Nouredine, O.	104	Pastene, C.	97
Novak, P.	341	Pattani, L.	180
Nunes, R.	181	Pedersen, E.	138
Nyamori, V.	279	Peikrishvili, A.	166, 186
Nykl, P.	214	Pelit Arayıcı, P.	271
		Pelleg, J.	27
Oancea, M.	282	Pengsuk, C.	173
Obreja, P.	262	Peres, L.	76
Oh, C.	46	Perez Rea, L.	189
Ohnishi, N.	9	Pertegas, S.	301
Okahisa, S.	32	Petica, A.	35

Petraccone, L.	274	Ricca, E.	274
Petralanda, U.	136	Riccardi, p.	25
Philippova, O.	243	Ricci, D.	201, 210
Piedade, A.	158	Riha, P.	56, 169, 301
Piedra Gil, H.	189	Rivera Armenta, J.	52
Pilloni, M.	232	Rives Monparler, A.	14
Pineda Hernández, M.	185	Rodionov, I.	98
Pinkas, I.	75	Rodrigues, W.	181
Pinna, N.	127	Rodríguez Ríos, D.	20
Pino Gaviño, J.	165	Roldan, A.	276
Pires, M.	181	Rosa, B.	181
Pligovka, A.	192	Rosei, F.	30
Podkovyrina, Y.	161, 285	Rossi Albertini, V.	218
Pokorny, M.	6, 227, 257	Rovira, C.	78
Polozov, V.	26	Roy, A.	41
Popov, A.	259	Russo, P.	127
Popovitz Biro, R.	75	Ryzhii, M.	207
Potemski, M.	336	Ryzhii, V.	207
Pradas, S.	14	Ryzhikov, I.	26
Pramanik, S.	41	Ryzhova, E.	98
Prato, M.	201, 210, 284	Rähn, M.	325
Preda, N.	81	Saade, H.	275
Prepelita, P.	226	Sabrina, S.	196
Principe, M.	345	Sahli, S.	199
Prodjosantoso, A.	115	Sakamoto, Y.	120
Purcell Milton, F.	225	Sambandam, A.	45
Pérez Corte, J.	24	San Martín, E.	189
Pérez Sánchez, G.	24	Sanchez Cabezas, S.	14
Qiao, N.	209, 338	Sanchez Góngora, M.	189
R. Domenegueti, R.	131	Sanchez Montoto, A.	14
Radmilovic, V.	91	Santhosh Kumar, D.	43
Ramazanov, T.	310	Saparpakorn, P.	10
Ran, R.	212	Sari, A.	59
Ranjan, P.	75	Sarikurt, S.	82
Ranoszek Soliwoda, K.	216	Sasar, M.	67, 193
Rashid, Z.	305	Sasnouski, I.	54
Raynaud, P.	199	Sauerova, P.	257
Re, F.	116	Sawosz, E.	175, 187
Redjda, N.	195	Scano, A.	232
Rehman, S.	264	Scarpellini, A.	201, 210
Respaud, M.	76	Scavo, M.	126
Reyhani, A.	294	Schledjewski, R.	301
Rezania, H.	308	Scotognella, F.	284
Rezende, M.	97	Scrobota, I.	183
Reznickova, A.	292	Scrosati, B.	323
Rezvani, E.	328	Seemen, H.	325
		Sekikawa, T.	9

---

Semenova, A.	147	Sovkova, V.	314
Sen, S.	100	Sriprachuabwong, C.	10
Seo, C.	303	Srisa Art, M.	101
Seo, J.	290	Srivastava, T.	100
Serano, R.	225	Stange, D.	226
Sevik, C.	82	Stastny, P.	315
Shalev, g.	86	Stavarache, I.	226
Shamsi, J.	89	Stellacci, F.	248
Shao, J.	18, 38, 58	Stern, R.	325
Sharifi, s.	200	Stoica, T.	226
Sharma, M.	63	Stratakis, E.	218
Shaymanov, A.	98	Striccoli, M.	126, 220
Shekarforoush, E.	235	Strojny, B.	175, 187
Shilyaeva, Y.	134, 254	Stéphan, O.	3
Shokri, A.	70, 270	Suchocki, A.	259
Shur, M.	207	Suchy, T.	257
Shvets, I.	328	Sugak, D.	259
Sid, N.	332	Sugimoto, H.	150
Siepi, M.	274	Sugiyarto, K.	115
Siew Wei, Y.	298	Sugurbekova, G.	328
Silakov, G.	134	Suharoschi, R.	183
Sillence, M.	156	Sun, C.	5
Silva, F.	318	Supova, M.	257
Silva, R.	131, 158	Svachova, V.	316
Sim, H.	28	Svir, K.	313
Sinder, M.	27	Svorcik, V.	292
Sindona, A.	25	Sybachin, A.	121
Sirigu, G.	284	Sysa, A.	134
Slav, A.	226	Syvorotka, I.	184
Slimi, O.	146	Szczepaniak, J.	175
Slobodian, P.	56, 169, 301	Szemraj, J.	216
Smaine, F.	299	Sánchez Segura, L.	20
Smrcek, S.	214	Talbi, L.	160
Sohn, A.	317	Tamm, A.	325
Sohn, h.	286	Tananaev, P.	98
Sokolovsky, V.	27	Tavadze, G.	186
Sokovnin, S.	79	Taylor, A.	332
Soldatov, A.	161	Techasakul, S.	173, 180
Soldatov, M.	285	Tehrani, A.	205
Solleti, G.	43	Tenne, R.	75
Song, R.	264	Teodorescu, V.	226
Song, S.	28, 288, 300	Terzis, A.	12
Song, W.	21	Tiour, F.	59
Song, Y.	260	Token, M.	172
Sonmez, M.	197	Toma, L.	113
Sosnowska, M.	175	Tomaszewska, E.	216
Soulantica, K.	76	Tomescu, R.	262

---



Tomovska, R.	8	Wang, S.	260
Tonooka, Y.	32	Weigand, B.	12
Tottereau, O.	195	Weishaupt, K.	12
Touam, T.	30, 145, 146, 154	Wibawa, A.	341
Trapella, C.	210	Wierzbicki, M.	175, 187
Triggiani, L.	220	Wilson, D.	131
Trujillo, W.	165	Winum, J.	299
Trunec, M.	315, 316	Wisitsorrat, A.	10
Trusca, R.	197	Wojdyla Cieslak, A.	332
Tseng, S.	13	Wongravee, K.	101
Tuantranont, A.	10	Wu, J.	12
Tudoroiu, L.	197	Xie, X.	9
Turcu, F.	267	Xodo, L.	138
Ualibek, O.	328	Yakavets, I.	118
Ubizskii, S.	184, 259	Yamshchikov, V.	48
Urso, C.	284	Yang, G.	12
Ushakova, E.	73	Yankovskij, G.	98
Valenta, J.	150	Yankovsky, I.	118
Van Den Berg, a.	250	Yaroslavov, A.	121
Van Der Boom, M.	75, 234	Yavuz, C.	237
Vargas Aparicio, J.	189	Yazdani, A.	70, 200, 270, 311
Vasile, E.	113, 151	Ye, J.	42
Vasylechko, L.	184	Yeon, C.	304
Veeranarayanan, S.	120	Yerlanuly, Y.	23
Velasco Santos, C.	52	Yilmaz, E.	271
Velebny, V.	6, 227	Yoo, C.	137
Vengoechea, F.	189	Yoo, J.	137
Venkateswara Rao, K.	43	Yoon, H.	137
Vermillac, M.	221	Yoon, K.	66
Veuillen, J.	336	Yoon, Y.	290
Večeřa, Z.	107	Youcef, F.	199
Vicini, S.	244	Youn, d.	304
Vijayaraj Kumar, P.	298	Yu, J.	11
Villa, S.	126	Yun, S.	304
Villaescusa Alonso, L.	14	Yuri G, R.	77
Visan, T.	190	Zabinski, P.	91
Vischio, F.	126	Zaborova, O.	121
Vlk, M.	214	Zaca Morán, P.	24
Vlková, D.	36	Zaina, S.	20
Vocetkova, K.	314	Zakhlebayeva, A.	192
Vogel, S.	138	Zarria Romero, j.	165
Vojtova, L.	316	Zavelani Rossi, M.	284
Volovlikova, O.	134, 254	Zeman, T.	107
Vomiero, A.	128	Zergoug, M.	196
Vrabcova, L.	150	Zhang, R.	127
Wang, C.	18, 57, 58, 203	Zhou, K.	338

Zhou, L.	38	Zorin, V.	118, 217
Zhu, W.	5	Zucchini, E.	201
Zhunisebekov, A.	310	Zulfikar, M.	302
Zhydachevskyy, Y.	259	Zulkifili, A.	42
Zidek, O.	6, 227		
Zong, Y.	50	Żyła, G.	188

